USMCA 2019

18th INTERNATIONAL SYMPOSIUM
ON NEW TECHNOLOGIES
FOR URBAN SAFETY OF MEGA CITIES IN ASIA

9-10 December 2019
Yangon, Myanmar

11-12 December 2019
Technical tour / Bagan, Myanmar

USMCA 2019

ICUS Report 2019-(serial No. 81)

the 18th International Symposium
on New Technologies
for Urban Safety of Mega Cities in Asia

October 9-12, 2019
at
Yangon Technological University, Myanmar

Organized by
Yangon Technological University, Myanmar

&

International Center for Urban Safety Engineering,
Institute of Industrial Science, The University of Tokyo, Japan

Sponsored by

Super Global University (SGU) Project of UTokyo

Cooperated by

Japan International Cooperation Agency (JICA),
SATREPS Office

SYMPOSIUM ORGANISERS

■ CHAIRPERSON & CO-CHAIRPERSON

Prof. Nyan Myint Kyaw	Chairperson, Head, Dept. of Civil Engineering, Yangon Technological University (YTU), Myanmar
Prof. Kimiro Meguro	Co-chairperson, Director, ICUS, IIS, The University of Tokyo (UTokyo), Japan

■ STEERING COMMITTEE

Prof. Myint Thein	Rector, YTU, Myanmar
Prof. Sint Soe	Rector, Mandalay Technological University, Myanmar
Mr. Aung Myint	President, Fed. MES, Myanmar
Prof. Mehedi Ahmed Ansary	Bangladesh University of Engineering Technology (BUET), Bangladesh
Prof. Sudhir Misra	Indian Institute of Technology Kanpur, India
Prof. Emeritus Taketo Uomoto	UTokyo, Japan
Prof. Toshiharu Kishi	Director General, IIS, UTokyo, Japan
Prof. Wei Cheng Fan	Director, CPSR, Tsinghua University, China
Prof. Pennung Warnitchai	Head of Dept, of Civil and Infrastructure Engineering, Asian Institute of Technology (AIT), Thailand
Prof. Emeritus Yoshifumi Yasuoka	UTokyo, Japan
Dr. Haruo Sawada	President, Forestry and Forest Products Research Institute, Japan

■ TECHNICAL COMMITTEE

Dr. Khin Than Yu	Former Pro-rector, YTU, Myanmar
Prof. Tun Naing	Head, Dept. of Engineering Geology, YTU, Myanmar
Prof. Theingi Shwe	Head, Dept. of Architecture, YTU, Myanmar
Prof. Sao Hone Pha	Director, RS&GIS Research Center, YTU, Myanmar
Prof. Kiang Hwee Tan	National University of Singapore, Singapore
Prof. Pradeep Kumar Ramancharla	International Institute of Information Technology, Hyderabad, India
Prof. Kimiro Meguro	Director, ICUS, IIS, UTokyo, Japan
Prof. Reiko Kuwano	ICUS, IIS, UTokyo, Japan
Prof. Wataru Takeuchi	IIS, UTokyo, Japan

■ ORGANIZING COMMITTEE

Prof. Htin Lin	Dept. of Mechatronic Engineering, YTU, Myanmar
Dr. Kyaw Zaya Htun	Deputy Director, RS&GIS Research Center, YTU, Myanmar
Dr. Kyaw Zin Latt	Lecturer, Dept. of Engineering Geology, YTU, Myanmar
Ms. Tomoko Matsushita	Project Researcher, ICUS, IIS, UTokyo, Japan

■ CONTACT PERSON

Ms. Eiko Yoshimoto	Project Specialist, ICUS, IIS, UTokyo, Japan

PREFACE

On behalf of the Organizing Institutes of the 18th International Symposium on New Technologies for Urban Safety of Mega Cities in Asia (USMCA2019), I express our sincere welcome to all symposium participants and distinguished keynote speakers.

In the Asia and Pacific-Rim regions, rapid economic development and population growth and concentration are fast accelerating the pace of urbanization. Unfortunately, the rapid expansion of infrastructure for urbanization is not adequately balanced with appropriate measures for their maintenance and management; thus, big urban disasters have resulted.

The International Center for Urban Safety Engineering (ICUS) was established in 2001 at the Institute of Industrial Science (IIS), the University of Tokyo (UTokyo). The objectives of ICUS are to carry out advanced researches on urban safety and to implement safer cities especially in Asia and the Pacific-Rim region in the 21st century. For over a decade, ICUS has been actively tackling advanced researches, as well as the enhancement of networking, information collection and dissemination in order to fully realize ICUS's vision. As a part of ICUS activities, ICUS has been annually co-organizing USMCA since 2002 with its partners in the Asian region.

In December 2019, ICUS jointly held the 18th USMCA in Yangon, Myanmar, with Yangon Technological University (YTU). This was the second USMCA in Yangon. YTU and ICUS jointly established the 5-year project in 2014 under the scheme of SATREPS (Science and Technology Research Partnership for Sustainable Development) with the support from JST (Japan Science and Technology Association) and JICA (Japan International Cooperation Agency). The title of the project is "Development of a Comprehensive Disaster Resilience and Collaboration Platform in Myanmar" and its aims are to reduce future damage caused by floods including storm surges and earthquakes in Yangon City and the Bago River Basin, and to increase the resilient capacity of the target areas. In order to achieve the goal mentioned above, research activities have been carried out from the three viewpoints, i.e. structural measures (hardware), non-structural measures (software) and human capacity development. The year 2019 was the final year of the project, we had planned the SATREPS especial sessions. In the sessions, approximately 30 papers were presented. Including these papers, during the two-day symposium, 85 papers in eight parallel sessions were presented and four keynote lectures were delivered. We also had research exhibitions in 10 booths. Totally about 150 people from 12 countries participated in the symposium. Following the symposium, two-day survey visit to Bagan, old capital city, were conducted with over 60 participants.

The objective of the USMCA symposium is to bring together decision makers, practitioners and researchers involved in the field of urban safety to share their expertise, knowledge and experience in tackling the critical issues for safer cities in Asia and the Pacific Rim regions. It also provides an environment to create and reinforce collaborative networks among experts in the fields relevant to urban safety. The symposium focuses on urban safety and disaster mitigation, infrastructure management, and environment informatics.

I would like to thank all the members of the Steering, Technical and Organizing Committees as well as the Symposium Secretariat for their hard work, time and effort in putting this symposium together. I would also like to thank all our sponsors, especially Super Global University (SGU) Project of UTokyo that supported us to prepare this Proceedings. Thanks are also due to all those who have contributed towards making this symposium successful.

Professor Kimiro MEGURO
Director of ICUS, IIS, The University of Tokyo
(Co-Chairman of Organizing Committee, USMCA2019)

PROGRAM OVERVIEW

<table>
<tr><th colspan="3">Monday, 9 December</th></tr>
<tr><td>08:00 - 09:00</td><td colspan="2">Registration in front of Assembly Hall</td></tr>
<tr><td>09:00 – 09:50</td><td colspan="2">◆ Opening Ceremony at Assembly Hall
1. Welcome Address Prof. Myint Thein Rector, YTU
2. Opening Address Prof. Khin Than Yu
3. Address by Co-Chair Prof. Kimiro Meguro, UTokyo</td></tr>
<tr><td>09:50 – 10:30</td><td colspan="2">Group Photo – Exhibitions & Coffee Break</td></tr>
<tr><td>10:30 – 11:30</td><td colspan="2">◆ Keynote Speech at Assembly Hall
1. Prof. Kimiro Meguro, Director,ICUS, IIS, UTokyo
Development of a comprehensive disaster resilience system and collaboration platform in Myanmar
2. U Saw Htwe Zaw, Vice Chairman, Myanmar Earthquake Committee
Earthquake risk in Yangon</td></tr>
<tr><td>11:30 – 12:30</td><td colspan="2">Lunch at top floor</td></tr>
<tr><td>12:30 – 14:30</td><td>◆ Session A: at Conference Room
INFRASTRUCTURE MANAGEMENT: MAINTENANCE AND SUSTAINABILITY / CONSTRUCTION MATERIALS AND TECHNOLOGY
Session Co-Chairs:
Dr.Koji Matsumoto, Hokkaido Univ.
Prof. Pennung Warnitchai AIT</td><td>◆ Session B: at Seminar Room 1
URBAN SAFETY & DISASTER MITIGATION: DISASTER MANAGEMENT, RECOVERY AND REHABILITATION PLANNING, ENVIRONMENT INFORMATICS: TRANSPORTATION / BAGAN HERITAG
Session Co-Chairs:
Prof. Pradeep Kumar Ramancharla IIIT Hyderabad
U Saw Htwe Zaw, MEC</td></tr>
<tr><td>14:30 – 15:15</td><td colspan="2">Coffee Break & Exhibitions</td></tr>
<tr><td>15:15 – 17:05</td><td>◆ Session C: at Coference Room
URBAN SAFETY & DISASTER MITIGATION: DISASTER MITIGATION & URBAN PLANNING / EMERGENCY RESPONSE
Session Co-Chairs:
Dr. Tsukasa Mizutani, UTokyo
Dr. Htay Win, YTU</td><td>◆ Session D: at Seminar Room 1
SPECIAL SESSION: SATREPS/ DISATER MANAGEMENT / DISASTER MITIGATION AND URBAN PLANNING
Session Co-Chairs:
Prof. Takaaki Ikeda, NUT
Prof. Theingi Shwe, YTU</td></tr>
<tr><td>18:00 – 20:00</td><td colspan="2">Banquet at Lakeside Lawn, Inyalake hotel</td></tr>
</table>

Tuesday, 10 December		
09:00 – 10:40	◆ **Session E:** at Conference Room **URBAN SAFETY & DISASTER MITIGATION: RISK ASSESSMENT** *Session Chair:* *Dr. Makoto Fujiu Kanazawa Univ.* *Prof. Tun Naing, YTU*	◆ **Session F:** at Seminar Room 1 **SPECIAL SESSION: SATREPS/ TRANSPORTATION, INFRASTRUCTURE MANAGEMENT** *Session Co-Chairs:* *Dr. Junichi Susaki, Kyoto Univ.* *Direcotr Sao Hone Pha, YTU*
10:40 – 11:10	Coffee Break & Exhibitions	
11:10 – 12:50	◆ **Session G:** at Conference Room **ENVIRONMENT INFORMATICS: GIS/REMOTE SENSING, TRANSPORTATION, WATER RESOURCES, INFRASTRUCTURE MANAGEMENT** *Session Chair:* *Dr. Yudai Honma, UTokyo* *Prof. Khin Maung Zaw, YTU*	◆ **Session H:** at Seminar Room 1 **SPECIAL SESSION: SATREPS/ WATER RESOURCES, DISASTER MITIGATION AND URBAN PLANNNING** *Session Chair:* *Prof. Osamu Murao, Tohoku Univ.* *Prof. Kyaw Kyaw, YTU*
12:50 – 14:00	Lunch at top floor	
14:00 – 15:00	◆ **Keynote Speech** at Assembly Hall **1.** Dr. Takayuki Miyoshi, Urban and Spatial Development Division, Nippon Koei Co., Ltd. **Bagan Tourism Development Project (2014-2018)** **2.** Dr. Toe Aung, Director, Yangon City Development Committee **Urban safety for Mega City, Yangon**	
15:00 – 15:30	Coffee Break & Exhibitions	
15:30 – 16:30	◆ **Closing Ceremony** at Assembly Hall 1. **Young Award Ceremony** 2. **Announcement of USMCA2020** Prof. Pennung Warnitchai AIT 3. **Closing Speech** Prof. TunNaing, YTU 4. **Closing Speech** Prof. Kimiro Meguro, UTokyo	
18:30 -	Farewell Dinner at 9th floor Esperade lake view hotel	
Wednesday, 11- Thursday, 12 December		
Technical Tour at Bagan		

CONTENTS

SESSION B:

URBAN SAFETY & DISASTER MITIGATION: DISASTER MANAGEMENT, RECOVERY AND REHABILITATION PLANNING, ENVIRONMENT INFORMATICS: TRANSPORTATION / BAGAN HERITAGE

SESSION C:

URBAN SAFETY & DISASTER MITIGATION: DISASTER MITIGATION & URBAN PLANNING / EMERGENCY RESPONSE

SESSION D:

SPECIAL SESSION: SATREPS/ DISATER MANAGEMENT / DISASTER MITIGATION AND URBAN PLANNING

SESSION E:

URBAN SAFETY & DISASTER MITIGATION: RISK ASSESSMENT

SESSION H:

SPECIAL SESSION: SATREPS/ WATER RESOURCES, DISASTER MITIGATION AND URBAN PLANNNING

KEYNOTES

MyAnmar Nippon Zero-casualty Engineering Network (ANZEN) Project Science and Technology Research Partnership for Sustainable Development (SATREPS)

Kimiro MEGURO[1] and Khin Than Yu[2]
[1] Director and Professor, ICUS, Institute of Industrial Science, The University of Tokyo, Japan
meguro@iis.u-tokyo.ac.jp
[2] Ex-Pro-Rector, Yangon Technological University, Myanmar

ABSTRACT

Myanmar is a country where natural hazards, such as cyclones and earthquakes, occur frequently, but preparations for natural hazards are not enough. Cyclone damage occurs every year, and the three major cities of Myanmar, Yangon, Naypyidaw, and Mandalay are all located along the Sagaing fault, which is a major active fault.
Furthermore, with the support of many countries through the transition to democratization, development of urban areas is rapidly progressing. But due to the lack of consideration for disasters, these developments has been increasing the vulnerability against natural hazards and there is high possibility to have serious damage in future. When a city is developed once, it is difficult and needs more time and budget to reduce disaster risk. Now is a very important time to improve the city's disaster resilience, and missing this opportunity will create major problems in the future.
Thus, we have established this project with the aim of reducing future damage caused by floods including storm surges and earthquakes in Yangon City and the Bago River Basin. In order to achieve the goal mentioned above, from the three viewpoints, i.e. structural measures (hardware, maintenance technology based on vulnerability assessment of structures and maintenance management technology), non-structural measures (software, near real time flood inundation simulation system using monitored rainfall, disaster response support system) and continuation environment of research activity, we designed the 5-year (2014-2020) project under the scheme of SATREPS* (Science and Technology Research Partnership for Sustainable Development) with the support from JST (Japan Science and Technology Association) and JICA (Japan International Cooperation Agency). Nick name of our project is ANZEN (MyAnmar Nippon Zero-casualty Engineering Network) SATREPS project. The meaning of ANZEN is safety and security and it corresponds to our goal that we want to implement safer and securer Yangon society.
The research flow is as follows: 1) Create an integrated inventory database composed of structures, soil and ground information, rainfall, traffic and people flow, etc. by using the equipment provided by the project and by collecting existing data. Next, 2) Using these data, create a physical model to estimate damage due to flood and earthquake. 3) By combining this physical model with the future urban development model, prepare an environment in which the future urban planning can be examined from the amount of damage that changes due to different urban development scenarios. As final research results, 4) Develop a near real-time flood inundation simulator for the Bago River Basin,

a support system for disaster management planning and disaster response, and a technology for monitoring, maintaining and repairing infrastructure and buildings to reduce their damage. And the last, 5) In order to promote the understanding of project, continuation of research activities, and continuous utilization of the research results, develop lectures on urban safety in YTU, establish a Research Center, and a consortium aiming industry-government-academia collaboration.
As the year of 2019 is the final year of our 5-year project, we already obtained a lot of research results and these results will be introduced at the USMCA 2019.

Keywords: SATREPS Project, ANZEN SATREPS Project, Disaster Resilience, YTU and UTokyo

*: The SATREPS project is a project supported by JICA and JST. The project aims to achieve the following three points through collaboration between JST and JICA. Since April, 2008, 145 projects have been implemented in 51 countries around the world. Our project, ANZEN SATREPS project is the first adopted one in Myanmar. The total research fund is about 500 million yen and annual budget is 100 million yen (35 million yen from JST, 60 million yen from JICA)

1. Strengthening international cooperation on science and technology development between Japan and developing countries
2. Acquisition of new knowledge and technologies that lead to the resolution of global issues and the improvement of science and technology, and creation of innovations through them
3. Capacity development

Bagan Tourism Development Project (2014-2018)

Takayuki Miyoshi
Urban and Spatial Development Division, Nippon Koei Co., Ltd.
miyoshi-tk@n-koei.jp

ABSTRACT

Bagan became the UNESCO World Heritage Site in 2019. Before the nomination, JICA conducted technical transfer project for tourism development with the cooperation of the Myanmar Government. Through 14 pilot projects for tourism management, infrastructure and human resource development, JICA established a tourism management plan toward sustainable tourism.

SESSION A

INFRASTRUCTURE MANAGEMENT: MAINTENANCE AND SUSTAINABILITY / CONSTRUCTION MATERIALS AND TECHNOLOGY

Management method of inspection information for station facilities in Tokyo Metro stations

Kazuya KUSABA[1], Kotaro KURAMOTO[2],
[1] Chief of Architectural Section Infrastructure Maintenance Department,
Tokyo Metro Co.,Ltd., Japan
k.kusaba@tokyometro.jp
[2] Deputy Manager of Architectural Section Infrastructure Maintenance Department,
Tokyo Metro Co.,Ltd., Japan

ABSTRACT

Tokyo Metro comprises 9 lines, 195.1km of commercially operating track, and 179 stations, with a ridership of about 7.42 million persons per day.
The Tokyo Metro is the oldest subway system in Japan. When the Tokyo Metro began operations, the station buildings were finished paint on the civil engineered structures or other simple materials. Now, almost all the stations are given full interior finishing, and there are various disaster prevention equipment.
Falling and floating of them and equipment failures lead to operational problems and injuries to station customers. To prevent these accidents, maintenance of the station facilities is carried out by the following procedure.
1 Inspection and soundness judgment of station facilities
2 Management of inspection information
3 Implementation of repair
This report describes the management method of inspection information for station facilities carried out by Tokyo Metro, and the effects.

***Keywords**: Subway station, Maintenance, Inspection method, Soundness Judgment,*

1. INTRODUCTION

In Japan, the inspection of external walls is mandatory due to the high risk of falling objects, there is no legal requirement for the inspection of interior materials. However, Tokyo Metro is voluntarily performing inspections, because a falling object in a station can cause tremendous inconvenience to station users.
About interior finish, in addition to the annual visual inspection, we do contact inspection once in two years. About station equipment, we set inspection cycle of each equipment and carry out it. Based on the results of this inspection, we make a soundness judgment and carry out repair or follow up.
Previously, the information of these inspections was kept in documents, but it is a huge amount, so there is a concern that items to be observed may be overlooked.
Therefore, in order to eliminate the accident caused by the overlooking, we constructed an efficient management method of the follow-up observation items with a tablet and cloud system.

2.INSPECTION ITEMS AND METHOD OF STATION FACILITIES

Inspection items have been defined for all materials in all parts, including contact inspection and numerical measurement. Some of the major items are described in Figure 1.

Table 1. Major Inspection Items of interior finish

Part	Spaces	Objects	Scope of inspection	Inspection methods	Inspection scene	Inspection items
Ceiling	Platform Concourse Room for human occupation	Spandrel, aluminum panel, etc.	100%	Prodding (@900mm)		・Detachment of clip ・Installation condition of suspending bolts ・Missing screws, etc.
		Ceiling substrate	Partial	Visual inspection from all inspection hatches		・Embedding condition of inserts ・Detachment of clip, etc. ・Lifting of structural concrete (hammering tests within the reach)
		Inspection port	100%	Opening + contact inspection		・Detachment of clip ・Installation condition of suspending bolts ・Other, including wobbliness
	Concourse	Cross parting	100%	Retightening of screws		・Loosening/corrosion of screws ・Expansion of screw holes
	Track area	Mortar	100%	Hammering		・Lifting, bulging ・Cracks/fractures ・Other, including wobbliness

Part	Spaces	Objects	Scope of inspection	Inspection methods	Inspection scene	Inspection items
Wall	Platform Concourse	Tile Mortar	100%	Hammering		・Lifting/bulging ・Cracks/fracture ・Movement during contact inspection
		Metal plate Stone	100%	Pulling with suckers		・Wobbliness ・Missing screws ・Corrosion
Wall	Platform	Suspended wall	100%	Retightening of screws and pushing in		・Loosening of screws ・Condition of screw holes ・Chipping and cracking of board
Floor	Platform Concourse	Floor stone	100%	Visual		・Differences in level ・Chipping and cracking ・Wear
		Tactile paving	100%	Visual		・Differences in level ・Wear ・Discoloration
Incidental facilities	Platform Concourse	Three-sided door frames, coping (stone, metal)	100%	Shaking		・Wobbliness ・Chipping and cracking
		Signs	100%	Shaking		・Wobbliness ・Chipping and cracking
		Toilet booths	100%	Shaking		・Wobbliness ・Missing screws ・Corrosion

In addition to these inspections, we also inspect water supply / drainage facilities, Entrance/exit facilities and disaster prevention facilities to maintain their functions.

Table 2. Inspection of other facilities

facilities	Item	Cycle of inspection	Inspection scene	Inspection items
Water supply/drainage facilities	Tank to catch water	Once a year		・disinfection ・cleaning ・water analysis
	Booster pump	Once a year		・visual inspection ・function test
Entrance/exit facilities	Automatic door	3 times a year		・visual inspection ・operation test ・controller check ・mover check
	Shutter	Once a year		・visual inspection ・operation test ・controller check ・mover check
Disaster prevention facilities	Fire alarm	Twice a year	 	・visual inspection ・equipment check ・operation test
	Fire extinguishing Equipment	Twice a year		・equipment check ・performance test
	Anti-inundation Measure Equipment	Once in 2 years		・component inspection

3.EVALUATION CRITERIA

We use a 6-level evaluation to eliminate the effect of bias among individuals, so that the progression of deterioration may be monitored under standardized conditions(Table 3). In addition, a time limit for repair was defined for each level to ensure the timely implementation of necessary repairs.

Table 3: Risk Levels

Soundness	The impact of driving safety on safety	Measures
AA	threaten	Immediate repair
A1	Threaten early	Repair within 1 year
A2	Threaten in the future	Observation Repair within 3 years is advisable
B	If progressed, move to A	Observation Monitoring of the progression of deterioration
C	No effect so far	Observation
S	No abnormality	No abnormality

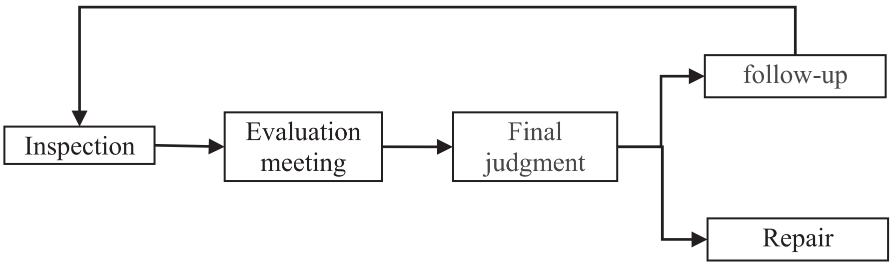

Figure 2: Flow from Inspection to Repair

4. INSPECTION INFORMATION MANAGEMENT METHOD

Although it was managed on paper media, there was a possibility that various problems would occur due to the huge amount of information (Table 4).

Table 4: problem on paper-based management system

Content	amount	Possibility of problems
Data storage	179 stations Filing book About 90 books	Increased storage space
Items at inspection	Number of drawings (10~ 20 sheets) Past inspection data (250sheets) Inspection tool (camera/ Test hammer/ measure etc.)	Oversight of follow-up items
Report creation time	2 months after inspection	Delay in construction planning
Inspection item	Per station250 items = 44,750 items at 179 stations	Neglect to do necessary repairs

Therefore, in order to maintain right situation, we started inspection with a tablet and management method with cloud system (Figure 3).

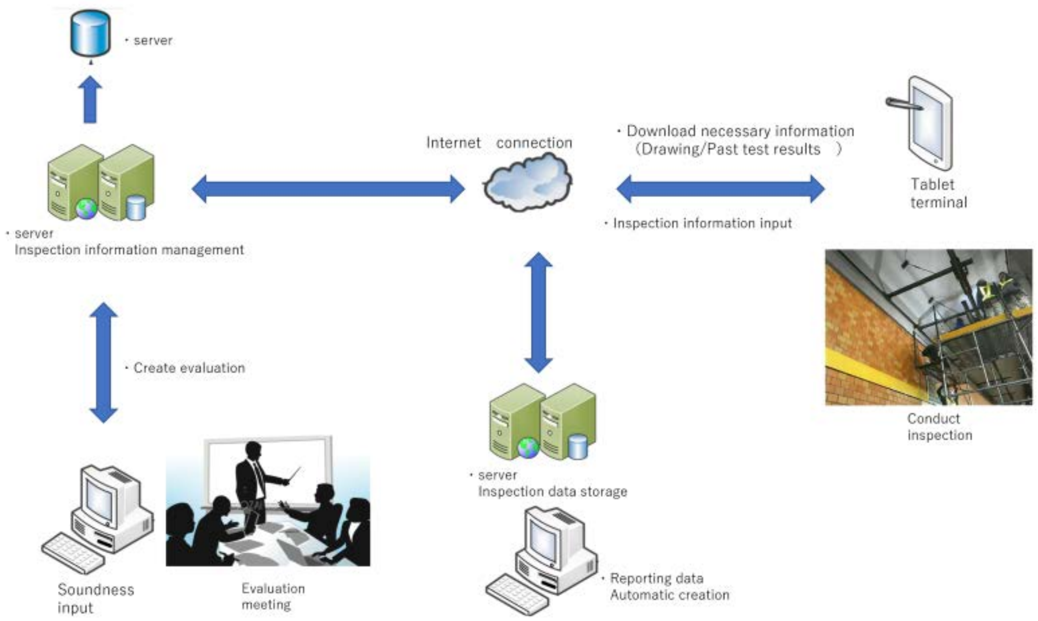

Figure 3: Information Management method with Cloud system

5. CASE (INSPECTION WITH TABLET)

5.1 Download past examination information to tablet

Download the floor plan and past inspection information (follow-up items) of the station to be inspected before the inspection starts in advance

5.2 Field inspection

5.2.1 Tablet input of results of palpation / sounding test

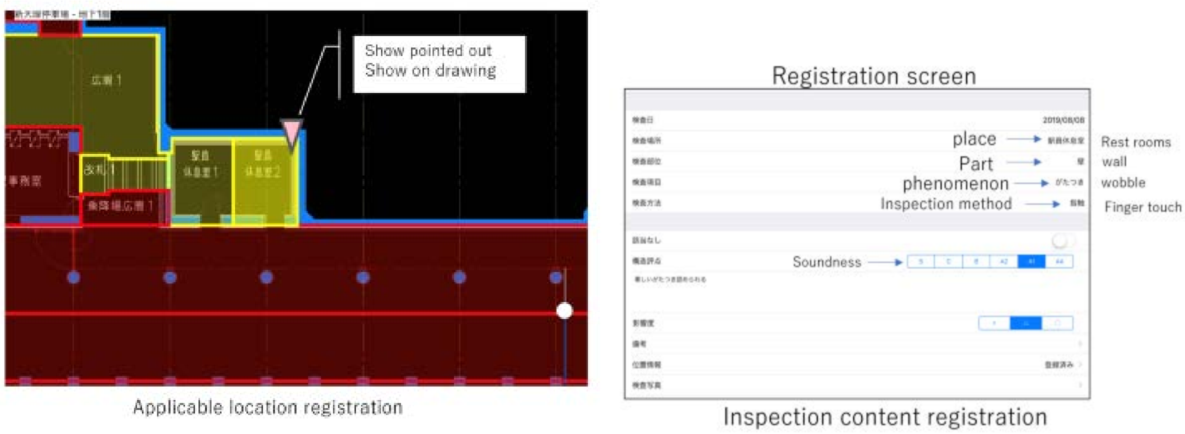

Figure 4: Input screen of inspection result and soundness

If an abnormality is found, it is registered in the tablet according to the criteria in Table 3 (Figure 4).

5.2.2 Check the progress and register the soundness of follow-up items

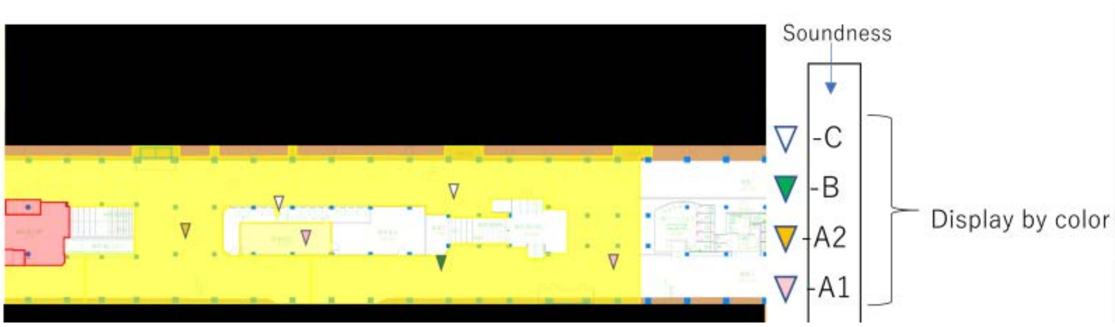

Figure 5: screen of follow-up items

The past examination information is displayed as points on the tablet plan view, and the contents are displayed by tapping the points.
As a result of the inspection, the health information is automatically registered in the server via the Internet line from the tablet for items that have been judged as AA (emergency measures) as a result of the inspection, and the person in charge of the inspection confirms the order for emergency measures construction

5.3 Determination of soundness

Regarding the soundness level, we will determine the final soundness level of the inspection information conducted in the local area, taking into consideration the structure and impact on the customer, and carry out repairs according to the soundness level.

5.4 Flow until construction

The determined soundness level is repair work or follow-up depending on the level (Fig. 2). For repair work, the inspection information is sent to the repair work implementer and the work is performed. When carrying out construction work, it was possible to monitor the progress of construction of parts that required repair as a result of inspection in cooperation with the construction management system.

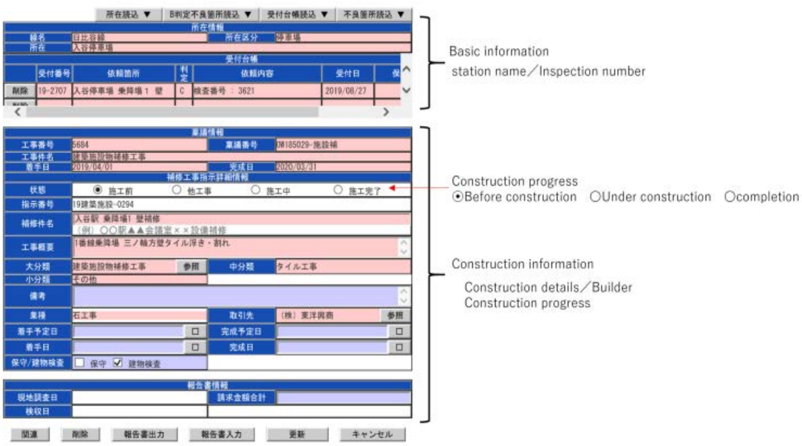

Figure 6: Screen of construction management system

6. EFFECT

By managing cloud-based inspections and inspection data from tablets based on paper-based inspections, as shown in (Table 5), it is possible to reduce the storage location, the amount brought in at the time of inspection and the reporting time, as described in (Table 4). Management issues have also been resolved. In addition, by managing the inspection information in the cloud, all employees involved in building maintenance can check the inspection information in real time, leading to more accurate building maintenance.

Table 5: effect

problem			effect
Content	amount	Possibility of problems	
Data storage	179 stations Filing book About 90 books	Increased storage space	Server room installation only No storage space expansion
Items at the time of inspection	Number of drawings(10~20 sheets) Past inspection data(250sheets) Inspection tool(camera/ Test hammer/ measure etc.)	Oversight of follow-up items	Displays all station drawings and past inspection information on a tablet There are 0 paper items (drawings and inspection information)
Report creation time	2 months after inspection	Delay in construction planning	Immediate reporting after inspection
Inspection item	Per station250 items = 44,750 items at 179 stations	Neglect to do necessary repairs	Reliable repair work

7. PRESENT ISSUES

By managing inspection information in the cloud, management of accurate inspection information has been performed. However, there are many inspection items and criteria when inputting inspection information using a tablet, and the tablet operation is partly complicated. In some cases, it may take time to enter inspection information. In the future, we want to improve the visibility and operability of the screen so that the tablet can be operated intuitively.

2-DIMENSIONAL PAVEMENT CONDITION EVALUATION BY SPATIAL FREQUENCY ANALYSIS OF POINT CLOUD DATA

T. MIZUTANI[1], T. ISHIDA[2], K. SUZUKI[3], Y. TAKAHASHI[4], Y. NAGATA[5], H. KAWAMURA[6]

[1] *Associate Professor, Institute of Industrial Science, , The University of Tokyo, Tokyo, Japan, mizu-t@iis.u-tokyo.ac.jp*
[2] *Professor, Department of Civil Engineering, School of Engineering, The University of Tokyo, tetsuya.ishida@civil.t.u-tokyo.ac.jp*
[3] *Aero Asahi Company, Tokyo, Japan, kiyoshi-suzuki@aeroasahi.co.jp*
[4] *Aero Asahi Company, Tokyo, Japan, youji-takahashi@aeroasahi.co.jp*
[5] *Shutoko Engineering Company Limited., Tokyo, Japan, y.nagata@shutoko-eng.jp*
[6] *Shutoko Engineering Company Limited., Tokyo, Japan, h.kawamura@shutoko-eng.jp*

***Keywords**: 2-Dimensional Pavement Condition Evaluation, Short Time Fourier Transform, Spatial Frequency Analysis, Point Cloud Data, Mobile Mapping System*

In this research, we propose the usage of On-Vehicle Ranging Laser System, so called "Mobile Mapping System (MMS)" (Figure1) to conduct 2-dimensional pavement condition evaluation. MMS can obtain 3-dimensional coordinate data (3-D point cloud data) of surrounding objects by measuring while rotating Lasers and driving (Figure2 and Figure3). After extracting only road surface data, we mainly detect local deterioration two-dimensionally by removing noise and unnecessary deformation on road surface via Short-Time Fourier Transform (STFT). STFT can be used to estimate Frequency Spectrum of non-stationary data. Considering space as time, road surface data can be also treated as non-stationary data. In this presentation, we report the detail of the signal processing using STFT and show its processing can detect the local deterioration on road surface with high-accuracy. In addition, we show the estimate result of IRI (road roughness index) and rutting (Figure4).

Figure 1: Mobile Mapping System (MMS)

Figure 2: 3-D Point Could Data Measured by Mobile Mapping System

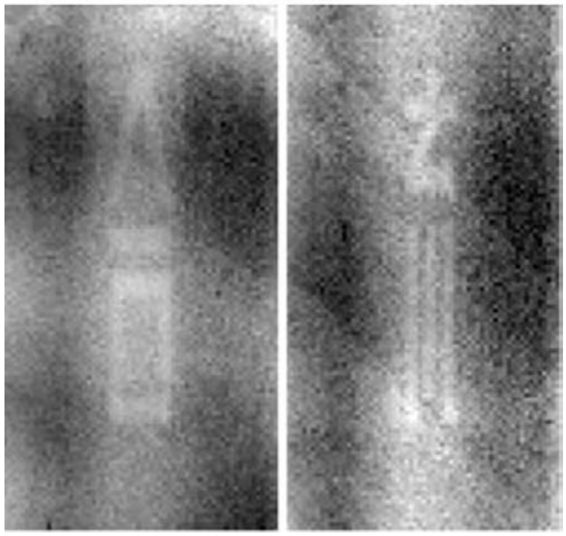

Figure 3: Road Surface Data Sample Extracted from 3-D Point Cloud Data[1]

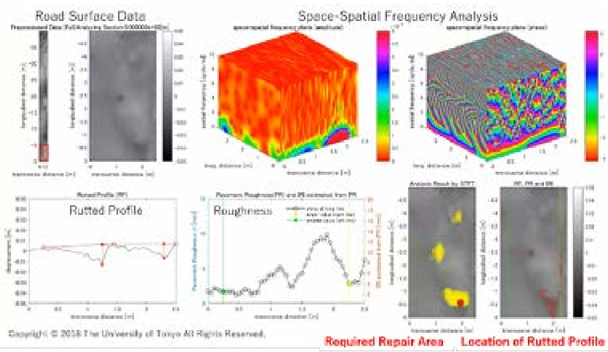

Figure 4: Spatial Frequency Analysis Result Sample

REFERENCES

[1] Hirotaka HIRANO, Tsukasa MIZUTANI, Tetsuya ISHIDA, Satoshi ANNAKA, Kiyosi SUZUKI, "Evaluation of Local Deterioration of Pavement Surface by Spatial Frequency Analysis Based on Short-Time Fourier Transform," Journal of Japan Society of Civil Engineers, Ser. E1 (Pavement Engineering), Volume 74, Issue 3, pp. I_113-I_120, 2018. (*in Japanese*)

Development of AR-based Training System for Tunnel Soundness Evaluation

Daisuke TANAKA[1], Yuuki ENOKIDANI[2], Naoya IMAIZUMI[3]
and Shinji KONISHI[4]

[1] Subhead of Structure Division Engineering Department, Tokyo Metro Co.,Ltd., Japan
d.tanaka@tokyometro.jp

[2] Chief of Structure Division Engineering Department, Tokyo Metro Co.,Ltd., Japan

[3] Deputy Manager of Structure Division, Engineering Department,
Tokyo Metro Co.,Ltd.,Japan

[4] Director of Structure Division, Engineering Department, Tokyo Metro Co.,Ltd.,Japan

1. INTRODUCTION

Tokyo Metro Co., Ltd. (Tokyo Metro) has been aiming to be a subway network offering excellent passenger satisfaction, based on the concept of "Satisfaction = Safety + Service." It has been accelerating several actions including earthquake measures and installation of platform doors, and has been proactively tackling difficult problems making use of advanced technologies and ideas. Faced with various issues related to facility maintenance, the company is continuously considering and promoting the introduction of new technologies to solve these issues.

2. PROBLEMS IN MAINTENANCE OF STRUCTURES

Tokyo Metro is operating in the Tokyo area with nine lines and a total operating distance of 195.1 km, carrying a daily average of 7.58 million passengers. The structures owned by the company include tunnels, viaducts, bridges, and earthwork, of which approximately 85% are located in tunnels.

For the maintenance of structures, regular inspections are conducted according to "Ministerial Ordinance to Provide Technical Standards on Railway" issued by the Ministry of Land, Infrastructure and Transportation, and actions including monitoring and repairs are planned and executed based on the results of inspections. The soundness of structures is guaranteed by ensuring the repetition of the inspection-planning-action cycle.

On the other hand, there are concerns that maintenance skills will decline as a result of the decreasing working population in an aging society, in addition to the retirement of experienced engineers. To maintain tunnels in sound conditions and continue stable operation in the future, it is important to address the problems concerning the improvement of efficiency in tunnel inspection and repair planning, and the training of maintenance engineers. As a solution to these problems, Tokyo Metro developed an AR (augmented reality) technology-based training system for tunnel soundness evaluation, aiming at the introduction of ICT（Information and Communication Technology） to tunnel inspection and the enhancement the technical abilities of young engineers

3. INTRODUCTION OF ICT IN TUNNEL INSPECTION

To ensure rapid, complete, and accurate execution and recording of inspection, Tokyo Metro introduced a light-weight tablet terminal to tunnel inspection work and developed inspection application (Photo 1) for better efficiency. The tablet terminal can display previous inspection information (type of deterioration and soundness rank) and photographs, and the whole work process from overwrite updating of records to taking photographs can be completely and accurately performed and recorded on the tablet terminal. In addition, the inspection results registered during the work in the tunnels are made available to relevant parties via a cloud server on the next day, enabling prompt sharing of information.

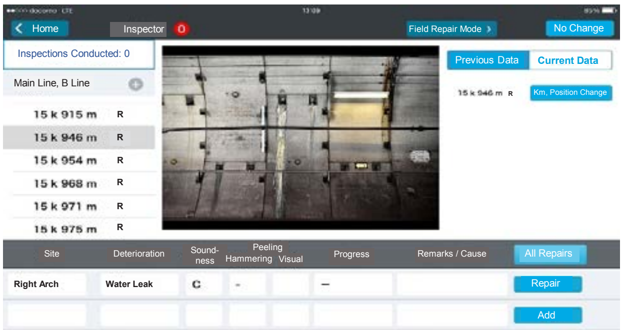

Photo 1: Inspection Application

4. INTRODUCTION OF AR-BASED TRAINING SYSTEM FOR TUNNEL SOUNDNESS EVALUATION

This system is an expansion of the application used in inspection work on structures. Used in the new and deterioration-free simulation tunnel and simulation bridge/viaduct (Photos 2 and 3) located in the Tokyo Metro Comprehensive Learning and Training Center, this application can reproduce deteriorations occurring in actual tunnels and bridges/viaducts on the mobile terminal screen.


Photo 2: Overall View of Simulation Tunnel


Photo 3: Simulation Viaduct

A feature of this application is the use of NFT (natural feature tracking), which recognizes the simulation tunnel wall itself as markers (Photo 4), while AR markers are installed on the simulation bridge/viaduct. This feature eliminates the need for placement and replacement of AR markers, which are necessary in conventional systems. The present report outlines the functions focusing on tunnel inspection. Ten points with deterioration (Photo 5) were prepared on the side surfaces (side wall and upper slab) of the tunnel with a total length of 180 m. The deteriorations reproduced using AR were six typical types of deteriorations occurring in the tunnels of Tokyo Metro, including cracking, peeling, lifting, cold joint, water leak, rebar exposure, and honeycomb.

Photo 4: Model Tunnel Wall without Deterioration

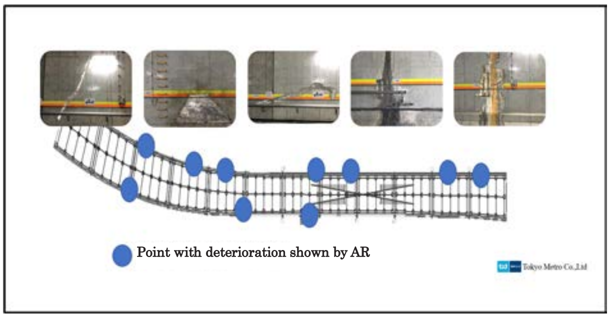

Photo 5: Deterioration Points in Tunnel

Photo 6: AR Reproduction of Deterioration, a Scene from Training

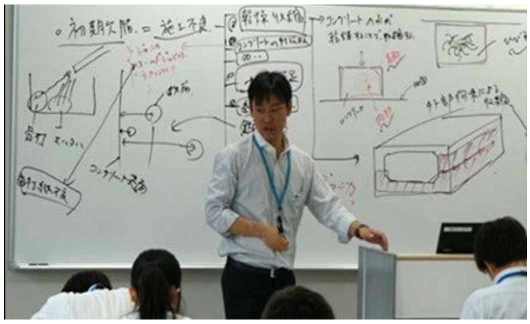

Photo 7: Guidance of Instructor

Holding the mobile terminal for training, the trainees experience the simulated inspection work according to the following flow of work. (1) They move to the point of deterioration in the simulation tunnel. (2) By aiming the mobile terminal at the wall surface, they take photographs of the simulated deterioration (Photo 6). (3) They enter information needed for maintenance, such as the type of deterioration, cause of deterioration, soundness evaluation, and remedial actions. (4) After entering the soundness evaluation for all deteriorations, they upload the input data to the cloud server. (5) They return to the classroom and receive guidance on how to look at, think about, and make judgments based on the input data on the PC client screen under the guidance of the instructor (Photo 7).

While the bridge and the viaduct are inspected using the same specifications as the tunnel, they are structurally more complicated than the tunnel. The positions that require attention (11 points on the bridge and 10 points on the viaduct) are, therefore, highlighted using AR reproductions of deterioration in these cases.
In addition, deteriorations on the bridge and the viaduct were more difficult to visualize than those on the tunnel, because many of the AR-reproduced deteriorations on these structures were given as illustrations, in contrast to those in the tunnel. For the purpose of the present report, AR-reproduced deteriorations were created based on the photographs of the points of interest to obtain more realistic reproductions (Photos 8 and 9).

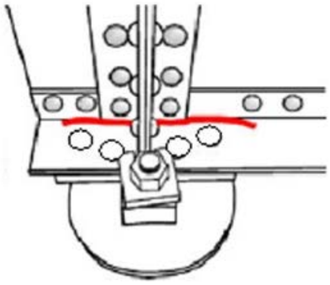

Photo 8: Illustration of Deterioration

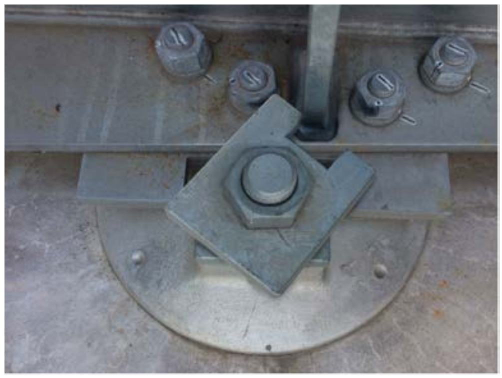

Photo 9: Reproduction of Deterioration

5. EFFECT OF USING AR-BASED TRAINING SYSTEM

Conventional teaching methods are hampered by the difficulty of providing on-site training due to safety reasons and time restrictions relating to train operation schedules (the hours from the last train to the first train) and limited space in the tunnel. Thus, training has chiefly been given on the desktop using texts and photographs. The introduction of this system is effective, since it can provide (1) simulated experience of actual inspection methods and procedures, (2) virtual confirmation of actual deterioration for better understanding, (3) safety training without time restrictions, and other advantages. In addition, a questionnaire asking the trainees about the effect of this application (Table 1) provided generally positive feedback. On the other hand, it also identified several areas of improvement, such as the trainees' request for a greater variety of types of deterioration that are reproduced using AR.

Table 1: Summary of Trainee Questionnaire

	Question	A	No.	B	No.	C	No.	D	No.	Total
1	Did you get realistic feel of structures and deterioration through application?	I very much think so.	18	I think so.	9	I generally do not think so.	0	I do not think so at all.	0	27
2	Was the application screen easy to use?		14		13		0		0	27
3	Was the application easy to operate?		16		11		0		0	27
4	Was it useful in understanding tunnel structure and deterioration?		17		10		0		0	27
5	Was it useful in understanding bridge/viaduct structure and the names of its members?		15		12		0		0	27
6	Was it useful in understanding deteriorations on bridge/viaduct and their causes?		15		12		0		0	27
7	Was it useful in visualizing the work you are going to be assigned to?		9		16		2		0	27
8	Do you want to use the training application in future training and work?		15		12		0		0	27
9	While one iPad units was shared by 2 trainees, do you think the use of 1 unit for each trainee would improve training effect?		8		7		9		3	27

6. CONCLUSION

The application presented here was introduced to the training of new employees and young employees in their second and third years in the company, and was found to be effective to a certain extent, as indicated by the answers of the trainee questionnaire. Going forward, Tokyo Metro aims to further diversify the content by adding more types of AR-reproduced deterioration, as well as different degrees of soundness for the same types of deterioration, with the goal of qualitatively improving human resource development.

Large Scale Ground Reinforcement for Improvement of Subway Stations

Shinji KONISHI[1], Tsuyoshi MORIYA[2], Ryuuji FUKUDA[3] and Tetsuya MURAKAMI[3]

[1] PhD, Director of Technical Standard Section, Improvement Construction Department, Tokyo Metro Co.,Ltd., Japan
s.konishi.r4r@tokyometro.jp

[2] Construction office Director, Improvement Construction Department, Tokyo Metro Co.,Ltd., Japan

[3] Construction manager, Improvement Construction Department, Tokyo Metro Co.,Ltd., Japan

ABSTRACT

Tokyo Metro Co.,Ltd. is advancing several improvement works of existing subway structures for mitigating congestion. Because Tozai line, which is one of the lines carrying out improvement work, was constructed in soft ground near sea, the improvement works of the line need large scale ground reinforcement under the condition that continuing operation service. This report describes ground improvement work of the Minami-Sunamachi Station and Kiba Station. About Minami-Sunamachi Station, the narrow existing tunnel station with one platform and two railway tracks are enlarged to large structure with two platforms and three railway tracks. To reinforce base ground and make underground beam, ground improvement was carried out under existing structures by the high-pressure injection and stirring method vertically and latitudinally. The Kiba Station which is consisting of two narrow shield tunnels are あ also under enlargement work now. The structural body which is composed of diaphragm walls and slabs are constructed surrounding existing tunnel station and segmental lining of the shield tunnels will be removed. Because the ground is super weak, ground improvement work is carried out now for reinforcing base ground and making underground beams. This report describes the works in details.

Keywords: *Subway Station, Improvement, Mitigating Congestion, Ground Improvement, High-pressure injection, underground beam*

1. INTRODUCTION

Tokyo Metro Co., Ltd. (hereinafter, "Tokyo Metro") opened the Tozai line in 1969, which extends for 30.8 km connecting Nakano Station in the west of Tokyo with Nishi-Funabashi Station in the east of Tokyo. The line offers through-services between three companies (Fig. 1). Of the 9 routes owned by Tokyo Metro, Tozai Line has the longest operating length and carries some 1.47 million passengers per day. With a congestion rate nearing 200%, this route also happens to be the most congested (Fig.2). The definition of ‘congestion rate’ in here is shown in Table 1. Specifically, there are significant train delays during morning rush-hours that are particularly chronic at the Nishi-Funabashi bound platform. Then, several measures have been implemented to alleviate this situation, such as upgrading of the Iidabashi Station to Kudanshita Station

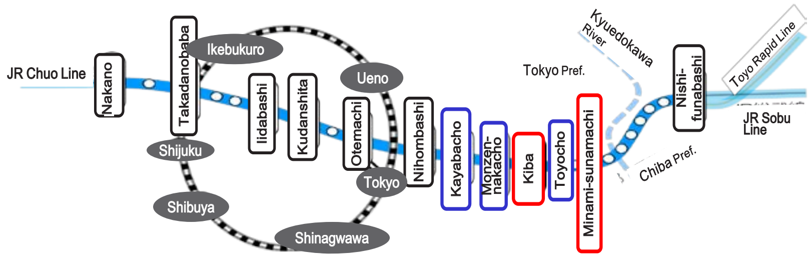

Figure 1 : Tozai line overview

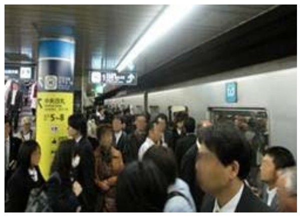

Figure 2 : Congestion on Tozai line

Table 1 : Definition of congestion ratio

Definition of Congestion ratio	
Congestion ratio means riding capacity. It shows situation that train can't be operated safely when passengers increase more than the number of people shown by riding capacity. The congestion ratio becomes 100% when all seats and standing space shown by hand straps and hand rails in the train are occupied.	
Congestion ratio	Standards of congestion ratio
100%	Passenger can sit a seat, hold a strap or a hand rail.
180%	Degree of congestion is that passenger's body's touch with each other. But, passenger can read a newspaper.
200%	Degree of congestion is that passenger's body's touch with each other and they have substantial oppressive feeling. However, passenger can read if it is a weekly magazine.
250%	Passengers slant and can't move every time train shakes. Also, they can't move their hands.

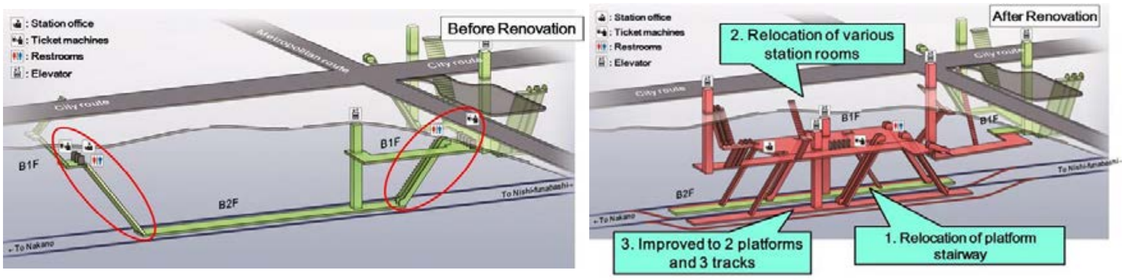

(a) Before renovation (b) After renovation

Figure 3: Minami-sunamachi station configuration

turnaround equipment and other major station improvement work. In short, improvement work has been carried out at each of Minami-sunamachi, Kiba, Toyocho, Monzen-nakacho, and Kayabacho stations. This paper describes details of the large scale ground reinforcement for improvement of Minami-sunamachi station and Kiba station.

2. MINAMI-SUNAMACHI STATION

2.1 Outline of improvement work

Minami-sunamachi Station has an island type single-platform with two-railway tracks (Fig.3(a)). The platform width is too narrow relative to the number of passengers using it, and people concentrate near the elevating equipment that connects the ticket gate to the platform. To address this, large-scale improvement work is being implemented to improve the safety of passengers on the platform, reduce congestion, and improve passenger convenience. Specifically, construction is increasing the number of platforms and tracks to realize a two-platform three-track configuration, as well as expanding the concourse floor and relocating platform stairs to the platform center (Figs. 3 (b), 4, 5) (Akagi, 2017). Doing this will allow city-bound trains at both stations to alternately arrive and depart from a single platform during morning rush-hour to shorten railcar dwell time and reduce train delays while also dispersing persons waiting to ride and increasing standby areas, thereby improving passenger safety.

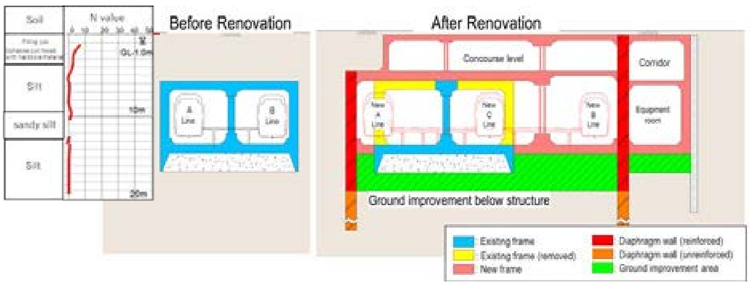

Figure 4: Cross-section of the station

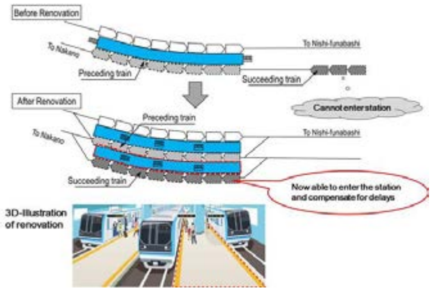

Figure 5: Layout of platforms

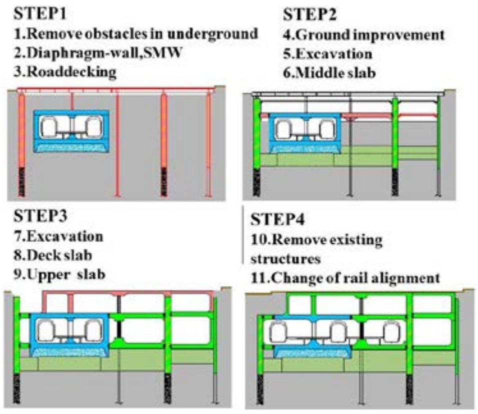

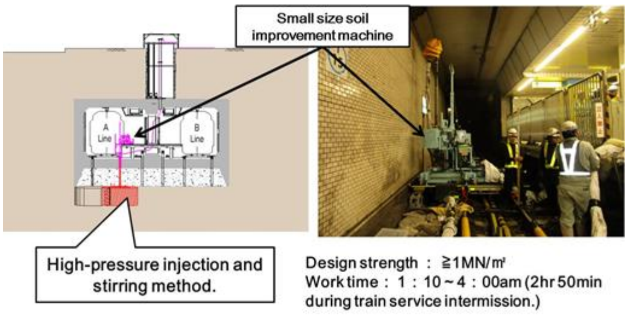

Figure 6: Construction steps

Figure 7: Ground improvement under structures

This area lies in the delta region of Sumidagawa River, Arakawa River and Edogawa River, which is composed of an alluvial soil deposit with N-values near 0. Improvement work adds new structures outside the existing construction which is still in use, and large diameter jet grouting of the foundation was used for ground improvement. Construction safety was ensured by completely enclosing the construction area with a solid diaphragm wall. Despite being large-scale excavation work, it was decided not to use the groundwater level lowering method due to the negative impact it would have on the surrounding environment. Fig.6 shows the construction steps.

2.2 Ground improvement

2.2.1 Vertical improvement

To reinforce base ground and make underground beam, ground improvement was carried out under existing structures by the high-pressure injection and stirring method. To prevent rebound of the existing tunnel by excavation, ground under the existing tunnel was improved from railway track floor and platform by the high-pressure injection in middle night before excavation of ground over the existing tunnel (Fig.7) because of expecting earth weight of the ground part. By the method, 520 columnar improving body's which are from 5.5m to 3.3m in diameter and from 3.1m to 2.0m in length were formed. Fig.8 shows layout of ground improvement columns. Fig.9 shows measurements of box element displacement before and after ground improvement. 1BL (the leftmost section outlined in red, see Fig. 8) on the plan view is the location of the intensive construction work that was performed in the initial stage of this project. Absolute displacement values reveal settlement of more than 15 mm. As a countermeasure, work was dispersed to limit localized settlement in spite of overall settlement. These countermeasures were successful, and it was possible to keep relative displacement below the primary control value through the

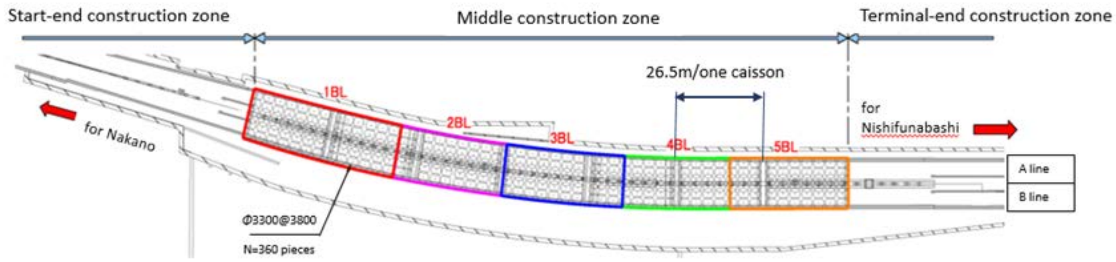

Figure 8: Layout of ground improvement

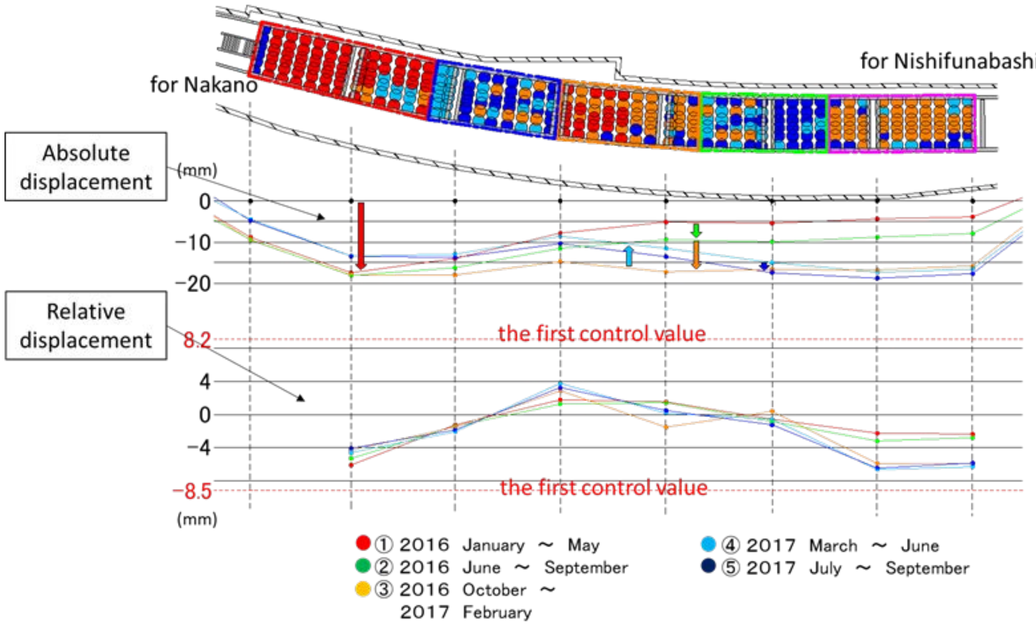

Figure 9: Box Element Displacement Results

end of the work. Nightly track measurements were also performed during the ground improvement period just as they were for the diaphragm wall excavation, and these measurements produced results within Tokyo Metro maintenance standards; thus, it was confirmed that the work had no effect on the tracks.

2.2.2 Longitudinal improvement

Moreover, when improvement work cannot be carry out from inner tunnel due to existing machine rooms and electric power equipment rooms, underground of the rooms were improved latitudinally by the high-pressure injection from two adits placed under existing station tunnel (Fig.10,11).

By the method, 90 columnar improving body's which are from 1.3m to 2.4m in diameter and 54m in length were formed and finished without bad influence on train operation for about 9 months. While the accuracy of drilling was set 150mm horizontally and 100mm vertically, 20% of columns had to be rebuild. Because a lot of concrete wastes, scraps of iron and wood are in under part of the caisson station, they caused to upset drilling direction. About measurement result of existing tunnel, the existing tunnel repeatedly deformed gently-uplift and settlement and converged about 4mm. The shape and strength of columns were checked by 10m length lateral boring for checking from the adits and vertical boring at destination point from the existing tunnel. Favorable result could be gotten from the borings.

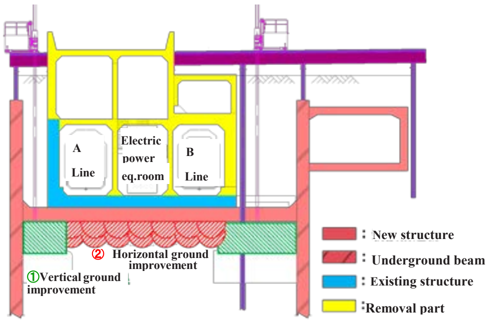

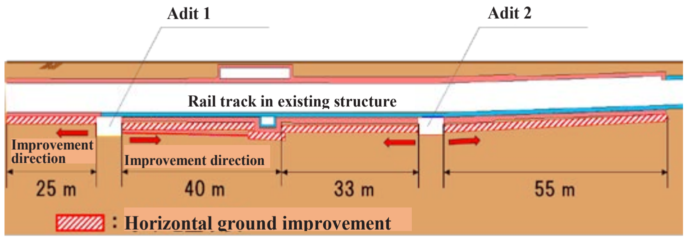

Figure 10: Cross-section of Longitudinal improvement

Figure 11: Profile of Longitudinal improvement

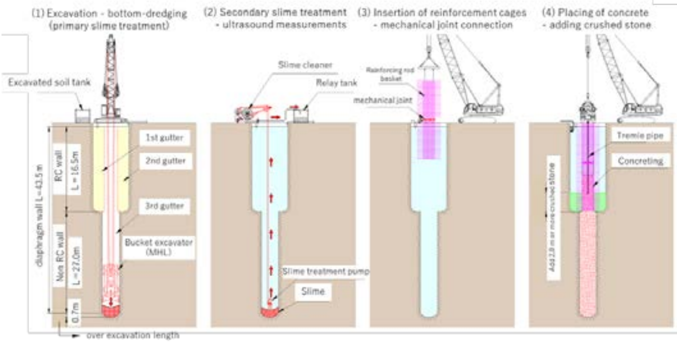

Figure 12: Forward Element Work Procedure

Figure 13: Element Work

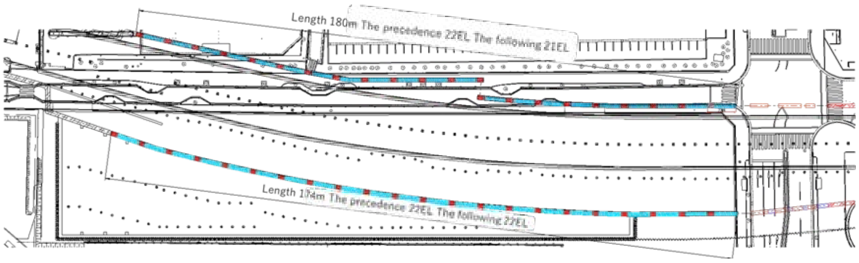

Figure 14: Element layout

2.3 Diaphragm Wall Work

Existing diaphragm walls that serve as structural sidewalls doubled as retaining walls. The diaphragm walls are 1.0 m and 1.2 m thick, and can be separated into two types of element: Primary element (roughly 2 m wide, roughly 44 m deep) and secondary element (roughly 6 m wide, roughly 17 m deep). A bucket excavator (MHL) was used to perform the excavation (Fig.12,13). Fig. 14 shows the element layout.

The ground around the construction site contains a thick layer of alluvial cohesive soil that is very soft (N = 0-1) and only gently supports the existing box elements. These conditions and the fact that element excavation was to be performed to a depth of 44 m prompted concern over slurry wall collapse in the ground behind the excavation areas. To address that concern, the stability of the slurry walls was calculated before beginning element excavation, and it was decided to construct soil walls (using the SMW method with no core material) to protect the slurry walls (Fig.15). There was also concern that the excavation of the ground around the station would cause horizontal displacement of that ground, which would in turn displace existing box elements. Clinometer measurements of ground displacement revealed that excavation caused horizontal displacement of 4 mm toward the excavation, and concrete placement caused 1 mm of displacement back toward the original position (Fig.16). In addition, settlement gauges

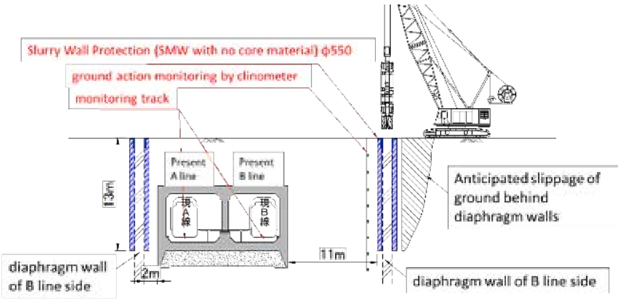

Figure 15: Slurry Wall Protection and Clinometer Installation Cross-Section

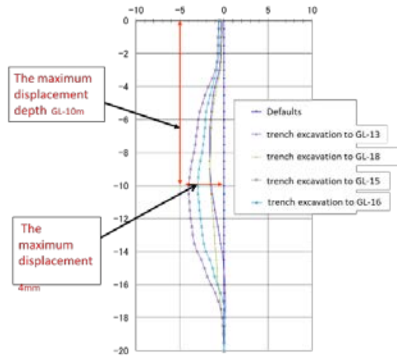

Figure 16: Horizontal Displacement of monitoring by Clinometer

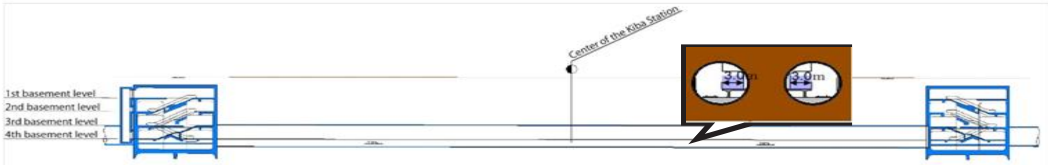

Figure 17: Kiba Station - Current Longitudinal Cross-section

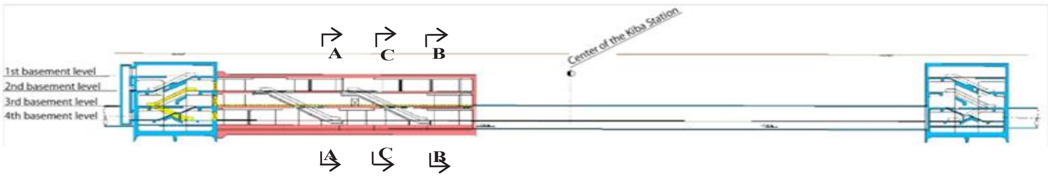

Figure 18: Kiba Station - Longitudinal Cross-section after Renovations

recorded settlement of up to 0.8 mm during concrete placement. Thus, the work caused minimal displacement to the surrounding ground. In addition, nightly track measurements during the construction period produced results within Tokyo Metro standards for track maintenance (less than 17 mm elevation difference and less than 20 mm alignment within a 10-m section); thus, it was confirmed that the work had no effect on the tracks.

3. IMPROVEMENT WORK OF KIBA STATION

3.1 Outline of Kiba station improvement work

Since opening for service in 1967, the passengers number of Kiba Station increase intensely and congestion occurs in recent years due to ongoing development around the station. In the Kiba Station, 187 m of the platform length of 220 m becomes a single-track shield portion (Fig.17). The platform width is 3.0 m on each side. As there is no passage in the intermediate portion, which connects both platforms, the lines of flow to respective platforms become intricate at both station ends. The platform is so narrow that passenger retention space becomes very small. As alighting passengers are large in number, a long queuing line forms on the platform. The station's stairs and escalators are located only in the shaft portion at both ends of the station, where passengers become concentrated., The long lines that form on the platform up to the center of the station during the morning rush hours do not shrink as trains arrive. For this reason, improvement work of Kiba station are advanced for enhancing passenger safety by widening the platform, mitigating congestion, and improving convenience by adding elevators and escalators from the platform to the ticket gate. In principle, improvement work is to be executed while maintaining normal operation of the revenue line.

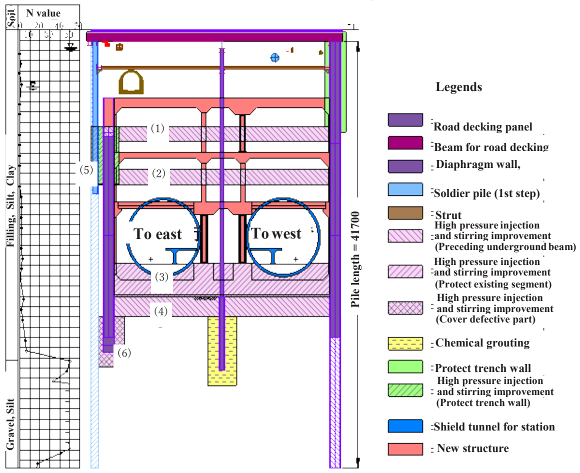

Figure 19: Outline of improvement work A-A cross-section

Table 2: Purposes of ground improvement

Position	Name	Purposes
(1)	Upper preceding underground beam	Secure formation level, Prevent deformation of retaining wall
(2)	Lower preceding underground beam	Secure formation level, Prevent deformation of retaining wall
(3)	Ground improvement of basement	Prevent station falling
(4)	Ground improvement of basement	Prevent heaving
(5)	Protecting trench wall	Prevent ground collapse near trench
(6)	Ground improvement at edge of earth retaining wall	Countermeasure for artesian groundwater

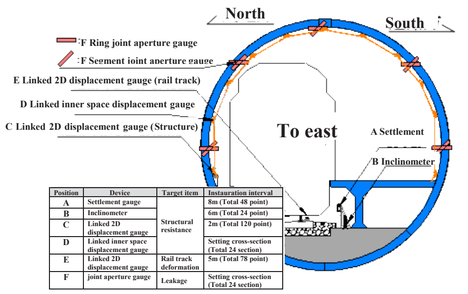

Figure 20: Layout of measurement devices

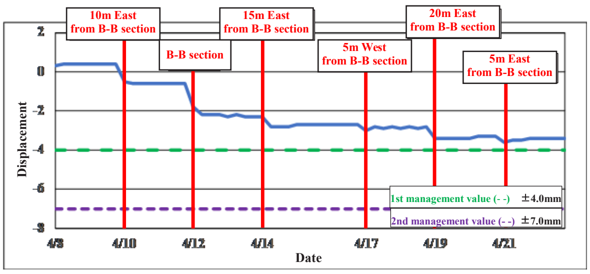

Figure 21: Measurement result of Settlement

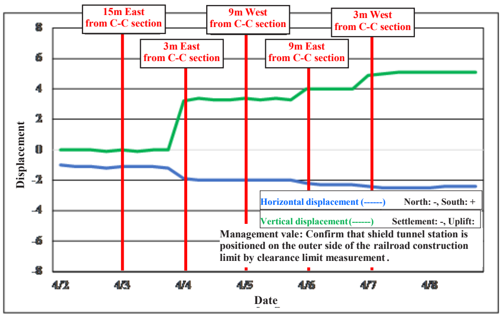

Figure 22: Deformation result of inside cross-section at tunnel crown

Therefore, plan is to construct the new structure around the existing shield in advance, and to subsequently remove the existing segments (Fig.18) (Hiromoto, 2017). Since the ground around Kiba Station is extremely soft, the work was planned according to inverted liming method based on using diaphragm walls as the tunnel body and ground improvement method. This is being done to reduce to a minimum any effects on neighboring buildings and existing shield station during the excavation work. The work sequence for improvement of Kiba Station is as shown in Figure 6.

3.2 Ground improvement work of Kiba station

Use of the inverted lining method is planned to minimize displacement associated with excavation. Since the ground condition is extremely soft, the formation level will be secured for construction of upper slabs from top down method by providing preceding footing beams with ground improvement under the upper slabs, and by providing inverted lining middle slabs for the second basement level and below the lower slabs (Fig.19, Table2).

3.3 Measurement management of Kiba station improvement work

Automatic measurement devices are installed in existing shield tunnels station for monitoring deformation of them continuously. Fig.20 shows arrangement of the devices and purposes of them. Fig.21 and 22 show measurement results of settlement and deformation of inside cross-section of the tunnels. the point at B-B cross section in Fig. 19 settled on 2.2mm during ground improvement work shown in Table 2 (6). Then, the settlement continued during ground improvement work near B-B cross section and growled to 3.4mm. Large deformation of Inside cross-section was appeared on the crown of shield tunnel at C-C cross section. Tunnel at the point was moved upward on 5.2mm and horizontally on 1.9mm to North direction during ground improvement work at C-C cross section shown in Table 2 (2). Moreover, the influence continued during ground improvement work near C-C cross section. Finally, the upward deformation became 5.2mm and lateral deformation to North direction also reached 2.5 mm. However, volume of these displacement are within the displacement management value and there was no influence on our train operation by the work. From the results, it is considered that ground stress was released by cutting of the ground and lack of filling, and deformation of the shield tunnel station occurred due to the ground improvement work.

4. CONCLUSION

Two improvement works of underground stations in urban area under the condition that continuing operation service has been described. Obtained knowledges are shown in the following.

(1) The improvement work is advancing safely due to the management system to grasp even small deformation with continuous monitoring and detail measurement of rail track after ground improvement work every night.
(2) The improvement work is advancing without bad influence on surroundings and existing tunnels due to application of high-rigidity diaphragm wall, large scale ground improvement for basement and preceding underground beam.
(3) When ground was improved by the high-pressure injection and stirring method, the existing structure uplifted or settled just a little. It is important to set suitable construction speed and sequence considering cutting size, filling speed and hardening speed of filling material.

In any case, the two-improvement work is advancing safely now.

We hope this paper is a useful point of reference in the future planning, design and construction of large-scale rail operation improvement work projects in major cities.

REFERENCES

Akagi, H., 2017. Amazing underground construction technology in Japan, 9th International Symposium on Geotechnical Aspects of Underground Construction in Soft Ground – Negro & Cecilio Jr. (Eds)© 2018 Taylor & Francis Group, London, ISBN 978-1-138-29711-1, pp.3-19.

Hiromoto, K., Hashiguchi, H & Arai, Y., 2017. Large-scale improvement of converting a Japan's first subway station constructed by the shield tunneling method into that of an open-cut method: Kiba Station on the Tozai Line, 9th International Symposium on Geotechnical Aspects of Underground Construction in Soft Ground – Negro & Cecilio Jr. (Eds)© 2018 Taylor & Francis Group, London, ISBN 978-1-138-29711-1, pp.327-337.

EVALUATION OF IMAGE PROCESSING-BASED CRACK DETECTION UNDER REAL ENVIRONMENT FOR REMOTE IMAGING INSPECTION WITH AI

T. Fukuoka[1], T. Minami[2], M. Fujiu[3], and J. TAKAYAMA[4]

[1] Dr., Informatics, Kanazawa University, Geosciences and civil Engineering, Kanazawa, Japan,
[2] Master (Eng), Kanazawa University, Dept. of Environmental Design, Kanazawa, Japan
[3] Ph.D., Associate Professor, Kanazawa University, Geosciences and civil Engineering, Kanazawa, Japan,
[4] Dr., Eng., Professor, Kanazawa University, Geosciences and civil Engineering, Kanazawa, Japan,
Correspond to Dr., T. Fukuoka (tfukuoka@se.kanazawa-u.ac.jp)

Keywords*: crack detection, filming conditions, image recognition technology, deep learning*

1. GENERAL INSTRCUTIONS

Recently, the study of extending the service life of bridges has gained attention. In Japan, there are about 730,000 bridges with a length of 2 m or longer, and many of these were built during a period of high economic growth, and have now reached the end of their service life. Therefore, their rebuilding and the extension of their service life must be considered.

However, among local public organizations, there are we some that have insufficient manpower relative to the number of bridges to manage, as well as insufficient funding for maintenance. Thus, these organizations are unable to perform routine close visual inspections.

As issues with the continuing close visual inspection of bridges are surfacing, the remote imaging system is expected to become a new inspection method that replaces close visual inspection.

To develop an alternative method to the current close visual inspection [1], the practical potential of bridge inspections using images captured with a super-high-resolution camera was examined. Although a super-high-resolution camera enable us to take a wide area picture of a target bridge from a long distance, there is no discussion about an optimal filming conditions for AI crack detection. In order to evaluate the effectiveness of the filming conditions for AI crack detection, we take pictures of concrete structure with shifting filming conditions and comparing the results of crack detection.

2. EXAMINATION

In this paper, we evaluate an effectiveness of filming condition by shifting a distance of camera and change the light of field. We compare a precision and recall of crack detection rate for the evaluation.

We adapt semantic segmentation method as a crack detection method. We use DeepCrack [2] model for crack detection. This model can output crack area with pixel unit. We have trained this crack detection model with 137 images of crack on a concrete surface and 137 augmented images.

We use some picture of crack on concrete building as a test image. We set camera and take picture at some distance for evaluate an effectiveness of camera distance. Each picture describes a crack with different resolution. Fig 1 show an example of a different resolution of crack taken from different distance. To evaluate an effectiveness of light intensity, we set a floodlights near the crack. We compare a picture taken with a floodlights running and a picture taken without floodlights (Fig 2).

Figure 1. Example of zoom images of crack in a picture; taken from 5 m distance and taken from 30 m distance.

Figure 2. Example of competition of light intensity of images.

3. CONCLUSIONS

In Japan, there are about 730,000 bridges with a length of 2 m or longer. It is necessary to constant maintain them with low cost. A bridge inspections using images is one of a potential method which perform bridge inspection with low cost. However, an optimal filming condition for take a picture of target bridge is not discussed enough yet.

In this paper, evaluate an effectiveness of distance of camera and light intensity. We would evaluate another filming condition in the future work.

REFERENCES

[1] H. Minami, M. Fujiu, J. Takayama, S. Suda, S. Okumura, K. Watanabe.: A basic study on diagnostic imaging technology for bridge inspection using super high resolution camera, Journal of Sociotechnology Research Network, 15, pp. 54-64, 2018). (in Japanese)

[2] Z. Qin, Z. Zheng, L. Qingquan, Q. Xianbiao, W. Qian, W. Song.: DeepCrack: Learning Hierarchical Convolutional Features for Crack Detection, IEEE Transactions on Image Processing, 28(3), pp.1498-1512, 2019.

Subsurface Pipe Detection by 3D Convolutional Neural Network and Kirchhoff Migration

Takahiro YAMAGUCHI[1], Tsukasa MIZUTANI, Minoru TARUMI
[1]M.S., Department of Civil Engineering
School of Engineering, the University of Tokyo
Japan
tyamag@iis.u-tokyo.ac.jp

ABSTRACT

In this paper, the novel algorithm to detect and localize subsurface utility pipe from Ground penetrating Radar (GPR) image is proposed. Due to the highspeed and dense 3D monitoring, GPR is a promising tool. However, vast amount of radar image and the difficulty of interpretation are the bottlenecks of GPR method. In the research, we propose a new algorithm by the combination of 3D Convolutional Neural Network (3D-CNN) and Kirchhoff migration. A CNN architecture is optimized by about 3,000 pipe measurement data. CNN model classifies images as 3 categories, transverse, longitudinal and no pipe. The classification accuracy reaches about 92 %, 8 % higher than 2D-CNN in the case of transverse pipe. After box-by-box scan by 3D-CNN, Kirchhoff migration is applied to each detected box. By extracting the maximum intensity peak of each section image, the algorithm successfully visualizes pipes' 3D positions and inclinations with reasonable calculation time.

Keywords: Ground Penetrating Radar (GPR), subsurface utility pipe, 3D convolutional neural network (3D-CNN), Kirchhoff migration, infrastructure health monitoring

1. INTRODUCTION

Ground penetrating radar (GPR) is a promising tool for subsurface utility pipe detection under the road. Compared to other Non-Destructive Testing (NDT) method such as electrical and elastic wave exploration method, GPR mounted on vehicle scans under the road high-speed, up to 80 km/h without traffic control. The problem of the GPR method is, radar images are enormous in quantity and difficult for a nonprofessional to interpret. Therefore, one inspection by skilled inspectors takes about several months and ten-thousand dollars. An automatic anomalies detection algorithm has a possibility to significantly reduce inspection time and cost.

The positions of subsurface pipes need to be localized accurately and fast to help road administrators' decisions. The lack of old utility pipes information delays construction process, and in worst case, damages pipes to bring economic loss to the society. The deteriorated pipes cause subsurface voids, which brings serious accidents of road collapses. For example, in Japan, over 30 % of total 470,000 km sewage pipe is going to be over 50 years in 20 years. Furthermore, over 3,000 road collapses are caused by sewage pipes. To handle enormous amounts of utility pipes, accurate and fast automatic detection algorithm is needed.

In terms of subsurface utility pipes detection by GPR, most research focuses on migration and tomographic reconstruction, reflection pattern detection by Hough transform, neural network or other adaptive approaches, antenna polarization, and electromagnetic (EM) simulation. In terms of migration, Soldovieri *et al.* (2008) proposed Kirchhoff-based reconstruction algorithm utilizing truncated singular value decomposition (TSVD) for multimonostatic configuration. However, migration algorithm is ordinally not feasible for kilometer-order long distance measurement data because of calculation cost and time. In terms of reflection pattern detection, Gamba and Lossani (2000) extracted pipe feature by preprocessing filter and neural network algorithm with up to 80 % detection accuracy. Al-Nuaimy *et al.* (2000) proposed the combination of window function and neural network to successfully localize the area of pipe reflections.

In this paper, we propose a novel subsurface pipe detection algorithm based on 3D convolutional neural network (3D-CNN). 3D-CNN is utilized in medical imaging and human action recognition. In this research, 3D pipe geometrical characteristics are utilized to improve the classification accuracy. Kirchhoff migration, considered as one of the most standard and accurate migration algorithms in NDT practice is applied to each region detected by 3D-CNN. 3D map of subsurface pipe is constructed by the extracted maximum intensity peaks of each migrated image. The rest of the paper is followed by 5 sections. Section 2 denotes the configuration of the utilized GPR system and measurement data. Section 3 discusses the appropriate filters and model architecture for 2D-CNN pipe detection. Section 4 optimizes the 3D-CNN model. The accuracy of 2D and 3D-CNN are compared in this section. Section 5 proposes the methodology to plot 3D map of subsurface pipe. Section 6 summarizes the paper.

2. Measurement system and data

As shown in Fig. 1, the multi-channel vehicle-installed type GPR system manufactured is utilized in the research. 29 channels are spaced at 0.075 m intervals and scan pitch is set 0.07 m. The system adopts stepped-frequency method. Operating frequency range is 50 MHz - 3.03 GHz with frequency pitch 20 MHz. Direct coupling removal and

Table 1: Measurement data.

Date	Transverse Pipe (2D Image Num.)	Longitudinal Pipe (2D Image Num.)
2018/3/15	1,040 (30,160)	49[a] (112,572)
2018/3/19	688 (19,952)	-
2018/3/21	204 (5,916)	-
2018/3/22	709 (20,561)	29[a] (38,688)

calibration filter is applied to all the measurement data. The effects of ordinally GPR image preprocessing filters, gain filter and BackGround Removal (BGR) are discussed in the following section.

The measurement was conducted in Nagano prefecture, Japan, four days from March 15, 2018 to March 22, 2018 (Table 1). The total transverse pipe number extracted by inspectors is 2,641. The first three days data, about the three fourths of all the pipes were used as training data, and the last day data was used as test data. The total longitudinal pipe number is 78, much less than transverse pipe. However, each longitudinal pipe length ranges from several tens meter to several hundreds meter, about 5 - 50 times longer than the length of transverse pipe, which equals to the channel width. For the two types of pipe, the training image number is confirmed to be enough by checking the accuracy convergence.

In the case of transverse pipe, a 29 channel pipe was divided into 29 images for 2D image data, and images having certain channels for 3D image data. In the case of longitudinal pipe, start and end points were provided by inspectors. Assuming each pipe is linearly positioned from the start to end, 2D and 3D images were diagonally extracted. No pipe images were randomly extracted from the area without pipe reflection. The no pipe image data number is the same as the pipe image data number.

3. PREPROCESSING FILTER AND LAYER ARCHITECTURE

To optimize CNN model for subsurface pipe detection, the effects of preprocessing filters, hidden layer number and input image size are examined. In this research, GPU NVIDIA GeForce GTX 1080 Ti and CPU Intel Core i7-8700K is utilized for training. All the training programs are written by TensorFlow. It takes several ten minutes to several hours for all the training cases, not strongly depending on the difference of 2D and 3D possibly because of the optimized backpropagation algorithms.

3.1 Preprocessing filter

The effects of two common preprocessing filters in GPR method practice, gain filter and BGR are evaluated. Gain filter is applied in time domain to compensate for attenuation and free space loss. BGR is also applied in time domain to remove multiple

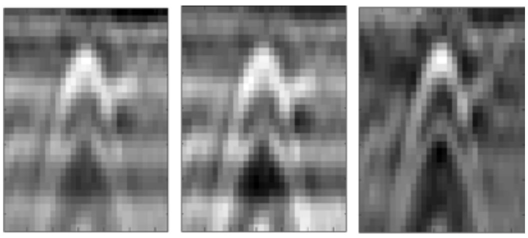

(a) (b) (c)

Figure 2: Preprocessing filter. (a) Raw image data. (b) Gain filter. (c) BackGround Removal (BGR).

Table 2: Preprocessing filter effect.

Preprocessing Filter	**Accuracy (%)**	**Precision (%)**	**Recall (%)**	**AUC**
No filter (proposed)	85.3	90.0	79.4	0.908
Gain	84.0	85.8	82.4	0.902
BGR	84.3	85.2	83.5	0.903

reflections between antennas and medium boundaries such as asphalt surface and soil layers. Figure 2 displays the images after gain filter and BGR. Table 2 shows the effects of the preprocessing filters on the transverse pipe classification accuracy. From Figure 2 (a) (b) and Table 2, the effect of gain filter is small when zooming in a hyperbola and found not to be important for the accuracy. On the other hand, the image clearness increases by BGR from Figure 2 (c). However, BGR has no effect on the accuracy from Table 2. This is because the models' filters automatically learned the target reflection patterns suppressing the multiple reflections. It is favorable because The parameters of the preprocessing filters need not be tuned for each measurement data.

3.2 Layer Architecture

The proposed model is shown in Figure 3. The model consists of 1 convolution layers and 1 fully connected layers). Input image size (N_1,N_2,N_3) represents depth, distance and channel direction pixels respectively. For 2D-CNN, all the input images and filters channel direction sizes are set 1, while each parameter is optimized in 3D-CNN as explained in the following section.

Table 3 explains the layer number effect on the transverse pipe classification accuracy. 2 layer model is the proposed model shown in Fig. 2. 1 layer model is discussed in previous research. For comparison, VGG16 model, 16 layer and InceptionV3, 48 layer are utilized. Support Vector Machine (SVM) model is adopted for comparison. From the results, the models learned certain abstract spatial features by deep layer structure, though the complicated models such as 4 layer and deeper layer model do not have an advantage in the context of subsurface pipe radar image classification. Because of the calculation cost, 2 layer is considered to be optimal in the research.

4. 3D-CNN INPUT IMAGE SIZE OPTIMIZATION

Table 4 shows the input image size effect on the accuracy. All the filter parameters are confirmed optimal in terms of the classification accuracy though the detailed explanation is omitted for the brevity of the paper. For each input image size, there is a tendency that optimal convolution filter size is almost constant because the scale of the target features for the convolution filters is constant.

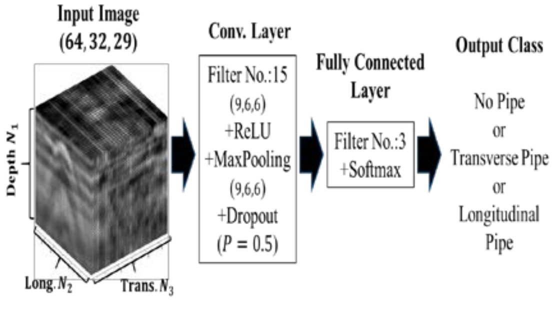

Figure 3: Proposed model.

Table 3: Model comparison.

Model	Accuracy (%)	Precision (%)	Recall (%)	AUC
SVM	72.5	67.9	77.1	0.805
1	62.1	67.5	46.9	0.627
2(Proposed)	85.4	86.2	84.8	0.927
4	84.7	85.9	83.1	0.915
VGG16	82.7	89.5	74.0	0.900
InceptionV3	74.3	75.1	72.7	0.724

In the case of image size (16,8), the accuracy is by about 3 % lower than the cases of image size (64,32). When the image size is equal to or larger than (64,32), the accuracy is about 85 % - 86 %. This is because the CNN model can recognize pipe reflection hyperbolic shapes when the image size is enough as observed in Fig. 3. Because of the calculation cost, the image size (64,32) is adopted in the research.

Table 5 exhibits the accuracy of each model by increasing channel direction input image size. From Table 5, even in the case of channel number 5, the accuracy increases by about 2 % compared to the most accurate 2D-CNN model. When the channel size is 29, the most accurate case, the accuracy increases by about 8 %. The accuracy monotonically increases with the increase of channel number. 3D-CNN model utilizes the succession of pipe reflection hyperbolics. Figure 4 shows the Receiver Operating Characteristic (ROC) curves of 2D and 3D-CNN. The performance of 3D-CNN is clearly improved comparing the curves of Figure 4 (a) and (b).

The same consideration is applied to longitudinal pipe case though the detailed discussion is omitted. From the results, When the image size is equal to (64,29), the accuracy is highest, about 90 %. Compared to the 2D-CNN case, the accuracy increases by about 2 % when the scan number is 32, and decreases when the scan number is larger than 32. This may be due to the inclination of pipe. When the scan number is too large, some longitudinal pipes protrude from the 3D-CNN boxes, reducing the relative volume of the pipes in the extracted boxes. To summarize the two cases, the channel number 29 is determined for the accurate transverse pipe detection and scan number 32 is determined for the accurate longitudinal pipe detection.

Table 4: Image size effect.

Input Image (N_1,N_2)	**Accuracy (%)**	**Precision (%)**	**Recall (%)**	**AUC**
(16,8)	82.8	83.7	81.9	0.904
(32,16)	84.7	85.4	84.0	0.923
(64,32) (proposed)	85.4	86.2	84.8	0.927
(128,64)	85.8	85.5	86.1	0.931

Table 5: Channel effect.

Input Image N_3	**Accuracy (%)**	**Precision (%)**	**Recall (%)**	**AUC**
1	85.4	86.1	84.8	0.927
9	87.8	88.6	87.2	0.952
13	89.9	90.5	89.3	0.963
29 (proposed)	92.9	94.6	91.1	0.976

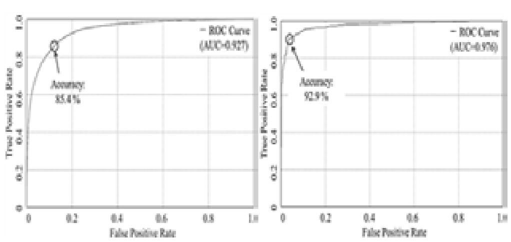

(a) (b)

Figure 4: ROC curve. (a) 2D-CNN. (b) 3D-CNN.

Table 6: Confusion matrix.

Predict Actual	**Accuracy (%)**	**Precision (%)**	**Recall (%)**	**Precision (%)**
No Pipe	1134	65	70	89.4
Trans.	32	676	1	95.3
Long.	97	2	1110	91.8
Recall (%)	89.8	91.0	94.0	Acc.: 91.6

The 3D-CNN model for three class classification, no pipe, transverse and longitudinal pipe is proposed by incorporating the optimum parameters of each direction pipe case. From the discussions of the previous two pipes' cases, the most appropriate 3D-CNN input image size for the two types of pipe is (64,32,29), corresponding to about 2 m depth, 2 m distance and 2 m channel range box assuming the soil permittivity is 3.

3D-CNN for the two types of pipe is developed by increasing the class number of the final softmax layer. Convolution layer filter number is doubled because the number of the features to be learned also increases by augmenting the class number (Figure 3). Table 6 exhibits the confusion matrix of the trained 3D-CNN. The total accuracy is about 92 %, an intermediate value between transverse and longitudinal pipe case. The numbers of the longitudinal pipe falsely detected as transverse pipe and vice versa are small, indicating the direction of pipe is accurately estimated when there is a pipe.

5. 3D MAPPING OF SUBSURFACE PIPE

Because the model is an object classifier for a provided image box, an appropriate object localization method needs to be developed. The pipes are detected by setting appropriate box-by-box scan parameters. Then, the pipes are accurately localized by Kirchhoff migration. In this paper, 3D map is shown for five transverse pipes case.

5.1 3D-CNN detection

In the case of radar image, images are monochrome, relatively large, include many clutters and the scale of target hyperbolics are almost constant, whose situation is completely different from a colored scenery photo. Furthermore, the target images are 3D in this research. Therefore, instead of Faster CNN and Single Shot MultiBox Detector (SSD), the most basic box-by-box scan method, conventionally called "exhaustive search" is adopted. By setting appropriate scan overlap parameters and probability thresholds of three classes, the pipes are accurately detected with reasonable calculation time.

Fig. 5 exhibits the same pipes 3D map by changing probability threshold P to 0.995 and 0.990 with the constant scan overlap 75 %. The boxes with solid and dashed lines correspond to detected transverse and longitudinal pipes respectively. Compared to

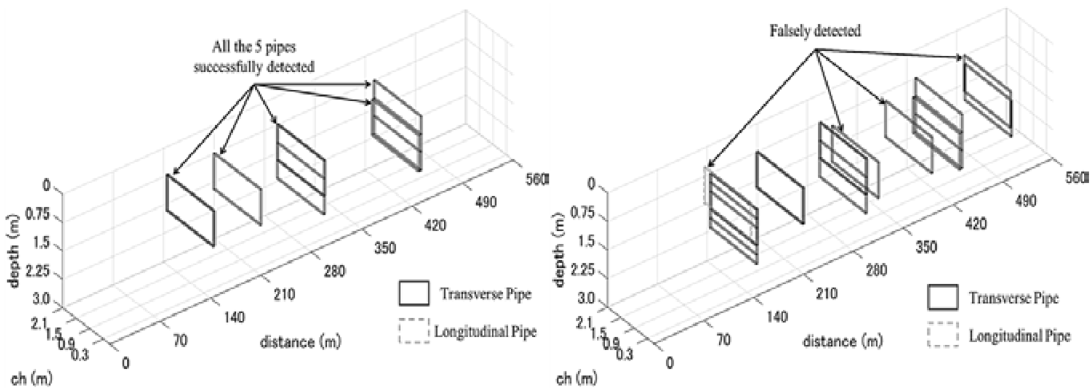

(a) (b)

Figure 5: Detected 3D-Region. (a) P=0.995. (b) P=0.990.

Figure 5 (a), false detection increases for P=0.990. In this measurement system and algorithm settings, the appropriate probability threshold P is 0.995. Practically, the appropriate probability threshold may be determined by the acceptable false negative rate required for the application.

5.2 Kirchhoff migration localization

In the proposed algorithm, migration is applied to each cross-section image perpendicular to pipe direction. In figure 6, Downward and upward ray distance $R_{\pm}$ and angle $\theta_{\pm}$ at point (x,z) of the image are a function of pipes' direction, transverse or longitudinal, detected depth dz and two antennas' offset 2h. After migration, the point of maximum absolute intensity in each image is plotted in 3D map as pipe's position.

Figure 7 shows an example of image before and after migration. Before migration, the algorithm fails to pick the apex of a hyperbola, where an upper edge of pipe is considered to exist. After migration, the pipe is successfully located. Figure 8 displays the extracted peaks. As shown in Figure 8, in some cases the algorithm fails to locate the pipes' positions without migration. On the other hand, after migration, pipes' positions and inclinations are visualized with centimeter-order variation around the line. 3D positions and inclinations of pipes can be inferred from the extracted peaks by Kirchhoff migration. The localization accuracy is enough from a practical point of view

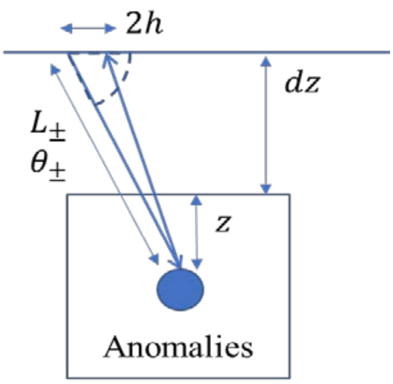

Figure 6: Kirchhoff migration.

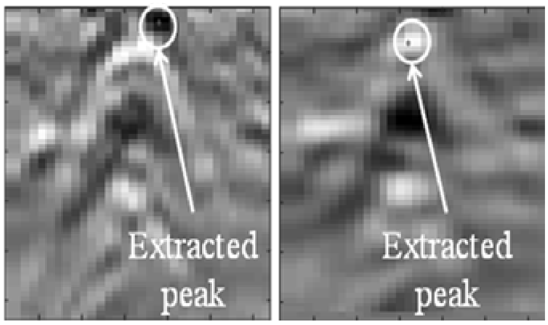

(a) (b)

Figure 7: Migrated image. (a) Before migration. (b) After migration

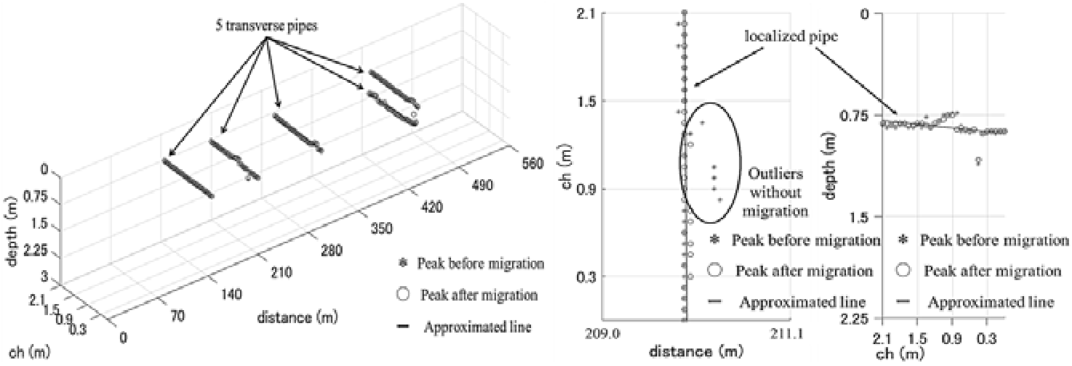

(a) (b) (c)

Figure 8: Kirchhoff migration results. (a) 3D map. (b) Top view. (c) Side view.

because actual pipes' diameter reaches to several tens centimeter. The total calculation time for migration is less than one minute for each case, extremely high-speed compared to conventional migration research framework.

6. CONCLUSION

In this paper, we proposed a novel subsurface pipe detection algorithm based on 3D-CNN and Kirchhoff migration. In terms of transverse pipe, 3D-CNN improves the classification accuracy by about 8 % compared to 2D-CNN considering 3D shape. The optimized 3D-CNN parameters in two directions are common, resulting in the three-class classification of the two types of pipe and no pipe image. By field measurement data examples, it is found the pipes are successfully detected from 3D map by box-by-box scan method. Position and inclination of pipe are visualized as the extracted peaks after Kirchhoff migration. The total calculation time is around ten minutes for 500 m image data. For future work, the authors are planning to apply the same 3D-CNN architecture for subsurface void detection. The material and diameter of pipes may be estimated at migration process.

REFERENCES

Daniels, D. J., 2004. *Ground penetrating radar*. the Institution of Engineering and Technology, London, UK.

Ministry of Land, Infrastructure, Transport and Tourism, *Utility Aging Countermeasures and Maintenance (in Japanese)*. Japan. Available: www.mlit.go.jp/common/001020125.pdf, Accessed on: Sep. 28, 2019.

Soldovieri, F., Brancaccio, A., Prisco, G., Leone, G., and Pierri, R., 2008. A Kirchhoff-Based Shape Reconstruction Algorithm for the Multimonostatic Configuration: The Realistic Case of Buried Pipes. *IEEE Transactions on Geoscience and Remote Sensing*, 46.10, 3031-3038.

Gamba, P., and Lossani, S., 2000. Neural Detection of Pipe Signatures in Ground Penetrating Radar Images. *IEEE Transactions on Geoscience and Remote Sensing*, 38.2, 790-796.

Al-Nuaimy, W., Huang, Y., Nakhkash, M., Fang, M. T. C., Nguyen, V. T., and Eriksen, A., 2000. Automatic detection of buried utilities and solid objects with GPR using neural networks and pattern recognition. *Journal of Applied Geophysics*, 43.2-4, 157-165.

Böniger, U., and Tronicke, J., 2012. Subsurface Utility Extraction and Characterization: Combining GPR Symmetry and Polarization Attributes. *IEEE Transactions on Geoscience and Remote Sensing*, 50.3, 736-746.

Wang, T., and Oristaglio, M. L., 2000. 3-D simulation of GPR surveys over pipes in dispersive soils. *Geophysics*, 65.5, 1560-1568.

Ji, S., Xu, W., Yang, M., and Yu, K., 3D Convolutional Neural Networks for Human Action Recognition. *IEEE Transactions on Pattern Analysis and Machine Intelligence*, 35.1, 221-231.

Kamnitsas, K., Ledig, C., Newcombe, V. F. K., Simpson, J. P., Kane, A. D., Menon, D. K., Rueckert, D., and Glocker, B., 2017. Efficient multi-scale 3D CNN with fully connected CRF for accurate brain lesion segmentation. *Medical Image Analysis*, 36, 61-78.

FUNDAMENTAL STUDY ON DETECTION OF FLOATING AREA OF MORTAR SPRAYED SURFACE USING INFRARED CAMERA MOUNTED ON UAV AND AI

N.ISHIMURA[1], T.MINAMI[2], M.FUJIU[3], T.FUKUOKA[4], and J.TAKAYAMA[5]

[1] Undergraduate Student, Dept. of Environmental Design, Kanazawa University, Kanazawa, Japan,
[2] Master (Eng), Dept. of Environmental Design, Kanazawa University, Kanazawa, Japan,
[3] Associate Professor, Geosciences and Civil Engineering , Kanazawa University, Kanazawa, Japan,
4 Dr., Informatics, Kanazawa University, Geosciences and Civil Engineering, Kanazawa, Japan
[5] Professor, Geosciences and Civil Engineering, Kanazawa, University, Kanazawa, Japan
Correspond to Makoto FUJIU(fujiu@se.kanazawa-u.ac.jp)

***Keywords**: Floating Detection, UAV, AI, Mortar Sprayed Surface*

1. GENERAL INSTRCUTIONS

In Japan, many civil engineering structures were constructed during the period of high economic growth. The mortar spray slope was constructed in the late 1940's and aging is progressing all at once. At present, the maintenance management of the mortar spray slope is carried out in accordance with the General Inspection Implementation Guidelines (Draft) of the Ministry of Land, Infrastructure and Transport. In Japan, the number of civil engineering-related staff is decreasing and maintenance and renewal costs for civil engineering structures are increasing. So, it will be important to perform more appropriate maintenance within a limited budget and personnel.

In this research, using an infrared camera mounted on the UAV grasp the temperature change of an abnormal part where there is a float and a normal part. Finally aiming at automatic detection of the float using a machine learning image analysis system (AI). This paper aims to clarify the factors that affect the temperature of the slope surface by performing core sampling of the AI judgment location in order to improve the accuracy of AI that automatically detects the float behind the slope. As a pre-stage of AI automatic detection, the infrared image is judged by human visual inspection, and core sampling is performed at the point where the float is thought to be present. In this way, the accuracy of the floating inspection of the slope with an infrared camera is verified.

2. OVERVIEW OF CORE SANPLING EXPERIMENT

In this study, a core sampling experiment was conducted for the purpose of understanding the accuracy of the floating inspection of the slope using an infrared camera. Table 1 shows the target slopes and survey dates and conditions.

It is considered that there is a high possibility that the part showing the color with high temperature is floating. Three locations on each slope were selected: a location where it is considered there was a float, a location where it was not clear whether there was a float, or a location where it is considered there was no float.

Figure 1 shows the infrared image and visible light image of the slope along prefectural road 10. No. 1 is a place where it is not clear whether there is a float, No. 2 is a place where there is a float, and No. 3 is a place where there is no float.

Table 1. Core sampling experiment conditions

Target slope	Date	Weather Condition
Prefectural Road 207	2019/8/29 8am	Cloudy
Prefectural Road 10	2019/8/29 11am	Cloudy
Prefectural Road 209	2019/8/29 3pm	Cloudy with occasional rain

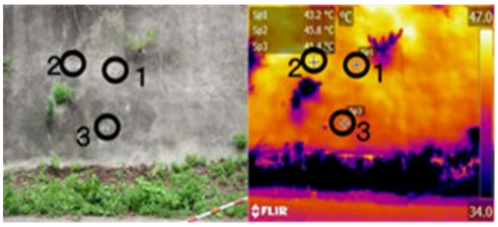

Figure 1. Visible light image and infrared image of slope along prefectural road 10

3. CONCLUSIONS

In this core sampling experiment, the deterioration of the slope was diagnosed using an infrared camera, and three cores with different possibilities of floating were collected. As a result of the core sampling experiment, it was confirmed that there were variations in the degree of consolidation and spraying thickness even on the same slope. It was also confirmed that there was a temperature difference on the surface of the slope even when there was no float behind the slope.

4. FUTURE TASKS

As a future problem, it was confirmed that the spray's thickness varies even on the same slope. When there is a temperature difference on the surface of the slope due to the difference in spray thickness, there is a possibility that AI may mistakenly recognize it as a temperature difference due to floating. Therefore, the relationship between the spray thickness and the surface temperature is clarified by continuously measuring the temperature of the mortar where the spray thickness is known.

REFERENCES

[1]Ministry of Land, Infrastructure, Transport and Tourism, 2013. https://www.mlit.go.jp/road/ir/ircouncil/pdf/roadstock11.pdf

DEVELOPMENT OF CRACK DETECTION AND SOUNDNESS DIAGNOSIS SYSTEM FOR REMOTE IMAGING INSPECTION WITH AI

Takahiro MINAMI[1], Makoto FUJIU[2] , Tomotaka FUKUOKA[3] Junichi TAKAYAMA[4]

[1] *Master (Eng), Kanazawa university, Dept. of Environmental Design, taketaka0503@stu.kanazawa-u.ac.jp*

[2] *Ph.D., Associate Professor, Kanazawa university, Geosciences and civil Engineering, fujiu@se.kanazawa-u.ac.jp*

[3] *Dr., Informatics, Kanazawa university, Geosciences and civil Engineering, fukuoka@se.kanazawa-u.ac.jp*

[4] *Dr., Eng., Professor, Kanazawa university, Geosciences and civil Engineering, takayama@staff.kanazawa-u.ac.jp*

***Keywords**: crack detection, soundness of bridge, image recognition technology, Automatic diagnosis, deep learning*

1. INTRODUCTION

Recently, the study of extending the service life of bridges has gained attention. In Japan, there are about 730,000 bridges with a length of 2 m or longer, and many of these were built during a period of high economic growth, and have now reached the end of their service life. Therefore, their rebuilding and the extension of their service life must be considered.

However, among local public organizations, there are some that have insufficient manpower relative to the number of bridges to manage, as well as insufficient funding for maintenance.

As issues with the continuing close visual inspection of bridges are surfacing, the remote imaging system is expected to become a new inspection method that replaces close visual inspection.

In this study, to develop an alternative method to the current close visual inspection, the practical potential of bridge inspections using images captured with a super-high-resolution camera was examined. With image recognition technology to prepare AI that identifies cracks, a method that delineates locations with cracks based on the entire image of a pier was proposed. Although the automation of the creation of the data of damage has been achieved, the automation of the diagnosis of the soundness level has not been conducted. In order to ensure the objectivity of the diagnosis results, in this study, in order to automate the soundness level evaluation, we analyzed the relationship between the data of damage and the soundness level evaluation value at the time of periodic inspections in the past.

2. CRACK MAP AT ROUTINE BRIDGE INSPECTION

At routine bridge inspection, inspecters detect crack and record the crack as crack map. And each crack maps was diagnosed soundness raiting from 1 to 4. Figure 1 shows crack map diagnosed soundness 1 or 2, in this study, relationship between crack characteristics gained from these crack map and soundness was analyzed. We focused on "Amount of cracks" and "Shape of cracks" as crack characteristics. Cross point, branch point and endpoint gained from crack map were considered as shape of crack, and we counted these amount using pattern matching. Figure 2 shows the result of amount of cracks for each crack maps, and Figure 3 shows the result of shape of cracks for each crack maps.

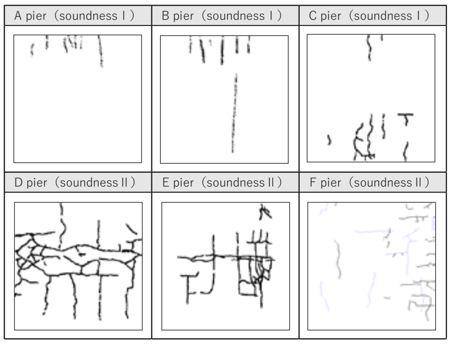

Figure 1 Crack maps used this study

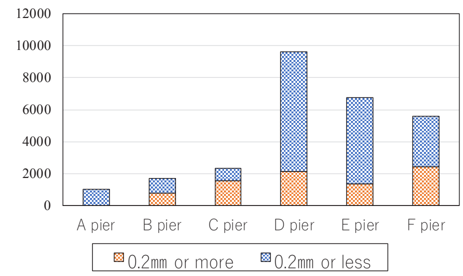

Figure 2 Amount of cracks

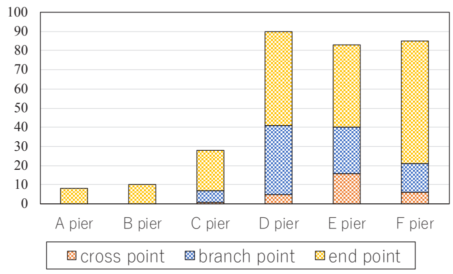

Figure 3 Shape of cracks

3. CONCLUSIONS

Regarding the amount of cracks, it was found that the total amount of cracks was higher in soundness level II than in soundness level I, and there was no significant difference in the amount of cracks with a crack width of 0.2 mm or more. As for the crack shape, it was found that the soundness level II was higher than the soundness level I in the number of cross point, the number of branch points, and the number of end points. In addition, the RC piers diagnosed as soundness degree I had a tendency to have one direction with few cross points and branch points.

REFERENCES

Yeum CM, Dyke SJ (2015) Vision-based automated crack detection for bridge inspection. Computer-Aided Civil Infrastruct Eng Vol.30, pp759–70

Electrochemical properties of reinforcing steel corroded by carbonation

Sothyrak RATH[1], Pakawat SANCHAROEN[2], Pitichon KLOMJIT[3] and Somnuk TANGTERMSIRIKUL[4]

[1]Graduate student, School of Civil Engineering and Technology, Sirindhorn International Institute of Technology, Thammasat University, Thailand
rathsothyrak2222@gmail.com

[2]Research assistant professor, Construction and Maintenance Technology Research Center, Sirindhorn International Institute of Technology, Thammasat University, Thailand
pakawat@siit.tu.ac.th

[3]Researcher, National Metal and Materials Technology Center, Thailand

[4]Professor, School of Civil Engineering and Technology, Sirindhorn International Institute of Technology, Thammasat University, Thailand

ABSTRACT

To repair corrosion of reinforced concrete structure due to carbonation, electrochemical properties of reinforcing steel corroded by carbonation is needed to be studied. In this study, reinforcing steel embedded in different concrete mix proportions were prepared including different types of binder as well as water to binder ratio. Specimens were exposed to accelerated carbonation environment and normal laboratory condition. The four-point probe was applied to investigate the electrical resistivity of concrete. Electrochemical impedance spectroscopy (EIS) and linear polarization resistance (LPR) were applied to investigate electrochemical behavior of steel bar in concrete at different exposure period. Results clearly show the effect of concrete mix proportions on carbonation resistance of concrete as well as electrochemical properties of reinforcing steel. From the results, compatibility design of patching repair can be well conducted in the future work.

Keywords: *carbonation, corrosion, durability, maintenance, electrochemical, electrochemical impedance spectroscopy, linear polarization resistance.*

1. INTRODUCTION

Corrosion of steel in reinforced concrete is now considered as the major problem causing premature deterioration of structures, especially for those exposed to aggressive environment (Bastidas et al., 2007). As a result, this problem leads to the considerable loss of society due to the maintenance and repair needs.

The embedded steel in concrete usually remains passive due to the formation of iron oxide layer that protect the steel from the chemical reactions. The formation of this layer depends on pH value in concrete pore solutions, normally in range from 12 to 13.8, and on electrode potential of rebar (Albani et al., 1990). This passive layer is easily dissolved when there is the presence of chloride or a drop of pH due to carbonation of concrete cover (Alonso et al., 2002, Huet et al., 2005).

Carbonation is the progressive neutralization of the alkaline constituents in concrete pore solutions by carbon dioxide in the air forming calcium carbonate. This reaction leads to the decrease of pH value to be around 9 that causes the unstable of passive layer when the carbonated surface zones reaches the depth of reinforcing steel (Katzer and Kobaka, 2006). The role of carbonation in the reinforced concrete deterioration has increasingly grown interest for two reasons: first, there are many aged RC structures that were built before considering durability design standards and have to be maintained. Second, the aim of reduction CO_2 emission, and using the supplementary cementitious materials (SCMs), such as fly ash (FA), limestone, ground granulated blast-furnace slag (GGBS) etc., to reduce environmental footprint (Stefanoni et al., 2018). However, the application of SCMs as a partial cement replacement material leads to lowering calcium oxide content resulting in reduction of pH of concrete pore solution. This can accelerate the corrosion initiation, with the presence of oxygen and water on the steel-concrete interface.
Many researchers (Montemor et al., 2002, Zornoza et al., 2009) has studied about the effect of carbonation on the corrosion of steel in concrete with and without fly ash substitution to cement.

The aim of this paper is to study the corrosion behavior of embedded steel bar in OPC based concrete sample with and without fly ash substitution, and water-to-binder ratios of 0.4 and 0.6 that are exposed to artificially carbonation (4% CO_2 concentration) and normal laboratory environment (0.03% CO_2 concentration). Electrochemical impedance spectroscopy and linear polarization resistance methods were applied to study the corrosion behavior of specimens during the carbonation process. The electrical resistivity of specimens during the carbonation process was also studied by using four-point probe method.

2. EXPERIMENTAL PROGRAM

Four different concrete mix proportions were studied in this experimental program (Table 1). Ordinary Portland Cement (OPC) type 1, conformed to ASTM C150 (ASTM, 2012), was used. Type 2-b coal fly ash, according to TIS2135, was used as a cement replacing material. Mix proportions varied water/binder ratios as 0.4 and 0.6 as well as fly ash replacement ratio as 0% and 30% by weight of binder. The coarse aggregate was crushed limestone with a maximum size of 10 mm, specific gravity of 2850 kg/m^3 and water absorption of 0.5%. The fine aggregate was river sand with specific gravity of 2670 kg/m^3 and 1.51% water absorption. The concrete mix proportion is shown in Table 1.
A grade SD40 deformed steel bar of 12 mm diameter was embedded in prismatic concrete specimen. The rebar was 150 mm in length, with only 60 mm length left and being exposed inside the concrete sample and the other area are coated with epoxy.

There are three types of specimens presented in this study such as: electrical resistivity, carbonation depth, and electrochemical measurement specimen that are shown in Figure 1(a), (b) and (c), respectively. The covering thickness of reinforcement is 20 mm.
All the specimens were coated its surfaces with epoxy on five surfaces (dash line), leaving only one top surface exposed to carbonation (solid line) as shown in Figure 1.

Table 1: Concrete mix proportion

Name	Water/ binder	Cement (kg/m³)	Fly ash (kg/m³)	Water (kg/m³)	Coarse aggregate (kg/m³)	Fine aggregate (kg/m³)
0.4OPC	0.4	397.6	0	159	1103.4	805.6
0.4FA30	0.4	262.1	112.3	149.8	1103.4	805.6
0.6OPC	0.6	318.4	0	191.1	1103.4	805.6
0.6FA30	0.6	212.9	91.2	182.5	1103.4	805.6

The concrete specimens were de-molded 24 h after casting. All specimens were cured in plastic wrap, kept in a normal environment room for 28 days. After finishing the curing period, the plastic wrap was removed and all specimens were kept in the normal room environment for other 30 days before exposing to accelerated carbonation (ACC) and laboratory environment (LAB). The ACC was done with 4% CO_2, 50 ± 5 % RH and, 40 ^{0}C, and the LAB (SIIT, Rangsit, Thailand) with 0.03% CO_2, 75 ± 5 % RH and, 36 ^{0}C.

The carbonation depth was done by spraying phenolphthalein on a freshly vertically-split section of concrete that recommended by RILEM CPC-18. The average value from five points measurement was used.
The electrical resistivity of concrete was measured by the Four-probe resistivity meter by putting its tips on the smooth exposed surface area of specimens. The average of four points measurement was used.
A standard three-electrode system with working electrode (WE), counter electrode (CE) and reference electrode (RE) was used for electrochemical measurement. The working electrode was the embedded steel bar with a stainless steel as counter electrode on the exposed surface of concrete specimen. Copper/copper sulfate (CSE) is used as reference electrode that was arranged as shown in Figure 2. A Metrohm Autolab potentiostat was used for electrochemical measurement.
The assessment of corrosion on steel bars over time was monitored using two techniques: (i) linear polarization resistance (LPR) to determine polarization resistance value (R_p) that is the slope of linear region of polarization curve. LPR measurement was performed by polarizing the steel $\Delta E = \pm 10$ mV from open circuit potential (OCP) with the scan rate of 0.1667 mV s^{-1}. The corrosion current density of steel bar, i_{corr} in µA/cm^2, was determine by using Stern-Geary equation (Stern and Geary, 1957), as shown in Equation (1)

$$i_{corr} = B/R_p \tag{1}$$

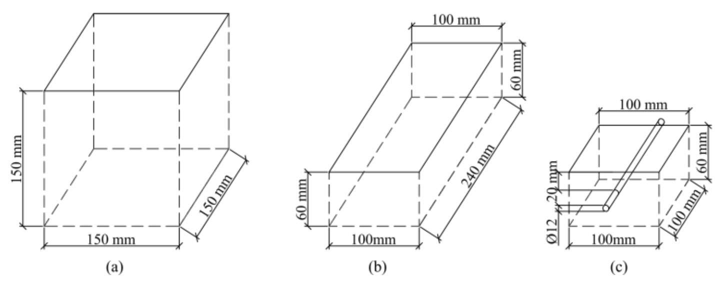

Figure 1: Schematic represents the specimens for: (a) electrical resistivity test, (b) carbonation depth test, and (c) electrochemical test.

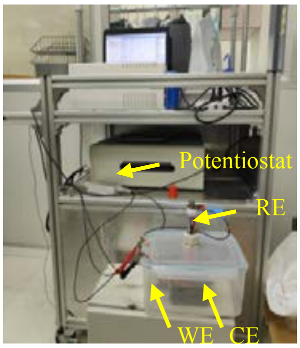

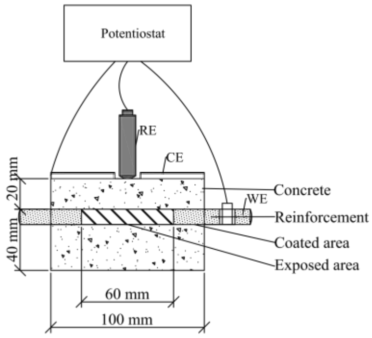

Figure 2: The setup of standard three-electrode system.

where the adopting tentative value B equal to 26 mV for active steel corrosion (Bastidas et al., 2008) and R_p is the polarization resistance in kΩ; and (ii) electrochemical impedance spectroscopy (EIS). EIS measurement was performed by applying ac perturbation of +10 mV from OCP with the frequency range from 10^5 Hz to 10^{-2} Hz and logarithmic sweeping frequency of 10 points per decade. The fitting data of impedance spectra was conducted by using the commercial software Nova 1.1. Results were the average of two replicate specimens with indicated standard deviation of the obtained results. All the tests were done at the age of 0, 10 and 27 days after exposing to carbonation chamber, respectively.

3. RESULTS AND DISCUSSION

3.1 Carbonation depth

The carbonation rate of the conventional concrete is described by carbonation rate coefficient (K_c), in mm/(day)$^{1/2}$, which is calculated from the parabolic law as shown in Equation (2), where x_c is measured carbonation depth (mm), and t is the time (days).

$$x_c = K_c\sqrt{t} \tag{2}$$

Figure 3 shows the carbonation depth versus square root of time for 0.4OPCA, 0.4FAA, 0.6OPCA and 0.6FAA concrete exposed to accelerated carbonation as well as the calculated carbonation rate coefficient, K_c. The carbonation rate coefficient of fly ash concrete shows higher value than that of OPC-only concrete, which is consistent with the trend of results by various researcher (Khunthongkeaw et al., 2006). At the same w/b ratio, the carbonation rate coefficient of fly ash concrete shows the value approximately two to three times as high as that of OPC concrete. This may be attributed to the fly ash concrete has lower amount of $Ca(OH)_2$ to react with CO_2, that resulted from the reduction of initial cement content as well as reduction of CH by pozzolanic reactions. Please be noted that carbonation depth of specimens exposed to normal environment cannot be measured as the exposure period is short.

3.2 Electrical resistivity

Figure 4 shows electrical resistivity versus time of concrete exposed to accelerated carbonation (0.4OPCA, 0.4FAA, 0.6OPCA, 0.6FAA) and a laboratory environment (0.4OPCL, 0.4FAL, 0.6OPCL, 0.6FAL). For the same w/b, the fly ash concrete shows higher resistivity than that of OPC concrete. This may attributed to the fly ash concrete has higher amount of C-S-H that clogs the bigger capillary pores and refining the microstructure (Mehta and Gjørv, 1982). For resistivity of OPC concrete in laboratory exposure (0.4OPCL and 0.6OPCL) seems to be slowly increased during the exposure time. This may be the hydration reactions cause refinement of pore size of concrete. The resistivity of OPC and fly ash concrete increases noticeably after being exposed to accelerated carbonation. This increasing may attributed to the deposition of $CaCO_3$ that reduce the porosity of concrete, which may came from the Equation (3) to (5). The Equation (4) and (5) are referred to carbonation of fly ash concrete.

$$Ca(OH)_2 + CO_2 \rightarrow CaCO_3 + H_2O \quad (3)$$
$$2SiO_2.3CaO.3H_2O + 2CO_2 \rightarrow 2SiO_2 + 3CaCO_3 + 3H_2O \quad (4)$$
$$4CaO.Al_2O_3.13H_2O + 3CO_2 \rightarrow 2Al(OH)_3 + 4CaCO_3 + 10\ H_2O \quad (5)$$

3.3 Polarization resistance measurement

Figure 5 shows the corrosion rate versus time of embedded steel in concrete exposed to accelerated carbonation and laboratory environment for 27 days. The Equation (1) was used to calculate this corrosion rate by adopting the constant value B equal to 26 mV. The effect of ohmic drop on the polarization resistance was not considered in this study. Most of the samples were in passive state. No corrosion has been occurred yet, except 0.6FAA and 0.6OPCA that corrosion rate was increased due to progress of carbonation depth. It should be noted that carbonation depth as shown in Figure 3 is still less than covering depth. For other specimens, the corrosion state are still in the passive state, even though they were exposed to accelerated carbonation. This is due to higher resistance against carbonation.

3.4 Electrochemical impedance spectroscopy

The equivalent circuit as shown in Figure 6 is used to fit the results of impedance spectra. This equivalent circuit consists of two constant phase elements (CPE and CPE_P) to consider two relaxation times. The couple CPE-R_c that performed at high frequency, referred to dielectric properties of concrete that consist of concrete resistance R_c. The CPE_P-R_P couple, low frequency range, characterizes corrosion process of steel/concrete interface that R_P is polarization resistance of reinforcing steel. Table 2 includes the fitting results by using equivalent circuit in Figure 6 with the measured impedance

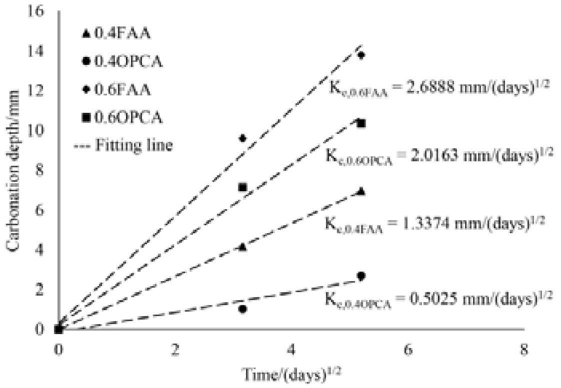

Figure 3: Carbonation depth of concrete in accelerated carbonation.

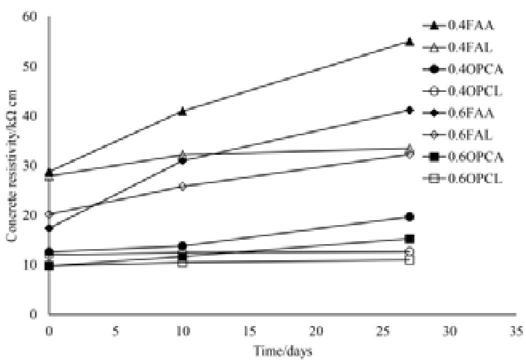

Figure 4: Concrete resistivity in accelerated and normal environment

results during the carbonation process. At high frequency, the concrete resistance, R_c, of fly ash and OPC concrete increased after accelerated carbonation, evident in Table 2, that this results conform to the trend of results from Wenner probe as discuss in part 3.2.

Compared to the steel embedded in partially carbonated fly ash concrete, the steel embedded in partially carbonated OPC concrete shows higher polarization resistance for both w/b ratio. This may attributed to the strength of passive film in which OPC concrete has higher alkalinity than fly ash concrete.

Comparing the 0.4OPCA to 0.6OPCA and 0.4FAA to 0.6FAA, the concrete with lower w/b ratio gives higher values of R_p. This may attribute to the higher amount of cement in the lower w/b ratio, as evident in Table 1. The decreasing of polarization resistance were observed when the accelerated carbonation time increased. This decrease may attributed to the decrease amount of $Ca(OH)_2$ in concrete by carbonation reaction that leads to lowering the pH in concrete pore solution which resulted in continually degraded the passive film which is represented as a polarization resistance.

For laboratory exposure, the polarization resistance values are continually increased. This may attribute to the hydration reactions are still continues that generating the hydration product, $Ca(OH)_2$, to reinforce the passive film that resulted in the increase of corrosion resistance. The R_P from OPC concrete are significantly increased, unlike the R_P from fly ash concrete. This may be because the OPC concrete has higher amount CaO than that of fly ash concrete or due to slower hydration reaction of fly ash concrete.

Table 2 shows the comparison between polarization resistance from LPR, denoted as $R_{p,LPR}$, and EIS, denoted as $R_{p,EIS}$. From this table, certain differences are evident. This differences may attributed to the very high IR drop, especially for fly ash concrete, furthermore, since the steel is in a very passive state, then the correlation between applied potential and measured current is far from linear (unstable of corrosion potential during the measurement). Therefore, the fitting results from LPR leads to some errors, as mentioned in previous researches (Kouřil et al., 2006, Serdar et al., 2017).

The comparison between the concrete resistance from Wenner probe test, denoted $R_{c,Wenner}$, and EIS, denoted $R_{c,EIS}$, is also shown in Table 2. It seems these two methods gives a comparable results, except for those of the specimens with higher carbonation depth. This may attributed to the influence of different layers of resistivity (carbonated-

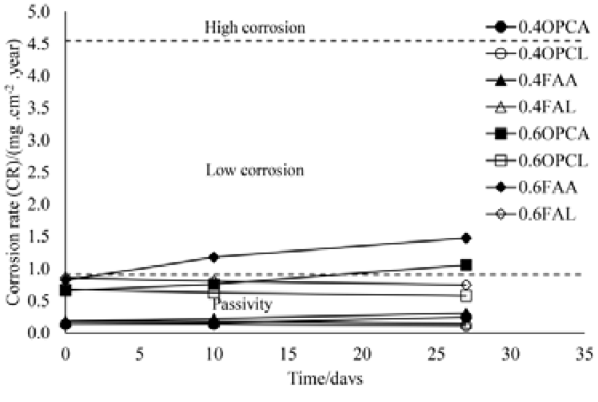

Figure 5: Corrosion rate versus time of embedded steel bar.

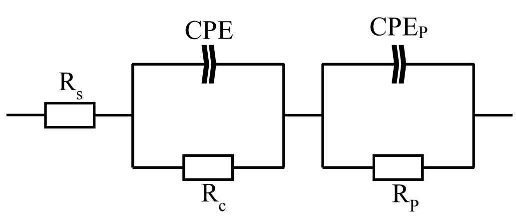

Figure 6: Electrical equivalent circuit used to fit the EIS data.

Table 2: Parameters of the tested results

Name	Sample age days	$\rho_{c,Wenner}$ kΩ cm		$R_{c,Wenner}$ kΩ		$R_{c,EIS}$ kΩ		$R_{P,LPR}$ kΩ		$R_{P,EIS}$ kΩ	
		Lab	Acc	Lab	Acc	Lab	Acc	Lab	Acc	Lab	Acc
0.4OPC	0	12	12.6	0.5	0.53	0.64	0.59	78.2	78.8	368.3	399.1
	10	12.5	13.8	0.52	0.58	0.73	0.85	79.4	67.9	474	298.5
	27	12.7	19.7	0.53	0.82	0.8	2.5	90.8	42.6	546.7	217.5
0.6OPC	0	9.8	9.8	0.41	0.41	0.62	0.62	15.4	15.9	285.9	311.3
	10	10.5	11.7	0.44	0.49	0.66	1.16	16.7	13.8	352.9	206.6
	27	13.8	15.3	0.58	0.64	0.73	1.5	18.1	9.9	469.1	131.8
0.4FA	0	27.9	28.8	1.17	1.21	1.29	1.5	57.8	57.4	212.5	209.58
	10	32.2	41	1.35	1.72	1.35	2.01	59.0	47.2	283.37	147
	27	33.5	55.1	1.4	2.31	1.53	2.71	71.0	34.2	399.6	99.21
0.6FA	0	20.2	17.4	0.85	0.73	1.2	1.38	12.2	12.7	158.7	157.7
	10	25.8	31	1.08	1.3	1.48	1.7	13.0	8.9	259.3	86.5
	27	32.3	41.2	1.35	1.73	1.8	2.02	14.0	7.1	283.3	56.9

Lab*: laboratory exposure
Acc*: accelerated carbonation exposure

and uncarbonated layer) of concrete that distorts the applied current of Wenner probe test (Gowers and Millard, 1999).

4. CONCLUSIONS

From the experimental results, the following conclusion would be made

i. The corrosion rates of embedded steel in OPC concrete were smaller than those of fly ash concrete with the same w/b ratio. The corrosion rate increases as an increase of w/b ratio.
ii. Effects of carbonation on electrical resistivity and polarization resistance of reinforcing steel can be clearly observed. Formation of calcium carbonate and reduction of alkalinity are the main causes.
iii. From the test results, a further study on compatibility patching repair for carbonation can be proposed.

ACKNOWLEDGEMENTS

The authors would like to express grateful appreciation to the National Metal and Materials Technology Center (MTEC) and the Center of Excellence in Material Science, Construction and Maintenance Technology Project, Thammasat University for their support during this research.

REFERENCES

Bastidas, D. M., González, J., Feliu, S., Cobo, A., & Miranda, J., 2007. A quantitative study of concrete-embedded steel corrosion using potentiostatic pulses. *Corrosion*, 63, 1094-1100.
Albani, O., Gassa, L., Zerbino, J., Vilche, J., & Arvia, A., 1990. Comparative study of the passivity and the breakdown of passivity of polycrystalline iron in different alkaline solutions. *Electrochimica Acta*, 35, 1437-1444.
Alonso, C., Castellote, M., & Andrade, C., 2002. Chloride threshold dependence of pitting potential of reinforcements. *Electrochimica Acta*, 47, 3469-3481.
Huet, B., L'Hostis, V., Miserque, F., & Idrissi, H., 2005. Electrochemical behavior of mild steel in concrete: Influence of ph and carbonate content of concrete pore solution. *Electrochimica Acta*, 51, 172-180.
Katzer, J., & Kobaka, J., 2006. The assessment of fine aggregate pit deposits for concrete production. *Kuwait Journal of Science and Engineering*, 33, 165.
Stefanoni, M., Angst, U., & Elsener, B., 2018. Corrosion rate of carbon steel in carbonated concrete – a critical review. *Cement and concrete research*, 103, 35-48.
Montemor, M., Cunha, M., Ferreira, M., & Simoes, A., 2002. Corrosion behaviour of rebars in fly ash mortar exposed to carbon dioxide and chlorides. *Cement and Concrete Composites*, 24, 45-53.
Zornoza, E., Payá, J., & Garcés, P., 2009. Carbonation rate and reinforcing steel corrosion rate of opc/fc3r/fa mortars under accelerated conditions. *Advances in Cement Research*, 21, 15-22.
ASTM,2012. Astm c150/c150m-12: Standard specification for portland cement. ASTM International West Conshohocken, PA, USA.
Stern, M., & Geary, A. L., 1957. Electrochemical polarization i. A theoretical analysis of the shape of polarization curves. *Journal of the electrochemical society*, 104, 56-63.
Bastidas, D., Fernández-Jiménez, A., Palomo, A., & González, J., 2008. A study on the passive state stability of steel embedded in activated fly ash mortars. *Corrosion science*, 50, 1058-1065.
Khunthongkeaw, J., Tangtermsirikul, S., & Leelawat, T., 2006. A study on carbonation depth prediction for fly ash concrete. *Construction and Building Materials*, 20, 744-753.
Mehta, P., & Gjørv, O., 1982. Properties of portland cement concrete containing fly ash and condensed silica-fume. *Cement and concrete research*, 12, 587-595.
Kouřil, M., Novák, P., & Bojko, M., 2006. Limitations of the linear polarization method to determine stainless steel corrosion rate in concrete environment. *Cement and Concrete Composites*, 28, 220-225.
Serdar, M., Poyet, S., L'Hostis, V., & Bjegović, D., 2017. Carbonation of low-alkalinity mortars: Influence on corrosion of steel and on mortar microstructure. *Cement and concrete research*, 101, 33-45.
Gowers, K., & Millard, S., 1999. Measurement of concrete resistivity for assessment of corrosion. *ACI Materials Journal*, 96,

SUFFUSION BEHAVIOR OF GAP-GRADED SOILS VIA SEGREGATION EXPERIMENTS

A. GHAEMI[1], R. KUWANO[2], M. OTSUBO[3]

[1] *Master Student, Department of Civil Engineering, The University of Tokyo, Japan,*
[2] *Professor, Institute of Industrial Science, The University of Tokyo, Japan,*
[3] *Research Associate, Institute of Industrial Science, The University of Tokyo, Japan*

Keywords: *Suffusion, Seepage flow, Permeability, Gap-graded soil, Segregation, Particle-size*

1. BACKGROUND

Suffusion has been identified as one of the lead causes of failure for many geo-hydro structures, particularly earth dams and railway embankments. A thorough understanding of the factors affecting suffusion is thus instrumental in preventing future failures from occurring and designing resilient infrastructure. Previous research has shown that the response of gap-graded soils undergoing suffusion is closely linked with the particle size ratio of the two constituent materials [1], as well as the percentage of fines in the composition [2]. The susceptibility of a gap-graded soil is defined by the ease with which the finer particles can be removed from the composite matrix. The present paper aims to identify the factors affecting the segregation behavior of different composite soils, particularly the effect of varying particle size ratio and absolute particle sizes.

2. EXPERIMENTAL PROCEDURE

A compacted homogenous layer of the coarser material (250 g) being overlain by a non-compacted homogenous layer of the finer material (200 g) in a cylindrical specimen is prepared. The gap-graded soils investigated are composed of silica sands (diameters from 0.5 to 1.8 mm) as the coarse-particle constituent material, in combination with various finer silica sands or powders. Greater gap ratios, ranging from 6 to 28, are examined in this study. These gap ratios are all above the classical boundary value of 4, which previous research has identified as the critical value for suffusion to occur [3].

Two types of experiments are performed in this study. (1) The dry segregation tests: the specimen being subjected to regular physical blows to the container in roughly equal amount from all sides, and the amount of mass removed from the specimen via a sieve on the bottom is measured. (2) The wet permeability tests: the fines removed from the specimen from the application of water pressure are measured.

3. RESULTS AND DISCUSSION

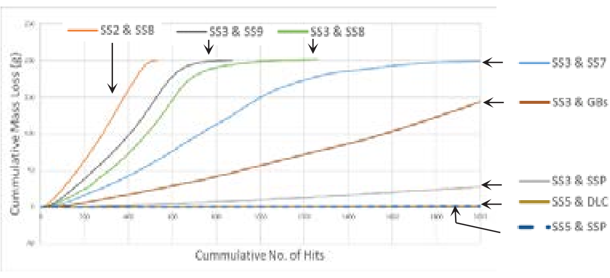

Figure 1 – Segregation rate under continuous vibrations

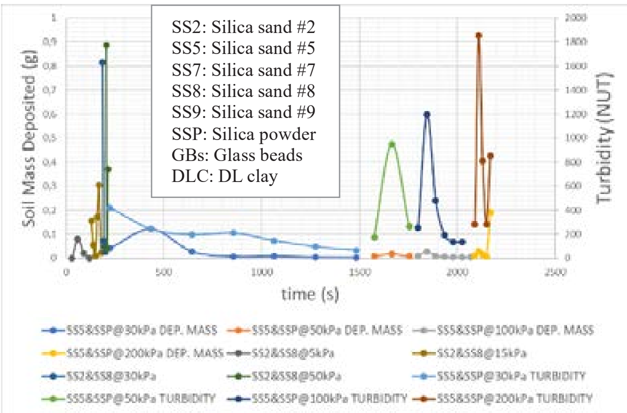

Figure 2 – Permeability test deposited mass and turbidity

Referring to Figure 1, for combinations of both larger coarse and finer silica sands it can be observed that the segregation rate gradually increases until it reaches a maximum and then slowly declines. For the largest gap-ratios all the finer material is segregated from the specimen within the range of applied vibrations. In comparison, the gap-graded soils composed of silica sand no. 5 and silica powder or DL clay, which have similar particle size ratios, show significantly smaller absolute segregation. This indicates that segregation behavior is governed not only by particle-size ratio, but to a greater extent than anticipated, also by absolute particle size of finer particles.

The permeability tests show that segregation under water is characterized by an initially large segregation which rapidly declined. Figure 2 shows that the mass of fines removed from the specimen is also significantly larger for larger relative particle size combinations.

4. CONCLUSIONS

Experimental results show that, additionally to the fines content and gap ratio, particle size is also a key factor in governing segregation behavior. Combinations of larger absolute particle size materials segregate more easily.

REFERENCES

[1] Honjo, Y. et al. (1996) Self-filtration behaviour of broadly and gapgraded cohesionless soils. Geofilters, BiTech Publishers, Montreal, Canada, 227-236.
[2] Liu, J. (2005) Seepage control of earth-rock dams: theoretical basis, engineering experiences and lessons (in Chinese), China Waterpower Press, Beijing.
[3] Kedzi, A. (1969) Increase of Protective Capacity of Flood Control Dikes. Dept. of Geotechnique. Technical Uni, Budapest, Hungary. Report no. 1 (in Hungarian).

MESO-SCALE DISCRETE ANALYSIS OF CONCRETE DAMAGED BY DELAYED ETTRINGITE FORMATION

K. MATSUMOTO[1], Y. MENG[2], and K. NAGAI[3]

[1] Associate Professor, Division of Engineering and Policy for Sustainable Environment, Faculty of Engineering, Hokkaido University, Sapporo, Japan
[2] Graduate Student, Department of Civil Engineering, The University of Tokyo, Tokyo, Japan
[3] Associate Professor, Institute of Industrial Science, The University of Tokyo, Tokyo, Japan
Correspond to Assoc. Prof. K. MATSUMOTO (km312@eng.hokudai.ac.jp)

Keywords*: Concrete, Delayed ettringite formation, Meso-scale discrete analysis, Rigid body-spring model, Initial strain*

1. INTRODUCTION

Delayed Ettringite Formation (DEF) occurs when primary ettringite melts under high temperature curing and reforms to secondary expansive ettringite after the concrete is hardened, resulting internal pressures. Up to the present date, the occurrence mechanism of DEF has been investigated in the material scale, however, the cracking mechanism has not been clarified. This study aims to investigate the cracking mechanism of concrete under DEF and its effect on the mechanical characteristics. A meso-scale discrete analysis method by Rigid Body-Spring Model (RBSM), in which coarse aggregates and mortar are separately modeled, is used for reproducing the expansive behavior in concrete.

2. OUTLINE OF ANALYSIS

Figure 1 show the model of concrete by RBSM. Elements are created by Voronoi meshing, in which shape of the element becomes random. Elements are rigid, but springs are interconnected between the elements. Coarse aggregates and mortar are separately modeled as an meso-scale analysis. This study adopted the material constitutive law used in the previous study [1]. Expansive strain is given to the mortar elements as an initial strain. To investigate the effect of non-uniformity of the expansion, region of the expansion is changed as an analytical parameter.

3. RESULTS AND DISCUSSIONS

Figure 2 shows the inner stress distributions and outer crack patterns when the average expansion strain is about 1%. When the expansion strain is given to only the inner part, both tensile stresses and cracking from the inside occur as observed in the experiment. However, when the expansion strain is given to all the region uniformly, macro cracks do not occur. It is because interface strength between aggregate and mortar is comparatively weak, resulting almost no restriction for mortar expansion.

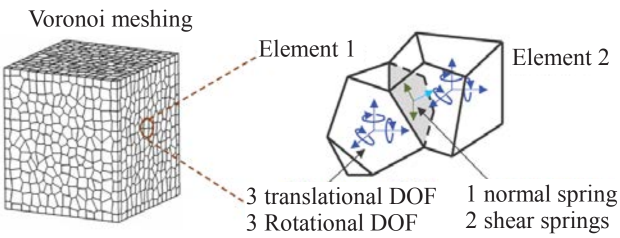

Figure 1. Model of concrete by RBSM

(a) Stress distributions

(b) Outer cracking patterns

Figure 2. Result of analysis after expansion

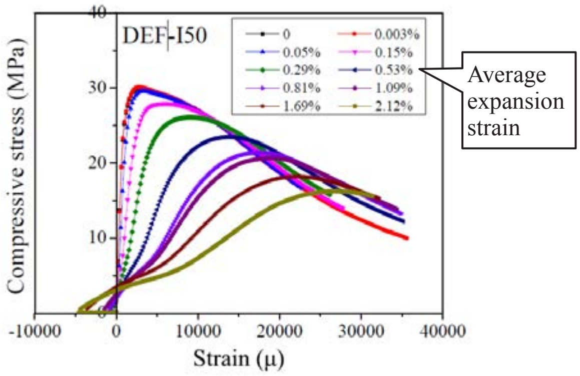

Figure 3. Stress-strain curves after expansion

Figure 3 shows average stress-average strain curves obtained by giving forcible displacement in compression after the concrete is non-uniformly expanded. It indicates that, with larger expansion, both compressive strength and elastic modulus become smaller.

4. CONCLUSIONS

1) By giving expansive strain to only inner region, concrete cracks induced by DEF can be reproduced.
2) Meso-scale discrete analysis using RBSM can simulate reduction of compressive strength and elastic modulus of concrete due to DEF.

REFERENCES

[1] K. Nagai, Y. Sato and T. Ueda, Mesoscopic Simulation of Failure of Mortar and Concrete by 3D RBSM, Journal of Advanced Concrete Technology, 3(3), 385-402, 2005.

Effect of stirrup confinement on residual bond performance of corroded RC by 3D RBSM

PUNYAWUT JIRADILOK[1], KUMAR AVADH[2] and KOHEI NAGAI[3]
[1]Project assistant professor, Institute of Industrial Science,
The University of Tokyo
Japan
punyawut@iis.u-tokyo.ac.jp
[2]Doctoral Student, Institute of Industrial Science,
The University of Tokyo
Japan
[3]Associate Professor, Institute of Industrial Science,
The University of Tokyo
Japan

ABSTRACT

The surface cracks from expansion of corroded rebar can be easily measured during field investigations. However, the internal condition and the residual capacity remain unrevealed. Therefore, it would be a very convenient system if the degree of deterioration of bond strength could be predicted by measuring these crack widths. The cracks induced due to corrosion in reinforced concrete structures are dependent on numerous parameters such as degree of corrosion, confinement offered by stirrups and concrete cover etc. Due to various uncertainties involved in corrosion of steel reinforcement it is very difficult to obtain a unifying relationship and understanding of the phenomenon from the experimental study. The aim of this research is to understand the effect of confinement provided by stirrups on corrosion cracks and bond strength using the 3D RBSM simulation technique. The reinforced concrete models with stirrup confinement are subjected to uniform corrosion process to induce the corrosion damage. The pulling-out simulations are then simulated to find the remained bond capacity. The simulation model is based on the experimental study performed by Lin et al., 2017 in which stirrup spacing and concrete cover are varied. The stirrup corrosion is not considered in this study. The relationship between the surface crack width, corrosion damage and the remained bond strength is analysed and discussed.

Keywords: simulation exercise, management by objectives, public relations, common operational picture, incident action plan

1. INTRODUCTION

Corrosion is one of the important issues in the field of structural monitoring and maintenance. Once the corrosion occurs, the reinforcement turns into voluminous corrosion product, which increases the internal pressure, and deteriorates the structure capacity. Even though several technologies had been developed for the inspection of the external condition of reinforced concrete structure, the internal condition and the residual capacity remains unrevealed.
Therefore, it would be useful if the degree of corrosion could be predicted by measuring the external observable condition of concrete. However, the cracks induced due to

corrosion in reinforced concrete structures are dependent on numerous parameters such as degree of corrosion, confinement offered by stirrups and initial corrosion expansion damage. Thus, it is important to improve the understanding of relationship between the corrosion crack damage, stirrup confinement and the residual capacity of damaged bond through numerical simulation.

To understand the internal condition of corrosion expansion damaged specimens, the simulation model is a beneficial tool. In this study, the numerical model called Rigid Body Spring Model is used to study the relationship between the corrosion expansion damage and surface crack width. Reinforced concrete models with different initial corrosion expansion damage and stirrup confinement are formed up for study the effect of each influent parameter. The corrosion expansion damage is induced into the model by expansive strain method. The pull-out was then performed to measure the residual capacity. Reinforced concrete models with different control parameters are simulated to investigate their effect on corrosion crack patterns. The simulation results were compared with the previous experiment for verification. The relationship between the surface crack width, corrosion degree, and the remained bond strength are analyzed and discussed. The object of this experiment was to clarify the relationship between each control parameter and understand the mechanism of bond failure after the corrosion of main tensile bar in specimens with and without stirrups using RBSM simulation tool. The paper will also describe the advantages of using RBSM in enhancing the ways to understand mechanical behavior or reinforced concrete reinforcing the results obtained from experimental study.

2. NUMERICAL MODEL

2.1 Rigid Body Spring Model

The numerical model used in this study is 3D RBSM, which is proposed by Kawai et al. (1977). A 3D reinforced concrete model is meshed into polyhedral rigid elements whose phases are interconnected by one normal spring and two shear springs (Fig. 1). Each rigid body has six degrees of freedom (i.e., three translational degrees of freedom and three rotational degrees of freedom with respect to some point within its interior) (Eddy et al.,2016). The response of the springs provides the interaction between the rigid elements.

To enable crack propagation in arbitrary directions, a random geometry, based on a Voronoi Diagram, is used for element meshing. The size of each concrete element is made approximately 1^3-2^3 cm^3, in reference to aggregate size, while the size of steel elements is set according to the geometric complexity of the rebar arrangement.

To represent the reinforced concrete, two types of elements are used, the rebar elements and the concrete elements as shown in Fig. 2 (a). Fig. 2 (b) shows the geometry of steel elements which is modelled in an accurate manner to properly account for the interlocking between concrete and rebars. The simulation system is developed in previous studies by Eddy et al. (2016).

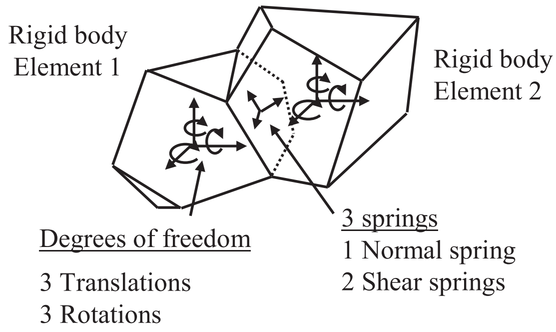

Figure 1: Concrete elements in RBSM

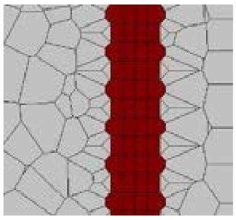

(a) Cross-section of steel and concrete elements

(b) 3D rebar shape (deformed bar)

Figure 2: Modelling of geometric shape of the rebar

2.2 Expansive strain model

In the 3D RBSM adopted in this study, the expansion resulting from corrosion products forming around rebars is modeled by inducing a strain at the interface between rebar and concrete. The expansive strain concept is previously developed by Matsumoto et al. (2015). This expansive strain is added only to the normal springs at the interface as shown in Fig. 3. Expansive strain concepted has been used to simulate the corrosion expansion damage of RC structural member in previous studies. (Jiradilok P. et al, 2019)

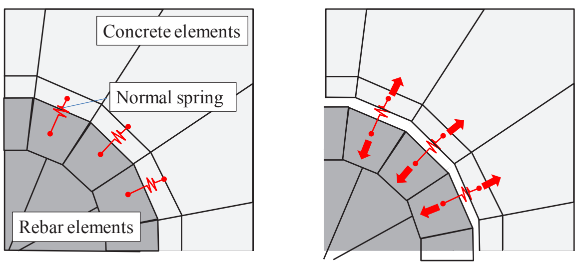

Figure 3: Interface between rebar and concrete and given initial strain

3. MODEL GEOMETRY

Table 1 shows the material properties of simulation model and Fig.4 shows the model geometry.
The specimen mode in this study is formed based on the previous experiment of Lin H. et al. (2017). Fig. 4 (a) and Fig. 4 (b) show the general geometry of the analyzed numerical models for the no stirrup specimen model and stirrup specimen model, respectively. The size of the model is 330×250×150 mm^3. The model contains 22,650 elements for non-stirrup case and 33147 elements for stirrup case. The specimen reinforced with one D20 rebar and two D8 rebars. The clear cover depth of main rebar is 30 mm. Unbond length of main rebar is set at 50 mm from the pull-out end and 80 mm from the free end. The stirrup confinement and initial crack damage are varied as the controlling parameters for this study. Two types of simulation models were formed up, the specimen with stirrup and without stirrup. In case of stirrups specimens, RB8 stirrups were placed at spacing of 200 mm to provide the confinement. To study the effect of different initial damage level, the surface crack width is varied from 0.0 mm (sound case), 0.5 mm, 1.0 mm and 2.5 mm. By varying these parameters, 8 simulation cases are investigated.

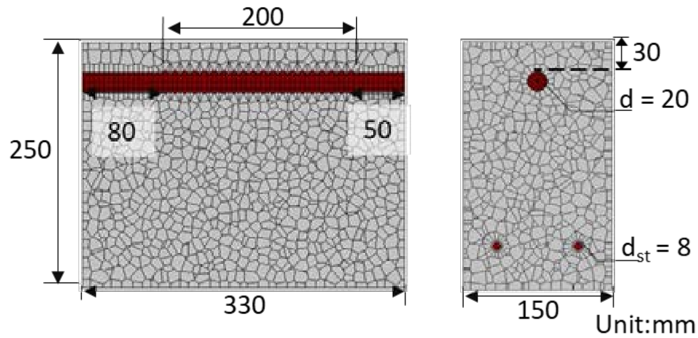

(a) Non-stirrup case specimen

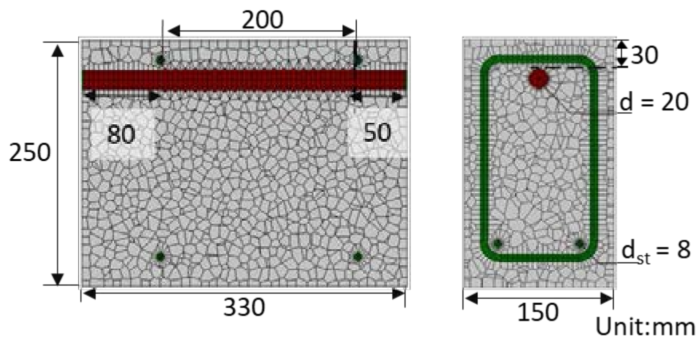

(b) Stirrup case specimen

Figure 4: Model geometry

Table 1: Simulation material properties

	Concrete	**Rebar**
Elastic modulus (MPa)	27000	200000
Poisson ratio	0.15	0.25
Tensile strength (MPa)	2.53	450

4. OUTLINE OF SIMULATION PROGRAM

The simulation cases with different control parameters are listed in Table. 2, including three different crack width with two stirrup confinement condition, LA0 (non-stirrup case) and LA200 (stirrup case). The simulation program is designed based on the previous study by Lin H. (2017). To consider the initial damage from corrosion expansion, the expansion simulation is performed to generate the initial damage before the pull-out simulation. The simulation process is divided into 2 stages, the expansion stage and the pull-out stage. During the expansion stage, only the main rebar is subjected to the expansion (the rebar with red color in Fig. 5).The uniform expansive strain is continuously given to the rebar-concrete interface along the bond length region of main bar at rate of 0.00005 strain/step until the crack width on top surface reaches the target crack width. Then, the pull-out is performed for finding the residual capacity of damage model by using displacement control pull-out simulation. The rebar is pulled at rate of 0.001mm/step from the side of 50 mm unbond length. The concrete elements at the pull-out surface are fixed in movement and rotational condition. The crack pattern for each case and the effect of each parameter on the residual capacity are discussed in the next section.

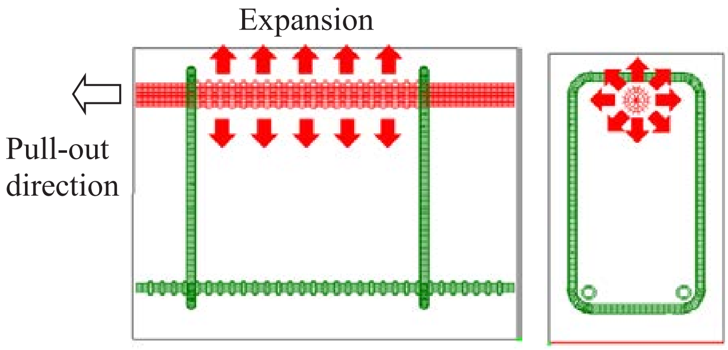

Figure 5: Simulation condition

Table 2: Simulation cases

Cases	Crack width(mm)	Confinement
LA0-0.0	0.0	Non-stirrup
LA0-0.5	0.5	
LA0-1.0	1.0	
LA0-2.5	2.5	
LA200-0.0	0.0	Stirrup
LA200-0.5	0.5	
LA200-1.0	1.0	
LA200-2.5	2.5	

5. SIMULATION RESULTS

5.1 Corrosion-expansion simulation

Fig. 6(a) and Fig. 6(b) shows the surface overview after the corrosion expansion simulation for non-stirrup and stirrup cases. The splitting crack appeared at the top of specimen along the bond length and 50 mm unbond length side, while the Y-shape crack can be observed above the unbond length of 80 mm. The similar crack patterns can be observed from both case specimens.

The crack width pattern along the transverse cross-section is shown in Fig. 7 for various crack widths. It could be clearly concluded that presence of stirrups reduces the rate of cracking as higher amount of expansive strain was required to obtain same value of crack width on the surface for specimen with stirrups as compared to the one without stirrup. Fig. 8 shows the expansion strain required for the surface crack achieving the target crack widths. In case of stirrup case, the required expansive strain is significantly higher than the non-stirrup case due to the stirrup confinement proving the counter force that restrains the opening of the crack. This result is not in accordance with the experimental study performed by (Lin et al., 2017) however, they have also mentioned that this requires further clarification experimentally. In previous experimental studies performed by (Lin and Zhao, 2016) and (Coronelli, Hanjari and Lundgren, 2013) effect of confinement provided by stirrups in reducing the magnitude of crack width for same degree of corrosion was clearly observed.

Hence RBSM can be effectively used to study the evolution of cracking patterns not only on the surface but also inside the specimen which cannot be achieved in experimental studies.

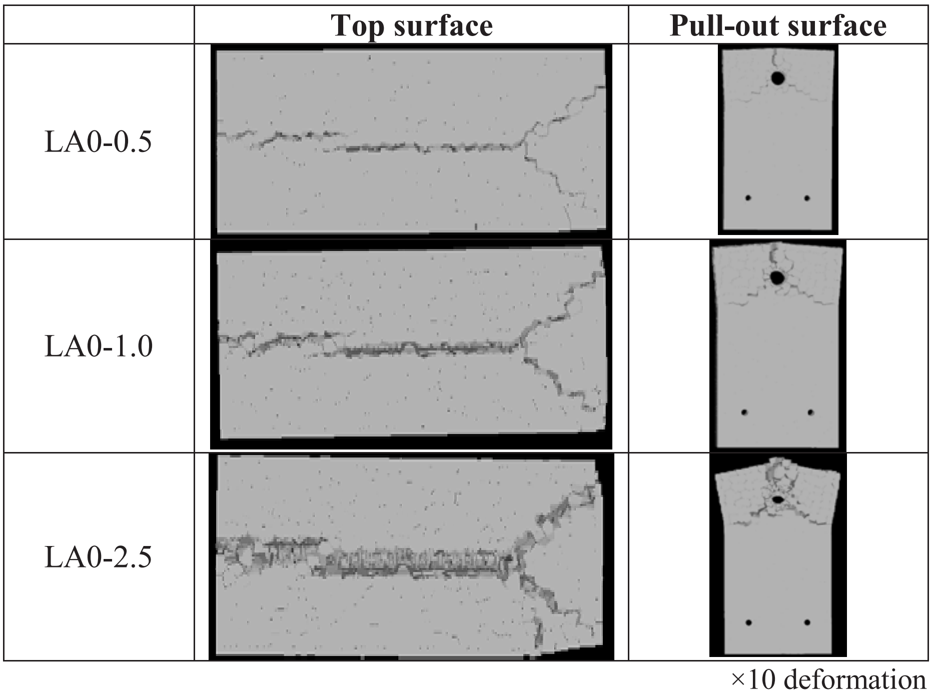

(a) Non-stirrup case

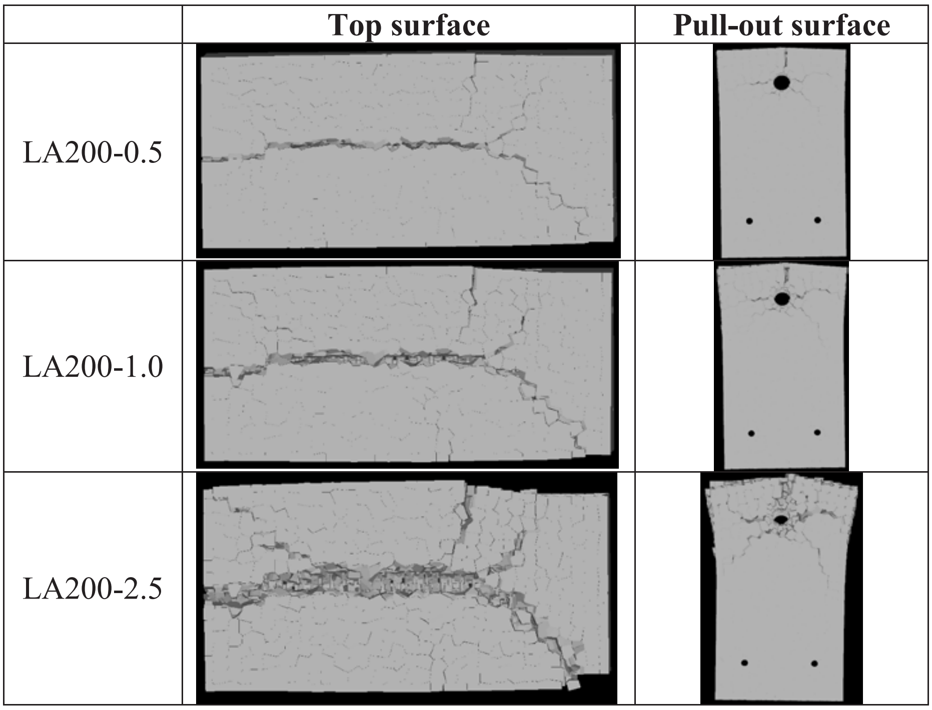

×10 deformation

(b) Stirrup case

Figure 6: Surface overview after corrosion expansion

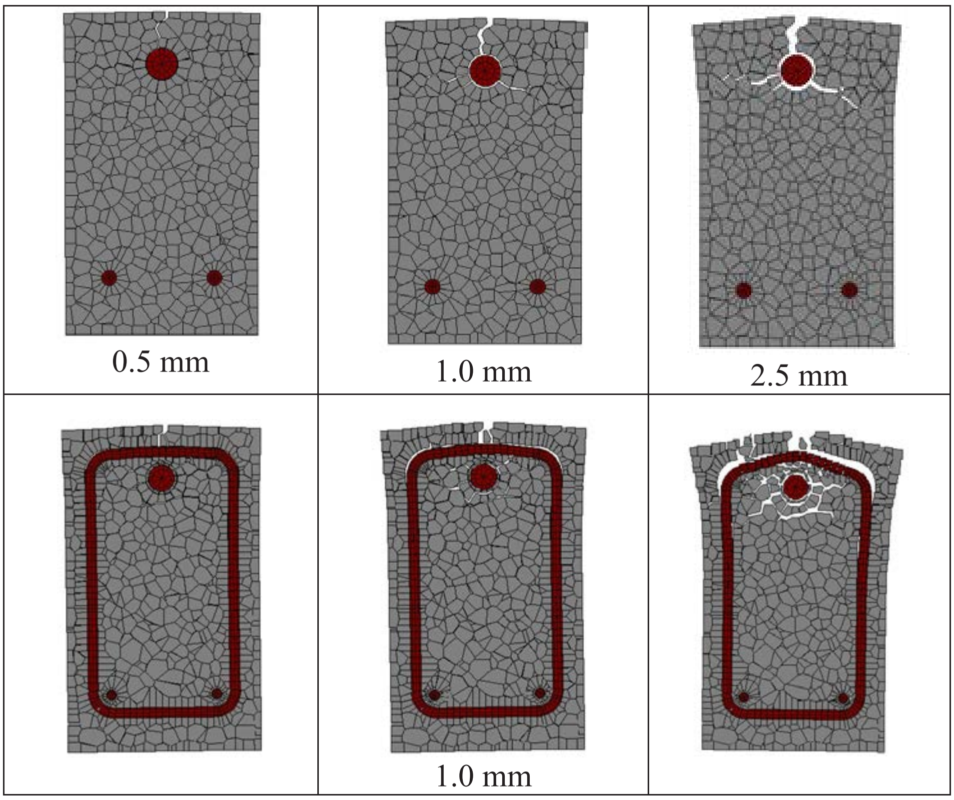

0.5 mm		2.5 mm

Figure 7: Crack evolution inside specimen during corrosion

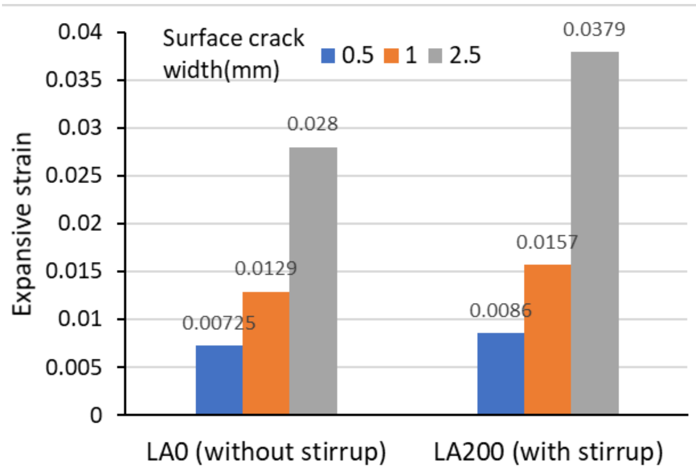

Figure 8: Required expansive strain for achieving target crack width

5.2 Pull-out simulation

In the experiment, the pull-out test method was performed under displacement control with a rate of 0.5mm/min applied monotonically. The average crack width was determined by measuring the longitudinal surface crack at every 20 mm and calculating it mean. In the simulation the average crack width was determined by measuring the movement of elements along the same transverse line and determining their average for all pairs of elements along the bonded length.

Fig. 9 shows the load-displacement curve for both the specimens for different crack widths. As expected and similar to the experimental results the peak load value for specimen with stirrups is higher for the corresponding crack widths than the specimen without stirrups. Using RBSM we can clearly visualize the stress distribution inside the specimen and realize that the red zones corresponding to compressive stress are formed near main tensile rebar and also stirrups. Form Fig. 10 we can compare the stress distribution for specimen with and without stirrups. Hence, using RBSM we can clearly study the distribution of stresses and understand the mechanism involved in bond failure. In this case we efficiently visualized the compressive stresses formed due to presence of stirrups surrounding the main tensile bar thus effectively providing confinement and enhancing bond behavior. We can clearly see the resistance offered by stirrups to the expansive pressure instigated due to corrosion of rebar which was not possible in the experimental study.

Table 3 lists the peak load value for the considered crack widths in both specimens. It was observed that the rate of decrease of peak load for similar crack width is higher in the specimen with stirrups as compared to specimen without stirrups. This is in coherence with the results given by (Lin *et al.*, 2017) in their paper as in line with the equation provided by them relating residual bond strength and crack width.

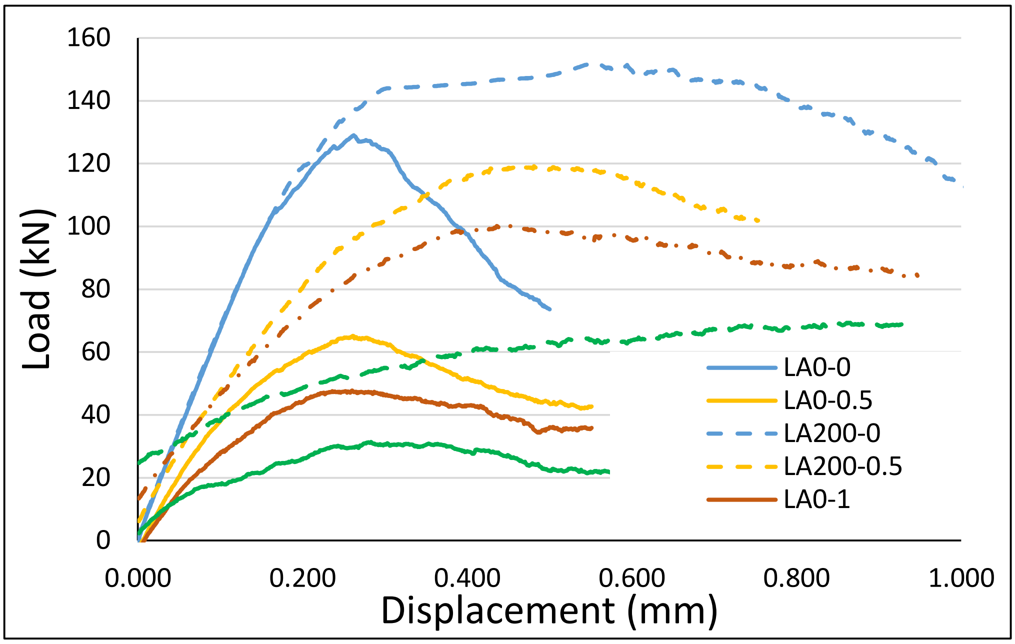

Figure 9: Load displacement curve obtained from simulation

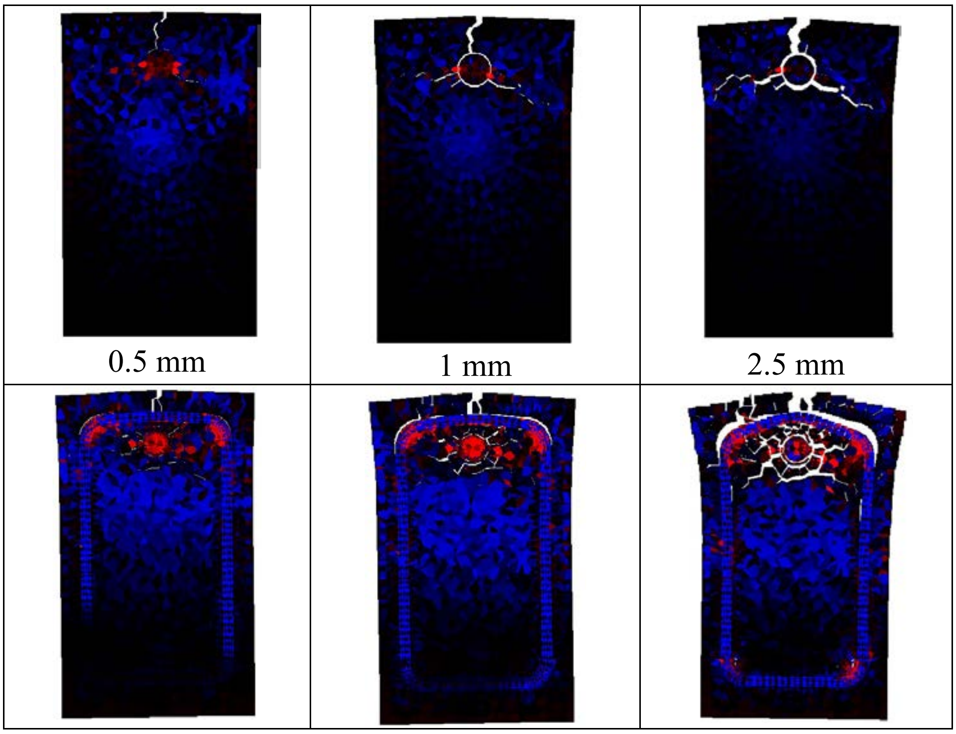

0.5 mm	1.0 mm	2.5 mm

Figure 10: Internal stress distribution diagrams obtained from RBSM

Table 3: Comparison of peak load and residual bond strength for corresponding crack widths

Crack Width (mm)	With Stirrups			Without Stirrups		
	Peak Load (kN)	Residual Strength ratio	Residual Strength from Equation	Peak Load (kN)	Residual Strength ratio	Residual Strength from Equation
0	128	1	1	149	1	1
0.5	64	0.5	0.5	119	0.8	0.81
1	47	0.37	0.26	100	0.67	0.68
2.5	31	0.22	0.11	70	0.47	0.47

6. CONCLUSIONS

Base on the simulation results, the following conclusion has been made:

1. It could be clearly concluded that the presence of stirrups reduces the rate of cracking as higher amount of expansive strain was required to obtain same value of crack width on the surface for specimen with stirrups as compared to the one without stirrup.
2. RBSM can be effectively used to visualize crack propagation and stress distribution inside the specimen, which cannot be done in actual experimental specimens.
3. The reduction in peak load obtained from RBSM simulation is similar to that obtained from the experimental study and also the equation provided by (Lin et al., 2017). This shows that RBSM can be used effectively to study the mechanism of bond failure.
4. It can be visibly observed from the plot that the degree of reduction in bond strength in the specimen with stirrups is much reduced as compared to the specimen without stirrups. Hence, we can conclude that the confinement provided by stirrups is important to reduce the risk of failure. Using RBSM we can clearly identify the zones of compressive stress formed surrounding the main tensile bar thus showing the increase in confinement because of stirrups. This is also in accordance with the experimental results obtained.

REFERENCES

Coronelli, D., Hanjari, K. Z. and Lundgren, K., 2013. Severely Corroded RC with Cover Cracking', *Journal of Structural Engineering*, 139(2), 221–232. doi: 10.1061/(ASCE)ST.1943-541X.0000633.

Eddy, L., Matsumoto, K. and Nagai, K., 2016. Effect of perpendicular beams on failure of beam-column knee joints with mechanical anchorages by 3D RBSM. Journal of *Asian Concrete Federation,* 2 (1), 56-66.

Eddy L. and Nagai K., 2016. Numerical simulation of beam-column knee joints with mechanical anchorages by 3D rigid body spring model. *Engineering Structures,* 126, 547-558.

Kawai T., 1977. New element models in discrete structural analysis. *Journal of the Society of Naval Architects of Japan*, 187-193.

Lin, H. and Zhao, Y., 2016. Effects of confinements on the bond strength between concrete and corroded steel bars. *Construction and Building Materials*, 118, 127–138. doi: 10.1016/j.conbuildmat.2016.05.040.

Lin, H., Zhao, Y., Ozbolt, J. and Hans-Wolf, R., 2017. Bond strength evaluation of corroded steel bars via the surface crack width induced by reinforcement corrosion. *Engineering Structures,* 152, 506–522.

Matsumoto, K., Osakabe, K. and Niwa, J., 2015. Effect of shrinkage and strength development histories on high strength concrete beams in shear. *13th fib Symposium Proceedings*, Copenhagen, Denmark.

Jiradilok, P., Nagai, K., and Matsumoto, K., 2019. Meso-scale modeling of non-uniformly corroded reinforced concrete using 3D discrete analysis. *Engineering Structures*, 197.

SESSION B

URBAN SAFETY & DISASTER MITIGATION: DISASTER MANAGEMENT, RECOVERY AND REHABILITATION PLANNING, ENVIRONMENT INFORMATICS: TRANSPORTATION/ BAGAN HERITAGE

Earthquake Countermeasures of Shinkansen and their Outcomes

Hiroto SUZUKI[1]
[1]PhD, Disaster Prevention Research Laboratory,
East Japan Railway Company
Japan
h-suzuki@jreast.co.jp

ABSTRACT

Japan is an earthquake prone area, and railway operators have been enforcing "hard" and "soft" earthquake countermeasures. JR East started anti-seismic reinforcement for viaduct columns, etc. in the wake of the Great Hanshin Awaji Earthquake (M7.3) in 1995. In the Niigata Chuetsu earthquake (M6.8) in 2004, a Joetsu Shinkansen train derailed but did not overturn, because anti-seismic reinforcement of the viaduct near the derailed point had just been completed. In the Great East Japan Earthquake (M9.0) in 2011, no fatal damage of RC structures occurred on Tohoku Shinkansen, nor did any commercially-operating Shinkansen trains derail. One factor is that, anti-seismic reinforcement had been completed for viaducts, etc. of the lowest seismic performance type in 2008. Enhancing seismic performance of structures is vital for safe train operation. Furthermore, Shinkansen is protected by the Earthquake Early Warning (EEW) system. The EEW system is a system for early detection of earthquakes, stopping trains based on observed values of seismometers installed along Shinkansen lines as well as the coastline. In the Great East Japan Earthquake, coastal seismometers detected the earthquake and all commercially-operating Shinkansen trains stopped safety. EEWS is also vital for safe train operation. After this, JR East started using ocean bottom seismometers in 2017 as a part of EEW system.

Keywords: *earthquake, countermeasures, anti-seismic reinforcement, Earthquake Early Warning System, Shinkansen*

1. INTRODUCTION

Japan consists of an island arc located off of the east coast of the Eurasian Continent. Around Japan, oceanic plates (the Pacific Plate and the Philippine Sea Plate) are subducted beneath continental plates (the North American Plate and the Eurasian Plate). Therefore, Japan is one of the most earthquake-prone areas in the world, and disasters caused by earthquake occasionally occur that incur damage on railways as well. Earthquake countermeasures are especially important for Japanese railways under such an environment. To prevent train accidents caused by earthquake, railway operators have been enforcing "hard" and "soft" countermeasures. Hard countermeasures include disaster reinforcement work such as anti-seismic reinforcement to help prevent earthquake disaster. Soft countermeasures consist of earthquake early warning (EEW)

Fig. 1: Viaduct slabs due to viaduct column damage (Right) and bridge beams fell down due to pier damage (Left) by the Great Hanshin Awaji Earthquake (M7.3) in 1995.

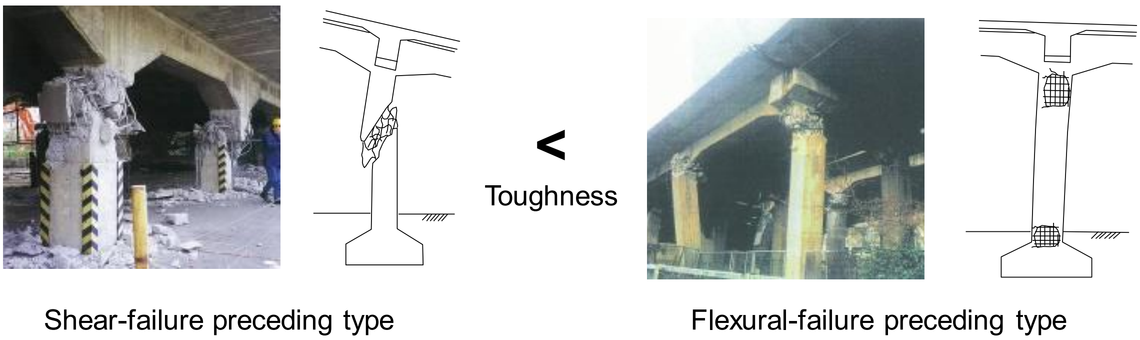

Fig. 2: Damage types of the viaduct columns and the piers

and train operation control in times of earthquake. Soft countermeasures cannot prevent earthquake disasters, but they can prevent train accidents.

There are seven Sinkansen lines networks in Japan, such as the Hokkaido, Tohoku, Joetsu, Hokuriku, Tokaido, Sanyou and Kyushu Shinkansen lines. The East Japan Railway Company (JR East) operates the Tohoku, Joetsu, and Hokuriku Shinkansen lines. This paper describes earthquake countermeasures and their outcomes, mainly for the Shinkansen of JR East, based on the experience of four large earthquake, namely as the Great Hanshin Awaji Earthquake (M7.3) in 1995, the Niigata Chuetsu earthquake (M6.8) in 2004, the Great East Japan Earthquake (M9.0) in 2011 and the Kumamoto Earthquake (M6.5) in 2016.

2. HARD COUNTERMEASURES

The following describes earthquake countermeasures and their outcomes, for the Shinkansen of JR East, based on the experience of four resent large earthquakes.

The Great Hanshin Awaji Earthquake (M7.3, inland earthquake) occurred at 5:46 on January 17, 1995. A maximum of 561 gal was observed by a wayside seismometer along the Sanyo Shinkansen (JR West). In this earthquake, as shown in Figure 1, viaducts and bridges of Sanyo Shinkansen suffered serious damage. Viaduct slabs fell due to column failure and bridge girders fell due to pier failure. Fortunately, no Shinkansen train accident occurred, because this earthquake occurred early in the morning before Shinkansen trains were operating, as Shinkansen service hours are from 6:00 to 24:00. The Sanyo Shinkansen resumed operation 81 days after this earthquake.

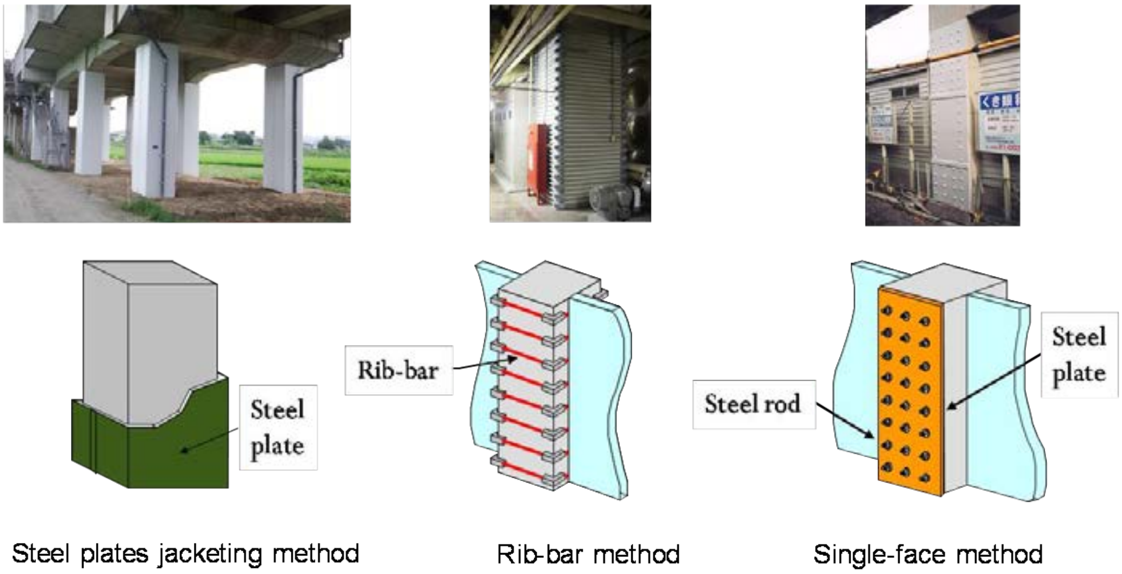

Fig. 3: Representative of anti-seismic reinforcement Methods

Fig. 4: Damage caused by the Niigata Chuetsu earthquake (M6.8) in 2004. Derailed Shinkansen train (left), viaduct damage (middle) and tunnel damage (right).

In the wake of this earthquake, JR East started anti-seismic reinforcement for reinforced concrete (RC) viaduct columns and bridge piers of Shinkansen and conventional lines. Anti-seismic reinforcement was started for viaduct columns and bridge piers of shear-failure type. Such viaduct columns and bridge piers fall in the category of the lowest seismic performance. As shown in Figure 2, the middle part of the viaduct column or bridge pier was damaged, with risk that the viaduct slab or bridge girder may fall. There are many seismic reinforcement methods for viaduct columns and bridge piers, including those shown in Figure 3 [1]. Among these, the most popular method is “Steel Plate Jacketing Method”, which is a method of enveloping up a viaduct column or bridge pier by steel plate. In the case of narrow space, “Rib-bar Method” is used, and in the case of existing facilities under viaduct, “Single- Face Method Method” is used.

Next, the Niigata Chuetsu Earthquake (M6.8, inland earthquake) occurred at 17:56 on October 23, 2004. A maximum of 846 gal was observed by a wayside seismometer along the Joetsu Shinkansen (JR East). In this earthquake, as shown in Figure 4, a Joetsu Shinkansen train derailed, being the first derailment of any Shinkansen train. Damage occurred on the viaduct and tunnel. Joetsu Shinkansen operation resumed 66 days after this earthquake.

The train derailed but did not overturn, because the viaduct near the derailed point had just completed anti-seismic reinforcement, and no damage was caused to the viaduct. This was an intended effect of the anti-seismic reinforcement. After this, JR

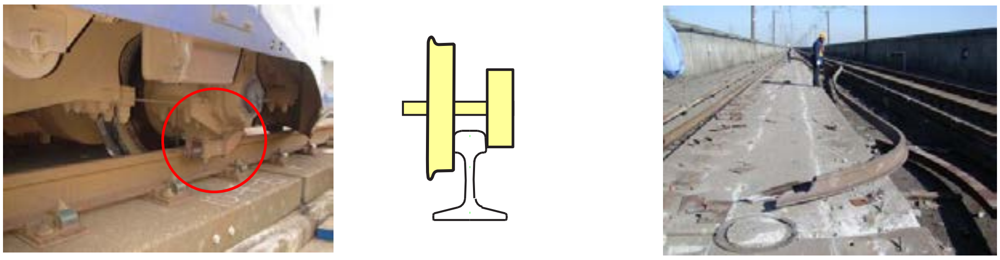

Derailed Shinkansen

Rail conditions after derailment

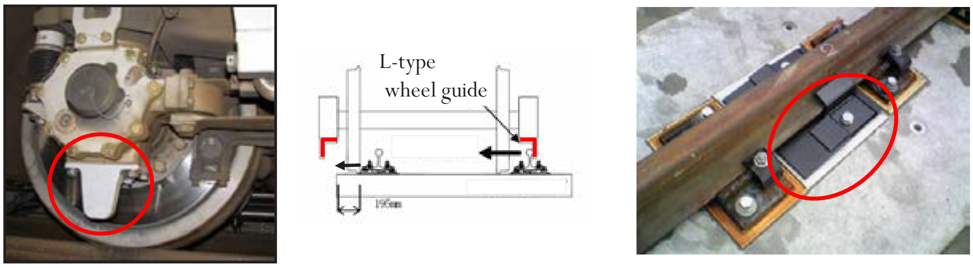

L-Type wheel guide

Rail overturning-prevention device

Fig. 5: Status after derailment and countermeasures developed in the wake of the Niigata Chuetsu earthquake (M6.8) in 2004

Damages of RC structures

Damages of electric poles

Derailed Shinkansen (No commercially operating)

Fig. 6: Damage caused by the Great East Japan Earthquake (M9.0) in 2011

East accelerated the pace of anti-seismic reinforcement. Another factor of the train not overturning was that a protruding wheel part caught on the rail when the train derailed, as shown in Figure 5 (upper left). This part had only been attached on particular railcars. So an L-type wheel guide [1] shown in Figure 5 (lower left) was developed to prevent railcars from deviating or flipping from the roadbed after a derailment. JR East started installing them on all Shinkansen railcars. On the other hand, the derailed Shinkansen caused the rail to come apart from its fasteners and fall over, as shown in Figure 5 (upper right). So a rail overturning-prevention device [1] was developed. This prevented overturning and deviating of rail in the case of rail fastener damage, which JR East started installing on railroad tracks.

Next, the Great East Japan Earthquake (M9.0, subduction-zone earthquake) occurred at 14:46 on March 11, 2011. This was a huge earthquake, at magnitude 9 and a maximum of 1,279 gal observed by a wayside seismometer along the Tohoku Shinkansen (JR East). No fatal damage of viaduct columns and bridge piers occurred on Tohoku Shinkansen, nor did any commercially-operating Shinkansen trains derail. Only flexural-failure type viaduct columns and bridge piers, the category of the next lowest seismic performance, were damaged; as shown in Figure 6 (left). This type of viaduct slabs or bridge girders in general do not fall. Many electric poles were damaged, as

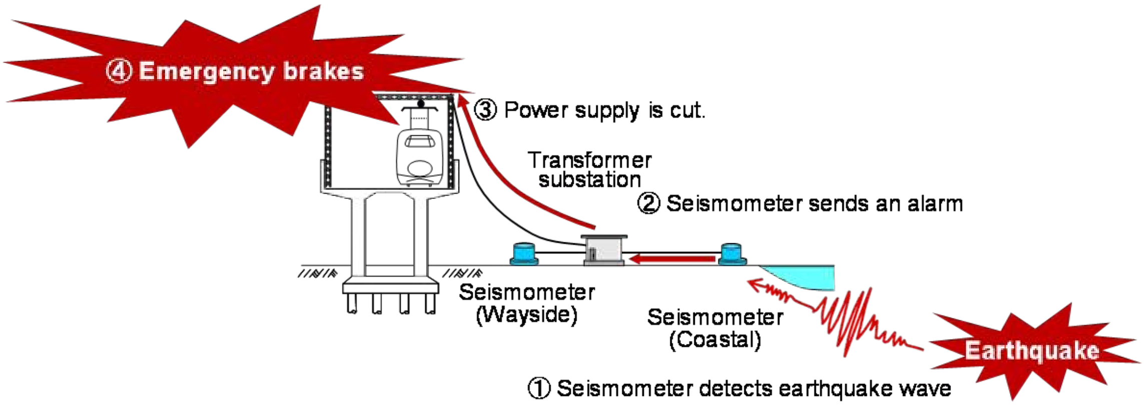

Fig. 7: Outline of earthquake early warning (EEW) system

shown in Figure 6 (middle). The Tohoku Shinkansen operation resumed 49 days after the earthquake, regardless of wide range damage.

One reason that commercially-operating Shinkansen trains did not derail is that no fatal damage of viaduct columns and bridge piers occurred, because anti-seismic reinforcement for shear-failure type viaduct columns and bridge piers (the lowest seismic performance type) had been completed in 2008. This was an intended effect of the anti-seismic reinforcement. After this, JR East accelerated anti-seismic reinforcement for flexural-failure type viaduct columns and bridge piers in order to further improve Shinkansen safety. In this earthquake, one Shinkansen trains not in commercial operation did derail, but did not fall from the roadbed. This train stopped franks to an L-type wheel guide sandwiching the rail, as shown in Figure 6 (right). In this way, the L-type wheel guide developed in the wake of the Niigata Chuetsu Earthquake proved effective immediately.

Next, the Kumamoto Earthquake (M6.5, inland earthquake) occurred at 21:26 on April 14, 2016. A maximum of 312 gal was observed by a wayside seismometer along the Kyushu Shinkansen Line (JR Kyushu). Viaducts and bridges of Kyushu Shinkansen were almost undamaged and cracks occurring only at 33 locations. The Kyushu Shinkansen operation resumed 14 days after this earthquake.

A major reason that viaducts and bridges were almost undamaged is that they were designed with the latest seismic design method defined in the wake of the Great Hanshin Awaji Earthquake. No commercially-operating Shinkansen trains were derailed, although one Shinkansen train not in commercial operation did derail.

JR East has been promoting earthquake countermeasures, the intended effects of which have already appeared. To enhance seismic performance of structures is vital for safe train operation.

3. SOFT COUNTERMEASURES

The following describes the Early Earthquake Warning (EEW) System [2] that is representative of soft countermeasures. The EEW system is a system for early detection of earthquakes, stopping trains based on observed values of seismometers. As shown in Figure 7, when acceleration of a seismic wave observed by a seismometer exceeds threshold, a warning is issued. The seismometer sends an alarm and power supply is cut and the emergency brakes are automatically applied and trains stop. There are two methods for issuing a warning [2, 3] : “P-wave warning” and “S-wave warning.” “S-wave warning” is issued when acceleration exceeds threshold and “P-wave warning” is issued according to earthquake information estimated by the initial part of P-wave.

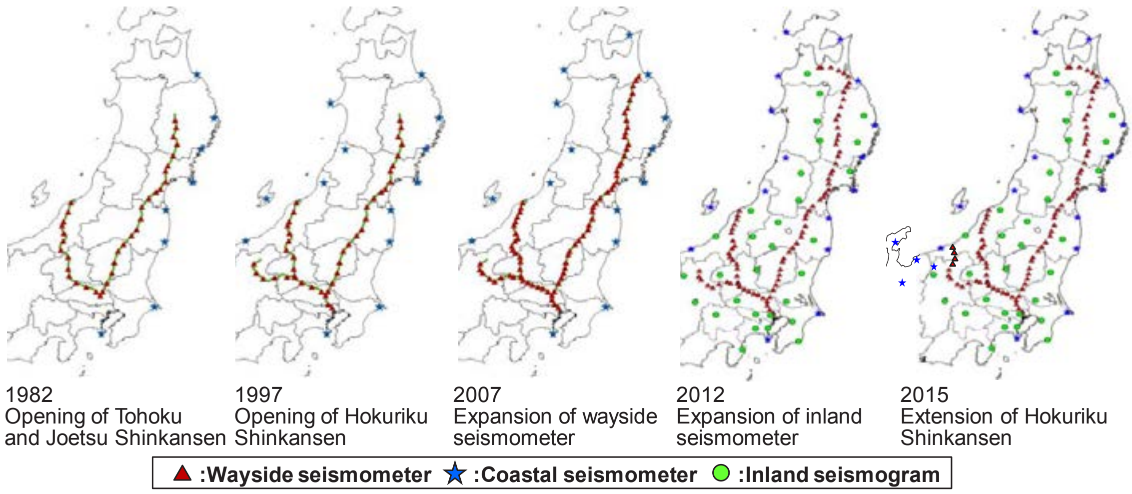

Fig. 8: Installation of seismometers on the Tohoku, Joetsu and Hokuriku Shinkansen

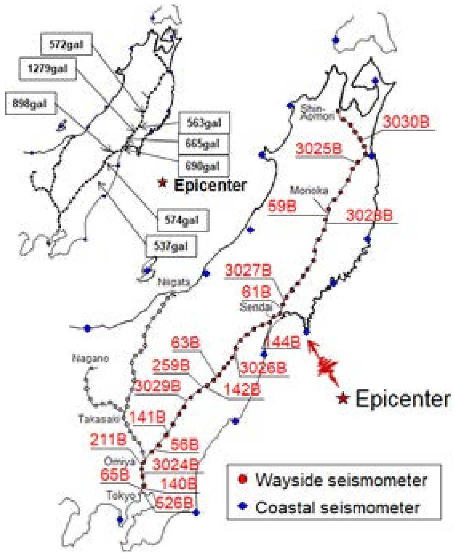

Fig. 9: Train location on the Tohoku Shinkansen at the time of the Great East Japan Earthquake

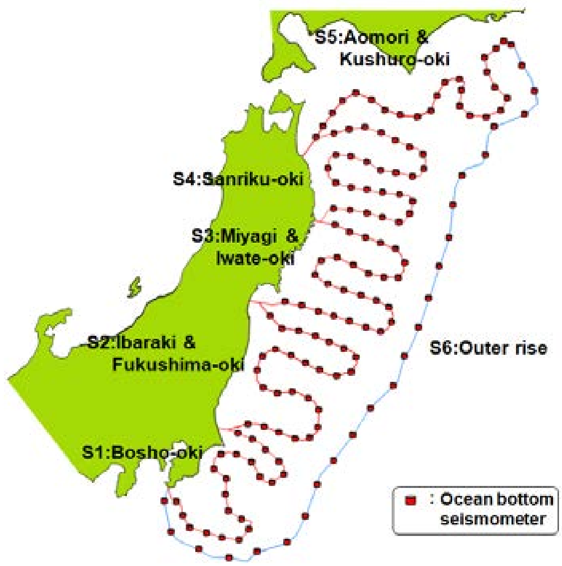

Fig.10: Locations of ocean bottom seismometers and epicenter of the Great East Japan Earthquake

In this system, there are three types of seismometers; “wayside”, “coastal”, and “inland.” Figure 8 shows the growth of the seismometer layout in the JR East EEW System. In 1982, when the Tohoku and Jouetsu Shinkansen lines opened, wayside and coastal seismometers were installed. Coastal seismometers were installed on the Pacific coast for early detection of subduction-zone earthquakes off the Pacific Ocean. At this point, S-wave detection was adopted, the threshold of which was 40 gal for both wayside and coastal seismometer. When the Hokuriku Shinkansen (Takasaki-Nagano) opened in 1997, seismometers were added wayside of the Hokuriku Shinkansen and along the coast of the Sea of Japan. In 1998, a P-Wave Detection System developed by Railway Technical Research Institute (RTRI) was introduced. The S-wave threshold of the coastal seismometer rose 120gal. In 2004, Newly P-Wave Detection System [3] developed by RTRI was introduced. In P-wave detection, epicenter and magnitude are estimated by the initial part of p-wave, and at-risk area, about 80 gal, is estimated by epicenter and magnitude, and warning is issued. In 2007, wayside seismometers were added and the Tohoku Shinkansen between Morioka and Hachinohe was extended. In 2012 inland seismometers were added for early detection of inland earthquakes, and JR East started using Earthquake Early Warning provided by Japan Meteorological Agency (JMA) as a part of EEW system. In 2015, the Hokuriku Shinkansen between Nagano and Kanazawa opened, and seismometers were added for this area.

Next is the intended effects of this system in the Great East Japan Earthquake. When this earthquake occurred, 19 commercially-operating train of Tohoku Shinkansen were running. Figure 9 shows their locations. Maximum acceleration was 1,279 gal along the Tohoku Shinkansen. In this earthquake, a coastal seismometer detected acceleration by earthquake exceeding threshold. A warning was issued 12-22 seconds before wayside seismometers detected acceleration exceeding threshold to suspend operations [4]. Emergency brakes were automatically applied and Shinkansen trains slowed down and stopped, and all commercially-operating Shinkansen trains stopped without derailment.

JR East began using the ocean bottom seismometers (OBSs) data of the Boso-oki (S1) sub-system shown in Figure 10 in November 2017, and data from the Ibaraki-oki to Kushiro-oki (S2, S3, S4, S5) sub-system in January 2019 for the Shinkansen EEW system. OBSs were installed along the Japan Trench by the National Research Institute for Earth Science and Disaster Prevention (NIED). Subduction-zone earthquakes along the Japan Trench, such as the Great East Japan Earthquake, may be detected earlier if the OBSs data are used for the EEW system. The threshold value of OBSs increases with distance from wayside.

Finally, this is the expected effect by using OBSs data for EEW System. In the case of the Great East Japan earthquake, by a simple calculation, OBSs are estimated to have been able to issue a warning about 25 seconds earlier than the S-wave detection of the coastal seismometer. Using the archive data observed by the OBSs, the effectiveness of using OBSs data for EEW system in the case of an earthquake occurring offshore of Fukushima Prefecture at 5:59 on November 22, 2016 (M7.4, subduction-zone earthquake) was verified. OBSs are estimated to be able to issue a warning about 12 seconds early than P-wave detection by a coastal seismometer of the conventional EEW system [5]. Thus, OBSs are expected to have a great intended effect on the early detection of subduction-zone earthquakes.

JR East has been using and improving EEW system, the intended effects of which have already appeared. To continue improving EEW system is vital for safe train operation.

4. SUMMARY

This paper describes earthquake countermeasures and their outcomes, mainly for the Shinkansen of JR East. Earthquake countermeasures implemented so far have been successful in preventing the derailment of Shinkansen and damage to structures, and contributed to safer train operations in times of earthquake. JR East will continue to develop hard countermeasures and introduce even more effective soft countermeasures for earthquakes.

This paper describs the importance of disaster prevention countermeasures using Japan’s Shinkansen as an example. In disaster prevention countermeasures, it is important to keep humble and learn from experience and implement countermeasures properly.

REFERENCES

[1] Horioka, K., 2013. Clarification of Mechanism of Shinkansen Derailment in the 2011 Great East Japan Earthquake and Countermeasures Against Earthquakes, JR EAST Technical Review-No.27, p13-16.

[2] Nakamura, Y., 1985. Earthquake warning system in Japan National Railways, Railway technology, Vol. 42, pp. 371-376, (in Japanese).

[3] Iwahashi, H., et al., 2004. Practical use of earthquake quick alarm system, RTRI Report, Vol. 18, No. 9, pp. 23-28. (in Japanese with English abstract)

[4] Yamamoto, S., and Tomori, M., 2013. Earthquake early warning system for railways and its performance, Journal of JSCE, Vol. 1, pp. 322-328.

[5] Miyakoshi, H. et al., 2019. Earthquake Early Warning for Shinkansen using Ocean Bottom Seismometer, 12th World Congress on Railway Research, Printing.

The Religious Buildings in Bagan and The 2016 M 6.8 Subduction Zone Earthquake In Myanmar

Hla Hla Aung

Senior Researcher

Myanmar Earthquake Committee, Federation of Engineering Societies

MES Building, Hlaing University Campus, Yangon, Myanmar

hhlaaung@gmail.com

ABSTRACT

The ancient city, Bagan (Pagan) is located in the heart of dry desolate desert-like plains in the Dry Zone of Myanmar, the very center of the country, along the bank of Ayeyarwaddy River covering an area of a little over 42 square kilometers, in the northwest of Mt.Popa. Bagan, the land of temples and stupas was shaken by a series of earthquakes since ancient time and the earliest record is about 25 November, 1372 and another event in 1550 A.D.by which event Shwe-gu-gyi temple was damaged. In 1975, the largest earthquake within 900 years, hit the city with magnitude 6.8, and many pagodas and temples were damaged within seconds. Some of pagodas are being left intact and withstand to maintain the role of its past glory as historical monuments in Southeast Asia. Due to another large earthquake, the Chauk earthquake in 2016 with M 6.8, approximate numbers of pagodas of (400) were damaged as the previous 1975 Bagan earthquake. Pagodas left intact and withstand as before. The 1975 Bagan earthquake and the 2016 Chauk earthquake are intermediate-depth subduction earthquakes and such inland intermediate-depth earthquakes are hazardous earthquakes for the area along the Rakhine Western Ranges (Indo-Andaman belt) under which the India plate is obliquely subducting beneath the Burma plate. Remote sensing + GIS technologies and geodesy survey are greatly needed for effective preparedness to keep the religious buildings to be able to withstand future earthquakes.

***Keywords**: religious building, earthquake, subduction, remote sensing, preparedness*

Introduction.

The ancient city, Bagan or Pagan is located at latitude 21°10’N, Longitude 94°51’E, in Mandalay Region, on the east bank of the Ayeyarwady River (Fig.1).

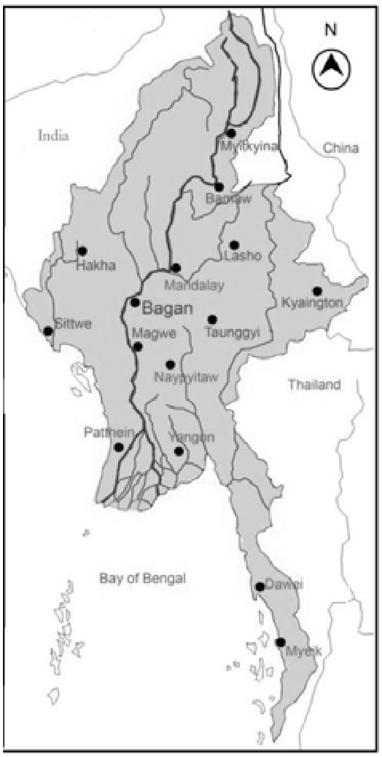

Fig.1.Location map of Myanmar in SE Asia showing geographical location of Bagan city.

Pagan became a capital city of the Burmese Empire and 55 kings ruled Pagan over a long period of 12 centuries according to local chronicles. Many Buddhist temples and pagodas were built on the stretches of sandy wind-swept plains and Pagan became a stronghold of Buddhism and was well known as the seat of Buddhist learning and culture among its contemporaries in SoutheasAsia.Myanmar is consist of five physiographic divisions: starting from the west(1) the Rakhine coastal plain, (2) the Rakhine ranges in N-S belt, (3) Central Myanmar lowland between Rakhine ranges and Shan Plateau, (4) Shan Plateau in the east, and (5) Kachin mountains in the north and north-east (Fig.2). Among these divisions, the Central Myanmar Basin is a lowland area and a flat land covered with mainly Tertiary sedimentary rocks of sandstone, siltstone, shale and clays and Quaternary sequences. Stretches of river alluvium exist in this division deposited by the major rivers of the Ayeyarwady and the Chindwin and their tributaries.

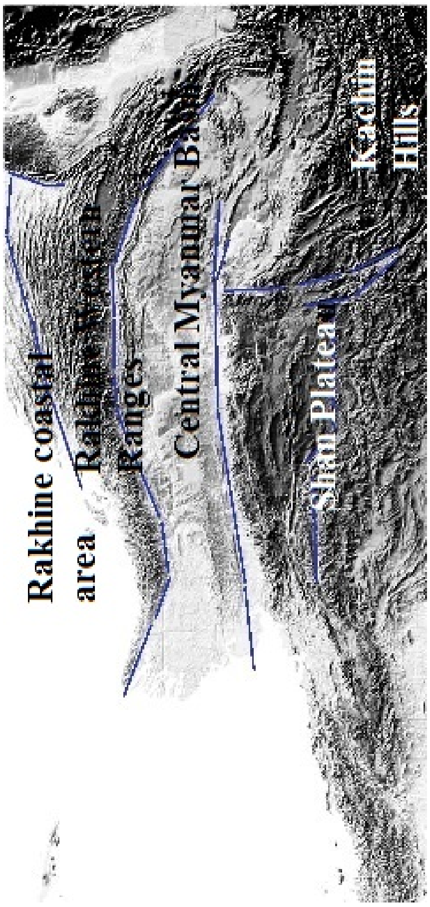

Fig.2.Satelliteimage of Myanmar Showing physiographic divisions.

Geological Setting

The Bagan is in a flat land area on the bank of the Ayeyarwady River.The Ayeyarwady River flows to the southwest direction from the confluence point of the Chindwin and the Ayeyarwady River and then to due south through the flat plain of the Dry Zone of Central Myanmar. There are few sandstone hills and cliffs along the bank of the river. These cliffs are covered with red gravels and sheets of gravel stretch over the plateau surface for a vast area indicating that the area must have been once the higher level of the present river. Beyond the confluence point, at the places of Naung-oo, Pagan, Sale and Chauk area, the river formed a terrace system consists of 5 terraces. In the section, Terrace 5 is 12 meter above the level of the Ayeyawady river and upward to Terrace 4, 3, 2, and 1 successively and at the top is covered with coarse red gravels on hill tops. This terrace system shows up clearly, particularly in the area between Sale and Chauk. It consists of sand and fine sand, similar to the present-day sediment load carried by the Ayeyarwady River, red gravels and red sand. It contains stone implements of the Late Paleolithic, and it is followed by aeolian sand, the loess-like "Pagan Silt". The aeolian sediment are formed by the accumulation of wind-blown silt, sand and less clay. It consists of a pebble-bearing gravel at the base, above which come fluviatile and finally aeolian sands, coarse red gravels of "Nyaung-U-Red Earth" which covers it. This horizon is several meters thick and causes a miniature badland topography (Bender,1983). Most of the Buddhist temples and stupas were built on the stretches of sandy wind-swept plains. Bagan sits on Quaternary strata above sandstone and shale of the Upper Irrawaddy Group and Pegu Group.

Tectonic Setting

Tectonically Myanmar is made up of a mosaic of tectonostratigraphic terranes: four tectonic terranes and three accreted belts. They are as follow:

(1) Rakhine Coastal Plain terrane (RC),
(2) Rakhine Western Range terrane (RWR),
(Indo-Andaman Belt)
(3) Central Burma Basin terrane (CBB),
(4) Shan Massif terrane (S) and,
(5) Kachin terrane (K)
(6) Shan Boundary Belt
(7) Than Lwin Belt

The geology of Bagan area consists of Holocene surficial deposits of gravel, sand, silt and clay. The underlying rock formations that crop out around the Bagan area are mostly sandstone, siltstone and shale of the Pegu Group of Oligocene-Miocene and the Irrawaddy Group of Pliocene-Pleistocene. In the west of Bagan, there is the steeply dipping eastern flank of the N-S extent of 2000 km long strip of Rakhine Western Ranges which was produced by collision between the India and Burma plates at about 46 Ma. India plate is subducting obliquely beneath Burma plate along Sunda subduction zone. Northward and northeastward movement of India oceanic crust is the most important part for tectonics of Myanmar in Tertiary time.

Fig.3. Satellite image showing epicentral
Location of 2016 Chauk earthquake.

A large amount of the motion is driving the uplift of the Rakhine Western Ranges since the Miocene time. The northeastward convergence of the Indian oceanic crust beneath the Burma continental plate is still active. This active tectonic activity below Rakhine ranges has been causing the intermediate focus seismicity along the belt from the Naga Hills in the north to the Chin Hills and the Arakhan ranges to the south. The Yakhine Western Range is a subduction-related outgrowth continent, composed of two different geologic units, normally a broad flysch belt which constitutes the main section, and a narrow, intermittently out-cropping zone of metamorphic rocks and ophiolite.This ophiolites were considered to be the remnants of Neo-

Tethys seafloor obducted during subduction. Structural trend swings from the NE-SW direction in the Naga Hills to NW-SE along the Rakhine Range and Chin Hills. Kabaw Fault System demarcated this terrane from Central Myanmar Basin terrane. The Central Myanmar Basin or Central Lowland area is a flat land covered with mainly Tertiary sedimentary rocks of sandstone, siltstone, shale and clay.

Archaeological Techniques & Religious buildings in Bagan

The stupas and temples were erected mostly from the 11^{th} to 13^{th} centuries but the Bagan dynasty began from 108 A.D. ruled by 55 kings for 12 centuries according to local chronicles. But epigraphically evidence supported that the dynasty began with the reign of King Anawrahta (1044-1077 A.D.). Some believed that most of the temples and stupas in Bagan must have been built during a few centuries about more than 13,000 stupas and temples, but today only about 5000 (recorded 4474 structures) are remained but total 3122 in the list of the archaeological department. The rest structures must have been disappeared due to weathering through times and some believed to have dismantled a considerable number of monuments to collect materials for building forts by invaders. Since then the great mass of the religious edifices were left to decay and ruin some by human vandalism. Technology of many multi-storeyed temples and stupas was technically most advanced as these temples and stupas in Bagan area still intact to the original locations. The structures are not only advanced in engineering aspects but also soil mechanic aspects. The kind of construction techniques, typical of Bagan period which were not found in middle ages all over the world involved the use of load bearing system which can resist the weight of the stately religious buildings, the use of vaults and arches to create lighting effects

Fig.4. A photo showing a proportionate geometry between the height of the structure and the depth of foundation

inside the buildings with changing effects between darkness and brightness through sunlight. The foundation geometry of ancient buildings in Bagan area has all essentials with very deep foundation with a proportionate between the height and depth of the structure as seen in the figure(Fig.4) and for an example of Me-Taw-ya temple with a foundation of 3 meter-5 meter deep (Fig.5). The temples are built using a multi-layered technique in order to maintain the stability of the temples and stupas for long term in the future. Apart from the best preserved temples but also they are elegant and harmonious dimension of the architectural style.

Fig.5. A photo of a temple Me-taw-ya showing the height and the depth of foundation (3m-5m) (Maria Leitzia et al.2018)

Earthquake Disaster & Preparedness

Bagan, the land of temples and stupas was shaken by a series of earthquakes since ancient time and the earliest records are about 25 November, 1372 , 14 July 1485 A.D. and another event in 1550 A.D.by which event Shwe-gu-gyi temple was damaged. In 1975, the largest earthquake within 900 years, hit the city with magnitude 6.8, and many pagodas and temples were damaged within seconds. Some of pagodas are being left intact and withstand to maintain the role of its past glory as historical monuments in Southeast Asia. The 8th July1975 Bagan earthquake of magnitude 6.8 occurred at 21°50' N and 94°70'E is an intermediate-depth subduction earthquake with a depth of 112 km (ISC) and focal mechanism is reverse faulting (USGS). Due to another large earthquake, the 24th August 2016 Chauk earthquake at latitude 20°919'N – longitude 94°579'E with M 6.8, approximate numbers of pagodas of (400) were damaged as the previous 1975 Bagan earthquake.

Focal mechanism was reverse faulting (USGS). Due to this event, damage to the ancient monuments was about 90 per cent and it was felt through the Central Myanmar, Rakhine area, northeastern India and Bengladesh.

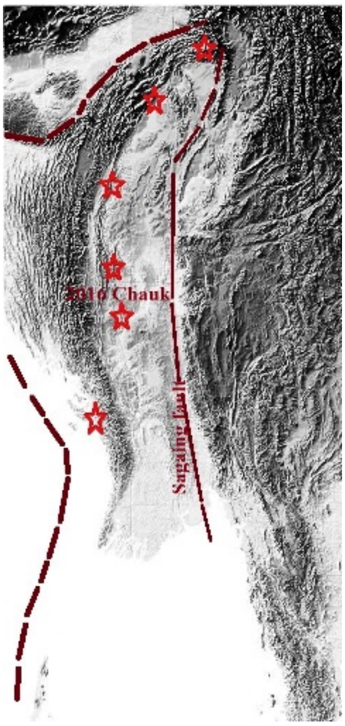

Fig.6. Epicentral locations of significant inland subdu*cti*on zone earthquakes along Rakhine Western Ranges in Myanmar.

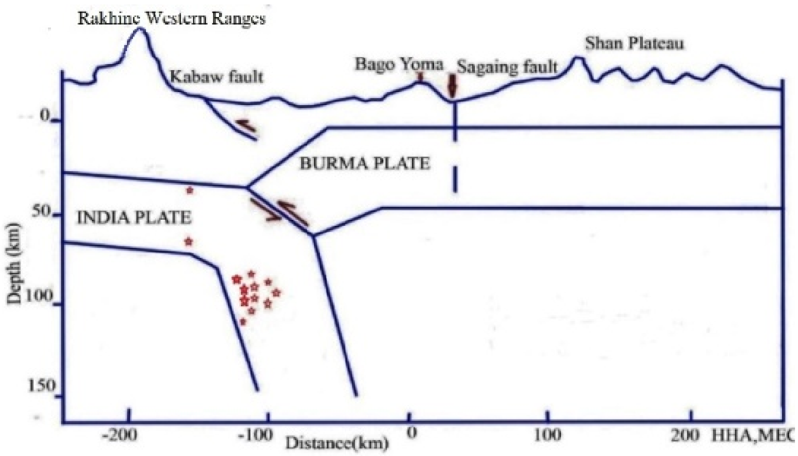

Fig.7. A section across latitude 20°N Showing intermediate-depth earthquakes within the India oceanic plate and surface profile from west to east through Central Myanmar Basin.

In Bagan and its environs, upper portion of stupa, temples and pagodas have fallen down. By judging the damages of the religious buildings only at the uppermost part and felt report of local people in Bagan indicate that the ground motion was strong enough to fling up the area as the fault moved vertically beneath it. The April 2016 Mawlaik earthquake (M 6.9,134 km depth) ruptured the Tripura segment, the August 2016 Chauk earthquake (M 6.8, 84.1km depth) and the January 2018 Kauk-tu earthquake (M 4.9,76.1km depth) ruptured the Arakan segment and the October 2016 Tamathi earthquake (M 4.8, 97.5 km depth) ruptured the Naga segment respectively (Fig.6 and 7). Each of the segments corresponds to the segments of Sunda megathrust segments as follow (from north to south): the Naga segment, the Tripura segment and the Arakan segment (Dasgupta et al.1984). Such deformation style may be characteristics of the environments under the extensional or compressional stresses that occurred within the downgoing slab of the India plate..

Discussion

Myanmar region is resting on three plates: India, Burma and Indochina so that many areas in Myanmar area at risk from future earthquakes. The inland intermediate-depth earthquakes are hazardous earthquakes for the area along the Rakhine Western Ranges (Indo-Andaman belt) under which the India plate is obliquely subducting beneath the Burma plate. To mitigate the seismic risk to these stupas and temples in Bagan, effective earthquake preparedness and recovery, rehabilitation, reconstruction should be introduced for Build-Back-Better. In preparedness, acquired satellite imagery and geospatial information will be carried out to produce rapid maps that can support government, disaster management agencies and first responders for damage assessment especially in remote areas and overall picture during and post disaster situation. In that case, we need to develop a way of detecting earthquake source from satellite image and to apply the same technique to detect the damages.

References

1. Aung,H.H., 2013. *Tectonic Styles and Deformation Patterns of Terranes in Myanmar.* Watah Press, Yangon, Printed in Myanmar
2. Aung,H.H., 2015. *Myanmar Earthquakes History,* Wathan Press, Yangon, Printed in Myanmar
3. Curray, J.R., et al.2005, *Tectonics and history of the Andaman Sea region*,J.Asia Earth Science XX1-42
4. Kyaw Lat: *Art and Architecture of Bagan and historical back ground with data of important Monuments.*Mudon Sarpay, No 501-D, Mahabandula Housing, Yangon
5. 5.Leyton,F., Javier Ruiz, Jaime Campos, Edger Kausal, 2001: *Intraplate and interplate earthquakes in Chilean subduction zone: A theoretical and observational comparison,* Physics of the Earth and Planetary Interiors,175(1): 37-46, June, 2009.
6. Maria Letizia Amadori et al. (2018) *Integrated scientific investigations on the constitutive materials from Me-taw-ya Temple, Pagán Valley, Burma (Myanmar),* Measurement, vol.131, January2019, pg.737-750
7. Mukhopadhyay, M. and Dasgupta, S.1988, *Deep structure and tectonics of the Burmese Arcs constraints from earthquake and gravity data,* Tectonophysics,149 (1988) 299-322 Elsevier Science Publisher B.V, Amsterdam, Printed in the Netherlands.
8. Mondal, M.; Cecillia M.G. Mchugh; Goodbred, S.; Akhter, S.H 2014.; *Paleoseismic Records of 1762 and similar Prior earthquakes along the SE coast of Bengladash*: Conference paper AGU Fall Meeting 2014
9. Rangin C.,1996-1999.*Deformation of Myanmar, Results of GIAC Projects,* GIAC Conf. (Yangon,Myanmar)
10. Ruff, L.J., 1996*, Large Earthquake in Subduction zones: segment interaction and Recurrence Time* Department of Geological Sciences,University of Michgan, Ann Arbor, Michigan
11. Satyabala, S.P.,2003 *The Historical Earthquakes of India,* National Geophysical Research Institute, Hydrabad-500 007, India

12. Steckler, M. et al., 2008, *Collision of the Ganges Brahmapudra Delta with the Burma Arc: Implication for earthquake hazard;* Earth and Planetary science Letters 273 (3-4): 367-378 Sept.2008
13. Stein,S.and Wysession,M., 2003,*An Introduction to Seismology, Earthquakes and Earth Structure* Blackwell Publishing,350 Main Street, Malden, MA 02148-5020, USA
14. Syed Humayun Akhter, the 5th International Workshop on Seismotectonics and Earthquake Risk Management 2015, Abstract Volume,Yangon, Myanmar
15. *Pictorial Guide to Bagan* ,Ministry of Culture, Archaeology and National Museum Department ,The Union of Myanmar, Yangon.
16. Thein Lwin, Deputy DG, Department of Archaeology and National Museum, Nay Pyi Taw, Myanmar Symposium on Earthquake and Related Risks Reduction 2016 .
17. Tettoni: *Burmese Design & Architecture,* published by Periplus Editions (HK) Ltd.2000, Printed in Singpore.

Investigation on Ancient Brick Masonry and Repair Mortar Properties in Post-Earthquake Rehabilitation Process of Ancient Bagan Monuments

T.M. SAN[1], K.KYAW[2]
[1]PhD, Civil Engineering Department,
[2]Professor, Civil Engineering Department,
Yangon Technological University,
Myanmar
eimon007@gmail.com[1], kyaw.u.kyaw@gmail.com[2]

ABSTRACT

Most of the monuments in Bagan are Brick masonry and few are stone masonry. All of these monuments are vulnerable to both disaster and natural degradation. After 2016 Chauk Earthquake, most of the monuments were damaged and post-earthquake rehabilitation work is required. In order to make proper conservation and repairing work, it is important to know the properties of ancient bricks and repair materials. Therefore, the physical, and mechanical properties and Energy Dispersive X-ray analysis of the ancient bricks from different monuments of 11 AD, 12 AD, 13 AD and 18 AD were investigated. It is important to use the similar materials in the repairing of ancient monuments so that the physical properties and chemical characterization of the new brick from the modern brick mill near Bagan was also performed. Then, the chemical properties and acid digestion tests of ancient mortars were experimented in the laboratory. The evaluation of the physical properties results showed that ancient bricks were in good range of water absorption. The compressive strength of the ancient bricks were various due to the location of the sample, but most of the ancient bricks have high compressive strength. The chemical characterization results showed that the composition of the ancient bricks and modern bricks were similar but not identical. The chemical composition results of ancient mortar showed that lime-based mortar was used in ancient mortars. The binder to aggregate ratio of mortar samples was different on the purpose of usage. Based on the results, the suitable proportion of mortar was proposed and, the properties of repair masonry properties were scientifically experimented.

***Keywords:** ancient monuments, brick masonry, physical properties, mechanical properties, chemical properties, repair mortar.*

1. INTRODUCTION

In Myanmar, earthquakes frequently occur and these bring little to severe damage to ancient monuments in Bagan so that conservation work has been carried out from the colonial period to until now. After 2016 Chauk earthquake, 389 numbers of monuments was listed as damaged monuments as shown in Figure 1. However, only 39 numbers were considered in severe conditions [1]. Reviewing the lessons learned from the Chauk earthquake, it can be seen that the compatibility of new and old materials is very important in conservation work. Not only for the rehabilitation of damaged monuments but for seismic risk analysis of ancient monuments, but the actual material properties of ancient materials are required. The ancient bricks and mortars from damaged monuments were collected and experimented in Structural Engineering laboratory of Yangon Technological University. Physical and mechanical properties of ancient bricks such as unit weight, absorption rate, compressive strength and flexural strength were investigated. The chemical properties of ancient bricks were also analysed by Energy Dispersive X-Rays analysis. Then, the chemical properties of ancient mortar such as chemical composition, and morphology were also examined. After that, acid digestion tests of ancient mortar samples were carried out in order to know the proportions. In practice, there is a proportion used by mason of repair work in rehabilitation although the scientific investigation is lack in this repair mortar. Reviewing the acid digestion tests results and Bagan style mortar used in reconstructed work, the suitable proportion is proposed and the experiments for physical and mechanical properties of repair mortars and bricks is carried out.

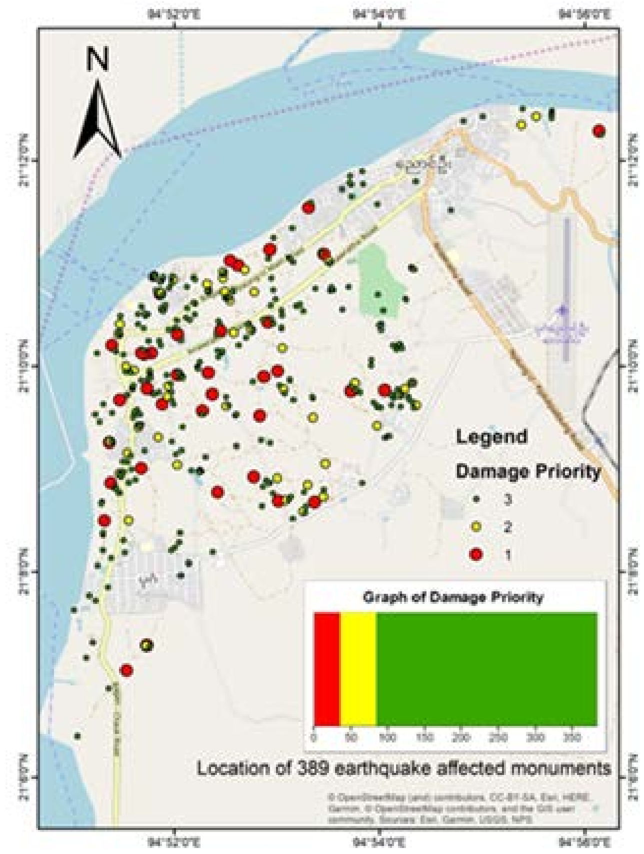

Figure 1. Location Map of Damage Monuments

2. CHARACTERIZATION OF ANCIENT BRICKS

The ancient bricks from Bagan monuments have different sizes. The average size of ancient bricks varies from (400 mm × 180 mm × 40 mm) to (290 mm × 160 mm × 30 mm). Modern brick's size in Myanmar is generally (225 mm × 115 mm × 75 mm). That is why the size of modern brick is unsuitable with repair work of damaged monuments. Then, another point should keep in mind is that the compression or bearing capacity of repair mortar should have a compatibles strength with brick. The ancient brick sizes vary from monuments to monuments. Even in the same monument, the brick sizes are different from the purpose of usage. Some of the bricks have a concave surface at the base and plain surface at the top. The depth of the curve varied from 2.5 to 3 cm. Although the bread and width of the modern brick are smaller than the ancient bricks, the depth of the modern brick is greater than the old ones. In Table 1, the list of samples is presented. The physical properties of bricks such as unit weight and absorption rate of ancient bricks and new bricks experimented according to ASTM C-67 and the results were shown in Figure 2.

Table 1. Sample Lists of Ancient Bricks and Modern Brick

No	Monument name	Constructed period	Sample description
1	*Abae* Yadanar (AY)	11AD	Only one brick of full size (ancient brick)
2	Ananda-Ok-Kyaung(AOK)	(1776-1785)	broken bricks (some are more than the half size of the actual brick size of the monastery) (ancient brick)
3	Mingalar Zedi (MGL)	13AD	Broken bricks under the ground which are larger than the half of the original size(definitely ancient brick)
4	MyayPon TharPhayarHla (MPT)	12AD	full-size bricks appropriate for tests (not certain ancient or new brick)
5	Pu Htoe Thar Myar (PHTM)	13 AD	Full-size bricks appropriate for tests (ancient brick)
6	Pyat Sa Shwe Gu (PSSG)	12 AD	Half-size brick appropriate for the test (ancient brick)
7	SatanarGyi (STG)	13AD	Full size and half size of bricks free from cracks (ancient brick)
8	Sulamani (SLMN)	13AD	full-size bricks and half size bricks appropriate for tests (ancient brick)
9	Modern Brick (MB)	Currently, use	full-size bricks appropriate for tests (new brick from mail)

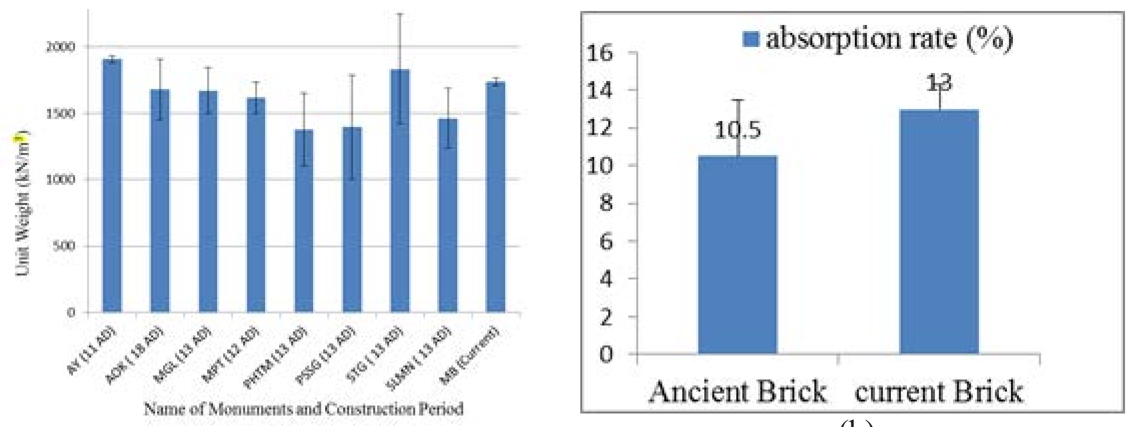

(a) (b)

Figure 2. Physical Properties of Ancient and Modern Bricks
(a) Unit Weight (b) Absorption Rate

The mechanical properties of ancient bricks are concerned for the structural analysis of ancient monuments. So, the compressive strength of ancient bricks and modern bricks were also examined and the results were shown in Figure 3.

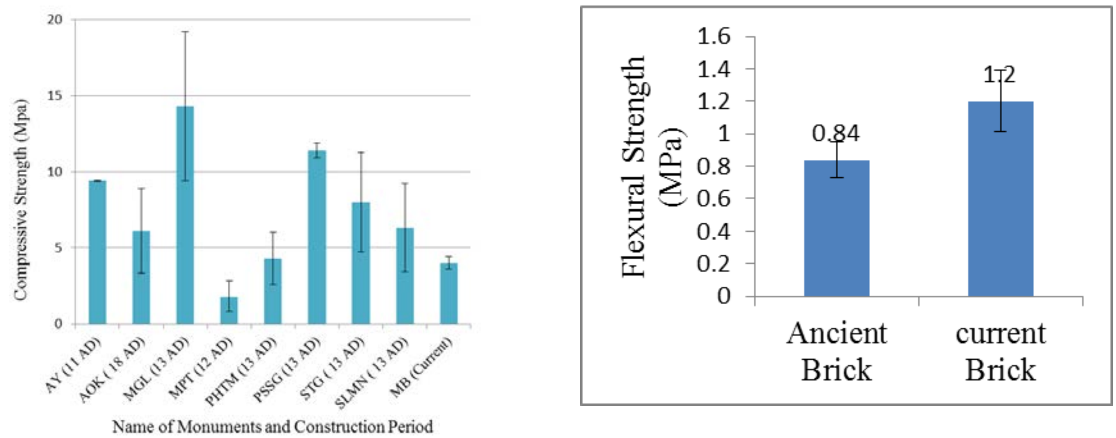

(a) (b)

Figure 3. Mechanical Properties of Ancient and Modern Bricks
(a) Compressive Strength (b) Flexural Strength

In order to know the quantitative results of the chemical composition of brick, Energy-Dispersive-X-ray-Fluorescence (EXDRF) test is performed on the bricks. The results of most of the bricks showed a very high amount of silicon dioxide followed by aluminium oxide, iron III oxide, and potassium oxide. The chemical compositions of ancient and modern bricks are similar.

2. CHARACTERIZATION OF ANCIENT MORTAR

Ancient mortar samples from damaged monuments were collected and chemical analysis such as EDXRF analysis, acid digestion tests, and Scanning Electron microscopy experiments were carried out. From the EDXRF results, most of the ancient mortars contain Calcium oxide as the main constituents followed by silicon dioxide, Sulphur trioxide, and Iron III oxide and potassium dioxide. The average comparison results for ancient stucco, mural painting plaster and cement mortar from rehabilitation work are shown in Figure 4.

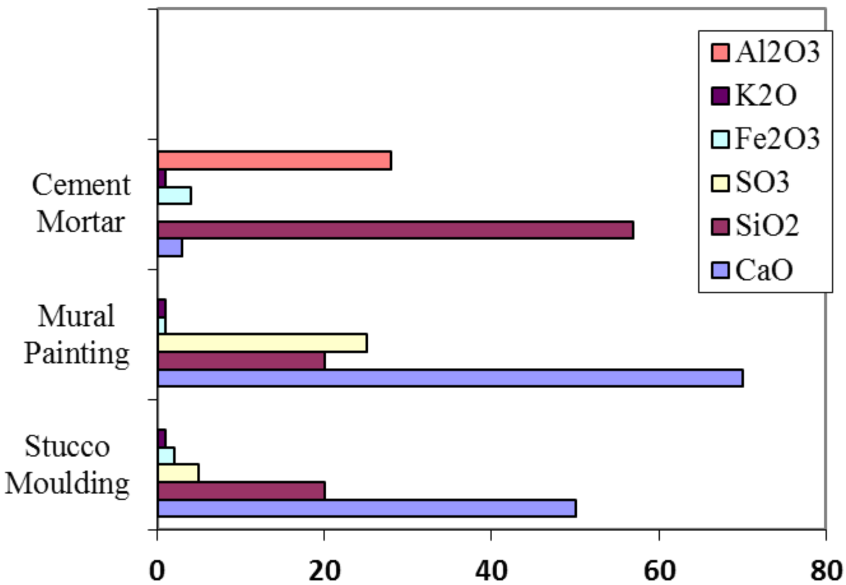

Figure 4. Oxide Compositions of Ancient Plasters and Cement Mortar from Intervention Work

Form the SEM images, the morphology of ancient mortar showed that the present of lime. Due to these results, the ancient mortars were considered as lime-based mortar. Then, acid digestion tests on different samples are carried out and the binder to aggregate ratios are presented in Table 2.

Table 2. Samples of Acid Digestion Tests

Monument name	Constructed period	Location and appearance	Aggregate percentage	Binder percentage
Sula Mani (SLMN/LM)	12 AD	from the south wall of level 1	68%	32%
Ananda-Ok-Kyaung (2162/ LM)	(1776-1785)	from the southern wall of monuments	49%	51%
448 (448-/LM)	13 AD	from intervention place	82%	19%

3. EXPERIMENTAL STUDIES ON REPAIR MORTAR PROPERTIES AND MASONRY UNITS

From the chemical composition and the acid to binder proportion results of ancient mortar form Bagan monuments; one can notice that the results differed depending on the purpose of usage. Moreover, the plenty of monuments for rehabilitation and repair works and the management problem brings to use the different proportion of materials in repair mortar. The lack of scientific investigation on repair mortar in practical works brings various problems such as the difference in colour, mechanical properties, physical properties of old and new masonry works. This condition can lead to serious damages in natural disasters such as earthquakes because of the different earthquake resistance of the old and new mortar and bricks. In order to overcome such problems, the preparation of repair mortar based on experimental results and current practice of mortar proportion in Bagan was carried out. The major materials of mortar such as lime, sand, brick dust and organic materials from Bagan were collected from reconstruction sites of some monuments. The required test on raw materials from Bagan was carried out and the results showed that these materials are good for repair work. To prepare mortar, the ingredients such as lime, sand, brick ducts, U-shit fruit, and jaggery were prepared first. Brick prisms were made with bricks of same sizes of ancient ones which are purposely manufactured for reconstruction and repair parts.

3.1 Experimental studies on repair mortar properties and masonry units

For compressive strength and bending strength of bricks, 5 specimens for each test were prepared according to ASTM C-67. For mortar cube strength, 50 mm cube of mortar of 15 specimens were prepared for 28 days, 45 days and 60 days results. A period of 28 days, the mortar samples were at the stage of forming solid so that tests were carried out for 45 days and 60 days periods. The compressive strengths of brick and mortar are shown in Table 3.

Table 3. Compressive Strength of Brick and Mortar

Specimen	Compressive Strength (MPa)		
	Brick	Mortar	
		45 days	60 days
1	7.3	0.7	0.9
2	11.0	0.7	1.2
3	2.2	0.7	0.9
4	14.3	0.7	1.1
5	8.0	0.7	0.5

For the compressive strength of masonry, 5 solid unit prism specimens (305 × 305 × 152 mm) of height to thickness ratio 2 were prepared and tested according to ASTM C-1314. The bricks of the same size with ancient bricks and the repair mortar were used to construct these prisms. The construction sequence of prisms, transporting of prisms, curing, and preparation for testing was conducted according to standards. The testing procedure is also according to ASTM C 1314. The compressive strength of all of the prisms with respective strain values is presented in Figure 5. The compressive strength of masonry prisms varies from 0.5 MPa to 2.3 MPa with the minimum strain values of 0.009 to maximum strain value of 0.025.

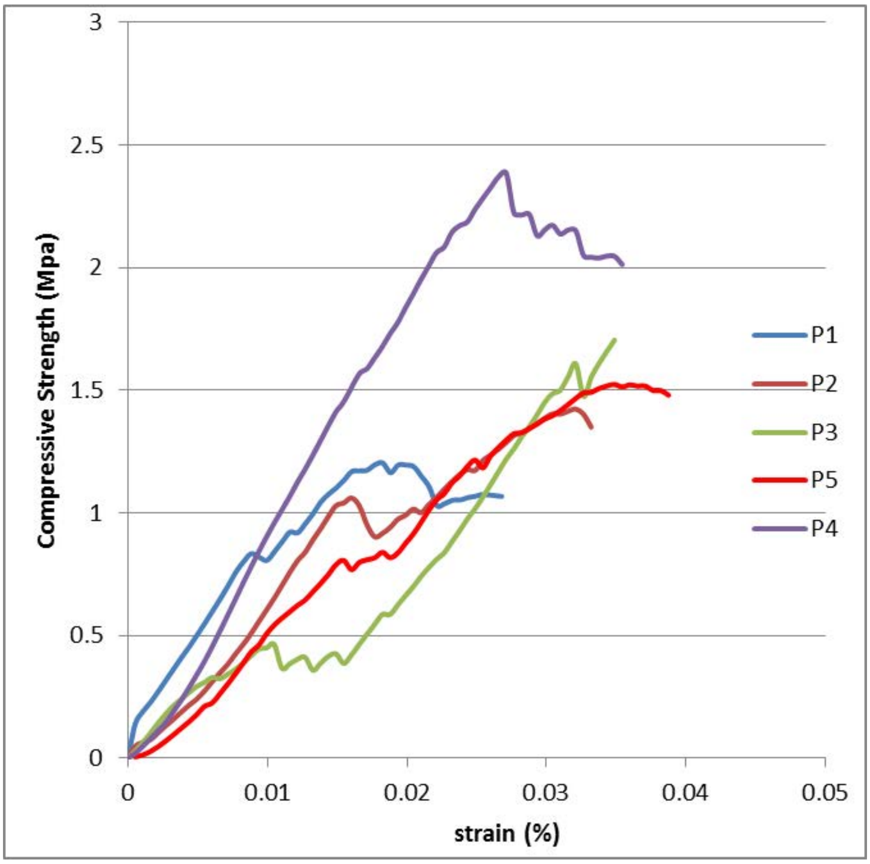

Figure 5. Stress-Strain Curve of Compressive Strength Test of Prisms

For the flexural test, 5 prisms with the length of 480 mm" were prepared and tested according to ASTM C-518. For diagonal shear strength, 5 prisms were prepared and tested according to ASTM C-519 but the sample size is small enough to fit the testing machine. The sample size of 305 × 305 × 152 mm walls was tested for diagonal shear test. The loading apparatus for flexural test and diagonal shear test of the masonry prisms are shown in Figure 6.

(a)

(b)

Figure 6. Loading Apparatus (a) Flexural Test (b) Diagonal Shear Test

The flexural strength of specimens was shown in Table 4. This value of repair masonry is very much lower than that of other type of mortar.

Table 4. Flexural Strength of Masonry Units

Specimen	Flexural Strength (MPa)
F1	0.03
F2	0.07
F3	0.07
F4	0.05
F5	0.10

From the test results, the diagonal shear strength of masonry prisms is very small. The values of 5 samples were shown in Table 5. The experimental results show that the strengths of masonry units with traditional lime mortar were very much less than that of other types of masonry units with different mortar.

Table 5. Diagonal Shear Strength of Masonry

Specimens	Shear Modulus (MPa)	Shear Stress (MPa)	Shear Strain
D1	16	0.2318	0.0149
D2	37	0.3798	0.0103
D3	20	0.3425	0.0169
D4	13	0.2073	0.0160
D5	52	0.1800	0.0034

4. CONCLUSION

Most of the compressive strength of ancient bricks is higher than that of modern bricks. The chemical analysis results of ancient mortars show that lime-based mortar was used in the ancient monuments. The use of organic materials in ancient mortar cannot be traced from chemical analysis of this study. However, the binder to aggregate ratios of mortar is different based on the purpose of usage. So, Bagan style repair mortar composed of lime putty, sand, brick dust, and organic material which is used in rehabilitation work of Post-earthquake Bagan monuments have also experimented in laboratory. The compressive strength and flexural strength of repair mortar and masonry units showed that they are compatible in strength with ancient masonry units for local repair work.

REFERENCES

[1] Myanmar Earthquake Committee, “Rapid visual survey for damages of monuments and buildings due to Chauk Earthquake,” Report of Myanmar Earthquake Committee, 2016.
[2] “ASTM. Standard test method for sampling and testing bricks and structural clay tile. C 67-02, ASTM International,” West Conshohocken, United States, 2002.
[3] “ASTM. Standard Test Method for Examination and Analysis of Hardened Masonry Mortar. C 1324-03, ASTM International,” West Conshohocken, United States, 2003.

LESSONS LEARNT FROM THE DAMAGE AND RESPONSE OF THE 2016 KUMAMOTO EARTHQUAKE IN JAPAN

K. MEGURO[1]

[1] *Director/Professor, International Center for Urban Safety Engineering (ICUS), Institute of Industrial Science (IIS), The University of Tokyo (UTokyo), Tokyo, Japan,*
meguro@iis.u-tokyo.ac.jp

Keywords*: 2016 Kumamoto Earthquake in Japan, foreshock, main shock, aftershock, Level 1 and 2 ground motions, Disaster response activities*

1. 2016 KUMAMOTO EARTHQUAKE DISASTER

At 21:26 (Japan local time) on Thursday, April 14, 2016, an earthquake (M6.5), which was thought main shock at that time but later was called the foreshock, occurred in Kumamoto Prefecture, Kyushu Island, Japan. Due to the earthquake, severe ground motion with seismic intensity 7 of JMA (Japan Metrological Agency) scale, the highest among 10 levels of the scale, was recorded. At 1:25 (Japan local time) on Saturday, April 16, 28 hours later, another earthquake (M7.3) attacked the area affected by the fore shock with again, seismic intensity 7 of JMA scale. With these two earthquakes and other a series of aftershocks (seismic intensity 6+: twice, seismic intensity 6-: 3 times), approximately 200,000 buildings were damaged. Totally, 50 persons were killed and among them, 10 were due to landslide and 37 were due to building damage (7 by a foreshock, 30 by a main shock). Furthermore, over 200 people were killed by indirect causes, such as stress and aggravation of illness during the life in refugee centers. In this paper, I will introduce the lessons learnt from damage due to the 2015 Kumamoto Earthquake and its disaster response activities.

2. EFFECTS OF A SERIES OF STRONG MOTIONS

With Japanese aseismic design code of infrastructure and building structures, we consider two different levels of ground motions i.e. Level 1 and Level 2. The Level 1 ground motion may attack the structure once or twice while it is in use. But the structure must be functional even after the earthquake. While the Level 2 ground motion, it is considered the ever severest motion attacked the target area in the past. Therefore, we assume that the Level 2 ground motion may not attack the target structure more than twice during the time of its use. And the structure may have some damage but should not injure and kill the users. Seismic intensity 7 of JMA scale is considered Level 2 ground motion. However, in case of the Kumamoto earthquake, a series of strong ground motions including twice seismic intensity 7 ground motion, attacked the affected area and many structures were damaged. Therefore, from now on, we should consider the phenomena that multiple very strong ground motions attack the structure and development of a methodology and implementation system for quick and accurate inspection to evaluate the remaining seismic capacity of exposed structure by these ground motions. While, the idea that a series of strong ground motions increased the number of fatalities is not correct. According to the questioner survey (CIDIR Newsletter, Vol. 32, 2016.6.1) carried out for the people in the affected area, it was found the following facts. At the time of the fore shock (9:26 PM on April 14), 87.2 % of the people were at their own homes (people at company or school: 4.3%, people on the way to the home:4.0 %, etc.). While at the time of main shock (1:25 AM April 16), 22.0 % of the people were at their own homes (people at public refugee camp: 28.7 %, people at their friends' home: 11.3 %, people outside of their home including staying in their cars at parking, etc.: 31.2 %). This is the evidence that many people with damaged residential houses (relatively lower seismic capacity ones) moved to public refugee camps and friends' houses (relatively higher seismic capacity ones) and evacuate to outside of the structures for fear of additional damage due to strong aftershocks. If the main shock attacked the area in midnight on the 16th without the foreshock on the 14th April, nearly 100% of the residents (most of them were sleeping), were in their residential buildings, including low earthquake resistant capacity.

Although in both the foreshock on 14th and the main shock on 16th, seismic intensity 7 of JMA scale was recorded, it was found based on the analysis that main shock ground motion was much stronger than the foreshock motion. Main shock ground motion had power that could make similar magnitude damage due to the combined power of the foreshock and main shock ground motions. Therefore, when we estimate the number of deaths in this situation from the total number of buildings collapsed (approximately 8,400 buildings) assuming the same ratio between the number of collapsed buildings (approximately 105,000 buildings) and that of death toll (approximately 5,500) in case of the 1995 Kobe earthquake, the number of deaths becomes 440.
Moreover, when the occurrence time of the earthquake is considered (Kobe 5:46 am, Kumamoto 1:25am), the number of death might become more as search and rescue condition of the Kumamoto earthquake was worse. Based on these facts, it can be told that the foreshock on 14th contributed a lot to reduce the casualties and it has great meaning of an alert to the people.

3.LESSONS LEARNT FROM DISASTER RESPONSE ACTIVITIES

(1) <u>Lessons on "push-type support"</u>

In the Kumamoto earthquake disaster, the national government of Japan implemented "push-type support" for the first time to support human resources and supplies

1) Lessons for both supporter and recipient
- Standardization of disaster response operations (country, prefectures, municipalities) and training

2) Lessons for supporting side
- Undeveloped criteria for implementation of "push-type support"
- About relief supplies:
  a) Simplification of complicated procedures from procurement to shipment
  b) Examining the method of transporting relief supplies to the affected areas
  c) Securing the goods tracing method to grasp their position in transit and the inventory status of goods
  d) Planning and development of the last one mile from the regional logistics base to the evacuation center
  e) Construction of a logistics system that allows country, prefectures, municipalities, manufacturers, and logistics operators to share information on order status, manufacturing status, transportation status, etc., and practical training for implementation
  f) Development of a supply capacity map by goods to enable efficient transportation of goods from nearby areas.
- About human resources support:
  a) Inadequate advance care for temporary staff(on-site dispatch with insufficient prior explanation regarding work contents)
  b) Issues related to temporary staff's working environment, living environment, working conditions, etc.
  c) Development and maintenance of a temporary staff list including past disaster response experience, information on work place and place of birth (persons who are from affected area or had work experience in the area could work efficiently)

3) Lessons for recipient
- Insufficient capacity to receive support due to lack of experience
  a) Lack of extraction of disaster response work that the recipient wants external supporters to do
  b) Securing space for external support activities
  c) Improvement of living environment for supporters in the affected areas

Figure 1 Lessons learnt from the 2016 Kumamoto Earthquake Disaster and Its Response Activities

without waiting for requests from the affected areas. This support has achieved certain degree of the results, such as promoting disaster response of the confused local governments and resolving the shortage of major supplies such as water and food in the affected areas. However, from a series of reviews, various issues as shown in Figure 1 can be pointed out.

(2) <u>Impact of Merge of municipalities in Heisei Era</u>

In addition, the effects of merge of municipalities in the Heisei Era have had a major impact on the issues related disaster response as described below.

The number of the municipalities in Japan was about 3,350 at the end of the Showa Era (late 1980'), become 1,741 due to the merger in Heisei Era. The number becomes nearly half and area becomes large, but in terms of population, the municipalities with a population of 100,000 or less is 85% of the total, with the population of less than 30,000 is 53% and with a population less than 10,000 is 27%. The number of governmental officials has been reduced by the merger, and their number per population has decreased from before the merger. As a result, the current number of officials working at disaster management department in municipalities is around 10 for a population of 100,000, about 2 to 4 for 30,000, and 1, 2 concurrent staff working at other department at the same time for less than 10,000.

Earthquakes, typhoons, and heavy rains (called hazards) occur regardless of the spatial extent and administrative boundaries of the basic municipality. The merger has reduced the resources for disaster response, but the frequency and scale of hazards has not decreased. Rather, it is increasing considering the current seismological environment surrounding Japan and the dangers of extreme torrential rains and huge typhoons associated with global warming.

Comparing the current disaster response conditions based on the population of local governments, the number of disaster-stricken population decreases in local governments with a small population. However, since the population density is low, it is often widely distributed, so the damage distribution is wide for the number of affected population. Also, damaged areas including infrastructure damage, landslide disasters, forests and farmland are often widespread even if the population is small. Therefore, in Japan, a society with a declining birthrate and an aging population, the disaster response of small population municipalities will inevitably become stricter in the future.

In this situation, the points I consider important are described below from the perspectives of "damage reduction" and "future disaster response enhancement".

- **To reduce damage in future**

The first is the viewpoint of future damage reduction. According to Mr. Hiroya Masuda, the population of local municipalities will continue to decline in the future, and marginal settlements will occur in various places and face the danger of disappearance. Under such circumstances, instead of letting the change in population naturally leave the number and distribution of conventional villages as they are, the risk of disaster in each region is evaluated, and it is important to guide the people from high risk areas to lower risk areas. This measure can be implemented effectively in a society with a declining population, and this will make it possible to create a happy environment for both people who move in and who receive them.

At this time, the important point is that it will be difficult for both the government and citizens to make a big financial burden. Therefore, it is important to move them to the spaces with low risk of disaster that become open due to depopulation, at the timing such as when moving or rebuilding houses in citizens' life plans. In this way, even if there is no special countermeasure cost or budgetary measure, the disaster risk and damage amount of the local government as a whole will be greatly reduced, and the disaster response environment will be greatly improved. Different from the past, considering the financial condition of Japan, it is impossible to take measures to protect a small number of people, living in areas with a high disaster risk, spending an enormous cost.

・ **To strengthen disaster response capabilities**

Next is the strengthening of disaster response capabilities. My conclusion is that we should revise the Disaster Basic Act and establish a new system that changes the responsibility for disaster response from municipalities to prefectures. Based on the experience of the 2011 Great East Japan Earthquake Tsunami Disaster, despite the jurisdiction moved from the Ministry of Health, Labor and Welfare to the Cabinet Office, the prefectural governor is still responsible for responding to the Disaster Relief Act.

Actual experience is important for appropriate disaster response, but even in Japan, which is often called a department store for disasters, the frequency is not high if the time and area are limited. Therefore, it is difficult for the municipality officials of disaster management departments in each municipality to have actual experience during their several years working term at the department. As a result, large-scale disaster response in municipalities is “always the first experience” and starts with the situation “I don’t know what to do”. Given the environment surrounding the current and future municipalities, there is no question how difficult it is to accumulate and inherit disaster response experiences and lessons individually in over 1,700 municipalities in Japan.

On the other hand, a prefecture that bundles dozens of municipalities experiences at least one or two disaster responses per year. Even for a term of several years, all persons of the disaster management department can experience of disaster response from several to ten times. Pre-disaster countermeasures should be promoted mainly by municipalities that know the region well because there is time. However, in the local government with a small population, it is not easy to appropriately manage up to tens of times more people than the persons who regularly manage, including external support staffs and volunteers, for the first time disaster response. In the future, disaster response know-how and lessons should be accumulated and inherited in prefectures, and a system should be built to manage disaster response in the affected municipalities.

However, since the number of persons at disaster management departments in prefectures is small, it is important to secure the number of personnel by exchanging personnel with municipalities and to build a human network through exchanges during normal times. When a disaster occurs, the prefecture will visit the municipality and manage the disaster response, and the municipality will be responding to the disaster under the control of the prefecture, with the people who have experienced personnel exchanges as the contact. It is necessary to establish such a system on the scale of the nation and to connect prefectures with each other for the huge disasters, due to such as Tokyo Metropolitan inland earthquake and Gigantic earthquake along the Nankai Trough earthquake.

Also, out of the disaster response work that the local government is currently in charge of, consider the experience and expertise, it is also important to extract the work that can be outsourced, and entrust this to a professional contractor or highly specialized volunteer. By doing so, it becomes possible to reduce the disaster response work that the local government should tackle.

Reforming awareness is also important when dispatching support staff to the affected areas. In other words, damaged area support is important not only for the affected area, but also as an opportunity for local government officials, who are dispatched to the affected area, to learn disaster response. On the other hand, whe a large number of officials are dispatched, the work of the dispatching local government becomes difficult, so a nationwide system that uses healthy OBs and OGs (retired staff) to make up for this should be constructed.

Nishihara Village was a successful example in the Kumamoto earthquake disaster response. Village staffs dispatched to Higashimatsushima City, one of the severely damaged areas by the Great East Japan Earthquake and Tsunami disaster, could play an active and important role in this earthquake disaster response. They engaged in disaster response in Higashimatsushima City and learnt a lot disaster response and built a network with affected municipality. When the Kumamoto earthquake occurred, mayor of the Nishihara village moved them, who were working other departments, back to the disaster management department to respond earthquake disaster. In addition, immediately after the earthquake, Higashi Matsushima City officials came to Nishihara Village to support disaster response activities. This is the reason why Nishihara Village's disaster response has become more efficient despite the severe damage.

In order to enhance the disaster response capabilities of the entire country, it is important for people outside the disaster-stricken area to learn by sharing past lessons and supporting disaster-stricken areas when disasters occur in various places. If this is not successful, we should recognize that the future disaster response for huge disaster, such as the Tokyo metropolitan inland earthquake and Gigantic earthquake along the Nankai Trough, will be "a tough battle without practice".

4. TOWARDS FUTURE LARGE-SCALE DISASTER RESPONSE

We learned many challenges and lessons from the damage and disaster response in case of the 2016 Kumamoto earthquake. However, the biggest lesson is that there is no way to achieve an efficient disaster response for expected huge earthquake disasters, such as due to the Tokyo Metropolitan inland earthquake and the gigantic earthquake along the Nankai Trough, by only reviewing a series of responses to the Kumamoto earthquake disaster (Figure 2). For disasters of these scales, we should consider both the available resources and the scale of the damage as well as the season, the time of occurrence, multiple large earthquakes with a certain time interval, complex disaster combined with other disasters, etc. Based on these conditions, it is necessary to plan and implement drastic measures, including the measures described in Chapter 3 of this paper.

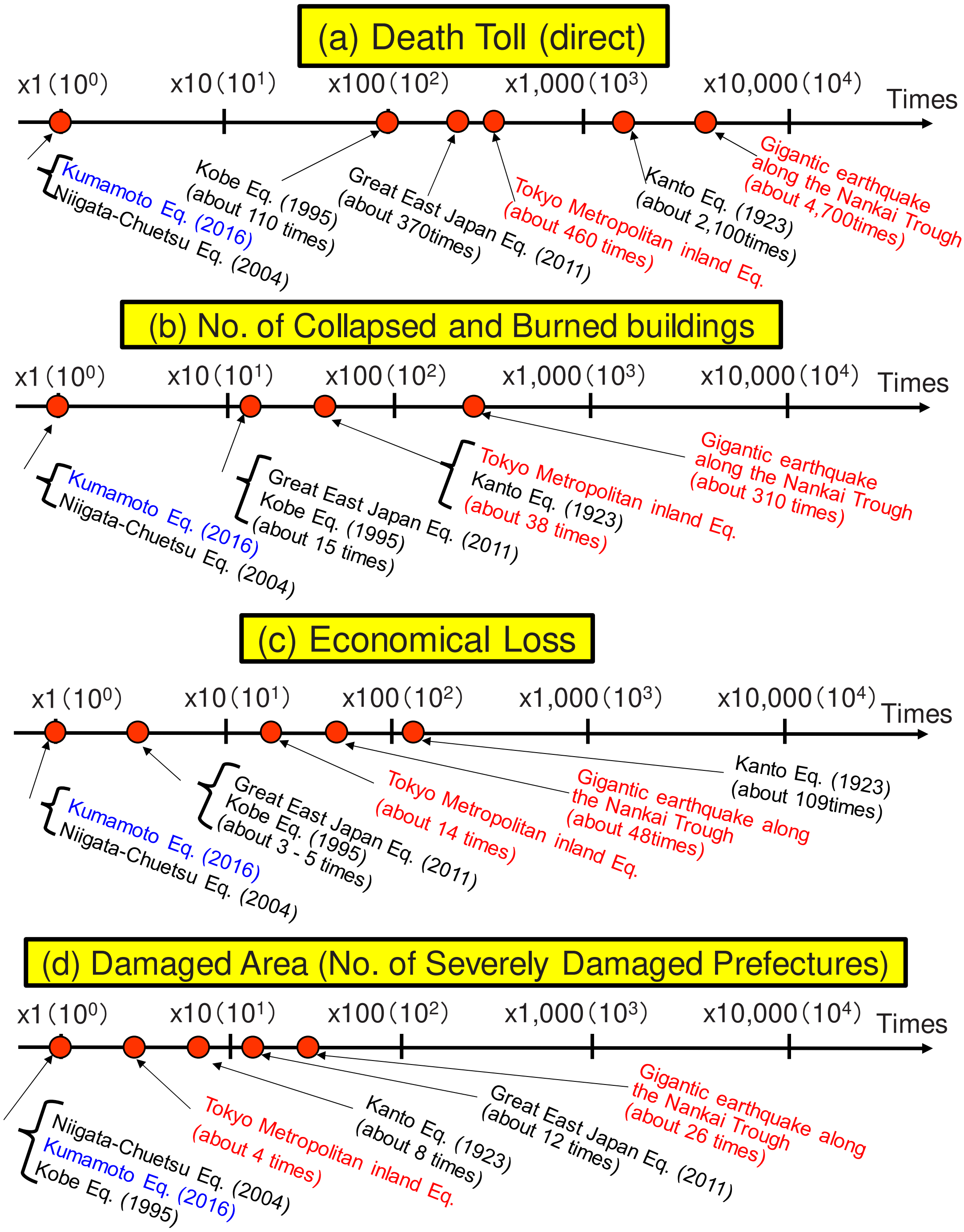

Figure 2 Comparison of the Kumamoto earthquake damage with other earthquake damages in Japan

MICROMECHANICAL INSIGHT INTO STABILITY OF SUBSURFACE CAVITY

M. OTSUBO[1], **U. ALI**[2], **and R. KUWANO**[3]

[1] *Research Associate, Institute of Industrial Science, The University of Tokyo, Tokyo, Japan,*
[2] *Graduate Student, Institute of Industrial Science, The University of Tokyo, Tokyo, Japan,*
[3] *Professor, Institute of Industrial Science, The University of Tokyo, Tokyo, Japan,*
Correspond to Dr. M. OTSUBO (otsubo@iis.u-tokyo.ac.jp)

Keywords: *Subsurface cavity, Cave-in, Discrete element method, Laboratory model test*

1. INTRODUCTION

Modern cities face an increasing number of road cave-in problems, primarily due to defects in buried structures caused by damaged or aged sewer pipes, or by improper works during poorly controlled constructions. Such defects in underground structure may trigger internal erosion of surrounding soils due to seepage action by underground water or heavy rainfall, eventually resulting in formation of subsurface cavities.

To prevent catastrophic road cave-in accidents, non-destructive technique such as ground penetrating radar (GPR) that can find a subsurface cavity and visualize its shape is often used in practice. However, our current knowledge is insufficient to judge confidently whether an existing cavity is stable or about to collapse due to lack of fundamental understanding on the stability of the ground having a subsurface cavity. The present research aims to develop a numerical simulation method to assess stability of subsurface cavity based on its geometrical information obtained using GPR technique.

2. MODEL TEST OBSERVATION

Prior researchers have investigated how a subsurface cavity is formed and expanded influenced by water flow using laboratory model test (Fig. 1) [1]. Ohara (2019) has reported that the stability of the ground with a cavity is related to both the width of cavity and the depth of the soil cover above cavity, and the geometrical data can be used for a risk assessment [1]. However, the observation from the model test was limited to the ground deformation and the resistance against vertical loading; thus, fundamental understanding of mechanical responses, e.g. stiffness or strength, is required.

Figure 1. Subsurface cavity observed in model test experiment (after Y. Ohara, 2019)

3. DISCRETE ELEMENT METHOD

Discrete element method (DEM), is a powerful tool to analyze responses of individual particles. To hold a subsurface cavity firmly, this research implemented a new contact model that considers inter-particle capillary forces where the degree of saturation is an additional input parameter [2] in LAMMPS code [3].

DEM simulations were performed using assemblies of both spherical and non-spherical particles in a rectangular box where the particles located inside a specified region of specimen were deleted to mimic the formation of a cavity (Fig. 2). The results revealed that inter-particle capillary force, particle size and shape are keys to assess the stability of soil structure with a subsurface cavity.

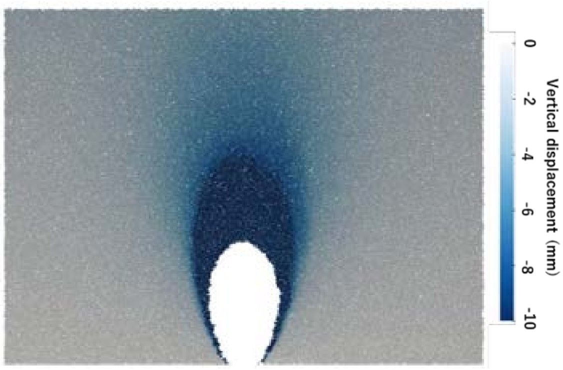

Figure 2. Example of present DEM simulation.

3. CONCLUSIONS

The present study aims to develop a numerical method to evaluate the stability of the soil having a subsurface cavity. The DEM simulations can effectively capture the microscopic response observed in the model test. Physical parameters relating to the particle-scale responses that cannot be measured from the model test will be analyzed further in the on-going research to improve the risk assessment technique for cave-in problems.

REFERENCES

[1] Y. Ohara (2019) A study on the process of expansion and collapse of subsurface cavities for risk evaluation of road cave-ins, *Master Thesis, The University of Tokyo*.

[2] U. Ali, M. Otsubo, R. Kuwano (2019) Implementation of suction-tension model for cavity simulations using DEM. *Proceedings of 54th Japan National Conference on Geotechnical Engineering*, 809-810.

[3] Plimpton, S. (1995) Fast parallel algorithms for short-range molecular dynamics. *Journal of Computational Physics*. 117, No. 1, 1-19.

ANALYSES ON LANDSLIDE EXTRACTION BY SYNTHETIC APERTURE RADAR SINGLE LOOK COMPLEX IMAGES

P. GE[1], H. GOKON[2], K. MEGURO[3], and S. KOSHIMURA[4]

[1] Ph.D. Student, Meguro Laboratory, Institute of Industrial Science, the University of Tokyo, Tokyo, Japan,
[2] Associate Professor, School of Knowledge Science, Japan Advanced Institute of Science and Technology, Ishikawa, Japan,
[3] Professor and Director, ICUS, Institute of Industrial Science, the University of Tokyo, Tokyo, Japan,
[4] Professor, International Research Institute of Disaster Science (IRIDeS), Tohoku University, Sendai, Japan,
Correspond to Ms. P. GE (gepl@iis.u-tokyo.ac.jp)

***Keywords**: landslide, synthetic aperture radar (SAR), single look complex (SLC), intensity, phase, receiver operating characteristic analysis (ROC)*

1. INTRODUCTION

The 2018 Hokkaido Eastern Iburi Earthquake, which occurred on September 6, triggered more than 6,000 landslides over an area of 20×20 km [1], disrupting transportation, communication, as well as electricity and power service. A rapid mapping of the massive earthquake-induced landslides was important for directing rescue efforts and limiting resource allocation delays. Synthetic aperture radar (SAR) is a potential tool for quick landslide mapping even in harsh weather due to its large cover, quick response, no contact, as well as light and weather independence capabilities. However, relevant studies were still limited to individual landslides or catchments with limited accuracy [2]. This study analyzed the potential of SAR single look complex (SLC) images acquired before and after the disaster for the massive earthquake-triggered landslide extraction.

2. RESEARCH AREA AND DATA

The research area was around Atsuma Town, Iburi, Hokkaido, where numerous landslides were induced in the 2018 Hokkaido Eastern Iburi Earthquake. Applied SAR dataset were two pre-event and one post-event ALOS-2 images acquired in the affected areas with an off-nadir angle of 37.8 degree from left looking. All three images were L1.1 SLC products represented by complex I and Q channels to preserve magnitude and phase information. The image acquisition mode was stripmap ultra-fine mode single polarization (UBS), with a 3m spatial resolution and a HH polarization mode. What is more, a landslide inventory map created by [3] was employed as ground truth data for result evaluation.

3. PARAMETER CALCULATION

Potential parameters that can be derived from the three SAR images and have the capability to measure ground changes were first selected according to SAR imaging principals. Determined parameters included the intensity difference, correlation coefficient, correlation coefficient difference, and normalized coherence difference. SNAP software was then employed to process the original complex images for basic intensity and coherence information extraction. And ArcGIS 10.5 was then applied for the final calculation of these potential parameters.

4. PARAMETER ANALYSIS

After calculating the potential parameters, qualitative observation was first performed by overlapping the landslide ground truth data to the calculated SAR parameter images. It indicates that the intensity difference displays clear lower and higher values in landslide areas (Figure 1) as triggered landslides smoothed the hillside areas and roughened the foothill areas. Besides, the correlation coefficient, correlation coefficient difference, and normalized coherence difference images all show lower values in landslide regions due to the landslide-induced ground changes. Quantitative analysis was then executed through receiver operating characteristic (ROC) analysis to evaluate and compare the landslide mapping performance of these parameters. It demonstrates that the intensity difference and correlation coefficient difference have better capability for landslide mapping in these forest areas compared with other parameters.

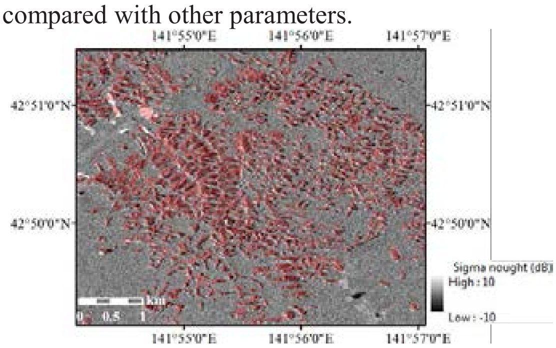

Figure 1. Intensity difference image overlapped by ground truth landsides (red color: ground truth landslides)

5. CONCLUSIONS

SAR SLC images have certain capability for massive landslide detection as several derived parameters, especially the intensity difference and correlation coefficient difference, showed clear different characteristics in landslide and non-landslide areas.

REFERENCES

[1] H. Yamagishi, F. Yamazaki, Landslides 15 (2018) 2521–2524.
[2] T. Konishi, Y. Suga, Eur. J. Remote Sens. 51 (2018) 205-221.
[3] S. Zhang, R. Li, F. Wang, A. Iio, Landslides 16 (2019) 1691-1708.

A FEASIBILITY STUDY ON THE SCALING OF OPERATIONAL MODE SHAPES OF BUILDING USING A SHAKER

G.K. Chaitanya[1], M. Numada[2], and K. Meguro[3]

[1] *Project Assistant Professor, Institute of Industrial Science, University of Tokyo, Japan,*

[2] *Associate Professor, Institute of Industrial Science, University of Tokyo, Japan*

[3] *Professor, Institute of Industrial Science, University of Tokyo, Japan*

Correspond to G.K. Chaitanya (chaitugk@iitbombay.org)

Keywords*: Operational Modal Analysis, FDD, Identification, mode shape scaling*

1. INTRODUCTION

There are many methods to support numerical modeling of existing structures for understanding the condition of the structures [1]; however, there is high uncertainty in estimation of the material properties. Estimating material properties and conditions of structures from vibration tests are gaining popularity, and one of the challenging aspects is obtaining scaled mode shapes [2]. This research explains a procedure for scaling of mode shapes with which operational mode shapes could be scaled to satisfy the unit modal mass property of the system.

2. METHODOLOGY

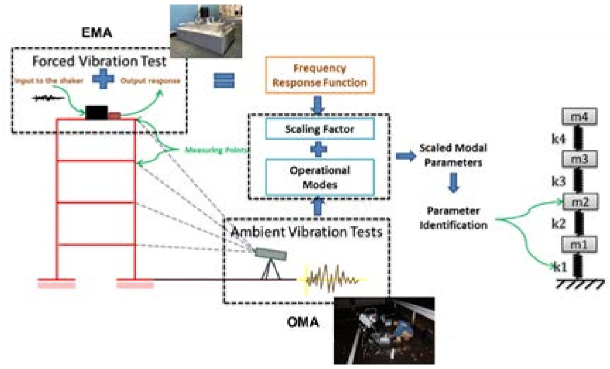

Fig. 1 Overall methodology of scaling of mode shapes

Fig. 1 shows the overall methodology where ambient vibration tests are conducted to obtain the operational mode shapes. As the outcome of these results are unscaled mode shapes, a method for scaling with a minimal forced vibration test using a shaker.

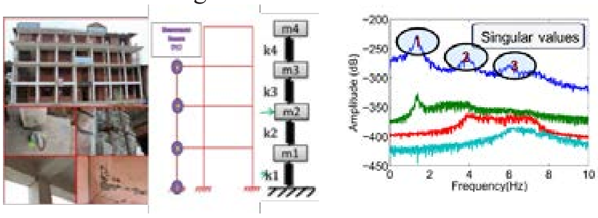

Fig. 2 Measurement and experimentation of a building

A simplified numerical model is developed with a mass-spring-damper system for a four storey building (Fig. 2). Whitenoise of 0-300Hz is applied, and the amplitude of the response equivalent to measured response using microtremor for buildings in Nepal. The natural frequencies and operational mode shapes are obtained using frequency domain decomposition (FDD). The shaker excitation (white noise) is applied in the same system at one location in the building, and the input and output are recorded. This response is further used to estimate the scaling factors (Fig. 3) for the operational modes calculated earlier.

3. RESULTS AND DISCUSSIONS

The determination of scaling factors is done, and it can be seen that the accuracy of estimation has been evaluated with its variation with amplitude of shaking, duration of shaking, and RMS ratio of response from the simulation and measured, as shown in Fig. 4.

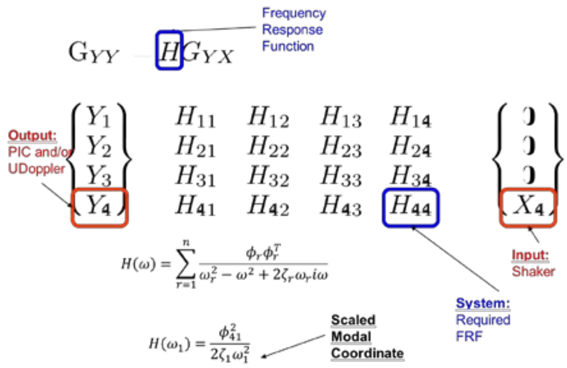

Fig. 3 Scaling of mode shapes using shaker response

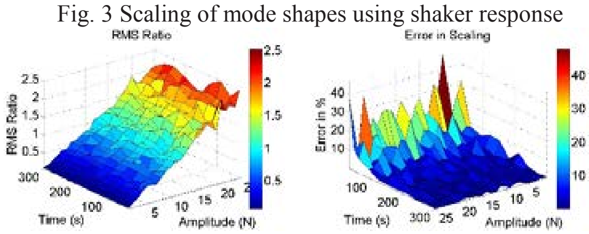

Fig. 4 Parametric study of RMS ratios and error in scaling

The results show that longer duration of shaking and measurement is critical in reducing the scaling error, and higher amplitudes do not contribute to the accuracy of scaling; however it is essential in this case of a building to ensure an RMS ratio to be higher than unity for scaling.

4. CONCLUSIONS

A minimalist procedure using a vibrating shaker is suggested for modal testing to scale operational mode shapes obtained from the operational modal analysis. We recommend this procedure for further evaluation and development of a multi-frequency shaker.

REFERENCES

[1] Klaus G T and Norris S. (1995) Non-destructive damage evaluation of a structure from limited modal parameters. *Earthquake Engineering & Structural Dynamics*, 24(11):1427.

[2] Heylen W., Lammens S., and Sas P. (1997). Modal analysis theory and testing Leuven, Belgium.

A STUDY ON THE METHODS OF UNDERSTANDING VULNERABLE PEOPLE'S NEEDS USING SATELLITE SAR IMAGE

YUMA MORISAKI[1], MAKOTO FUJIU[2], RYOICHI FURUTA[3],

TAKASHI SAKAI[4], KAZUHIRO NAGAKI[4], JUNICHI TAKAYAMA[5], and YUTO SHIOZAKI[6]

[1] Doctoral Course Student, Dept. of Environmental Design, Kanazawa University, Japan,
[2] Associate Professor, Geosciences and Civil Engineering, Kanazawa University, Japan,
[3] Remote Sensing Technology Center of Japan, Japan,
[4] Master Course Student, Dept. of Environmental Design, Kanazawa University, Japan,
[5] Professor, Geosciences and Civil Engineering, Kanazawa University, Japan,
[6] Specially Assistance Professor, Dept. of Environmental Design, Kanazawa University, Japan,
Correspond to Ass. Prof. Makoto FUJIU (fujiu@se.kanazawa-u.ac.jp)

***Keywords**: large-scale earthquake disaster, vulnerable people, satellite SAR image, understanding location information and needs*

1. BACKGROUND OF THIS STUDY

In Japan, large-scale earthquake disasters frequently occur. When a large-scale earthquake disaster occurs, it becomes difficult to collect the victim's needs, and at the same time the realization of detailed support for the victims also becomes difficult. Especially, vulnerable people, for example elderly person, sick person, pregnant, it is necessary to quickly grasp the location information and needs. And efficient system is needed about quick and detailed assistance from third party to vulnerable people. In this research, we propose a method of understanding various vulnerable people's needs and location information using satellite SAR images. In this analysis, as a basic study for understanding location information and needs, we proposed an object with a shape and size that can be recognized by SAR.

2. ANALYSIS PROCEDURE OF THIS STUDY

In this research, satellite images acquired from ASNARO-2 are used. ASNARO-2 is a SAR satellite operated by NEC. In this analysis, satellite images observed from Spotlight mode with 10km observation width and 1m resolution are used. In this study, as a basic study for a major research goal, we propose a target that can be observed by ASNARO-2.

Figure 1 shows the target proposed in this study. The proposed target has an aluminum disk on the bottom and a petal-like partition on it. When the interval (inner angle) of the partition is set to 60 degrees and 40 degrees, hexagonal or nonagonal "petals" are formed. Unlike the shape of a typical corner reflector, this shape has very little direction dependency. These targets were devised and set at the ASNARO-2 observation. The experiment date is June 25, and the target is ideally arranged for the angle of incidence of the microwave emitted by ASNARO-2.

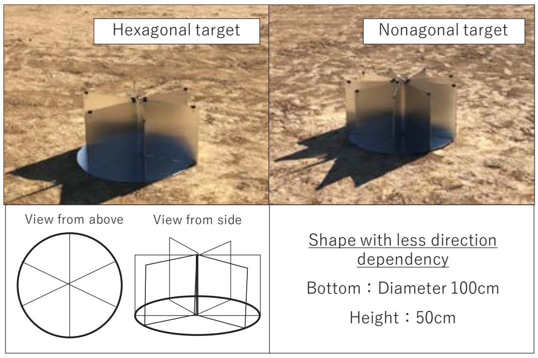

Figure 1. Target details

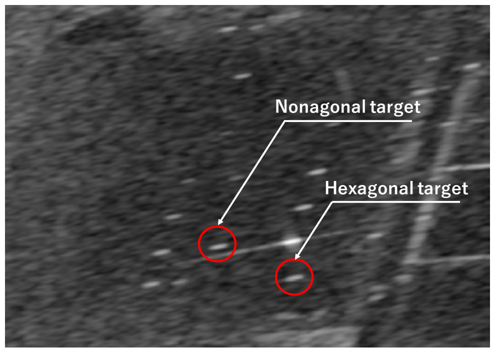

Figure 1. Target details

3 RESULT OF EXPERIMENTS

Figure 2 shows the results of a target visibility experiment. The visibility of the hexagonal and Nonagonal targets can be confirmed. In addition, comparing the visibility of hexagonal and nonagonal targets, there is a difference in the backscatter indicating the reflection intensity.

4 CONCLUSION AND FUTURE WORKS

As a result of experiments and analysis, the object which we proposed was able to be recognized in SAR observation.In the future, we will conduct experiments in various areas considering land surface condition, geographical features, etc. in order to examine the versatility of the object. In addition, we aim at the construction of bulk management visualization system that information of location information and needs.

SURVEY OF RECONSTRUCTION PROJECTS IN JAPAN AND MAKING THE DATABASE FOR DISASTER RESPONSE WORK

R. ITOH[1], **K. MEGURO**[2], **and M. NUMADA**[3]

[1] *Graduate Student, Department of Civil Engineering, The University of Tokyo (UTokyo), Tokyo, Japan,*

[2] *Director/Professor, International Center for Urban Safety Engineering (ICUS), Institute of Industrial Science (IIS), UTokyo, Tokyo, Japan,*

[3] *Associate Professor, ICUS, IIS, UTokyo, Tokyo, Japan,*

Keywords*: Reconstruction, Recovery, Restoration, Construction cost, Disaster response, Local government*

1. GENERAL INSTRCUTIONS

When local governments suffer large-scale natural disasters, they should first estimate the costs to make plans for recovery and reconstruction after assessing the damage. The cost estimation work for reconstruction will be normally carried out by the government officials. But due to lack of experience of disaster response, it is usually very difficult for them to do properly.

Japan is sometimes called department store of natural disasters. Even in Japan, it is practically impossible for all officials to have actual experience of disaster response, considering the relation among the frequency of big disaster, area of municipality, and their working duration of disaster management section. Also, it is very rare that the local government had similar disaster experiences and their records. Moreover, the number of local government staff is decreasing due to the decrease in public works, then when a disaster attacks certain municipality, many staff from other municipalities are dispatched to disaster-affected municipality to support it [1]. When they suffer damage, they look for past construction cases for restoration work of individual damaged parts, build up construction costs based on them, and estimate a cost for reconstruction. This work is very time-consuming and is one of the causes of delaying the initial movement of disaster recovery. A delay in the initial recovery from disasters not only promotes the anxiety of the people in the affected area, but may also delay the completion of recovery and increase construction costs.

In addition, in the areas where large-scale earthquake and tsunami damage is currently expected, it is considered that prior reconstruction is necessary. However, the discussion of plans in the absence of a specific amount of budget lacks feasibility.

Table 1. Number of dispatched local government staff in the 2011 Great East Japan Earthquake and Tsunami disaster [2]

Date	Number of officials dispatched	
	Cumulative number	Currently number
1st Jul. 2011	56,923	2,460
1st Oct. 2011	73,802	1,211
1st Jun. 2012	79,107	804

2. OBJECTIVE

In this research, we aim to support local governments for disaster response operations or making a prior reconstruction plan that can quickly and easily create cost estimates for disaster recovery. For that purpose, we investigate the contents and amount of budget of each construction of the reconstruction projects in the past large-scale disasters, such as the 2011 Great East Japan Earthquake and Tsunami disaster.

3. METHODOLOGY

First, as a preliminary survey, we investigate businesses that are relatively easy to obtain materials. Usually, governments release the contents of the bid and contract. We extract the work related to disaster recovery and reconstruction from all the construction works. From the publicly available information, the name, location, type of industry, amount of budget, etc. of each construction can be obtained. We examine the forms of damages, construction methods, and types of materials related to construction, etc.

Next, we collect the information not disclosed. Since the format and contents differ depending on the organization, we need to collect the missing information by asking the organizations to provide inquiry materials. In addition to public information, we also collect detailed information about each construction, such as accumulated contents and damage status of the construction site. Create questionnaires that make it easy to get answers when surveying each local government and to summarize at the time of tabulation.

Finally, we create the database. By linking damage scale and construction scale, construction scale and cost, the cost of recovery and reconstruction work can be calculated from the damage situation. Unit price and damage scale will be variables for construction cost calculation.

4. CONCLUSION

Study results and conclusion will be introduced at USMCA 2019 in Yangon.

REFERENCES

[1] Mori Yoshihisa (2015), Recent efforts in public procurement, *JICE report,* No.28, pp. 64-67

Reference to a website:

[2] "Efforts by the Ministry of Internal Affairs and Communications to support local governments affected by the Great East Japan Earthquake", Ministry of Internal Affairs and Communications, http://www.soumu.go.jp/menu_kyotsuu/important/70131.html (accessed 2019-9-28)

A STUDY ON ANALYZING ROAD NETWORK PATTERNS AND PROXIMITY GRAPHS IN TERMS OF EFFICIENCY IN ROAD TRANSPORTATION

Daisuke WATANABE

Associate Professor, Department of Logistics and Information Engineering,
Tokyo University of Marine Science and Technology, Japan
daisuke@kaiyodai.ac.jp

***Keywords**: Road network patterns, Proximity graphs, Route Factor*

1. INTRODUCTION

The road transportation system under the disaster situation is very important for emergency vehicles like fire engines and ambulances and trucks for relief supplies, and the road network pattern directly affect the efficiency for the movement of them. The purpose of this paper is to evaluate the travel efficiency of road network pattern using Route Factor by considering relationship between neighborhood intersections. The proximity graphs like Delaunay triangulation (DT), Gabriel Graph(GG) and Relative Neighborhood Graph(RNG) are used to analyze the road network pattern of major cities in United States of America as network construction model.

2. MODEL DESCRIPTION

A graph defined by the proximity of points on a plane exemplified by DT and a minimum spanning tree(MST) is generally called a proximity graph and there are many applications in engineering, particularly to morphological problems[1]. By creating a proximity graph based on road points extracted from an existing road network and then comparing a graph edge to an actual road network, we can clarify the principles for creating a road segment[3].

Ten cities representing the east coast, inland, and west coast regions were chosen for this study. The Census TIGER/Line is used as the data source for the inner city road networks of U.S. cities.

Network Distance is calculated as the distance of shortest path of two points on the Network. Route Factor(RF) that is the major index for travel efficiency is calculated as the ratio of Network Distance to Euclidean Distance[2]. Demand points are 1000 points which are randomly generated along road network. Travel Demand is defined as the pair from all nodes to all nodes except oneself (Total: n(n-1) =999000 OD pairs)

3. CONPUTATIONAL RESULT

As shown in Figure 1, Route Factor(RF) in All Cities shows the following relationships: RF(DT) < RF(GG) < RF(Road) < RF(RNG) < RF(Rectilinear). Route Factor on Road network is intermediate of that of GG and that of RNG in almost all cities. Travel Efficiency on Road network is intermediate of GG and RNG except San Diego. The highest city in travel efficiency is New York. High travel efficiency correlates with High connectivity and High density road network.

As shown in Figure 2, the distribution of Route Factor(RF) of Road network in New York is the

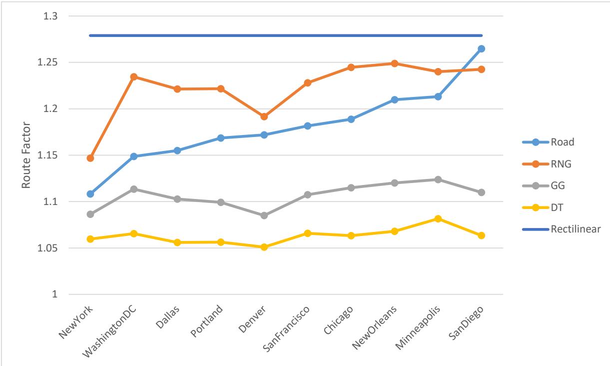

Figure 1. Route Factor of each graphs in all cities

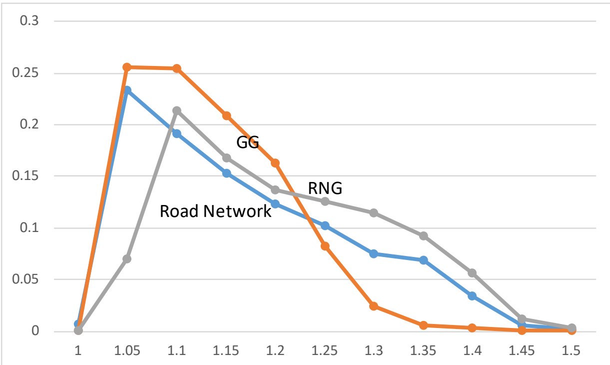

Figure 2. Distribution of Route Factor(RF) in New York

intermediate of that of RNG and that of GG. This fact shows that travel efficiency on the road network in New York is very close to that on RNG and GG.

4. CONCLUSION

In this research, we evaluate the Road Network Patterns in US major 10 cities using Proximity Graphs with Road intersections in terms of travel efficiency. As a result, travel efficiency on Road network is very similar to that on some proximity graph like RNG and GG.

REFERENCES

[1] A. Okabe et al: Spatial Tessellations: Concepts and Applications of Voronoi Diagrams, Wiley, 2000.

[2] D. Watanabe: Evaluating the configuration and the travel efficiency on proximity graphs as transportation networks, FORMA, 23(2), 81-87, 2008.

[3] D. Watanabe: A Study on Analyzing the Grid Road Network Patterns using Relative Neighborhood Graph, Lecture Notes in Operations Research, 12, 112-119, 2010.

Statistical Analysis of Relation between Seismic Motion and Viaduct Damage in Considering Efficacy of Seismic Reinforcement

Shoichi Uemura, Hiroto Suzuki and Hiroyuki Miyakoshi [1]
[1]R＆D Center of JR East group,
East Japan Railway Company,
Japan
s-uemura@jreast.co.jp

ABSTRACT

East Japan Railway Company has been conducting seismic reinforcement of reinforced concrete viaduct columns and piers. In order to ensure the safety of a train when an earthquake occurs, train operation control such as stopping and/or restricted speed are carried out based on observed values of seismic motion. Train operation control criteria is based on eathquake resistance of structures. Therefore, if the eathquake resistance of structures is improved by seismic reinforcement, train operation control criteria value may be increased. So, for this research, we used statistical analysis to evaluate the relation between seismic motion and structural damage and how structural reinforcement may have improved eathquake resistance. As a result, reinforcement may be a major factor in improving the structures to seismic motion and reduced potential for damage.

Keywords: railway, seismic reinforcement, seismic motion, train operation control

1. INTRODUCTION

East Japan Railway Company (hereinafter called "JR East") started conducting seismic reinforcement of reinforced concrete viaduct columns and piers (hereinafter called "RC columns) in the wake of the 1995 Southern Hyogo Prefecture Earthquake (Great Hanshin-Awaji Earthquake) as a "hard" earthquake countermeasure. Seismic reinforcement for tens of thousands of RC columns has been completed, with construction still in progress. Seismic reinforcement of a viaduct is to strengthen the shear and resilience by enveloping the RC columns in a steel plate, RC, etc. In order to ensure the safety of a train when an earthquake occurs, train operation control such as stopping and/or restricted speed are carried out based on observed values of seismic motion as a "soft" earthquake countermeasure. Train operation control criteria is based on eathquake resistance of structures. Therefore, if the eathquake resistance of structures is improved by seismic reinforcement to RC columns, train operation control criteria value may be increased. So, for this research, we used statistical analysis to evaluate the relation between seismic motion and structural damage and how structural reinforcement may have improved eathquake resistance.

2. OUTLINE AND METHOD OF EARTHQUAKE COUNTERMEASURES

2.1 Seismic reinforcement (“hard” earthquake countermeasures)

(1) Seismic reinforcement design
Seismic reinforcement to RC columns is designed so that conditional expression 1 and 2 are satisfied against two directions of seismic motion (Figure 1).

$$\gamma_i \cdot \mu_{rd} / \mu_{dd} \leqq 1.0 \tag{1}$$
$$\gamma_i \cdot V_d / V_{ud} \leqq 1.0 \tag{2}$$

where μ_{rd} : design response plasticity, μ_{dd} : design toughness rate, γ_i : structure factor, V_d : design shearing force(=Mu/La) , Mu : flexural capacity, La : shear span and V_{ud} : design shear capacity. μ_{rd} is calculated by equation 3

$$\mu_{rd} = 1/2 \cdot (K_{hE}^2 / K_{hy}^2 + 1) \tag{3}$$

where K_{hE} : response acceleration in case of elastic behavior and K_{hy} : design horizontal seismic coefficient.

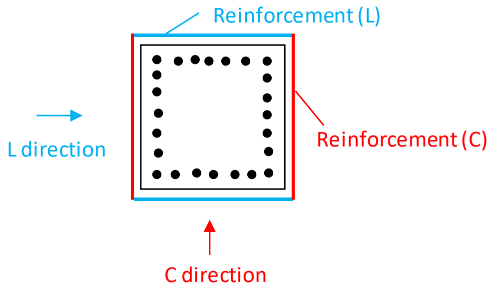

Figure 1: Seismic reinforcement concept of conditional expression 2

(2) Seismic reinforcement method
A seismic reinforcement method, enveloping the RC columns in a steel plate as shown in Figure 2(a), has been adopted at many sites. However, in cases where there are obstacles attached to RC columns that are difficult to remove, or where equipment that is difficult to relocate is in close proximity, a one-sided seismic reinforcement method is adopted (Figure 2(b)). If structural requirements are satisfied, three-sided seismic reinforcement (Uemura, 2013) can be adopted to RC columns integrated with retaining wall.

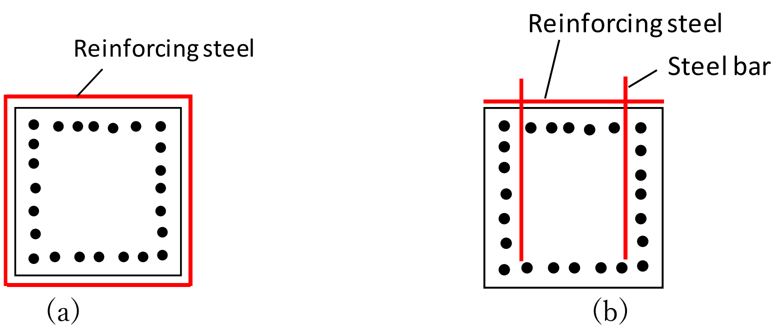

Figure 2: A seismic reinforcement method

2.2 Train operation control ("soft" earthquake countermeasure)

Spectrum intensity (Housner, 1952) (SI) is used in train operation control as an index of seismic motion highly correlated to damage. The interval between seismometers along a rail line is in the order of tens of kilometers. Table 1 shows operation control classifications and operation control threshold values for conventional lines in earthquakes. Seismic design sections are those where structures were designed and constructed under the seismic design standard established in 1979 (hereinafter called "1979 standard"), having high eathquake resistance. Rockfall sections are mountainous sections with a risk of rockfall in earthquakes. Ordinary sections are those that do not fall under either rockfall sections or seismic design sections, and sections made of viaducts designed and constructed under standard prior to the 1979 standard are classified as ordinary sections.

Table 1: Operation control classification and operation control threshold value for conventional lines in earthquake

Operation control classification	Rockfall section	Ordinary section	Seismic design section
Speed restriction (kine)	3 to under 6	6 to under 12	9 to under 18
Operation suspension (kine)	6 or greater	12 or greater	18 or greater

3. ANALYSIS METHOD

Structures analyzed were rigid frame and girder RC viaducts on JR East conventional and Shinkansen lines designed and constructed under standards prior to 1979. Study was carried out in the following procedure.

- Establishing structural unit of viaducts as a basic factor of analysis
- Selection of earthquakes as subject of study
- Classification of structural unit based on seismic conditions, namely eathquake resistance of RC column, seismic motion and seismic structural damage
- Tabulation of structural units falling under each seismic condition
- Analysis of relationship between seismic motion and seismic damage due to difference in the eathquake resistance of RC column

4. SETTING STRUCTURAL UNIT OF VIADUCT

The concept of establishing a structural unit for the viaduct is shown in Figure 3. Rigid frame viaducts are composed of integral structures made up of columns, beams, and slabs (these structures hereafter called, "blocks") and adjustment girders, so we considered blocks and adjustment girders to each be a distinct classifications in this research. For girder RC viaducts, we considered a span to be a distinct classification.

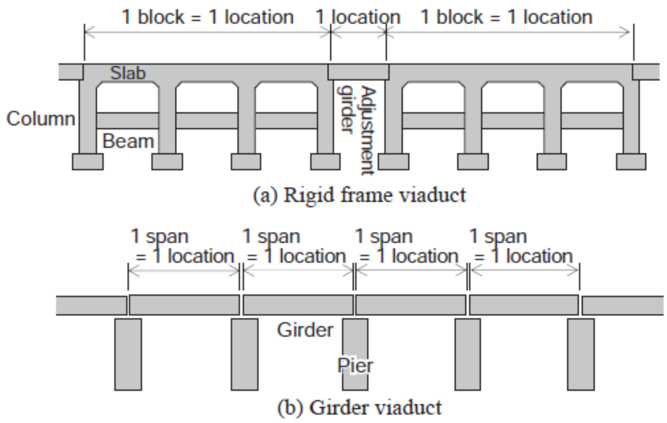

Figure 3: Concept of viaduct classification in statistical analysis

5. SEISMIC CONDITION OF STRUCTURAL UNIT

5.1 Selection of subject earthquake

In this study, we used the five earthquakes shown in Table 2 beginning with the 2004 Mid Niigata Prefecture Chuetsu Earthquake in which damage to JR East railway facilities was suffered.

Table 2: Earthquake studied

Earthquake name	Moment magunitude	Date of occurrence
Mid Niigata Prefecture Chuetsu Earthquake	6.6	23-Oct-04
Chuetsu Offshore Earthquake	6.6	16-Jul-07
Iwate-Miyagi Nairiku Earthquake	6.8	14-Jun-08
Great East Japan Earthquake(mainshock)	9	11-Mar-11
Great East Japan Earthquake(aftershock)	7.1	7-Apr-11

5.2 Eathquake resistance of RC columns

The structural units are classified into three types based on eathquake resistance of RC column: ”reinforced,” ”reinforcement unnecessary,” and ”requiring reinforcement.” Structural units confirmed to have RC columns with certain eathquake resistance in seismic assessment were classified as “reinforcement unnecessary.” Structural units in which seismic reinforcement was conducted on all RC columns were classified as “reinforced.” Structural unit in which seismic reinforcement was not conducted on any of the RC columns despite need for reinforcement were classified as “requiring reinforcement.”

5.3 Seismic structural damage

Structural units are classified based on seismic structural damage caused by the five earthquakes shown in Table 2. Structural units suffering seismic structural damage obstructing train operation is classified as “damaged.” Other structural units are classified as “undamaged.” The total number of “damaged” structural units was 128.

5.4 Seismic motion

In order to evaluate the seismic motion of each structural unit, it is effective to use a method of estimating spatial distributions of seismic motion (Yamazaki, 1998). Figure 4 shows an image of estimating spatial distribution of seismic intensity. First, we calculated seismic intensity at engineering bedrock by dividing seismic intensity observed in the individual earthquakes by site amplification. Then, we spatially interpolated seismic intensity at engineering bedrock to find spatial distribution. Spatial interpolation was performed by the Simple Kriging method (Wackernagel, 2003), which can take into account the tendency of seismic motion to attenuate according to the distance from the hypocenter. Finally, we multiplied the area-wide distribution of seismic intensity at engineering bedrock by site amplification to estimate spatial distribution of seismic intensity at ground surface. For seismic intensity, we used SI values that JR East uses in train operation control. For values observed by seismometers, we used those of the K-NET and KiK-net strong-motion seismograph networks of the National Research Institute for Earth Science and Disaster Resilience (NIED) and those for train operation control used by JR East. For site amplification, we used site amplification factors (Fujimoto, 2006) of the subsurface ground per 250 m mesh for all of Japan estimated from geomorphologic classification (Wakamatsu, 2013). As for structural units classified into SI values of less than 10 kine, not even slight damage occurred, so they were omitted from statistical analysis. As a result, seismic motion was evaluated for a total of 23847 structural units.

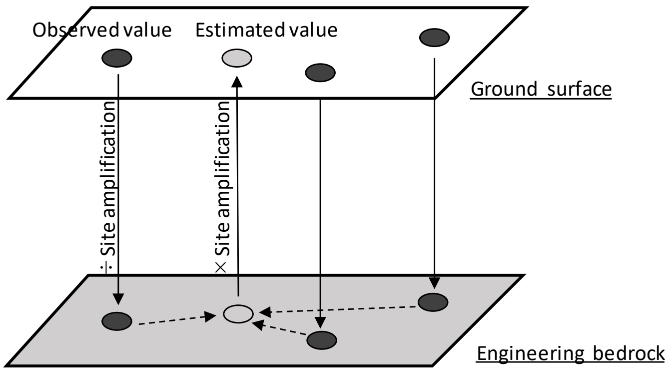

Figure 4: Image of estimating spatial distribution of seismic intensity

6. ANALYSIS OF RELATIONSHIP BETWEEN SEISMIC MOTION AND DAMAGE

Figure 5 shows the relation between damage rate and SI value for the eathquake resistance of each RC column classification. Damage rate is the ratio of the number of damaged structural units to the total number of structural units and defined by the following equation.

$$\text{Damage rate(SI)} = \text{(Number of damaged structural units less than SI value)} / \text{(Number of structural units less than SI value)} \times 100 \quad (4)$$

Damage rate is lowest in the classification “reinforced” and heightens in the order of “reinforcement unnecessary” and “requiring reinforcement.”
Lower-limit value of damage is 26.7 kine for “requiring reinforcement,” 36.6 kine for“reinforcement,” and 28.8 kine for “reinforcement unnecessary,” The classification “reinforced” showed the highest lower-limit value of damage, becoming lower in the order of “reinforcement unnecessary” and “requiring reinforcement.” Moreover, the lower-limit values of damage above were higher than the 21.8 kine lower-limit value of damage investigated when setting current operation threshold values of ordinary sections(Shimamura, 2004) shown in Table 1. From the above results, we found that reinforcement may be a major factor in improving the structures resilience to seismic motion and reduced potential for damage.

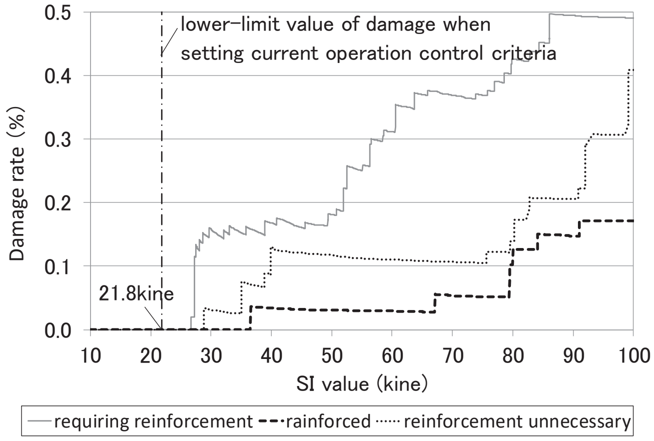

Figure 5: Relation between SI value and damage rate

7. CONCLUSION

To increase train operation control criteria value in viaduct sections where seismic reinforcement has been completed, we used statistical analysis to evaluate the relation between seismic motion and structural damage and how structural reinforcement may have improved eathquake resistance. Analysis was carried out by classifying structural conditions as “reinforcement unnecessary,” ”reinforced,” and ”requiring reinforcement” for railway structures experiencing seismic activity from five relatively recent earthquakes, producing the following results:

・Damage rate is lowest in the classification “reinforced,” and heightens in the order of “reinforcement unnecessary” and “requiring reinforcement.”

・The classification “reinforced” showed the highest lower-limit value of damage, becoming lower in the order of “reinforcement unnecessary” and “requiring reinforcement.”

From above results, it was found that reinforcement may be a major factor in improving the structures resilience to seismic motion and reduced potential for damage. In the future, we intend to clarify the physical aspects by structural analysis using the numerical model.

REFERENCES

Fujimoto, K., Midorikawa, S., 2006. Relationship between Average Shear-Wave Velocity and Site Amplification Inferred from Strong Motion Records at Nearby Station Pairs (in Japanese), Journal of Japan Association for Earthquake Engineering, Vol. 6, No. 1, 11-22.

George W. Housner, 1952. Spectrum Intensity of Strong Motion Earthquakes, Proceedings of 1952 Symposium on Earthquake and Last Effects on Structures, 72-88.

Hans Wackernagel, 2003. Multivariate Geostatistics, Morikita Publishing Co., Ltd.

Shimamura, M., Suzuki, H., 2004. Railway Traffic Control Based on Earthquake Monitoring (in Japanese), Proceedings of the 11th Japan Railway Engineering Symposium, 2289-2292.

Uemura, S., Tukisima, D., Koda, K., 2013. Seismic reinforcement of viaduct columns integrated with retaining walls (in Japanese), Summary of the 68th Annual Conference of the Japan Society of Civil Engineers, 157-158.

Wakamatsu, K., M.Matsuoka, 2013. Nationwide 7.5-Arc- Second Japan Engineering Geomorphologic Classification Map and Vs30 Zoning, Journal of Disaster Research, Vol. 8, No. 5, 904-911.

Yamazaki, F., Onishi, J., Tayama, S., Takano, T., 1998. Development of Fragility Curves for Expressway Structures in Japan (in Japanese), Proceedings of the 10th Earthquake Engineering Symposium, 3491-3496.

SESSION C

URBAN SAFETY & DISASTER MITIGATION: DISASTER MITIGATION & URBAN PLANNING / EMERGENCY RESPONSE

EVALUATION OF EVACUATION PATH DURING EARTHQUAKE DISASTER CONSIDERING RISKS OF A FALLING OBJECT AND CROWD CONDITION

K. TAKADA[1], K., MIYAUCHI[2] and M. NISHINO[3]

[1] Professor, Tokyo Denki University, Hatoyama-tyo, Japan;
[2] Doctoral Student, Tokyo Denki University, Hatoyama-tyo, Japan;
[3] Undergraduate Student, Tokyo Denki University, Hatoyama-tyo, Japan
Correspond to Prof. K. TAKADA (takada67@gmail.comg)

***Keywords**: earthquake disaster, falling objects, crowd condition, evacuee assignment*

1. BACKGROUND

Falling object from walls and roofs may injure evacuating people during earthquake disaster. Meanwhile, density of evacuating people on the road would be a key factor to decide safety level of evacuation route. Therefore, the safety level of evacuation route should be evaluated by considering the risk of falling objects and the density of evacuating people on the road.

In this study, Senju district in Adachi ward, Tokyo is focused on because there would be congested by the evacuating people after an occurrence of Tokyo metropolitan earthquake. An index presenting the risk level of falling objects was developed. Moreover, the evacuation route choice model was estimated by applying multinomial logit model and probability to be chosen for the evacuating route was calculated by the estimated model. In consequence, it is shown that decrease in density level could contribute to increase safety level in the evacuation.

2. DEVELOPMENT OF INDEX

Figure 1. shows the ideal situation during earthquake disaster. h[m] and b[m] indicate height and width of building respectively, L[m] and W[m] indicate length and width of road respectively, and V[m/s] indicates moving speed of evacuating people. Influenced area of falling objects is shown by shaded rectangles in Figure 1.

The influenced area of falling objects depends on height of the buildings as described in eq. (1). The initial horizontal speed is assumed to be 1.11[m/s] as mentioned in the report [1]. By integrating eq. (1) regarding the height, the risk of falling object from whole surface of the wall is derived as shown in eq. (2).

$$x = \sqrt{h}/2 \qquad (1)$$

$$\mathrm{R(h)} = \frac{1}{3}\sqrt{h^3} \qquad (2)$$

Moving speed is assumed by eq. (3) by utilizing a concept of Fruin [2]. Here, D is derived by eq.(4). Q is number of evacuating people on road link.

$$V=1.36-0.341D \qquad (3)$$

$$D=Q/WL \qquad (4)$$

Finally, the risk of falling object of road link is derived by eq.(5). K_0 is unit risk per second and T[s] is duration while evacuation people stay in the road link.

$$K = K_0\mathrm{T} = \left(\sum \frac{1}{3}\sqrt{h^3}b\right)T \qquad (5)$$

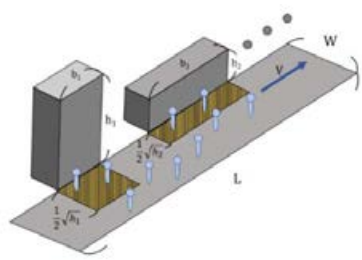

Figure 1. Ideal situation during earthquake disaster

3. EVACUATION ROUTE CHOICE

Questionnaire survey was conducted. Each respondent was requested to fill in the expected evacuation path on the map under certain conditions as shown in Table 1. Evacuation path choice model was estimated by multinomial logit model. Shortest path, a path through national road, and other path which was mentioned by respondents were included in choice set. The estimation result is shown in Table. 2.

Table 1. Condition setting

	Road congestion	Spreading fire	Falling objects
Condition 1	○	×	×
Condition 2	×	○	×
Condition 3	×	×	○
Condition 4	○	○	○

Table 2. Evacuation path choice model

	Explanator variables	unit	Estimates	t -value
congestion	Path length for female	km	-5.78	-1.17
	Total length of the road with more than 5.0m width	km	13.65	2.31
	Detour rate for the shortest path for female	%	-0.19	-0.32
spreading fire	Path length for female	km	-4.6	-0.72
	Total length of the road with less than 3.0m width	km	-8.62	-3.71
	Detour rate for the shortest path for female	%	1.05	2.15
falling object	Risk of falling object		-0.81	-1.04
	Total length of the road with more than 5.0m width	km	13.12	2.43
	Detour rate for the shortest path for elder person (over 70)	%	1.6	2.34
Log-likelihood			0.43	
Samples			148	
Hit ratio		%	61.5	

REFERENCES

[1]The Japan Building Disaster Prevention Association

[2]Fruin, John J. Pedestrian Planning and Design. New York: Metropolitan Association of Urban Designers and Environmental Planners, Inc., 1971.

A case study on land-use and transport relationship in Yangon

Hnin Su Mon WIN[1] and Theingi SHWE[2]
[1]Ph.D. Candidate, Department of Architecture,
Yangon Technological University,
Myanmar
hninsu.hsmw.ytu@gmail.com
[2]Professor and Head, Department of Architecture,
Yangon Technological University,
Myanmar

ABSTRACT

As Yangon is one of the busiest and major commercial cities with the most populated division throughout the country, it suffers lots of pressures for the city's development, especially for city's transportation and land utilization issues. This article describes a study on the current planning of land utilization and transport relationship in Yangon. The paper begins with an examination of the continuing tensions between land-use and transport planning and contains identifying issues of planning frameworks by the local government. Then, the linkage between transportation and land use evaluation process applied urban volume rate and road area ratio. The result suggests that the existing land-use and transport planning system needs to integrate to achieve better city planning design and minimize the current traffic problems.

Keywords: *Land-use Planning, Transport Planning, Urban Volume, & Split Model*

1. INTRODUCTION

Because of the accelerated process of urbanization and demand for urban transportation systems has been dramatically increased and changes in land utilization is a major phenomenon especially in the major cities. Currently, Yangon faces a high tension of traffic pressure for the development of the city and lack of integration between land-use and transportation. This paper is aiming to research this area to realize the current condition of the urban transport systems, effective coordination and interaction between land-use and transportation system and mutual relations system are significant.

Like other major cities from developing countries, it generates four major issues for the development of Yangon city: increased population, housing demand, employment locations and movement problems which are inter-related each other. Among these four issues, a linkage between transportation system and land-use regulation system of Yangon city has been studied in this paper to examine the current tensions as well as finding out the existing condition between supply _ the capacity of road networks, and demand while a study on the land utilization frameworks and transport planning. However, there are several methodologies and valuation tools have been advocated to assess the case studies, research methodology to evaluate the coordination between transportation and land-use will be calculated with urban volume rate and road area ratio calculation methodologies to identify the supply and demand conditions of transport network situation.

1.1. Physical Growth Pattern and Population of Yangon

Since 2005, Yangon, the former capital of Myanmar, had been officially marked as the second capital city of Myanmar after the development of the new capital city: Nay Pyi Taw which is an administrative capital city is located in lower Myanmar. According to the historical records, the city had been founded by King Alaungpaya after conquered Dagon, a small fishing village, in 1755 and retitled it "Yangon – means the end of strife". After being a colonized country by the British in 1885, they constructed Yangon (formerly known as Rangoon) as a new city design with a grid plan on delta land by a Bangel Engineer Lit. Fraser. The city was only 86.20sq.km in 1940 and it was originally planned for only 50,000 populations. And then it was expanded towards the north and became 208.51sq.km in 1974. Later, it grew towards east and west directions with 346.13sq.km in 1985 (Moe, 1992 & YCDC, 2012) as shown in (Figure 1). The physical development of the city has been strongly affected by its original location and geography which is located between the Hlaing River, Pazundaung Creek, and Yangon River. The city population has increased also increased from 50,000 populations in 1941 to nearly 5.2 million people in 2018.

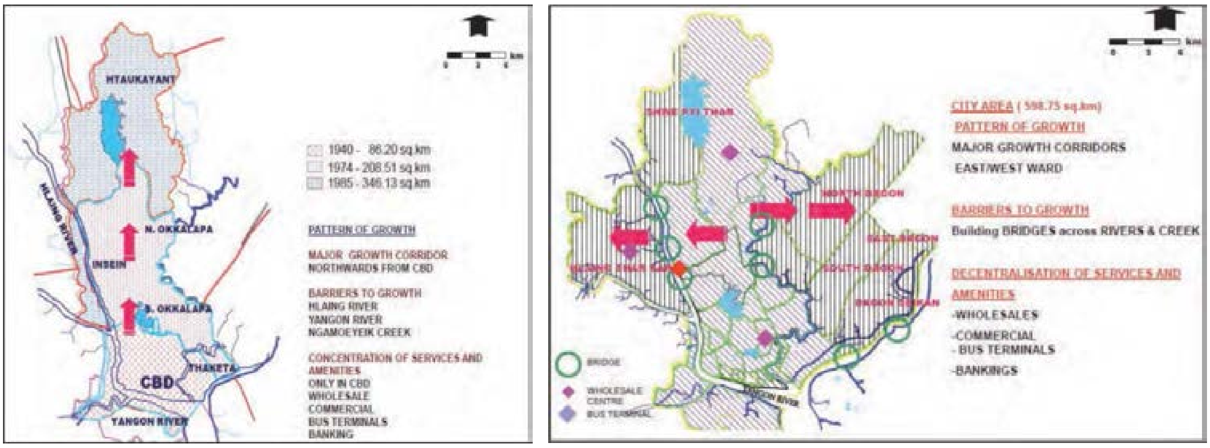

Figure 1: Physical Growth Pattern of Yangon City (DHSHD, 2000)

2. NATURE OF LAND-USE AND TRANSPORT RELATIONSHIP AND APPLIED METHODOLOGY

As many scholars claim that land use and transportation has a strong link where people settle in certain places where facilities are closely located such as houses and workplaces, amenities as well as health care and educational facilities. However, the choice of settling places is not satisfactory when the levels of transportation facilities are poor and unreliable, squatters and informal settlements occur. Besides, the level of income, mode of choice and route choice, trip distribution and travel duration between two destinations points influence the mechanism of the entire urban transportation system. Nonetheless, travel behavior plays a vital role as it may change the result of the entire framework between land use and transportation by the nature of its society.

According to Mackett (1985), he defines a framework as shown in (Figure 2) for land use and transportation cycle based on form, function, land use and transport. He also claims that activities may change rapidly when policy change while the physical infrastructure has a slow response during the mismatch responses of planning stages. Moreover, (Figure 3) represents the relationship between land-use and transport system.

	Forms	Functions
Land Use	Buildings & Physical Infrastructure	Activities (Residing, shopping, working, travel, etc.)
Transport	Channel	Flows

Figure 2: Framework for analysis of cities (Mackett, 1985)

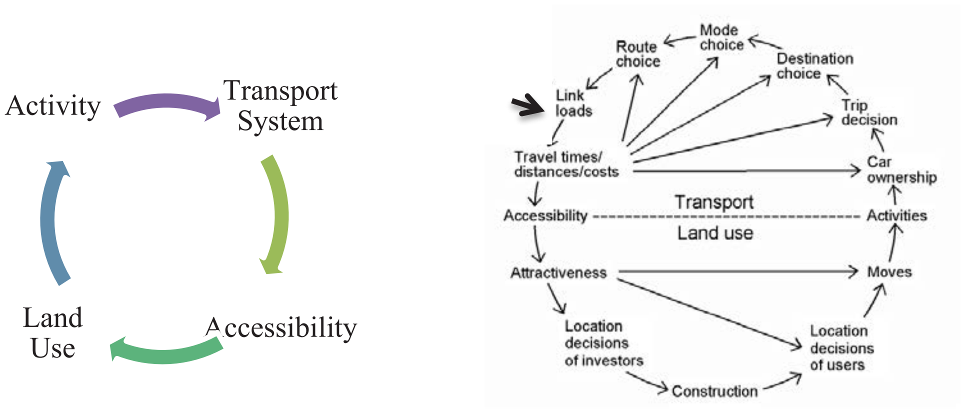

Figure 3: Land-use Transport Cycle

Similarly, based on the findings of Ewing et al. (1994) sprawl dwellers compensate for poor accessibility by linking more trips in multipurpose tours. Also, gender difference and dual worker households may affect travel activity patterns. Trip-chains are, therefore, an example of travel behavior that could be investigated to better understand the land use and transportation linkage.

However, it can be argued that people who live near the transits oriented or neo-traditional development generate shorter trips and frequent usage than the outer urban rings or outskirts areas while neo-traditional design contains a town center, connected grid street patterns, proximity between land use, on-street parking for narrow residential streets and small residential lots with public parks and open spaces. Many studies identify that there is a strong relationship between land use characteristics and travel behavior. Kitamura et al (1997) argue that person trip generation is largely determined by demographic and socioeconomic characteristic but not associated with the land-use characteristics. In contract, Frank and Pivo (1994) and Cervero and Radisch (1996) indicate that density and mixed land use area related to mode choice for both work and shopping trips while neighborhood characteristics were found to exert their strongest effect on local non-work trips including walk trips as substitutes for auto trips. According to the elements of a city plan by Frederick Law Olmsted, Jr. mentions the three main divisions of city planning and which are circulation of both transportation and communication, the lands devoted to all other public purposes, and the land to private ownership.

To calculate urban volume (equation 1) and road area ratio (equation 2) has been utilized as followings:

$$R_1 = \frac{C_{building}}{C_{land}} \text{, where,} \quad (1)$$

R_1=urban volume rate, $C_{building}$=urban building area (m^2), C_{land}= urban land area (m^2)

$$R_{21} = \frac{C_{road}}{C_{building}} \text{, where,} \quad (2)$$

R_2=road area ratio, C_{road}=road-used land (m^2), $C_{building}$=urban-used land area (m^2)

Model split indicator has also been applied to investigate the interaction between mode of choices, and the study of existing land-use mapping from YCDC to understand the formation of trip attraction points to move around the city.

3. INSTITUTIONAL DEVELOPMENT OF LAND-USE AND TRANSPORT PLANNING IN YANGON

Land-use zoning map of Yangon contains major six categories: residential, commercial, industrial, agriculture, government and institutional, special zonings such as religious, green and blue, heritage, etc. Land-use planning of Yangon can trace back till the development of Rangoon Development Trust Act (RDT Act-1920) which can be divided into four periods: from 1920 up to Second World War, post-war Independence period (1948-1962), the period from 1962-1988, and 1988-1992 (Moe, 1992).

After 1988, largest land use development projects in the history were planned and implemented in 1990, compromising four new suburban townships each accommodation over 150,000 populations by the State Law and Order Restoration Council and the scheme was responsible by the Department of Human Settlement and Housing Development (DHSHD) which was similar to that of the late 1950s squatter resettlement programs, except the scale and the magnitude. In addition, Thein Gyi Shopping Center Project was implemented by YCDC to provide over 100,000 sq.ft for both shopping space and office space similarly and completed in 1994. Although wholesale business center and warehousing used to be located in the west end of CBD, starting from 1990, these activities have been moved toward the north and north-east area. Private sector housing can be found in inner urban areas such as Sanchaung, Ahlone, Tamwe and Pazundaung Townships with new 3-4storey walk-up apartments although it is originally intended for low-density single family houses. Another transport-related project is Yangon International Airport and runway extension project as well as bridges across Bago and Hlaing Rivers which have a significant impact on the city.

Transport planning of Yangon city can be divided into three major functions: Transport Infrastructure, Operation, and Traffic Management under the management of Urban and Regional Planning Division of DHSHD and later Roads and Bridges Department of YCDC. The Yangon City Transport Management Committee (Central) has the highest authority especially for the public transport provision operations in the city which is now chaired by Mayor of Yangon City and responsible for the overall public transport system in the city on daily basis.

4. STUDY ON THE CURRENT SITUATION OF LAND-USE AND TRANSPORTATION IN YANGON

Current Yangon City is composed of 4 districts with 33 townships under the management of Yangon City Development Committee (YCDC) whereas the whole Yangon region contains a total 45 townships. The Central Business District (CBD) area, the old Fraser Plan, with 6 townships, has 33.2 sq.miles. The current land utilization of 15 townships including CBD, is shown in (Figure 4). Residential and employment densities also influence the transport and land-use interaction as well as trip length, mode of choice and trip frequency.

Although there is different mode of transport systems in the city, the majority of the city's transport share is owned by public bus transport system and it is managed by Yangon Region Transport Authority (YRTA). The model share of transportation in Yangon City is shown in

(Table 1) while water-bus transport service is private investment, unlike, sub-urban rail and circular rail transportation which is managed by a government sector, Myanma Railway.

Descriptions		
1	A	Low Rise Residential
1	B	Mid Rise Residential
1	C	High Rise Residential
1	D	Mix Use Residential
2		Commercial
4	A	Port & Related
4	B	Government & Institute
4	C	Military
5	A	Green & Blue
5	D	Religious

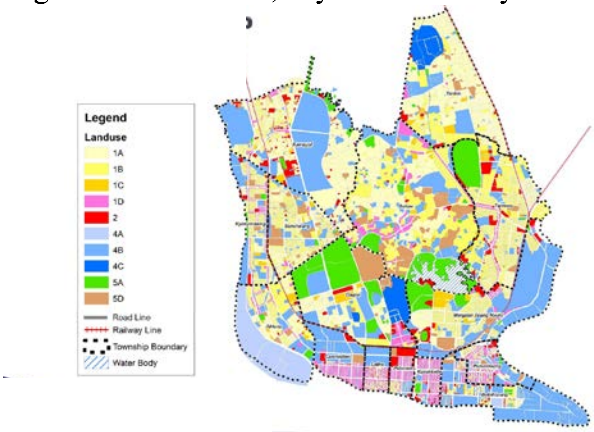

Figure 4: Current Land Use Map of 15 Townships in Yangon (Kyi, 2017)

Table 1: Mode of Transportation & Model Share (YCDC & DRTA, 2000) (JICA, 2014)

No.	Mode of Transport	Model Share (%) [2000]	Model Share (%) [2014]	Current Mode of Transport Remarks
1.	Buses (Public Transport)	87.7%	63%	Over 300 routes with over 5000 buses – over 1.2millions passengers/day
2.	Sub-urban Rails & Circular Rails	2.1%	1.4%	38 stations 29.5 miles for circular train – nearly 92000 commuters/day
3.	Water Bus & Fairies	1.3%	3.2%	7 stops (from CBD to Insein Township – 7 stops + weekend special trips to Kyauktan
4.	Motorcycles	N/A	9.3%	Limited use – 31 out of 33 townships legally prohibited
5.	Bicycles	N/A	N/A	Limited use inside CBD
6.	Taxi & Private cars	8.9%	21.4%	Available but more expensive than any others
7.	Others	N/A	1.7%	Limited use of trishaws inside CBD

As a result of the dominant use of buses for transport communication, most of the traffic solutions occur especially on the road networks. While many people moving towards CBD and inner urban area and old suburb area to access a variety of facilities such as better job opportunities, shopping centers, movie theatres, and other recreational facilities from the new suburb area as well as peripheral areas where accessible amenities are less favorable.

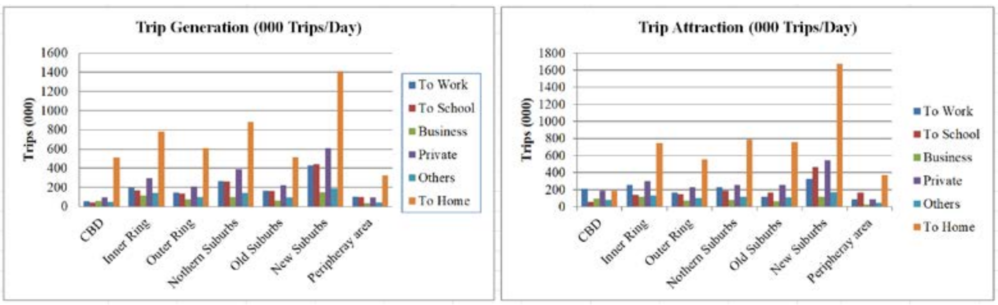

Figure 5: Trip Generation and Trip Attraction by Urban Area (YUTRA, 2014)

4.1 A Case Study of CBD Area

Taking CBD area (6 townships) as an example to validate the model, and the result is as shown in (Table 2) although the Seikken Township data is not available as the majority of the land use categories is for port, factory, and storage areas. Table 3 describes the result of the township data for urban volume rate and road area ratio by utilizing ArcGIS Earth, visual survey analysis methods has been applied and is shown in (Table 2).

Table 2: CBD Area Urban Volume Rate and Road Area Ratio

Township	**Total Urban Land Area (m^2)** (MIMU,2019)	**Total Street Area (m^2)** (ArcGIS Earth)	**Building Coverage Area (m^2)**	**Urban Volume Rate (R_1)**	**Road Area Ratio (R_2)**
Lanmadaw	1300000	133253.6	1166746.4	0.90	0.10
Latha	603000	118758.9	484241.1	0.80	0.20
Pabedan	617000	76907.9	540092.1	0.88	0.12
Kyauktata	701000	89785.2	611214.8	0.87	0.13
Botahtaung	1170000	136717	1033283	0.88	0.12
Seikken	2600000	N/A	N/A	N/A	N/A

4.2 Problems resulting from the Fragmented Land Use and Transport Planning

When a city's population grows, its physical boundaries need expansions and there is no difference in Yangon. The overall distance from the CBD to pre-1980s peripheral settlements were at the manageable level which is around a 7-mile radius. Later it has been expanded especially to the north and north-east area was less the physical barriers than others and after 1988, development of new peripheral settlements along the north, northeast and north-west area: Shwe Pyi Thar, Hlaing Thaya and Dagon Myothit including both north and south and also Shwe Paukkan. As these developments are originally targeted for industrial land use with about 1000 acres each although these developments are not fully establishment-level yet resulting in the excessive journey to work time for those who have been living in these areas whatever their reasons. Also, the employment opportunities in these townships are especially for the blue-collar workers: construction labours, textile workers, and others who need manual labour jobs causing the job market still much depend on CBD and inner urban areas. Unlike, people who live in suburbs area have their private transport in the developed world but Yangon in completely contrast and majority of people entirely to rely on public transport system while the travel cost is also higher and lack of basic social facilities and demand on the transport systems and (Table 3) shows the data of travel distance and travel duration between CBD and its new suburbs areas. Nearly 25 percent of a day has been used for travelling is not a healthy solution for the city as well as for the residents.

Table 3: Travel duration and cost between CBD & new peripheral Areas

No.	**Township**	**Distance from CBD**	**Maximum Travel Duration (Peak & Off-peak)**	**Travel Cost**
1	Shwephithar	16 miles	3hr & 2hr	200-300 kyats
2	Hlaingtharyar	14 miles	3.5hr & 2.5hr	200-300 kyats
3	Dagon Myothit (North)	14 miles	3.2hr & 1.7 hr	200-300 kyats
4	Dagon Myothit (South)	12 miles	2 hr & 1.5hr	200-300 kyats

Note : Peak hour – between 7am - 9am and 5:15pm – 6:30pm

5. CONCLUSIONS

In summary, land-use and transport planning practices need to integrate for the sustainable development of the city planning, for example, the later development of Yangon city is facing lots of pressure on the transportation as a result of neglecting on the land-use categories and development plans by both government and private sectors. Utilization land-use transport models are essential to spatial planning of urban area for all type of land uses.

REFERENCES

Frederick Law Olmsted, Jr. 1916. *Introduction, Basic Principles of City Planning* John Nolen (ed.), *City Planning: A Series of Papers Presenting the Essential Elements of a City Plan,* NY: D. Appleton and Company, 1-18.

ALMEC Corporation, Oriental Consultants Co., Ltd and Nippon Koei Co., Ltd (2014) *Project for Comprehensive Urban Transport Planning of the Greater Yangon (YUTRA) Final Rreport*, Vol 1.

Srinivasan, S., 2000. *Linking Land Use and Transportation: Measuring the Impact of Heighborhood-scale Spatial Patterns on Travel Behaviour*. PhD Dissertation. Department of Urban Studies and Planning, Massachusetts Institute of Technology: USA.

Than Moe. 1992. *Integrated Land Use Transport Planning in Yangon*. MSc. Dissertation. University of Wales College of Cardiff. Department of City & Regional Planning: Wales.

YCDC, 2012. *Facts about Yangon*.

Yujie Sun, Wenxin Qiao, Yongsheng Zhang and Yang Yang, 2015. GIS-based urban land use and traffic coordination evaluation system, *Applied Mechanics and Materials*, Vol 738-739 Trans Tech Publications, Switzerland, 204-208.

Zaw Zaw Aye, 2001. *The Transportation Management System in Yangon: A Focus on Easing the Traffic Congestion.* Master Thesis, Asian Institute of Technology, School of Environment, Resource & Development: Thailand.

BASIC ANALYSIS OF AIRCRAFT DIVERT DESTINATION SELECTION DURING LARGE-SCALE NATURAL DISASTERS USING AIR TRAFFIC CONTROL DATA ~CONSIDERRING THE VULNERABILITY OF THE AIRPORT~

R. FUJII[1], M. FUJIU[2], Y. MORISAKI[3], J. TAKAYAMA[4], and Y. SHIOZAKI[5]

[1] Undergraduate Student, Dept. of Environmental Design, Kanazawa University, Kanazaawa, Japan,
[2] Associate Professor, Geosciences and Civil Engineering, Kanazawa University, Kanazaawa, Japan,
[3] Doctoral Course Student, Dept. of Environmental Design, Kanazawa University, Kanazaawa, Japan,
[4] Professor, Geosciences and Civil Engineering, Kanazawa University, Kanazaawa, Japan,
[5]Specially Assistant Professor, Geosciences and Civil Engineering, Kanazawa University, Kanazaawa, Japan,
Correspond to Makoto FUJIU (fujiu@se.kanazawa-u.ac.jp)

Keywords*: Airport, Aircraft, Divert, Disaster*

1. INTRODUCTION

In recent years, there have been many natural disasters in Japan, causing tremendous damage. Among them, damage to the airport function has also occurred. Due to Typhoon No. 21 on September 4, 2018, Kansai International Airport was flooded, and it took 10 days to recover the domestic flight due to the damage of the power outage. Also, on September 6, 2018 at 3:07:59, the Hokkaido Iburi Eastern Earthquake occurred, and the maximum seismic intensity recorded seismic intensity 7. New Chitose Airport became inoperable due to the damage caused by large-scale blackouts and earthquake damage, and it took time to recover. If an airport is damaged in the aviation field where high safety standards are required, it will have a major impact not only on the airport facilities but also on the operation of the aircraft. Based on the above, more effective measures such as reselection of divert destinations and improvement of CIQ facilities are required. As a pre-stage for the construction of these countermeasures, it is considered necessary to grasp the flight status of the aircraft at the time of the disaster. Therefore, the purpose of this study was to understand the flight situation of the aircraft using the aircraft track data and clarify the danger at the time of disaster occurrence. As an example, we analyzed based on the assumption that Tokyo International Airport was damaged.

2. ANALYSIS

In this analysis, we analyzed Tokyo International Airport, which has the largest number of aircraft departures and arrivals among airports in Japan, in order to understand the aircraft that should be dealt with in the event of a disaster.

CARATS Open Data was used as usage data. CARATS is an abbreviation for Collaborative Actions for Renovation of Air Traffic Systems. This is a wake of aircraft nationwide created from radar data, etc., and includes data for approximately 640,000 flights for 24 weeks from 2012 to 2015. Reserch and development is expected to realize the long-term vision of CARATS, which is used for applications such as discovery of problems and facts useful for improving the operation of air traffic management, analysis of factors, and evaluation of proposed operation improvement methods.

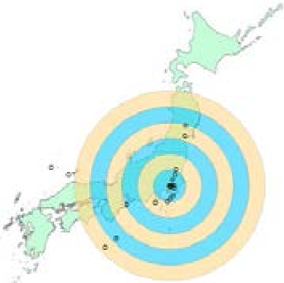

Figure 1. Aircraft Flight Position

It was assumed that New Chitose Airport was hit by a large-scale blackout due to the Hokkaido Iburi Eastern Earthquake last year, but Tokyo International Airport was in the same state. The analysis was carried out based on the assumption that the control work would be impossible due to a power outage at 22:30, targeting the 22:00 range with many landing aircraft at Tokyo International Airport. We used all flight data from 18:00 to 24:00 on March 7, 2013 from CARATS Open Data. The data of the aircraft heading to Tokyo International Airport at 22:30 was extracted from a huge amount of aviation data.

3. CONCLUSIONS

Figure 1 shows the flight position of the aircraft near Tokyo International Airport at 22:30. The control area of each airport is within a radius of 9km. In this analysis, at 22:30, 2 aircraft were in control of Tokyo International Airport and 18 aircraft were flying to Tokyo International Airport. If the control tower of Tokyo International Airport becomes temporarily inoperable, 2 aircraft in flight in the control zone are waiting for instructions such as landing, so immediate action is required. Since the other 18 aircraft cannot land at Tokyo International Airport, it is necessary to allocate a divert destination. Assuming that the control work becomes impossible due to a power outage, etc., the assumption is insufficient, suggesting the need to take immediate measures. As future tasks, we will expand the target time and analyze at other airports to understand the flight status of the aircraft in more detail.

REFERENCES

[1] Ministry of Land, Infrastructure, Transport and Tourism, http://www.mlit.go.jp/common/001264807.pdf

DEVELOPMENT OF AGENT-BASED FLOOD EVACUATION SIMULATION FOR SUPPORTING LOCAL GOVERNMENT EVACUATION PLANNING

J.H. KIM[1], T.S. EDA[2], I.P. HARADA[3], K.H. AYUKAWA[3], T.H. MUKAI[4], T.A. KATO[5]

[1] *Project researcher, KATO Takaaki Lab(Social Safety System),Institute of Industrial Science, the University of Tokyo, Tokyo, Japan,*
[2] *Research Fellow, KATO Takaaki Lab(Social Safety System),Institute of Industrial Science, the University of Tokyo, Tokyo, Japan,*
[3] *Senior Reseacher, Intrabasin Communications Division,Foundation of River & Basin Integrated Communications, Japan*
[4] *Director, Intrabasin Communications Division,Foundation of River & Basin Integrated Communications, Japan*
[5] *Professor, International Center for Urban Safety Engineering(ICUS),Institute of Industrial Science, the University of Tokyo, Tokyo, Japan,*
Correspond to J.H. KIM (kimjah@iis.u-tokyo.ac.jp)

***Keywords**: Flood evacuation analysis, Evacuation planning, Planning support system, Individual evacuation timeline, Agent-based simulation*

1. INSTRCUTIONS

The recent precipitation pattern shows increase in occurrence of concentration rainfall and the intensity of rain is getting stronger. Furthermore, due to the influence of recent climate change, there are greater worries toward more flood damages and large-scale damages.

To prevent such damages, considering the experience of flood damage mentioned above and prospect of climate change, the central and local governments are reviewing various measures to prevent large-scale flood damage. However, there are no quantitative evaluation or verification method or tools for quantitative analysis needed to establish evacuation plans in local government level, there are great difficulties for each local government to establish concrete and comprehensive evacuation plans.

Thus, the purpose of this study is to develop a flood damage evacuation simulator that can support the establishing of evacuation plans by local governments through evaluation of the characteristics of the area such as the status of the shelter, population density, road network structure, etc. and quantitative assessment of evacuation timing.

2. BUILD SIMULATION MODEL

The simulations built in this study were conducted on the entire municipalities and surrounding areas in order to consider wide-area evacuation from the results of previous studies, which were mostly conducted on a part of the area or analyzing evacuation capacity within the area. In this way, it was possible to express large-scale evacuation according to the occurrence of large-scale flooding and to verify the evacuation situation according to evacuation timing by enabling quantitative analysis according to the timing of evacuation.

Concretely we choose to find a shelter by car and walk on foot. We make it considerably in the capacity of shelter by classifying district internally and externally. Also, we make it review the status of refuge in accordance with traffic jam and congestion with numbers of refugees by considering the capacity of refuge flow with the road network's structural characteristics.

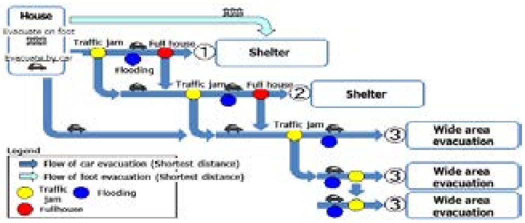

Figure 1. Building a Simulation Model: Evacuation Behavior Flow

3. COMPOSITION OF THE SIMULATION

This study bases on three-step analysis to establish evacuation plans. The first step is to carry out basic analysis with GIS in order to understand regions. The second step is to implement analysis(simulation zero) that introduce the worst case using simulation, and to understand characteristics of regional evacuation problems.

On third step, figure out(simulation A) the city structural feature for the capacity of evacuation and the flow, and act, and execute the verification(simulation B)on each scenario for establishing ideal evacuation plans such as evacuation tools, demand control on its target population and the timing, and so on, based on it.

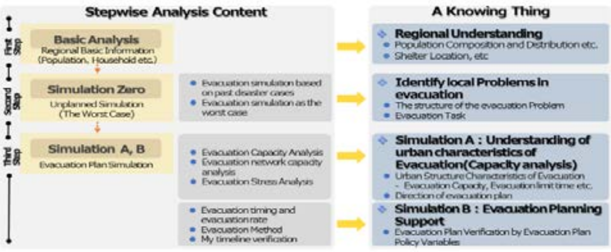

Figure 2. Evacuation Plan Establishment Using Flood Evacuation Simulation

4. CONCLUSIONS

This study developed a simulator that makes a quantitative measurement of evacuation conditions possible, considering space characteristics of regions such as shelters, road networks, population distributions on the rate of timing in beginning evacuation, in order to support establishing proper evacuation plans while reviewing those of massive flood damage.

From the scenario analysis of JOSO City derived from this simulator, we were able to identify the maximum capacity of an ideal(safe) evacuation on foot and via cars taking into account the structural characteristics of the city. This is considered to be an important indicator in establishing an evacuation plan. Based on this, various evacuation measures, such as a reduction in evacuation demand or the dispersion of evacuees across time and space, were reviewed. This is expected to help local governments establish a practical evacuation plan.

REFERENCES

[1] Toshitaka Katada, Noriyuki Kuwasawa, Satoru Shida, Masaru Kojima, Scenario Analysis on Evacuation Strategies for Residents in Big Cities During Large-Scale Flood, Journal of Japan Society of Civil Engineers, Ser. B1 (Hydraulic Engineering), Vol. 69 Issue 1, April, 2013.
[2] Jyun-ichi Tomatsu, Michiyuki Hirokane, Tanaka yuudai, Evaluation of The Validity for Flood Disaster Measures by An Evacuation Simulation, Japan Society for Fuzzy Theory and Intelligent Informatics 28th Fuzzy System Symposium, September, 2012.
[3] Cabinet Office, Large-scale flood measures guidelines in the metropolitan area, 2012.

HOW MUCH DOES SOCIAL NETWORKING SERVICE AFFECT THE EVACUATION EFFICIENCY? - A STUDY USING AGENT-BASED SIMULATION

T. MINAMI[1], T. KATO[2]

[1] Graduate Student, Department of Urban Engineering, School of Engineering, the University of Tokyo, Japan,
[2] Professor, Institute of Industrial Science, the University of Tokyo, Japan,
Correspond to T. MINAMI (minami-t@iis.u-tokyo.ac.jp)

Keywords: *evacuation, decision making, agent-based simulation, social networking service*

1. INTRODUCTION

Recently SNS (Social Networking Service) is widely used when people communicate with each other. It is also applicable to post-disaster situations. At 2011 Great East Japan Earthquake, 16.7 % of people living near Tokyo used Twitter to get information about evacuation centers [1]. While SNS can be helpful in finding uncrowded centers, there are also some risks that a specific information is explosively spread in short time, which contrarily brings disorder.

In this research, by running a simulation model of people's evacuation behavior which includes information exchanging activity, we investigate the effect of SNS on the overall efficiency of the evacuation.

2. METHODOLOGY

We create an agent-based evacuation simulation model where each person agent will evacuate to an evacuation center, introducing in it an SNS-like information exchanging system. By running it for some SNS use scenarios, we examine the change of the efficiency in some aspects.

3. SIMULATION DESIGN

In 500x500 space, we place 5,000 people and 25 evacuation centers randomly (Fig.1). When a disaster occurs, each person starts to find an evacuation center to be in. Only 20% of the people know the nearest center at the beginning and the remainder will follow the leader.

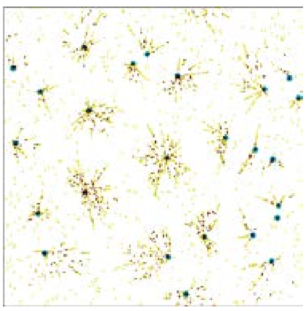

Figure 1. An example of the simulation execution

R_{use} is a parameter which stands for the SNS utilization rate. A person who uses SNS can communicate the congestion information to his/her followers.

When an evacuee arrives at a center, he/she decides whether to enter or not, considering the crowdedness. If the congestion rate exceeds his/her tolerance, he/she does not enter and sets the new destination. If he/she is an SNS user, he/she will also decide whether to send the congestion report to the followers or not.

SNS users can also read the *timeline* where posts from people whom they follow are listed. Based on the congestion information there, they can change the destinations. They can also *repost* (forward the post he/she received to his/her followers) some information, which enables a single congestion report to reach many people.

4. RESULTS

In order to evaluate the effect of SNS, we change the SNS utilization rate R_{use} from 0% to 100% by each 10%. We run each scenario in 10 different patterns of evacuation center distribution (D.P. = Distribution Pattern).

The average evacuation time (AET) tends to decline when R_{use} goes from 0% to 20%. However, when it goes to higher than 20%, AET stays flat or sometimes increases. The maximum evacuation time (MET) has the same trend, and the gap between the most and the least time-consuming D.P. is reduced as R_{use} increases (Fig.2).

For the population balance among centers, the final variance σ_f clearly becomes lower in every D.P. as R_{use} goes up. In particular, the D.P. 6, where the variance is the highest at $R_{use} = 0\%$, has the largest decrease (Fig.3).

These results indicate that the initial disparity among areas which derives from the geographical characteristics can be flatten by the information spread through SNS.

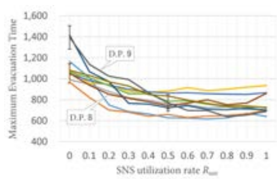

Figure 2. R_{use}- MET relation

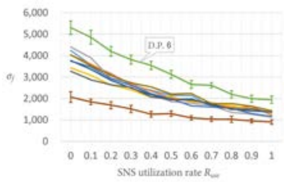

Figure 3. R_{use}-σ_f relation

5. CONCLUSIONS

In this research, we gained the following conclusions:

1) SNS can help to redress the population balance among evacuation centers.

2) SNS can also reduce the evacuation time when its utilization rate is low. However, it sometimes brings the adverse effect when the utilization rate is high. We need to take it into consideration to make an evacuation plan.

REFERENCES

[1] T. Kawai, H. Fujishiro, Use of Twitter in the disaster information after the Great East Japan Earthquake. Corporate communication studies, 17 (2013) 118–128.

COLLAPSE ANALYSIS OF R.C BUILDINGS SUBJECTED TO BLAST LOAD USING AEM

M. Pavan Kumar[1], **G.K. Chaitanya**[2] **and K. Rambabu**[3]

[1] *Ph.D Scholar, Department of Civil Engineering, Andhra University, India,*

[2] *Project Assistant Professor, Institute of Industrial Science, University of Tokyo, Japan*

[3] *Professor, Department of Civil Engineering, Andhra University, India,*

Correspond to Prof. M. Pavan Kumar (pavanidea@gmail.com)

Keywords: *Collapse analysis, AEM, blast load, debris analysis*

1. INTRODUCTION

There is a considerable demand to study the blast phenomenon to understand the mechanism and provide essential guidelines on keeping critical buildings blast resistant or blast-proof. One of the principal activities in this field is to study and understand the behavior of a building when subjected to a blast. This study provides a methodology to study the collapse behavior of a building.

2. METHODOLOGY

We propose a comprehensive collapse assessment method by simplifying numerical blast mechanism into (1) collapse of the structural component; (2) debris analysis and (3) residual capacity of remaining building.

2.1 Collapse evaluation of the structural part

In this study, the energy absorbed by the building due to blast load is calculated using $\int a^2 dt$. This form of intensity represents the overall duration, amplitude and frequency change of building due to blast.

2.2 Debris analysis of the building

The debris is calculated using the number of disintegrated elements from the building. In this analysis, the percentage of the collapse of the structural part of the building at every storey level is obtained. Further, the velocities of disintegrated elements are studied

2.3 Residual capacity of the undamaged part

To understand the residual capacity of the undamaged frame, inter storey drifts are calculated at each storey.

3. NUMERICAL SIMULATION

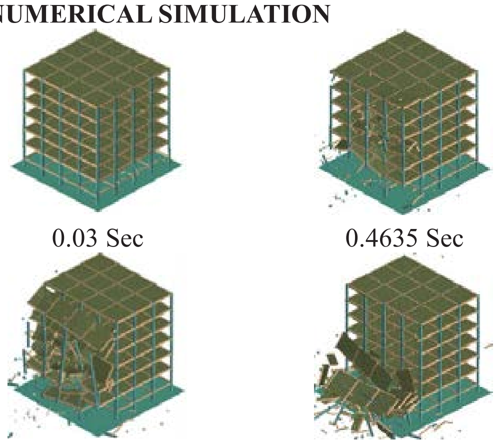

Fig.1 Collapse analysis of a building

A typical RC building as a case study has been considered, which has 6 storeys and 4 bays in each direction, a bay width of 4m, storey height of 3m, and foundation depth of 3m. The numerical analysis is based on AEM. The input blast load was fixed surface blast load of charge weight 2500kg TNT at a range of 10m.

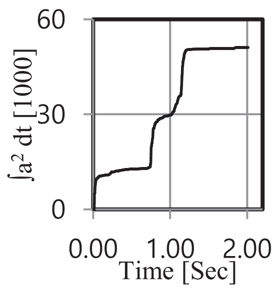

Fig. 2 Collapse

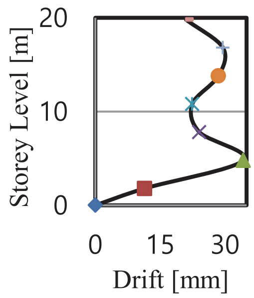

Fig. 3 Residual

4. RESULTS AND DISCUSSIONS

The overall damage could be seen in Fig. 1. The Collapse analysis is shown in Fig. 2 where, the maximum energy is absorbed before 0.1 and is further saturated. A jump in energy release at 1.15 seconds and 1.70 seconds which attributes to heavy damage and physical collapse of components. The debris analysis as inTable 1, shows that the structural debris is from slabs. This is due to exposure of slab directly to blast. Residual Capacity is shown in Fig 4 and the maximum inter storey drift ratio in this case is 1.15% which is lesser than 4%, recommended by FEMA 356 for collapse prevention.

Table 1: Debris of structural part of SFR

Storey Level	Debris (%)		
	Beam	Columns	Slabs
Plinth Lvl.	20.01	20	N/A
Stilt floor	19.72	20	25
Gr.floor	19.72	20	25
1st floor	19.72	20	25
2nd floor	19.72	20	25
3rd floor	19.72	20	25
4thfloor	19.72	20	25

5. CONCLUSIONS

In this research a comprehensive method has been proposed to analsyse the blast which addresses the collapse part, severity of flying debris, blockage, and also the strength and integraty of undamaged building. This assessment has various applications especially in providing guidelines for blast protection of RC buildings.

REFERENCES

[1] B.M. Luccioni, R.D. Ambrosini and R.F. Danesi, "Analysis of Building Collapse under Blast Loads", Engineering Structures, Vol. 26, Issue 1, January 2004, pp. 63 – 71, ISSN: 0141-0296.

[2] T. Ngo, P. Mendis, A. Gupta and J. Ramsay, " Blast Loading and Blast Effects on structure", The University of Melbourne, Australia, 2007.

EVALUATION OF URBAN SUNSHINE ENVIRONMENT BY SHADOW SIMULATION

Hiroko WATANABE[1], Yudai HONMA[2], Kentaro HONMA[3] and Kotaro IMAI[4]

[1] Student, Graduate School of Engineering, the University of Tokyo, Tokyo, Japan,
[2] Associate Professor, ICUS, IIS, the University of Tokyo, Tokyo, Japan,
[3] Associate Professor, IIS, the University of Tokyo, Tokyo, Japan,
[4]Professor, IIS, the University of Tokyo, Tokyo, Japan

Keywords: *sunshine environment, shadow simulation, skyscraper*

1. INSTRCTION

In this study, to clarify the sunshine environment formed by multiple buildings, we create a shadow simulation to analyze the city's sunshine environment. We focus on the overlap of the shadows of skyscrapers and other buildings and evaluated quantitatively.

In Japan, the sunshine is regarded as important as a living environment. In the high economic growth period of the 1960s, the construction of condominiums spread throughout Japan. Many middle- high-rise buildings were built and conflict occurred between the inhabitants and construction companies concerning the right to sunshine. Hence, as a measure to provide a right to sunlight the Building Standard Law was revised. As a result, disputes concerning the rights to sunlight have subsided and now are on a downward trend. However, even now, middle-high-rise buildings and skyscrapers are being built and the problem with sunlight has not disappeared. Therefore, it is meaningful to know how the sunlight environment in cities changes due to the presence of the middle-high-rise buildings and skyscrapers that are increasing in urban areas.

2. SIMULATION

A shadow simulation is conducted in the Nishi-Shinjuku area of Tokyo. Candidate points that may cause a shadow of the target building group are placed on the grid at 1 m intervals. Next, each candidate point is subjected to shadow judgment based on the result of intersection judgment between the sun position and the building wall at that time. These are not limited to buildings that bring shadow directly, but by judging all buildings. Here, building height is calculated from number average floor height of 3.5 m in 23 wards of Tokyo [1] by the number of floors data. We acquire necessary data from the building GIS data and ZmapTownII (2016) [2] in the relevant area. We set the target date and time from 8:00 am to 4:00 pm on the winter solstice day and accumulate the measured values every 15 minutes.

We consider the influence of shadow by skyscrapers from the viewpoint of both increase time and overlap time. Figure 1 shows the equal time shadow diagram. Figure 2 shows the addition-time-shadow diagram, and Figure 3 shows the superposition-time-shadow diagram.

3. CONCLUSIONS

In this study, we focus on the composite shadow made from skyscrapers and low to high-rise buildings. We evaluated the effect of skyscraper shadow on the sunshine environment of the block in terms of both the addition-time-shadow and the superposition-time-shadow.

First, superposition-time-shadows has a stronger impact to congested buildings area than addition-time-shadow does. Second, the effect of superposition-time-shadow is almost as same as that of addition-time-shadow in throughout the day.

REFERENCES

[1] Yasunobu Ashie, and Takayuki Tokairin: Examination of building heights for various building types in Tokyo 23-wards: laser measurement data, Air-conditioning and Sanitary Engineers of Japan (Transactions of the Society of Heating), 2006, 31(115), pp.51-54, 2006 (In Japanese).

[2] Housing map database Zmap-TOWNII, Official homepage.https://www.zenrin.co.jp/product/category/gis/basemap/zmaptown/index.html, May 17, 2019.

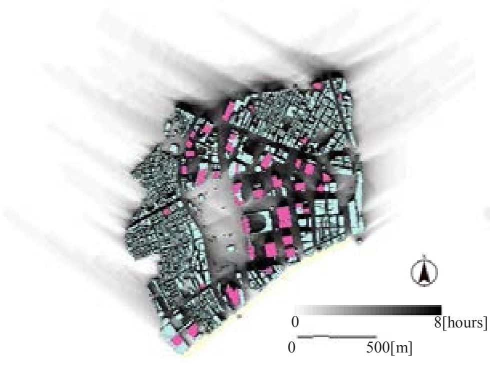

figure 1. The equal time shadow diagram

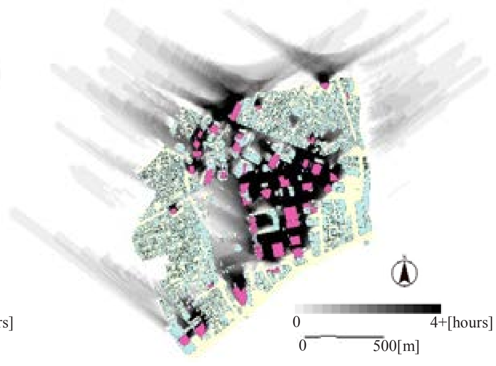

figure 2. The addition-time-shadow diagram

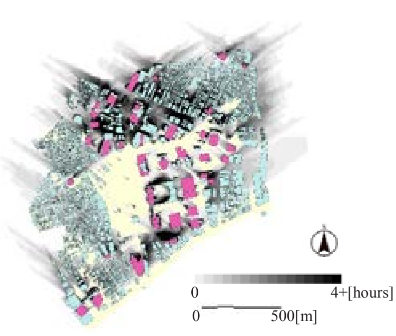

figure 3. The superposition-time shadow diagram

NUMERICAL STUDY ON EFFECT OF NEW SEISMIC RETROFITTING METHOD TO MITIGATE THE DAMAGE IN NON-DUCTILE RC FRAME WITH MASONRY INFILL WALLS

S.C.SADINENI[1], K.MEGURO[2]

[1]PhD student, Department of Civil Engineering, the University of Tokyo, Japan
[2]Director/Professor, ICUS, IIS, the University of Tokyo, Japan
Correspond to S.C.SADINENI (silpa@iis.u-tokyo.ac.jp)

Keywords: *Non-ductile, reinforced concrete, masonry infills, seismic retrofitting, disaster risk mitigation*

1. INTRODUCTION

Reinforced concrete (RC) frame with masonry infill wall construction is the most common type of construction in urban India (Figure 1). Majority of these buildings are insufficiently designed and detailed.

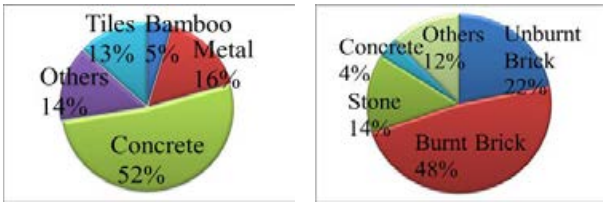

(a) Roof material (b) Wall material

Figure 1. Census urban housing data, India, 2011

Past earthquakes exposing the seismic deficiencies of these collapse prone buildings have increased the necessity for cost effective and adaptable retrofitting methods. Considering the challenges, a new method has been proposed (Figure 2) to improve the seismic performance of these buildings by a) eliminating the undesirable frame-wall interaction and b) providing the PP-band mesh in out-of-plane direction.

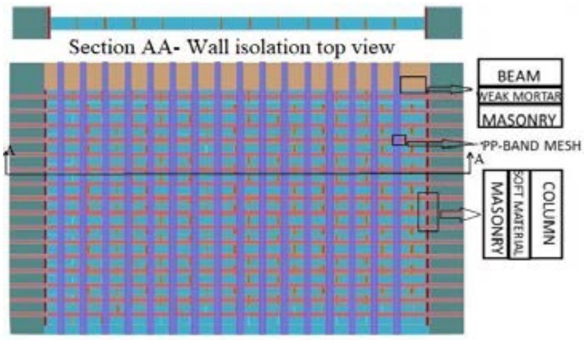

Figure 2**.** Layout of PP-band mesh detailed wall isolation method

2. NUMERICAL SIMULATIONS

In this study, seismic performance of four non-ductile 2-story frame buildings with different infill arrangement (Table 2) subjected to ground motion (Kocaeli earthquake) was determined using the three-dimensional Applied Element Simulation [2].

Table1.Non-ductile detailing of the RC frame

Section	**Dimensions (mm)**	**Longitudinal bars**	**Tie**
Column	230×230	4#12mm	#8mm@200
Beam	230×300	4#12mm	#8mm@200

Table 2: Collapse simulation of the building with different infill arrangements

	Case	Intial stage	Final stage
1	Bare Frame		
2	Tight- fit Infill	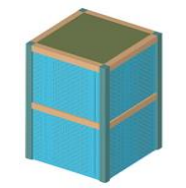	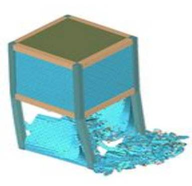
3	Isolated Infill	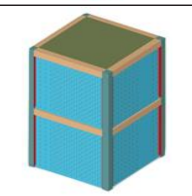	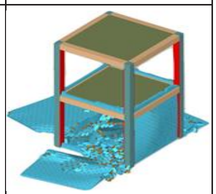
4	Retrofitted Infill	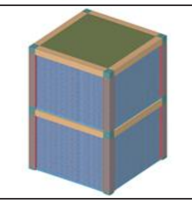	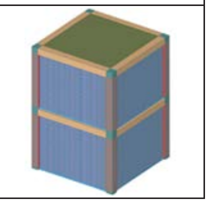

Based on the primary survey, typical features of 2-story RC buildings in India have been used for the analysis (Table 1). As shown in Table 2, Case (1) & (2) failed due to the brittle failure of columns. In Case (3), out-of-plane collapse of the walls was observed and no severe damage in Case (4).

3. CONCLUSIONS

Results showed that the infill arrangement with proposed retrofitting method prevented the brittle shear failure of the columns and out-of-plane collapse of walls.

REFERENCES

[1] National Disaster Management Guidelines – *Seismic Retrofitting of Deficient Buildings and Structures*, Government of India, 2014.

[2] Meguro, K. & Tagel-Din, H. S. (2002). Applied Element Method Used for Large Displacement Structural Analysis. *J. Nat. Disaster Sci. 24*, 25–34.

DEVELOPMENT OF GROUT FOR FILLING SUBSURFACE CAVITY

T. TAN[1], R. KUWANO[2], N. KOSAKAI[3], and M. KINJOU[4]

[1] *Student, Department of Civil Engineering, Graduate school of the University of Tokyo, Tokyo, Japan,*
[2] *Professor, Institute of Industrial Science, The University of Tokyo, Tokyo, Japan,*
[3] *Executive Officer, Cement-Related Product Department, Sumitomo Osaka Cement, Chiba, Japan,*
[4] *Cement-Related Product Department, Sumitomo Osaka Cement, Chiba, Japan.*

Keywords*: Grout, Subsurface Cavity, Permeation, Unconfined Compression Test, Re-excavability*

1. BACKGROUND

Sinkholes often occur in Japan due to aging of underground infrastructure such as sewer pipes. As a countermeasure, backfilling using excavation method has been carried out to repair them. However, this method takes huge amount of time and cost. Hence, maintenance using backfilling with cavity filling material is relatively cost-effective. The performance of grout (cavity filling material mixing with water) is highly affected by its material fluidity and the strength. In this study, permeation behavior of grout to surrounding ground was investigated to ensure there is no leakage into sewer pipes. Besides, formulation design of grout with unconfined compression tests were carried out and the optimum strength was aimed to ensure the re-excavability. The main objective is to develop new grout for filling subsurface cavity.

2. PERMEATION TEST

In the cross section of ground model shown in Figure 1, backfilled grout permeated through the surrounding ground and drained into the sewer pipe. This condition is simulated through one-dimensional column permeation test shown in Figure 2.

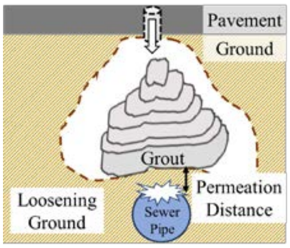

Figure 1. Ground Model

2.1 Procedure

Cylinder-shaped ground model was built with 50% and 80% of relative density. Next, the grout was poured into the model to a height of 20 cm. The permeation distance was measured after 8 hours. As shown in Figure 2, by adjusting the density of ground model, the loosening ground between sinkhole and sewer pipe can be simulated.

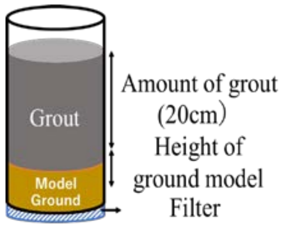

Figure 2. Permeation Test

3. UNCONFINED COMPRESSION TEST

In order to discover strength trends due to difference in design formulation, unconfined compression tests with different conditions have been carried out. Condition 1 in which different composition of main mixture and admixture (calcium carbonate or fly ash) were mixed, while curing methods of air curing or water curing are varied in condition 2. Unconfined compressive strengths of specimens were measured in 3 days, 7 days and 28 days.

3.ANALYSIS ON RESULT

In permeation test, difference in relative density did not show significant difference in permeation distance. However, the effect of particle size is not negligible as permeation distance increased with the particle size.

In the unconfined compression test results shown in Graph 1, formulation where only main mixture was used shows a relatively higher strength. Besides, curing method did not show a big difference in the strength.

Table 1. Test Conditions and Permeation Distance

	Silica No.5		Silica No.3	
Relative Density, Dr (%)	50	80	50	80
Void ratio	0.81	0.73	0.83	0.73
Permeation Distance (cm)	0.3	0.2	1.0	0.8

Graph 1. Unconfined Compressive Strength Trends

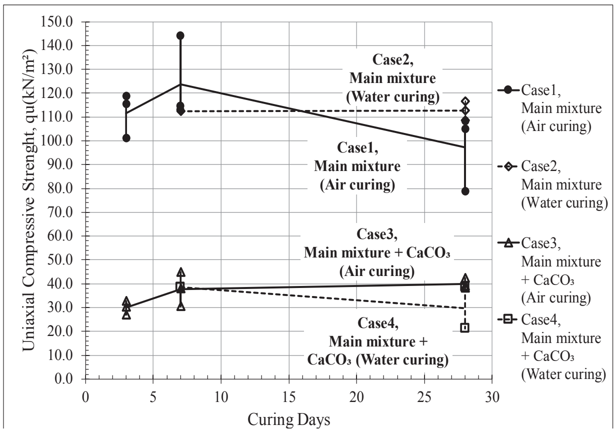

4.CONCLUSIONS

Permeation of grout did not show a big permeation distance. Grout do not drain into sewer pipe if the damaged part is covered with sand. However, this is only limited to homogeneous sand particles. On the other hand, formulation with only main mixture showed a higher strength compared to admixture design. Further research samples are needed to determine the optimal compressive strength in order to ensure the re-excavability of grout.

REFERENCES

[1] W. Fukatani, T. Sakakibara, Study on the Use of Mort ar Mixed Backfill Soil for Sewer Installation, Technical Note of NILIM, No.531, pp. 34-60.

RETURNING HOME BEHAVIOR ANALYSIS OF NEW CHITOSE AIRPORT USERS WHO WERE AFFECTED BY THE 2018 HOKKAIDO EASTERN IBURI EARTHQUAKE

G. HAYAMIZU[1], **Y. MORISAKI**[2], **T. MINAMI**[3], **M. FUJIU**[4], **Y. SHIOZAKI**[5], **and J. TAKAYAMA**[6]

[1] *Master Course Student, Dept. of Environmental Design, Kanazawa University, Kanazawa, Japan,*
[2] *Doctoral Course Student, Dept. of Environmental Design, Kanazawa University, Kanazawa, Japan,*
[3] *Doctoral Course Student, Dept. of Environmental Design, Kanazawa University, Kanazawa, Japan,*
[4] *Associate Professor, Geosciences and civil Engineering , Kanazawa University, Kanazawa, Japan,*
[5] *Assistant Professor, Geosciences and civil Engineering , Kanazawa University, Kanazawa, Japan,*
[6] *Professor, Geosciences and civil Engineering , Kanazawa University, Kanazawa, Japan,*
Correspond to Makoto FUJIU (fujiu@se.kanazawa-u.ac.jp)

***Keywords**: The 2018 Hokkaido Eastern Iburi Earthquake, blackout, Traffic paralysis, Questionnaire survey, Traffic behavior*

1. INTRODUCTION

In Japan, the 2018 Hokkaido Iburi Eastern Earthquake is a disaster that caused many traffic problems. The 2018 Hokkaido Iburi Eastern Earthquake occurred at 3:07 on September 6, 2018, with the Middle East of the Iburi region as the epicenter. A maximum seismic intensity of 7 was observed in Atsuma town. In addition, in Hokkaido, it was the first earthquake disaster in which seismic intensity 7 was observed. Due to the influence of this earthquake disaster, Blackout is occurred across Hokkaido. As for traffic, all JR lines in Hokkaido, including the Hokkaido Shinkansen, were stopped operation. As for aviation, the collapse of the ceiling and water leakage occurred in the terminal building (New Chitose Airport Building Co., Ltd 2018) due to the seismic intensity of 6 upper hit the New Chitose Airport. As a result, all flights were stopped operation on September 6(Cabinet Office in Japan 2018). From the above, it can be said that Hokkaido was isolated area after the disaster due to difficult to get traffic information. New Chitose Airport is a very important airport in the domestic aviation network. The reason is that New Chitose Airport has routes to 22 airports in Japan. According to the result of the 5th Nationwide Intercity Person Trip Survey conducted in 2010. The transportation share is 95% by air, 3% by rail, and 2% by ship when moving central Hokkaido to outside Hokkaido. From the above, it is considered that a lot of people who planned to move to outside Hokkaido using New Chitose Airport were existed.

2. SUMMARY OF QUETIONNAIRE SURVEY

In this study, web-based questionnaire survey was conducted using monitors of Macromill, Inc. The target of the questionnaire survey is a very limited people because they are victims of a sudden disaster and live outside Hokkaido. Therefore, we used web-based web-based questionnaire survey that can expect many samples in a short survey period. to secure as many samples as possible. The survey period was from October 3rd to October 12th, 2018. Screening was performed on 30,000 samples, and the number of samples in this survey was 49 samples.

3. BASIC TABULATION OF QUESTIONNAIRE SURVEY

Figure 1 shows the difference between the planned means of transportation outside Hokkaido and the actual means of transportation outside Hokkaido after the disaster. The questionnaire screening is limited to respondents who were scheduled to take an air flight from New Chitose Airport to their home on September 6-8, 2018.

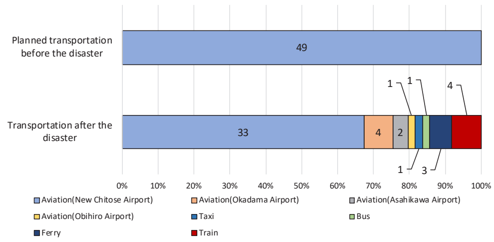

Figure 7. difference between the planned means of transportation and the actual means of transportation outside Hokkaido

3. CONCLUSIONS

The 2018 Hokkaido Iburi Eastern Earthquake occurred at 3:07 on September 6, 2018, with the Middle East of the Iburi region as the epicenter. In this study, A web questionnaire survey was conducted immediately after the disaster. A survey target lives in outside Hokkaido who had planned to use New Chitose Airport. In Figure 7, after the disaster, 16 out of 49 respondents (about 32.7%) moved outside Hokkaido using various transportation other than New Chitose Airport. From the two viewpoints of cost and time to return home, it became clear that the time and cost were greatly changed due to the change of transportation until going home.

REFERENCES

[1] New Chitose Airport Building Co., Ltd (2018), Report of The 2018 Hokkaido Eastern Iburi Earthquake
[2]Cabinet Office in Japan (2018), Annual report of The 2018 Hokkaido Eastern Iburi Earthquake

BASIC STUDY ON THE DIFFICULTY OF EVACUATION IN THE REGION THAT CONSIDERED GEOGRAPHICAL CHARACTERISTIC

T. SAKAI[1], **Y. MORISAKI**[2], **M. FUJIU**[3], **J. TAKAYAMA**[4], **Y. SHIOZAKI**[5], **K. YANAGIHARA**[6], **T. NISHINO**[3], **M. SAGAE**[7] **and K. HIRAKO**[8]

[1] Master Course Student, Dept. of Environmental Design, Kanazawa University, Kanazawa, Japan,
[2] Doctoral Course Student, Dept. of Environmental Design, Kanazawa University, Kanazawa, Japan,
[3] Associate Professor, Geosciences and Civil Engineering, Kanazawa University, Kanazawa, Japan,
[4] Professor, Geosciences and Civil Engineering, Kanazawa University, Kanazawa, Japan,
[5] Specially Assistance Professor, Dept. of Environmental Design, Kanazawa University, Kanazawa, Japan,
[6] Associate Professor, Dept. of Health Science, Kanazawa University, Kanazawa, Japan,
[7] Professor, Dept. of Economics and Management, Kanazawa University, Kanazawa, Japan,
[8] Specially Assistance Professor, Organization of Frontier Science and Innovation, Kanazawa University, Kanazawa, Japan,
Correspond to Takashi SAKAI bass0418@stu.kanazawa-u.ac.jp)

***Keywords**: large-scale earthquake disaster, KDB data, vulnerable people, evacuation difficulty, regional evaluation*

1. Introduction

In the 2011 off the Pacific coast of Tohoku Earthquake, mortality rate of elderly people over 60 years old were accounted for 66% of the overall mortality rate in Iwate, Miyagi, and Fukushima Prefecture. In the event of a large-scale earthquake disaster, there are major problems with evacuation for the elderly and people with disabilities. On the other hand, it was obliged to create a list of people who needed special assistance for evacuation in the event of a disaster. However, it was not used in the 2016 Kumamoto Earthquake. In other words, there are still problems in the evacuation system for those people. To improve this situation, it is indispensable to examine the actual situation of evacuation, such as "how much live in which area" and "what kind of difficulties may be hit by during evacuation". Therefore, in Komatsu City, Ishikawa Prefecture, we used the National Health Insurance database to examine the number of people who were considered difficult to evacuate at the time of disaster.

2. Visualization of evacuation difficulty

In this analysis, "Distance from house to designated refuge", "Percentage of roads with a slope of 8% or more in roads in town", and "Number of intersections per 1 m of road" were used as geographical difficulties during evacuation. Principal component analysis was conducted for these three variables. Figure 1 shows a visualization of the first principal component. The primary principal component score was defined as representing "evacuation difficulty". The "ratio of roads with a slope of 8% or higher in roads within town letters" was selected with reference to Nitta et al[1].

There are 365 people in Imae town, 259 people in Ataka town, 187 people in Mukaimotoori town, and many people who need assistance for evacuation. Therefore, it is necessary to deal with a large number of supporters who need evacuation behavior at the time of disaster. Further, Imae town and Ataka town, which are located in urban areas and have many supporters who need evacuation action, have a low evacuation difficulty in Komatsu City.

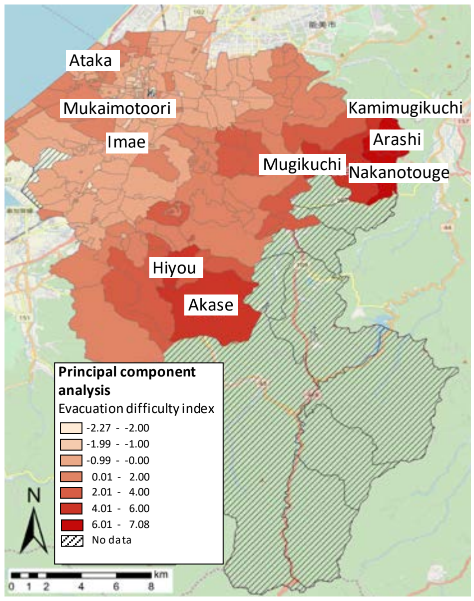

Figure 1. Visualization of evacuation difficulty

On the other hand, Nakanoiso town, Arashi town and Akase town are located in the suburbs, and there are few people who need evacuation action. However, it became clear that evacuation difficulty was high in those areas.

3. CONCLUSIONS

In this analysis, we conducted principal component analysis using KDB data and the geographical difficulty index during evacuation. And, we conducted a regional evaluation on the difficulty of evacuation during a disaster. The relative difference of geographical difficulty in the region became clear. However, we used three regional difficulty variables. Therefore, we would like to increase the number of variables in the future in order to evaluate geographic difficulty in more detail.

REFERENCES

[1] Y. Nitta, K. Koyama, H. Inoi, A. Nakahira: The burden of elderly and disable walker on a slope, Proceedings of Civil Engineering Planning (CD-ROM), 2004.

SESSION D

SPECIAL SESSION: SATREPS/ DISATER MANAGEMENT /

DISASTER MITIGATION AND URBAN PLANNING

Determination of site condition based on microtremors survey in three selected townships of Yangon, Myanmar

Tun NAING1, Su THINZAR[2], Aung Myo ZAW[2],
[1] Professor, Department of Engineering Geology,
Yangon Technological University, Myanmar
tunnaing1972@gmail.com
[2] Assistant Lecturer, (Engineering Geology), Department of Petroleum Engineering,
Technological University (Mandalay), Myanmar
[3] Ph. D Student, Geology Department, University of Yangon, Myanmar

ABSTRACT

Site condition is one of the major issues during an earthquake especially for the cities which are situated in young sedimentary rock and recent alluvium areas like Yangon. Most of the townships of Yangon are located in soft alluvial plain which is mainly composed of sand, silt and clay, underlain by young sedimentary rock. Moreover, the seismogenic Sagaing Fault is passing through about 40 km in the east of Yangon and it had experienced several destructive earthquakes in the past. Studied townships: Mingalartaungnyunt, Dagon and Ahlon are major townships of Yangon with high historical value besides their dense population. To understand the potential site condition or site effects in those townships during an earthquake, the microtremors survey and analysis had been conducted at 136 sites. The analysis reveals that the fundamental frequency of horizontal to vertical spectral ratio (HVRs) of microtremors is generally ranging from 1.25Hz to 2.65 Hz, while the peak amplitude is between 0.7 and 3.9. Based on combined analysis of secondary boring data and the inversion process from fundamental frequency and peak amplitude of microtremors HVRs, the sediment thickness is between 45m to 125m in general and the shear wave velocity of upper 30m depth (Vs30) is ranging from 200m/s to 680m/s. The outcomes of this research are major input parameters for future seismic risk analysis and development of township level earthquake resilience management system in Yangon.

Keywords: site condition, microtremors, HVRs, fundamental frequency, Vs30

1. INTRODUCTION

Yangon is the most socio-economically important city of Myanmar besides its highest density of population especially in downtown area. The old and historical buildings are concentrated in major parts of Yangon including the studied townships. The major seismogenic Sagaing Fault is passing through 40 km east of Yangon and it had caused several destructive earthquakes in the past. The damage and losses will be high due to its old buildings and substandard structures if there is an earthquake in future generated by the nearest Sagaing Fault segment to Yangon. The local soil effect or site effect is one of the important factors for observed damages during an earthquake. The adequate information of subsurface soil condition is one of the important requirements for determination of the site effects and microtremors survey had been carried out in Mingalartaungnyunt, Dagon and Ahlon townships to fulfill this requirement.

2. LOCATION AND SIZE OF RESEARCH AREA

Yangon is situated at the confluence of Hlaing River and Bago River on the eastern margin of the Ayeyarwady delta. The studied townships; Mingalartaungnyunt, Dagon and Ahlon shown in Figure 1 are major townships of Yangon City regarding to their population density, socio-economic conditions and existence of Yangon Region Government Head Office and Shwedagon pagoda.

According to the 2014 Myanmar Population and Housing Census, 2015, Mingalartaungnyunt Township has the areal coverage of 5.06 km^2 and population of 132,494. Dagon Township has the area of 4.7 km^2 and population of 25,082 while Ahlon has the area of 3.626 km^2 and the population of 55,482.

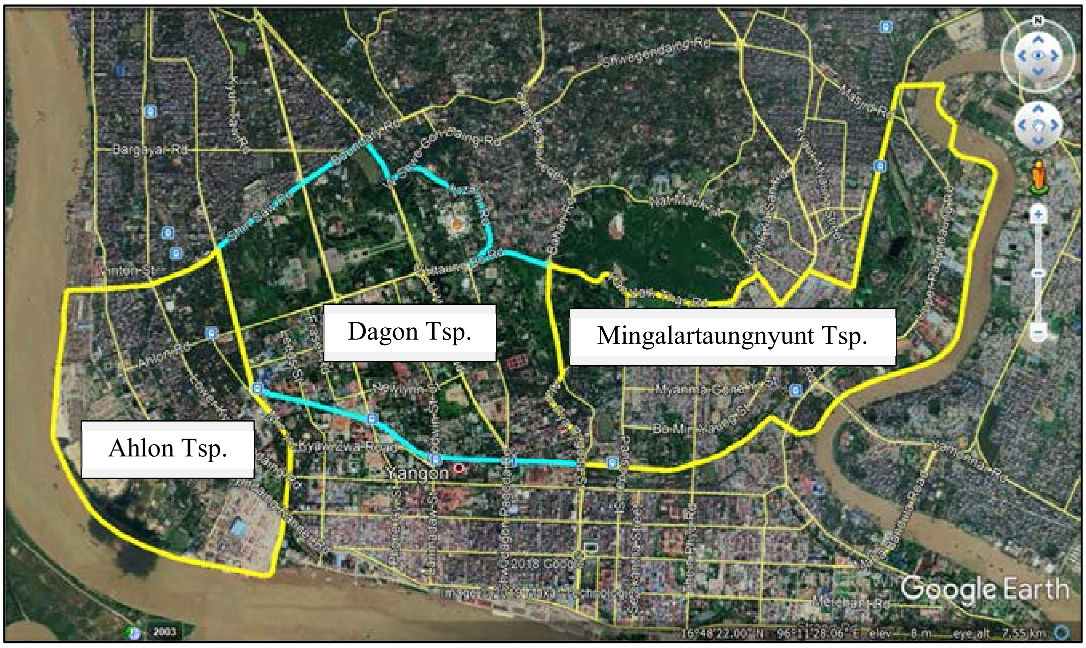

Figure 1: Location of studied townships

3. MICROTREMOR SURVEY AND ANALYAIS

The studies of Nakamura (1989) have indicated that the horizontal-to-vertical (H/V) spectral ratio of microtremors, conveniently observed at a site with only one three-component sensor, may approximate the amplification factor of the site for vertically incident *S* wave.

After a number of studies on the microtremor H/V spectra, it has been widely confirmed that the peak frequency of the microtremor H/V spectrum at a site corresponds nearly to the natural site frequency (Nakamura, 1989). Shear wave velocity of all layers, the variation of thickness of the layers can be estimated through the inversion of microtremor H/V spectrum assuming that it reflects the fundamental-mode of Rayleigh wave (Hiroshi Arai and Kohji Tokimatsu, 2005).

3.1 Microtremor survey

The single station microtremor surveying was carried out at 136 sites throughout the study townships by using SMAR-6A3P model microtremor equipment as shown in Figure 2. The measured sites in each township are: 52 sites in Mingalartaungnyunt Township, 44 sites in Dagaon Township and 40 sites in Ahlon Township as shown in Figure 3.

Figure 2: SMAR-6A3P model microtremor equipment

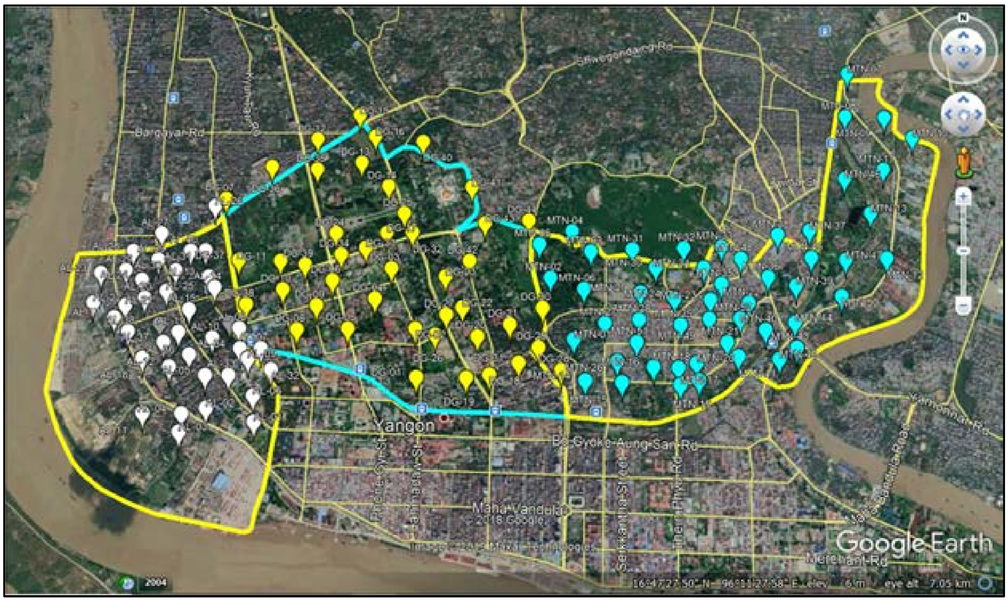

Figure 3: Location of microtremor measured sites

3.2 Data analysis

The horizontal to vertical spectral ratio, H/V ratios of NS/UD and EW/UD components were calculated first and the ratios of both components were then averaged to determine the final observed microtremor H/V ratio. The data analysis generally includes the separation of recorded acceleration time historical data for each component, division of windows for every 40.96s of recorded data, determination of Fast Fourier Transform spectrum and calculation of microtremor H/V spectral ratio for each measured site. The observed microtremor spectra always shows two peaks; one at lower frequency while the other at higher frequency ranges as shown in Figure 4. The low peak amplitude suggests that the impedance contrasts between the underlying soil layers are small and the high peak amplitude suggests that the impedance contrasts between the underlying layers are large (Tun Naing et al., 2013).

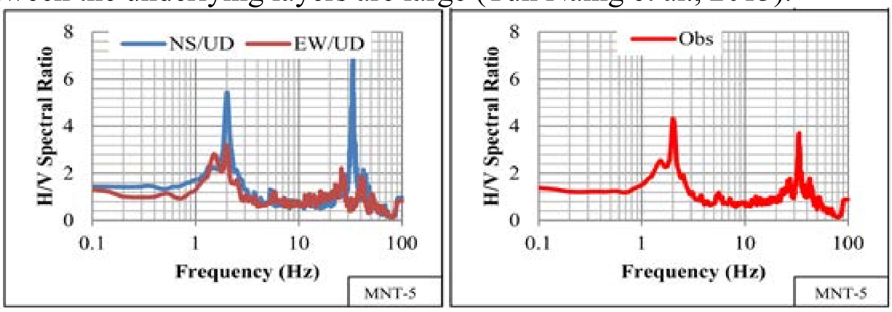

Figure 4: Microtremor H/V Ratios of NS/UD, EW/UD Components and Observed Spectra at some selected sites

3.3 Shear wave velocity inversion

The inversion of shear wave or S-wave velocity structures had been focused on the H/V ratio's peak at low frequency (generally 1.2 – 2.65 Hz) by trial and error method. The H/V are the primary concern and all spectra for two horizontal components are average and then take the ratio to one vertical component because it does not need to separate site effects for two components at a site (Kawase et al., 2011). Therefore, the mean H/V of NS/UD and EW/UD is used for S-wave velocity inversion and results at DG-19 are shown in Figure 5 and Table 1.

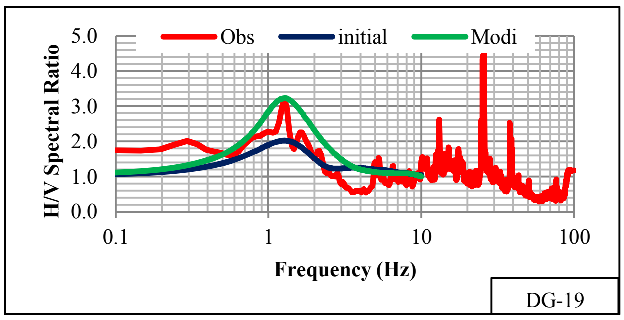

Figure 5: Observed microtremor H/V spectrum and calculated H/V spectra for initial and final model at DG-19

Table 1: Parameters of initial and modified soil model of DG-19

Layer	Thickness (m)		Vp* (m/s)		Vs** (m/s)		Unit Wt. (g/cm^3)	
	Initial	Modi.	Initial	Modi.	Initial	Modi.	Initial	Modi.
1	10	7	1536	1293	320	180	1.94	1.86
2	12	12	1633	1365	380	220	1.97	1.88
3	13	15	1710	1502	430	300	1.99	1.93
4	14	18	1741	1664	450	400	2.00	1.98
5	22	22	1815	1815	500	500	2.02	2.02
6	30	30	1957	1957	600	600	2.06	2.06
Elastic Half space	-	-	2219	2219	800	800	2.12	2.12
*Primary Wave Velocity **Shear Wave Velocity								

The modification of initial soil model by increase or decrease of soil parameters of each soil layer gives the best fit theoretical H/V spectra (green spectrum in Figure 5).

4. RESULTS AND DISCUSSIONS

The fundamental frequency of soil, potential soil amplification, soil thickness above the weathered bedrock and average shear wave velocity of upper 30 m depth zone are main results of this research.

4.1 Fundamental frequency of underlying soil

Generally, the fundamental frequency is related to the thickness of soil layer at the microtremor measured sites. The frequency of the fundamental peak of observed microtremor H/V ratio is regarded as the fundamental frequency of underlying soil layers. The fundamental frequency of studied townships is ranging from 1.25 Hz and 2.65 Hz as shown in Figure 6 and soil thickness is between 45 m and 125 m as shown in Figure 7.

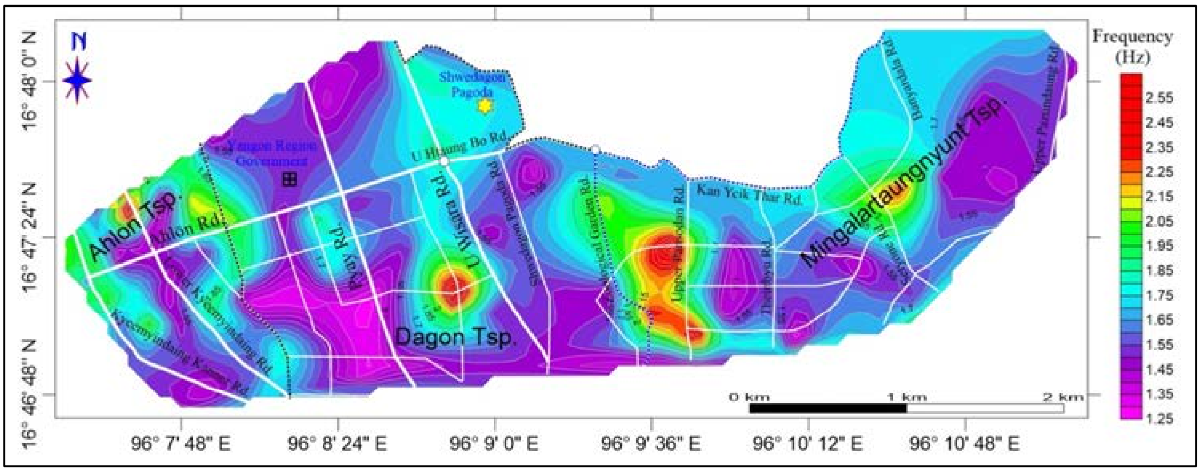

Figure 6: Map of fundamental frequency of underlying soil in studied three townships

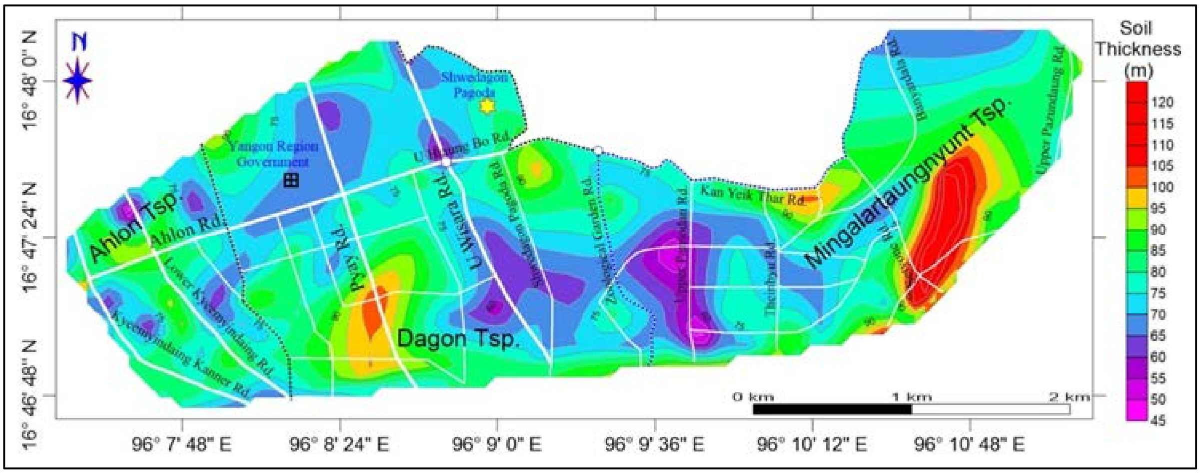

Figure 7: Map of soil thickness in studied three townships

In Figure 6, the red color represents the highest frequency zones while purple color is the lowest frequency zones. The thicker soil layers are observed in lower frequency zones and thinner sediment layers are encountered in higher frequency zones as shown in Figure 7. It is more dangerous for high-rise building in lower frequency zones of thick sediments than low-rise buildings while the latters are more liable to severe damage in high frequency zones of thinner sediments.

4.2 Potential soil amplification

The peak amplitude of H/V spectral ratios can be used to estimate the potential amplification of underlying soil. The potential soil amplification map of the studied townships is shown in Figures 8.

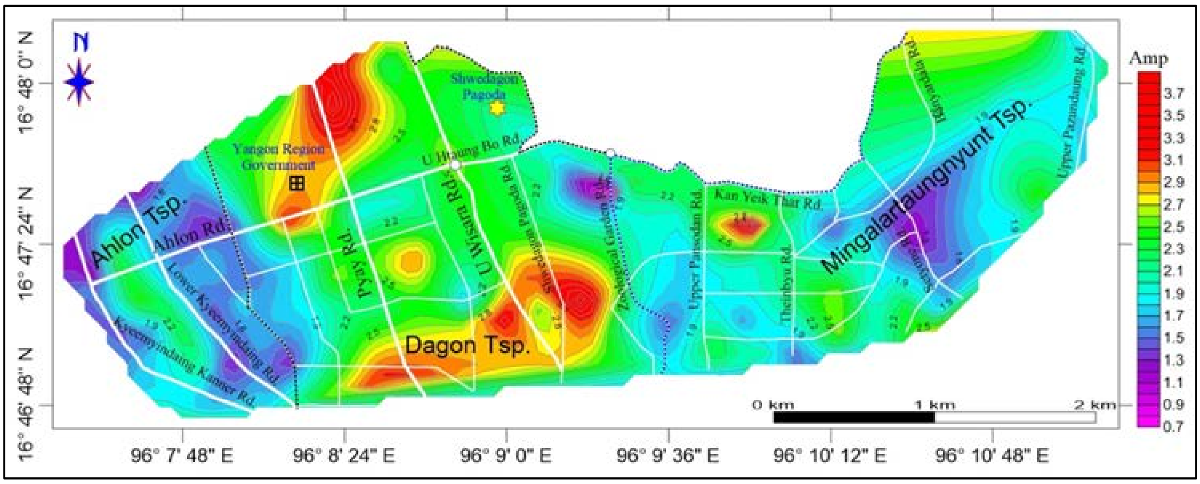

Figure 8: Map of potential soil amplification in studied three townships

The red color in Figure 8 represents the highest potential soil amplification zones and it is well observed in northern and southern parts of Dagon Township where softer soil layers will be encountered. The purple color is the lowest amplification zones and well observed in Ahlon Township and south-eastern part of Mingalartaungnyunt Township where denser soil layers are dominated. The stronger ground shaking therefore can be expected in higher amplification zones due to softer soil layers there rather than lower zones during an earthquake.

4.3 V_s^{30}

The average shear wave velocity of upper 30 m depth zone, V_s^{30}, of each site had been determined by using the following equation (MNBC, 2012) based on modified soil model.

$$\overline{v_s} = \frac{\sum_{i=1}^{n} d_i}{\sum_{i=1}^{n} d_i / v_{si}} \tag{1}$$

Where,

d_i = thickness of i^{th} soil layer

v_{si} = shear wave velocity in i^{th} soil layer

n = number of soil layer

Based on the results from 136 sites in three townships, the V_s^{30} map was prepared as shown in Figure 9 and it ranges from 200 m/s to 680 m/s.

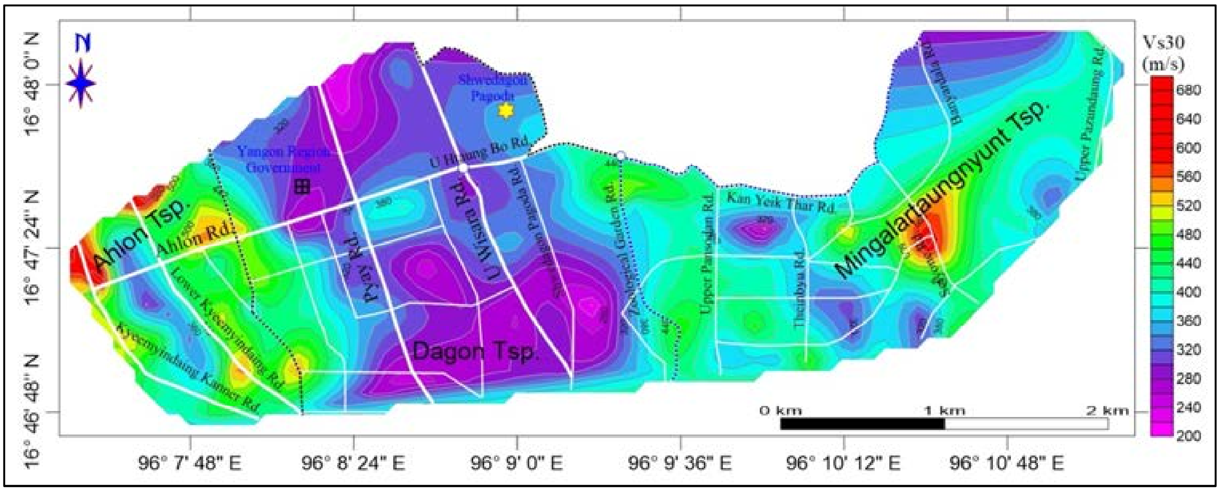

Figure 9: V_s^{30} map of studied three townships

Figure 9 shows that most parts of Dagon Township are covered by lower V_s^{30} zone while higher V_s^{30} covers most parts of Ahlon and Mingalartaungnyunt townships. Longer and stronger ground shaking can be expected in lower V_s^{30} zone than higher zone.

5. CONCLUSION

This research mainly focused on the determination of ground information in Mingalartaungnyunt, Dagon, Ahlon townships and the microtremor survey had been applied as the main tool. Based on results from overall research works, the following facts are highlighted.

1. The primary outcomes of this research are fundamental frequency map, potential soil amplification map, map of sediment thickness, V_s30 map and related soil profiles.

2. Fundamental frequency is generally ranging from 1.25 Hz to 2.65 Hz. Generally, the lower frequency zones are dangerous for high-rise buildings and higher frequency zones are dangerous for low-rise buildings.

3. Higher ground motion and shaking can be expected in the zones with higher potential soil amplification where the soil layers are softer than others places.

4. S-wave velocity is ranging from 200 m/s to 680 m/s in general and the higher shear wave velocity is observed at the sites with lower peak amplitude of H/V ratios and weaker ground shaking can be expected. Meanwhile, the lower shear wave velocity is observed at the sites with higher peak amplitude of H/V ratios and stronger ground shaking can be expected.

5. The outcomes of this research are the important input parameters for better urban planning and development of a comprehensive disaster resilience system in Yangon.

REFERENCES

Arai, H. and Tokimatsu, K., 2005. S-Wave Velocity Profiling by Joint Inversion of Microtremor Dispersion Curve and Horizontal to Vertical (H/V) *Spectrum. Bulletin of the Seismological Society of America,* Vol.95, No.5, pp. 1766-1778.

Kawase, H., San'chez-Sesma, F.J. and Matusushima, S., 2011. "Effect of Surface Geology on Seismic Motion: Application of the H/V Spectral Ratios for Earthquake and Microtremor Ground Motion" *4th IASEI / IAEE international Symposium, University of California Santa Barbara, USA*, page 1-13.

Ministry of Immigration and Population, 2015. The Union Report: the 2014 Myanmar Population and Housing Census, Census Report Volume 2.

MNBC, 2012. Provisional Myanmar National Building Code, Federation of Myanmar Engineering Societies, Myanmar.

Naing, T., Kawase, H., Matsushima, S., Thant, M., Mon, S. T., Tin, T. H. and Oo, K., K., K., 2013. S-Wave Velocity Profiles Based on the HVRs in Bago, Myanmar for Seismic Hazard Mapping, *Proceeding, International Symposium on Earthquake Engineering, JAEE*, Vol.2.

Nakamura, Y., 1989. A method for dynamic characteristics estimation of subsurface using microtremor on the ground surface. ser.*Rep. Railway Tech. Res. Inst., Jpn*, vol30 (1), 25–33.

INVESTIGATION OF DISASTER RESPONSE ACTIVITIES OF ADMINISTRATION OFFICES OF YANGON CITY

H. GOKON[1], T. KATO[2], M.M. MON[3], T. NAING[4], M. NUMADA[5] and K. MEGURO[2]

[1] *Associate Professor, School of Knowledge Science, JAIST, Ishikawa, Japan,*
[2] *Professor, ICUS, IIS, The University of Tokyo, Tokyo, Japan*
[3] *Master Student, Yangon Technological University, Myanmar*
[4] *Professor, Yangon Technological University, Myanmar*
[5] *Associate Professor, ICUS, IIS, The University of Tokyo, Japan*
Correspond to H. Gokon (gokon@jaist.ac.jp)

***Keywords**: disaster response activities, flow chart of disaster response, Yangon city*

1. INTRODUCTION

Myanmar has been threatened by natural disasters (e.g. the 2008 Cyclone Nargis). Each administrative organization in Yangon City has taken various measures against natural disasters, but activities of who did what and when were not clearly recorded well. There is also a big difference between the disaster response operations in terms of both quantity and quality of information. At the township level in Yangon City, Kikuchi et al.(2018) investigated three regional disaster prevention plans, but the structure of disaster prevention-related work in Yangon City as a whole has not yet been clarified. The objective of this study is to analyze the actual situation of undocumented disaster response by conducting interview surveys with the Relief and Reconstruction Bureau in Yangon City about disaster response operations conducted before, after, and after the disaster.

2. METHOD

Based on interviews in Yangon City and existing disaster prevention documents, we analyzed the overall picture of disaster response operations. The field survey was conducted in two parts: June 15 to July 31 and December 6 to 15 of 2017. For the interview, we asked the staff who worked for 30 years to the Department of Rehabilitation and Rehabilitation (RRD, now renamed to DDM) of the Ministry of Social Welfare and Rehabilitation in Yangon City.

(1) Understanding the overall picture of disaster response operations

First, we interviewed the general picture of the disaster response work about the name of the administrative organization related to the disaster related work and the documents related to disaster prevention when a disaster occurred in Yangon City.

(2) Survey of organizations in charge of disaster response operations

Based on the survey results in (1) and the regional disaster prevention plan in Myanmar and Japan, a checklist was prepared to investigate disaster prevention operations including the information of before and after the disaster, the recovery and reconstruction period, and members involved in the disaster prevention and recovery. We interviewed the staff again. The survey items before the disaster were 75 items, and the survey items after the disaster were 113 items. The 25 administrative organizations including ministries and city committees were included in the interview sheet.

(3) Investigation of disaster response work flow

In order to clarify the flow of disaster response operations, a workflow was created for responses after the disaster. Based on the interview survey results, an outline of the work flow was created, and the staff of the Relief and Reconstruction Bureau confirmed each one to correct and improve.

(4) Confirmation of the validity of the survey results

We conducted interviews with RRD and GAD at the township level, and verified the validity of the survey results in (2) and (3).

3. RESULTS AND DISCUSSIONS

As a result of interviews, it was found that at least 12 ministries and 12 disaster prevention committees were involved in disaster response work in Yangon City. As a document related to disaster prevention, the RRD in Yangon City has Myanmar Action Plan on Disaster Risk.

As a result of the investigation of the number of operations using the disaster response operation checklist, we were able to quantitatively analyze the disaster response operation burden of each ministry. In addition to RRD and GAD, the Fire Department, Yangon City Development Committee, the police, the Ministry of Insurance, and the Red Cross have more work than other ministries.

4. SUMMARY

We conducted a survey and analysis of the actual situation of disaster response operations in Yangon City. As a result, the ministries and agencies that are deeply involved in disaster response work and the overall picture of the disaster response work flow were clarified.

REFERENCES

[1] Rena Kikuchi, Muneyoshi Numada, May Myat Mon, Tun Naing, Khin Than Yu and Kimiro Meguro: A Comparison of Disaster Management Plans for Both Japan and Myanmar, Journal of Disaster Research (JDR), Vol. 13, No.1, 2018

Slope modeling for future slope stability in Hakha City, Chin State, Myanmar

May Myat MON[1], Tun NAING[2], Kyaw Zin LATT[3], Muneyoshi NUMADA[4], Khin Than YU[5], Kimiro MEGURO[6]

[1] Master Student, Dept. of Engineering Geology, Yangon Technological University, Myanmar, casperrosey@gmail.com

[2] Professor, Dept. of Engineering Geology, Yangon Technological University,Myanmar

[3] Lecturer, Dept. of Engineering Geology, Yangon Technological University, Myanmar

[4] Lecturer, International Center for Urban Safety Engineering, the University of Tokyo,Japan

[5] Pro-Rector, Yangon Technological University, Myanmar

[6] Professor, International Center for Urban Safety Engineering, the University of Tokyo, Japan

ABSTRACT

Hakha City has to face one of the major geo-hazards, landslide, during the raining season of every year. Mudstone and siltstone are mainly observed in most of the slopes and sometimes thin layers of sandstone are intercalated. High and deep weathering of rocks and heavy rainfall are major controlling factors besides slope gradient. The landslides in August, 2015 had affected large parts of Hakha, especially in Zaythit ward, Myohaung ward and the wards along Dauchim road. The landslide inventory survey had been conducted based on field survey and historical records to understand the distribution and types of landslides. Soil and rock samples were collected at some selected slopes and engineering geological properties such as shear strength parameters, moisture content, Atterberg's Limits and so on, were determined to understand the behaviors of slope materials. Moreover, Twenty nine ground control pints were constructed throughout the Hakha city for aerial survey to obtain good accuracy of ground elevation model. The digital elevation model, DEM, is final outcome of this survey and this DEM will be the great help for the construction of slope profile or slope configuration of interested slopes in Hakha city. The slope modeling is conducted in this research based on the laboratory tests results and DEM maps for future landslide or slope instability as a result of stress exceeding the shear strength of the slope material. The excess stress could be added with increasing pore water, excessive overburden pressure due to external load, and so on. Moreover, poor soil condition, weathering, slope geometry, soil stratification, discontinuities in the rock body are some other common factors for slope instability in Hakha.

Keywords: *landslide hazard, highly deformed, deeply weathered, slope modeling, future landslide assessment*

1. INTRODUCTION

The proposed research area, the new Hakha City region, is located in the Chin Hills which forms part of Western Fold Belt. Devastating landslides occurred in this area in

August 2015, followed by severe landside damage along the Falam-Hakha road and some places of Hakha city. Due to this disaster, some parts of Hakha city were going to be resettled in a new location. Most of the areas around Hakha City are hilly and contain high topographic features with steep slope.
The characteristic of slope materials is one of the major controlling factors of landslide in this city. The stability of existing slopes is important issue for the development of this city and the detailed slope stability analysis is required for the critical slopes inside the city based on geology and engineering geological properties of slope materials. For those reasons, the soil samples were collected at some selected critical slopes and various laboratory tests were conducted to determine the physical and mechanical properties of soil. Slope modeling is important issue to understand the mechanism to assess the future landslide.

1.1 Location and Size

The study area, Hakha city is the capital of Chin State which is situated in Western Ranges of Myanmar. The Hakha City is located at 22°40′37.94″ N and Longitude 93°35′9.94″ E as shown in Figure 1. The area coverage of Hakha city is 32.37 km^2 and the population is 24,926 according to the 2014 Myanmar Population and Housing Census situation.

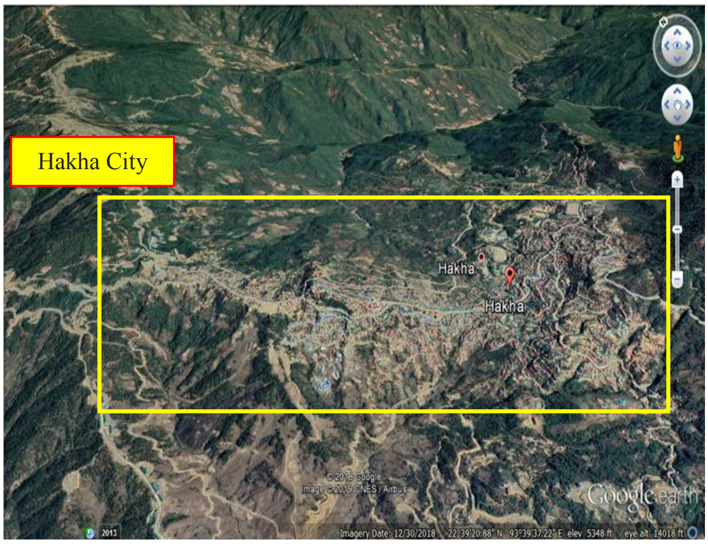

Figure 1: Location Map of Study Area

2. GEOLOGICAL CONDITION OF THE STUDY AREA

The study area is composed of the flysch types of sedimentary and metasedimentary rocks. It can be divided into three different rock units according to lithology, stratigraphic position and faunal content: the Falam Mudstone-Micrite Formation, the Chunsung Mudstone Turbidite Formation, and the Kennedy Sandstone Formation.

2.1 Weathering Condition of Rock

Weathering of rocks in the slope is one of the influential factors for a landslide. The rocks in Hakha are highly and deeply weathered due to high intensity of annual rainfall and deformation of rocks (Figure 2).

Figure 2: Weathering condition of rock in slopes of Hakha city

2.2 Deformation of Rock

The rocks in Hakha area are young sedimentary rocks of Upper Cretaceous to Eocene age. The rocks are mainly mudstone, silty mudstone, slaty mudstones and sandstones, and they are generally regarded as soft rocks. The active subduction and collision of Indian plate and Myanmar minor plate have caused those soft rocks highly deformed and brecciated (Figure 3).

Figure 3: Deformation in rocks of Hakha area

3. SLOPEMODELING FOR FUTURE SLOPE STABILITY

The field survey and observation mainly consists of geological observation, engineering geological observation at selected slopes in Hakha and aerial survey by drone.

3.1 Soil Sampling and Laboratory Testing

The disturbed soil samples were collected from 30 selected slopes of Hakha city for identification of material types and laboratory testing. Sealed plastic bags and PVC pipes with proper caps were used to store the collected samples. The locations of collected soil samples are shown in Figure 4.

Figure 4: Locations of Collected Soil Samples

The collected soil samples were tested the following physical and mechanical tests to determine the engineering properties of soil in the slopes of Hakha city.

1. Sieve Analysis
2. Atterberg's Limited Test (Casagrande)
3. Standard Compaction Test (Proctor Test)
4. Moisture Content Test
5. Specific Gravity Test
6. Direct Shear Test

The grain size distribution test was conducted according to ASTM - D422 to classify the soil type in Hakha and the grain size distribution curves are drawn.

The soil in the slopes of Hakha can generally be regarded well graded soil because gravel, sand, silt and clay are well observed although the majority are sand and silt and minor amount of gravel and clay.

Atterberg's Limits tests were conducted according to ASTM – D2216. The flow curves of liquid limit determination at some selected slopes. The liquid limit at L1 is 52.0 % and Plastic Limit is 34.95 % while the Plasticity Index (PI) is 17.05 %.

This test was conducted according to ASTM-D698 using collected disturbed samples. The optimum moisture content and maximum dry density of soil were determined through this test.

(a)

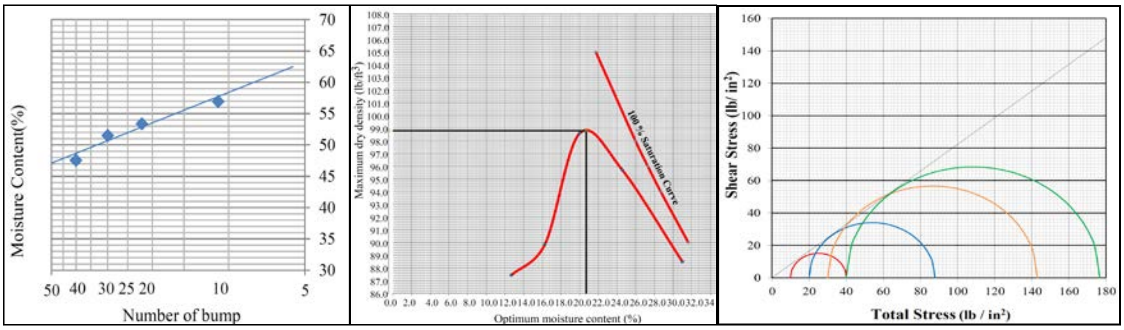

(b)

Figure 5: (a) Soil Testings, (b) Some Laboratory Test Results

Table 1. Summary of Laboratory Test Results

Slopes	Atterberg's Limits			Sieves Analysis				Dry density	Moisture Content	Strength Parameters		Soil Types
	LL	PL	PI	Gravel	Sand	Silt	Clay		w	Triaxial		
	%	%	%	%	%	%	%	g/cm³	%	c (kPa)	ϕ (°)	
1	52	34.95	17.05	13	52	15	20	2.12	16.572	0	38.5	SC
2	38	25.01	12.99	25	26	18	31	2.05	16.133	341	30.5	CL
3	41	27.93	13.07	15	47	11	27	2.05	20.184	163	10°	SC
4	51	33.38	17.62	8	22	37	33	1.92	25.223	283	16.5	MH
5	59	37.97	21.03	5	14	41	40	1.80	31.974	59	6	MH
10	38	24.41	13.59	1	8	52	39	1.87	22.423	107	18	CL
11	39.5	24.12	15.38	10	32	25	33	1.83	19.645	34	3	CL
12	51	33.65	17.35	4	8	43	45	1.81	27.506	165	8.5	MH
13	45.5	28.31	17.19	3	31	28	38	1.83	19.548	159	6.5	CL
14	38.5	25.88	12,62	29	27	25	19	1.91	19.828	69	17	GC
15	55.50	38.73	16.77	1	8	53	38	1.66	35.749	131	19	MH
16	31.00	21.21	9.79	13	54	19	14	2.25	12.821	99	11	SC
17	56.50	40.84	15.66	19	25	30	26	1.55	30.348	93	28	MH
18	38.00	23.48	14.52	28	38	16	18	2.25	13.608	159	21.5	SW
19	32.00	17.38	14.62	24	52	13	11	2.53	10.495	138	17.5	SW
20	55.00	37.09	17.91	27	22	33	18	1.77	26.574	138	25.5	MH
21	44.50	30.92	13.58	20	33	27	20	1.95	17.044	59	14	SM
22	45.50	33.06	12.44	15	39	23	23	1.96	14.592	52	23.5	SM

23	44.50	31.78	12.72	18	23	46	13	1.64	24.061	45	3	ML
24	41.50	27.68	13.82	22	22	32	24	1.90	16.553	21	12	ML
25	25.00	16.55	8.45	8	27	43	22	2.18	15.935	72	8	ML

3.2 Aerial Survey by Drone

Twenty nine ground control points (Figure 6) were constructed throughout the Hakha city (both old and new cities) for aerial survey to obtain good accuracy of ground elevation model. The ground control points were constructed based on government bench mark which was located at the top of Mt. Rung by RTK survey instruments using GNSS solution.

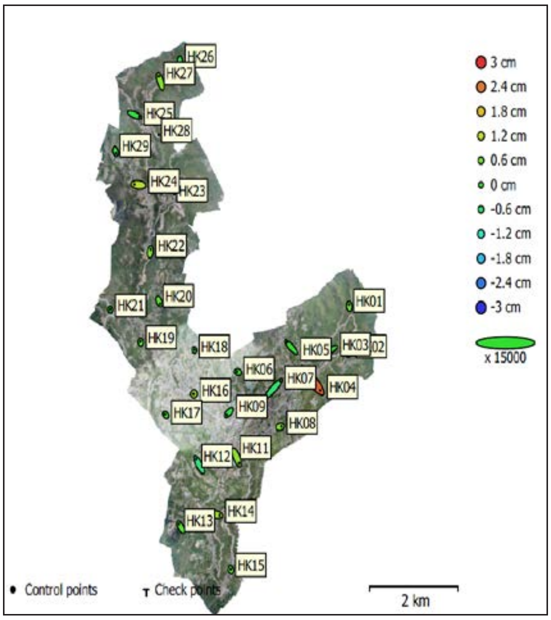

Figure 6: Location of Ground Control Points in Hakha

Phantom 4 Drone was used to take the aerial photographs from the altitude of 266 m and total 4684 images with ground resolution of 6.76 cm/pix were taken. The drone was taking the images along the total numbers of 66 flight paths and some aerial surveying activities.
The digital elevation model, DEM (Figure 7) is final outcome of this survey and this DEM will be the great help for the construction of slope profile or slope configuration of interested slopes in Hakha city.

Figure 7: Digital Elevation Model (DEM) of Hakha City

According to Figure (6), the lowest elevation of Hakha city is 1319 m above mean sea level and it is around the eastern most part of old city. The highest elevation is 2106 m and it is in the northern most part of new city. The profiles of interested slop can be generated from obtained DEM of Hakha city. The profile along the AA′ section in Figure (7) is shown in the following Figure (8,9,10,11,12).

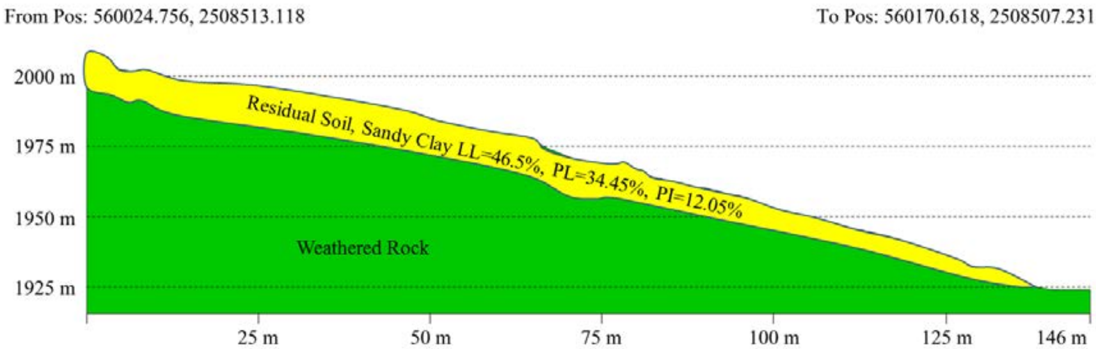

Figure 8: Slope Profile along the Line L-7

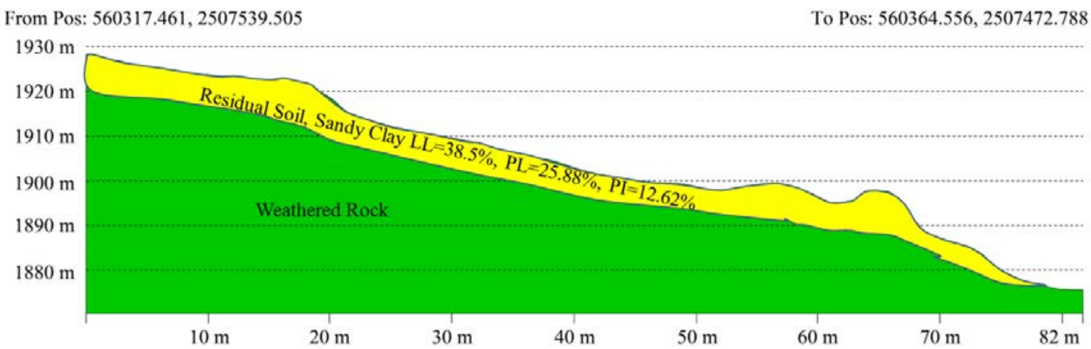

Figure 9: Slope Profile along the Line L-14

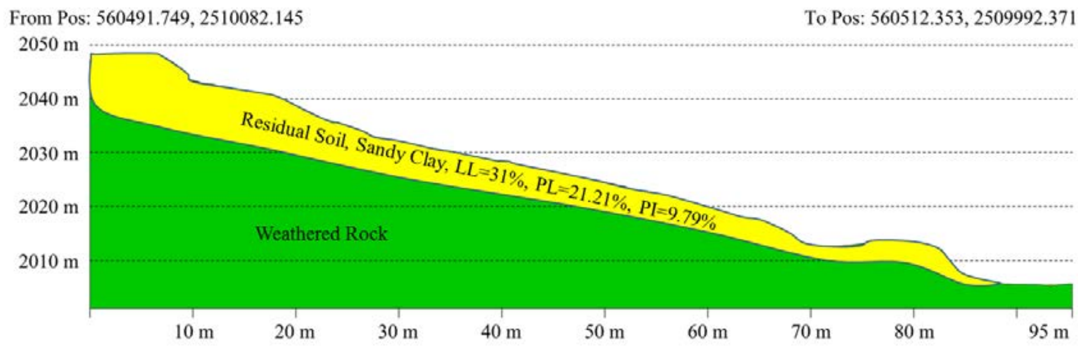

Figure 10: Slope Profile along the Line L-16

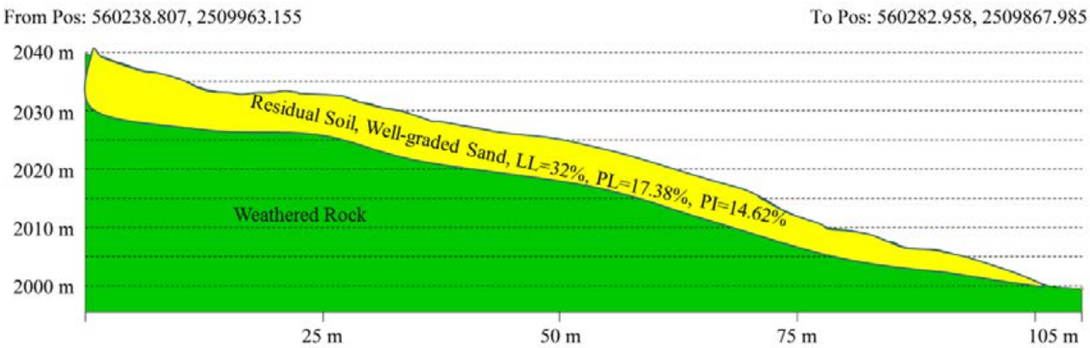

Figure 11: Slope Profile along the Line L-19

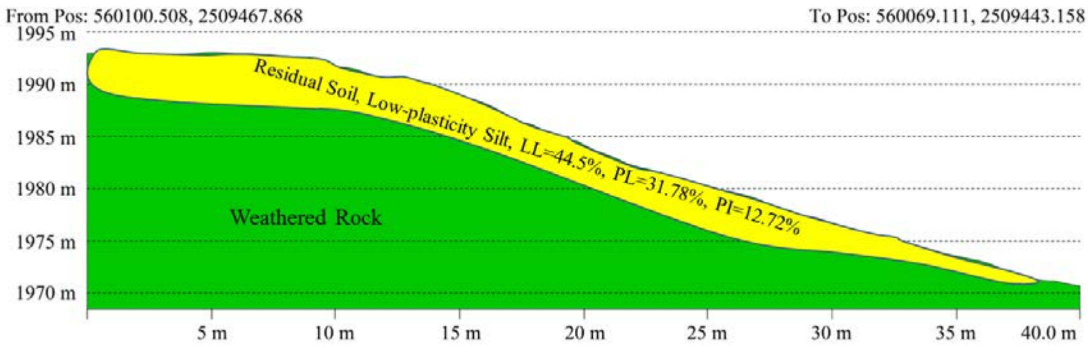

Figure 12: Slope Profile along the Line L-23

4. DISCUSSION

According to sieve analysis, the soil from the selected areas is mainly composed of 26% of clay, 30% of silt, 29% of sand and 15% of gravel in average. The dry density is relatively low. Most of the slopes are composed of low to high plasticity silty (ML-MH) and clayey (CL) soil.

The liquid limit is ranging from 25% to 59% and the high liquid limits can be observed in slopes 1, 4, 5, 12, 15, 17 and 20. The plastic limit is between 16.55% and 38.73% and the plasticity index ranges from 8.45% to 21.03%. The moisture content in soil is from 10.5% to 35.7% at the time of sample collection in May and the moisture content will be higher in the middle of raining season.

The soil from slopes 1, 2, 17 and 20 give relatively high angle of internal friction (>25˚) while those from slopes 3, 5, 11, 12, 13, 23 and 25 give low angle of internal friction

(≤10˚). The cohesion is ranging from 0 to 341 kPa and 114 kPa in average. The shear strength of soil in some slope can be very low where both cohesion and angle of internal friction are low.

The determined slope models together with unit weight of soil, shear strength parameters; cohesion (c) and angle of internal friction (ϕ), and classified soil types and their thickness will be the main input parameters for future detailed slope stability analysis in future.

5. CONCLUSION

Based on the field observation and recent research work, it is the urgent need to conduct the systematic study and analysis of landslide potential for sustainable development of the region.

It is obvious that Hakha city has two important influential factors for landslide; high relief and high weathering together with extremely deformed rocks in the slopes. Besides that, heavy rain fall and poor land use are triggering factors of landslide and slope failures in Hakha area.

The soil is composed of high percentage of clay and silt which are low permeable. Therefore, the percolated rain water inside the slope cannot be drained completely in a designated period. Consequently, the pore water pressure inside the slope gradually increases and finally the high uplift pressure caused landslides and other slope failures in Hakha. The determined physical and mechanical properties of slope materials are fundamental parameters for engineering geological modeling of critical slopes for future slope stability analysis.

Soil types and related properties were determined for thirty selected slopes of new Hakha city. Digital Elevation Model and contour map with five meter interval had been successfully created for Hakha city (both old and new) based on results of aerial survey by drone.

Slope profiles had been successfully modeled based on Digital Elevation Model and laboratory test results of related soil samples.

REFERENCE

M.S. Islam, M.A. Hussain, Y.A. Khan, M.A.I. Chowdhury and M. B. Haque, “Slope Stability Problem in the Chittagong City, Bangladesh,” *Journal of Geotechnical Engineering (JoGE)* vol. 1(3), 2014, pp. 13-25.

D. B. E. Putra and T. Choanji, 2016. ‘Preliminary Analysis of Slope Stability in Kuok and Surrounding Areas,” *J. Geoscience, Engineering, Environment, and Technology*, vol. 1, 2016, pp. 4144.

R. Anbalagan, “Landslide hazard evaluation and zonation mapping in mountainous terrain”, Eng Geol. 32, 1992, pp. 269–277.

P. Aleotti, R. Chowdhury, “Landslide hazard assessment: summary review and new perspectives,” *Bull Eng Geol Environ*, 58, 1999, pp. 21–44.

H. X. Lan, C. H. Zhou, L. J. Wang, H. Y. Zhang and R. H. Li, “Landslide hazard spatial analysis and prediction using GIS in the Xiaojiang watershed, Yunnan, China,” Eng Geol. 76, 2004, pp. 109–128.

Chin Committee for Emergency Response and Rehabilitation (CCERR), “The Chin State Floods & Landslides: A Community-Led Response and Assessment,” Report, Dec. 2015.

M. H. Nyo, R. S. Grant, M. T. Aye, and Y. L. Yee, “Rodent population outbreaks associated with bamboo flowering in Chin State, Myanmar,” Researchgate, 2010.
Ministry of Immigration and Population, “The 2014 Myanmar Population and Housing Census,” The Union Report, Census Report Volume 2, May 2015.
Department of Geological Survey and Mineral Exploration and United Nations, “Geology of the Falam – Kalemyo area northern Chin hills” 1977.

SOIL-STRUCTURE-INTERACTION EFFECTS ON THE DAMAGE STATE OF TYPICAL BUILDINGS IN YANGON

Khin Myat Kyaw[1] **and K. MEGURO**[2]

[1] Graduate Student, Civil Engineering Department, The University of Tokyo (UTokyo), Japan
[2] Director/Professor, International Center for Urban Safety Engineering, Institute of Industrial Science, U Tokyo, Japan
Correspond to Khin Myat Kyaw (khinmyatkyaw2012@gmail.com)

Keywords: *soil-structure-interaction, damage state, vulnerability, microtremor measurement*

1. INTRODUCTION

Building damage mechanism during an earthquake event relies on the different factors such as the intensity of the event, seismic resistant capacity of the building and underlying soil condition. In case of vulnerability assessment work, normally soil part is neglected assuming the building is situated on firm base. However, soil behavior during shaking plays a vital role in the collapse mechanism of the building [1]. Because of the soil flexibility underneath the building, the natural period gets longer resulting in enhanced effective damping ratio and increased displacement demand [2]. Nakhaei found out that the damage index of the short period buildings significantly increases on softer soils and the effect is more prominent in the structures with high aspect ratio. [3]. The above-mentioned studies show that the soil structure interaction (SSI) effect is important for the damage estimation of the building in the vulnerability assessment process.

2. COLLECTION OF BUILDING INFORAMTION AND NUMERICAL MODELING

Yangon with its rapid urbanization and increased population, construction industry rapidly developed during the recent years. According to building types information from YCDC (2016), timber, RC and brick-nogging types occupied the highest percentage in the order of approximately 51, 41, and 3 %, respectively. Timber, brick-nogging and some low-rise RC buildings are non-engineered constructions and the recorded building information and material properties are not available. Therefore, field work on building information collection and material testing were conducted for the selected buildings. Samples for material property testing were collected from the existing buildings which were about to be demolished. It was resulted using the ASTM standard testing procedures that the mean compressive strength of masonry block is around 680 psi and that of Inn/ Kanyin wood is 4,400 psi.

Figure 1. Material Testing Works for Masonry and Wood

Initial analysis is started with two-storeyed brick-nogging building situated in Shwe Pyi Thar township in Yangon. For the SSI numerical model, substructure approach is adopted through ASCE 41-13 procedure by considering the shallow foundation as rigid. Translational and rotational stiffness were calculated taking the soil shear wave velocity values as 200 m/s and poisson's ratio to be 0.3.

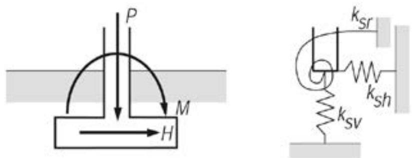

Figure 2. Uncoupled Spring Model using ASCE 41-13 Procedure

Microtremor measurement was also conducted in the modeled building to know the natural frequency of the soil and building. Modal analysis results were enumerated in the Table below.

Table 1. Modal Analysis Result of Two-storeyed Brick-nogging Building using Uncoupled Spring Model and Microtremor Measurement

Period Fixed Base	Period Linear Base	Period Nonlinear Base	Period Microtremor Measurement
0.84 s	0.93 s	0.93 s	0.95 s

3. CONCLUSIONS

It can be seen from the initial modal analysis of two storeyed brick-nogging building, the natural period gets longer, and it approximately matches the microtremor measurement result. Building responses and damage pattern comparison for different buildings through nonlinear dynamic analysis will be discussed later in the USMCA 2019 presentation.

REFERENCES

[1] Chopra A. and Yim S.C., *ASCE Journal of Structural Engineering*, 111(4), (1985), 906-930.
[2] John P. Wolf, *Dynamic Soil Structure Interaction*, Prentice-Hall, Englewood Cliffs, New Jersey, (1985)
[3] Nakhaei M. and Ghannad M.A., *The effect of soil structure interaction on damage index of buildings, Journal of Structural Engineering*, 30, (2008), 1491-99.
[4] Gazetas, G., *Journal of Geotechnical Engineering*, 117(9), (1991), 1363-1381.
[5] ASCE/SEI 41-13, *Seismic Evaluation and Retrofit of Existing Buildings*, Reston, Virginia, 2013.
[6] Nakamura, Y., *A Method for Dynamic Characteristics Estimation of Subsurface Using Microtremor on the Ground Surface, Quarterly Report of Railway Technical Research Institute* 30, (1989), 25–33.

One-dimensional seismic response analysis by equivalent linear method in Kyauktada, Pazundaung and Botahtaung Townships,Yangon, Myanmar

Su THINZAR[1]and Tun NAING[2]
[1]Assistant Lecturer (Engineering Geology), Department of Petroleum Engineering, Technological University (Mandalay), Myanmar
tharyar.stz@gmail.com
[2]Professor, Department of Engineering Geology, Yangon Technological University, Myanmar

ABSTRACT

Yangon had experienced several earthquakes in the past because it is located in the moderate seismic prone area and the seismogenic Sagaing Fault is passing through about 40 km away from Yangon in the east. The studied Kyauktada, Pazundaung and Botahtaung are major townships of Yangon and are located mostly in soft alluvial plain of sand, silt and clay where strong ground motion can be expected. The microtremors survey had been conducted at 84 sites throughout the studied townships. One-dimensional seismic response analysis by equivalent linear method had been performed based on the shear wave velocity structures and subsurface soil profiles derived from microtremor survey and boring data. The peak ground acceleration (PGA), the peak ground velocity (PGV), the response accelerations and the predominant period are main outcomes of response analysis. The PGA values are ranging from 0.16g to 0.28g while the PGV values are between 0.75cm/s and 1.55cm/s. The response acceleration at 1.0s ranges from 0.07g to 0.19g and it is ranging from 0.58g to 1.10g at 0.2s.

Keywords: response analysis, microtremors survey, PGA, PGV, response accelerations

1. INTRODUCTION

Yangon is the most important city in Myanmar for the public commercially and educationally. One of the remarkable historical events that Yangon had experienced in the past is Bago Earthquake (7.3Mw) which was due to the Sagaing Fault on May 5 of 1930. At that time, the death toll in Bago was 500 and 50 in Yangon. There will be several folds in death tolls and damages in Yangon when that earthquake recurrences due to high population density, many substandard buildings and a large number of old buildings. High amplification of underlying soil can cause stronger ground motion in Yangon because several large townships, including studied townships are located in soft alluvial plain which is mainly composed of sand, silt and clay.

The shear wave velocity structures and engineering properties of underlying soil layers are main input parameters for seismic response analysis. Therefore, the shear wave velocity structures and engineering properties of each soil layer in studied townships were determined by combining the microtremor survey results and secondary boring data. Another main input parameter is the earthquake bedrock motion and however, no recorded bedrock motion is available for Yangon area. The computer code prepared by Ohsaki in 1979 was used to generate synthetic bedrock motion.

2. AERIAL COVERAGE OF STUDIED AREA

The studied area; Kyauktada, Pazundaung and Botahtaung Townships are located in shouth eastern part of downtown Yangon as shown in Figure 1 and bounded by Yangon River in the South and Pazundaung Creek in the East. Kyauktada Township has the population of 3,700 while 3,100 in Pazundaung Township and 40,995 in Botahtaung Township according to 2014 Myanmar Population and Housing Census (Ministry of Immigration and Population, 2015). The area coverage of Kyauktada Township is 0.6 km^2, Pazundaung Township is 1.01 km^2 and that of Botahtaung Township is 2.4 km^2, and 4.01 km^2 in total.

Figure 1: Location map of Kyauktada, Pazundaung and Botahtaung townships (Google Earth Image, 2019)

3. SEISMICITY OF YANGON

The historical earthquakes, geologic and tectonic settings around the city highlight that Yangon is located in a moderate seismic prone area (Su Thinzar et al., 2018). The Seismogenic Sagaing Fault, the most active seismic source in Myanmar, is passing through about 40 km away in the east of city (Soe Thura Tun, 2007). The most well-known earthquake for Yangon area is Bago earthquake of 7.3 Mw, on May 5 of 1930.

4. DETERMINATION OF INPUT PARAMETERS

The input parameters, especially the underlying soil information for seismic response analysis had been determined by microtremor survey throughout the studied townships. The survey results were combined with available secondary boring data.

4.1 Microtremor survey

According to Nakamura, 1988, the microtremors are low amplitude ambient seismic noises generated by natural disturbances and microtremor survey has been used as a tool to estimate seismic response of underlying soil layers. Based on the diffuse field theory, Kawase et al., 2011, proved that the microtremor H/V spectral ratios correspond to the square root of the ratio of the imaginary part of horizontal displacement for a horizontally applied unit harmonic load and the imaginary part of vertical displacement for a vertically applied unit load.

The microtremor single station measurements had been conducted at 84 sites in three townships: 20 sites in Kyauktada Township (green colour), 20 sites Pazundaung Township (blue colour) and 44 sites in Botahtaung Township (orange colour) as shown in Figure 2. By using SMAR-6A3P seismometer, it was measured for 20 minutes at each site and the sampling rate is 200 Hz/s. The horizontal to vertical spectral ratio (H/V ratio) was calculated for each site. The required input soil information for 1D seismic response analysis were obtained by inversion of shear wave velocity structures from H/V ratio.

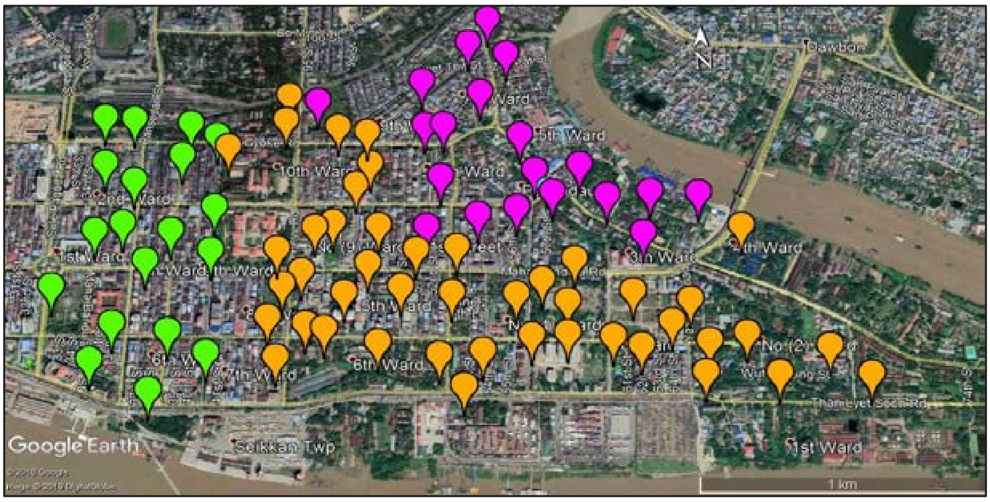

Figure 2: Locations of microtremor measurements in studied three townships

4.2 Input earthquake motion

As the recorded bedrock motion for Yangon is not available, the synthetic waveform of 1930 Bago earthquake was generated by Ohsaki's (1979) computer code based on magnitude of 7.3 Mw, assumed focal depth of 20 km, and epicentral distance of 42 km for earthquake input motion (Su Thinzar et al., 2018) as shown in Figure 3.

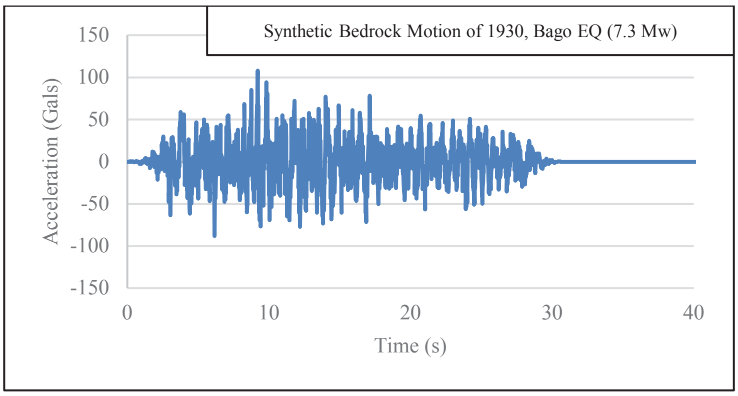

Figure 3: Synthetic bedrock motion for studied townships

The maximum acceleration of synthetic earthquake bedrock motion in Figure 3 is 108 gals or 0.11 g.

5. 1D SEISMIC RESPONSE ANALYSIS

1-D seismic response analysis was conducted by equivalent linear method, using DYNEQ computer program, coded by Yoshida et al. in 2004 for each site where microtremor was measured. DYNEQ is a computer code for the earthquake response analysis of the level ground in frequency domain based on the equivalent linear method and multiple reflection theory. Since multiple reflection theory is an exact solution of the governing equation (wave propagation equation), it has an advantage that incident and reflected waves can be separated, input wave can be specified at any point and any types of wave (incident, composite, or reflected), and any types of wave can retrieve at any location, which is impossible in the nonlinear analysis, and some of them are important in the engineering practice (Yoshida et al., 2004).

The shear wave velocity of 800 m/s was used for elastic half space or weathered bedrock below all soil layers (Hirokawa, 2016). The shear wave velocity, thickness and unit weight of each soil layer, the number of soil layers, and earthquake bedrock motion are the main inputs parameters of response analysis. Theoretical amplification characteristics from layer of elastic half space or weathered bedrock to surface had been determined for consideration of the strong ground motion due to lose alluvium sediments.

6. RESULTS AND DICUSSION

The major results of this research are spectral response spectrum (response accelerations for 1s and 0.2s), peak ground acceleration (PGA) and peak ground velocity (PGV).

6.1 Response spectrum

The response spectrum is used extensively in earthquake engineering practice. The response spectrum describes the maximum response of a single degree-of-freedom (SDOF) system to a particular input motion as a function of the natural frequency (or natural period) and damping ratio of the SDOF system (Kramer, 1996). Some response spectra under 3 materials (soil) damping conditions; 2% damping, 5% damping and 10% damping are shown in Figure 4. It is obvious that the greater soil damping will reduce the response acceleration more. The response acceleration at 5% soil or material damping is generally used for earthquake resistant design consideration.

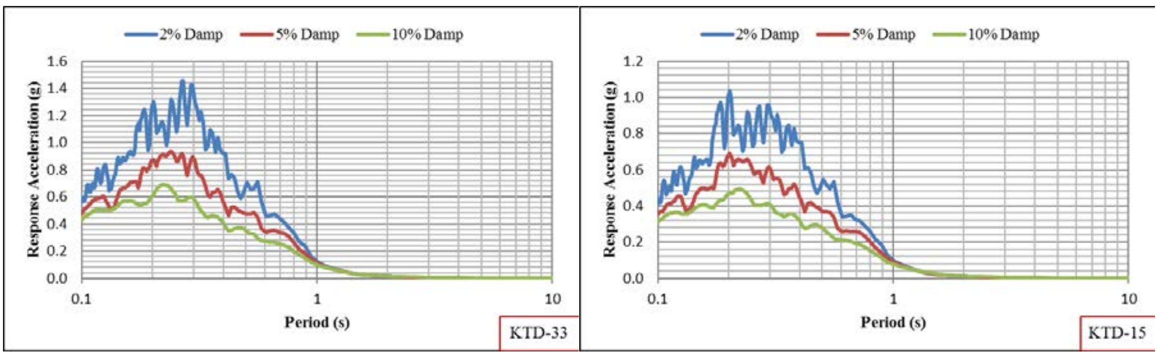

Figure 4: Spectral response spectra at some selected sites in studied townships

The maps of response accelerations for 1s and short period 0.2s were prepared based on the response spectra at 5 % damping and are shown in Figure 5 and Figure 6.

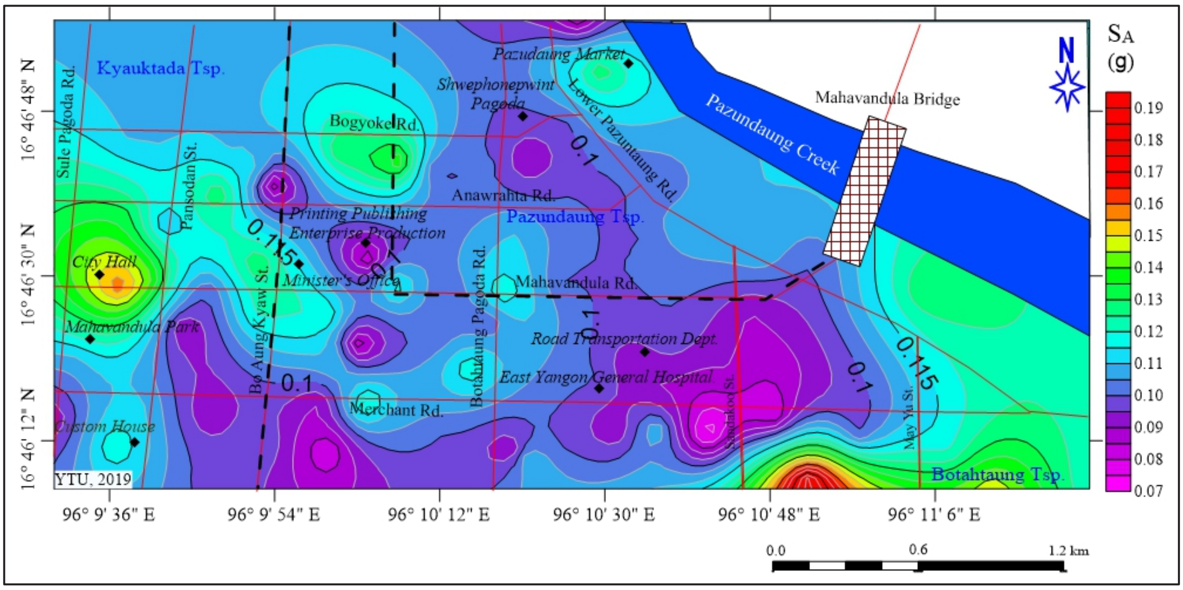

Figure 5: Map of response acceleration at 1s for Kyauktada, Pazudaung and Botahtaung Townships

The response acceleration at 1s is ranging from 0.07g to 0.19g as shown in Figure 5 and it can be regarded the acceleration is low at 1s. Relatively, higher acceleration (green to red) zones are around the city hall in western part and the highest one (yellow to red zone) in south-eastern part of the area. The purple colour zones represent the lower response acceleration at 1s.

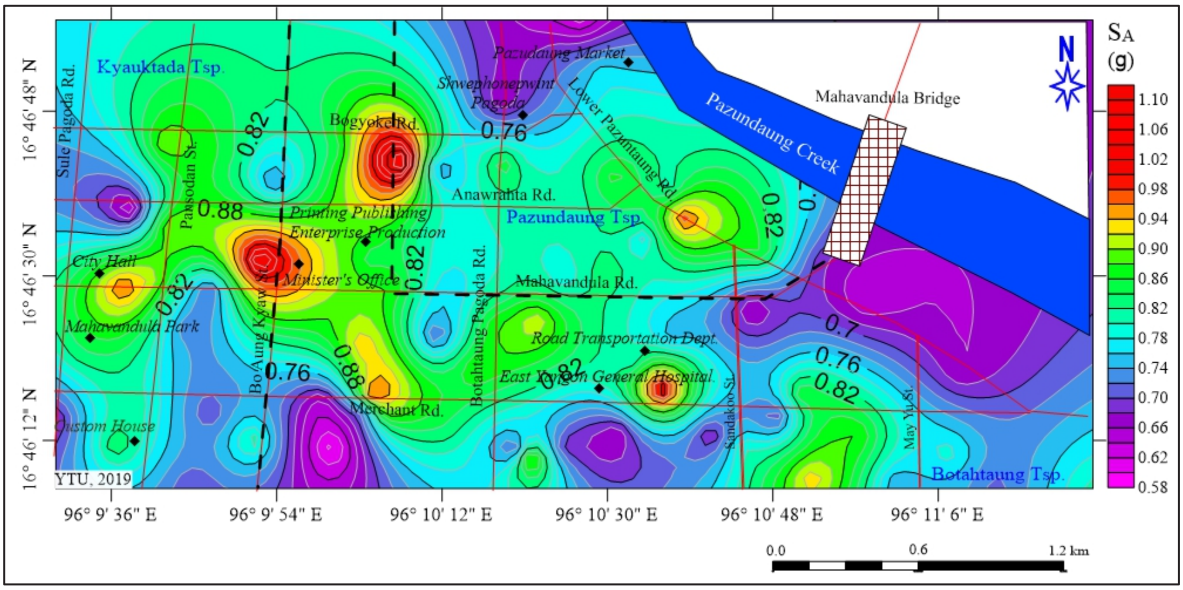

Figure 6: Map of response acceleration at 0.2s for Kyauktada, Pazundaung and Botahtaung Townships

The response acceleration at 0.2s ranges from 0.58g to 1.10g as shown in Figure 6 and most of the areas are covered by higher acceleration. The various structures may response at higher response acceleration in the areas (green, yellow and red zones) along Thein Phyu Road, between Sule Pagoda Road and Lower Pazundaung Road and along the Merchant Road.

6.2 Peak ground acceleration, PGA

Ground motions with high peak ground accelerations are usually, but not always, more destructive than motions with lower peak accelerations. Very high peak accelerations that last for only a very short period of time may cause little damage to many types of structures (Kramer, 1996). The most commonly used measure of amplitude of a particular ground motion is peak ground acceleration, PGA and it is the absolute value of horizontal acceleration (Kramer, 1996). The PGA is always used to describe the ground motion because of its natural relationship to inertial force induced in certain types of structures (Kramer, 1996). The acceleration time histories of some selected sites are shown in Figure 7 and the PGA map is shown in Figure 8.

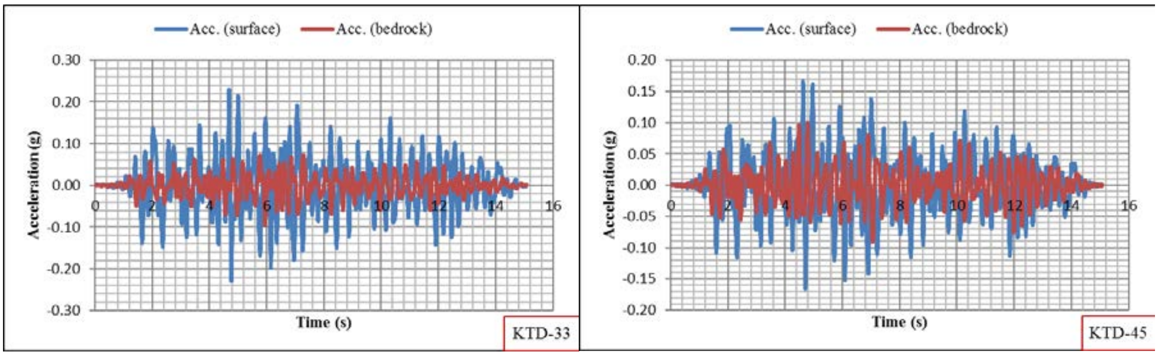

Figure 7: Acceleration time histories at some selected sites in studied townships

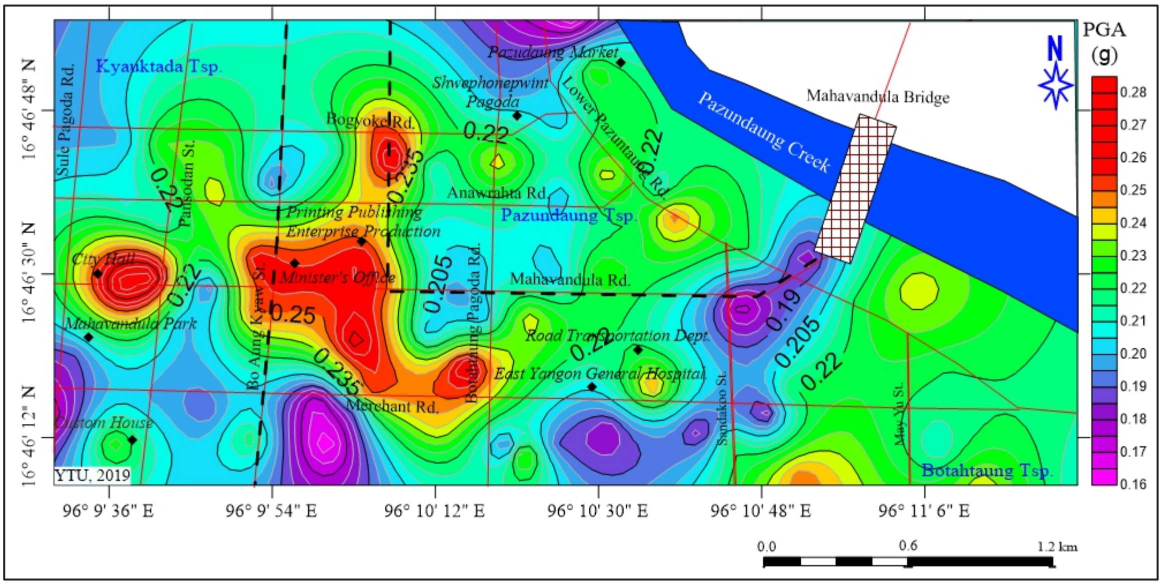

Figure 8: PGA map of Kyauktada, Pazundaung and Botahtaung townships

As shown in Figure 8, the PGA values are ranging from 0.16g to 0.28g in the studied townships. The red colour represents the highest PGA zones and the lowest PGA zones are in purple colour. The highest PGA zones can be observed around city hall, along the sections of Merchant Road, Mahavandula Road between Bo Aung Kyaw Road and Botahtaung Pagoda Road. The stronger ground shaking can be expected in those higher PGA zones then lower PGA zones.

6.3 Peak ground velocity, PGV

The peak ground velocity (PGV) is another useful parameter for characterization of ground motion amplitude. Since the velocity is less sensitive to the higher-frequency components of the ground motion, the PGV is more likely than the PGA to characterize ground motion amplitude accurately at intermediate frequencies (Kramer, 1996). For structures or facilities that are sensitive to loading in this intermediate-frequency range (tall or flexible buildings, bridges, etc.), the PGV may provide a much more accurate indication of the potential for damage than the PGA (Kramer, 1996). The following Figure 9 shows surface velocity time histories of some selected sites in studied townships.

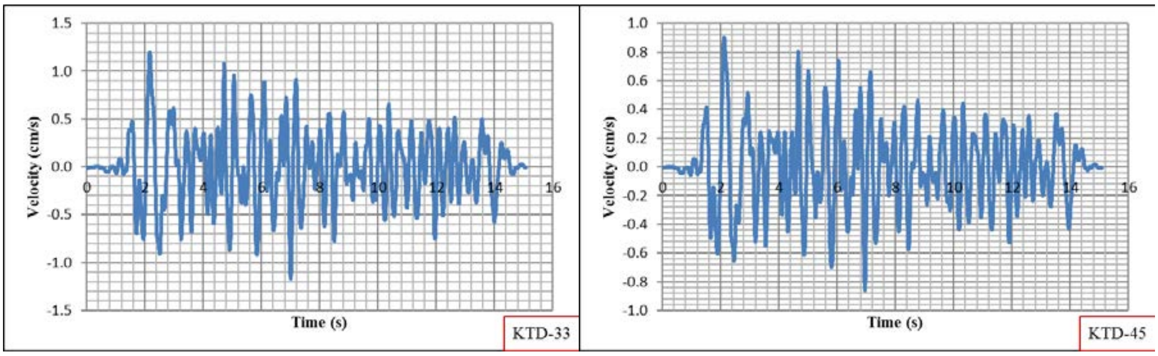

Figure 9: Velocity time histories at some selected sites in studied townships

The map of peak ground velocity (PGV) was prepared for studied townships based on the velocity time histories of 84 sites as shown in Figure 10.

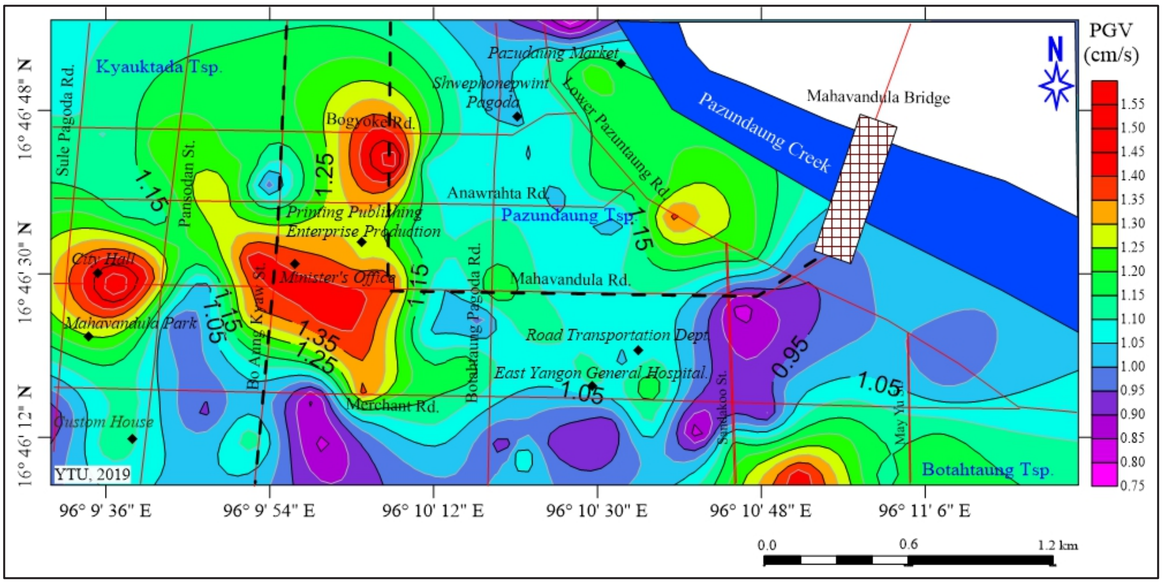

Figure 10: PGV map of Kyauktada, Pazundaung and Botahtaung townships

The PGV values are between 0.75 cm/s and 1.55 cm/s as shown in Figure 10 and the distribution PGV values is similar to that of PGA values; the highest PGV zones are around city hall, along the sections of Merchant Road, Mahavandula Road between Bo Aung Kyaw Road and Botahtaung Pagoda Road. The relatively larger damage can be expected in higher velocity zones than the other parts of the townships.

7. CONCLUSION

Kyauktada, Pazundaung and Botahtaung are important townships of Yangon due to existence of buildings with high historical and cultural values such as ministers' Office and City Hall. Although Yangon is located in moderate seismic prone region, the seismic risk can be quite high because of its high population and substandard buildings. Therefore, 1D seismic response analysis by equivalent linear method was carried out at 84 sites, using DYNEQ computer code to support detailed hazard information for future seismic risk analysis.

The PGA, values are between 0.16g and 0.28g while the PGV values range from 0.75 cm/s to 1.55 cm/s. The PGA and PGV distribute similarly; the highest zones were observed around city hall, along the sections of Merchant Road, Mahavandula Road between Bo Aung Kyaw Road and Botahtaung Pagoda Road.

Most parts of three townships are covered by high spectral response acceleration at 0.2s and the acceleration is relatively low at 1s. It can be regarded that the seismic risk of buildings in the areas with high PGA, PGV and response acceleration will be relatively higher than the buildings in other places.

REFERENCES

Google Earth Image, 2019. [Online]. Available: http://www.google.com/

Hirokawa, Y., Matsushima, S., Kawase, H., Naing, T., and Thant, M., 2016. Estimation of underground structures in Yangon City, Myanmar using single-station and array microtremors, *Proceeding of International Symposium on Earthquake Engineering,* JAEE, Vol.1.

Kawase, H., Sánchez-Sesma, F. J. and Matsushima, S., 2011. Effects of Surface Geology on Seismic Motion: The Optimal Use of Horizontal-To-Vertical Spectral Ratios of Earthquake Motions for Velocity Inversions Based on Diffuse Field Theory for Plane Waves, *Bulletin of Seismological Society of America*, Vol 101, pp 201-214.

Kramer, S. L., 1996. *Geotechnical Earthquake Engineering*, Prentice Hall, New Jersey.

Ministry of Immigration and Population, 2015. The Union Report: *the 2014 Myanmar Population and Housing Census*, Census Report Volume 2.

Nakamura, Y., 1988. *A method for dynamic characteristics estimation of surface layers using microtremor on the surface*, RTRI Report 4, 18-27.

Ohsaki, Y., 1979. Guideline for evaluation of basic design earthquake ground motions, Appendix to Regulatory Guide for seismic Design of Nuclear Power Facilities, Japan.

Thinzar, S., Naing, T. and Latt, K. Z., 2018. Determination of Ground Motion Parameters by 1D Equivalent Linear Method in Botahtaung Township, Yangon, Myanmar, *Proceedings of 9th International Conference on Science and Engineering*, Yangon Technological University, Yangon, Myanmar.

Tun, S. T., 2007. Tectonic Map of Myanmar and Surrounding Region, Myanmar Geosciences Society, MGS.

Yoshida, N. and Suetomi, I., 2004. DYNEQ: A computer program for dynamic response analysis of level ground by equivalent linear method," version 3.25.

OVERVIEW OF URBAN GROWTH AND YANKIN REDEVELOPMENT

TOWARDS SUSTAINABLE LAND USE PLANNING IN YANGON

S.S.MOE[1], T.G.SHWE[2]

[1] Associate Professor, Department of Architecture, Yangon Technological University, Yangon, Myanmar,
[2] Professor, Department of Architecture, Yangon Technological University, Yangon, Myanmar,

***Keywords**: Urban Growth, Urban Congestion, Sustainable Land Use Planning, Environmental Impact, Yankin Redevelopment, Yangon.*

1. INTRODUCTION

Yankin is one of the most populated townships of inner urban ring area in Yangon. Nowadays, it is rapidly change to modern city by building with multistoried high-rise buildings and it has been transforming to be a commercial hub of Yangon. Within its parameter some important buildings are existed. These are Central Bank of Myanmar, Yangon Head Quarters (existed on Industrial Road), CB Bank HQ (existed on Sayarsan Road), Yoma Bank HQ, Ooredoo Telecom HQ in Myanmar Plaza (existed on Kabar Aye Pagoda Road), Telenor HQ (existed on No 1. Industrial Road0, Myanmar International School (existed on Maw Ya Waddy Street), Yankin Children Hospital (existed on Kanbae Road). Urban facilities like international school, vocational training centers in the field of Health, IT and Finance among other education and training are grouping each other. So, Yankin Land use is tremendously changed to second CBD of Yangon (central business distrait). This condition is that all the elements need to develop the next generation of Entrepreneurs and leader of Myanmar. These urban facilities are offices which include Grade A office buildings for the multinationals and SOHO (Small Office Home Office) for entrepreneurs and Shared office for the startups and IT mall among other malls to be invited for entrepreneurs who are starting business using information technology. Beside that hotels, condominium, exhibition and conference center to be included.

2. POPULATION, POPULATION GROWTH AND HOUSEHOLD

According to the census record in 2014, there are 14,637 households in Yankin township and population is about 70,946 persons, including in promotion of male 32,724 persons and female 38,222 persons. Male to female ratio is approximately 1:1.2. In figure 2.1 shows the increasing of population from 2015 to 2017. Fig 2.2 shows the population and Number of households in each ward. Fig 2.3 shows the population per square mile in each ward.

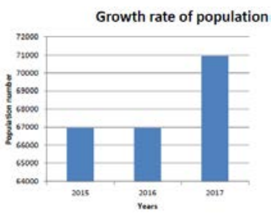

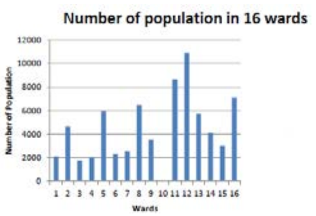

Fig (2.1) Growth rate of population in township
Fig (2.2) Number of population in township

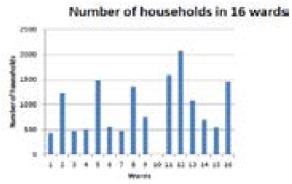

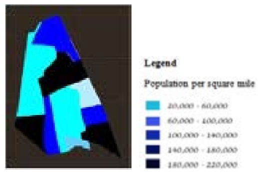

Fig (2.2) Number of household in township
Fig, (2.3) Density Map

3. CAUSE AND CONSEQUENCES

Currently, in Yangon development trends is going to build in mixed-use projects neglecting the inhabitants behavior, comfort and traffic congestions are causing lack of proper zoning plan for long turn development. According to site layout and synergy, using urban center with ground floor retail facing the street residential and/or office on upper levels. These may include one or multiple blocks. Each developer must normally stand on its own experiences based on area market demand. Traffic impact is the major factor of Yangon City. Future mixed use development projects should be study and access trip generation and by using shared parking, considering internal trip capture, site layout and walking distances.

4. CONCLUSION

There is a clear conclusion arising from this study that point towards the development of idea for land use potential in Yangon. Yangon is one of the most important commercial centers and city has also grown rapidly in recent years. Unplanned and rapid urbanization increase population as well as number of vehicles, poor traffic management and poor road condition. Shopping malls or shopping centers are nowadays arising to build in Junction area and near junction area. In this study some land use changed development projects are made a case studies and detail analysis are going upon them. However, it is clear from the information in this conclusion that the primary uses today and foreseeable mixed use developments are retail, restaurant, residential and office. Available resource should be concentrated on those uses, but any procedures developed should be adaptable to all common land uses. According to this some area should be controlled. Some should be promoted and some should be freeze.

REFERENCES

[1]San San Moe, “The Current Trends of Urban Development in Yangon City and Its Implication on the Environment” GMSARN International Online Journal Vol-3/ No.4, March, 2010 pg. 40-49 (www.gmsarn.org)

[2]Yangon City Development Committee. 2016. Yangon City Comprehensive Land Use, Zoning and Urban Design Review Working Committee.

ESTIMATION OF SITE AMPLIFICATION FACTOR IN YANGON CITY

Takumi MATSUMOTO[1], Takaaki IKEDA[2], Hideomi GOKON[3], Atsuya MINAGAWA[4]
TUN NAING[5], and Osamu MURAO[6]

[1] Graduate student , Civil and Environmental Engineering, Nagaoka University of Technology, Niigata, Japan,
[2] Professor, Civil and Environmental Engineering, Nagaoka University of Technology, Niigata, Japan,
[3] Associate professor, Knowledge Management, Japan Advanced Institute of Science and Technology, Ishikawa, Japan,
[4] Graduate student , Civil and Environmental Engineering, Nagaoka University of Technology, Niigata, Japan,
[5] Professor, Engineering Geology, Yangon Technological University, Yangon, Myanmar,
[6] Professor, International Research Institute of Disaster Science, Tohoku University, Miyagi, Japan,
Correspond to Matsumoto (s163310@stn.nagaokaut.ac.jp)

***Keywords**: site amplification factor, vulnerability evaluation, microtremor, H/V spectral ratio,soil classification*

1. BACK GROUND

Our research focuses on seismic risk assessment in Yangon, Myanmar. There is plate boundary around Myanmar, and the Sagaing fault runs in the central part, so the earthquake risk is very high. The ground motion due to an earthquake may cause greatly damage. In this study, for the purpose of seismic vulnerability evaluation of surface ground, we estimated the site amplification factor (ARV) based on average shear wave velocity in Yangon.

2. ESTIMATION MEATHOD OF ARV

The target area was 568 wards of Yangon, and the ARV was estimated from three methods. Fig.1 shows the site amplification factor of each ward determined from the estimated values of three methods. Each estimation method is explained below. The accuracy of ARV was improved by estimating it in order of 1), 2) and 3).

1) Simplified Method

In Tokyo, 12 types of soil classification are defined from geomorphologic and geologic characteristics, and the ARV of peak ground velocity is determined for each soil classification[1]. In this study, the soil classification of Yangon was determined based on it of Tokyo, and the ARV was simply estimated. Yangon was classified into 4 categories from geoinformation. Tab.1 shows the soil classification and characteristics of Yangon.

Table 1. The soil classification and characteristics of Yangon based on it of Tokyo

Classification	ARV	Characteristic
Plateau 1	1.6	Diluvium, Gravel
Plateau 2	1.7	Diluvium, Clay
Valle-plain 2	1.8	Sediment, Soft layer 3-8m
Alluvial plain 2	2.3	Alluvium, Soft layer 0-10m

2) Microtremor measurement

The ARV shows strong correlation with the shear wave velocity[3]. Therefore, this study estimated the ARV using the formula with the average shear wave velocity as the parameter (Eq. (1)) proposed by Matsuoka and Midorikawa (1994).

$$\log ARV = 1.83 - 0.66 \log AVS \qquad (1)$$

The average shear wave velocity was calculated from the predominant frequency of surface ground estimated by the H/V spectral ratio of microtremor. Microtremor measurement was conducted at 140 sites at intervals of about 2 km.

3) Boring data

The average shear wave velocity was calculated from boring data in Yangon, and the ARV was estimated by Eq.(1). The ground with N-Value less than 50 was regarded as surface ground, the predominant frequency of surface ground was calculated based on N-Value.

Figure 1. Site amplification factor of Yangon

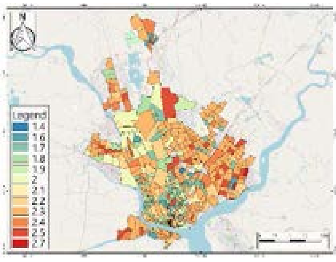

3. CONCLUSION

The accuracy of the estimation was improved by comparing the results of each method. By using microtremor measurement and boring data, the ARV reflecting the predominant frequency and ground structure at each site was indicated.

REFERENCES

[1] Maruyama, Y., Fushioka, S., Yamazaki, F., Evaluation of Site Amplification in the Survey of District-based Vulnerability to Earthquake Disaster Performed by Tokyo Metropolitan Government, Institute of Social Safety Science, No.16, 2012
[2] Nakamura, Y., Basic Sturacture of the H/V Spectral Ratio, The Society of Exploration geophysicists of Japan, 2008
[3] Midorikawa, S., Matsuoka, M., Sakugawa, K., SITE EFFECTS ON STRONG-MOTION RECORDS OBSERVED DURING THE 1987 CHIBA-KEN-TOHO-OKI, JAPAN EARTHQUAKE, japan Association for Earthquake Engineering, No.9, 1994

STUDY ON AMPLIFICATION FACTOR OF MAXIMUM ACCELERATION FOR SEISMIC HAZARD ASSESSMENT

Atsuya MINAGAWA[1], Takaaki IKEDA[2], Hideomi GOKON[3], Takumi MATSUMOTO[4], and Tun NAING[5]

[1] Graduate student, Nagaoka University of Technology, Japan,
[2] Professor, Nagaoka University of Technology, Japan,
[3] Associate Professor, Japan Advanced Institute of Science and Technology, Japan,
[4] Graduate student, Nagaoka University of Technology, Japan,
[5] Professor, Yangon Technological University, Myanmar,

Keywords: *Vulnerability assessment, Maximum acceleration, Maximum velocity, Hazard map*

1. INSTRCUTION

Our research focuses on the evaluation of amplification characteristics for earthquake risk assessment in Yangon city, Myanmar. The earthquake risk is very high because there is the Sagaing fault longitudinally cutting in central Myanmar, and a plate boundary in the vicinity of this country. The amplification characteristics of the ground are evaluated using topography classification, soil profile, microtremor and so on. It is possible that the ground surface shake greatly affects the damage caused by the earthquake. The amplification characteristic of the ground in our research has been mainly the evaluation of the maximum velocity in the surface ground. In this study, it is aimed to evaluate the amplification characteristics of maximum acceleration and to investigate the effectiveness of earthquake risk control in Yangon.

2. METHODS

2.1 Methodology

First, the acceleration and velocity amplification factors are obtained using the vertical array observation records where seismometers are installed on the base and the ground surface. However, since there is no vertical array seismic observation in Yangon City, we use the records of vertical array observations in Japan.

Since the amplification factor is affected by the ground motion level, multiple seismic records with different ground motion levels are used. The velocity time history waveform is calculated by integrating the acceleration time history waveform[1)].

2.2 Calculation of amplification factor and relational expression

It was found that the geological condition is mainly sand and clay by the geologic columnar section of Yangon, and the surface layer is a very soft ground with a surface N value of 50 to 25m and 45m. Figure-1 shows a geologic columnar section of Yangon. Therefore, the measurement points similar to the geological condition of Yangon was selected from the geological condition and S-wave velocity of the geologic columnar section using the strong motion data of the strong motion observation network (KiK-net[2)]) in Japan.

KiK-net has about 700 observation facilities nationwide, and each observation facility has an observation well.

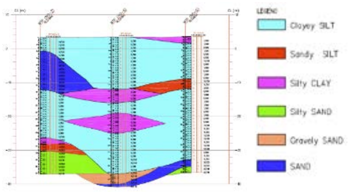

Figure-1 The geologic columnar section of Yangon

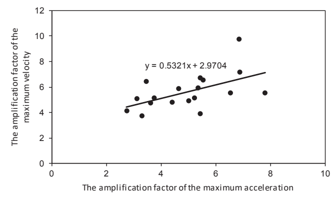

Figure-2 the relationship of amplification factor

Strong-motion seismometers are installed on both the surface and underground. The selected locations were AICH06 which observed maximum accelerations of 5.2, 5.3, and 5.6 gal, and AICH09 which observed 5.0, 5.2, and 5.2 gal, and AKYH17 which observed 5.0 gal three times.

3. RESULTS

Figure 2 shows the amplification factor of maximum acceleration on the horizontal axis and the amplification factor of maximum velocity on the vertical axis, and shows the relationship linearly. At the present stage, there are only 18 measurements, but it can be inferred that there are correlations between them.

4. CONCLUSIONS

Although the calculation of amplification factor in this research is not a method to carry out in detail, it is necessary to investigate as a new evaluation object of the amplification characteristic of the future ground using the relationship between both of them. The plan is to expand the usefulness of research on amplification characteristics in Yangon.

REFERENCES

[1] Kazuyuki IZUNO, Ritsumeikan University, "Integral.xlsm" program for integrating the acceleration waveform in the frequency domain (2015)
[2] National Research Institute for Earth Science and Disaster Resilience (2019), KiK-net, National Research Institute for Earth Science and Disaster Resilience

Developing Evacuation Areas in Yangon for Emergency Response with GIS system

Ms. Eiei TUN[1], Ms. Tintin AYE[2]

DR. Takaki KATO[3] and Ms. Tomoko MATSUSHITA[4]

[1]Student, Satreps Group of Urban Planning,

Department of Architecture, Yangon Technological University, Yangon

eiei.cocci@gmail.com

ABSTRACT

Yangon is facing fire disaster as highest risk and evacuation areas will become major issues to provide in new planning. Currently, there is no usage of green spaces as evacuation areas in Yangon. The objective of having an evacuation area includes quickly and safely moving population away from the danger zone into shelters to reach in time by the shortest way, to allocate disaster prevention evacuation areas depending on population density. The minimum standard of evacuation areas for each ward will be produced as a hypothesis of the study. The evacuation service areas analysis will reveal the lack of green spaces in each ward and also define suitable locations with a focus on emergency safe and accessibility as one of the disaster facilities of green spaces. Network analysis through GIS, evacuation service areas, recommended evacuation routes, and risk level can be determined based on risk level and human's walking speed. The questionnaire surveys of government offices which perform mainly in reducing disaster risks will enhance for accurate outcomes. The output indicates the vulnerable areas of Yangon, introduction of green areas as emergency shelters and enhancement of emergency modified evacuation methods to increase resilience in city planning.

Keywords: *Risk assessment, Emergency response, Evacuation Service Areas, Geographic Information System, Evacuation Routes.*

Introduction

Myanmar, also known as Burma, is one of the developing countries in Southeast Asia with the population density of 56 million. The rapid growth of urbanization has been occurred in Yangon when reviewing last 10 years to until now. Yangon has been experienced changes of land utilization over 60 years after colonial period. The growth in population and physical assets in hazard-prone areas, lack of basic infrastructure and access to affordable land, extreme poverty and substandard structures of buildings increases the vulnerabilities of the urban population. Moreover, there is important need to include emergency evacuation areas in new town planning. Currently, the green area per person of Yangon is 0.37 square meter per person according to JICA study and it is noticeable minimum when compared to other developing countries. The important factor is the rule and regulation on urban planning. Most of the urban planners predicted that Yangon may become mega city in 2040. The integrated guideline and recommendations will be new evaluation and changing of integrated town planning.

The first step towards the urban resilience planning is to ensure that affected people are evacuated in a short time to safe assembly points and shelters during the disasters. To ensure an efficient disaster management, the shelter locations should be strategically allocated within minimum evacuation distance and time. The increased recognition of green and open spaces is one of the strategies to the urban expansion characteristics. The open space network makes contribution to urban resilience.

Literature Review and Study Framework

Planning emergency shelters in advance is an effective approach to mitigate the damage caused by natural disasters.

Pre-identification of suitable shelter to be used in evacuations

This section should plan for the pre-identification of suitable accommodation for evacuees within the safety zone. Shelter provides for the temporary accommodation of evacuees. It provides the basic personal needs which arise at an individual level during an emergency. Identification of appropriate shelter areas should be based on safety, availability of facilities, accessibility, capacity, and numbers of persons. Location will depend on the type and severity of the hazard, as well as potential secondary hazards. According to particular situations and contexts, new levels and types of risk may quickly emerge requiring evacuation to new areas due to secondary hazards such as fire following earthquakes. Sites should be identified in the planning stages. Issues in the use of public facilities, such as schools, must be considered when identifying potential evacuation centers. This will include analyses of the potential negative impacts of the use of public facilities on host communities.

Emergency Response Preparedness System of Myanmar

The Humanitarian Country Team (HCT) of Myanmar drafted and regularly updated an Inter-Agency Contingency Plan (IACP). The IACP was designed to support the Government of the Union of Myanmar in preparing for, and responding to, any of the hazards that may affect Myanmar. In 2014, the HCT decided to apply the new guidance for Inter-Agency Response Preparedness (ERP) as an action-oriented approach to enhance readiness for humanitarian response. This methodology replaces the previous IACP. The ERP approach seeks to improve effectiveness by reducing both time and effort, enhancing predictability through establishing predefined roles, responsibilities and coordination mechanisms. The Emergency Response Preparedness Plan (ERPP) has four components which have similarities with the previous IACP: i) Risk Assessment and Monitoring, ii) Minimum Preparedness Actions, iii) Contingency Response Planning, and iv) Standard Operating Procedures for the Initial emergency response.

The overall goal is to mitigate the impact of disasters and save as many lives as possible from preventable causes. [8]

Current Conditions of emergency evacuation system of Yangon

The survey is extracted through the discussions with the government officers who play mainly in the disaster management cycle. The Government offices include urban planning group of Yangon City Development Committee, Ministry of Social Welfare, Relief and Resettlement, and Myanmar Red Cross Society. The major aim is to improve the emergency evacuation system as a response for disaster management. The survey is composed with main 11 questions to reveal the current emergency response system of Yangon.

Firstly, the action plan is effected and losses time, livelihood and infrastructure development for post disaster emergency responses. YCDC has to coordinate with other relevant ministry and public official for rehabilitation services. The contingency Plan of Myanmar aim for multi hazards such as earthquakes, storms, flooding and etc. Types of disasters are classified from small to large scale. The Disaster risk management system includes responses for basic facilities such as food, wastes and relief goods. The evacuation teams need support with equipment for rescue and research. The major contribution of food supply and basic utility will serve for the evacuees. Non- food items such as sanitary (wash-kit) for 10,000 people store for disaster preparedness. Total warehouses of both government and of NGOs are totally around 30 numbers in Yangon. Starting from 2015, priority needs for emergency evacuees target for 22,000 residents per year in MRCS. Each warehouse of the relief and resettlement has emergency food for minimum 150 to 300 people normally. For non-food items, each warehouse contains 10,000 people. In each evacuation team, the equipment include Telephone, Based VHF Machine, Radio with battery, camera, carry box, advanced first aid kits, T-shirt, cap, back pack, touch, calculator, notebook and pen, VHF Icon, Life Jacket, Rain coat and sleeping bag. During 2011-2014, MRCS have already trained 712 volunteer by 25 team trainings in different states and region in Myanmar. YCDC takes emergency preparedness by serving duties and responsibilities of drainages, collecting garbage, checking the building resistance, etc.

Secondly, project areas include non-structural, structural, small-scale disaster risks reduction, health care and early warning system under MRCS. A national disaster response team has been set up by the Myanmar Red Cross society in the country that will be able to give immediate attention and assistance to emergencies and disasters in the country. Major response preparedness is to understand disaster management and awareness, simulation and drill.. It also includes Disaster risk reduction, preparedness for safe public facilities and shelter. Contingency plan as major response preparedness should include temporary shelter such as schools, monasteries and open spaces such as football field for each township. The minimum requirements of each temporary shelter need to analyze and provide for the international standard of shelter requirements in future. Depending upon the township disaster management committee, MRCS, YCDC and community leaders including the residents, the most vulnerable areas are evolved. The suitable locations for temporary emergency evacuation are based on the township population and township risks level.

Mostly, the evacuees keep at the religion building, temporary shelters, schools and stadiums and their relationship resident. Besides, undergraduate schools serve as evacuation areas and MRCS can support basic facilities of children mainly and the aids to be use as evacuation shelter. The affected people usually get Diarrhea, dengue, respiratory tract infection are diseases after disasters. The participants were trained on how to manage disasters and emergency situations and also to equip them with the right skills on how to deal with diseases like Malaria, Cholera, Ebola, Yellow Fever and other epidermal related diseases.

Thridly, the missing of the affected people is usually facing when making evacuation during disasters. Besides, transportation such as the direction of exit way, how to go and run to shelter to reach safely, how to stay and which places can be saved for their live, etc., and Financial difficulties are the difficulties for the evacuation team. Besides, home ownership becomes major problem when providing the shelters and also the basic facility during disaster. After disaster, the difficulties become the camp management, contributed relief goods to disaster affected people, health and nutrition of refugee, resettlement after disaster. Between the government offices and NGO, the cooperation and coordination, define duties and responsibilities, time-frame, budget become major tasks for resettlement. When they make evacuation for relocation the affected people, the organization usually face the scarce land for relocation the evacuees. There is no special evacuation place in Yangon.

Thirdly, the renovation of infrastructure, resettlement, employment opportunity, mental secure, etc., become the important tasks to carry after the disasters. Emergency facilities such as medicals, evacuation places, hospitals, and search and rescue equipment become essentially need to reduce the disaster risks. The above results reflect the current emergency evacuation process of Yangon. Nearly all of the organizations express the whole process of disaster management cycle from their current position. According to the survey, the lack of planning leads to scattered processes. Therefore, the integrated emergency evacuation management plan should be developed. Additionally, the ongoing process should be taken from the determination from several coordination workshops.

Method

The author would like to study the township level as a typical one by using the capacity constraints and accessibility constraints to reduce the disaster risks level. The spatial analysis using database link with Geological Information System (GIS) will utilize to highlight vulnerable areas of township. The study was based on township report and 2014 Housing Census. The next section provides our results and discussion. The paper concludes with a summary of the results showing that vulnerability townships areas for emergency evacuation.

The framework and processes of analysis in the present research are as shown below.

1) Calculation the coverage areas within 1km from centroids of each ward. A map produces the area in square-meter per person to know the coverage amount of evacuees in shelters.
2) Calculation of the linear distance between each ward and each emergency shelter
   The linear distance between the center of each ward and each emergency shelter will be calculated by using the normal people walking rate at 4km.

Basic Data Sets Used

Background Data

The South Dagon Township is located with the Dagon Seikkan Township on the East side, Hle-gu on the north, Tharkata and Thingangyun Townships on the south and North and East Dagon Myottit Townships on the west. The study area is located along the No (2) Main Road. The major roads of Pyi Htaung Su and Kyan Sit Thar Road are connected neighborhood townships. The railroad is passed through 26 ward and 22 ward within the township.

Green and Open Spaces Locations

The data of existing green areas including parks, playgrounds and green area are supported by Yangon City Development Committee (YCDC) and places of worships are extracted from JICA Study of 2012. The facility and the attributes of the existing data set are the major keys for analysis. The total 68 number of parks and playgrounds are under controlled by Yangon City Development Committee (YCDC) as public ownership. The existing places of worships will also be used as potential shelters for evacuation according to the questionnaire survey. The total 93 numbers of places of worships exist inside the South Dagon Myotthit Township. The locations will be analyzed to find out the shelter coverage area per person. In the immediate aftermath of a disaster, particularly in extreme climatic conditions where shelter materials are not readily available, coverage area less than 3.5 square meter per person become appropriate to save life and to provide adequate short-term shelter to the greatest number of people in need. In such instances, the shelter response should be designed to reach 3.5sq.meter per person as possible, as longer durations may begin to affect the health and well-being of the people accommodated. [2] [6]

Response Capacity Evaluation

The distribution of emergency shelters will be displayed on the digital map by using GIS tool. In the present research, the places of worships as emergency shelters are newly added to emergency shelters. The places of worships were utilized as emergency shelters in the past disasters. For a shelter to meet the basic facility, the number of people in a shelter should not exceed the shelter's maximum capacity. There are two kinds of analysis for the evacuation coverage area.

For the first one, a proximity feature (emergency shelters) that is within 1km from centroid of each ward is selected and 'n' value (the total number of evacuation shelter within 1km) is obtained. For each ward, the n value will be the average of the number of emergency shelters within 1km.The 1km is a standard of the human walking distance. Following the same series, the population within 1 km from centroids of each ward will be produced. The results of total emergency shelters will be divided by the total population. The result will show the vulnerable wards which lack evacuation areas.

For the second, the 1km rings from the centroids of green areas including parks, playgrounds and places of worships will be produced. These intend to know the capacity of each emergency shelters which can hold during disasters. According to the above two analysis, the minimum capacity of evacuation areas will be produced as responses of emergency disaster risks management.

Response Coverage Evaluation

In the present research, the linear distance between each district and each emergency shelter will be calculated by using a tool of GIS. The residential data is extracted from the 2012 JICA study. The data identify a total of 6097 residential communities.

There are two types of road generally: major and minor. The counted roads are 2 lanes and above. The origin destinations (OD Cost Matrix) analysis of parks, playgrounds and green areas has done using the velocity equation. The standard human walking rate of 30 mile per hour is using to produce the minimum time taken for the evacuation. The OD cost matrix analysis, using the tool of GIS; a proximity feature of emergency shelter as destination analyzed with centroids of each household as origins and show the shelter demand.

Results and Discussions

For the analysis of evacuation areas for South Dagon Myotthit Township, the existing of green areas and places of worships in each ward are taking into account as first. The results show that about 50 percent of the total wards of green areas lack in evacuation areas for the evacuees. And, there are two wards which lack the place of places of worships. This study will show in the fig a and b as below.

The response capacity analysis shows that the green area and places of worships area per person in each ward. According to the figures of c and d, the results show the emergency evacuation area per person. The maximum evacuation area per person of green spaces is 10.814 sqm for No.25 ward and the minimum is 6.431sqm for No.26 ward. For the places of worships, the maximum is 34.77 sqm in Ywar Thar Gyi ward and minimum one is 10.22 in Nol.66 ward. The total coverage wards for green and places of worships are ward No.26 (6.431sqm), No.25 (21.144sqm), No.66 (10.22sqm), No.63 (13.67sqm), No.57 (17.71sqm) and Ywar Thar Gyi Ward (48.43sqm). The red circle shows the wards where coverage area is between 0 to 5sqm. About 50 percent of the total wards lack in evacuation areas for the evacuees. But , there are only two wards which lack the place of places of worships.

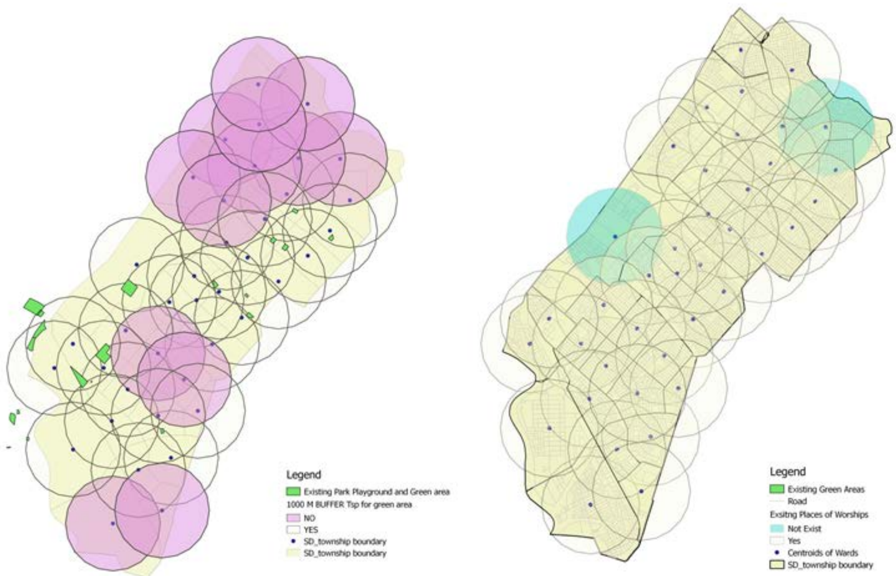

Fig.a and b show the existing green areas and places of worships in South Dagon Myotthit Township.

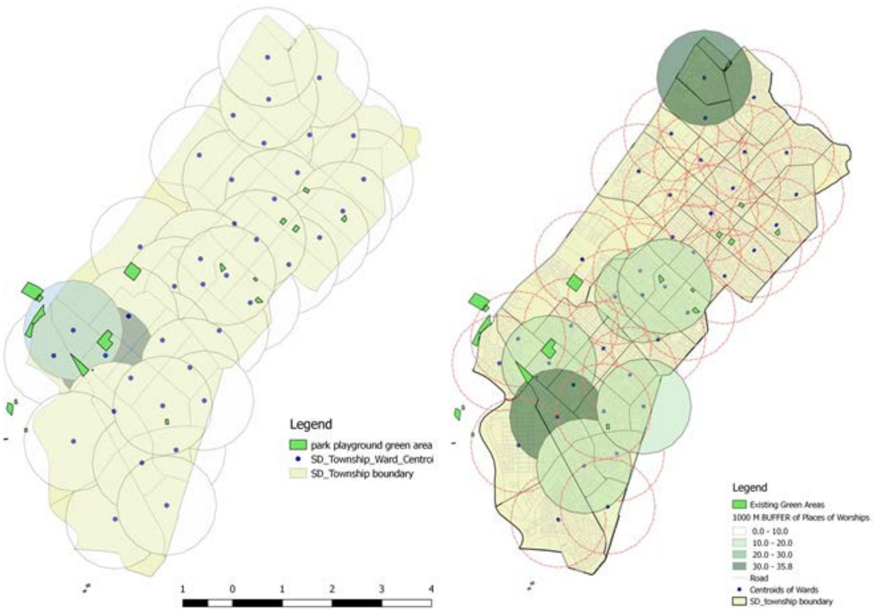

Fig.c and d show the coverage area density of green area and places of worship per person in South Dagon Myotthit Township

The Accessibility Analysis for the Emergency Evacuation Response

The accessibility analysis states that people cannot arrive to evacuation areas within 10 minutes and only 30 minutes may be coverage to be safety. The first 10 minute show that few residents can arrive to evacuation areas. In order to avoid the chaos situations at the evacuation stage, the route capacity should have the sufficient wide for the refugees to pass. Smaller capacity than the required ones becomes a high risk of evacuation route, because it will delay the evacuation clearing time and it may produce greater chaotic conditions. Currently, the roads of South Dagon have not standard width for fire fighters. Most residential houses located at the lower level of ground and do not have platform to walk.

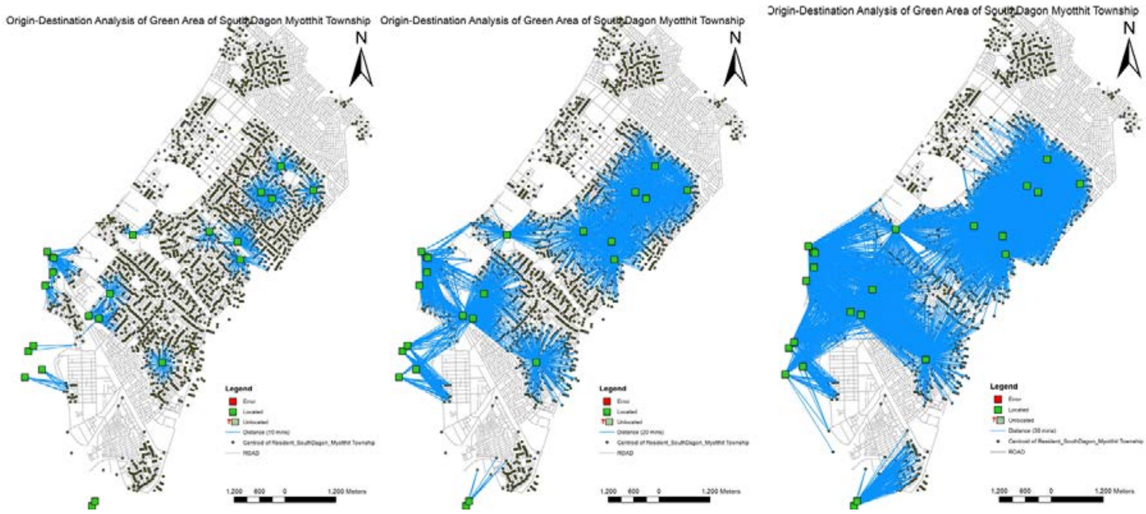

Fig.a show coverage area of green areas in South Dagon Myotthit Township.

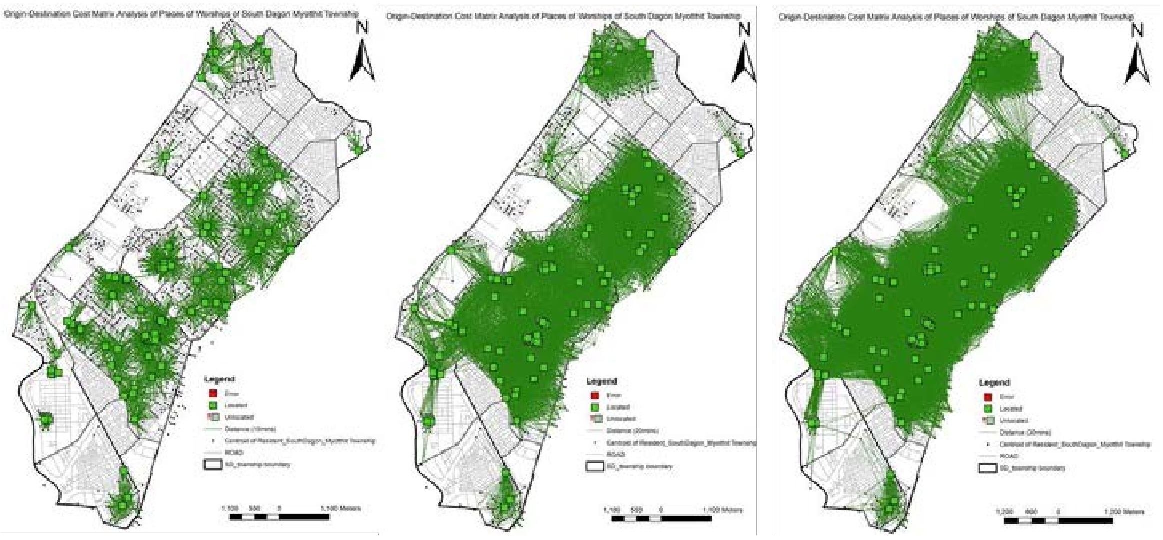

Fig.b show coverage area of places of worships in South Dagon Myotthit Township.

Discussion and Conclusion

On the basis of the present analysis, the authors would like to recommend that each ward within the townships should have coverage within 7 to 15 minutes. Result indicated that most residents in South Dagon Myotthit Township have not been covered by evacuation places yet. Blocking main roads was resulting in the deduting of covered evacuation coverage area.

However, the suitable evacuation should be allocated within the limited time as further research. The promotion of facilities of green evacuation areas will be promoted from the dangerous diseases. The research for the time varying shelter demand analysis to a location-allocation model for emergency management will be proceed with further research.

REFERENCES

[1] Open Space Suitability Analysis for Emergency Shelter after an earthquake By J. Anhorn and B. Khazai

[2] Yangon Region, Eastern District Dagon Myothit (South) Township Report

[3] Sendai Framework for Disaster Risks Reduction 2015 – 2030

[4] Study on Green and open spaces as emergency shelters by Dr. Yasmin Bachattara, Tokyo University

[5] 2014 Myanmar Population and Housing Census

[6] Yangon Master Plan JICA 2012

[7]Planning Emergency Shelter for Urban Disaster Resilience: An Integrated Location-allocation Modeling Approach, Laijun Zhao, Huiyoung Li, Yan Sun, Rongbing Huang, Qingmi Hu, Jiajia Wang and Fei Gao

[8] Emergency Response Preparedness Plan, Myanmar (version 1.0, updated in June 2014)

[9] Determining Evacuation Service Areas and Evacuation Route Risk Level as Disaster Mitigation Plan using GIS – based Software in Hyuga, Japan

[10] Mulit Hazard Contigency Plan , Myanmar Red Cross Society

A STUDY OF EVACUATION RISK IN THE CENTRAL BUSINESS DISTRICT OF YANGON CITY AND DISCUSSION ON THE ROLE OF BACK DRAINAGE SPACE

T. MATSUSHITA[1], A. KUBOTA[2], and K. MEGURO[3]

[1] *Project Researcher, International Center for Urban Safety Engineering, Institute of Industrial Science, the University of Tokyo, Japan, matsu-t@iis-u-tokyo.ac.jp (corresponding author)*
[2] *Project Professor, Department of Urban Planning, the University of Tokyo, Japan, ak@td.t.u-tokyo.ac.jp*
[3] *Professor & Director, International Center for Urban safety Engineering, Institute of Industrial Science, the University of Tokyo, Japan, meguro@iis.u-tokyo.ac.jp*

***Keywords**: Back Drainage Space, Yangon, evacuation risk*

1. BACKGROUND AND OBJECTIVE

This study focuses on the role of a unique urban space called Back Drainage Space (BDS), a 15-foot wide back alley with surface drainage and underground sewage facilities which was built behind buildings to provide sufficient light and air to keep the city sanitary and protect it from flood and fire. It was implemented by the British during the colonial period and in the early days, the space was not only used as drainage space but it served as a social space for the residents. However, starting in the 1980s, BDS became cluttered with garbage. Today there are 182 BDSs in the Central Business District (CBD) of Yangon, but they have been underutilized for nearly three decades. From 2011-2015, Myanmar went through a series of political reforms towards democratic government and as a part of the transformation, Yangon City Development Committee (YCDC) decided to improve the BDS environment. A large scale cleaning and repairing of the BDS started in 2015 (Figure 1). In 2017, a social enterprise called *Doh Eain* initiated a project called Alley Garden Project (AGP) to improve BDS and promote its use as a space for the community. As a result, eight BDSs have been transformed via collaboration between the community and the government by 2019. Impact study was carried out by the authors and the result has indicated that the use of the BDS has increased and people's perception of it has been improved [1].

2. PROBLEM STATEMENT

Despite the positive effects and prospects of BDS brought by the project, a majority of BDSs remain underutilized. Based on the previous studies conducted by the authors, three reasons why BDSs have not been utilized are that 1) the spaces have been filled with garbage and/or privatized and difficult to manage among the residents; 2) physical access from a building or street to BDS is limited due to a lack of staircase and locked gates prescribed by law; and 3) the use of BDS is prohibited by YCDC law [2]. However, the city accepts the use of some BDSs transformed by AGP because it is for a "public good" and its usefulness is recognized. The authors consider BDSs as significant assets as they have a potential to become shared urban space in the CBD where very little open space for the people exists. But in order for the BDS to be used as shared urban space, above-mentioned issues need to be resolved and a sustainable management system needs to be developed. This study focuses on a physical aspect of accessibility as it can pose a serious risk in the case of disaster if no appropriate evacuation scheme is in place, especially since the CBD is the oldest and most densely populated commercial center in Yangon. The authors conducted surveys to grasp the actual condition to identify issues and discuss possible resolutions in relation to the role of BDS.

3. SURVEY METHOD

A field survey was conducted to check structural and non-structural conditions related to accessibility, both from a building to BDS and BDS to a street in February 2019. Total of 115 BDSs in 4 townships (TS) in CBD, namely Lanmadaw TS (LMTS), Latha TS (LTTS), Pabedan TS (PBTS) and Kyauktada TS (KTTS) where BDSs are concentrated were surveyed. 88 out of 115 BDSs are "full-length BDSs" described in item no.5 in Table 1 meaning they have a full block length of 820 ft. The results from these 88 BDSs were used to calculate values represented in item no.6 to 10. It should be noted that the survey was conducted using methods available to the authors thus the values were obtained from different sources and assembled for this analysis. The number of access points (staircases and ladders) were obtained through visual surveys conducted by the authors, which were difficult at times due to inaccessibility of some of the BDS, while the building data including the number of buildings, usage and floor numbers were acquired from dataset created by JICA project [3].

4. FINDINGS

For an access from building to BDS, three typical configurations are observed; 1) steel staircase built in an alcove, 3) steel ladder attached on a wall surface and

Figure 1: Transformation of BDS (from left: BDS as a social space (photo by Yangon Heritage Trust), BDS as T rash Alley, BDS clean-up effort by the city, BDS transfor med through Alley Garden Project (photo by Doh Eain)

Table 1: Existing condition of BDS in 4 Townships

1.Township (TS)	LMTS	LTTS	PBTS	KTTS
2.No. of conventional HH / TS*1	6978	4292	6563	6120
3.Total no. of surveyed wards*2	7	9	11	9
4.Total no. of BDS surveyed / TS	33	23	29	30
5.No. of "full-length" BDSs / TS	18	21	24	25
6.Average no. of buildings / BDS	**50**	42	34	**28**
7.Average no. of staircase / BDS	12	10	7	9
8.Average no. of ladders / BDS	6	3	0	2
9.Average no. of access / BDS	18	13	7	11
10.% of accessibility to BDS / TS	**36%**	31%	**21%**	**37%**
11.% of residential use building*3	**88%**	87%	81%	**74%**
12.% of building 1-4F	**51%**	58%	63%	**69%**
13.% of building 5F+	**48%**	41%	36%	**30%**
14. Average no. of exit to street	**4.4**	2.6	2.4	2.4
15. % of BDS w/ N-S exit	**90%**	0%	0%	5%

*1 "Conventional household (HH) includes "one or more persons who are either related or unrelated and share living quarters and meals" according to 2014 Census [4];
*2 Authors surveyed wards with BDS only;
*3 This includes four categories of residential buildings that are residential-detached house, residential-apartment, residential-mixed apartment, and residential–mixed detached house.

Figure 2: Typical conditions of access points (from left: deteriorated staircase in alcove; ladder attached to the wall surface; concrete staircase locked with steel fence)

staircase made of concrete (Figure 2). The survey findings are summarized in Table 1 which shows that on average, 9.5 staircases and 2.8 ladders were observed as access points per BDS, where the average number of buildings facing BDS turned out to be 38.5. In all, on average, 12 points of access from 39 buildings to the BDS were observed, which means 31.3% of buildings facing the BDS have a second means of egress. However, the condition of most of these access points are neither in use nor in a state of being used safely due to severe deterioration and a lack of proper maintenance. Some of the residents are privatizing the alcove as their storage which disturbs the path. Steel staircase and ladder are often rusted and broken while new staircase made of concrete seems sturdier but often enclosed and locked with steel fences on the ground floor for a security reason.

For an access from BDS to a street, there are 6 exit points at maximum, 2 at longitudinal, N-S direction and 4 at cross sectional, E-W direction. 90% of BDS in LMTS had N-S exits while only 0-5% for other 3 TSs. On average, LMTS had nearly double the number of exit points (4.4) compared to other 3 TSs (2.4~2.6).

With respect to the differences observed between TSs, PBTS had lowest accessibility rate (AR) of 21% among 4 TSs. On the contrary, LMTS had a high AR (36%) and a largest number of buildings per BDS (50 buildings), while KTTS also had high ARC (37%), but with a smallest number of buildings (28) per BDS. Likewise, LMTS had a higher ratio of the residential use (88%) and larger number of buildings with 5-stories and more (48%), while KTTS had a lower ratio of residential use (74%) and smaller number of buildings with 5-stories and more (30%). Thus it can be said that two TSs - LMTS which is more residential, dense, taller neighborhood and KTTS which has lower buildings with wider frontage –had high AR despite of their contrasting characteristics. These findings are insufficient to conclude whether or not there is a correlation between AR and other characteristics of the built environment and further investigation is needed.

4. ANALYSIS & DISCUSSION

According to the authors' previous studies [1], three challenges concerning the improvement of the accessibility are 1) physical difficulty to create space for installing new staircase, 2) financial difficulty and 3) managerial difficulty in consensus building among multi-unit owners of a building. This study attempted to verify the actual condition by finding facts about staircase and exit points of evacuation and comparing between TSs. And it was found that although 31.3% of buildings have a second means of egress, the majority of them are unusable because of neglect and privatization by the residents. This may be due to a lack of incentive for the residents to commit to the BDS environment because the law does not allow its use and in reality, they can survive without using it. Nonetheless, as stated earlier, BDS can become shared urban space to benefit the city and the residents' safety also depends on its usability in the case of disaster. In order to create an incentive, it is important that the BDS becomes a legally usable space which has been demonstrated by AGP. If the BDS can be used as an amenity space, it will increase a utility value and may incentivize the residents to use the space and eventually improve the environment including the accessibility. Therefore it can be concluded that the usability of the BDS is a critical factor in creating a safe urban environment and the improvement of the BDS environment and its accessibility need to be studied in parallel.

ACKNOWLEDGEMENT

We would like to thank the residents, local authorities and volunteers for their cooperation in this study. The field study was made possible by the opportunity provided by SATREPS program supported by JICA and JST.

REFERENCES

[1] Matsushita, T. et al., "Impact Evaluation of Alley Revitalization Project in Yangon and Investigation of Potential as Urban Commons," Great Asian Streets, National University of Singapore, December 14-16, 2018.

[2] YCDC "YCDC Law" Chapter 29, No. 315, 2018

[3] Yangon Regional Government, YCDC, "Yangon Mapping Project," 2019.

[4] Department of Population, Ministry of Immigration and Population, "The 2014 Myanmar Population and Housing Census," May 2015.

SESSION E

URBAN SAFETY & DISASTER MITIGATION: RISK ASSESSMENT

LONG TERM MEASURES FOR EARTHQUAKE DISASTER SAFETY IN DEVELOPING COUNTRIES OF ASIA

PRADEEP KUMAR RAMANCHARLA[1]

[1] *Professor, EERC, IIIT Hyderabad, India*

ramancharla@iiit.ac.in

Keywords: *Earthquake safety, Risk Index, Vulnerability, Mitigation*

1. ABSTRACT

Due to rapid urbanization in many cities in the world, in last few decades, there is a tremendous pressure on housing industry to cater to the needs. This fast pace of construction activity with no planning has led to uneven growth of low-to-medium rise buildings in tier II cities and medium-to-highrise buildings in tier I cities, causing serious threat to life and property during disasters. The same is clearly evident from the losses during earthquakes in the recent past including twin major earthquakes in Nepal. Therefore, it is necessary to carry out Long term mitigation measures for Earthquake Disaster safety.

Earthquake Disaster Management has 6 stages, namely, prediction, mitigation, preparedness, recovery, rehabilitation and reconstruction. Out of these six, three are pre-event and the other three are post-event. For long term disaster risk mitigation, there is a need to emphasize on mitigation and preparedness measures. In this paper a newly developed method for the assessment of earthquake safety index is proposed. This method consists of the combination of three major components viz., Hazard, Exposure and Vulnerability. In addition to these, it also includes physical, social, economic and other vulnerability parameters. Each of these parameters is sub-divided and depending on the city, usage and built environment, a weightage factor is assigned to each of the components which constitute Safety Index. Similar concept has been worked out in various cities by UNDP, FEMA, etc., worldwide in last decade. As a first attempt in India, it is proposed to evaluate risk in the form of index, by developing an appropriate model for Disaster Mitigation Indexing for Bhuj. This kind of indexing will be helpful for the administrative bodies in comparing the overall risk across number of cities or region and also in prioritization of cities to implement appropriate disaster mitigation and preparedness measures.

2. INTRODUCTION

Earthquake disaster risk assessment is urgently required to mitigate possible losses in future disasters. Quantitative assessment of earthquake risk is necessary to confirm qualitative intuition of the severity of the problem. And, this quantitatively method of assessing earthquake risk of cities/towns located in Seismic Zones III, IV and V will help understand relative earthquake risk across not only the cities but also the districts. Therefore, a simple measure, called the Earthquake Disaster Risk Index (EDRI), is proposed to estimate broadly the earthquake risk of a city and a district; this is not meant to be used for estimating the earthquake risk of individual houses. The objectives of the proposed work are;

- Provide a systematic method to compare broadly the earthquake disaster risk across many cities or districts;
- Create awareness in cities with low seismicity that even a small earthquake event can cause a major disaster owing to characteristics of the built environment in the cities;
- Sensitize governments and decision makers to take appropriate actions towards reducing earthquake risk, and judiciously use the available limited resources (manpower and money);
- Identify effectiveness of the specific measures adopted in the construction of buildings, by re-evaluating the EDRI periodically over the years; and
- Prioritize cities and districts for launching earthquake risk mitigation program.

Figure 1. Street view of market of Bhuj city

3. METHODOLOGY

Risk index has been computed using the combination of hazard, vulnerability and exposure parameters of the Bhuj city. The main purpose of the visit was to conduct the rapid visual survey (RVS) of buildings to help understand the distribution of risk at city level. But, considering the time required for survey and field data conversion in a computer for further analysis, the decision was taken to capture the visual inspections in the form of photographs. These photographs of buildings were analysed later for calculating the risk of individual building. As a result, the team could do the risk calculations and results analysis in a systematic format in a computer. Various parts of new and old settlements of the city was surveyed and photos of building stock in those area were captured.

$$Risk = Hazard \times Exposure \times Vulnerability \quad (1)$$

4. CASE STUDY OF BHUJ CITY

Bhuj is the one of the largest cities in Gujarat in terms of population as well as in area especially in Kachchh region. As per Census of India 2011, Bhuj city has about 32,681 buildings which include the residential, commercial and office buildings. Based on the basic load resisting system or framing system and construction technology, 28% buildings are of stone masonry, 27% of brick masonry, 52% reinforced concrete (RC) and rest 7.5% of other category buildings are standing till the date.

26 January 2001 Bhuj earthquake has completely changed the mindset of private and government construction work in and around the city. In order to compute the risk index of the city, a field survey was conducted by IIIT Hyderabad. After collection of building information of bhuj city, next step was the calculation of risk of individual building, and risk of city. IIIT Hyderabad team had prepared an approximate procedure to calculate the risk of city based upon the risk of individual buildings in the city.

Table 1. Risk Index of all Surveyed Buildings and Risk Index of Bhuj City

Housing Typology	EDRI Calculation of Surveyed Buildings (SB)				EDRI Calculation from Census		
	Number of Buildings N_i		$EDRI_{Vulnerable}$	$EDRI_{SB}$	Number of Buildings N_{iTown}	Sum of Risk (Town)	$EDRI_{Town}$
RC Building	580	111.23	0.19	0.18	11,298	2,167	0.17
Brick Masonry Building with RC Roof	142	18.30	0.13		6,585	849	

Bhuj city has low mean *EDRI* score for Brick Masonry Building with RC Roof compared to RC Buildings; the same trend is reflected in the standard deviation of *EDRI* score. The reason for large standard deviation in RC Buildings is its poor earthquake resistance as seen in the 2001 Bhuj Earthquake. On the other hand, most Brick Masonry Buildings performed poorly during 2001 Bhuj Earthquake and were re-constructed with earthquake resistant features, leading to decrease in mean *EDRI* value and lesser deviation.

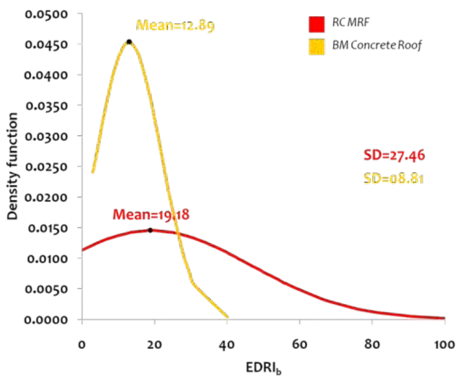

Figure 3. Distribution of *EDRI* score

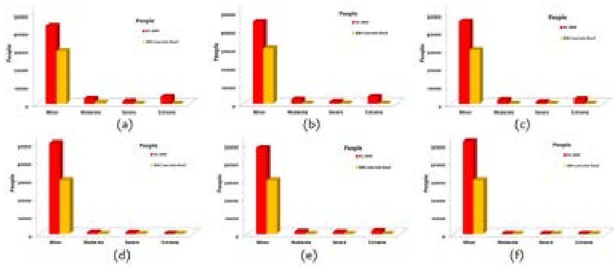

Figure 4. Loss of life scenario: (a) Present, (b) After Exposure Issues rectified, (c) After Exposure + Life Threatening Factors rectified, (d) After Exposure, LTF and Architectural Features rectified, (e) After Exposure, LTF and Structural Aspects Rectified, and (f) After all Aspects are rectified

5. CONCLUSIONS & RECOMMENDATIONS

This paper aims to arrive at long term mitigation measures. For that purpose, a methodology was developed and the same was tested on Bhuj city as a case study. The following recommendations were given to local bodies to reduce risk of the city:

- Locate staircase properly while planning and separate it structurally to reduce significantly possible damage in building.
- Orient structural members properly to contribute to lateral stiffness and uniform stiffness along both principal plan directions to avoid twisting of building during horizontal shaking.
- Modify local building byelaws to provide sufficient gap between buildings to reduce damage in buildings due to pounding effects.
- Prevent any new construction or extension of existing buildings of *gamtal* areas. Propose new policy to encourage owners to move out of unsafe buildings. Encourage new housing schemes or loan for new building construction in other locations.
- Retrofit important buildings (including multi-storey buildings) urgently.
- Train private and government engineers in design and detailing, and artisans in construction of earthquake resistant buildings.
- Generate awareness in public to accelerate disaster mitigation and preparedness programs.

6. REFERENCES

- Ramancharla Pradeep Kumar and C. V. R. Murty: Earthquake Safety of Houses in India: Understanding the Bottlenecks in Implementation, ICJ, Vol. 88, No. 9, Sept 2014.
- Srikanth T., Kumar R. P., Singh, A. P., Rastogi, B. and Kumar, S. (2010) "Earthquake Vulnerability Assessment of Existing Buildings in Gandhidham and Adipur Cities Kachchh, Gujarat (India)", European Journal of Scientific Research , Vol.41 No.3, pp.336-353, ISSN 1450-216X, http://www.eurojournals.com/ejsr.htm
- Jain, S.K. (2010), Seismic Assessment & Retrofitting of RC Frame Buildings, Rebuild, Vol. 4, 1, pp. 6-8.

A STUDY ON DEFINITION TO NATURAL DISASTER-DANGEROUS POINTS ON ROAD THAT AIM TO UPGRADE THE EVALUATION OF DISASTER RESISTANCE ON ROAD-NETWORK

S. OSAWA[1], J. TAKAYAMA[2], M. FUJIU[3], and Y. SHIOZAKI[4]

[1] Doctor Course Student, Kanazawa University, Kanazawa, Japan,
[2] Professor, Kanazawa University, Kanazawa, Japan,
[3] Associate Professor, Kanazawa University, Kanazawa, Japan,
[4] Assistant Professor, Kanazawa University, Kanazawa, Japan,
Correspond to Assoc. Prof. M. FUJIU (fujiu@se.kanazawa-u.ac.jp)

***Keywords**: road disaster prevention plan, disaster resistance, road-network evaluation, dangerous point on road*

1. INTRODUCTION

Japan is prone to various natural disasters. Even recently, large-scale earthquakes and heavy rains have occurred, and they cause great damage. It is necessary to quickly deal various disaster responses to mitigate the disaster damage. It is also an important challenge that define response details and its procedures clearly and ensure that stakeholders have informed them. On the other hand, to be implemented these responses, it is essential to transport physical resources and personal resources to disaster-response bases. It is recognized that keeping the connection between disaster-response bases under natural disaster is more important in various disaster responses in Japan from these facts and past disaster experiences. From these social backgrounds, many methods to assess the disaster resistance of road-network that aiming to keep connectivity on road-network under natural disaster have been proposed. The perfection as evaluation method of disaster resistance on road-network is often argued while argumentation about "what kind of road-conditions have influenced the possibility of road-damage in natural disaster" of conditions for the appropriate application of these methods is not enough. The purpose of this study is proposing the definition method for dangerous points on road that possible to be damaged in natural disaster.

2. METHODOLOGY

It has been often discussed that the damage state and/or cause of damage by natural-disasters. On the other hand, little work has been done on application these knowledges of previous studies in the research field of road structures to assessment the disaster resilience of road-network. The problem seems to lie in the fact that the application policy is not established.

To propose such an application policy for road-network assessment, investigation reports of natural-disasters that occurred in the past in Japan are referenced as research sources in this study. The advantage that using these reports is completeness of past damage cases. To achieve the purpose of this study, what types of road-structure and what its elements are vulnerable to natural-disaster is summarized in first step. In next step, text mining techniques are used for analyzing the factors that related to vulnerability.

Figure 1. An example of road collapse.

Figure 2. An example of tsunami damage

3. CONCLUSIONS AND FUTURE WORKS

In the future, we will collect and organize quantitative and qualitative data such as individual specifications and surroundings of each structure and the scale of the external forces that acted on each of these organized damage forms and factors, and statistically analyze them. The aim is to extract elements that have a relationship with damage. In addition, it is a future task to show the requirements of the hazard points for disasters that should be considered in the evaluation of the functionality of the road network against natural disasters based on the extracted elements from the damage form, damage factor, and disaster scale.

Seismic Vulnerability Assessment of Lifeline System in Myanmar

AYE AYE MAR[1], KYAW KYAW[2], TAKESHI KOIKE[3]
[1] PhD candidate, Department of Civil Engineering, Yangon Technological University, Myanmar
ayeayemar.civil@gmail.com
[2] Professor, Department of Civil Engineering, Yangon Technological University, Myanmar
[3] *Academic Advisor, JICA EEHE Project, Yangon, Myanmar*

ABSTRACT

Lifeline earthquake disaster brings not only property loss but also functional damage to urban activities and socioeconomic loss. In this research, one of the water supply network system of Gyobyu in Yangon region is proposed for the seismic vulnerability assessment based on the three limit states: immediate occupancy (IO), life safety (LS), and collapse prevention (CP) corresponding to the three earthquake levels: maximum operated earthquake (MOE), design basis earthquake (DBE), and maximum considered earthquake (MCE), respectively. This research aims to assess the condition of the supply of water distribution system of downtown area after the earthquake and to evaluate and assess the probability of failure of structural components for each failure mode. To find out the failure mode of each structural component, the seismic performance of the pipes are assessed by the pipe damage mode such as leakage, pull-out and buckling failures at the joint based on the seismic design guideline from American Lifelines Alliance (ALA). It can be said that the proposed seismic risk procedure is quite useful and applicable to all large cities, located in earthquake-prone areas of the world and it can help decision-makers who work with disaster prevention and reduction of urban lifeline system for the better plan in the future.

Keywords: water supply system, vulnerability assessment, three earthquake levels, probability of failure, seismic design guideline

1. INTRODUCTION

Lifeline systems are often grouped into six principal types of systems: electric power, gas and liquid fuels, telecommunications, transportation, wastewater facilities, and water supply. According to earthquake survey in recent decades, the correlation and coexistence of the lifeline system are the important factors to result in their big losses.

Myanmar is one of the earthquake-prone regions as it is located in the eastern part of Alpide Earthquake Belt, between the eastern end of Himalaya Arc, the collision zone of Indian and Asia Plates, and the northern segments, highly active portions of Sunda Arc. The most significant and active fault in Myanmar is the Sagaing fault shown in Figure 1, a 1500km long tectonic fault that passes through the cities of Nay Pyi Taw, Bago, Sagaing, Mandalay, and close to Yangon, as in [1].

Yangon, the second city of Myanmar, is situated in the southern part of the Central lowland and it is tectonically bounded by the Indian-Burma plates subduction in the west, Sagaing fault which is located about 40km in the east of Shwedagon pagoda, West Bago Yoma fault in the north, Kyaykkyan fault in the north-east, and the Andaman rift zone in the south, as in [2].

Figure 1: Fault Hazard Map in Myanmar

In this paper, one of the water supply network system of a hospital in Yangon region is proposed for the seismic vulnerability assessment based on the three limit states: immediate occupancy (IO), life safety (LS), and collapse prevention (CP) corresponding to the three earthquake levels: maximum operated earthquake (MOE), design basis earthquake (DBE), and maximum considered earthquake (MCE), respectively.

2. DECRIPTION AND SELECTION OF STUDY AREA

The present water supply system of Yangon which has been operated over 100 years, all pumping stations in reservoirs and main transmission pipes have already aged and beyond its lifespan, because of the long economic sanction to Myanmar. Gyobyu pipeline was constructed in 1940 and has been operating for over 70 years. After that, this pipeline suffered Taikkyi earthquake effect on March 2017. According to the report of Yangon City Development Committee (YCDC), over 200 numbers of pipe supports damaged between Gyobyu reservoir and near Phugyi reservoir (10.5miles). Water supply is vital to the function of an industrialized society and important to emergency response and recovery after earthquakes.

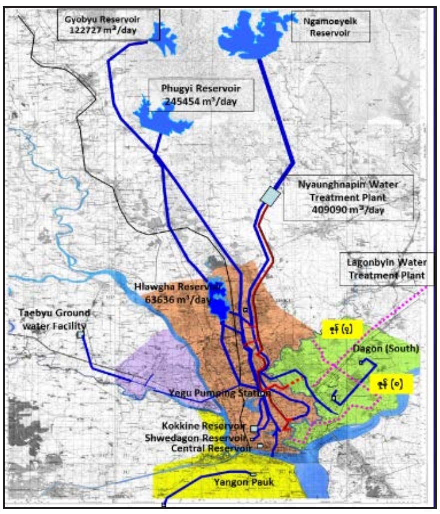

Figure 2: Schematic Configuration of Existing Water System of Yangon (JICA, 2012)

There are mainly four reservoirs shown in Figure 2: Gyobyu reservoir, Ngamoeyeik reservoir, Phugi reservoir, and Hlawgha reservoir, which supply the water by the various types of transmission main pipes and distribution pipelines to the citizens in Yangon area, as in [3]. Among them, Gyobyu reservoir is proposed as a source point and Kokkine reservoir in Bahan Township is selected because it is one only one above-ground pipeline in Yangon. The water transmission pipeline, however, in Yangon, is installed on the ground supported by the concrete foundation from the reservoir to the downtown terminal point by segmented steel pipe having concrete lining with dresser coupling joint.

3. METHODOLOGY

The basic information to assess the seismic vulnerability of the lifeline system is more detailed classified into two types of data: earthquake hazard data and lifeline systems vulnerability data. These parameters are used in the safety and vulnerability assessment of the water supply system. Generally, it includes seismic hazard analysis for Sagaing fault based on the probabilistic way, the basic concept of the seismic design method of the water supply system, and vulnerability assessment of the system at the three different seismic performance levels.

Based on Probabilistic Seismic Hazard Analysis (PSHA), the following earthquake motions are defined: MOE – 50% in 50 years, DBE – 10% in 50 years, and MCE – 2% in 50 years corresponding to the three limit states: immediate occupancy (IO), life safety (LS), and collapse prevention (CP), respectively [4] and their corresponding pipe joint criterion for their performances is formulated based on the Japan Water Work Association (JWWA) guideline [5] as shown in Table 1. By analyzing microtremor data value from the microtremor measurements along the pipeline, the soil profile types existing along the study area are chosen based on the code, ATC-40. The probabilities of damage mode in each segment are estimated from the fragility curves for structural components at the three different limits in each area.

Table 1. Design Formula of Pipe Joints for Wave Effect due to Design Earthquake

Design Earthquake	**Limit state**	**Mechanical Joint**		**Continuous Joint**	
		Straight pipe	**Geometrical pipe**	**Straight pipe**	**Geometrical pipe**
MOE	IO	$\Delta.\frac{2\pi l}{L}$	Δ	$\alpha_s.\varepsilon_G$	$\alpha_B.\frac{2\pi\Delta}{L}$
		$\frac{2\pi l}{L}.arctan\frac{2\pi\Delta}{L}$	$arctan\frac{\Delta}{W}$	None	$arctan\frac{\Delta}{W}$
DBE	LS	$\Delta.\frac{2\pi l}{L}$	Δ	$\alpha_s.\varepsilon_G$	$\alpha_B.\frac{2\pi\Delta}{L}$
		$\frac{2\pi l}{L}.arctan\frac{2\pi\Delta}{L}$	$arctan\frac{\Delta}{W}$	None	$arctan\frac{\Delta}{W}$
MCE	CP	$\Delta.\frac{2\pi l}{L}$	Δ	$q.\alpha_s.\varepsilon_G$	$C_B.\alpha_B.\frac{2\pi\Delta}{L}$
		$\frac{2\pi l}{L}.arctan\frac{2\pi\Delta}{L}$	$arctan\frac{\Delta}{W}$	None	$arctan\frac{\Delta}{W}$

4. STRUCTURAL SAFETY ASSESSMENT

In this study, the earthquake magnitude of 6.51M, 7.34M, and 7.87M for the return period of 73, 475, and 2475 years are estimated by using Figure 1. The PGA at bed rock of 0.087g, 0.178g, and 0.281g for the MOE, DBE, and MCE are estimated with the assumption of R=54km for Taikkyi and Hmawbi area. The PGA at bed rock of 0.319g, 0.284g, and 0.448g for the MOE, DBE, and MCE are estimated with the assumption of R=36km for Mingalardon area. Then the PGA at bed rock of 0.096g, 0.196g, and 0.308g for the MOE, DBE, and MCE are estimated with the assumption of R=50km for Mayangone, Bahan and Yankin area.
Moreover, a simple procedure to evaluate the soil amplification factor of surface strata is developed based on the response spectrum method by INOUE et al. Finally, the PGA at ground surface of 0.208g, 0.427g, and 0.674g for the MOE, DBE, and MCE are taken by multiplying the PGA at bed rock with the soil amplification factor of 2.4 and 2.2 for Taikkyi and Hmawbi respectively. The PGA at ground surface of 0.16g, 0.33g, and 0.53g for the MOE, DBE, and MCE are taken by multiplying the PGA at bed rock with the soil amplification factor of 1.37, 1.71, 1.83 and 1.76 for Mingalardon, Mayangone, Bahan and Yankin respectively. Based on the response acceleration spectrum S_A, the response velocity spectrum S_v, can be theoretically formulated as shown in Table 2.

A simplified methodology for the seismic vulnerability assessment of water distribution networks are determined. The results of axial and bending damage mode of pipes in each township are compared with the critical seismic performance at the three limit states. From which, the pipe damage mode such as leakage, pull-out and buckling failures at the joint will be revealed.

Table 2. Analysis of Response Velocity Spectrum, S_v

Earthquake	Response Velocity Spectrum , $S_v = \frac{T}{2\pi}.S_A$ (m/s)					
	Taikkyi	Hmawbi	Mingalardon	Mayangone	Bahan	Yankin
MOE	0.259	0.219	0.172	0.24	0.25	0.258
DBE	0.383	0.336	0.187	0.281	0.281	0.289
MCE	0.661	0.548	0.44	0.593	0.597	0.617

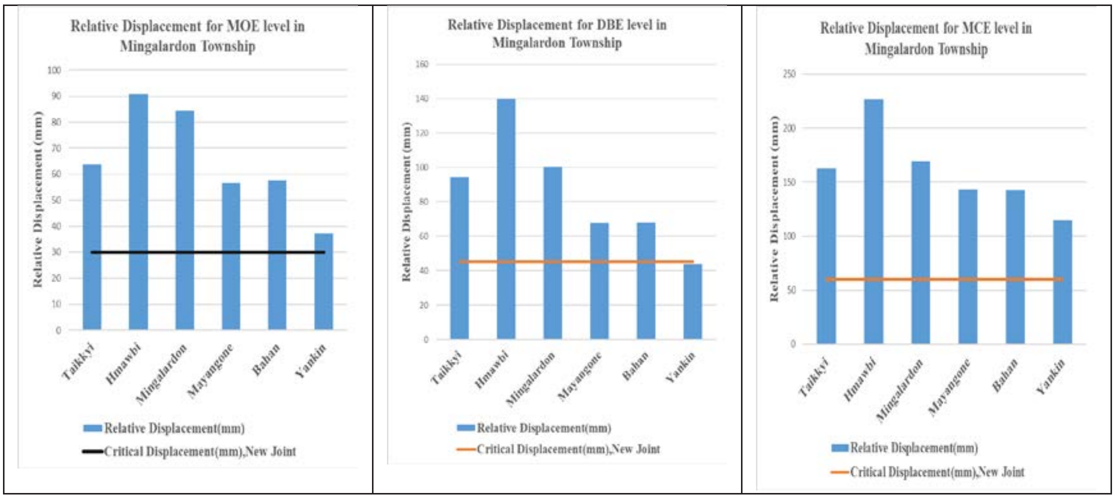

Figure 3: Axial Damage Mode of Mechanical Joint Pipes (MS) in Six Townships at MOE, DBE, and MCE

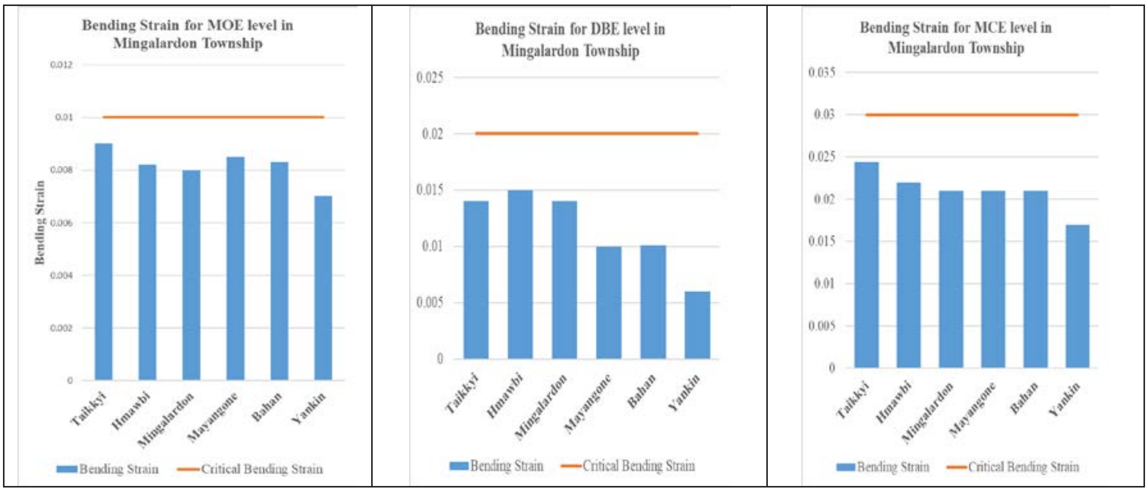

Figure 4: Bending Damage Mode of Mechanical Joint Pipes (MS) in Six Townships at MOE, DBE, and MCE

Figure 3 and 4 show the axial and bending damage mode of pipe at the three seismic performance levels in six townships. Based on the results of damage mode of pipes, the axial displacement of mechanical joint pipes are more than the critical limits whereas the bending strain of mechanical joint pipes are controlled within the critical limits.

In estimation of probability of failure mode from fragility curves, the probability of failure of continuous and mechanical joint pipes at the three seismic performance levels in six townships, as shown in Figure 5 to 10, show that most of the mechanical joint pipes have 100% probabilities of failure in three seismic levels.

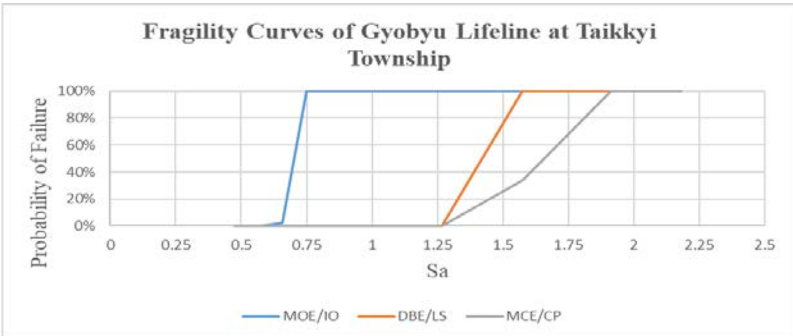

Figure 5: Probability of Failure of Continuous Joint Pipes (MS) in Taikkyi at MOE, DBE, and MCE

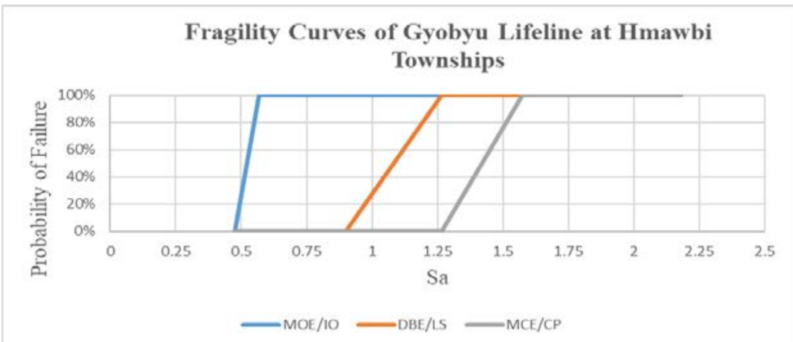

Figure 6: Probability of Failure of Continuous Joint Pipes (MS) in Hmawbi at MOE, DBE, and MCE

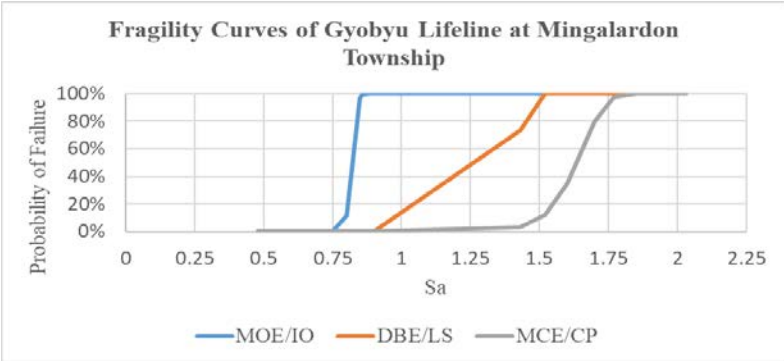

Figure 7: Probability of Failure of Continuous Joint Pipes (MS) in Mingalardon at MOE, DBE, and MCE

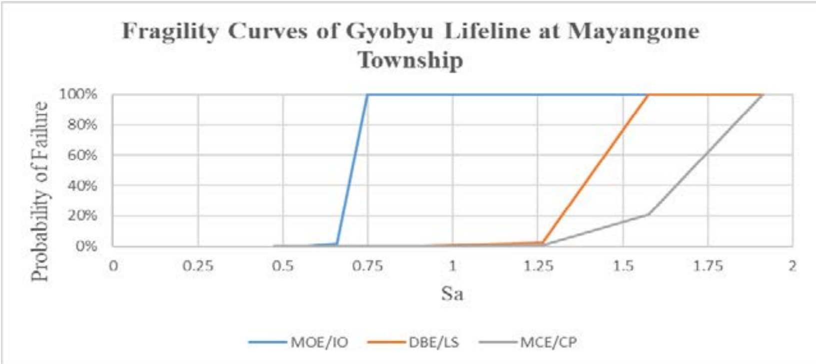

Figure 8: Probability of Failure of Continuous Joint Pipes (MS) in Mayangone at MOE, DBE, and MCE

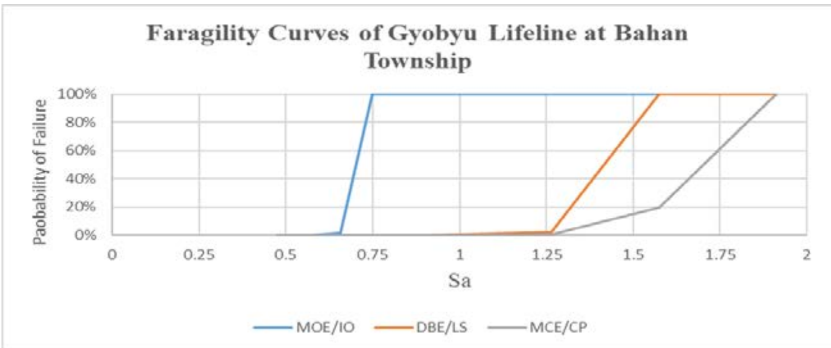

Figure 9: Probability of Failure of Continuous Joint Pipes (MS) in Bahan at MOE, DBE, and MCE

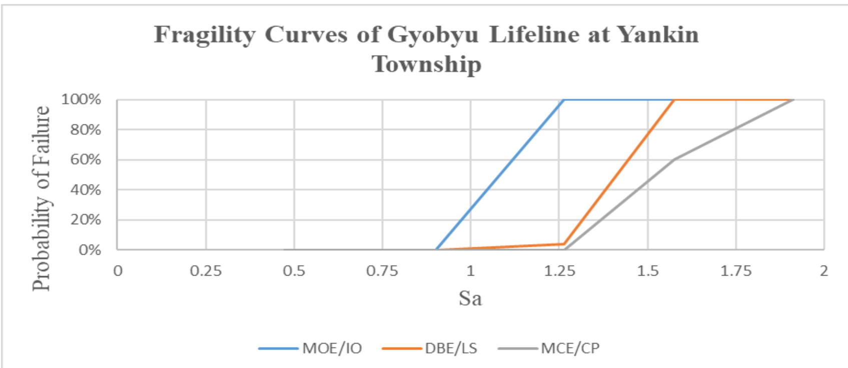

Figure 10: Probability of Failure of Continuous Joint Pipes (MS) in Yankin at MOE, DBE, and MCE

5. CONCLUSIONS

The analysis results for each failure mode of the system are mainly depending upon the shear wave velocities, response velocity spectrum, and network data of the system. From the evaluation of the axial damage mode of pipe joints for each township, it can be examined that the more the displacement in mechanical joint. Moreover, all mechanical joint pipes have 100% probabilities of failure in three seismic levels. It shows the alert for aging pipes, especially mechanical joint pipes, should be replaced with newly developed pipes based on the seismic design guideline and seismically resilient water pipes together with non-leakage joint mechanism are needed when the current water supply system is upgraded to a new system.

REFERENCES

The Sagaing Fault, Myanmar (Burma) [Online]. Available: http://www.sagaingfault.info/

Myo Thant, "Probabilistic Seismic Hazard Assessment for Yangon region, Myanmar," Report of Department of Geology, University of Yangon, Myanmar, December 21, 2012.

Situation of Water Supply System of Yangon City and its Future Demand, Yangon City Development Committee [Online]. Available: http://www.ycdc.gov.mm /

Maung Tint Lwin, *A Simplified Seismic Performance based Method for Steel Moment Resisting Frames using Building Design Data Bank,* Ph.D Thesis, Yangon technological University, Yangon, September, 2015.

Khin Aye Mon, T.Koike, G.Nishikawa, L.E.Garciano, and J.Kiyono, *A Simplified Seismic Design Method of Water Lifelines in Developing Countries*, AUN/SEED-Net Project, 2015-2017Yi, H. L.2012.

A funfamental study on dynamic wave propagation in the soil around a cavity

Yusuke Nakata[1], Reiko Kuwano[2], Masahide Otsubo[2], Umair Ali[1]
[1] Graduate Student, Graduate school, The University of Tokyo, Japan
[2] Professor, Institute of Industrial Science, The University of Tokyo, Japan
[3] Research Associate, Institute of Industrial Science, The University of Tokyo, Japan
y-nakata@iis.u-tokyo.ac.jp

ABSTRACT

Recently, an increasing number of sinkhole problems in developed cities have been reported. To prevent a sinkhole, it is necessary to detect a subsurface cavity in its earlier stage. Although dynamic wave survey is often used to investigate the stiffness or structure of the ground, it is not always valid for detection of subsurface cavities. If ground motion sensors are installed in buried pipes, detecting a subsurface cavity based on vibration characteristics of surrounding ground would be feasible. In this study, with the aim of improvement in cavity detection method, laboratory model tests were conducted to investigate wave propagation through the model ground during the process of cavity growth. In the model tests, nano-order compression waves were excited and received with piezoelectric transducers and the time and frequency domain analyses of the received signals were performed. As a result, a decrease in both wave velocity and lowpass frequency (f_{lp}) was observed as a cavity grew due to the expansion of the loosened area around the initial cavity. Discrete element method simulations were also conducted with the presence of a subsurface cavity and a decrease in f_{lp} was observed due to the diffraction of propagation path.

Keywords: subsurface cavity, dynamic measurement, disk transducer, discrete element method

1. INTRODUCTION

Recently, an increasing number of sinkhole problems in developed cities have been reported. Sinkholes occur as the final phase of subsurface cavity growth; thus, improvement of cavity detection method is required. Dynamic wave survey is widely used to investigate the stiffness or structure of the ground, whereas characteristics of dynamic wave propagation around a cavity are not well understood. Kominami et al. (2018) reported that this method is not always valid for the detection of a subsurface cavity. According to Fujii et al. (2019), the ground-penetrating radar method, which is currently used for finding cavities beneath the road surface in Japan, is practically conducted only for cavities that are located shallower than 1.5 m from the ground surface. However, no efficient method to find a cavity at a deeper elevation has been established. As the cavities are often formed due to the failure of deeper underground structures, if ground motion property can convey information about the nearby subsurface cavity, detecting cavities in deeper ground is maybe possible by installing motion sensors on underground structure. In this research, with the aim of improving the cavity detection method using a dynamic wave propagation method, laboratory model tests, and discrete element method (DEM) simulations were conducted with the presence of a subsurface cavity.

2. MODEL TEST

2.1 Model preparation

A cylindrical transparent chamber was used to reduce the effect of reflected waves due to sidewalls. The chamber was 30 cm in diameter with a capacity of water supply through the holes on the bottom plate (Figure 1). Uniformly graded silica sand No. 5 having a median particle size of 0.5 mm, was used in the model test. The sand was pluviated from a specific elevation to achieve a specimen height of 20 cm with a relative density of 50%. Two pairs of disk transducers (DT) were placed on the bottom plate and the top surface of the sandy ground (Figure 1). The DTs including both P- and S-type piezoelectric elements were developed based on Suwal & Kuwano (2013). The dimension of each piezoelectric element was 30 mm × 30 mm × 2 mm (thickness). A thin coating of epoxy resin was applied to the surface of the elements to prevent damage due to water and abrasion caused by angular sand grains. The elements were placed inside acrylic frames and supported using silicone and epoxy resin. Uniform load of about 2.7 kPa was applied on the surface of the sandy ground to ensure firm contacts between the sand grains and the surface of DT.

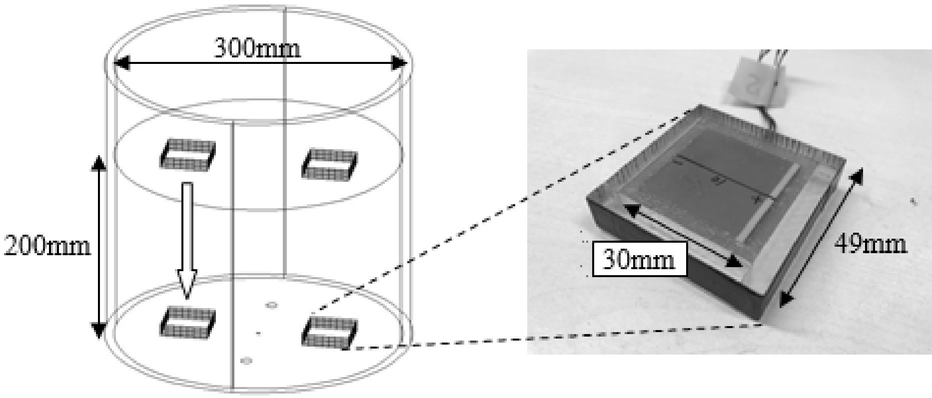

Figure 1: Schematic of soil chamber and disk transducer

A single period of sinusoidal pulse having input frequencies of 2~30 kHz was given from the DT at the ground surface (transmitter) and received at the DT on the bottom plate (receiver). An input voltage of 140 V was sent to the P-type element to generate compression (P-) waves and the excited P-mode displacement on the surface of the disk transducer was about 8~12 nm.

The chamber design and experimental procedure broadly followed Kominami (2018). On the bottom plate, there are three holes; two larger holes are for supply and drainage of water and the other hole located at the center is for drainage of soil with pore water (Figure 2). The saturation condition of the sand was controlled by raising and lowering a water tank connected to the chamber through the bottom plate. By opening the initially closed hole at the center where the water level was initially adjusted to be 10 cm or 15 cm from the bottom, the soil was drained with water and cavity was formed in the ground. Dynamic wave measurements were performed at five stages of the ground condition as below (Figure 3):

1. Dry: after the surface load was applied to the dry ground
2. Saturated: after increasing the water level to the surface

3. No cavity (unsaturated): after lowering the water level to the bottom
4. Cavity S (unsaturated): after the first cycle of drainage of both water and soil
5. Cavity L (unsaturated): after the second cycle of drainage of both water and soil

For each condition of the five stages, wave velocity and frequency distribution of inserted and received waves were analysed.

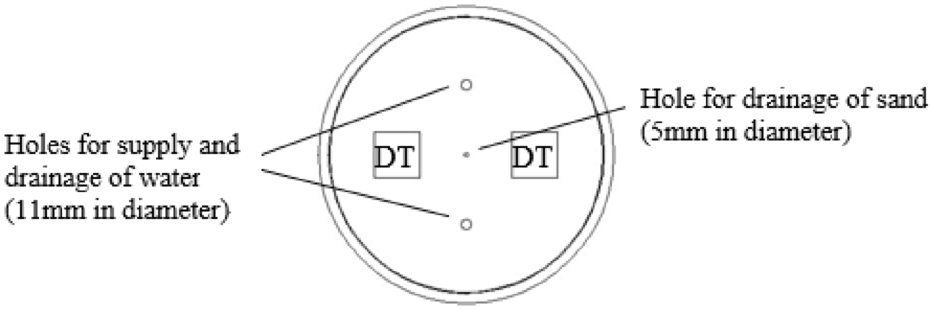

Figure 2: Bottom plate

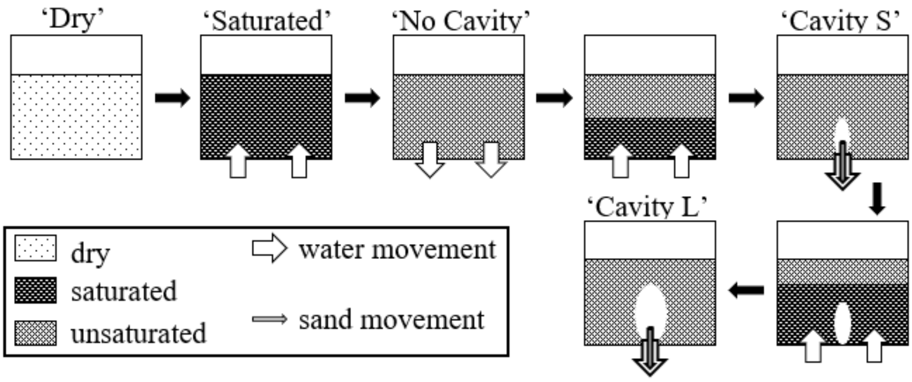

Figure 3: Flow of experimental procedure

After performing the wave measurement for 'Cavity L', the ground was cut vertically into half to observe the cross-section of the cavity (Figure 4). The volumes of cavities were estimated from the drained sand and the volume of 'Cavity L' was observed five times as large as that of 'Cavity S' (Figure 4). The shape of 'Cavity S' was inferred from the volume of the drained sand with an assumption that both 'cavity S' and 'Cavity L' had a similar shape. The wave measurements were conducted along the vertical line connecting the transmitter DT and the receiver DT, located 2 cm off from the side of 'Cavity L' (Figure 4).

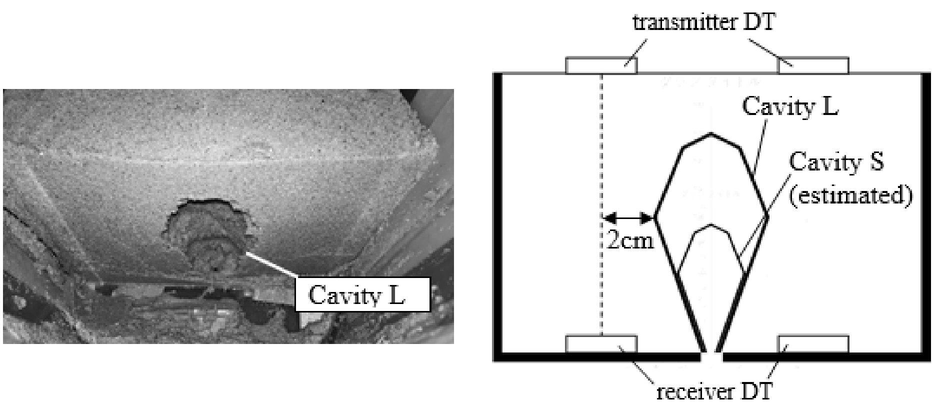

Figure 4: The cross-section of the cavities

2.2 Results and discussion

The data of compression (P-) waves measured along the vertical line (dotted line in Figure 4) were analyzed. The time domain responses are shown in Figure5(a) where the amplitude of receiver responses was normalized by the maximum amplitude for 'No Cavity' case. It is found that attenuation was considerable for 'Saturated' and 'Cavity L' cases. P-wave velocity (V_P) was calculated from the rising points of the input and output signals and V_P data are listed in Figure 5(b) for the five stages of the ground condition. As the condition changed from 'Dry' to 'Saturated' V_P decreased, while V_P increased from 'Saturated' to 'No Cavity'. This variation can be attributed to the variation in the effective stress that varies with the change in pore water pressure. As the cavity expanded, V_P decreased continuously although the wave path was 2cm off from the cavity in "Cavity L". V_P for 'Cavity L' was lower than that of 'No Cavity' by 27%. This reduction is probably explained by the expansion of the loosened area in the soil around cavity as V_P is lower for looser soil (Otsubo et al., 2017). It was found from this result that growth of a cavity can be correlated with the change in V_P around the cavity.

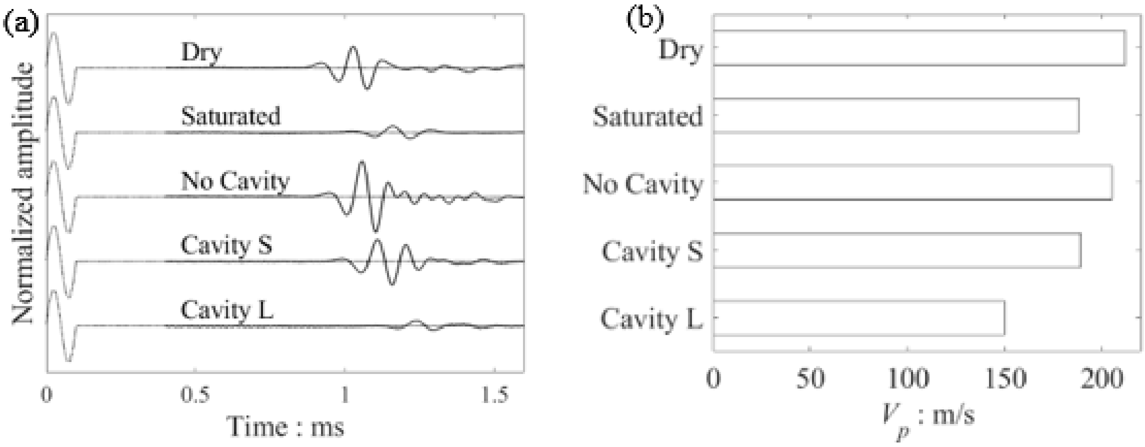

Figure 5: (a) Time-domain responses of P-waves (amplitude of receiver responses was normalized by the maximum amplitude for 'No Cavity' case) (b) V_P for each condition

The amplitude of frequency spectra (fast Fourier transforms of received signal / transmitted signal, FFT_{out}/FFT_{in}) with frequency for the four conditions excluding 'Saturation' are shown in Figure 6(a). The input wave frequency was 30 kHz for the frequency domain analysis to excite a broad range of frequencies. The lowpass frequency, the maximum frequency that can pass through the ground (f_{lp}) is quantified by considering a threshold amplitude of 8×10^{-4} for the experiment. The f_{lp} values of each condition are illustrated in Figure 6(b). As Otsubo et al. (2017) described, f_{lp} has a consistent relationship with stress or density. The present experiment revealed that f_{lp} decreases when the model ground becomes fully saturated; in contrast, f_{lp} increases when the model ground becomes unsaturated, exhibiting a similar variation with V_P. However, the increase in f_{lp} due to shift from 'Saturated' to 'No Cavity (unsaturated)' was relatively larger than that for V_P; this is probably caused by the capillary force generated between contacting particles during the unsaturation process. In the process of cavity expansion, f_{lp} decreased as the size of cavity increased similar to the variation in V_P. The f_{lp} value for 'Cavity L' was smaller than that for 'No Cavity' by 60% and the decreasing rate of f_{lp} was significant compared to that of V_P. Thus it is inferred that growth of a cavity can be assessed from f_{lp} around the cavity more sensitively than measurement of wave velocity.

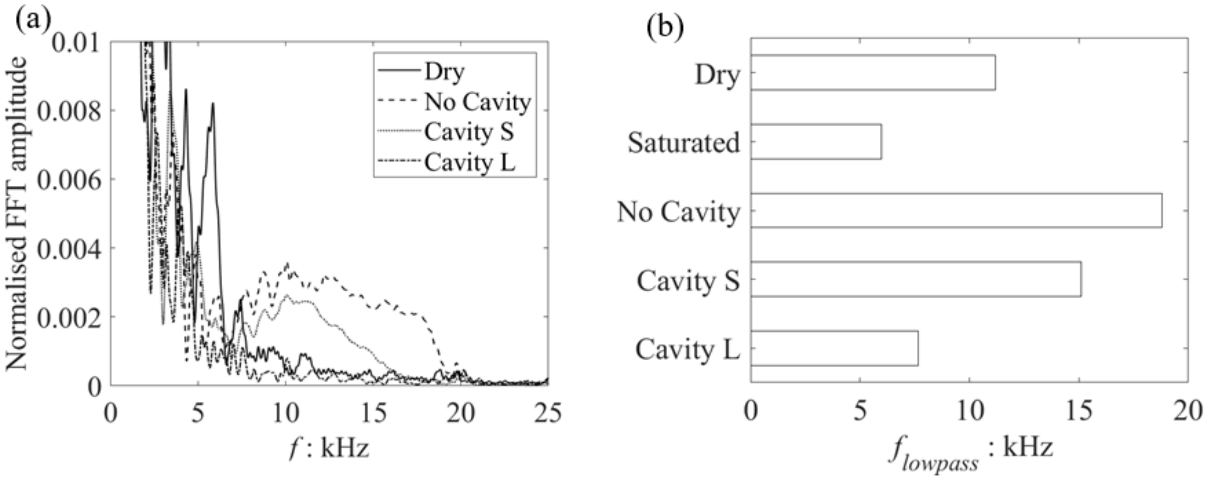

Figure 6: (a) Frequency spectra of received waves and (b) lowpass frequency

3. DEM SIMULATION

To understand the mechanism of the decrease in V_P and f_{lp} around a subsurface cavity, DEM simulation was conducted considering the situation of the model test. Particle-scale analyses using DEM enable observation of phenomena that cannot be measured in the laboratory experiment including wave reflection and diffraction.

3.1 Model preparation

Ali et al. (2019) revealed that the inter-particle cohesion due to unsaturated pore water is necessary to simulate a subsurface cavity. In this research, a simplified unsaturated model implemented by Ali et al. in the open-source LAMMPS code (Plimpton, 1995) was used. The contact theory follows the Hertz-Mindlin model but an inter-particle suction of 5 kPa was considered to stabilize the model with a cavity. Note that the value of suction adopted is much larger than the realistic value. The size of spherical particles was 1.2 – 2.2 mm in diameter, Young's modulus, Poisson's ratio, and the specific gravity were 71.6 GPa, 0.23, and 2.5, respectively.

The dimensions of the model ground were 200 mm in width (X), 20 mm in depth (Y) and 180 mm in height (Z) and it was prepared using an air-pluviation method under gravity. Periodic boundary was applied for the Y-axis direction and rigid boundary conditions for the X- and Z-axis directions. Firstly, the inter-particle friction was set to 0 so that a dense condition was achieved (void ratio of 0.572). Secondly, the inter-particle suction was applied to mimic the unsaturated condition in the laboratory model test. Lastly, the inter-particle friction was increased to 0.5 and particles located in the area of 40 mm × 100 mm (Cavity S) or 60 mm × 150 mm (Cavity L) crossing the periodic boundary were removed from the simulations to produce a cavity.

After the ground had become stabilized, P- wave was generated either right above the cavity or right above the receiver region (Figure 7). Particles located inside a square of 50 mm (width) × 10 mm (thickness) were considered as a transmitter and a receiver (Figure 7). The particles inside the transmitter region were excited downward following single period of cosine pulse having a frequency of 20 kHz and a double amplitude of 200 nm (see Figure 9 for particles displacement). No viscous damping was considered during the wave propagation simulation.

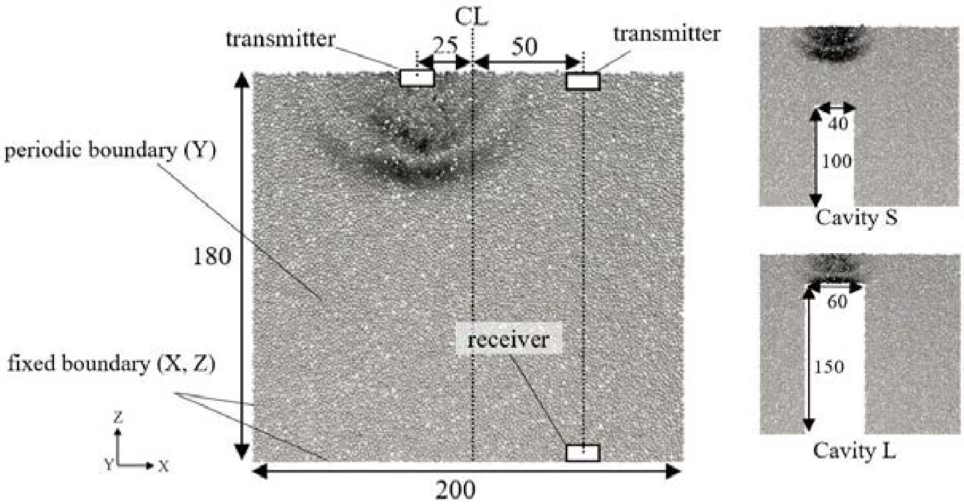

Figure 7: Outline of the model

3.2 Results and discussion

When P-wave was transmitted from right above the receiver, no distinct difference in received waves was observed irrespective of the difference in cavity size. This is probably due to the suction force that is beyond realistic value, and therefore the influence of a cavity on the surrounding soil, i.e. loosening effect, was not measurable. Therefore, the consequences when the transmitter right above the cavity was excited are described below.

For ‘No Cavity’ case, the radial propagation of P-waves was observed as illustrated in Figure 7. As the effective confining pressure increases with depth, a gradual increase in wave velocity was observed at a deeper elevation. Reflection was observed at the walls and at the boundary between soil and cavity. Diffraction phenomenon was also observed around the cavity (Figure 8). The time domain and frequency domain responses of the transmitted and received waves are shown in Figure 9. The time domain displacements are calculated as the mean displacement of the particles inside the region. In the frequency analysis, time domain response until 1.5 ms was processed. f_{lp} was estimated by considering a threshold amplitude of 1×10^{-2} for DEM data.

The rising point of the received waves is slightly delayed for ‘Cavity L’, where the shortest travel path is diffracted and extended (Figure 9(a)). As for f_{lp}, a slight decrease for ‘Cavity L’ was observed (Figure 9(b)). The overall distribution of frequency at large amplitudes was also lowered for ‘Cavity L’ compared with the other conditions.

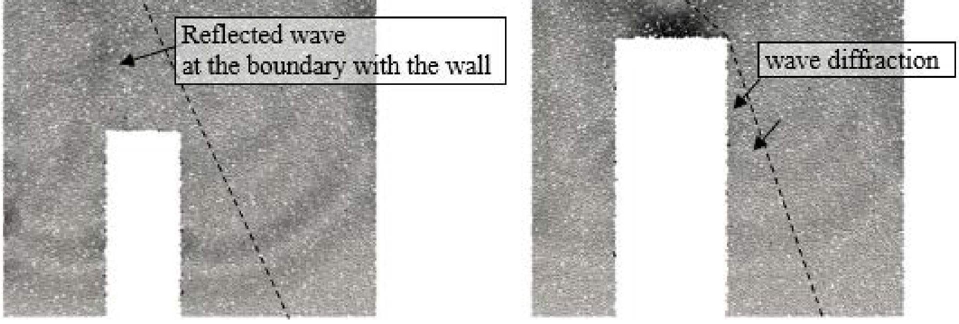

Cavity S Cavity L

Figure 8: Reflected wave and diffraction wave

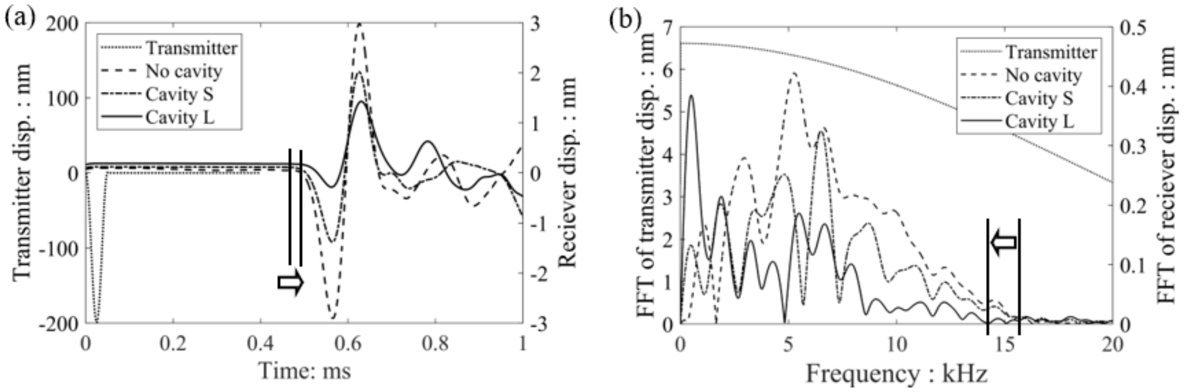

Figure 9: (a) Time – displacement and (b) frequency spectra of waves

This study also analyzed the arrival time of P-waves which were reflected vertically at the ceiling of the cavity. The arrival time was measured at the transmitter and it was 0.495 ms for ‘Cavity S’ and 0.225ms for ‘Cavity L’. These are almost proportional to the distance between the transmitter and the ceiling of the cavity, which is 80 mm for ‘Cavity S’ and 30 mm for ‘Cavity L’. This indicates that the reflection waves from the ceiling of a cavity can be effective to estimate the depth of the subsurface cavity.

4. CONCLUSIONS

This study investigated characteristics of compression wave propagation in the soil around a cavity using laboratory model tests and DEM simulations. Based on the model tests, the following conclusions can be drawn:

- Characteristics of P-wave propagation are affected due to a subsurface cavity nearby.
- Both V_P and f_{lp} decrease as a cavity grows.
- Decrease in f_{lp} is more sensitive compared to V_P when the cavity size increases.

Based on the DEM simulations, the following conclusions can be drawn.

- f_{lp} decreases due to diffraction of the propagation path around a cavity.
- Reflection of P-waves at the ceiling of a cavity is evident.
- An improved DEM model considering loosening and arching effects is required.

REFERENCES

1. Kominami, N., 2018. *The relationship between sinkholes and waterpaths and the effectiveness of underground water sound*, Master thesis, University of Tokyo, Tokyo, Japan.
2. Fujii, K., Kitamura, K., Kojima, Y., Kuwano, R., Yonemoto, Y., Achievements of Collaborative Study on Effective Measures for Prevention of Road Cave-in in FUJISAWA city, *Proceedings of 54th Japan National Conference on Geotechnical Engineering.* 1443-1444.
3. Hardin, B.O. & Richart, F.E., 1963. Elastic wave velocities in granular soils. *J. Soil Mech. Found. Div.* 89, No. 1, 33-65.
4. Otsubo, M., O’Sullivan, C., Hanley, K. J. & Sim, 2017. Influence of packing density and stress on the dynamic response of granular materials, *Granular Matter* 19:50.
5. Ali, U., Otsubo, M., Kuwano, R., 2019. Implementation of suction-tension model for cavity simulations using DEM. *Proceedings of 54th Japan National Conference on Geotechnical Engineering*, 809-810.

6. Plimpton, S., 1995. Fast parallel algorithms for short-range molecular dynamics. *Journal of Computational Physics*. 117, No. 1, 1-19.
7. Suwal, L. P. & Kuwano, R., 2013. Disk shaped piezo-ceramic transducer for P and S wave measurement in a laboratory soil specimen. *Soils Found*. 53, No. 4, 510-524.
8. Dutta, T. T., Otsubo, M., Kuwano, R. & O'Sullivan, C., 2019. Estimating stress wave velocity in granular materials: Apparent particle-size dependency and appropriate excitation frequency range, *Géotechnique Letters*. 9 (3), 1-26.

UNSATURATED SHEAR CHARACTERISTICS OF EXTREMELY LOOSE VOLCANIC SOIL CAUSING SLOPE DISASTER

Itsuki Sato[1] **and Reiko Kuwano**[2]

[1] *Doctoral Student, The University of Tokyo, Institute of Industrial Science, Tokyo, Japan, i-sato@iis.u-tokyo.ac.jp*
[2] *Professor, The University of Tokyo, Institute of Industrial Science, Tokyo, Japan, kuwano@iis.u-tokyo.ac.jp*

Keywords*: Volcanic soil, Cementation, Particle crushing, Landslide, Slope disaster*

1. INTRODUCTION

Slope Disasters that flow a long distance with destructive energy at very gentle slopes are sometimes observed. In such cases, the trigger layer is often volcanic soils with extremely high void ratios, induced by earthquake or heavy rainfall. The loose structure of such volcanic soils are retained by weak cementation or composed of crushable particles having intra voids. Although the cause of destructive long-distance flow has been explained by liquefaction, trigger layer was not always fully saturated, i.e. liquefaction is not a major cause. Thus, this study considers deformation and strength characteristics of unsaturated soils. Focusing on the fact that slope disasters such as long-distance flow or gentle slope flow are triggered by loose volcanic soil layers, artificial loose soil samples consisting of silt and cement were prepared [1]. Triaxial tests with unsaturated condition were performed to discuss how air trapped in voids affects the shear strength properties.

2. TEST RESULTS

Artificial pumice specimens (Φ=5cm, H=10cm) with cementation and crushable particles were prepared. Unsaturated CU tests were conducted at different confining pressure and initial water content by using double cell method (Table1).

Table 1. Experimental cases

Test	Ad-100	Ad-300	A60-CU100	A60-CU300	A70-CU100	A70-CU300
Sr(%) before consolidation	0	0	60	60	70	70
Consolidation pressure(kPa)	100	300	100	300	100	300
Preconsildation pressure(kPa)	20	20	20	20	20	20
ρ_s (g/cm3)	2.69					
Void ratio, e	2.06 ~2.02					
Volumetric strain at consolidation ε_{vol} (%)	3.2	6.1	3.2	15.2	4.7	18.1
Sr(%) after consolidation	0	0	63	76	75	93

3. CONCLUSIONS

Figures 1 and 2 show experimental results. Artificial pumice exhibits a high shear strength and a low compressibility when cementation is maintained. However, once cementation is lost, a high compressibility is observed. Although the specimen is not fully saturated, after the shear strength reached its peak and the cementation was lost, a brittle behaviour was observed in which the shear strength converges to a residual state, called steady state.

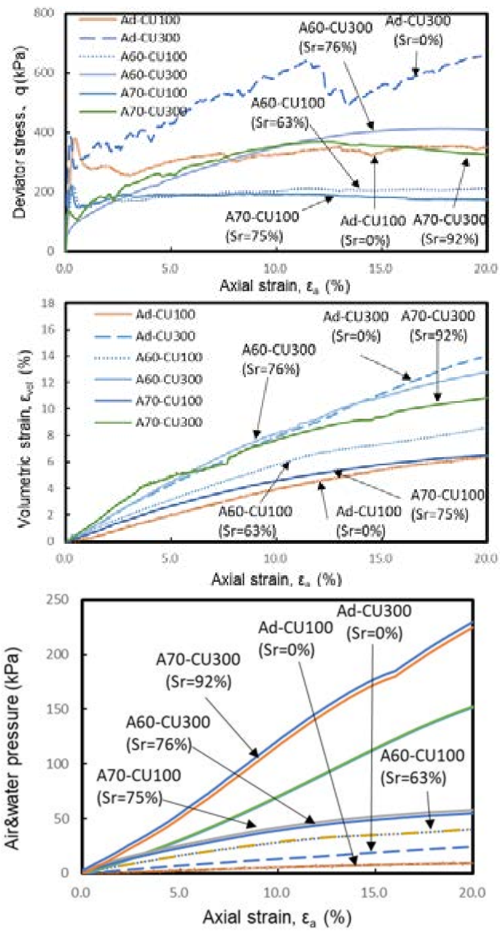

Figure 1. Unsaturated CU test results.

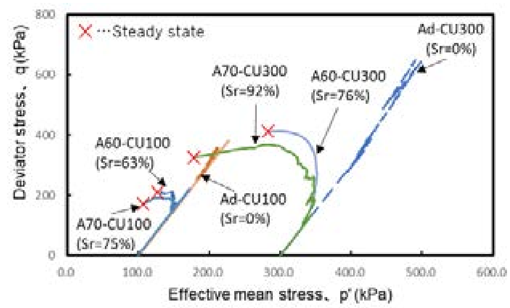

Figure 2. Stress path

REFERENCES

[1] I. Sato, R. Kuwano (2019) Vulnerability of volcanic loose soils having cementation and crushable particles, International Symposium on Deformation Characteristics of Geomaterials (IS-Glasgow 2019), E3S Web of Conferences, 92, 09001.

Relationship between inequality, education, and disaster experience at the household level in Yangon City, Myanmar

Kota HORIUCHI[1] and Michael HENRY[2]
[1]Master student, Graduate School of Engineering,
Hokkaido University, Japan
kt_horiuchi@eis.hokudai.ac.jp
[2]Associate Professor, Faculty of Engineering,
Hokkaido University, Japan

ABSTRACT

The Government of Myanmar issued The Myanmar Sustainable Development Plan (MSDP) in August 2018. The MSDP is designed to achieve ensuring balance between development in the economic, social and environment spheres. In this research, as the economic, social and environmental aspects, income inequalities, education attainment levels, and disaster experience, are focused on. This is because Myanmar is a nation having the possibility of various natural disasters, and the income inequality and the education attainment levels can be considerable in households units. The objective of this research was to clarify the relationship between income inequality and the damage of water-related disaster while examining the relevance of the income inequality and the education attainment levels, and to consider the relationship the education attainment levels and experience of disaster. From analysis of these relationships, it was revealed that there are relationships between the HIS Zone and experience of disaster, between education and the HIS Zone, and between income and the education. Therefore, it is concluded that the education has a relationship with the experience of disaster, and the income influences the experience of disaster through the education and the HIS Zone.

Keywords: sustainability, education, income, disaster

1. INTRODUCTION

Myanmar is proceeding the development system in the government, and has experienced rapid economy and political growth in recently years. According to the World Economic Outlook Database (International Monetary Fund, 2019), the economic growth rate of Myanmar keeps advancing from 5% to 8% in recently 7 years. However, it has been appearing the imbalances growth in Myanmar so much as to concentrate on the economic and political growth. To address the imbalances, the Government of Myanmar designed "The Myanmar Sustainable Development Plan (MSDP) (The Government of the Republic of the Union of Myanmar , 2008) in order to ensure the right balance between economic, social development, and environmental protection.

Myanmar also have a possibility to suffer from various natural disasters. According to the hazard profile of Myanmar (Government of the Union of Myanmar, 2009), it is classified the disasters in Myanmar to the cyclone, droughts, earthquakes, fires, landslides, high tide, and tsunami. Furthermore, these disasters frequency are not low, and a lot of local people suffer from these disasters every year. Especially for the water-related disasters, such as cyclone and flood, the damage of them are more severe than other disasters. For example, in cyclone Nargis, which occurred in 2008, the number of dead and missing exceeded 140,000 people, according to the Learning from Cyclone Nargis (Nizar Mohamed, 2009). Therefore, it is quite important problem to be solved, and safety from disaster is an important social and environmental aspect for sustainability.

With these conditions of Myanmar in mind, this research focused on the social and environmental aspects for attaining sustainability. In social and environmental sphere, income inequalities, education achievement levels, and disaster experience and damage were focused. The objective of this research was to clarify the relationship between income inequality and the experience and damage of water-related disaster, while also examining the effects of the education attainment levels on the experience and damage of water-related disaster. It will be able to contribute to suggest some strategies to accomplish sustainable development in Myanmar.

2. SURVEY METHOD AND SAMPLE CLASSIFICATION

2.1 Investigation method

In order to clarify the relationship between water-related disaster and income inequality, and education attainment levels, it was used the data of Household Interview survey (HIS) in Yangon city, conducted by Japan International Cooperation Agency (JICA) in "Strategic Urban Development Plan of Greater Yangon" in 2012. The detail of HIS is summarized in Table 1. In this survey, 10,069 households answered, which is equal to 1.0~1.2% of population of Yangon City in 2012. As for survey items, this research utilized the data of household socioeconomic conditions, such as income inequality and educational achievement levels, and experiences of water-related disaster and property of damage. The data which was used in this research was summarized in the Table 2.

Table 1: Summary of questionnaire (Japan International Cooperation Agency, 2013)

Method	Interview Survey
Term	22 Sep 2012 – 16 Nov 2012
Target	Household in Yangon City
Number of Sample	10,069 Household

Table 2: Survey items

Classification	Questionnaire contents	Response categories
Income inequality	Household income per month	Below 25,000 to Above 1,000,000
Educational levels	Education attainment level	University degree or higher, High school, Middle school, Primary school or lower
Experience of water-related disaster and property of damage	Experience of disaster	Experience, No experience
	Property damage by cyclone	Very serious, Serious, Slight, None
	Property damage by flood	Very serious, Serious, Slight, None

2.2 Investigation area

HIS was conducted in 18 townships groups (HIS Zone), which compose Yangon city, and the number of sample households and proportion to the actual households in each HIS Zone are summarized and shown in Table 3. The distribution of sample was decided by the population in 2011.

Table 3: Characteristics of townships in Yangon in 2011

HIS Zone	No. of the sample households	HIS Zone	No. of the sample households	HIS Zone	No. of the sample households
A	495 (1.22 %)	G	675 (1.00 %)	M	1,123 (1.00 %)
B	546 (1.08 %)	H	533 (1.00 %)	N	596 (1.00 %)
C	556 (1.14 %)	I	489 (1.00 %)	O	805 (1.00 %)
D	411 (1.13 %)	J	571 (1.00 %)	P	700 (1.39 %)
E	397 (1.00)	K	431 (1.00 %)	Q	500 (1.70 %)
F	492 (1.00 %)	L	380 (1.00 %)	R	300 (2.08 %)

2.3 Definition and classification of sustainability indicators

To consider the sustainability in Yangon City, the data of household income, education level and the experience and damage of disaster were selected as indicators of three sustainability pillars: Economy, Society, and Environment. In addition, HIS Zone was also considered as an indicator to reveal the actual Myanmar's sustainability condition depending on the residence areas.

As for the income and education levels, it was classified into the four groups as shown in Table 4. In this research, it was defined that the highest education level in the household member as the household education level, because it is expected that the person who has the highest education level will support the other household members. Among 10,069 households of data, 9,518 data were valid and 551 data was not considerable because of the lack of the income and education responses. The distributions of income and education levels in household data are summarized in Table 4. Regarding with the relationship between the income and education levels, a correlation coefficient was 0.378609, and it can be said that there is a weak relevance. Thus, it was available to analyze both of indicators.

As for the experience of water-related disaster, it was classified as shown below in Table 5. Among 10,069 households of data, 9,518 data was also available to analyze the relevance of the experience of water-related disaster to the income levels and the education levels. Meanwhile, as for the responses for cyclone or flood damage, the total number of household data was restricted because they only include the people who have experienced each disaster. The available household number of who have ever experienced cyclone was 6,228. Among them, 5,072 households have ever experienced cyclone damage. On the other hand, 237 households have ever experienced flood and 94 households have ever experienced flood damage. The number of households that have ever experienced flood together with flood damage was closed to 1.0~2.0% of total households, so it was omitted in the below discussion. The classification of the experience of cyclone or flood damage and the property of damage of them were summarized in Table 6.

Table 4: Classification of household income and education level

Income			Education		
Classification (kyat/month)	**Number**	**Ratio**	**Classification**	**Number**	**Ratio**
Low income (0 ~ 100,000)	1,712	17.99%	Upper primary school	1,155	12.13%
Middle income (100,001 ~ 200,000)	3,829	40.23%	Middle school	2,516	26.43%
High income (200,001 ~ 500,000)	3,144	33.03%	High school	1,608	16.89%
Extremely high income (500,001 ~)	833	8.75%	Above university	4,239	44.54%
Total	9,518	100.00%	Total	9,518	100.00%

Table 5: Classification of experience of water-related disaster

Experience of water-related disaster		
Classification	**Number**	**Ratio**
Yes	6,617	69.52%
No	2,901	30.48%
Total	9,518	100.00%

Table 6: Classification of experience and property damage due to cyclone and flood

Cyclone						
Experience of cyclone damage				**Property damage**		
Classification	**Number**	**Ratio**		**Classification**	**Number**	**Ratio**
Yes	5,072	81.44%		Very serious	751	14.81%
				Serious	2,044	40.30%
				Slight	2,277	44.89%
No	1,156	18.56%		Total	5,072	100.00%
Total	6,228	100.00%				

Flood						
Experience of flood damage				**Property damage**		
Classification	**Number**	**Ratio**		**Classification**	**Number**	**Ratio**
Yes	94	39.66%		Very serious	26	27.66%
				Serious	20	21.28%
				Slight	48	51.06%
No	143	60.34%		Total	94	100.00%
Total	237	100.00%				

3. ANALYSIS RESULT

In this research, it was analyzed the relationship between the experience of water-related disaster, the income level, the education levels and the HIS Zone at the beginning. Then, the households that have experienced disaster were divided to the group of cyclone, flood and others, and analyzed the relationship between the experience of cyclone damage, the income levels, the education levels, and the HIS Zone in the group. Next, the experience of cyclone damage were distributed as property of damage, such as very serious, serious, and slight. The relevance of the property of damage of cyclone to the income levels, the education levels and the HIS Zone was calculated in the group.

In each analysis, Cramer's V was calculated in order to evaluate the degree of influence between each indicators. The degree of relationship with Cramer's V is shown in Table 7, and the equation of Cramer's V is shown below. The evaluation criteria in Cramer's V is objective, so it was modified to this analysis to reveal the relationships of them.

Table 7: Degree of the relationship of Cramer's V

Cramer's V	The degree of relationship
0.31 ~	Relative strong relation
0.21 ~ 0.30	General relation
0.11 ~ 0.20	Weak relation
0.01 ~0.10	Very weak relation
0	No relation

The equation of Cramer's V

$$\text{Cramer's V} = \sqrt{\frac{\chi^2}{n(k-1)}}$$

χ^2 = Chi-square value
n = Sample size
k = Number of category

3.1 Relation between experience of water-related disaster and socioeconomic condition

The relevance of the experience of water-related disaster to socioeconomic condition, such as the income levels, the education levels and the HIS Zone, was analyzed by Cramer's V. This analysis was conducted with targeting the group that was composed with 9,518 households of Table 5, and cross-tabulation data which shows the distribution of households is summarized in Figure 1. The Cramer's V are summarized in the Table 8.

The proportion who have ever experienced water-related disaster became lower as the income levels and the education levels rise. From the analysis of Cramer's V, the relationship with the HIS Zone and the experience of disaster, with the income and education levels, and with the HIS Zone and the education levels were considered as general relation.

Table 8: Results of Cramer's V in the group that have experienced water-related disaster (N=9,518)

	Income	Education	HIS Zone	Experience of disaster
Income				
Education	0.225998			
HIS Zone	0.189938	0.216482		
Experience of disaster	0.104956	0.125452	0.261187	

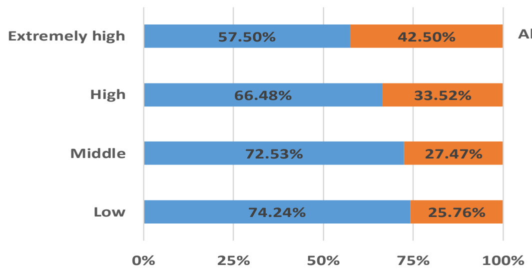

(a) Divided by income levels

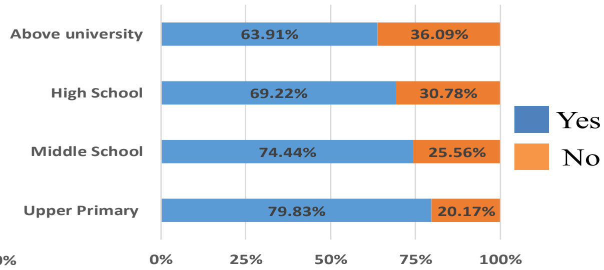

(b) Divided by education levels

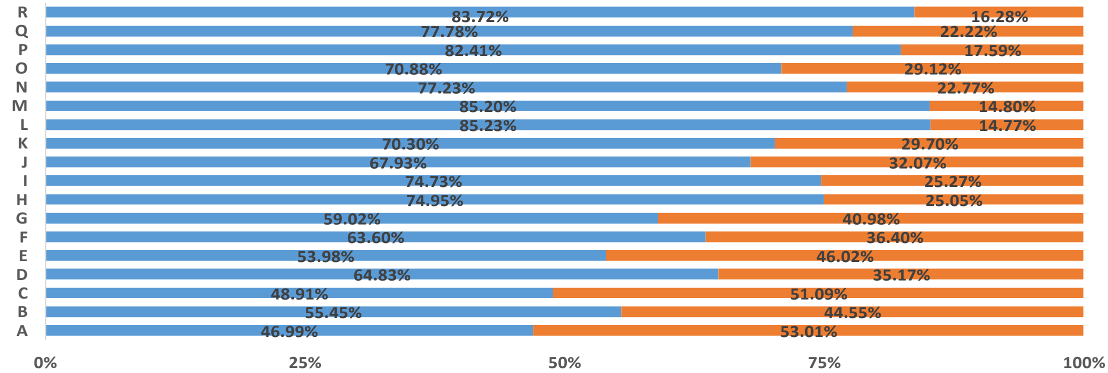

(c) Divided by HIS Zone

Figure 1: Experience of water-related disaster (N=9,518)

3.2 Relation between experience of cyclone damage and socioeconomic condition

Table 9: Results of Cramer's V in the group who have experienced cyclone (N=6,228)

	Income	Education	HIS Zone
Experience of cyclone damage	0.104827	0.104734	0.307632

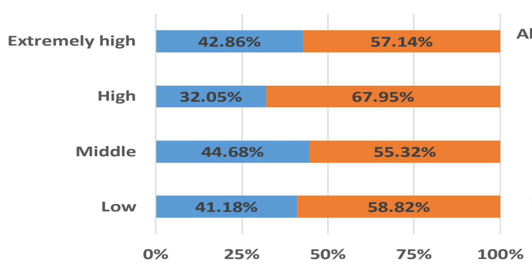

(a) Divided by income levels

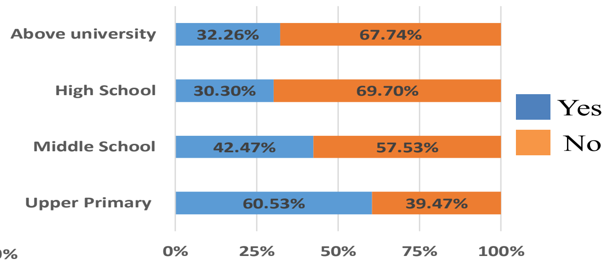

(b) Divided by education levels

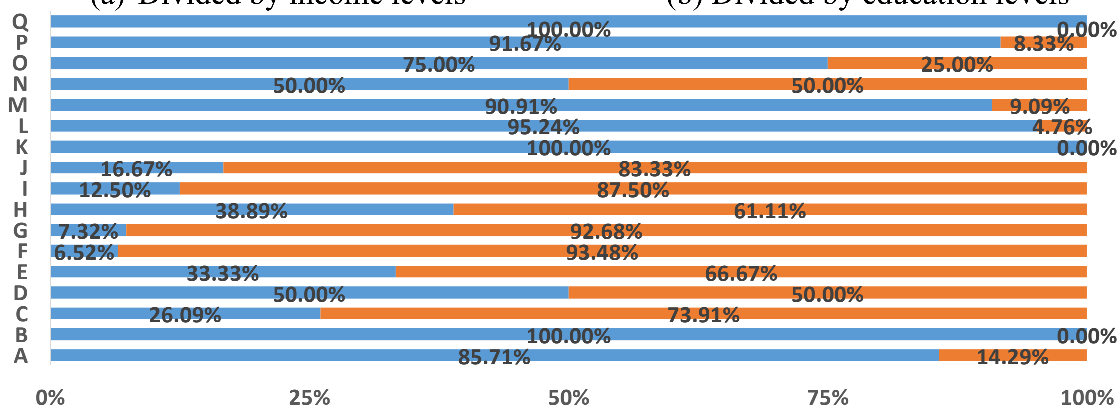

(c) Divided by HIS Zone

Figure 2: Experience of cyclone disaster damage (N=6,228)

The relevance of the experience of cyclone to socioeconomic condition, such as the income levels, the education levels and the HIS Zone, was analyzed. This analysis was conducted with targeting the group that was composed with 6,228 households of Table 6 of cyclone, and cross-tabulation data which shows the distribution of households is summarized in Figure 2. Cramer's V are summarized in the Table 9. The relationship with the income levels and the education levels, with the income levels and the HIS Zone, with the Education levels and the HIS Zone were omitted above table.

There are no distribution of who have experienced disaster damage in all income levels. However, the proportion became lower as the education levels rise. From the analysis of Cramer's V, the relationship with the HIS Zone and the experience of cyclone damage was recognized as relative strong relation in Cramer's V. On the other hand, it was not appeared the relationship of the experience of cyclone damage and the income levels and the education levels.

3.3 Relation between property cyclone damage and socioeconomic condition

The relevance of the property of damage of cyclone to the income levels, the education levels, and the HIS Zone was analyzed, and summarized in the Table 10. This analysis was conducted with targeting the group that was composed with 5,072 households of Table 6 of cyclone, and cross-tabulation data is summarized in Figure 3.

Table 10: Results of Cramer's V in the group who have experienced cyclone damage (N=5,072)

	Income	Education	HIS Zone
Property damage of cyclone	0.089718	0.084117	0.221662

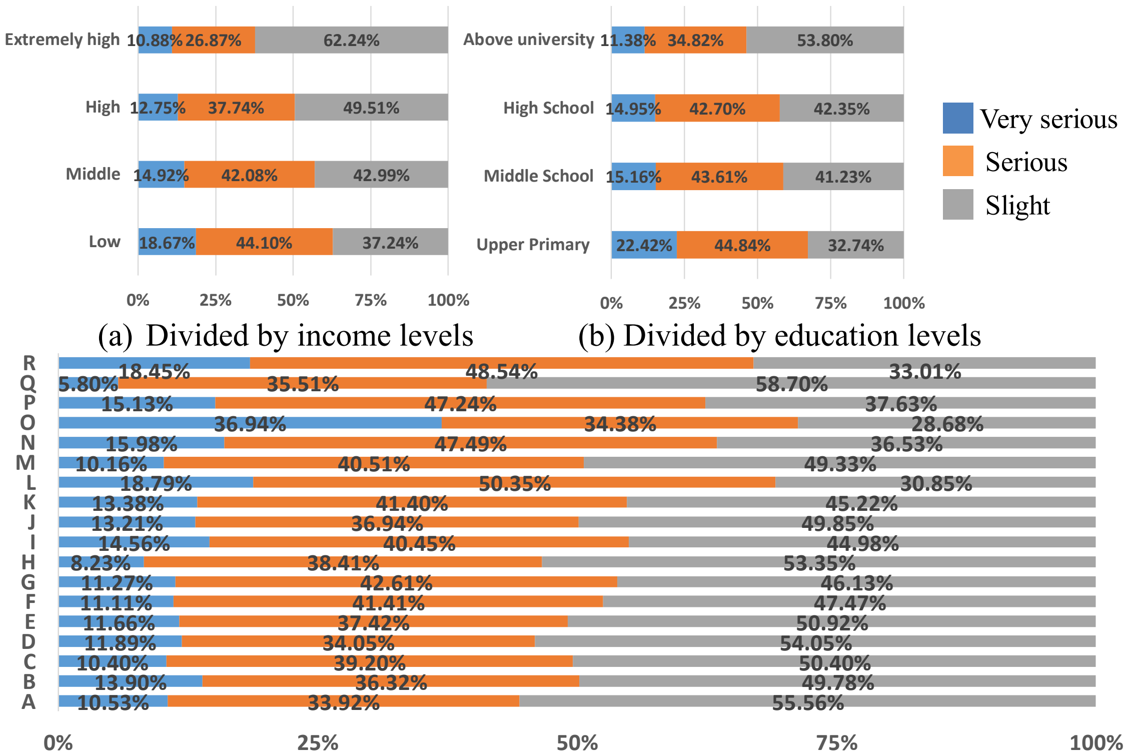

(a) Divided by income levels (b) Divided by education levels

(c) Divided by HIS Zone

Figure 3: Property of cyclone damage

The proportion of who experienced slight damage was higher as the income and education levels rise. However, it was recognized that just only the HIS Zone have relationship with the property of cyclone damage in Cramer's V.

4. CONCLUSION

From the results, it is revealed that the HIS Zone has the strongest factor for the disaster experience, especially cyclone, among almost the income levels or the education levels. Then, it is obvious that the HIS Zone and the education levels have relationship. Furthermore in the property damage due to cyclone, it is clear that the HIS Zone has relationships with property of cyclone damage and the education levels. Therefore, it can be said that the education levels influence on the HIS Zone and the HIS Zone decides the disaster experiences and the damage of cyclone. It can be assumed that households who have higher education levels prefer to stay in the areas that have less possibility to be exposed to the dangerous and damage of disaster, such as cyclone.

In addition, the income levels influence on the property damage of cyclone through the HIS Zone. It was not found the directly relationship with the income levels and the disaster experiences, however, it can be concluded that the income levels have also influences for the disaster experience if other aspects of disaster were analyzed with the income levels because the influential role of the HIS Zone for the property of damage.

ACKNOWLEDGEMENT

This research was supported by the Science and Technology Research Partnership for Sustainable Development (SATREPS) program, which is sponsored by the Japan Science and Technology Agency (JST) and Japan International Cooperation Agency (JICA). The copyright of this Household Interview Survey data belongs to Japan International Cooperation Agency (JICA). The authors would like to express their gratitude to Dr. Akiyuki Kasasaki of The University of Tokyo and Mr. Naoki Yamashita of Nippon Koei Co, for permission to use this data.

REFERENCES

International Monetary Fund, 2019. Myanmar: Gross domestic product, constant prices (Percent change), *World Economic Outlook Database,* The United Stated of America.

The Government of the Republic of the Union of Myanmar, 2018. *Myanmar Sustainable Development Plan (2018-2030)*, Myanmar

Government of the Union of Myanmar, 2009. *Hazard profile of Myanmar*, Myanmar.

Nizar Mohamed, 2009. *Learning from Cyclone Nargis*, United Nations Environment Programme Kenya.

Japan International Cooperation Agency, Nippon Koei Co., Ltd., NJS consultants, Ltd., YACHIYO Engineering Co, Ltd., International Development Center of Japan Inc., Asia Air Survey Co., Ltd., ALMEC Corp. 2013. *A Strategic Urban Development Plan of Greater Yangon : Final report 1, Appendix, Appendix 2*, Japan.

Development of Subsurface Cavity Potential Map for Effective Road Cave-in Countermeasures

Ryoko SERA [1], Reiko KUWANO [2],

[1] *Manager, Operational Headquarter, GEOSEARCH Co.,LTD., Tokyo, JAPAN, r-sera@geosearch.co.jp (corresponding author)*
[2] *Professor, Institute of Industrial Science, The University of Tokyo, Tokyo, JAPAN, kuwano@ iis.u-tokyo.ac.jp*

Keywords: *subsurface cavity; road cave-in; regional characteristics; factor analysis; evaluation of potential*

1. BACKGROUND

Preventing road cave-in is key to keeping road traffic functions. Since the 1990s, several Japanese public administrations began subsurface cavity surveys utilizing ground-penetrating radar technology. The trigger of starting surveys was a social issue known as the "cave-in syndrome" that a fact of multiple road cave-ins in Tokyo in 1988. From then on, the surveys have been conducted regularly all over Japan that focuses on cavities due to damage of aged buried infrastructures, influenced by high-density underground development, and fluctuation of groundwater level. In recent years, emergency surveys were carried out after large earthquakes to ensure disaster recovery activities. Such unique and state-of-the-art technologies for the prevention of cave-in have been innovated through various experiences over 30 years. Especially, it is important that the survey technology of subsurface cavities be improved in accuracy and speed, and the early detection will lead to a reduction in road maintenance costs. Besides, survey data analysis and cave-in mechanisms have been discussing and the development of repair material for cavities has progressed based on field investigations. Regarding the evaluation of cavity/cave-in, each data of the subsurface cavity was used for prediction of risk to cave-in itself, but this is the first attempt to evaluate the regional area using the cavity survey data and the environmental factors of cavities.

Figure 1: Photo of a self-propelled cavity exploration car named "SKELE-Car"

2. PURPOSE OF DEVELOPMENT OF THE POTENTIAL MAP

Cave-in potential map is an information-sharing tool. The purpose of the development of that map is to understand the regional condition. It shows the potential of cavities in regional using the cavity survey data and the environmental factors of cavities. For keeping road functions against cave-ins, it is necessary to consider the road network around the cavities. The regional assessment of the potential of the cavity/cave-in and the map showing it gives some benefits. It takes appropriate measures not only for regular situations but also for emergency situations such as large-scale natural disasters. In addition, these approaches will support discussion at other local governments that starting new measures for cave-in as experienced cases.

3. CONTENTS FOR DEVELOPMENT THE MAP

The beginning of cave-in is a small ground phenomenon. One of the factors forming cavities can be considered as a washout of soil particles through a broken sewer pipe or joint. Fig. 2 shows photos as actual examples of the factor of cavities in Fujisawa city. In addition, another main factor is the consolidation settlement of soil particles in the subgrade; loosen the soil around the underground structure and fluctuation of groundwater level. In many cases, some contributing factors influence each other forming cavities.

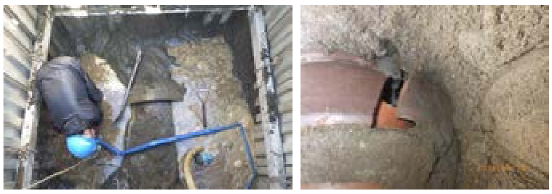

Figure 2: Photos at detail investigations of the cavity and a broken sewer pipe by aging [2]

The development of the potential map prototype was conducted in collaboration with Fukuoka City[1] and Fujisawa City[2] [3]. Each city has different localities, with different city development scales, underground usage, the history of the survey of the subsurface cavity, and the factors of cavity. The content used to develop the potential map prototype is as follows:

1. Databases of cavity survey / including information of repair and factors of cavity
2. Governmental manage data / GIS; roads, sewage
3. GIS data; landform, geology
4. The databases of the cave-in
5. Monitoring survey data of cavities
6. Detail investigation data of causes of cavity
7. Governmental manage data; groundwater level

The contents of 1-3 were used for development in Fukuoka City, and 1-7 were used for development in Fujisawa City. Using these contents, the main regional environmental factor and appearance rate of the cavities in each area were analyzed, and the method for evaluating the potential of cave-in was studied.

4. PROTOTYPE CAVE-IN POTENTIAL MAP OF FUJISAWA CITY

The cave-in potential of Fujisawa city was set by using four factors belonging to each divided grids; type and age of sewer pipe, the number of sewers attaching pipe, groundwater level, and surface geology. The threshold values are as follows:

-Sewer: Confluence type laid in 1950-80s
-Number of sewer attaching pipes: more than 300 /m^2
-Groundwater level/reference value: shallower than GL-3m
-Surface geology: Sandy

After making sure for appropriateness by sensitivity analysis of four potential factors in each, the regional occurrence tendency of cave-ins was analyzed by overlaying each four-factor maps with the cave-in and cavity location map. A knowledge that cavities often occur under overlapped multiple factors was reflected in this evaluation as a new attempt. Fig. 3 shows the combination of cave-in factors and grade of potential/probability of occurrence of Fujisawa City.

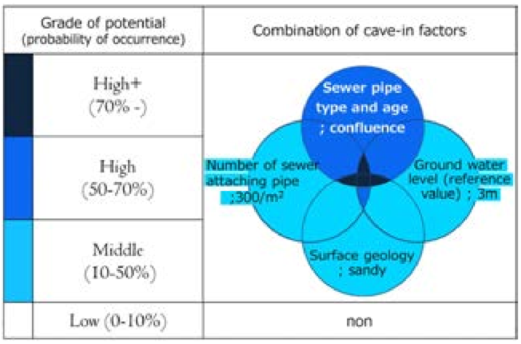

Figure 3: Combination of cave-in factors and grade of potential/probability of occurrence of Fujisawa City [4]

Fig. 4 shows the cave-in potential map as a prototype of and occurrence tendency of cavity/average number in a unit length of road.

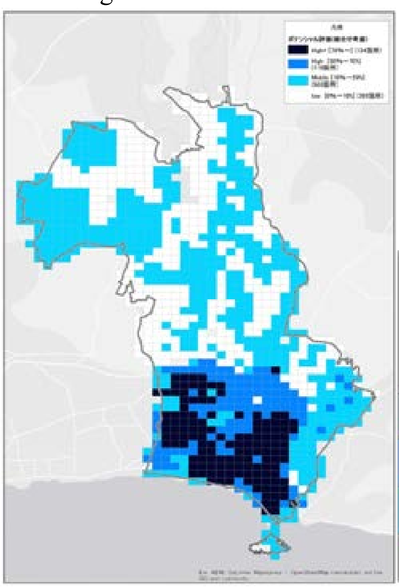

Grade of potential (probability of occurrence)	Occurrence tendency /average number in unit length of road	
	Cave-in number/km	Cavity number/km
High+ (70% -)	1.4	4.6
High (50-70%)	0.7	2.4
Middle (10-50%)	0.2	0.4
Low (0-10%)	0.1	0.3

Figure 4: Cave-in potential map as a prototype of and occurrence tendency of the cavity of Fujisawa City [4]

Furthermore, assuming the potential value as Y and the occurrence frequency of cave-ins/ cavities as X, the following approximate expression and correlation coefficient were obtained was obtained:

Cave-in: $Y = 0.460x - 0.085$, $R^2 = 0.9180$
Cavity: $Y = 1.508x - 0.352$, $R^2 = 0.8977$

This highly accurate formula suggests “if one cave-in occurs, there will be 3 to 4 cavities”.

5. CONCLUSION

This is the first attempt to evaluate the area by the cavity information. And it was able to get the realistic result with the output named cave-in Potential Map.

Subsurface Cavity Potential Map is achieved by reliable cavity survey data over several years. The evaluation got possibility by analysis and quantification of regional factors from field investigations and governmental manage data. It is necessary to understand that the quality of an evaluation depends on "the accuracy of cavity survey" and "determining the cause of cavity“. Preventing road cave-in is key to keeping road traffic functions and it also will be a disaster-resistant system. This MAP can be used by any city around the world, for all road administrators; National roads, prefectural roads, for all administrative departments; roads, sewage, disaster prevention, and not limited to one region, can be expanded into zones.

REFERENCES

[1] Ryoko SERA., R. KUWANO, and M. HOTTA, (2019). *Development of subsurface cavity potential map for prevention of road cave-in*, The 16th Asian Regional Conference on Soil Mechanics and Geotechnical Engineering (16ARC), Taipei.

[2] Hiromitsu NISHIYAMA., H. YOKOTE, M. HARIGAYA, R. KUWANO, and H. MIKI, (2019). *Achievements of Collaborative Study of Effective Countermeasures for Prevention of Road Cave-in in Fujisawa City*, Japan Society of Civil Engineers 2019 Annual Meeting, TAKAMATSU, VI-292.

[3] Kunio FUJII., K. KITAMURA, Y. KOJIMA, R. KUWANO, M. ABE, and M.OKAMURA, (2019). *A Discussion about Effective Countermeasures against Road Cave-in in Fujisawa City based on Monitoring Survey of Subsurface Cavity by Public-Academia-Private Collaborative Study*, Japan Society of Civil Engineers 2019 Annual Meeting, TAKAMATSU, VI-293.

[4] Ryoko SERA., R. HIRATA, Y. YAMAMOTO, R. KUWANO, S. YONEMOTO, and N. KUROSAWA, (2019). *Development of Cave-in Potential Map of FUJISAWA City by Public-Academia-Private Collaborative Study*, Japan Society of Civil Engineers 2019 Annual Meeting, TAKAMATSU, VI-294.

Issues on Crisis Management ~especially counterterrorism~ at the Tokyo Olympic Games

ITO Tetsuro

Visiting Professor, ICUS, IIS, the University of Tokyo, Japan

Keywords: *Olympic Games, Terrorism, Risk management, Crisis management*

1. Introduction

In 2020, Tokyo Olympic Games will be held in Japan. In the big sporting events such as the Olympic Games, so many issues on crisis management emerges compared with other normal sporting events.

This paper describes empirical analysis about why some particular big sporting events such as Olympic Games cause crisis management issues, and what kind of threats are there, and what the features of threat are, and terrorism is the biggest issue among these threats.

The Analysis are about the methods of risk management such as preparations for threats, prevention of crisis and mitigation of damage, and methods of crisis management for minimization of damage, prevention of expansion of damage and chain expansion of crisis.

This paper describes about 2020 Tokyo Olympic Games and analyses cause of threats, issues on crisis management and resolution of crisis in the Games.

2. The Issues and Countermeasures in the Big Sports Event

	Issues	Countermeasures
1	Security	Counterterrorism Cyberterrorism Measures Public Law and Order
2	Traffic Management	Transportation Measures Traffic Jam Measures
3	Crowd Control	Crowd Control in the Stadium Crowd Control outside of the Stadium
4	Abnormal Events	Safety Measures in the Emergencies and the Natural Disasters Heat Stroke Measures

3. The biggest issue on crisis management at Tokyo Olympic Games is the terrorism.

The reason why the terrorism becomes biggest issue is Olympic Games is big sport event which attracts international focus. Therefore terrorist can appeal their opinion and thoughts and existence to the whole world in front of numerous media coming from the world.

There have been many terrorism incidents at the O lympic Games in the past. In late years a terrorist incidents by the influence of the Islam extremism occur worldwide, and not only the things affected by the Islam extremism but also the terrorism with the group which the name has not been yet known may be expected in future.

And it is necessary to assume the terrorism by every means of tools such as using drones and cyber terrorism. And the targets of terrorism have spread to soft targets from conventional targets.

4. What are important to counter the crisis? ~Risk Management and Crisis Management~

[1] Risk Management as the Prior Measures to Crisis

To take prior countermeasures to crisis is very important to prevent crisis and to mitigate the damage. The important things to build countermeasures are 1. The assumption of various type of crises. 2. Examination of various countermeasures to crises. 3. The decision of a countermeasure and to start the preparations and execute countermeasures to crisis.

[2] Crisis Management in the period of before the time of Olympic Games and at the time in the mid of Olympic Games.

It is very important to investigate the countermeasures to various hazards which will happen in the period of the time before Olympic Games and at the time in the mid of Olympic Games. The important things are 1. Who will prepare and execute the countermeasures to crises? 2. Who will play the role of countermeasures when emergency situation outbreaks? 3. What kind of crisis management will be executed? 4. Who will be the decision maker of the countermeasures to the crisis? 5. Is enough training accomplished for a state of emergency?

4. Who is the main player to prepare and execute the countermeasures to the each crisis?

In the big sporting event there are many interested party of the event not only the persons concerned with sports itself but also the central and local government, media, sponsor, the public etc. It is very important to establish a system to prepare, examine, execute the countermeasures to crises in advance. The important things are to decide earlier who is the main player of risk management for each crisis? It is also very important to build the close cooperation system for risk management and crisis management.

5. Conclusion

Big sport event such as Olympic Games become a huge society phenomenon beyond contents in itself of the competition. The crisis to surround the big sporting event became huge too. Risk management and crisis management are very important to prevent or avoid crisis and to mitigate the damage. Early establishment of the system to prepare, examine, execute countermeasures to crisis is crucial for close cooperation between concerned organizations of big sporting event.

SESSION F

SPECIAL SESSION: SATREPS/ TRANSPORTATION,

INFRASTRUCTURE MANAGEMENT

Analysis of transit behaviors using mobile call detail records

Kyaing[1], Ko Ko Lwin[2], Yoshihide Sekimoto[2]
[1]Civil Engineering Department,
Yangon Technological University,
Myanmar
[1]kyaingkyaing63@gmail.com
[2,3]Institute of Industrial Science (IIS), University of Tokyo, Tokyo,
Japan
[2]kokolwin@iis.u-tokyo.ac.jp
[3]sekimoto@iis.u-tokyo.ac.jp

ABSTRACT

Rapid urbanization and modernization are increasing around the world including Myanmar. Mobile call detail records (CDRs) provide new opportunities to measure the transport demands and problems in transportation planning. This research aims to analyze the transit behaviors of mobile phone user based on their call activities. O-D pairs were computed for the whole city and extracted O-D pairs, which fall inside the buffer region, based on their Cell ID locations for rail users. Logical assumptions are specified to extract all users. This results indicated that the four categories of transit usage such as rail users, non-rail users, other modes to rail and rail to other modes. Among the four categories, non-rail users are the highest proportion and rail users are the lowest proportion. This study is very useful in future travel demands to support a better new transport system in Yangon City.

Keywords: call detail records, origin-destination, rail users, non-rail users, transit behaviors

1. INTRODUCTION

In order to satisfy the needs for rapid urbanization and motorization, the city should be well-planned with a variety of facilities. Among the needs, transportation infrastructure plays a vital role in economic growth of country. The current urbanization and motorization are becoming worse and worse day by day on the existing transport infrastructure in Yangon city. The deteriorating of urban transport situation has become a serious concern socially, politically and environmentally. In order to provide a well transportation planning, it is necessary to understand transit behaviors.

To analyze the transit behaviors, many data sources and information are required. Today, especially in developing countries, the process of obtaining relevant real-world indicators is a hard task that needs a lot of expertise and resources. Household travel interviews and census survey data or traffic counts represent traditional tools to analysis travel demand. Interview and surveys, however, are costly and rare especially in Myanmar.

The roadside and household surveys involve expensive data collection, limiting sample sizes and lower update frequencies. Moreover, they are prone to sampling biases in reporting. The census data is also hard to obtain to analysis travel demand. Due to the expensive roadside surveys and infrequent data collection of census data, CDRs data have become a powerful tool to analyze travel behavior patterns that are useful for transportation planning. Therefore, this study concentrates to analyze transit behavior using mobile call detail records in Yangon urban area.

The structure of this paper is organized as follows: related relevant study backgrounds are presented in Section 2. Section 3 states why the study area is selected as a case study. Section 4 briefly describes data to be used in this study and how to extract origin-destination pairs and transit behavior of travelers. Transit behaviors of the study area are discussed in Section 5. Finally, conclusions and future works are presented in Section 6.

2. PREVIOUS STUDIES

The number of researchers studied the various topics using mobile call detail records. Sampling biases and reporting errors occur in traditional approaches (Hajek, 1977: Kuwahara and Sullivan, 1987; Groves, 2006). Automated registration plate scanners (Castillo et al. 2008) and mobile traffic sensors such as portable GPS devices (Parry and Hazelton, 2012: Morimura and Kato, 2012: Herrera et al. 2010) can be used for origin-destination estimation in more recent approaches. The mobility patterns of phone users are linked to human mobility behavior. Lwin et al. (2018) analyzed the hourly link population and flow directions of Yangon city from mobile CDRs data. This dataset was intended to optimize bus routes, solve traffic congestion problems, and enhance disaster and emergency preparedness. Kyaing et al. (2017) analyzed human mobility patterns for different regions in Myanmar based on CDRs data. In this study, average distance travelled, preferred days of long distance users and human mobility patterns at different times of same place and same time at different places were analyzed for two major cities. The results indicated the similarities and differences in mobility patterns for both cities. Zin et al. (2018) also estimated the origin-destination trips in Yangon by using CDRs data. This study described the originating and destination trips from each township in weekday and weekend. And then, the estimated values are compared with the JICA O-D trips at 2013 for validation purpose. Kyaing et al. (2017) forecasted the trip generation by using CDRs data. In this study, regression models were described for forecasting of trip generation.

Rose (2006) and Caceres et al. (2008) described other issues to be considered that may affect the accuracy of transport mode prediction. These factors are market penetration, customer profile and network infrastructure of the mobile network operator supplying the billing information, citizens who do not carry or have their mobile devices turned off during travelling. Traffic data estimations were analyzed using a variety of metrics extracted from mobile phone networks by Caceres et al. (2008). The development of origin-destination matrices for traffic flow estimates, travel speed, travel time calculations, and traffic volumes were also presented. Transportation mode inference was examined from mobile billing records based on travel time by Wang et al. (2013). Mode share of driving and public transportation for a given origin and destination are determined and walking trips are not taking into account in this study. H. Ishizuka et al. (2015) proposed an automated method to generate an alignment of cell towers for a specific transportation route using unsupervised machine learning techniques. They focused on distinguishing different types of motorized transport such as train, bus, and subway. Their proposed system can estimate a specific name of transport line which a user rode on by sequence matching between cell tower sequences of a user and pre-learned cell tower sequences for each route.

In this study, transit behaviors of travelers were analyzed using mobile call detail record for urban area of Yangon City.

3. STUDY AREA

Yangon has an area of 598.750 km2 with a population of 5.211 million in 33 Townships of the urban area. The current urbanization and motorization are becoming worse day by day on the existing transport infrastructure in Yangon city. Traffic congestions, long travel time, low travel speed and traffic accidents are subjected in most parts of the days. Average travel speed being even below 10 kph in central business district. In order to provide good transportation planning, it is necessary to measure transit behavior of Yangon City. Therefore, the urban area of Yangon was selected as a case study. The location of the study area and its road network is shown in Figure 1.

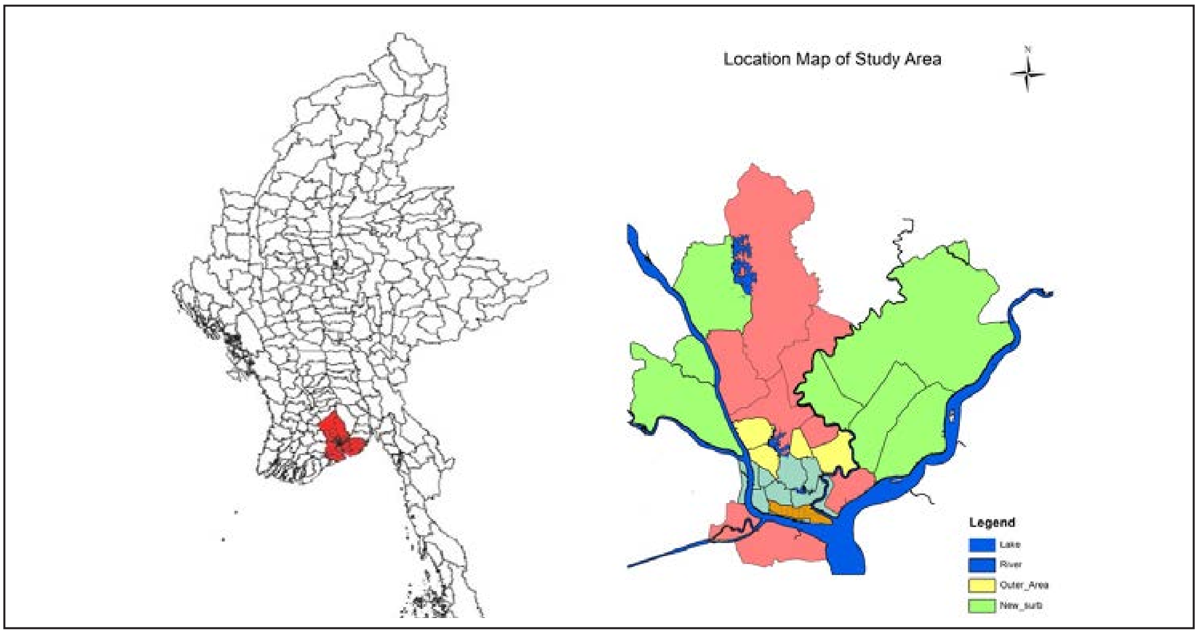

Figure 1: Location of the study area

4. METHODOLOGY

4.1 Data

Call Detail Records (CDRs) data are used to estimate of origin-destination trips and to investigate the travel behavior of the phone uses. The CDR data containing all mobile phone voice calls and data means such as short message service (SMS) and internet service were collected from base transceiver stations (BTS) towers which are located in the study area from 1st December 2015 to 7th December 2015. It was provided by Myanma Posts and Telecommunications (MPT), which is one of the biggest mobile operators in Myanmar. There are 657 BTS towers of MPT services and 132 traffic analysis zones in 33 townships of study area.

Distribution of traffic analysis zones and township boundary and BTS towers in traffic analysis zones are shown in Figure 2(a) and Figure 2(b) respectively. Individual phone numbers were anonymized by the operator before leaving their storage facilities and were identified with a security ID (hash code) to safeguard personal privacy. CDRs data contain Timestamp (date and

time), Caller's ID, Call duration in second and Caller's connected cell tower ID. The location of a user can be determined from the Cell ID that provides the ID of BTS station that is communicating with the user.
In addition, secondary data such as road network map of Yangon City was also used to analyze travel distance for each O-D pair trip.

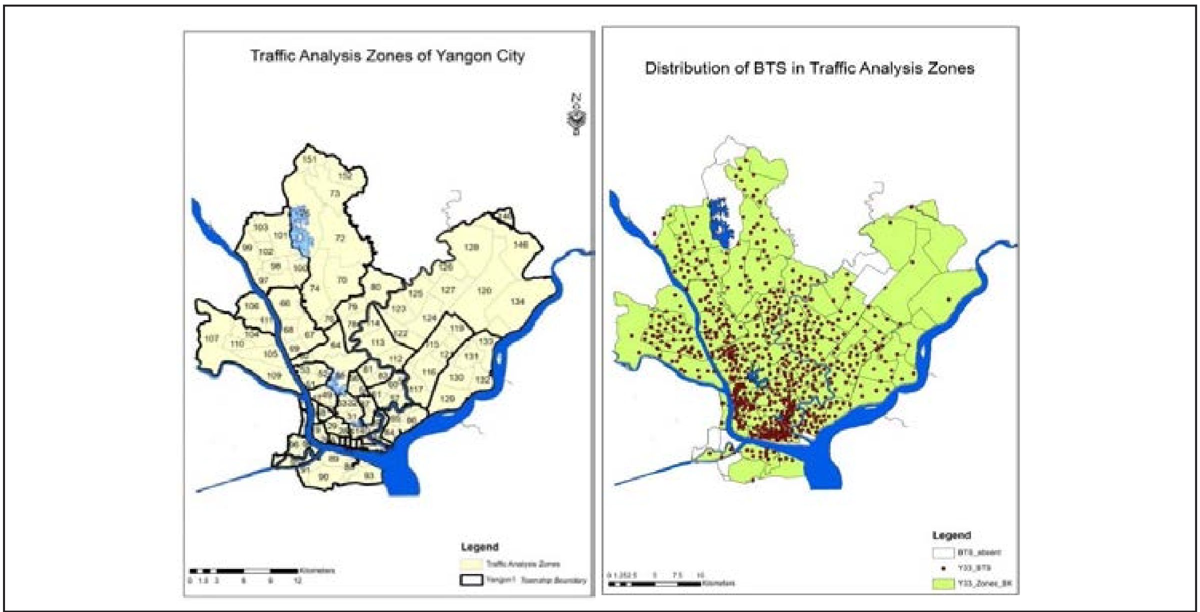

Figure 2(a). Distribution of traffic analysis zones, (b) Distributions of BTS

4.2 Method

In this paper, various transportation modes were identified and transit behavior were analyzed using mobile call detail records in Yangon.

4.2.1 Identification of trip

Cell phone usage of each region can be used to generate trip numbers of this region within certain time frame and time windows. For each mobile user, it is assumed that a trip is made between two consecutive calls occurring within a limited time window with different BTS. The number of trips (flows) can be analyzed as the movement of people who travel from starting point in the origin region and ending in the destination region. In this study, origin and destination zones the cells defined by the base stations and convert the O-D trip to be between Traffic Analysis Zones (TAZs) instead of between cells.
Therefore, time window is necessary to be defined for the determination of O-D trip. Generally, time window interval is defined according to travel behavior of study area. The time window is represented by the travel time to make a O-D trip. Time window is identified as 3 hours in this analysis.

4.2.2 Pre-processing of CDRs data

Pre-processing of CDRs data was done to extract O-D pairs based on BTS stations. Firstly, all missing data were removed and error in BTS file, missing BTS name, wrong coordinates and townships names were corrected in this analysis. And, Cell ID numbers were formatted to string. Geographic locations (Longitude, Latitude) were added to each cell IDs after formatting.

CDRs data alone could not know the location of a person because it is only CELLID with the mobile subscriber. Therefore, the geolocation of CELLID needs to join with latitude and latitude to trace the location. Both formatted voice and data usage were merged by individual subscribers. From these CDRs data, PID, DTIME, and CELLID data were only used in this analysis.

4.2.3 Processing of CDRs data

O-D pairs were extracted for three hours' interval such as 06:00-09:00, 09:00-12:00, 12:00-15:00, 15:00-18:00, 18:00-21:00 for only Tuesday for typical weekdays and Sunday for the weekend. 3-hour interval was identified based on hourly variation of human mobility pattern for the study area. As a time window determination, travel time between origin and destination were extracted for all trips travelled by each user for the whole day. It is found that travel time between origin and destination trip is maximum 3 hours. Therefore, 3 hours is identified as time window in this study.
And, travel distance, duration and travel speed were calculated for each O-D pair with the road network of Yangon City. In this study, BigGIS RTX Research Toolbox (Lwin et al. 2018) was used to process CDR data cleaning, formatting, Cell ID geolocation, OD pair generation, network distance measurement, and speed calculation.

4.2.4 Identification circular railway user from CDRs data

Circular railway line has predefined 200 m or 400 m buffer for service area to determine mode share of rail users as shown in Fig.4.

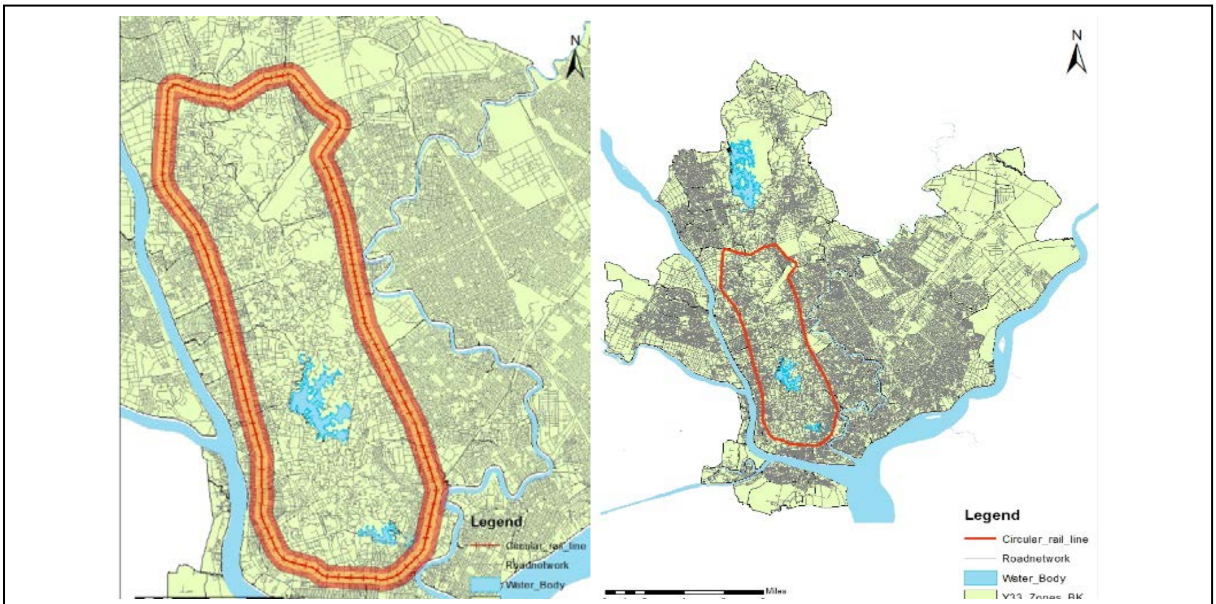

Figure 4. Rail (buffer 200 m or 400 m) and road network of study area

According to questionaries' survey, 200 m buffer is predefined as rail user service area in this study. O-D pairs were computed for the whole city and extracted O-D pairs, which fall inside the buffer region, based on their Cell ID locations for rail users. True and false status are specified as logical assumptions to extract rail users. True is specified as if calling fall inside the buffer region and false is identified as if calling fall outside the buffer region. Therefore, it can be identified as circular railway user if both origin and destination of traveler's status are "True" (both calling fall inside of the buffer area). The numbers of O-D pairs for rail users were extracted using SQL queries. After that, mode share was computed for rail users.

4.2.5 Identification of transit mode from CDRs data

Users were divided into four categories such as circular railway to other mode, other mode to circular railway, circular railway users, and non-circular railway users.
If origin of traveler's status is "True" (calling fall within buffer area) and destination of traveler's status is "False" (calling fall outside of buffer area), transit behavior is defined as circular railway to other mode. If origin of traveler's status is "False" (calling fall outside of buffer area) and destination of traveler's status is "True" (calling fall within buffer area), transit behavior is defined as other mode to circular railway. If both origin and destination of traveler's status is "False" (both calling fall outside of the buffer area), transit behavior is defined as non-circular railway users. Finally, analyzed data are discussed for future transportation planning of study area.

5. RESULTS AND DISCUSSIONS

Transit behavior of travelers were determined using CDRs data in study area. Table 2 shows the transit behavior of travelers on weekday and weekend.

Table 2. Transit behavior of travelers

Day	Mode	Time interval				
		06:00-09:00	09:00-12:00	12:00-15:00	15:00-18:00	18:00-21:00
Weekday	Other Mode to Circular Railway (%)	6.68	7.07	7.22	7.34	6.55
	Circular Railway users (%)	1.75	2.10	2.18	2.24	1.87
	Circular Railway to Other Mode (%)	6.49	7.07	7.22	7.39	6.81
	Non Circular Railway Users (%)	85.08	83.77	83.37	83.03	84.78
Weekend	Other Mode to Circular Railway (%)	5.90	6.38	6.63	6.69	6.16
	Circular Railway users (%)	1.55	1.74	1.76	1.76	1.69
	Circular Railway to Other Mode (%)	5.92	6.42	6.58	6.75	6.35
	Non Circular Railway Users (%)	86.63	85.46	85.03	84.80	85.80

From this Table, it is found that railway users are around 2 %, other mode to railway users is about 7 %, circular railway to other mode is also 7 % and non-circular rail users is about over 80 % on weekday. On weekend, railway users are around 2 %, other mode to railway users is about 6 %, circular railway to other mode is also 6 % and non-circular rail users is about over 80 %. Non-circular railway users are the highest between 06:00-09:00 and 18:00-21:00 interval of the day. It can be inferred that public bus and private car/taxis are the primary responsible for their work trip. But, other remaining transit behavior of users are totally different in these time intervals. Weekday and weekend transit behavior are very similar although actual values are may not be the same.

There are some limitations of CDRs data used in this study. While CDRs data were used in this research, it in tracing location, O-D (Origin-Destination) trips are based on call activities. Therefore, although people are moving from one place to another place, this trip cannot account for a trip if he/she does not use the mobile phone in this analysis. Positions may also change slightly due to load balancing. And, routes were estimated based on the shortest-path analysis. Travel distances were measured based on this analysis, and also speeds were calculated using these distances. This study can be analysed with CDRs data from only MPT is available although there are three telecommunications in Myanmar such as Ooredoo, Telenor and MPT services due to difficulties in data acquisition of privacy issues.

6. CONCLUSIONS

In this study, it is found that non-circular railway users are the highest and followed by other mode to circular railway and circular railway to other mode. Other mode to circular railway and circular railway to other mode users are similar proportions and rail users is the least proportion among all of transit because of its inconvenience and uncomfortable. In addition, most of the people can choose only private car, taxi and public bus to arrive their destination according to road network as shown in Fig.1. Rail network is provided only circular pattern of urban area and is not provided north-south and east-west directions across Yangon City. Therefore, new transit system should be provided to balance the demand and existing transit systems should be improved to reduce private car usage. If public transport services such as bus and rail can be improved, many challenges and issues can be solved in urban area of Yangon.

This method can be easily applied for the large population of the large-scale area such as country/state/division/township levels. Therefore, it is a cost-effective solution to complement traditional survey without time consuming. These data are very helpful in the prediction of passenger demand for transport services. We hope that this study will help to improve new transport services of Yangon City traffic planning and public facility management.

As for further studies, the results were validated by Person Trip Survey for Comprehensive Urban Transport Plan of the Greater Yangon and route trips through road network based on their mode choice and traffic assignment will also be analyzed to measure traffic congestion on a roadway system.

REFERENCES

Castillo, Enrique del et al. 2008. *Trip matrix and path flow reconstruction and estimation based on plate scanning and link observations*, Transportation Research Part B. Vol 42, Issue 5, pp 455-481.

G. Rose, 2006. *Mobile phones as traffic probes: practices, prospects and issues,* Transport Reviews, vol. 26, no. 3, pp. 275–291.

H. Ishizuka, N. Kobayashi, S. Muramatsu and C. Ono, 2015. *Classifying the mode of transportation using cell tower alignments,* Vol. 2015-MBL-74, No. 57, Vol. 2015-UBI-45, No. 57.

Hajek. J. J. 1977. *Optimal Sample size of Road-side-interview Origin-Destination surveys* (No. RR 208).

Kyaing, D.; Lwin, K.; Sekimoto, Y. 2017. *Human Mobility Patterns for Different Regions in Myanmar Based on CDRs Data,* IPTEK J. Proc. Ser. 2017.

Kyaing, D.; Lwin, K.; Sekimoto, Y. 2017. *Estimation of Trip Generation by Using CDRs Data,* Proc. Sep. 2017, volume 11.

Lwin, K., Sekimoto, Y., & Takeuchi, W., 2018. *Development of GIS Integrated Big Data Research Toolbox (BigGIS-RTX) for Mobile CDR Data Processing in Disasters Management,* Journal of Disaster Research, 13(2), 380-386. doi:10.20965/jdr. 2018.p0380.

Lwin, K.K., Sekimoto, Y., Takeuchi, W. 2018. *Estimation of Hourly Link Population and Flow Directions from Mobile CDR,* ISPRS-International Journal of Geo-information, 7, 449. https://doi.org/10.3390/ijgi7110449

Morimura, T., Kato, S., 2012. *Statical origin-destination generation with multiple sources,* In: 21st International conference on in pattern recognition (ICPR), November 11-15, Tsukuba, Japan.

Wang, M.H, Schrock, S., Vander Broek, N. and Mulinazzi, T., 2013, *Estimating Dynamic Origin-Destination Data and Travel Demand Using Cell Phone Network Data,* International Journal of Intelligent Transportation Systems Research, Vol 11, N°2, 2013, pp. 76-86

Zin, T.; Kyaing, D.; Lwin, K.; Sekimoto, Y. 2018. *Estimation of Originating-Destination Trips in Yangon by Using Big Data Source*, J. Disaster Res. 2018, 13, 6–13.

Economic and operational analysis of public transportation in Pathein township

Emmanuel[1] and Kyaing[2]
[1]M.S candidate(Transportation Engineering), Civil Engineering Department,
Yangon Technological University, Yangon, Myanmar
immanuelfalam1995@gmail.com
[2]Associate Professor, Yangon Technological University, Yangon, Myanmar,
kyaingkyaing63@gmail.com

ABSTRACT

It is essential to have economical public transport mode due to undeniable issue for the current and future populations. Pathein include one of the most populous cities in Myanmar without the good quality services of public transportation. The problem of the study area is irregular headway cause the less reliability on transit system, poor mobility, poor performance quality in transit operation system. The travel characteristics and willingness-to-pay data were collected using questionnaires survey at the check points with road side interview in which random and purposive sampling utilized. Using the data collected from an experimental survey, analysed with logit model, benefit-cost and net benefit analysis. This study will drive to the more convenience and safety public transportation mode by specific consideration on economical factors and improvement of operation system. According to willingness to pay of people and peak passenger demand, estimate the suitable headway within 15-20 minutes operate with fourteen vehicles per day. The route distance will be 28.86 km between Pathein and Kangyidaunk. This study can assist the decision maker to supply the better public transportation mode for Pathein township and especially helpful for the operators to achieve the higher benefit by improving the service quality of public transportation.

Keywords: transit, mobility, logit model, benefit-cost analysis, willingness to pay.

1. INTRODUCTION

Transportation plays the important role in the livability of a community the factors that influence a community's quality of life. Rural residents are more reliant on personally-owned, single driver automobiles for transportation than their urban counterparts. However, it is impossible many rural residents are only relying on this mode of transportation. Personal vehicles may be expensive to purchase and maintain, and some residents cannot have drivers' licenses. Efficient and affordable transportation is the main feature in economic growth in rural areas and helps ensure that people can obtain services and participate in public life. Public transportation provides people with mobility and access to employment, community resources, medical care, and recreational opportunities in their communities. Attracting people to use the public bus has never been easy. Private vehicles have typically offered better alternatives than the public bus at the cost of environmental problems. The challenge is even greater in rural areas and small cities where factors such as diverse activity locations, abundant parking lots, and nonexistence of traffic jams have justified the use of private car as a commuting mode. In general, factors affecting ridership will be determined by the demand for services, the level of service provided, and the cost of service. Demand for services can be estimated based on population and demographic characteristics. It is expected that demand will be greater in areas with a higher population and that concentrations of transportation-disadvantaged populations will create greater demand. In Myanmar, Ayarwady region include one of the high number of registered vehicles above five lakh in the year of 2019 meanwhile increasing population. To protect the negative impact of increase vehicles, public transportation sector include in the vital portion. The public transportation system in Pathein township operates with the old vehicles and without any improvement on the performance quality. Therefore, this research will focus on the improvement of public transit system of the study area.

2. PROBLEM STATEMENT AND OBJECTIVES

2.1 Problem statement

Transit service exists in a dynamic environment, in which changes in passenger demand occur regularly. Nowadays, the transportation system in Myanmar has been well developed due to the rapid urbanization and growing economic prosperity. People can travel smoothly not only local but also international. Different modes of transport in Myanmar are air transport, rail transport, road transport and water transport. Currently, road transportation is the main transportation system such as car, bus, taxi, bike and railway are the main transport alternatives in Pathein township in which private bicycle and bike is common mode for almost every household. This kinds of mix transport system cause congestion on the road especially the area where without separate bicycle or bike lanes. The public transportation system in Pathein township, operates with the old age vehicles without any improvement on the performance quality. The impact of using old age vehicles affect on travel speed, safety, convenience, more fuel consumption, body stiffness.

Among the various problem, this study will focus to improve the existing public transportation on the following factors:

1. Unfrequently headway
2. Less regular public transit users
3. Long waiting time during off peak period
4. Overtaking problem during the busiest time

2.2 Objectives

The general objective of this study contain to improve the transit operation system by determined regular headway based on peak passengers demand meanwhile reduce the long waiting time during the off peak period, to investigate the convenience and comfortable transit mode for the connection of urban and rural area by making economic analysis.

The specific objectives to fulfill the purpose of the study are as follow:

1. To calculate the proper headway for improving transit performance depends on passenger demand and define the bus fare.
2. To displace the new vehicle to the existing modes
3. To estimate net present value (NPV), for the propose transit mode.
4. To estimate internal rate of return (IRR)
5. To estimate cost-benefit ratio (B/C)

3. STAGES OF THE STUDY

In order to achieve the aim and objectives of this research the work is divided according to the following chart can be seen in Figure.

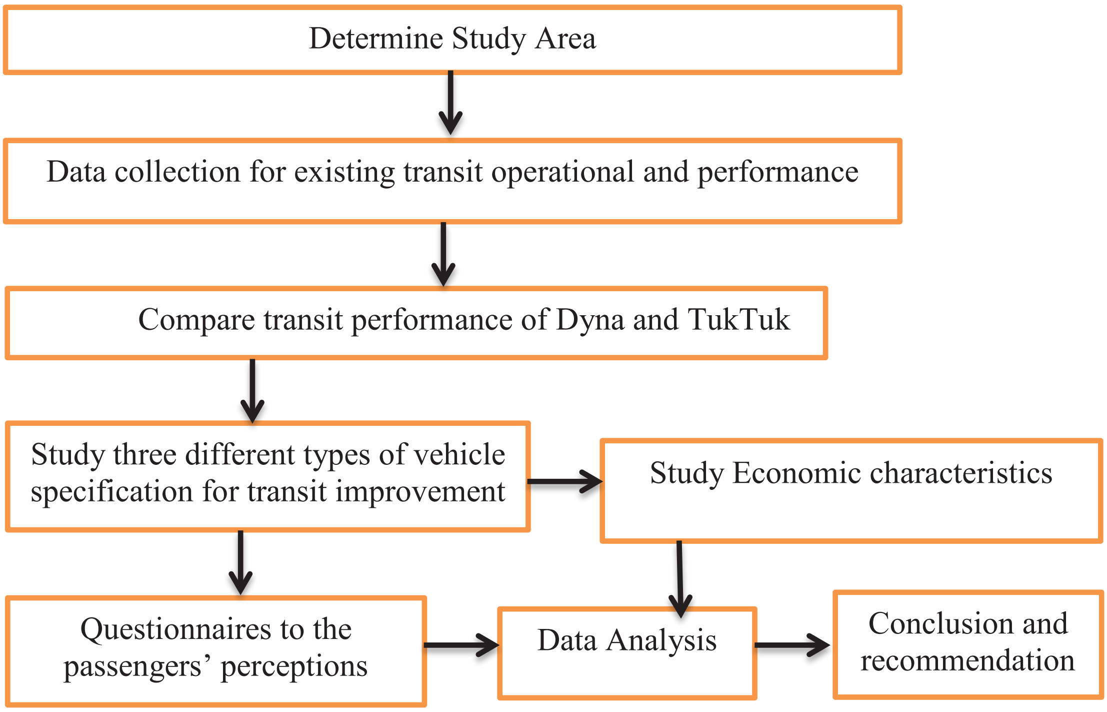

Figure: Methodology Flow Chart

3.1 Implementation of the study method

Firstly, determined the study area then made the literature review on transit system and its operational, economical characteristics. The literature review seek for case studies applied in cities of developing countries especially in the cities that have similar conditions. The second phase related to collect the operational data and the socioeconomic characteristics on the existing transit modes users around the study scope includes the passengers, drivers, operators point of views. Chosed the most suitable mode for the study area. The third phase involves analysed the collected data by logit model to describe the most association variables which concern with the behavior of the transit users. Compare the performance of existing transit system. In the fourth phase contain the detailed study for the propose vehicle specification and analysed according to the operation system. Using the fundamental transportation calculations and other economical calculation method. Finally, summarized the main findings and conclusion from the study.

3.1.1 Effective Parameters in calculation sample size and benefit-cost analysis

The questionnaire design was developed to collect the data from the following portions;

1. Socioeconomic characteristic of the transit users
2. The existing transit operational performances

$$n = N/(1 + N\,e^{\wedge}2) \qquad (1)$$

Where; N is the total population
n is the number of sample size
e is the standard confidence level 95%

Net Present Value (NPV)

Net present value is present value of all future cost and benefits. In this method the stream of costs / benefits associated with the project over an extended period of time is calculated and is discounted at a selected discount rate to give the present value. Benefit are treated as positive and cost as negative and the summation gives the net present value (NPV). Any project with positive NPV is treated as acceptable.

$$\text{NPV} = \sum_t \frac{B(t)-C(t)}{(1+i)^\wedge t} \quad (2)$$

Cost benefit Ratio (CBR)

Cost benefit ratio is the ratio of total present benefit and the total present cost.

$$\text{CBR} = P_B/P_C \quad (3)$$

Discount rate

Discount rate represents the time value of money. Selecting a discount rate is key assumption for benefit – cost analysis. Higher the rate the tougher it is for a project to be economically justified since costs typically are incurred in early years (and less heavily discounted while benefits occur over longer timeframe). In discount rate the following risk factors include:

(i) the risk free interest rate

(ii) tare of inflation. It is measured by either by consumer price index or GDP deflator

(iii) market risk, industry risk, firm specific risk, project risk, social risk, political risk, exchange rate risk.

Internal Rate of Return

To calculate IRR, which allows the discount rate to be varied until it results in a net present value of 0, such that NPV =0

3.1.2 Effective Parameters in calculation of operational system

Headway is a measurement of the distance or time between vehicles in a transit system. The minimum headway is the shortest such distance or time achievable by a system without a reduction in the speed of vehicles. Headway is a key input in calculating the overall route capacity of any transit system.

$$\text{Headway} = \frac{Seating\ capacity * load\ factor * 60}{peak\ hour\ demand} \quad (4)$$

Cycle time is the number of minutes needed to make a round trip on the route, including layover/recovery time. Cycle time is important for several reasons, including playing a part in the formula used for determining the number of vehicles needed to provide a given level of service on a route.

$$\text{Cycle Time} = 2 * \text{Length} * 60 / \text{Speed} \quad (5)$$

4. CASE STUDY

According to collected field data, there were more than fifteen bus stops along the study route but only the busiest bus stops were used to collect data. Two types of vehicles run on the study route which are Tuk Tuk and Dyna. Total length of this transit line is about 28 km from the origin to destination. Female respondents' interesting is about thirty percent more than male because female mostly rely on public transit according to different types of trip purpose. Generally, the ages between eighteen and thirty years, under eighteen years, above sixty years are the daily users of public transportation for education trips, work trips, social trips etc. In the weekend, about fourty percent of destination is at the city center of Pathein to go shopping trips. From about 400 questionnaire data, 92% of respondents agree to change the transit mode to get the more safety, high speed, low operating costs.

Variables

Occupation	X1
Trip origin from KGD	X2
Trip origin from KK	X3
Waiting time at bus stops	X4
Travel Frequency	X5
Willingness of waiting time reduce	X6

Let L= mode change system with Hijet, Bi (i=0, 1, 2, 3, 4, 5,6) are coefficients of the Binary Logistic Regression model to be estimated from the data. Then according to standard theory of logistic regression, the value of Logit is given by:

$$L = \ln(\text{odds}) = \ln(p/1-p) = B0 + B1X1 + B2X2 + B3X3 + B4X4 + B5X5 + B6X6 \quad (6)$$

Table 1. Variables in the logit equation.

	B	S.E.	Wald	df	Sig.	Exp(B)
X1	-1.699	0.428	15.751	1	0.000	0.183
X2	-1.5	0.497	9.095	1	0.003	0.223
X3	-1.833	0.452	16.489	1	0.000	0.160
X4	-0.962	0.497	3.744	1	0.053	0.382
X5	0.97	0.367	6.996	1	0.008	2.638
X6	-1.644	0.584	7.914	1	0.005	0.193
Constant	2.224	1.044	4.537	1	0.033	9.248

The equation of the logistic regression line is given by:

$$L = 2.224 – 1.699\ X1 - 1.5\ X2 - 1.833\ X3 - 0.962\ X4 - 0.97\ X5 –1.644\ X6 \quad (7)$$

The main findings of this mode change (Hijet) analysis are; strongly association of transit mode change for students' occupation and passengers from Kankone and Kangyidaunk residents, significant association on the travel frequency and waiting time at bus stops of the current transit system and people who willingness to reduce waiting time at bus stop.

5. DETAIL CACULATION OF NPV AND BENEFIT-COST RATIO

According to the described equations, net present value, cost-benefit ratio, internal rate of return will calculate for the transit improvement of the study. The cost will be considered with Myanmar kyats.
Description of project characteristic and cost for one vehicle per year;
Assumptions;
Discount rate = 17%
Fixed cost per vehicle include: purchase cost = 9,500,000 MMK
License registration fees = 200,000 MMK
Annual variable costs for one vehicle;
Commercial license = 96,000 MMK /year
Maintenance cost = 360,000 MMK /year
Engine oil cost = 379,218 MMK /year
Fuel consumption rate per year = 3717 liters
= 870 MMK/ liter
= 3,233,790 MMK
Driver wages = 200000 MMK/month = 2,400,000 MMK /year
Gate fees = 1000 MMK/day = 36,500 MMK/year
Milliage depreciation cost (life time for pickup truck 5 years) = 1,900,000MMK
Insurance rate = 1.7% *purchase = 161,500MMK
Assume revenue only from bus fare ;
Hijet car capacity = 11 persons
Bus fare = 300 kyats/trip
Number of round trips = 6 trip/day
Number of operating vehicles =14veh/day
Capacity factor = 0.8
Total revenue =11 x 14 x 300 x 6 x 0.8 x 365 = 80,942,400 MMK/year
Concept of fuel,
17 km = 1 litre
Travel distances = 173.16 km/day
= 63203 km/year
Concept of engine oil cost calculations,
Assume, the engine oil must be refill after every five thousand kilometer used.
5000 km = 30,000 kyats
So, 1 km = 6 MMK,
For 63203km, engine oil cost =379,218 kyats/year
Assume: capital cost include all fixed cost.
Annual variable cost include:
(1) Commercial license,
(2) Maintenance cost,
(3) Engine oil cost,
(4) Fuel cost,
(5) Driver wages,
(6) Gate fees,
(7) Milliage depreciation cost,
(8) Insurance rate.
The ridership for origin to destination is 1.5 times the capacity depends on the following reasons: (1) many villages along the study route, (2) boarding and alighting at the villages.

Table 2. The investment cost and benefit estimation

Year	Investment or Cost (C)	Profit or Benefit (B)	Net Benefit (B-C)	PV factor 1/(1+i)^t	PV
0	MMK 164,900,000	MMK -	MMK (164,900,000)	1.0000	MMK (164,900,000)
1	MMK 124,537,140	MMK 165,564,000	MMK 41,026,860	0.8547	MMK 35,065,692
2	MMK 124,537,140	MMK 165,564,000	MMK 41,026,860	0.7305	MMK 29,970,677
3	MMK 124,537,140	MMK 165,564,000	MMK 41,026,860	0.6244	MMK 25,615,963
4	MMK 124,537,140	MMK 165,564,000	MMK 41,026,860	0.5337	MMK 21,893,986
5	MMK 124,537,140	MMK 165,564,000	MMK 41,026,860	0.4561	MMK 18,712,808
6	MMK 124,537,140	MMK 165,564,000	MMK 41,026,860	0.3898	MMK 15,993,853
7	MMK 124,537,140	MMK 165,564,000	MMK 41,026,860	0.3332	MMK 13,669,960
8	MMK 124,537,140	MMK 165,564,000	MMK 41,026,860	0.2848	MMK 11,683,727
TOTAL	MMK 1,161,197,120	MMK 1,324,512,000	MMK 163,314,880		MMK 7,706,667

NPV = 7,706,667 MMK
B/C = 1.14
IRR = 18.5%

Table 3. Internal rate of return estimation

Discount rate	NPV
20%	(28,325,219.68) MMK
17%	7,706,667 MMK
IRR	18.50%

6 DISCUSSION AND CONCLUSION

6.1 Discussion

According to the economic analysis, the result net present value is positive with discount rate 17%. It means the project is acceptable. The benefit-cost ratio is greater than 1 with 17% discount rate. So that this investment for mode change with Hijet should accept to get healthy and good public transportation system in Pathein township especially around the study area.

6.2 Conclusion

Based on the survey result, females are more interesting on questions. The most users' occupation is student because the study route location pass through more than five basic schools and universities in Pathein township. The data shows the trip purpose of other transit users include, recreational trip, work trip, shopping trip, social visit, education trip etc. Among these, education trip is the most significant trip depends on the data collection.

In the collected data the most of respondent do not need to wait the long period during peak hour but the long waiting time during off peak hours. From this research, estimated the proper headway for peak period and off peak period to solve long waiting time. The willingness to pay for the mode change to Hijet vehicle was 300 kyats that is the most significant value the passenger want to pay per trip.

The result of this data the peak passenger volume is 122 per hour so that fourteen vehicles need to operate daily with 15-20 min headway during peak and off period. The travel speed range is between 30 – 50 km/hr considered for both urban road and rural area road.

Moreover, according to the people travel characteristics, socioeconomic factors, their perception on the existing transit system, most of people would like to mode change with reduce not only bus fare but also waiting time at bus stops. So that to solve the current problem, the vehicle should be good fuel efficiency, high speed, drive safely and faster than the existing mode. In order to fulfill this option the Hijet vehicle is proposed from this research.

REFERENCES

D.Bharathan, L Chaney, R.B. Farrington, J. Lust bader, M.Keyser, and J. Rugh. *An overview of vehicle test and analysis from NREL'S AIC fuel use reduction research*.

Elana S. Prassas, Roger P.Roess. *Engineering economics and finance for transportation infrastructure.* Springer tracts on transportation and traffic STTT.

John Wiley and Sons, Inc., Hobokon, New Jersey. *Urban transit systems and technology*. Published simultancously in Canada.

Jeremy Mattson. *Estimating Ridership of Rural Demand-Response Transit Services for the General Public.* National Center for Transit Research

Rakesh Bewal. *People's perception of public transport services in Oman.* https://www.researchgate.net/ publication/260190662

Steve Abley, Paul Durdin and Malcolm Douglass (2010). *Integrated Transport Assessment Guidelines*, Report 422, Land Transport New Zealand (www.nzta.govt.nz); at www.nzta.govt.nz/resources/research/reports/422.

Todd Litman. *Transportation cost and benefit analysis: techniques, estimates and implications.* https://www.researchgate.net/ publication/ 235360398

Utpal Dutta. *A Framework to Identify Economic and Community Benefits of the Proposed BRT System in Southeast Michigan.* Copyright © 2017 by author and Scientific Research Publishing Inc. Published: June 12, 2017.

American Association of State Highway and Transportation Officials (2010). *A Manual of User Benefit Analysis for Highways,* 3rd Edition. https://bookstore.transportation.org/collection_detail.aspx?ID=65.

Basic Speed/Fleet Size Relationships. H:\Projects\Transit course\Fleet relationships.doc 11/14/2006

ANALYSIS ON THE EFFECT OF LAND USE AND SOCIOECONOMIC CHARACTERISTICS ON TRAVEL BEHAVIOR

T. AUNG[1], KYAING[2], K.K. LWIN[3], and Y. SEKIMOTO[4]

[1] Ph.D. Candidate, Department of Civil Engineering, Yangon Technological University, Yangon, Myanmar,
[2] Associate Professor, Department of Civil Engineering, Yangon Technological University, Yangon, Myanmar,
[3] Project Assistant Professor, IIS, The University of Tokyo, Tokyo, Japan,
[4] Associate Professor, IIS, The University of Tokyo, Tokyo, Japan,

Keywords*: land use, socioeconomic, modal split, commuting distance, multiple linear regression.*

1. INTRODUCTION

Yangon, the former capital of Myanmar and the capital city of Yangon region is located in lower Myanmar at the convergence of the Yangon and Bago Rivers about 30 km(19 mi) away from the Gulf of Martaban. It has the population of over five million in urban areas and the City has an area of about 600 square kilometers. Therefore, the population density of Yangon City in urban area is about 8600/km^2. As many people from the rural areas and other regions come to Yangon City for their better life and opportunities, the population and the city area have grown significantly since 1948. Due to these rapid growths in population and urban structure, debates around urban form sustainability have grown and focus on the shape and size of cities, their relationships with daily travel patterns and solutions to the challenges of urban sprawl and decentralization. This study aims to investigate the effect of land use and socioeconomic effect on the travel behaviors of Yangon city. To evaluate the effect of land use and socioeconomic factors on travel behaviors, socioeconomic attributes, land use attributes and trip attributes provided from JICA (Japan International Cooperation Agency) Survey (2014) were used. By using multiple regression model based on these data, it can be examined how journey to work travel behavior is affected by land use and socioeconomic factors.

2. METHODS OF ANALYSIS

Modal split (public transportation and private car usage) were used as transport performance indicators to investigate the interaction between travel behavior and land use for journey to work. Journey to work is chosen because it is strongly influenced by mode choice and it is easier to undertake due to its regularity and adjustment. Two dependent variables were analyzed by using multiple linear regression in SPSS software according to independent variables, including socioeconomic index for areas (SEIFA), income, occupation, population density, distance from CBD and car ownership. The socioeconomic data, land use data and transport data were collected from JICA survey which took place in 2014. In Yangon City, the main modes of transport are private cars and buses.

3. RESULTS AND DISCUSSIONS

According to this study, it was found that the main mode used for intra trips in all areas except New Suburb region is the walking mode and in New Suburb region, other modes such as motorcycle and bicycles are the main modes. People mostly use buses for inter-zonal trips and the second most mode is private car and taxi in CBD areas, inner city and outer city areas.

The factors affecting the usage of private car and public transportation are analyzed by using multiple regression model and the influenced factors for both modes are shown in Table.1.

Table.1. Regression Analysis for Public Transportation and Private Car Usage

Public Transportation		Private Car	
Variables	Coefficient	Variables	Coefficient
Constant	-2.450	Constant	1.683
Bluecollar	0.337	CBD Distance	-0.094
Whitecollar	0.821	Pop Density	-0.051
Low HH Income	0.333	Low HH Inome	-0.112
2 Cars+	-0.970	2 Cars+	0.713
Adjusted R^2	0.957	Adjusted R^2	0.852

Based on these results, it can be found that low income households mostly use public transportation rather than the private car and taxi while the households which own more than two private car prefer to use private car as it has positive relationship with private car. The blue collar staff and white collar staff prefer to use public transportation as it can reduce the cost of the travel.

3. CONCLUSIONS

From this analysis, it can be found the factors which influenced the travel behaviors and by promoting the public transport facilities and network, it will be a remedial measure to reduce the traffic congestion on roads.

REFERENCES

[1] Wegener, M., and Fuerst, F. (2004): Land-Use Transport Interaction: State of the Art. SSRN Electronic Journal.10.2139/ssrn.1434678.

[2] Alqhatani, M., Bajwa. S., and Setunge, S., (2012). “Land Use Transport Interaction: A Comparison of Melbourne and Riyadh.” The 8th International Conference on Traffic and Transportation Studies, Changsha, China, procedia - social and behavioral sciences 43, pp, 3-13.

Optimization Model to Estimate Cognitive Distances for Cognitive Maps from Travel Data

Hiroyuki HASADA[1] and Yudai HONMA[2]
[1] Graduate Student, Graduate School of Engineering, the University of Tokyo, Japan
hasada-hiroyuki649@g.ecc.u-tokyo.ac.jp
[2] Associate Professor, ICUS, IIS, the University of Tokyo, Japan

ABSTRACT

Maps are critical elements for us to recognize a travel distance between two arbitrary points. In fact, we utilize a variety of maps, such as map-apps or route-maps, to travel as efficiently as possible. On the other hand, such "best" route, which we believe it is the shortest, frequently contains some errors because of the accuracy of maps or the limitation of our recognition. From this point of view, many earlier studies discussed cognitive distances on mental maps, but it is difficult to measure them quantitatively from large amount of data. In this study, we propose a new optimization model to estimate cognitive distances from travel data. The travel data contains route information, and it can be regarded as a result of their best selection in mind. Conversely, it must be possible to estimate cognitive distances that their choice becomes the best as a result. Based on this idea, we fix a network topology and prepare variables for each link to express cognitive distances. The objective function of our model is to minimize the difference between the graph-distance of the selected route and that of the shortest path. For numerical examples, we solved the problem on small networks and verified the accuracy of estimation by fluctuating the correct distance. This study has great potential; we can reflect our activities to market areas and urban planning with obtained cognitive distances in an area, or we can illustrate cartograms based on them. Solving our problem in large networks and real travel data, including probe data, is essential future work.

Keywords: *cognitive distance, travel data, optimization, cartogram*

1. INTRODUCTION

When we go to a destination, we don't always go along the shortest route a map indicates. For example, we often take a detour to avoid stairs and steep slopes. We sometimes take a familiar route, not unfamiliar one off the beaten path. These behavior shows that the image of a city we have is distorted from an ordinary map. The goal of our study is to obtain and visualize this distorted image.

One of methods to show distortions of cities, many what we call time-space maps, such as maps by Sugiura (2014), were made. Most of the time-space maps were made by drawing isolines in or distorting original maps in terms of only travel time from a point (Shimizu, 1992). It is comparatively easy to make these time-space maps, but travel time between any points are ignored in these maps. On the other hand, some studies, such as by Kilchenmann (1972), located points on a two-dimensional plane in terms of travel time between any points, by using Multi-Dimensional Scaling (MDS). Since the distances shown in these studies focus on travel time, objective data, the distances are contrast to subjective distances in our image of cities.

In addition, many studies, such as by Lynch (1960), obtained distances between points and image of space we recognize. According to Montello (1991), methods to measure cognitive distances are broadly divided into five classes: psychophysical ratio scaling, psychophysical interval and ordinal scaling, mapping, reproduction and route choice. Studies have used an appropriate class of methods to purpose of the studies and data. Psychophysical ratio scaling and psychophysical interval and ordinal scaling are methods to measure the distances participants themselves express cognitive distances at the ratio, interval or ordinal level. For example, Katayama et al (2001) used psychophysical ratio scaling in order to identify some factors of physical environment that influence pedestrian's cognitive distances. Mapping is a method to regard distances between points on the maps, what we call mental maps, that participants draw as cognitive distances. Xu et al (2001) measured cognitive distances in a simulated circulated space with this method after participants walk in the space. Reproduction is a method to measure the distances that participants reproduce target distances on a straight line. Yanase et al (2006) measured cognitive distances generated by ascending and descending stairs with this method. The above four classes of methods have a problem that it is difficult to obtain data from many participants, because these methods put a great strain on them. Route choice is a method to measure an ordinal scale of cognitive distances on the basis of route choice data. This method has the assumption that humans usually choose to travel along the shortest routes which they believe require the least effort. This method needs route choice data of subjects and puts a little strain on them. This is the reason why it is comparatively easy to measure cognitive distances many subjects have. However, Gärling (1988) pointed the problem that humans should choose routes which require the least effort in terms of not only cognitive distances but also other factors like costs.

The purpose of this study is to propose an optimization model to estimate cognitive distances from route choice data, travel data, and visualize cognitive maps as distance cartograms. We define cognitive distances as subjective distances derived from data of our actual movement. The cognitive distances we define express accessibility in cities determined by various factors such as psychological cognitive distances and cost. Although the cognitive distances we define have the problems from the point of view of psychology, the cognitive distances and the cognitive maps from them can show our image of cites distorted from ordinary maps.

Few studies are available that show methods to compute cognitive distances from big travel data. In this study, we verify accuracy of the model we propose by using large amount of hypothetical travel data. This study contributes to computation of cognitive distances from large amount of actual travel data. Since it become much easier to obtain big travel data than before due to recent development of information and communication technology, this model is useful for expression of image of cities many people have. This image not only shows aspects and characteristics of cities but also enables us to design cites adapted to our movement and sense. For example, location of public facilities and stores can be made more appropriate on the basis of this image. In addition, since this model can be applied to any scale of space, this model is useful for expression of image of interior space of buildings. The image of interior space has not been so available and can be utilized for better building layouts.

2. OPTIMIZATION MODEL

The optimization model we propose has the following three assumptions. The first assumption is that travelers move on a network composed of nodes and links. This means that this model can be applied to not only cities but also buildings, for example, by regarding rooms as nodes. The second assumption is that all travelers go along the path which they believe is shortest in terms of cognitive distances. This means that travelers sometimes make a detour in terms of actual distances. The third assumption is that cognitive distances does not depend on travelers. In other words, all travelers recognize the same set of cognitive distances corresponding to the links. Although in fact cognitive distances vary a little between travelers, they have a common tendency as Lynch (1960) described. Lynch emphasized the importance to see "public image" of cities. The tendency of the cognitive distances is certainly the "public image" distorted from maps.

The optimization model is formulated with two design goals. The first goal is to make the path where a traveler moves in fact on each travel shortest in terms of cognitive distances, based on the second assumption. This goal is incorporated by minimizing difference in terms of cognitive distances between the length of the path where each traveler moves and the length of the shortest path from origin to destination. The second goal is to make a cognitive distance of a link closer to an actual length. This goal comes from the property of cognitive distances estimated from travel data. Since travel data determines only an ordinal scale of cognitive distances, it is necessary to determine a numeric scale in order to visualize a cognitive map. In this model, the value which changes smallest from an actual distance is calculated as the cognitive distance of each link, because cognitive map on the basis of this shows the least extent of distortion of "public image" distorted from maps. Formulation of the model is as follows and notation defined for this model follows.

$$\text{Minimize} \quad M\sum_{p\in P} w^p\left(\sum_{(i,j)\in\Pi} x_{ij}^p l_{ij} r_{ij} - u_{o(p)\delta(p)}\right) + \sum_{(i,j)\in\Pi}\left(r_{ij}-1\right)^2 \tag{1}$$

$$\text{subject to} \quad u_{hi} - u_{hj} \le l_{ij} r_{ij} \qquad \forall h \in O, (i,j) \in \Pi \tag{2}$$

$$u_{hi} \ge 0 \qquad \forall h \in O, i \in N \tag{3}$$

$$u_{hh} = 0 \qquad \forall h \in O \tag{4}$$

$$r_{ij} > 0 \qquad \forall (i,j) \in \Pi \tag{5}$$

Indices

p index of travels
h index of origin nodes on travels
i, j indices of nodes

Sets

P set of travels
Π set of links
N set of nodes
O set of origin nodes on travels

Variables

r_{ij} a ratio of a cognitive distance between nodes i and j to an actual length l_{ij}

u_{hi} potential (= path length) of node i,which origin is a node h

Parameters

M a big penalty to prioritize determination of an ordinal scale of cognitive distances

w^p weight of travel p

x_{ij}^p 1 if a traveler on travel p pass a link between nodes i and j, 0 otherwise

l_{ij} an actual length of a link between nodes i and j

$o(p)$ an origin node on travel p

$\delta(p)$ a destination node on travel p

The first term of objective function (1) minimizes the difference in terms of cognitive distances on each travel between the path length where each traveler moves and the shortest path length. The path length where each traveler moves is obtained to calculate the sum of only the link length which the traveler pass in fact. $x_{ij}^p l_{ij} r_{ij}$ is the length of the link between nodes i and j in terms of cognitive distances if the link is passed, and 0 otherwise. The shortest path length is obtained in a variable $u_{o(p)\delta(p)}$ by using the dual of the shortest path problem. Formulation of the dual is shown below and is the LP to maximize potential u_{hk} of destination node k,which origin is an origin node h, in the network. The difference between potential of node i and node j is always no more than the path length l_{ij} between the nodes, where constraints (7) hold. Therefore, maximizing u_{hk} is equivalent to finding the greatest lower bound for the length of the shortest path from origin to destination. In the first term of objective function (1), the shortest path lengths are obtained by minimizing $-u_{o(p)\delta(p)}$. Constraints (2)−(4) correspond to constraints (7)–(9). M is a penalty large and used in objective function (1) to prioritize minimizing the differences between the path lengths where travelers move and the shortest path lengths. This is because determination of an ordinal scale of cognitive distances from travel data is prior to determination of a numeric scale.

$$\text{Minimize} \quad u_{hk} \tag{6}$$

$$\text{subject to} \quad u_{hi} - u_{hj} \leq l_{ij} \quad \forall (i,j) \in \Pi \tag{7}$$

$$u_{hi} \geq 0 \quad \forall i \in N \tag{8}$$

$$u_{hh} = 0 \tag{9}$$

The second term of objective function (1) minimizes the square of the difference on each link between 1 and a ratio of a cognitive distance to an actual length. The reason why the ratio is used is to evaluate distortions of long links and short links equally.

3. VERIFICATION METHODS

3.1 Materials

To verify accuracy of the model we propose, we prepared an idealized network of a city. The network consists of 25 nodes and 43 links (Figure 1). The nodes are given position coordinates and actual lengths of the links are given Euclidian distances of end nodes.

We generated hypothetical travel data in the following three steps. Step 1: we changed the actual length of each link at random. These changed lengths are equivalent to public image of the network. Each of the changed lengths are obtained by multiplying a random number which follows a gamma distribution. An average of the distribution is 1 and a

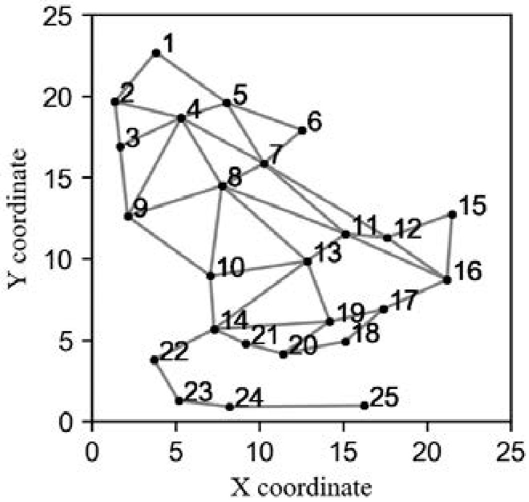

Figure 1: Idealized network composed of 25 nodes

variance is 0.5. Step 2: we generated pairs of origin and destination nodes at random. The number of the O-D pairs is parametric in order to verify whether the model can be applied to large amount of travel data. We set the values of the number of the pairs to 10, 100 and 1000, and repetitions of the pairs are allowed. Step 3: we obtained the shortest path, travel data, in the network composed of the changed lengths for each of the O-D pairs generated by using Dijkstra method. In this study, weights of all travels are 1.

3.2 Verification from three points of view

We verify accuracy of the model from three points of view: lengths of the links, travel data and cartograms. In terms of lengths of the links, we estimate lengths of the links, which are equivalent to cognitive distances, from the hypothetical travel data by using the optimization model and compare the estimated lengths and the changed lengths, which were used to generate the hypothetical travel data. In terms of travel data, we generate travel data in the network which links have the estimated lengths. We obtain the shortest path for each of the O-D pairs which were used to generate the hypothetical travel data by using Dijkstra method. We compare the travel data generated in the changed and estimated networks. In terms of cartograms, we visualize the changed and estimated network as cognitive maps. We use metric MDS to locate nodes on a two-dimensional plane. Metric MDS is optimization problem designed to approximate given dissimilarities t_{ij}, the shortest path lengths between any nodes in this study, to direct distances $\widehat{d_{ij}}$ between any located nodes on a two-dimensional plane and minimize called stress σ defined as shown in (10) (Leeuw, 2009). We solve this problem by using SMACOF (Scaling by MAjorizing a COmplicated Function). We compare obtained cartograms visualizing the changed and estimated networks.

$$\sigma = \sum_{i<j\in N} \left(t_{ij} - \widehat{d_{ij}}\right)^2 \tag{10}$$

Figure 2 shows the flowchart of verification methods explained above. We verify accuracy of the model by generating O-D pairs at random 10 times where the number of O-D pairs is each value.

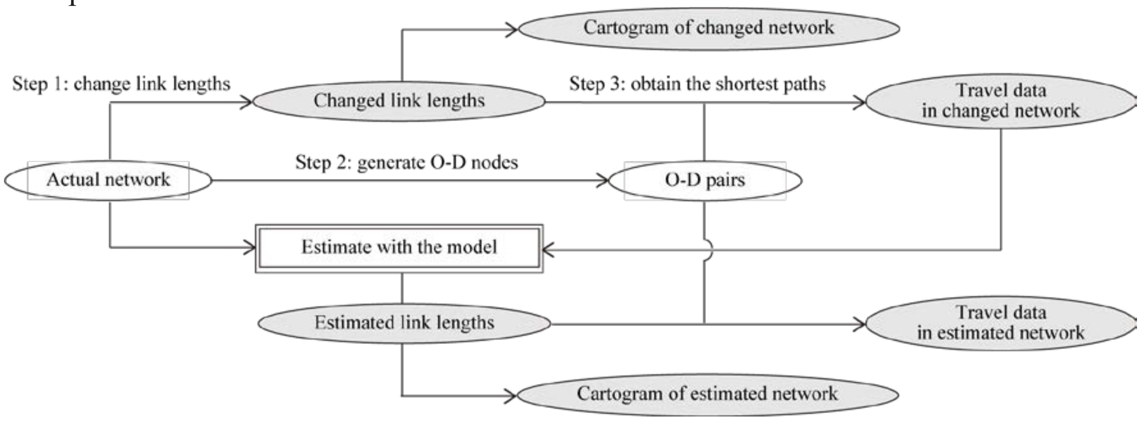

Figure 2: Flowchart of verification methods

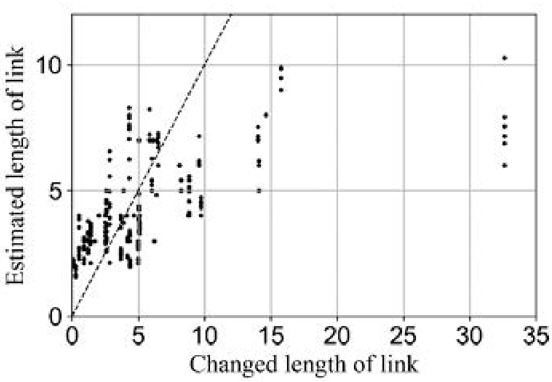

Figure 3: Changed and estimated lengths of links (10 O-D pairs)

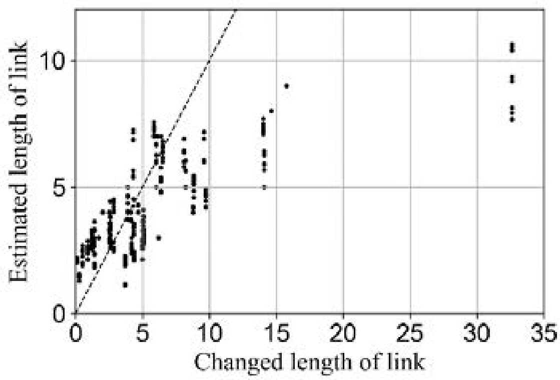

Figure 4: Changed and estimated lengths of links (100 O-D pairs)

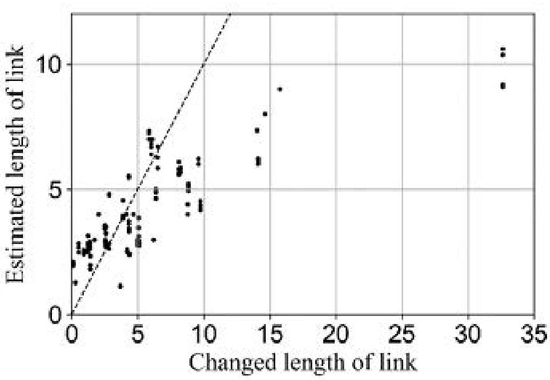

Figure 5: Changed and estimated lengths of links (1000 O-D pairs)

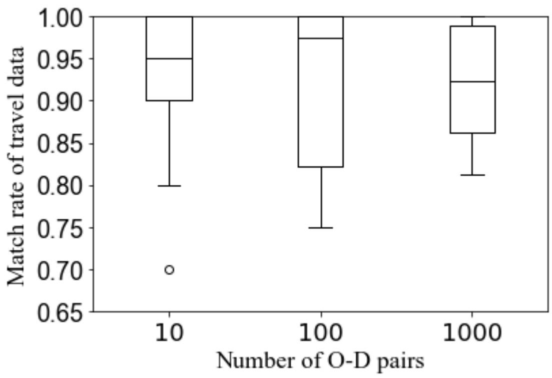

Figure 6: Match rate of travel data where 10, 100 and 1000 O-D pairs

4. RESULTS

Figure 3, 4 and 5 show comparison of lengths of the links. Figure 3, 4 and 5 are scatter plots of the changed and estimated lengths of the links in the 10 times estimations where the number of the generated O-D pairs is 10, 100 and 1000. In these figures, dashed lines show that changed length equal to estimated length and points near the dashed lines mean that lengths are estimated well. We obtained the result that the model we proposed estimates cognitive distances relatively well. In addition, as the amount of travel data is large, the accuracy of the estimation improves a little.

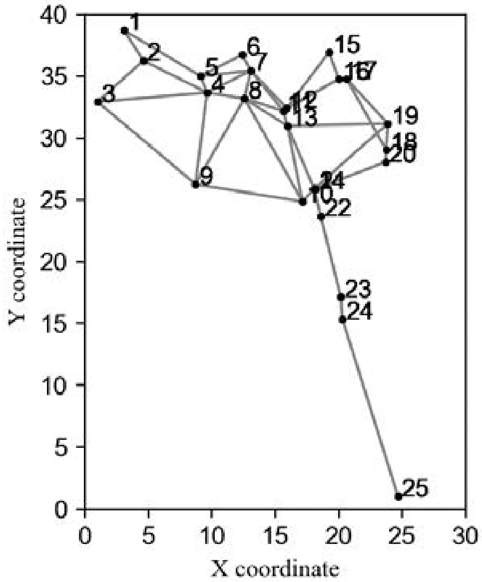

Figure 7: Cartogram visualizing changed network

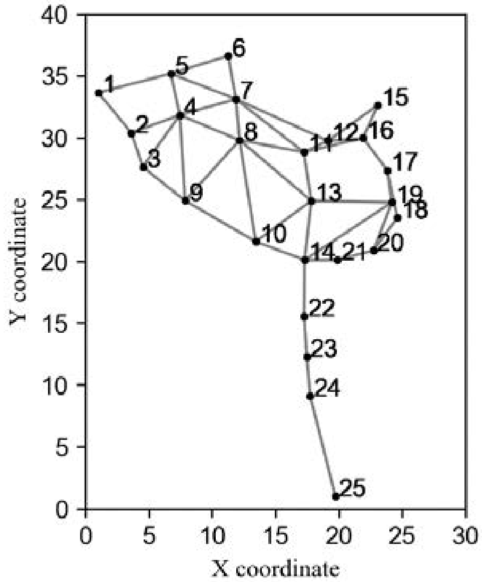

Figure 8: Cartogram visualizing estimated network (10 O-D pairs)

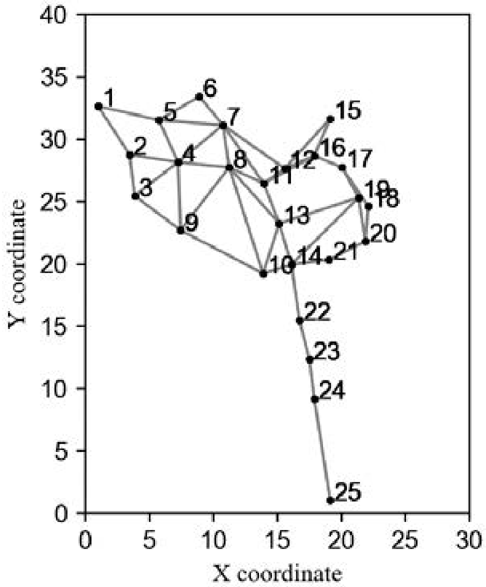

Figure 9: Cartogram visualizing estimated network (100 O-D pairs)

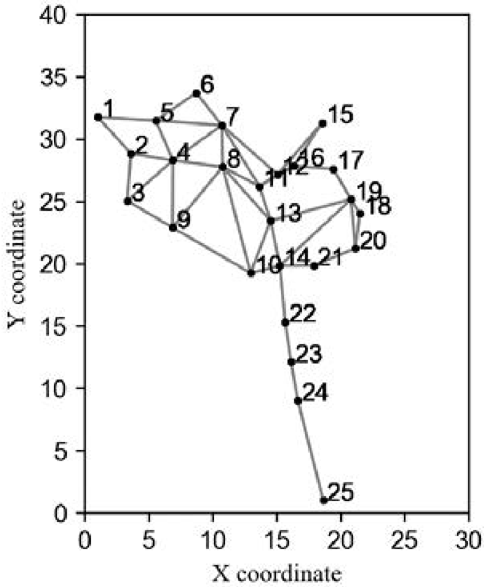

Figure 10: Cartogram visualizing estimated network (1000 O-D pairs)

Figure 6 show comparison of travel data. This figure is a box plot of match rate of travel data where the number of the generated O-D pairs is 10, 100 and 1000. In this study, match rate of travel data is defined as a ratio of the number of the O-D pairs where the shortest paths are the same in the changed and estimated networks to the total number of O-D pairs. We obtained the result that travel data reproduced is relatively correct. In terms of not matched travels, the shortest paths are just a little different but have the almost same distances.

Figure 7 to Figure 10 show cartograms. Figure 7 is a cartogram visualizing the changed network. Figure 8, 9 and 10 are cartograms visualizing the estimated networks where the number of the generated O-D pairs is 10, 100 and 1000. We obtained the result that cartograms visualizing the estimated networks, estimated cognitive map, become closer to a cartogram visualizing the changed network, correct cognitive map, where the amount of travel data is large. In these cartograms, node 23, 24 and 25 are far from the others because travels from these nodes to the others always have much longer path lengths than direct distances.

5. CONCLUSIONS

This study proposed the optimization model to estimate cognitive distances from travel path data. This model is designed to make the path where a traveler moves shortest on each travel in terms of cognitive distances and then make cognitive distances closer to actual lengths of the links. In addition, we demonstrated the usefulness of this optimization model. We verified the accuracy of this model from three points of view: lengths of the links, travel data and cartograms. Although we used an idealized network and hypothetical travel data, this verification is enough to show that this model enables us to estimate cognitive distances and cognitive maps visualizing our distorted image of cites from only travel data. When further studies estimate cognitive maps with this model from real big travel data captured with positioning system such as GPS, real characteristics of cites are visualized and the usefulness of this model will be shown more. In addition, this model has the possibility to express image of interior space of buildings and contribute to realization of cites and buildings adapted to our movement and sense.

REFERENCES

Cadwallader, M., 1975. A Behavioral Model of Consumer Spatial Decision Making. *Economic Geography* 51, 339-349.

Katayama, M., and Ohno, R., 2001. A Study of Pedesrian's Cognitive Distance of a commuting Route. *The Architectural Institute of Japan's Journal of Architecture and Planning* 66(549), 193-198.

Leeuw, D. L. and Mair, P., 2009. Multidimensional Scaling Using Majorization: SMACOF in R. *Journal of Statistical Software*, 31(3), 1-30.

Lynch, K., 1960. *The image of the city*. MIT press, Massachusetts.

Gärling, T., and Gärling, E., 1988. Distance minimization in downtown pedestrian shopping. *Environment and Planning A*, 20(4), 547-554.

Montello, R. D., 1991. The measurement of cognitive distance: Methods and construct validity. *Journal of Environmental Psychology* 11(2), 101-122.

Okamoto, K., 1982. A Review of Cognitive Distance Studies. *Japanese Journal of Human Geography* 37(5), 429-448.

Shimizu, E., 1992. Time-space Mapping and Its Application in Regional Analysis. *Infrastructure Planning Review* 10, 15-29.

Sugiura, K., 2014. *Folds of Time, Wrinkles of Space… Attempts to Make [Time-Space Maps] (in Japanese)*. Kajima Institute Publishing, Tokyo.

Xu, H., Matsushita, S., and Nishide, K., 2001. Characteristics of Cognitive Maps: Simulation study on pedestrian path choice and spatial cognition (Part II). *The Architectural Institute of Japan's Journal of Architecture and Planning* 66(545), 173-179.

Yanase, R., and Sakita, M., 2006. A Study on Cognitive Distance Generated by Ascending and Descending Stairs: Fundamental study for the spatial planning of large-scale architecture based on a distance Part2. *The Architectural Institute of Japan's Journal of Architecture and Planning* 71(601), 33-38.

Mathematical Relationship between Minimization of Travel-time and Detouring Behavior on Grid Networks: A Case Study of Yangon Downtown

Yudai HONMA[1] and Kimiro MEGURO[2]
[1] Associate Professor, ICUS, IIS, the University of Tokyo, Japan
yudai@iis.u-tokyo.ac.jp
[2] Professor, Director of ICUS, ICUS, IIS, the University of Tokyo, Japan

ABSTRACT

The downtown of Yangon-city is a typical grid-like network, and it is a very congested area in terms of both blocks and streets. In this study, we focus on the mathematical relationship between the shortest time route and deviation behavior on grid networks and clarify the fact that the bottlenecks in secondary streets would be serious elements to reduce the network's potential in downtown Yangon. Road patterns of Yangon-city downtown are tricky because the traffic capacity of north-south streets and that of east-west streets are quite different. Lots of secondary North-South streets are much narrower than arterial East-West streets. This capacity difference makes the traveler incur a longer distance. The mechanism of this phenomenon is as follows. (i) travelers try not to use secondary North-South streets as much as possible. (ii) This principle makes traveler detour from the shortest-distance route. (iii) Such deviation behavior accelerates the flow volume increase of streets. What we emphasize though the study is that significant unbalance of streets would accelerate further traffic congestions.

Keywords: downtown Yangon, grid network, deviation, bottleneck

1. INTRODUCTION

Yangon city, Myanmar, has large road networks that are crowded with traffics. Notably, the downtown area in Yangon city always suffers heavy traffics, and we need a long time to move within the area. The road network in the downtown area is a typical grid-like network with hierarchical road types, and it is difficult to move smoothly on the secondary narrow streets. Apparently, the reason is huge illegal parking cars in the street by road users. It is essential to clarify how these undesirable behaviors make worse the potential of the Yangon road network.
There are two most common measures to evaluate the ability of road networks, “travel distance” and “flow volume” (Vaughan 1987). It should be noted that travel distances and flow volumes have clear theoretical relationships (Koshizuke 1999). Precisely to say, as travel distances in an area become longer, flow volumes also become larger. It is natural because both measures indicate the activeness of movement. Therefore, there are plenty of earlier studies which focus on distances and/or flow volumes on road networks. For example, Fujita and Suzuki (2003) focus on the idealized circular-radial network and analytically derive both average distance and flow volumes. Meanwhile, there are other studies that assume other types of networks. One example of a grid network would be

held by Koshizuka (1996), and the analysis based on Euclidian distance was done by Ghosh (1951). Furthermore, Kurita (2001) assumed a circular disk city and compared several types of idealized road patterns. Similarly, Ukai and Toriumi (2017) defined n-directional distance and theoretically analyze the distance distribution in a circular region. Likewise, Miyagawa (2014) has assumed hierarchical road networks in his studies.
In this research, we focus on both distance and flow volumes on the road network in downtown Yangon. We explicitly consider the hierarchical structure of the road network and consider the difference in travel speed between arbitral streets and secondary streets. Then, we calculate the distance of the shortest-time route in various speed settings. These calculations clarify that unfavorable deviation behaviors increase as the speed of secondary roads decreases. All of These results points out the fact that the bottlenecks in secondary streets would be serious elements to reduce the network's potential in downtown Yangon.

2. FORMULATION

2.1 Basic Concepts

First, we explain about grid network. The glid network can be categorized as one of the road metrics. As another typical road metrics, there is the circular-radius network. As shown in Figure 1, the downtown area of Yangon city can be regarded as a typical grid network.
In the grid network, the route which connects two points in the shortest-distance is rather simple. Usually, it consists of two directional and orthogonalized movements within only a few turning like Figure 2-(b). The important point is that even if we assume a hierarchical grid network like Figure 2-(a), the characteristics of the shortest-distance route is still simple.
On the other hand, the route which connects origin-destination in the "shortest-time" is more complicated. Since it is deeply related to the travel speed of each link, it becomes prominent with a hierarchical grid network. As described in Figure 2-(c), they also consist of two-directional and orthogonalized movements, but the number of turns would be multiple times.
The most important point in this study is that these two routes are different, and the difference becomes larger when the travel speed of each link is different like the hierarchical road network. Obviously, the shortest-distance route is not the "shortest" in terms of "time". Likewise, the shortest-time route is not the "shortest" in terms of "distance". It means that we cannot simultaneously optimize both measures. In the following subsection, we formulate these phenomena and examine the unfavorable influences on the road networks. Hereafter, we abbreviate the shortest-distance route as the SD route and the shortest-time route as the ST route.

2.2 Mathematical models

Let us suppose a directed graph $G(N, E)$ as a road network where N is a set of nodes and E is a set of links. Furthermore, we denote each link as $e \in E$, and d_e indicates the travel-distance of link e and t_e indicate the travel-time of link e.
A mathematical problem to solve the SD route from origin $o \in N$ to destination $d \in N$ is as follows:

$$\text{min. } \sum_{e \in E} d_e \, x_e^{\text{SD}} \tag{1}$$

$$\text{s.t. } \sum_{I(i)} x_e^{\text{SD}} - \sum_{O(i)} x_e^{\text{SD}} = \begin{cases} -1 & (i = o) \\ 0 & \forall i \in N \setminus \{o, d\} \\ -1 & (i = d) \end{cases} \tag{2}$$

$$x_e^{\text{SD}} = \{0,1\} \ \forall i \in N \tag{3}$$

where $x_e^{\text{SD}} = 1$ if link e is used as a part of the SD route, and 0 otherwise. Furthermore, $I(i)$ is a set of inflow links of the node i, and $O(i)$ is a set of outflow links of the node i.

Expression (1) is the objective function, and it calculates the distance of the route. Constraint (2) is a flow-constraints and it assures the route connectivity. Constraint (3) is for 0-1 variables.
Similarly, the following problem is to solve the ST route from origin $o \in N$ to destination $d \in N$:

$$\text{min. } \sum_{e \in E} t_e \, x_e^{\text{ST}} \tag{4}$$

$$\text{s.t. } \sum_{I(i)} x_e^{\text{ST}} - \sum_{O(i)} x_e^{\text{ST}} = \begin{cases} -1 & (i = o) \\ 0 & \forall i \in N \setminus \{o, d\} \\ -1 & (i = d) \end{cases} \tag{5}$$

$$x_e^{\text{ST}} = \{0,1\} \ \forall i \in N \tag{6}$$

where $x_e^{\text{ST}} = 1$ if link e is used as a part of the ST route, and 0 otherwise.

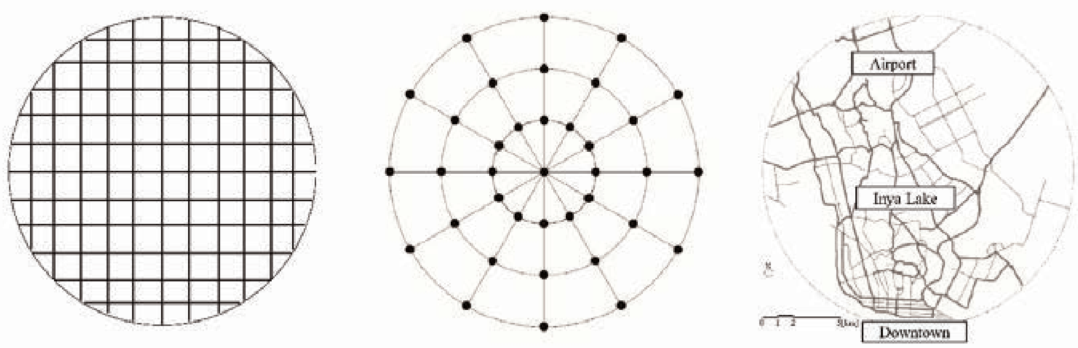

(a) Grid network (b) Circular-radial network (c) Yangon city

Fig. 1. Types of road networks

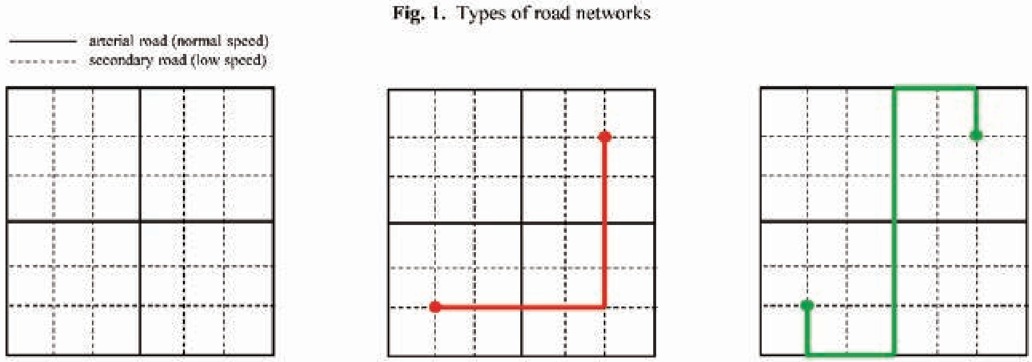

(a) hierarchical grid network (b) shortest-distance route (c) shortest-time route

Fig. 2. The shortest-distance route and the shortest-time route in a hierarchical grid network

2.3 The relation between the SD and ST route

Note that the "shortest" route under any measures does not pass through the same link twice. Therefore we can express both the SD route and the ST route as a set of links as follow:

$$R_{od}^{\mathrm{SD}} = \{e | \forall e \in E, x_e^{\mathrm{SD}} = 1 \text{ for OD pair } (o, d)\} \quad (7)$$
$$R_{od}^{\mathrm{ST}} = \{e | \forall e \in E, x_e^{\mathrm{ST}} = 1 \text{ for OD pair } (o, d)\} \quad (8)$$

In addition, we define a function to calculate the total distance (time) as a function of route R_{od} as follows:

$$Distance\left(R_{od}\right) = \sum_{e \in R_{od}} d_e \, x_e \quad (9)$$
$$Time\left(R_{od}\right) = \sum_{e \in R_{od}} t_e \, x_e \quad (10)$$

Now, we obtain two inequalities which are quite important in the study:

$$Distance(R_{od}^{ST}) \geq Distance(R_{od}^{SD}) \quad (11)$$
$$Time(R_{od}^{ST}) \leq Time(R_{od}^{SD}) \quad (12)$$

First, Inequality (11) indicates a situation that will be happened in the real world. In general, people tend to use the ST route than the SD route because they can empirically recognize the travel speed of each link. Then, (11) indicates that people need to incur more distance the SD distance. Such "deviation" behavior from the SD route increases in traffic volume. Meanwhile, (12) corresponds to another scenario that people single-

Fig. 3. Road networks and OD points in downtown area

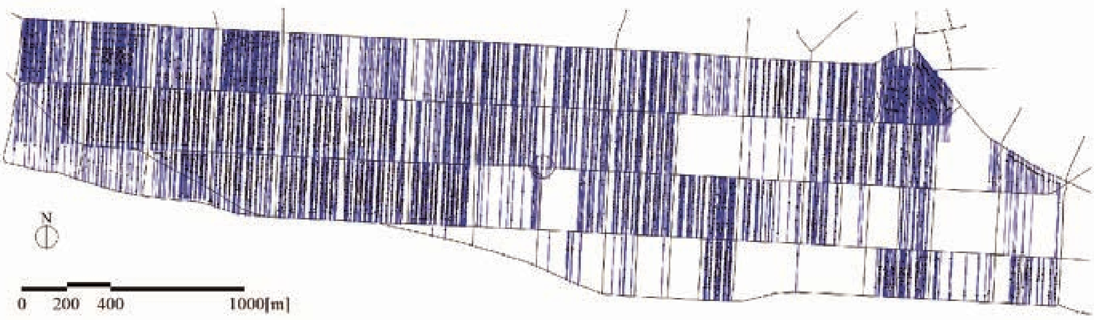

Fig. 4. Idealized access to arterial West-East streets

mindedly use the SD route. In that case, as (12) shows, people are obliged to bear more travel-time than the ST route.

3. NUMERICAL RESULTS

3.1 Network and Demand Data

The road network we used for the downtown area of Yangon is described in Figure 3. As shown, it is a typical grid-like network, but the efficiencies in moving between West-East and that of North-South are very different. Precisely to say, there are many "narrow and secondary" North-South streets which are not recorded in our GIS Data. Since the span of arterial North-South streets is long, these secondary roads are frequently utilized to help the North-South movement. However, at the same time, lots of cars are parked on the secondary roads, and the travel speed of their roads is quite slow. Meanwhile, the span of arterial West-East streets is relatively short, and there is no secondary street.

In this numerical example, we regarded the exact locations of building as Origin-Destination (OD) points, which are also shown in Figure 3. There are 5558 OD points, and therefore the total number of OD pairs is $(5{,}558 \times 5{,}557)/2 = 15{,}442{,}903$. In addition, to describe the movement using secondary North-South streets, we assume that each OD point can vertically access the nearest arterial West-East streets as shown in Figure 4. As a result, the movements are somehow idealized but we believe that it highly simulates the real situations.

We calculated both the ST routes and the SD routes for all pairs. For arterial roads, we assume that the travel speed is v_1 =20[km/h]. Meanwhile, to examine the impact of slow-down in secondary North-South streets, we prepared the following six cases, $v_2 = \{20,10,8,6,4,2,1\}$[km/h].

3.2 Results based on the route of the shortest time

We discuss the results based on the route of the shortest time route.

Figure 5 shows the distance distribution of the shortest time route at various speeds of v_2. Similarly, Figure 6 shows aggregated flow volumes on the networks. Remind that the ST route is equivalent to the SD route when all link speed is the same ($v_1 = v_2$ =20km), that is, Figure 5,6-(a) shows the most favorable case in terms of traffics. Meanwhile, as shown in Figure 5,6-(b) and (c), both travel-distance and aggregated flow volumes are increased as a result of decreasing of the secondary links speed v_2. These are the results of deviation behavior form the SD route. Especially from Figure 6-(c), we can confirm that the arterial North-South street on the center is much more congested then Figure 6-(a), and lots of other arterial North-South streets are more utilized as well. The facts indicate that the occurrence of bottlenecks on secondary streets will be a critical factor of deviation behaviors AND traffic increasing on arterial streets.

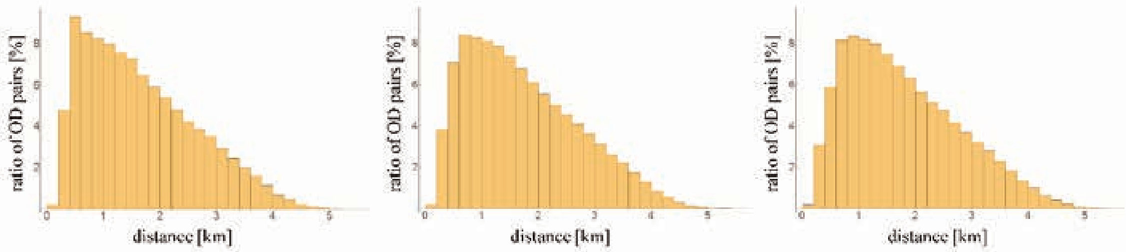

(a) Case of v_2=20[km/h] (b) Case of v_2=4[km/h] (c) Case of v_2=1[km/h]

Fig. 5. Distance distributions in various cases for the ST routes (v_1=20[km/h])

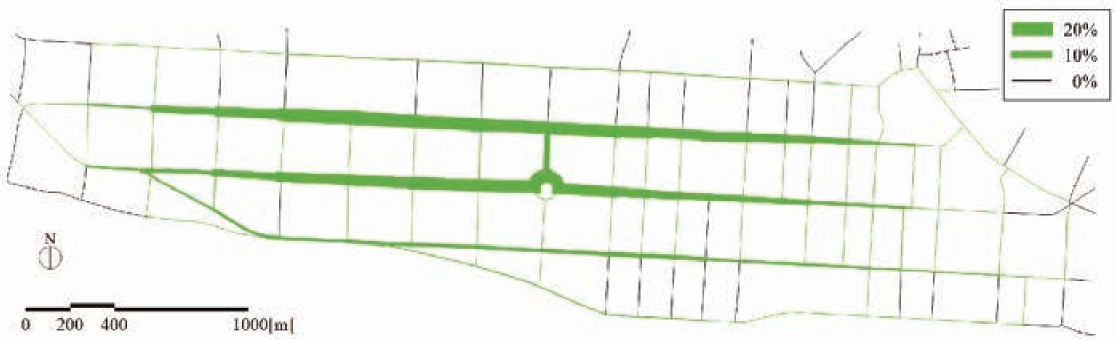

(a) Case of v_2=20[km/h]

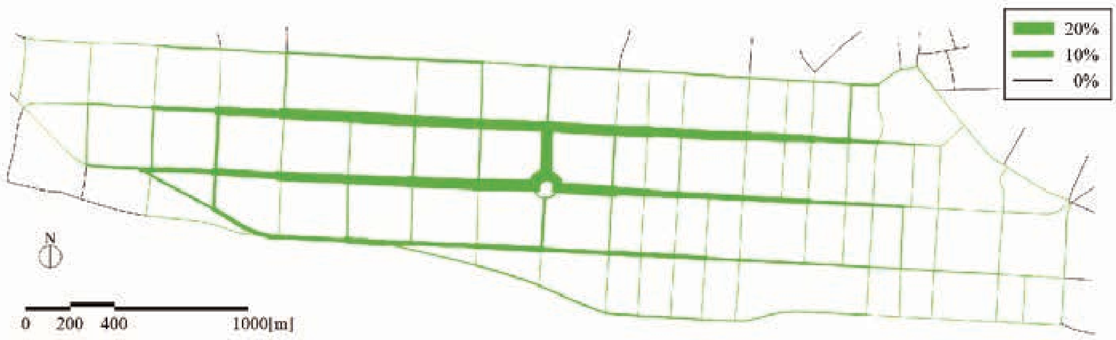

(b) Case of v_2=4[km/h]

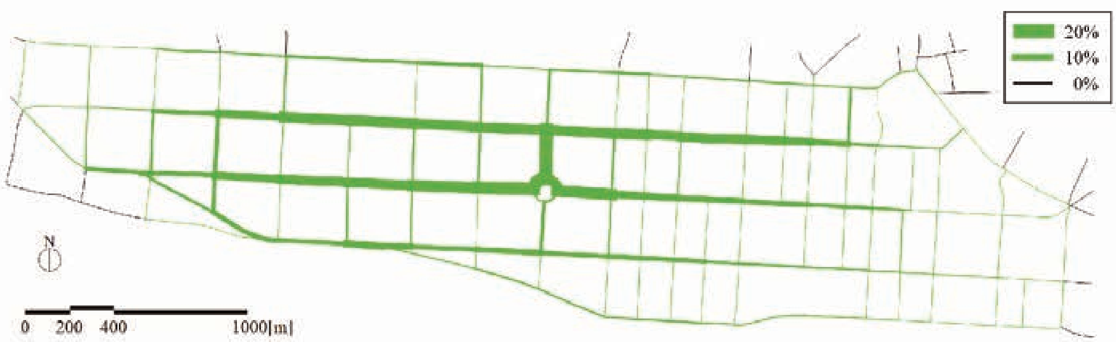

(c) Case of v_2=1[km/h]

Fig. 6. Aggregated flow volumes in various cases regarding the ST routes (v_1=20[km/h])

4. CONCLUSION

In this study, we numerically discuss the influence of bottleneck occurred in secondary North-South streets in downtown Yangon from the viewpoints of travel-time, travel-distance, and flow volume.

Since the road network is a typical grid-like network with a hierarchical road type, the ST route and the SD route would become different. Especially when we assume that people would use the ST route for movements, the above results showed the fact that the bottleneck in secondary North-South streets promotes people's deviation behavior and the increase of traffic volumes. Even if we assume that people follow the SD route, the slow-down of secondary streets contributes to the increase of travel time.

REFERENCES

R. Vaughan, 1987, Urban Spatial Traffic Patterns, Pion.

T. Koshizuka, 1999, "Comparison of Road Network Patterns with Respect to Travel Distance and Passing Volume," Journal of the City Planning Institute of Japan, Vol.34, pp763-768.

S. Fujita, and T. Suzuki, 2003, "Average Trip Length and Traffic Flow in a Disk City with Multi-ring Routes," Journal of the City Planning Institute of Japan, Vol.38, pp.421-426.

T. Koshizuka, 1996 "Comparison between Low and High Buildings with Respect to Travel Distance," Journal of the City Planning Institute of Japan, Vol.31, pp.31-36,.

B. Ghosh, 1951 Random distances within a rectangle and between two rectangles, Bulletin of the Calcutta Mathematical Society, Vol.43, pp.17-24.

O. Kurita, 2001, "Theory of Road Patterns for A Circular Disk City, Journal of the City Planning Institute of Japan," Vol.36, pp.859-864.

T. Ukai, and S. Toriumi, 2017, "Distribution of n-directional distance in a circular region," Journal of the City Planning Institute of Japan, Vol.52, pp.1327-1334.

M. Miyagawa, 2014, "Optimal allocation of area in hierarchical road networks," The Annals of Regional Science, 53, pp.617-630.

Optimization of building footprint extraction model with color and texture analysis in Yangon city

Hein Thura Aung[1], Sao Hone Pha[2]
and Wataru Takeuchi[3]

[1] Post-graduate Student, Department of Electronic Engineering,
Yangon Technological University, Myanmar
heinthuraung@ytu.edu.mm, heinthuraung@gmail.com
[2] Director, Remote Sensing and GIS Research Center,
Yangon Technological University, Myanmar
[3] Professor, Institute of Industrial Science,
The University of Tokyo, Japan

ABSTRACT

Automatic building footprint extraction using machine learning and deep learning saves a lot of time and human source, and makes future updates easier. Creation of training datasets for those learning algorithms is one of the most important steps in the extraction process especially when the feasibility of training samples is limited. In this research, different townships of Yangon City are clustered based on color and texture analysis. First, non-building areas of Yangon City are removed by using digital building model (DBM) which is derived from GeoEYE stereo RGB satellite image. Then, the whole Yangon City image is split according to the boundaries of thirty different townships. After that, for each image of each township, the average and standard deviation for color histogram analysis, and three features for textural analysis, mean Euclidean distance, variance, and skew, are calculated. Based on the color histogram and textural analysis, thirty different townships are clustered by using k-means clustering algorithm. By looking at the color analysis and clustering results, training dataset representation for the whole Yangon City such as from where the training images should be extracted, can be decided.

Keywords: GeoEYE RGB image, digital building model, GLCM, clustering, training dataset representation

1. INTRODUCTION

Yangon is the largest city in the country and formal capital of Myanmar. Its area is growing seven times in forty two years from 1973 to 2015 (Sritarapipat et al., 2018) without proper urban planning and management. Urban population has also increased about two and half times from 1972 to 2014 (Ministry of Immigration and Population, 2015). With that rate of increase, proper management of urban resource management such as food and water, transportation management, emergency response, disaster response and so on, are very important. Urban related database such as urban building maps are one of the essential things for urban related applications. Manual creation of urban building maps takes much more time and human resource, and more difficult in future updates. Automatic extraction needs image processing techniques, machine learning and deep learning algorithms.

In (Lopez et al., 2015, p. 201), (Oztimur Karadag et al., 2015) and (Kabolizade et al., 2010), several datasets such as optical image, light detection and ranging (LiDAR) dataset were used to detect building footprints. They combined several image processing techniques with machine learning algorithms such as support vector machine (SVM) classification. Their research works need multi spectral images including red, green, blue (RGB) and near infra-red (NIR) bands. In (Vakalopoulou et al., 2015) and (Zhang et al., 2016), they used convolutional neural network (CNN) to detect building footprints. CNN is deep learning algorithm which needs a lot of training samples. In (Zuming Huang et al., 2016) and (Chen et al., 2017), they used two datasets including near-red band and digital surface model (DSM). (Bittner et al., 2018) also used multiple datasets including RGB, IR bands and panchromatic images. All these research works are based on convolutional neural network (CNN) which is a very powerful deep learning algorithm. However, in order to CNN, a lot of training samples are required.

The research works in (Hein Thura Aung et al., 2018a) and (Hein Thura Aung et al., 2018b) indicate how training samples could affect the extraction performance of deep learning algorithm. Due to the high price of very high resolution satellite images, availability of training samples for automatic building footprint extraction is limited. So, in this research work, color and texture analysis of RGB GeoEYE satellite image are performed in order to optimize building footprint extraction model by selecting the most effective area as training samples.

2. METHODOLOGY

Figure 1 shows the flow chart of this research. As shown in Figure 1, the RGB image of GeoEYE satellite of the study area is masked with digital building model (DBM). The RGB image of the study area is columns and rows with meter spatial resolution. It is comprised of thirty townships including urban and suburban areas. The digital building model of the study area is columns and rows with meter spatial resolution.

Firstly, the non-building regions of RGB image of Yangon city is suppressed with a threshold value of DBM image. After that, the average of image histogram elements, mean and standard deviation of each band in the masked RGB is calculated. In order to compare the image histogram statistical elements of different townships, normalized difference indices for mean and standard deviation values between each pair of townships are calculated. And then, townships with highest frequencies of being enlisted in the lowest three normalized difference mean and standard deviation index values are considered.

For textural analysis, three texture features, mean Euclidean distance, variance and skew, are calculated. After calculation of three texture features, k means clustering is used in order to classify each texture feature image into five classes based on texture analysis values. After clustering, the distribution of each class in the image is used to consider the suitability of townships for training dataset.

2.1 Normalized Difference Index

As the townships in Yangon city have different columns and rows, it is very difficult to compare mean and standard deviation values alone. Instead, normalized difference mean index and normalized difference standard deviation index between each pair of townships are calculated as shown in equation 1 and equation 2.

(1)

(2)

For example, for calculation of normalized difference indices of Ahlone Township and Bahan Township, the subtraction of mean values of Ahlone and Bahan is divided by the addition of mean values of those two townships. Similarly, other pairs of townships are calculated. Higher index values indicate higher difference between two townships whereas lower index values represent lower difference.

After calculation of normalized difference indices for mean and standard deviation of each township, the frequencies of enlisted townships in the lowest three index values are considered for training dataset optimization.

2.2 Texture features

In this section, three texture features, mean Euclidean distance, variance and skew, are discussed.

2.2.1 Mean Euclidean distance (MED)

Mean Euclidean distance is the average of the differences between the center pixel of the moving window and other pixels in that window (ERDAS, Inc, 2010). Equation 3 shows the calculation of MED for a single band.

(3)

is the digital number (DN) value of a spectral band at pixel , is the DN value of the window's center pixel for a spectral band and is number of pixels in a window

2.2.2 Variance

Equation 4 shows how to calculate the variance (ERDAS, Inc, 2010). Variance is calculated as the average of the differences between mean value of a window and DN value of each pixel in the window.

(4)

is the DN value at pixel , is number of pixels in a window and is the mean of the moving window where .

2.2.3 Skew

Equation 5 shows how to calculate skew (ERDAS, Inc, 2010).

(5)

is the DN value at pixel , is number of pixels in a window, is the mean of the moving window where , and is variance.

2.3 K means clustering

K means clustering is partitioning a data set into distinct, non-overlapping clusters (James et al., 2013). K means clustering can be done by equation 6.

(6)

The term in the curly bracket represents the squared Euclidean distance. Firstly, a random number, from to , is assigned to each observations. denote clusters. is the number of observations in the cluster. Equation 6 represents to minimize the differences between the centroid of each of the K clusters and every observation i.e., each observation is assigned to the cluster whose centroid is closest in terms of Euclidean distance. A good clustering is one for which the within-cluster variation is as small as possible (James et al., 2013).

3. RESULTS

In this section, color and texture analysis results are discussed. Depending on the results of K means clustering, optimization of building footprint extraction model is also discussed.

3.1 Color analysis

For color analysis, normalized difference indices for mean and standard deviation between every pair of thirty townships are calculated. Figure 2 shows the frequencies of enlisted townships in the lowest three normalized difference mean and standard deviation index values.

As shown in Figure 2, Botahtaung and Dawbon townships include in the lowest three mean index values for five townships. Bahan, Dagon, Dagon Myothit (South), Hlaingtharya, Insein, Kyeemyindaing, Mingalardon and Tamwe are enlisted in the lowest three mean index values for four townships. Dagon Myothit (East), Mayangone, Mingalar Taung Nyunt, Sanchaung and Seikkan Townships have only once in lowest frequencies in the bottom three mean index values. For lowest three normalized difference standard deviation index values, Ahlone, Dagon Myothit (North), Kyeemyindaing, Latha and Thingangyun Townships have highest frequencies followed by Bahan, Botahtaung, Dagon Myothit (South), Insein, South Okkalapa, Seikkan, Thaketa and Yankin townships with being enlisted in four townships.

3.2 Texture analysis

Figure 3 shows some sample images how five classes are clustered depending on the MED values. Other texture features, variance and skew, have similar occurrence. Black areas represent masked area with DBM image. As shown in Figure 3, Class 1, 2, and 3 represent low texture areas such as rooftops and plane-like surfaces whereas Class

4 and 5 represent high texture areas such as boundaries and edges.

Figure 4 shows the distribution of each class in the texture image of MED. According to Figure 4, Dagon Myothit (Seikkan) and Seikkan Townships have lowest Class 4 distribution as Dawgon Myothit (Seikkan) is mostly suburban area and Seikkan is just a township with ports full of containers and fewer buildings than other urban areas. As a result of having fewer buildings and containers, those two townships have higher contribution for Class 1 and Class 2 which represent lower texture level.

Figure 5 shows distribution of five classes in Variance texture image. Similarly, Dagon Myothit (Seikkan) and Seikkan Townships have higher contribution for Class 1 and 2, whereas lower contribution for Class 4 and 5. Figure 6 shows distribution of five classes in Skew texture image. Similarly in MED and Variance texture images, Dagon Myothit (Seikkan) and Seikkan Townships have higher contribution of Class 1 and 2, and lower contribution for Class 4 and 5. For all three texture images, downtown areas such as Botahtaung, Latha, Mayangone, Kyeemyindaing and Dawbon and South Okkalapa Townships have high contribution in Class 4 and 5.

4. DISCUSSION

According to Figure 2, Botahtaung and Kyeemyindaing Townships have highest enlisted frequencies in the lowest three normalized difference mean and standard deviation index values. Both of them includes in urban areas where most of them are covered with buildings. Bahan, Dagon Myothit (South) and Insein Townships also have high enlisted frequencies. Dagon Myothit (South) and Insein Townships are sub urban areas which are covered with trees and buildings, and although Bahan Township is in urban area, it is also covered with trees and buildings. Kan Daw Gyi Lake which is one of the two major lakes, is also located in Bahan Township. Insein, Ahlone, Thingangyun and Latha Townships also have high enlisted frequencies. Those four townships are also covered with vegetation and buildings. Although Latha Township is urban area, half of it is covered with both tress and buildings and the other half is mostly buildings.

From Figure 4, 5 and 6, only Dagon Myothit (Seikkan) and Seikkan Townships have very different class distributions. Dagon Myothit (Seikkan) is mostly covered with bare lands with small vegetation and farms, and some buildings. Seikkan Township is mostly covered with impervious floor, containers and warehouses. Botahtaung and Kyeemyindaing Townships have similar distributions of classes for variance as shown in Figure 5 and 6, but they have different distribution for MED as in Figure 4. Only Bahan and Dagon Myothit (South) Townships have similar distribution for MED as shown in Figure 4, but all Bahan, Dagon Myothit (South) and Insein Townships have similar distributions for variance and skew as shown in Figure 5 and 6.

Latha and Thingangyun Townships have similar distributions for MED as in Figure 4, but all Ahlone, Latha and Thingangyun Townships have similar distributions for variance and skew as in Figure 5 and 6.

According to the color and texture analysis, training dataset should be selected from all or any of Botahtaung, Kyeemyindaing, Bahan, Dagon Myothit (South), Insein, Ahlone, Latha, and Thingangyun Townships.

5. CONCLUSIONS

In this research, monocular RGB GeoEYE satellite image is analyzed with image histogram statistics such as mean and standard deviation, and texture features which are mean Euclidean distance, variance and skew. According to the results, townships with similar spatial and spectral properties from visualization have similar color and texture statistical values. Some townships such as Dagon Myothit (Seikkan) and Seikkan Townships have different spatial and spectral properties, so they cannot be chosen for training dataset. The color and texture analysis of Yangon City gives eight different townships that are suitable for training dataset representation for the whole Yangon City. So, as future plan, some of those eight townships will be selected as training dataset and performance of pix2pix will be evaluated again.

REFERENCES

Bittner, K., Adam, F., Cui, S., Korner, M., Reinartz, P., 2018. *Building Footprint Extraction From VHR Remote Sensing Images Combined With Normalized DSMs Using Fused Fully Convolutional Networks*. IEEE Journal of Selected Topics in Applied Earth Observations and Remote Sensing 11, 2615–2629. https://doi.org/10/gd7zc2

Chen, K., Fu, K., Gao, X., Yan, M., Sun, X., Zhang, H., 2017. *Building extraction from remote sensing images with deep learning in a supervised manner*, in: 2017 IEEE International Geoscience and Remote Sensing Symposium (IGARSS). Presented at the 2017 IEEE International Geoscience and Remote Sensing Symposium (IGARSS), IEEE, Fort Worth, TX, pp. 1672–1675. https://doi.org/10.1109/IGARSS.2017.8127295

ERDAS, Inc, 2010. *ERDAS Field Guide*.

Hein Thura Aung, Sao Hone Pha, Wataru Takeuchi, 2018a. *Automatic building footprints extraction of Yangon City from GeoEYE monocular optical satellite image by* *using deep learning*, in: Asian Conference on Remote Sensing 2018. Presented at the 39th Asian Conference on Remote Sensing, Kuala Lumpur Malaysia, pp. 1987–1996.

Hein Thura Aung, Sao Hone Pha, Wataru Takeuchi, 2018b. *Performance evaluation of building footprint delineation in Yangon City using deep learning with different training datasets*, in: 9th International Conference on Science and Engineering. Presented at the 9th International Conference on Science and Engineering, Yangon Technological University.

James, G., Witten, D., Hastie, T., Tibshirani, R. (Eds.), 2013. *An introduction to statistical learning: with applications in R*, Springer texts in statistics. Springer, New York.

Kabolizade, M., Ebadi, H., Ahmadi, S., 2010. *An improved snake model for automatic extraction of buildings from urban aerial images and LiDAR data*. Computers, Environment and Urban Systems 34, 435–441. https://doi.org/10.1016/j.compenvurbsys.2010.04.006

Lopez, E.R., Santos, H.F., Ana, R.R.C.S., Samalburo, S.J.D., 2015. *Evaluation of Building Footprint Generation from LIDAR Data and Orthoimages using Object-based Image Analysis Technique*, in: 36th Asian Conference on Remote Sensing. Presented at the 36th Asian Conference on Remote Sensing, Manila, Philippines.

Ministry of Immigration and Population, M., 2015. *A changing population: Yangon region figures at a glance*. Department of Population, Myanmar.

Oztimur Karadag, O., Senaras, C., Yarman Vural, F.T., 2015. *Segmentation Fusion for Building Detection Using Domain-Specific Information*. IEEE Journal of Selected Topics in Applied Earth Observations and Remote Sensing 8, 3305–3315. https://doi.org/10.1109/JSTARS.2015.2403617

Sritarapipat, T., Takeuchi, W., The University of Tokyo 6-1 Komaba 4-chome, Meguro, Tokyo 153-8505, Japan, 2018. *Land Cover Change Simulations in Yangon Under Several Scenarios of Flood and Earthquake Vulnerabilities with Master Plan*. Journal of Disaster Research 13, 50–61. https://doi.org/10/gd52wk

Vakalopoulou, M., Karantzalos, K., Komodakis, N., Paragios, N., 2015. *Building detection in very high resolution multispectral data with deep learning features*, in: 2015 IEEE International Geoscience and Remote Sensing Symposium (IGARSS). Presented at the IGARSS 2015 - 2015 IEEE International Geoscience and Remote Sensing Symposium, IEEE, Milan, Italy, pp. 1873–1876. https://doi.org/10.1109/IGARSS.2015.7326158

Zhang, Q., Wang, Y., Liu, Q., Liu, X., Wang, W., 2016. *CNN based suburban building detection using monocular high resolution Google Earth images*, in: 2016 IEEE

International Geoscience and Remote Sensing Symposium (IGARSS). Presented at the IGARSS 2016 - 2016 IEEE International Geoscience and Remote Sensing Symposium, IEEE, Beijing, China, pp. 661–664. https://doi.org/10/gftsgh

Zuming Huang, Guangliang Cheng, Hongzhen Wang, Haichang Li, Limin Shi, Chunhong Pan, 2016. *Building extraction from multi-source remote sensing images via deep deconvolution neural networks*, in: 2016 IEEE International Geoscience and Remote Sensing Symposium (IGARSS). Presented at the IGARSS 2016 - 2016 IEEE International Geoscience and Remote Sensing Symposium, IEEE, Beijing, China, pp. 1835–1838. https://doi.org/10.1109/IGARSS.2016.7729471

MONITORING RESULTS OF PATHEIN BRIDGE TOWERS AND BEARINGS

KHIN MAUNG ZAW[1], WIN BO[2], AMY AUNG[2], K. MATSUMOTO[3], and K. NAGAI[4]

[1] Associate Professor, Department of Civil Engineering, Yagon Technological University, Yangon, Myanmar,
[2] Postgraduate Students, Department of Civil Engineering, Yagon Technological University, Yangon, Myanmar,
[3] Associate Professor, Division of Engineering and Policy for Sustainable Environment, Hokkaido University, Japan,
[4] Associate Professor, Institute of Industrial Science, University of Tokyo, Japan,
Correspond to Khin Maung Zaw (ukmzaw@gmail.com)

***Keywords**: Pathein Bridge, bridge monitoring, tower tilting, bearing movement*

1. INTRODUCTION AND BACKGROUND

Pathein Bridge is one of the most important bridges in Ayeyarwady Region, connecting its capital Pathein to western coastal areas and the southern part of Rakhine State. According to the 2012 bridge inspection report [1] of the Ministry of Construction, it was found that the bridge had lost a great deal of camber since completion, and it may be due to the tilting of main towers (shown in Figure 1.a) towards the river [2].

The bridge towers were built on the alluvial soil and, hence, the horizontal force of main cable may move concrete anchorage blocks or the tower foundation may rotate due to differential settlement. Most hangers were found to be inclined towards Pathein side (shown in Figure 1.b) [3]. Hence, in order to check whether tower tilting is still continued or not and whether the bearings (shown in Figure 2) are working properly or not, the monitoring system was installed on both sides of downstream towers including two inclinometers, two displacement transducers, temperature sensors and two portable data loggers.

(a) (b)

Figure 1: Inclination of (a) tower and (b) hanger of Pathein Bridge. [3]

2. RESULTS AND DISCUSSIONS

According to the results of regression analysis of monitoring data from November 2017 to April 2018, there is no significant change in the value of tower inclination degree. The results also indicate that the values of inclination degree are very small, and it may be due to the effect of temperature fluctuation. Hence, it can be concluded that the tower is in stable condition. The inclination degree of the tower along the bridge axis direction is about 0.0015 degree per degree centigrade, and along the transverse direction is about 0.0009 degree per degree centigrade (shown in Figure 3.a) [3].

(a) (b)

Figure 2: (a) Fixed bearing on Pathein side and (b) expansion bearing on Chaung Tha side. [3]

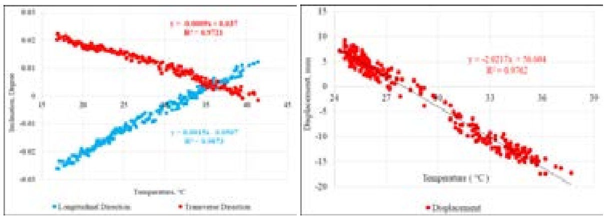

(a) (b)

Figure 3: (a) Tower inclination and (b) Bearing displacement with respect to temperature. [3]

According to the results of regression analysis, the rate of movement of expansion bearing is found to be about 2.02 mm/˚C (shown in Figure 3.b) but there is no significant movement of fixed bearing on Pathein side.

3. CONCLUSIONS

Pathein Bridge had lost a great deal of camber since completion and, hence, the monitoring system was installed on both sides of downstream towers in order to check the condition of tower tilting and the movement of bearings. According to the monitoring results, it can be concluded that the towers and bearings are in stable condition. The inclination degree of the tower along the bridge axis direction is observed to be about 0.0015 degree/˚C, and along the transverse direction is about 0.0009 degree/˚C. The rate of movement of expansion bearings is found to be about 2.02 mm/˚C and there is no significant movement of fixed bearing on Pathein side.

REFERENCES

[1] Japan Infrastructure Partners. Bridge Inspection Report to Ministry of Construction, Myanmar. 2012.

[2] K.M. Zaw, Y. Suzuki, and K. Sugiura. Proceedings of Construction Steel, JSSC, Vol.23 (2015) 364-371.

[3] Win Bo. Ph.D. Thesis, Department of Civil Engineering, Yangon Technological University. 2018.

SEISMIC HAZARD ASSESSMENT IN YANGON CITY USING THE EMPIRICAL EARTHQUAKE EVALUATION METHOD

Yoshito YOKOE[1], Takaaki IKEDA[2], Takumi MATSUMOTO[1], Atsuya MINAGAWA [1]

[1] *Graduate student , Civil and Environmental Engineering, Nagaoka University of Technology, Niigata, Japan,*
[2] *Professor, Civil and Environmental Engineering, Nagaoka University of Technology, Niigata, Japan,*
Correspond to Mr. Yokoe(s173282@stn.nagaokaut.ac.jp)

Keywords: *Ground motion simulation, Source model, EMPR, Scenario earthquake*

1. INTRODUCTION

Yangon city is the largest city in Myanmar with a population of about 5 million. Sagaing fault, which extends about 1500 km in the central part of Myanmar is located in near Yangon City (Figure 1[1)]), the risk of earthquakes in Yangon City is very high. It is necessary to take disaster measures before the next earthquake occurs. In this study, we attempt strong ground motion prediction for Yangon City against crustal earthquake along the Sagaing fault using the empirical ground motion prediction method[2)].

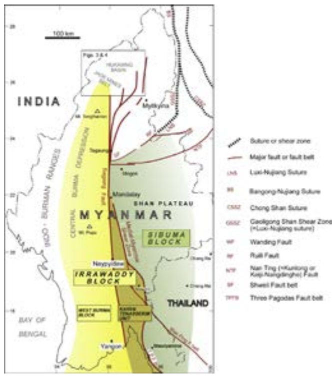

Figure 1. Outline map of Myanmar showing the two most significant strike-slip fault belts[1)]

2. SCENARIO EARTHQUAKE

Table 1 shows parameter of scenario earthquake. Magnitude was set to 7.3 based on the 1930 Pyu earthquake in Myanmar. Figure 2 shows location of scenario earthquake. Fault distance to target site is about 25km. Fault size was 30km × 15km. Fault length was estimated by Matsuda's method[3)]. Fault width was assumed half of fault length. Fault dip angle was set to 90 deg. assuming the strike slip earthquake.

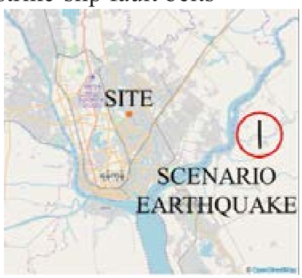

Figure 2. Location of the target site and scenario earthquake

3.METHOD AND RESULT

We used EMPR[1)] for predicting strong ground motion. It is nonstationary strong motion prediction models which was proposed by Sugito et al[2)]. It can be evaluated strong ground motion on engineering base with Vs=500-600m/s in consideration of fault rupture process.

In this study, we divided fault plane into 18 (6 × 3, see figure 2), and we calculated 18 series that changed the rupture starting point. Table 3 shows result of strong ground motion prediction. The maximum acceleration is 388.8 cm/s^2. Figure 3 shows acceleration waveform. The maximum acceleration of the surface ground exceeds 500 cm/s^2 assuming amplification factor of surface layer is 2.0.

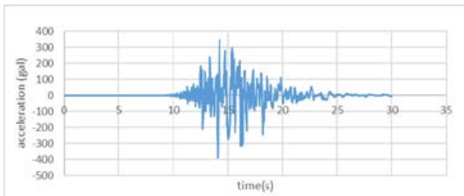

Figure 3. Predicting strong ground motion

Table 1. Source parameter of scenario earthquake

Location	16.8547N, 96.4283 E
Magnitude (Mw)	7.3
Size (L×W)	30km × 15km
Depth (Upper end of fault)	10km
Dip angle	90 degree
Seismic moment (M_0)	3.52 × 10^{19} Nm

Table 2. Result of strong ground motion prediction

	Max.	Ave.	Ave.+1σ
Acceleration (cm/s^2)	388.8	280.1	328.9
Velocity (cm/s)	43.2	28.4	35.6

REFERENCES

[1] Michael, F. R. et al.: The role of strike-slip faul ting in the history of the Hukawng Block and the J ade Mines Uplift, Myanmar, Proc. Geologists' Associ ation, 130, 2, 126-141, 2019.

[2] Sugito, M. et al.: Strong Motion Prediction on Rock Surface by Superposed Evolutionary Spectra, 12WCEE, 2000.

[3] Matsuda, T.: Magnitude and Recurrence Interval of Earthquake from a fault, zishin, 2, 28, 269-283, 1975(in Japanese).

EFFECT OF SURFACE GROUND CHARACTERISTICS ON STRUCTURAL DAMAGE

Haruki SUZUKI[1], **Takaaki IKEDA**[2] **and Yukiko KOJIMA**[3]

[1] Graduate student, Nagaoka University of Technology, Niigata, Japan,
[2] Professor, Nagaoka University of Technology, Niigata, Japan
[3] Assistant Professor, National Institute of Technology, Nagaoka College, Niigata, Japan
Correspond to Mr. Suzuki (s173253@stn.nagaokaut.ac.jp)

***Keywords**: Earthquake damage investigation, Effects of Surface Geology, 2019 off Yamagata Prefecture earthquake*

1. INTRODUCTION

On June 18, 2019, at 22:22 (JT), an Mw6.4 earthquake occurred off the coast of Yamagata Prefecture. A maximum acceleration of 1191.3 gal was also observed at a nearby seismic station. Strong ground motions were generated at near source area, but there was no major damage. Main damage is roof tiles damage of the wooden house. A damage rate of roof tile at Koiwagawa area was the highest in damage area. On the other hand, Oiwagawa area and Wasada area which are adjustment in Koiwagawa had minor damage. Therefore, in order to clarify the difference in damage between Koiwagawa, Oiwagawa, and Wasada, we investigated the ground conditions at each site.

2. INVESTIGATION SITE

The study sites are the Koiwagawa, Oiwagawa, and Wasada. Figure 1 shows the location of the epicenter and study sites. Considering the topographical conditions, surface layer at each site was composed by sandy soil mainly. As shown in Figure 1, the epicentral distance of study sites are almost the same, so the input ground motion is considered to be the same.

Figure-1 Location of epicenter and study sites

Kojima et al.[1)] has evaluated of the roof tile damage from an aerial photograph. They were reported that damage rate of roof tile was 28.6% in the Koiwagawa, 1.0% in the Oiwagawa and 2.6% in the Wasada. It was thought that damage of roof tile related to characteristics of surface layer.

Therefore, we conducted microtremor measurement at study site and evaluated predominate frequency of surface layer by H/V spectral ratio of microtremor measured. H/V spectral is Horizontal-to-Vertical spectral ratios. Frequency of peak H/V spectral ratio correspond to predominate frequency of surface layer.

3. RESULTS

From the H/V spectral ratio shown in Figure 2, H/V spectral ratio of Koiwagawa is dominant around 5 to 7 Hz, and Oiwagawa and Wasada are exceeding 10 Hz. The natural frequency of wooden houses is usually 2 to 10 Hz.

Predominate frequency of surface layer at Koiwagawa falls in the range of the natural frequency of wooden house. On the other hand, predominate frequency of other site is greater than natural frequency of wooden house. Therefore, it is thought that the damage situation of study sites was affected by ground charactristics.

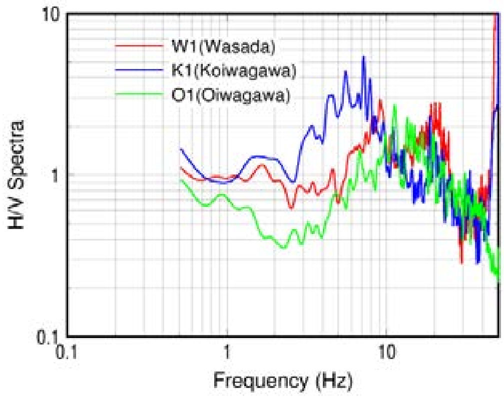

Figure-2 H/V spectral ratio of each area

4. CONCLUSIONS

In this earthquake, many roof tiles were damaged in near source area, but the damage was different at near sites, so the characteristics of the surface layer were evaluated by H/V spectral ratio of microtremor measured. As a result, it was found that there is a correlation between the predominate frequency of the surface layer and the damage situation.

REFERENCES

[1] Y. Kojima et al.: Damage investigation of 2019 off the yamagata prefecture earthquake, Proc. of the 39th JSCE Earthquake Engineering Symposium, 2019 (under submission, in Japanese).
[2] Nakamura, Y.: A method for dynamic characteristics estimation of subsurface using microtremor on the ground surface, Q. Rep. Railw. Tech. Res. Inst.,30,25–30, 1989.

SOURCE MODELING AND GROUND MOTION SIMULATION OF THE MID-SCALE CRUSTAL EARTHQUAKE

T. IKEDA[1]

[1] *Professor, Department of Civil and Environmental Engineering, Nagaoka University of Technology, Nagaoka, Japan*
Correspond to Prof. T. IKEDA (ikeda@vos.nagaokaut.ac.jp)

***Keywords**: ground motion simulation, source modeling, empirical Green's function method, mid-scale crustal earthquake*

1. INTRODUCTION

Recently, structure or lifeline system damages caused by the mid-scale earthquake were reported. Generally, damage scale by mid-scale earthquake was not so serious, but that earthquake is often generated. So it is important that study of the source modeling the mid-scale earthquake. In this study, we attempted to make a source model of mid-scale earthquake by the forward modeling[1] using empirical Green's function method[2].

2. SOURCE MODELING

Target earthquake is 2017 Nagano prefecture earthquake of Mw5.2 in Japan. Figure 1 shows locations of the epicenter and near seismic stations.

We set single strong motion generation area (SMGA) referred to observation waveform. As a result, we make a source model with single SMGA which located in near hypocenter (Figure 2). Figure 3 shows the synthesized acceleration waveforms, velocity waveforms and displacement waveform of EW component at each target stations compared with the observed ones. Synthesized acceleration waveform and velocity waveform at NGNH18 which is the nearest station were good agreement with observed ones. Especially, synthetic waveform can reproduce pulse waveform.

Figure 4 shows relationship between seismic moment and short period source spectrum. Scaling law was written in this figure[3]. Relation between seismic moment and short period source spectrum can be express scaling law.

3. CONCLUSIONS

We constructed the source model of the 2007 Nagano prefecture earthquake with Mw5.2. The source model has a single SMGA. Relation between seismic moment and short period source spectrum can be express scaling law[3].

REFERENCES

[1] Kamae, K. and Irikura, K., Source model of the 1995 Hyogo-ken Nanbu earthquake and simulation of near-source ground motion, BSSA, Vol.88, 400-412., 1998

[2] Irikura, K., Prediction of strong acceleration motion using empirical Green's function, Proc. 7JEES,151-156., 1986.

[3] Dan, K. et al., Short-period source spectra inferred from variable-slip rupture models and modeling of earthquake faults for strong motion prediction by semi-empirical method, Journal of Structural and Construction Engineering, AIJ, No.545, 51-62. 2001.

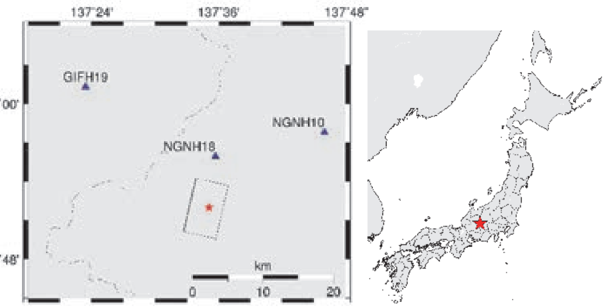

Figure 1. Location of the epicenter of the 2017 Nagano prefecture earthquake and seismic stations

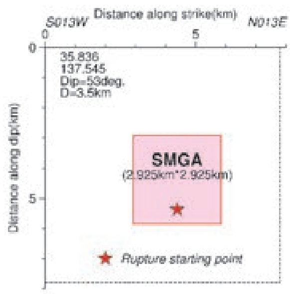

Figure 2. The source model of the 2007 Nagano prefecture earthquake which composed 1 SMGA

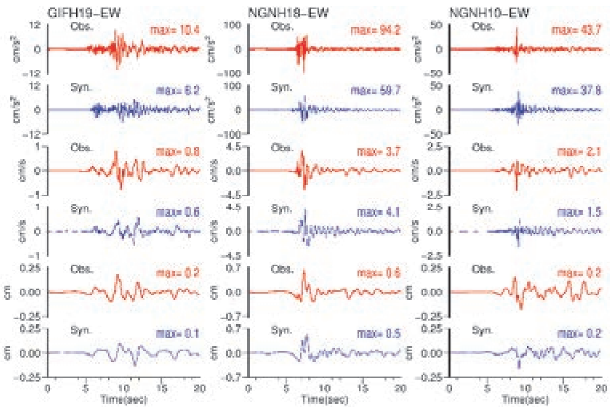

Figure 3. Comparison of the observed and synthetic waveforms of EW component at target station.

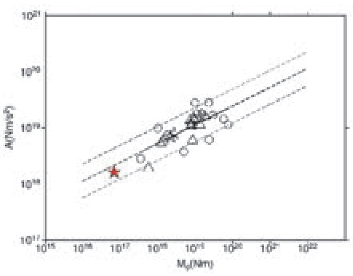

Figure 4. Relation between seismic moment and short period source spectrum.

SESSION G

ENVIRONMENT INFORMATICS: GIS/REMOTE SENSING, TRANSPORTATION, WATER RESOURCES, INFRASTRACTURE MANAGEMENT

Extraction of damage situation in Yamagata coast earthquake using UAV

Yukiya TANIGUCHI[1], C. K. Gadagamma[2] and Muneyoshi NUMADA[3]
[1]Student, Graduate School of Interdisciplinary Information Studies,
Institute of Industrial Science, the University of Tokyo, Japan
taniguchi-yukiya312@g.ecc.u-tokyo.ac.jp
[2]Project-Assistant Professor, Institute of Industrial Science,
The University of Tokyo, Japan
[3]Associate Professor and Director, Institute of Industrial Science,
the University of Tokyo, Japan

ABSTRACT

On June 28, 2018, a magnitude 6.8 earthquake occurred around the coast of Yamagata Prefecture. A seismic intensity of 6 or more was observed in Murakami City, Niigata Prefecture, and a seismic intensity of 6 or less was observed in Tsuruoka City, Yamagata Prefecture. Also, seismic intensity 5 was observed from Hokkaido to the central part of Japan. Around the epicenter, many houses were destroyed, along with landslides and liquefaction occurred. On the other hand, in recent years, surveys using UAV have been used at disaster sites. Also, aerial photographs from paragliders (Para-Motor, PM) allows for a wider range of surveys than UAV. In this study, aerial images of the affected areas were taken from UAV and paraglider at Koiwagawa and Nezugaseki in Tsuruoka City, which were damaged by the Yamagata-Oki earthquake. From the taken aerial images, a three-dimensional model was created, and the model was analyzed to extract damaged areas and mapped to GIS.

Keywords: Aerial image, GIS, Image analysis, Photogrammetry, Remote sensing, Image analysis

1. INTRODUCTION

On June 28, 2018, a magnitude 6.8 earthquake occurred on the coast of Yamagata Prefecture. In the vicinity of the epicenter, many houses were damaged, many people were injured, roads were depressed, and the landslides occurred. Tsuruoka City in Yamagata Prefecture is the top 10 largest area among all 1,741 municipalities of Japan. In such a wide disaster area, the distance from the city hall where the disaster response headquarters was established to the center of the damaged area is long way, so it is important how to grasp the disaster situation in the wide-area. Understanding the damage situation immediately after the disaster will lead to efficient initial responses.

In recent years, measurements and surveys using UAV have been used at disaster sites. By drawing a route for automatic navigation, aerial photographs with even side wrap and overlap are taken quickly in a short time. On the other hand, UAV is effective for certain limited objects such as bridges, but it is necessary to collect data over a wide area by flying for a long time in order to grasp the damage situation. In addition, incidents and accidents associated with the spread of UAVs are increasing, and the law strictly restricts UAV flight, and many other issues restrict an overall understanding of the disaster situation.

Therefore, in this study, the effectiveness of the motor paraglider is verified as a method of grasping the damage situation in a wide area. Table 1 shows a comparison for UAV and Para-Motor feature. A motor paraglider does not require a runway like an aircraft, and the takeoff and landing are available even on the flat ground with 30m to 40m length. Currently, motor paragliders can fly and take aerial images freely almost anywhere except for some prohibited areas such as around the airfield. Setting time to take-off is about 15 minutes, flight speed is about 35km / h, the noise is low same as 50cc motorbike. Moreover, flight in urban areas and residential areas is unrelated to noise. It is very low-cost, speedy, and can be surveyed in a wider range area than UAV.

In this study, by using UAV and Para-Motor (PM) at Koiwagawa and Nezugaseki in Tsuruoka City, damaged by the Yamagata-Oki earthquake, aerial images of the affected areas were taken to analyze the situations.

Table 1. A comparison for UAV and Para-Motor feature

	UAV	PM
Flight time	20 minutes	4 hours
Flight distance	4 km	10 km
Noise	-	Same as 50cc motorbike
License	Necessary depending on place	Necessary
Regulation by law	Civil Aeronautics Act	Nothing

2. METHOD

On July 1st and July 2nd, 2019, we deployed a UAV and a PM along the coast of Tsuruaoka and Nezugaseki where damages such as building collapses and landslides had occurred. Figure 1 shows the landslide points and the collapsed area of the buildings where aerial photographs were taken in this study. The red stars in Figure 1 show the place where the landslide occurred, and the yellow polygons are the areas where the collapse of the buildings occurred.

Figure 1. Disaster area in Tsuruoka

2.1. UAV

In order to grasp the damage situation of Nezugaseki, aerial images were obtained from UAV. A Phantom 4 Professional with a 4K camera was used as UAV. The flight altitude and lap rate were set up as uniform using the operation system *Litchi* which is automatic navigation application to construct 3D models with necessary figures. Figure 1 shows a route map of UAV by automatic navigation. The flight speed was 28 km / h and the flight time was 11 minutes.

2.2 Para-Motor (PM)

PM (Figure 3) was flied along coast of Tsuruoka city from the ground of Atsumi Junior High School by the route in Figure 4. The flight distance was 15.6km, the flight time was about 32 minutes. Aerial images were taken by *EOS 6D* at every second, the overlap was over 80%.

Figure 2. Automatic navigation map of UAV

Figure 3. Paramotor

Figure 4 Flight route of Paramotor

2.3 3D analysis

3D models were created by using PhotoScan in order to create the ortho photo combined from aerial images by UAV and PM.

2.4 Image analysis

In this study, it was focused on the threshold of RGB image to extract the damaged parts. All the damaged buildings were covered with blue sheets. For the RGB values of the blue sheets, blue has high reflection characteristics. Therefore, the pixels of the higher brightness of the blue threshold were extracted using raster calculation by ArcGIS. The brightness value of the blue color was set to 245 RGB values or more.

Also, it was focused on the reflection characteristics of the soil to extract landslide. The soil has high red reflection and low green reflection characteristics among RGB values. Therefore, landslides were extracted by subtracting Green from Red and showing the result with a value greater than 0 in the aerial images.

3. RESULTS

3. 1. 3D analysis

Figure 5 shows a 3D model of Nezugaseki created by aerial images from UAV. Figure 6 shows another 3D model of the area near Koiwagawa (coast of Tsuruoka-city) created by aerial images from PM. The 3D model acquired by UAV was combined with the entire shooting range, and a single orthoimage was created. The blue roof was applied to the blue part of the roof, and the building collapsed. The three-dimensional model is taken from the Para-Motor in Figure 6 is a combination of the shooting area on the south side from the Atsumi Junior High School at the takeoff point. Due to a large number of shots and the fact that the camera GPS was turned off, it was not possible to build the entire shooting area into a single orthoimage in this study.

3.2 Image analysis

Figure 7 shows the original images of building collapse and landslide used for image analysis. The image of the building was obtained from UAV, and the image of the sediment disaster was obtained from Para-Motor. Figure 8 shows the result of extracting the collapsed part of the building and the sediment disaster part from the RGB information by the GIS raster calculation committee. In the collapse of the building, the blue sheet area was extracted by focusing on the blue threshold. However, other parts with high blue thresholds, such as road white lines and white car bodies, have also been misrecognized. Figure 9 shows the same image extracted from the orthoimage constructed from the Nezugaseki 3D model. In Figure 9, in addition to the blue sheet, other parts having a high blue threshold were also extracted. Moreover, in the collapsed part of earth and sand fraud, it expressed with the spectrum in order with the low threshold among the extracted pixels. Focusing on the reflective properties of the soil, forest, and soil were distinguished by subtracting the green threshold from the red threshold.

Figure 5. 3D model of Nezugaseki

Figure 6. 3D model of are near Koiwagwa

Figure 7. Original images taken by UAV and Paramotor

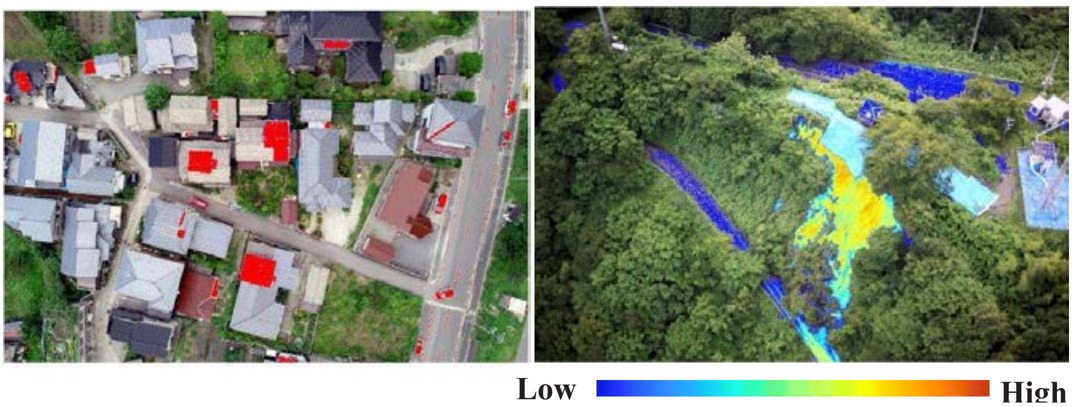

Figure 8. Extraction of damaged buildings and landslide

Figure 9. Extraction of damaged buildings by orthophoto

4. DISCUSSIONS

In both UAV and Para-Motor, it was possible to quickly obtain aerial images for grasping the situation at the disaster site. However, in UAV, from the viewpoint of battery capacity, the flight time was less than 20 minutes, at most about 30 minutes. Also, it is difficult to take an aerial shot at a distance of more than 1km from the operator from the viewpoint of laws and radio communication distance in Japan. However, Para-Motor was able to shoot at an altitude higher than UAV and a wide area over 10km. In the image analysis, the fossil is currently only the threshold value of the RGB image, so in the extraction of the collapsed part of the roof, in addition to the blue sheet, reactions such as cars and white lines with high blue threshold values were also seen.

5. CONCLUSION

In this study, the authors examined the effectiveness of UAV and Para-Motor with a real case of a disaster the Yamagata-Oki earthquake. UAV was able to take aerial photographs with a uniform lap rate by automatic navigation. On the other hand, a flight of less than 20 minutes and a radius of about several hundred meters was the limit. On that point, Para-Motor was able to fly for more than 30 minutes in this study. Depending on the type of engine, it is possible to fly for more than 4 hours. In the future, as a Para-Motor device, we plan to construct a sensor that can transmit disaster information in real time during aerial photography. Also, we will plan to build a mechanism that automatically estimates the damage status of a large area of images taken by a motor paraglider using AI.

ACKNOWLEDGMENT

The authors are grateful to HIROO NISHIMURA for operating and shooting of Para-Motor.

REFERENCES

K., Suzuki, and O. Kobayashi, 2007, Mechanism of Roll Control Response Characteristics in an Aircraft and a Paraglider, Transactions of the Japan Society for Aeronautical and Space Sciences, Vol. 55, No. 42, 337-343.

Mario A. R. E., Abrahim N., 2019, The uses of unmanned aerial vehicles –UAV's- (or drones) in social logistic: Natural disasters response and humanitarian relief aid, Procedia Computer Science, Volume 149, 375-383.

Leandro D. O. S., Renata A. D. M. B., Vânia B. G. C., 2017, The use of UAV and geographic information systems for facility location in a post-disaster scenario, Transportation Research Procedia, Volume 27, 1137-1145.

Study on Impacts of Parking on Congestion by Different Parking Management Systems

May Pyai Sone Win
ME (Transportation Engineering), Civil Engineering. Department
Yangon Technological University, Myanmar
Maypyisonewin1990@gmail.com

ABSTRACT

Parking demands daily increase especially in commercial zones within Yangon Central Business District (CBD). Along the CBD roads and streets, on-street parking types can be found mostly. The problems for parking users are long-rest parking, less parking information access, parking prices, scarce resources for new parking yard and loose rule and regulation. Consequence issues of on-street parking types are troubled on traffic congestion and road capacity in the streets. Therefore, to solve and reduce these issues, the parking management systems are required. The objective is to reduce the impacts of on-street parking in traffic stream.

The study area is selected to the most famous crowded market within CBD area called Thein Gyi Market. The market possesses on-street parking types and is complexed with many cargo trucks, shopping light-truck, cars and taxi on traffic stream the whole worked time and locates in the Shwedagon Pagoda; one of busiest roads of downtown. The data are collected with In-Out Survey for parking demand, measuring geometric characteristics of parking yards, questionnaires to shoppers, drivers and shop owners and cycle time in the selected signalized intersections for road capacity. Statistically analysis is made and then a relationship is derived between the parking management system and traffic capacity to reduce the impact of on-street parking on congestion.

The results of the study clearly indicate that the reduction in impact of on-street parking on congestion is greater when cargo trucks are restricted in on-street parking along the road with parking management systems. The study suggests possible reduction factors that can be used in road capacity estimations when on-street parking is allowed in an urban transport corridor. This study has potential to improve the parking management systems of on-street parking in CBD and then satisfy to the road users, shoppers and people annoying reduction due to traffic congestion.

Keywords: *on-street parking, traffic congestion, road capacity, land use, parking management systems*

1. INTRODUCTION

Parking is called the place to rest the vehicles at the time of intervals, the whole night, the whole day and so on. The drivers always stop the vehicles at the parking to go to their origins or destinations. Parking is one of the major problems that are created by the increasing road traffic. It is an impact of transport development. The availability of less space in urban areas has increased the demand for parking space especially in Central Business District. This affects the mode choice and also has a great economic impact. For solving the parking problems, parking

management includes as an important role. Parking management means the strategies like reducing the requirements of parking, making the effective use of existing parking, improving parking facilities, searching new parking resources, identifying the parking policies and rules for the government and so on.
The selected study area, Thein Gyi Market used to congest along the Shwedagon road due to on-street parking especially in peak hours. The Shwedagon road is the six lanes undivided one-way road and on-street parking takes half of the road lanes according to the data collection. This on-street parking type is 90 degree parking.

2. LITERATURE REVIEW

This section provides a brief literature review of land use and parking management strategy and its relation to traffic congestion.

2.1 Parking Concepts and Land Use

Parking facilities and programs are of considerable importance in traffic engineering. Most persons to urban and regional commercial centers are accessed primarily by cars. The viability of these areas depends on the availability of convenient parking facilities adjacent to or easily accessible to desired destinations, especially off-street parking facilities. Parking studies are parking demand, average peak period parking demand, peak period of parking demand, total parking demand, parking capacity, parking volume, parking supply analysis and parking duration. The commercial land use provides opportunities for a broad range of retail and service commercial and professional office as well as regional shopping demand.

2.2 Parking management strategy

Parking provision represents a major financial overhead, in terms of the additional land required, construction as well as its on-going maintenance and management. Restricted parking zoning management system is used and the traffic regulation order fails to define what a "restricted street" is and it does not prescribe that it is a contravention to park in a restricted street during prescribed hours.

3. METHODOLOGY

The figure illustrates the methodological flow chart for the study.

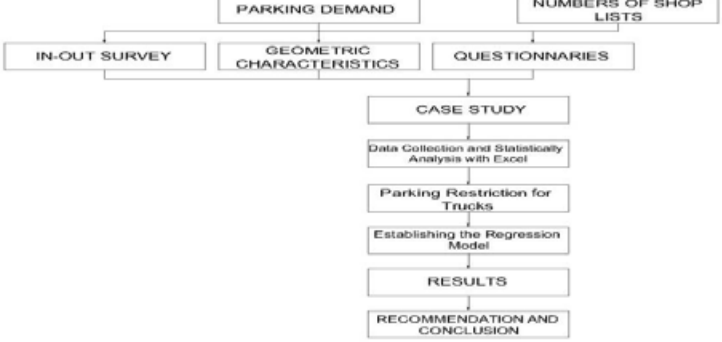

3.1 In-out Survey

In this survey, the occupancy count in the selected parking lot is taken at the beginning. Then, the number of vehicles that enter the parking lot for a particular time interval is counted. The number of vehicles that leave the parking lot is also taken. The final occupancy in the parking lot is also taken. Here the labor required is very less. Only one person may be enough. But we won't get any data regarding the time duration for which a particular vehicle used that parking lot. Parking duration and turnover is not obtained. Hence we cannot estimate the parking fare from this survey. For quick survey purposes, a fixed period sampling can also be done. This is almost similar to in-out survey. All vehicles are counted at the beginning of the survey. Then after a fixed time interval that may vary between 15 minutes to i hour, the count is again taken. Here there are chances of missing the number of vehicles that were parked for a short duration.

3.1.1 Key observation

The observations and findings of the in-out survey which assisted in the development of the survey methodology have been discussed in this section. The parking zones and major land uses present were initially documented prior to undertaking the survey, to ensure all movements related to parking were accounted.

4. Objectives and Problem statement

The main objective is to reduce the impact of on-street parking in traffic stream. The specific objectives are

- To reduce queue lengths of vehicles in a period of traffic signals in selected junctions
- To reduce the times of parking-waiting by stopping in traffic streams
- To reduce the inefficient use of existing parking.

The problem statements are

- Inadequate parking spaces
- Need for various acceptable parking management systems
- Scarce resources for new parking yard constructions and
- Loose rules and regulations.

5. ILLUSTRATIONS

41.2.2 Off street parking

In many urban centers, some areas are exclusively allotted for parking which will be at some distance away from the main stream of traffic. Such a parking is referred to as off-street

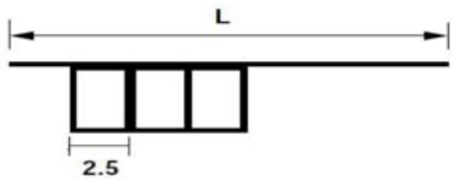

Figure 41:5: Illustration of 90° parking

Dr. Tom V. Mathew, IIT Bombay 41.3 February 19, 2014

5.1 Layout of illustrations

Regression Statistics	
Multiple R	0.68688
R Square	0.471804
Adjusted R Square	0.452597
Standard Error	2.709376
Observations	115

ANOVA

	df	SS	MS	F	gnificance F
Regression	4	721.269	180.3173	24.56399	1.53E-14
Residual	110	807.4788	7.340717		
Total	114	1528.748			

	Coefficients	andard Err	t Stat	P-value	Lower 95%	Upper 95%	ower 95.0%	Ipper 95.0%
Intercept	10.5895	1.339371	7.906318	2.22E-12	7.935177	13.24382	7.935177	13.24382
Arrival Time	-0.18889	0.10831	-1.74402	0.083948	-0.40354	0.02575	-0.40354	0.02575
Trip Purpose	-2.40547	0.342069	-7.03212	1.81E-10	-3.08337	-1.72757	-3.08337	-1.72757
Parking fees	0.155738	0.296	0.526141	0.599849	-0.43087	0.742342	-0.43087	0.742342
Type of vehicles	0.522934	0.36302	1.440508	0.152564	-0.19649	1.242355	-0.19649	1.242355

7. UNITS AND SYMBOLS

Y = Parking duration (hours)
X_1 = Arrival Time (hours)
X_2 = Trip Purpose
X_3 = Parking fees
X_4 = Types of vehicles

7.1 Equations

$$Y = 10.589 - 0.189X_1 - 2.405X_2 + 0.156X_3 + 0.523X_4 + 2.709 \quad (1)$$

Y = Parking duration
X_1 = Arrival Time
X_2 = Trip Purpose
X_3 = Parking fees
X_4 = Types of vehicles

REFERENCES

ON-STREET PARKING ON STATE ROADS; VIRGINIA P. SISIOPIKU, Ph.D.
Chapter-41. Parking Studies; Transportation Systems Engineering
Chapter-37. Capacity and LOS Analysis of a Signalized I/S; Transportation Systems Engineering
Chapter-34. Design Principles of Traffic Signal ; Transportation Systems Engineering

Chapter-4: Traffic Engineering Studies; Traffic and Highway Engineering, Fourth Edition, Nicholas J. Garber and Lester A. Hoel
Chapter-11: Parking: Studies, Characteristics, Facilities, and Programs; Traffic Engineering, Third Edition, Roger P. Roess, Elena S. Prassas, William R. McShane
Chapter-4: Traffic Engineering Studies; Traffic and Highway Engineering, Fourth Edition, Nicholas J. Garber and Lester A. Hoel
Impacts of On-street Parking on Road Capacity; http://www.atrf.info/papers/2015/files/ATRF2015_Resubmission_141.pdf

Economic Analysis of Highway Improvement

(Case Study: Yangon-Bago Highway)

Moe Thet Thet Aye[1], **Kyaing**[2]

[1] *Ph.D Candidate at Transportation Engineering, Department of Civil Engineering, Yangon Technological University, Yangon, Myanmar,*

[2] *Associate Professor, Department of Civil Engineering, Yangon Technological University, Yangon, Myanmar,*

Keywords: *Transportation, Economic Analysis, Cost, Benefit, B/C ratio, Net Present Value (NPV)*

1. INTRODUCTION

Economic analysis of highway is a multi-disciplinary activity involving highway engineers, economists and statisticians. Construction and maintenance of highways are financed by the government or authorized company, whereas the highway user is the general public. Costs go to the government or authorized company and the benefits go to the public. It is not concerned with the sources of financing, but only with an analysis of the costs and benefits to the road-user and the consequences to all sections of the society of a scheme, and establishing its economic viability. It is also essentially a study for the future and therefore, the analysis should estimate the future traffic, costs and benefits.

2. DATA COLLECTION

Nowadays, the Yangon-Bago Highway Road of 32 miles and 6 furlongs (52.7 km) is responsible with BOT system by Max Highway Company Limited. Therefore, traffic volume data and financial status of this highway are collected from this company.

3. BENEFIT-COST (B/C) RATIO METHOD

There are a number of variations of this method, but a simple procedure is to discount all costs and benefits to their present worth and calculate the ratio of the benefits to costs. Benefits are positive flows, while costs are negative flows. Thus, the savings in transport costs are considered as benefits. If the benefit-cost ratio is more than one, the project is worth undertaking. The advantage of the B/C ratio method is its simplicity; hence, it is widely used by highway engineers.

4. MAINTENANCE AND TRANSPORTATION COSTS

The cost of road maintenance is a function of pavement condition, the rate of deterioration and the maintenance standard applied by a road agency. Transportation costs comprise the costs of vehicle operation and travel time.

5. TRAFFIC GROWTH STUDY

Based on the traffic volume data between 2015 and 2018, the 3-year growth factor between 2015 and 2018 would be 1.749. Assuming linear growth in the future, the annual growth rate would be (1.749–1.0) /3 = 0.249, or 24.9% on this highway

Table 1. Maintenance Costs of Yangon-Bago Highway (Year 2015-2018)

Year	**Maintenance Costs (kyats million)**
2015-2016	3200.3
2016-2017	3143.8
2017-2018	1061.6
Total	7405.7

Table 2. Collected Toll Fees (kyats million) for Yangon-Bago Highway (Year 2018)

	Htauk Kyant Toll	Bago Toll
2018	5098.078	6110.8028

Table 3. Vehicle Operating Cost (VOC)

2018	To Bago	To Yangon
Annual Cost (kyats)	9,748,101,505	7,469,981,801
Total Annual Cost (kyats)	17,218,083,306	

All financial costs are converted into economic costs by applying a Standard Conversion Factor (SCF) of 0.85

From this analysis,

- Net Present Value (NPV) = 9527,548,680 kyats
- Benefit-Cost Ratio (BCR) = 1.63 %
- The rate of return considered desirable for transport infrastructure projects = 12 %.

6. CONCLUSIONS

The results of economic appraisal in most cases will show that the economic returns from road maintenance far exceed those from investments in new road construction. In countries where the road condition is generally good but with high volumes of traffic, economic appraisal will generally show that investments in capacity improvement will generate higher economic returns.

REFERENCES

[1] Henry Kerali. Economic Appraisal of Road Projects in Countries with Developing and Transition Economies. July 2003.

STUDY ON CHANNEL MIGRATION ASSESSMENT IN BRIDGE AREAS ALONG AYRYARWADY RIVER

MYINT MYAT OO[1], CHO CHO THIN KYI[2], and WIN WIN ZIN[3]

[1] Staff Officer, DUHD, Ministry of Construction, Nay Pyi Taw, Myanmar,
[2] Associate Professor, Civil Engineering Department, Yangon Technological University, Yangon, Myanmar,
[3] Associate Professor, Civil Engineering Department, Yangon Technological University, Yangon, Myanmar,

***Keywords**: Channel Migration, Bridge Sustainability, Erosion-Deposition, Remote Sensing, Satellite Imagery*

1. INTRODUCTION

Rivers and streams are self-regulatory in that they adjust their forms in response to environmental changes which may occur naturally or sometimes may be results of human activities. Both activities distort the natural quasi-equilibrium of a channel [1]. It is vital to monitor the migration of channel which can provide the important information for analysis of river morphology. River monitoring can also be recognized as a key issue for river management and training [2]. Recent developments in remote sensing technologies opened up unprecedented capabilities to perform high quality monitoring program for a wide range of environmental fields including river systems [3]. The goal of this study is to assist the bridge monitoring works by means of remote sensing and GIS techniques which are currently undertaking by Ministry of Construction with conventional techniques.

2. STUDY AREA

The Ayeyarwady River is the most important commercial waterway and the backbone of the country. It is originated from the confluence of Maikha and Malikha Rivers and flows relatively straight North to South before emptying through the Ayeyarwady Delta into the Andaman Sea. The total length of Ayeyarwady River is about 2,210 km and 15 bridges along the Ayeyarwady river according to Ministry of Construction. But Maubin Bridge and Daydaye Bridge are excluded from the study because both bridges and not located on the main channel of the Ayeyarwady River. All of Ayeyarwady bridges are constructed as steel truss bridges with concrete pier foundation. The lengths of bridges are ranged between 750 m and 4120 m.

3. METHODS AND MATERIALS

The data set of Landsat Imagery is obtained from the US Geological Survey (USGS) Global Visualization Viewer including the archives of Landsat 5 Thematic Mapper (TM), Landsat 7 Enhanced Thematic Mapper Plus (ETM+), and Landsat 8 Operational Land Imager acquired between 1987 and 2017. For the processing and analysis of satellite imagery, Google Earth Engine is used. In order to detect the changes of the channel between 1987 and 2017, the surface water of the river in each temporal image was extracted individually.

4. RESULTS AND DISCUSSION

The study period of my research is between 1987 and 2017. According to the study, the bridges along the Ayeyarwady River can be divided into three main groups, bridges in low, moderate and high migration areas respectively. Bridges located in the upper Ayeyarwady are fronting with the low channel migration, while bridges located in central Ayeyarwady and delta area are facing with the threats of high channel migration as shown in Table 1. Although most of the bridges are located on the least channel migration point of each bridge site, some of the bridge sites are not meet the criteria required for the best site for the bridge, for example, (i) Bo Myat Tun Bridge, (ii) Ayeyarwady Bridge (Nyaungdon), (iii) Ayeyarwady Bridge (Pakokku), and (iv) Ayeyarwady Bridge (Tigyaing). Among these bridges, Bo Myat Tun Bridge is a bridge which faced the obvious amount of threat from channel migration during the study period in which the channel near the Bo Myat Tun Bridge has the tendency of shifting to the right by means of erosion at the right bank and deposition at the left bank which is the major threat to bridge sustainability.

Table 1. Channel Migration of Ayeyarwady Bridges

Bridge	Migration	Location
Bala Min Htin Bridge	Moderate	Upper
AYY Bridge (Sinkhan)	Low	Upper
AYY Bridge (Tigyaing)	Moderate	Upper
Yadana Thinga Bridge	Moderate	Upper
AYY Bridge (Yadanabon)	High	Central
Innwa Bridge (Sagaing)	High	Central
AYY Bridge (Pakkoku)	HIgh	Central
Anawrahtar Bridge	High	Central
AYY Bridge (Magway)	High	Central
AYY Bridge (Malun)	Low	Central
Nawaday Bridge	High	Central
AYY Bridge (Nyaungdon)	High	Delta
Bo Myat Tun Bridge	High	Delta

5. CONCLUSION

In this study, the channel migration in bridges areas along Ayeyarwady River can easily be identified throughout the study period by using remote sensing and GIS techniques. Most of the high channel migration areas are found in delta and central Ayeyarwady. The channel migration in each bridge is subjected to various causes. This study is carried out based on the 30-m resolution Landsat imagery dataset and there will be better result for river monitoring if finer satellite images are available.

REFERENCES

[1] D. Rosgen, H.L. Silvey, Applied River Morphology, 2nd Edition, Wildland Hydrology, Colorado, 1996.
[2] R. Koech, P. Langet, L. Kumar, Monitoring River Channel Dynamics Using Remote Sensing and GIS Techniques, Geomorphology, Volume 325 (2018) 92-102.
[3] M.G. Tulbure, M. Broich, S.V. Stehman, A. Kommareddy, Surface water Extent Dynamics from Three Decades of Seasonally Continuous Landsat Time Series at Subcontinental Scale, Remote Sens. Environ, 2016.

IMPROVING HISTORICAL REANALYSIS DATASET FOR HYDROLOGICAL MODELLING BY INTEGRATING LIMITED OBSERVED DATA AND BIAS CORRECTION

S.S. BHAGABATI[1], A. KAWASAKI[2] and M. OGAWA[3]

[1] *Project Researcher, Department of Civil Engineering, The University of Tokyo, Tokyo, Japan,*
[2] *Project Professor, Department of Civil Engineering, The University of Tokyo, Tokyo, Japan,*
[3]*Associate Professor, International Education Center, Kanazawa University, Kanazawa, Japan*
Correspond to S.S.BHAGABATI (seemanta@hydra.t.u-tokyo.ac.jp)

Keywords*: Nineteenth century, historical analysis, bias correction*

1. INTRODUCTION

Droughts are natural disasters that affect agriculture, flora and fauna, natural resources as well as disrupt human livelihood. Globally they affect millions of people annually and over a million people had died as a result of droughts since 1974 [1]. Droughts are quite common natural disaster in India, with one drought in every three years in some part of India [2]. The biggest and most severe drought happened in the year 1876, claiming over 5 million lives, the effects of which lasted until the year 1878. It was termed as the "Great Famine".

2. METHODOLOGY

Although there has been some statistical analysis of the Great Famine, spatial analysis including the extent and severity has not been conducted. The primary reason being the lack of observed datasets in the Nineteenth century (as advanced hydrological models require multitude of datasets).

In recent years, multiple reanalysis datasets have been released which provides a continuous global gridded dataset for many different meteorological and hydrological parameters. Although, the availability of such data for the Nineteenth century is very limited. One such dataset which contains these datasets is the NOAA-CIRES Twentieth Century Reanalysis (V2c) (https://www.esrl.noaa.gov/psd/data/gridded/data.20thC_ReanV2c.html). It contains data for 1851-2012.

But upon conducting quality check for the recent years (unable to conduct quality check for earlier years due to lack of available/base data), by using JRA55 (https://jra.kishou.go.jp/JRA-55/index_en.html) as base data, it was found that it contains large bias.

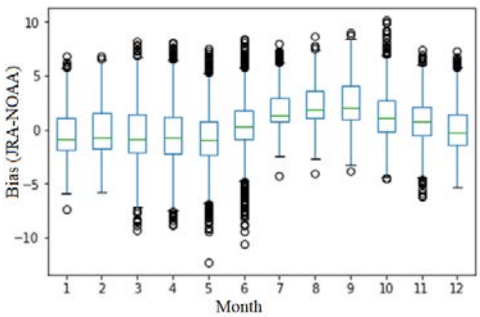

Figure 1. Box plot of bias of a location for 1991-2014

Fig 1 shows the box plot of the overall monthly bias for a location over for the time period 1991-2014. Upon further checking it was found that bias both temporal and spatial i.e., it has different characteristics of bias for different locations and time periods (figure 2)

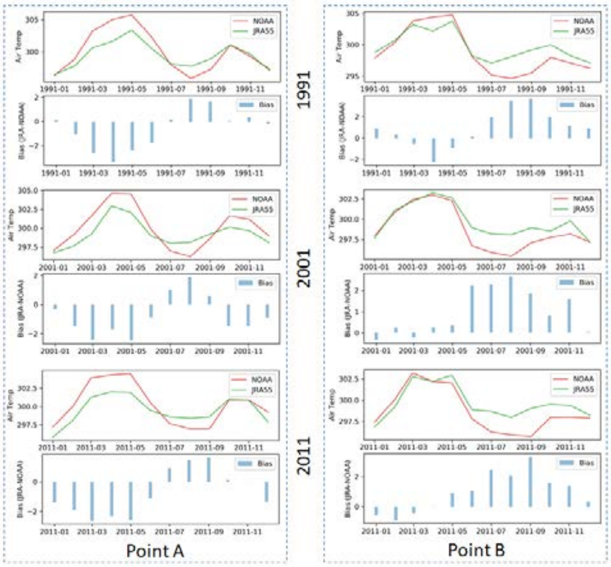

Figure 2. Comparison of spatial bias of two locations in the south-western India for the years 1991, 2001 and 2011.

3. CONCLUSIONS

In this research we are trying to bias correct a historical reanalysis dataset in order to use it to conduct advanced hydrological simulations, thereby reconstructing the Great Famine in the Indian sub-continent. So far, we have identified the characteristics of the different biases for the different grids over the Krishna River basin located in the western India. Next step is to develop an approach to use the current biases as a reference point to correct the NOAA dataset for nineteenth century. This is currently a work in progress.

REFERENCES

[1] United nations (UN): Trends in Sustainable Development 2008–2009. United Nations publication, United Nations Division for Sustainable Development (2008)

[2] M.K. Goyal, V. Gupta, S. Eslamian. Hydrological Drought: Water Surface and Duration Curve Indices. Handbook of Drought and Water Scarcity: Principles of Drought and Water Scarcity, 2017

Study on code of practices for quality control, health and safety management in construction industry

Htet Wai Yee Aung[1]
[1]Master of Science in Engineering, Construction Management,
Civil Engineering Department, Yangon Technological University,
Myanmar
htetwaiyee@gmail.com

ABSTRACT

Nowadays, Myanmar construction industry has developed in recent years but still need to improve the quality control, health and safety management in construction industry. Therefore, this paper mainly focuses on the study of the code of practices for the quality control and health and safety management in construction industry, Yangon, Myanmar. Firstly, field observation and questionnaires survey are carried out to know the existing quality control, health and safety management in some construction projects. After that the code of practices for quality control, health and safety management for the selected case study Reinforced Concrete Building project are prepared by using checklists. This paper provides the checklists for substructure, superstructure and finishing works in accordance with the approved code of practices such as Myanmar National Building Code and other international codes of practice such as American Society for Testing Materials, American Concrete Institute for quality control checklists, Work Health and Safety Code of Practice 2015 – Safe Work Australia and Occupational Health and Safety and Working Conditions 2019 for health and safety checklists. The findings of the study showed that some quality problems are occurred in construction projects that can damage the end user safety and lack of health and safety management can cause accidents or injuries for employees in project site. Similar dimensions and outcomes make it feasible to combine quality and safety management into a single high-performance system. As a result, the health and safety management can enhance the quality control system. From construction management point of view, time and cost can be saving and quality can be improved by combining the quality control and health and safety management as a single high performance system.

Key works: questionnaires survey, code of practices, quality control, health & safety management

1. INTRODUCTION

Quality control and safety management are increasingly important in construction industry. Quality Control is the part of quality management system focused on fulfilling quality requirements, whereas quality assurance is the part focused on providing confidence that quality requirements will be fulfilled. The Quality Management System (QMS) in construction industry refers to quality policy, planning, implementation, measure and evaluation, management reviews and continual improvement. Quality control is critically important to a successful construction project and should be adhered. Inspection during construction will prevent costly repairs after the project is completed [1]. A good quality control system can also be ensured the workplace safely. Thus the safety workplace gives the great quality from construction management view. From safety perspective – Workplace Health and Safety Management is prepared for the Occupational Health and Safety, Environmental Impact Assessment, preventive or mitigation measures are prepared for the Environmental Safety, Quality Assurance and Quality Control are prepared for the End user

Safety. In health and safety management systems – policy, organizing, planning, measuring, audits and review are concerned [2].

2. AIMS AND OBJECTIVE

(1) To understand the importance of quality control system and safety management in construction industry
(2) To know the code of practices which are widely used in Myanmar construction industry
(3) To improve the quality control and health and safety management that are based on code of practices.

3. EXISTING CONDITIONS OF QUALITY CONTROL, HEALTH AND SAFETY MANAGEMENT

There are nine selected case study projects which are situated in Yangon, Myanmar. All projects are constructed by local contractors. The case study projects are shown in table 1.

Table 1: Summary of case study projects

No	Company	Storey	Type	Location
1	Project 1	4-Storey	RC	Bahan Tp.
2	Project 2	4-Storey	Steel	East Dagon Tp.
3	Project 3	4-Storey	RC	Insein Tp.
4	Project 4	4-Storey	Steel	East Dagon Tp.
5	Project 5	3.5-Storey	RC	Thilawa Thanlyin Tp.
6	Project 6	4-Storey	Steel	East Dagon Tp.
7	Project 7	5-Storey	RC	Thanlyin Tp.
8	Project 8	4-Storey	Steel	East Dagon Tp.
9	Project 9	4-Storey	Steel	East Dagon Tp.

The observations of quality control and health and safety management for the selected case study projects are presented as follows: The questionnaire survey and results for quality data, survey results based on checklists for quality control in case study projects are presented. The questionnaire survey and results for health and safety management, survey results for accidents in case study projects are also presented in the following.

3.1 Questionnaire Survey and Results for Quality Control in Case Study Projects

There are two types of respondents participated in the questionnaire survey. They are workers and engineers. The respondent rate is 35% of workers and 65% of site engineers respectively.

3.1.1 Visual survey in case study projects

According to the visual survey, some of the quality defects were occurred in case study projects such as the honeycombs occurred in the wall, the concrete cracking occurred at apron and drain and the partition is damaged because of the poor quality are described in the following figures.

(a) (b) (c) (d) (e)

Figure 1: (a, b, c) Wall honey comb, (d) Concrete cracking at apron and drain, (e) Poor quality in partition

3.1.2 Surveyed Results for Quality Control in Case Study Projects

The quality data including policy, plan, procedure, checklists, inspection, testing and maintenance are surveyed from project 1, 2, 3, 4, 5, 6, 7, 8 and 9. The percentage of quality data in policy is 44.44, the percentage of plan is 44.44, the percentage of procedure is 44.44, the percentage of checklists is 56.56, the percentage of inspection is 66.67, the percentage of testing is 66.67 and the percentage of maintenance is 44.44. The surveyed data for citation projects are described in Table 2.

Table 2: Surveyed data for quality in case study projects

No	Company	Storey	Type	Quality Data						
				Policy	Plan	Proced -ure	Check list	Inspec -tion	Testing	Mainte -nance
1	Project 1	4-Storey	RC	✓	✓	✓	✓	✓	✓	✓
2	Project 2	4-Storey	Steel	✗	✗	✗	✓	✓	✓	✗
3	Project 3	4-Storey	RC	✓	✓	✓	✓	✓	✓	✓
4	Project 4	4-Storey	Steel	✗	✗	✗	✗	✓	✓	✗
5	Project 5	3.5Storey	RC	✓	✓	✓	✓	✓	✓	✓
6	Project 6	4-Storey	Steel	✗	✗	✗	✗	✗	✗	✗
7	Project 7	5-Storey	RC	✓	✓	✓	✓	✓	✓	✓
8	Project 8	4-Storey	Steel	✗	✗	✗	✗	✗	✗	✗
9	Project 9	4-Storey	Steel	✗	✗	✗	✗	✗	✗	✗
	Percentage of Quality Data			44.44	44.44	44.44	55.56	66.67	66.67	44.44

✓ YES ✗ NO

The project 1, 3, 5 and 7 are 100 % in quality data including inspection, testing, checklists, policy, plan, procedure and maintenance. The project 2 is about 42.86 % and the project 4 is about 28.57%. The project 6, 8 and 9 are zero percentage in quality data. The surveyed results for case study projects are described in Table 3.

Table 3: Surveyed results for the case study projects

No	Company	Storey	Type	Quality Data							%
				Policy	Plan	Proce-dure	Check-list	Inspect-ion	Test-ing	Maint-enance	
1	Project - 1,3,5,7	4-Storey	RC								100
2	Project-2	4-Storey	Steel								42.86
3	Project-4	4-Storey	Steel								28.57
4	Project-6,8,9	4-Storey	Steel								0

YES NO

3.1.3 Surveyed Results for Quality Control Based on Checklists in Case Study Projects

The checklists are also used to investigate the quality control in case study projects. The checklist for surveying and setting out, checklist for earthwork, checklist for backfilling, checklist for formwork and reinforcement, checklist for brick and block masonry, checklist for flooring, checklist for external and partition wall, checklist for plastering, checklist for painting, checklist for interior ceiling and checklist for fabrication work are used to determine the existing condition of quality control in case study projects. The surveyed results for quality control in case study projects are described in figure 2.

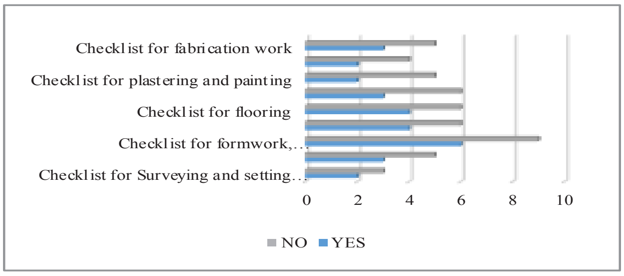

Figure 2: Surveyed results for quality control using checklists

According to the surveyed results from figure 2, most of the work activities are not complied with the prepared checklists and the checklists are not based on the code of practices. Therefore, as a result, the quality has damaged for these projects and the end user safety can be damaged.

3.2 Questionnaire Survey and Results for Health and Safety Management in Case Study Projects

There are two types of respondents participated in the questionnaire survey. They are workers and site engineers. The respondent rate is 96% of workers and 4% of site engineers respectively.

3.2.1 Surveyed Results for Safety

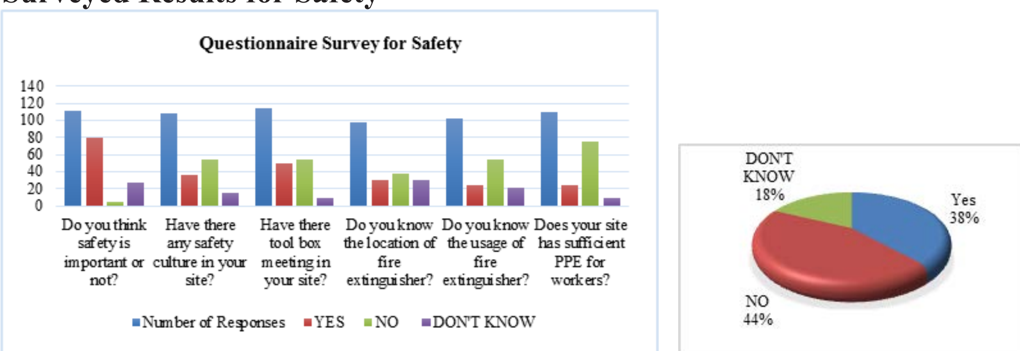

(a) (b)

Figure 3: (a, b) Questionnaire survey for safety

According to the surveyed results for safety from figure 3, the answers “NO” and “DON’T KNOW” from the respondents had more percentage than the answers who said “YES”. There have no safety culture and tool box meeting. Besides, the workers did not know exactly the location and usage of fire extinguisher. There have no sufficient personal protective equipment for workers. Only 38% of respondents said that their site provided about safety and about 44% of respondents said that their site did not provide safety. About 18 % of respondents said that they did not know about safety as shown in figure 3.

3.2.2 Surveyed Results for Health

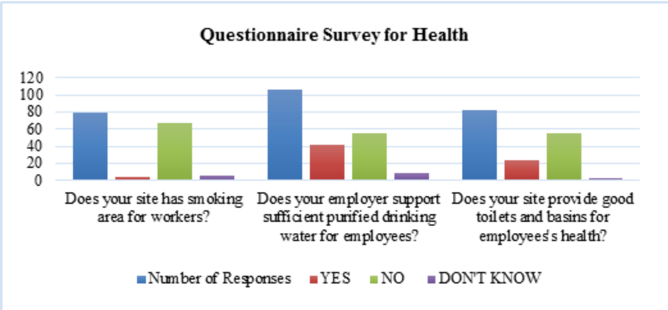

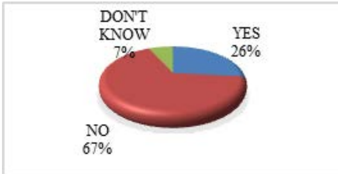

(a) (b)

Figure 4: (a, b) Questionnaire survey for health

According to the survey results for health from figure 4, there have no smoking area for workers, no sufficient purified drinking water and good toilets and basins for employees. Only 26% of respondents said that their site provided about health and about 67% of respondents said that their site did not provide about health and safety. About 7 % of respondents said that they did not know about health and safety as shown in figure 4.

3.2.3 Surveyed Results for Welfare

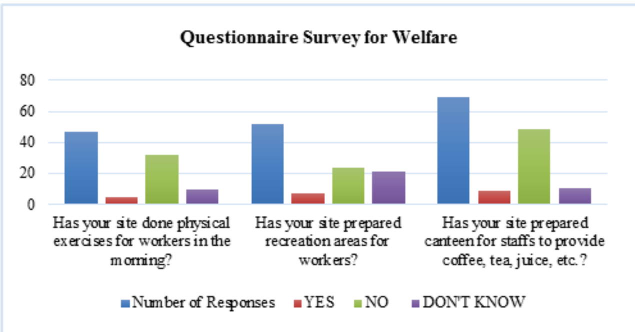

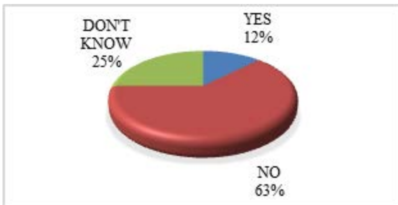

(a) (b)

Figure 5: (a, b) Questionnaire survey for welfare

According to the survey results for welfare from figure 5, there have no physical exercises and no canteens for workers. The welfare facilities are poorly prepared in the proposed site. Only 12% of respondents said that their site provided about welfare and about 63% of respondents said that their site did not provide about welfare. About 18 % of respondents said that they did not know about welfare as shown in figure 5.

3.2.4 Surveyed Results for Accidents in Case Study Projects

The accidents were found in case study project because there have no good health and safety management and without any remedial actions when causing the accidents. Some accidents such as falls from height, struck by a moving vehicle, struck by falling objects, rebar impalement hazard, scaffolding collapse, transportation accidents, slips, trips and falls, chemical burns and dermatitis from wet concrete were occurred. These surveyed results are described in figure 6.

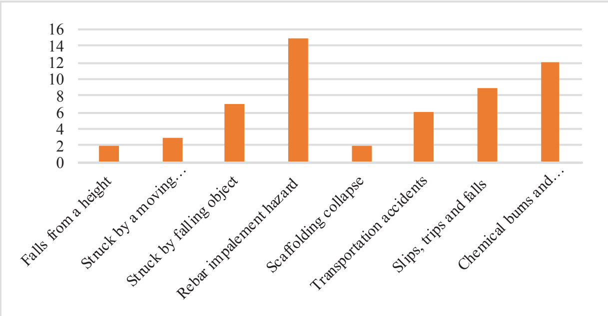

Figure 6: Surveyed results for accidents in case study project

4. IMPROVEMRNT OF QUALITY CONTROL, HEALTH AND SAFETY MANAGEMENT

The checklists for quality control and health and safety are prepared including substructure, superstructure and finishing of the selected case study project because inspection checklist forms are critical quality control tools for the entire construction industry. Then, health and safety management can enhance the quality control system. Besides, the checklists for quality control and health and safety are also based on the code of practices in order to improve the quality of construction projects and reduce quality deficiencies and some accidents in construction projects.

4.1 Case Study Project

The selected case study project is 4 stories RC residential building and located in Mingalardon Township, Yangon. In order to improve the quality control and health and safety management in this case study project, the quality control checklists and health and safety checklists for substructure, superstructure and finishing are prepared. These prepared checklists are also based on the code of practices such as Myanmar National Building Code and other international code of practices.

4.2 Preparation of Checklists for Substructure, Superstructure and Finishing

The checklist for surveying and excavation, the checklist for backfilling, the checklist for retaining wall, the checklist for rebar installation, the checklist for concreting work and the checklist for formwork are prepared for the substructure of the case study project that are described in table 4. The Checklist for Rebar installation (before, during, after), the Checklist for Formwork (before, during, after), the Checklist for Concreting (before, during, after) and the checklist for brick work are prepared for the superstructure of the case study project that are described in table 5. The Checklist for Roofing, Checklist for ceiling work, Checklist for Plastering, Checklist for Painting, Checklist for Electrical Installation Work, Checklist for Plumbing & Sanitary are also prepared for the finishing of the case study project that are described in Table 6. The quality control checklists are based on Myanmar National Building

Code, American Society for Testing and Materials and American Concrete Institute. The health and safety checklists are also based on the Myanmar National Building Code, Work Health and Safety Code of Practice 2015 (Safe Work Australia) and Occupational Safety, Health and Working Conditions, 2019.

Table 4: Preparation of checklists for substructure

Item	Checklist's Name	Code of Practices for Quality Control	Code of Practices for Health and Safety
SUB-STRUCTURE	1)Checklist for surveying and excavation	-Myanmar National Building Code, 2016 -American Society for Testing and Materials -American Concrete Institute	-Work Health and Safety Code of Practice 2015 (Safe Work Australia) -Occupational Safety, Health and Working Conditions, 2019
	2)Checklist for backfilling		
	3)Checklist for retaining wall		
	4)Checklist for rebar installation (before, during, after)		
	5)Checklist for concreting work (before, during, after)		
	6)Checklist for formwork (before, during, after)		

Table 5: Preparation of checklists for superstructure

Item	Checklist's Name	Code of Practices for Quality Control	Code of Practices for Health and Safety
SUPER-STRUCTURE	1)Checklist for Rebar installation (before, during, after)	-Myanmar National Building Code, 2016 -American Society for Testing and Materials -American Concrete Institute	-Work Health and Safety Code of Practice 2015 (Safe Work Australia) -Occupational Safety, Health and Working Conditions, 2019
	2)Checklist for Concreting (before, during, after)		
	3)Checklist for formwork (before, during, after)		
	4)Checklist for brick work		

Table 6: Preparation of checklists for finishing

Item	Checklist's Name	Code of Practices for Quality Control	Code of Practices for Health and Safety
FINISHING	1)Checklist for Roofing	-Myanmar National Building Code, 2016 -American Society for Testing and Materials -American Concrete Institute	-Work Health and Safety Code of Practice 2015 (Safe Work Australia) -Occupational Safety, Health and Working Conditions, 2019
	2)Checklist for ceiling work		
	3)Checklist for Plastering		
	4)Checklist for Painting		
	5)Checklist for Electrical Installation Work		
	6)Checklist for Plumbing & Sanitary		

5. CONCLUSION

From the Construction Management point of view – Time, Cost and Quality are the key elements. These key elements are also related to each other. From the time perspective – there have no frequent repair, reconstruction and maintenance for the defects because of the good quality control system. The time also saving because safety management can enhance the quality control system and can prevent the accidents and injuries of workers. From the cost perspective– the good quality control and health and safety management can reduce the cost overruns because there have no deficiencies or weakness about quality and no accidents or injuries to employee about health and safety. From the quality perspective – the project can achieve target quality goal within the target time and specified budget with safe environment for the employees throughout the whole project. By preparing the quality control checklists and health and safety checklists based on MNBC and other international code of practices can provide the good quality control and health and safety management for the construction industry. Besides, the checklists can be used in Myanmar construction industry because these checklists are based on Myanmar National Building Code that is intended to use for construction works in Myanmar.

ACKNOWLEDGMENT

The author would like to thank all of his teachers in Civil Engineering Department for their supporting, encouragement, useful suggestions, invaluable guidance and help till the completion of this journal.

REFERENCES

[1] Anon. “Project Management for Construction, Chapter (13) Quality Control and Safety during Construction” <http://www.cmu.edu>cee>PM book>.

[2] Phil Hughes and ED ferrette, “Introduction to “Introduction to Health and Safety in construction”, Fourth edition.

[3] Myanmar National Building Code, 2016.

[4] ASTM International, <https://www.astm.org>wiki>

[5]ACI Standard Adoption – American Concrete Institute, https://www.concrete.org>standard.

[6] Mr. Santash kumar Gangwar, 2019. “Occupational Health and Safety and Working Conditions.”

[7] Citation Case Study Projects from Ma Hsu Wutyee Htun, “Analyzing and Critical Thinking of Quality Problems for Construction Projects in Myanmar”.

DEVELOPMENT OF CUBIC SOIL CHAMBER FITTED WITH MULTI-DIRECTIONAL DISK TRANSDUCERS

Y. KAWAGUCHI[1], M. OTSUBO[2] and R. KUWANO[3]

[1] *Graduate Student, Institute of Industrial Science, The University of Tokyo, Japan,*
[2] *Research Associate, Institute of Industrial Science, The University of Tokyo, Japan,*
[3] *Professor, ICUS, Institute of Industrial Science, The University of Tokyo, Japan,*
Correspond to Y.KAWAGUCHI (y-kawa@iis.u-tokyo.ac.jp)

Keywords: *Elastic Wave Velocity, Model Experiment, Disk Transducer, Intrinsic Anisotropy, Dynamic Measurement*

1. BACKGROUND

It is empirically known that the soil stiffnesses in the vertical and horizontal directions are not identical. However, accurate measurement of multi-directional stiffness is difficult; thus, the mechanism of the stiffness anisotropy has not been fully understood. In many cases, naturally existing ground has inherent anisotropy depending on particle shape and deposition direction [1, 2]. Understanding fundamentals of the stiffness anisotropy enables accurate prediction of ground deformation, which contributes to reliable design of geotechnical structures.

2. SOIL CHAMBER

Aiming to develop a test device to evaluate the inherent anisotropy of the soil stiffness accurately, a cubic soil box equipped with disk-shaped piezoceramic transducers [3] in the three orthogonal directions was manufactured. Tested materials were air-dried Toyoura sand and glass beads, having the same median particle size of 0.24 mm and 0.20 mm but with different sphericity. Glass bead is spherical but Toyoura sand has oval shapes. The model ground was divided into 10 layers, and the dry material was compacted in each layer. An overburden load of 2 kPa was added vertically while the horizontal defamation was restricted, i.e. K_0 stress state. S- and P-wave signals in x, y and z axes were measured for each material.

3. COMPARISON OF S-WAVE VELOCITY

Focusing on the three types of shear wave components, S_{HH}, S_{HV}, S_{VH} (the first and second subscripts stand for the directions of propagation and oscillation), $V_{S,HH}$ for the glass bead sample is the largest, whereas $V_{S,HH}$ for the Toyoura sand sample is the lowest. This agrees with the observation in the field measurement that natural materials tend to exhibit a largest $V_{S,HH}$ amongst the three types [1]. Moreover, V_S is generally greater in the Toyoura sand sample than that in the glass bead sample in all axes although the density is larger for the glass bead sample. This may be due to effects of particle rigidity, the number of contact points between particles, particle shape.

4. CONCLUSIONS

This study investigated the inherent anisotropy of elastic wave velocity. The results revealed that non-spherical particles such as Toyoura sand exhibit a larger elastic wave velocity that propagates and oscillates along the horizontal plane although the horizontal stress is lower than the vertical stress.

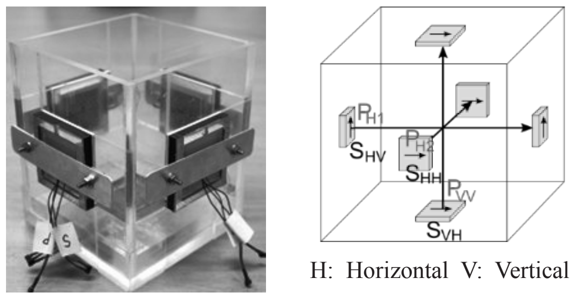

Figure 1. Soil chamber and direction of wave propagation

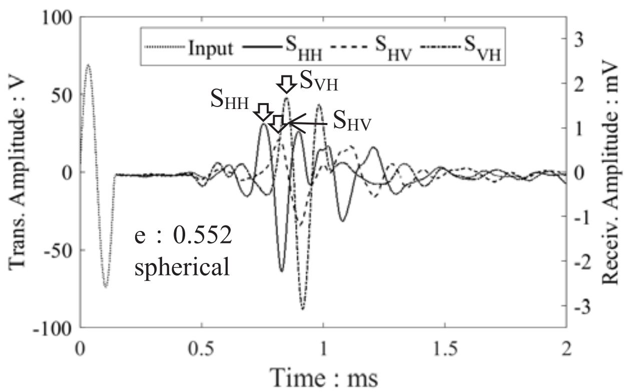

Figure 2. S-wave propagation in glass bead sample

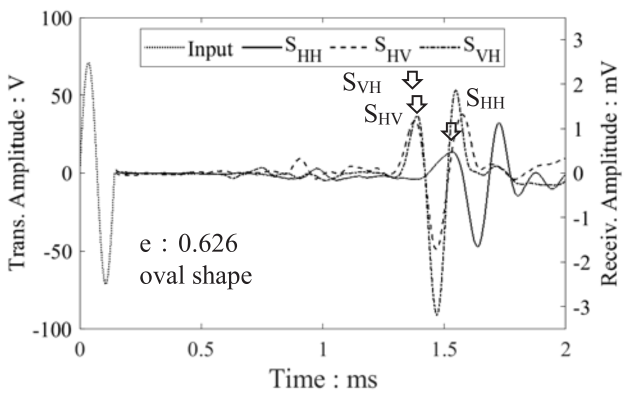

Figure 3. S-wave propagation in Toyoura sand sample

REFERENCES

[1] Clayton, C.R.I. (2011) Stiffness at small strain: research and practice. *Géotechnique*, 61(1), 5–37.
[2] Santamarina, J.C. & Cascante, G. (1996). Stress anisotropy and wave propagation: a micromechanical view. *Can. Geotech. Journal*, 33(5), 770–782.
[3] Suwal, L.P. & Kuwano, R. (2013) Disk shaped piezo-ceramic transducer for P and S wave measurement in a laboratory soil specimen. *Soils and Foundations*, 53(4), 510–524.

FORMATION AND EXPANSION OF SUBSURFACE CAVITY AND ITS POTENTIAL RISK OF COLLAPSINGR

R. KUWANO[1], **Y. OHARA**[2], **and N. KOMINAMI**[2]

[1] Professor, ICUS, Institute of Industrial Science, The University of Tokyo, Tokyo, Japan,
[2] Former Graduate Student, Dept. of Civil Engineering, The University of Tokyo, Tokyo, Japan,
Correspond to Prof. Kuwano (kuwano@iis.u-tokyo.ac.jp)

Keywords: *Sinkhole, Subsurface cavity, Ground cave-in*

1. INTRODUCTION

A sinkhole or ground cave-in is usually initiated by the formation of cavity in the ground due to soil loss. When the location of the cavity is deep in the ground, the detection of the cavity is not easy. Then it is possible that the hidden cavity expands to eventually cause sudden collapse. In this study, characteristics of formation/expansion of cavity and surrounding ground loosening were investigated by a series of model tests, aiming at evaluating potential risk of surface ground collapse.

2. MODEL TEST OBSERVATION

Two-dimensional as well as three-dimensional cavity formation tests were conducted using rectangular and cylindrical soil chambers having a small opening at the base. Uniform clean sands were used for tested materials. Water was supplied from either center or side of the soil chambers and soil with water was drained from the bottom opening. Test apparatus are shown in Figure 1.

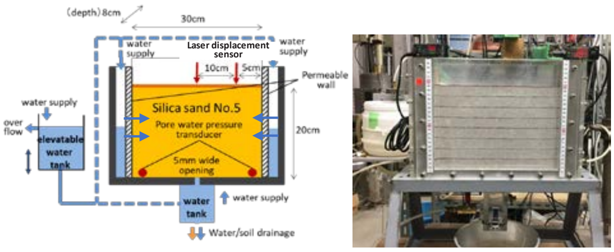

a) a rectangular soil chamber for two-dimensional tests

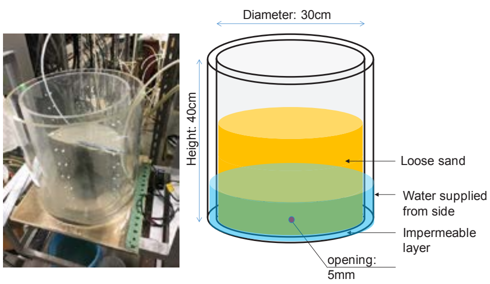

b) cylindrical soil chamber for three-dimensional tests

Figure 1. Test apparatus for cavity formation tests

A typical pattern of cavity formation and expansion from two dimensional tests are shown in Figure 2. When water drains quickly, a chimney-like narrow cavity formed. The ceiling of the cavity was around the same height of ground water level. If water stays in the cavity, fan-shape cavity develops and the width of cavity became larger. The cover soil lost its stability when the width of cavity grew too large.

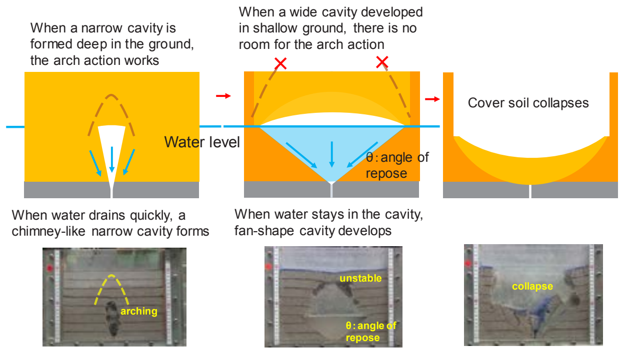

Figure 2. Cavity expansion process observed in two dimensional tests

Figure 3 shows cavity formation in three-dimensional tests. All cavities were chimney shape consisting of different diameters. Lower part had larger diameter, which seemed to be influenced by the water level.

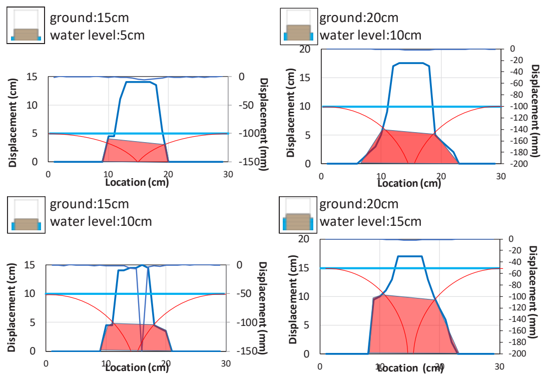

Figure 3. Cavity formation observed in three dimensional tests

3. CONCLUSIONS

The result of two and three dimensional cavity tests implied that the process of cavity formation can be divided into two part, the first part influenced by ground water level and the latter part affected by soil property. Approximate depths of the cavity ceiling can be estimated by the ground water level and the risk of collapse can be roughly evaluated by the ratio of depth of cavity ceiling and cavity width.

SHAKING TABLE TESTS ON EFFECT OF REINFORCEMENT STIFFNESS

ON SEISMIC STABILITY OF GEOGRID REINFORCED SOIL WALLS

J. KUWANO[1], and A.A. AJUDA[2]

[1] *Professor, Department of Civil and Environmental Engineering, Saitama University, Saitama, Japan,*
[2] *PhD student, Department of Civil and Environmental Engineering, Saitama University, Saitama, Japan,*
Correspond to Prof. J. KUWANO (jkuwano@mail.saitama-u.ac.jp)

Keywords: *geogrid, shaking table test, retaining wall, stiffness arrangement*

1. INTRODUCTION

Few studies are available for cases with multiple reinforcement stiffness values along the wall. This study attempts to investigate the effect of reducing the reinforcement stiffness value along the wall height in different manners under seismic load by means of shaking table test using a sinusoidal wave with a predominant frequency of 5 Hz.

2. TEST OUTLINE

Geogrid reinforced soil wall models were constructed in rigid container. 8 wall segments were placed on top of each other and no additional connection was made between the panels. One geogrid was connected to each pane. Length and stiffness of geogrid were changed. Wall 1: all 300 mm stiff geogrids, Wall 2: all 200 mm geogrids, Wall 3: 300 mm and 200 mm stiff geogrids alternatively, Wall 4: 200 mm stiff and soft alternatively, Wall 5: Top 4 stiff and bottom 4 soft 200 mm geogrids, and Wall 6: Top 4 soft and bottom 4 stiff 200 mm geogrids. The backfill and soil foundation were constructed using dry Toyoura sand to achieve the desired relative density of 90%.

3. EFFECT OF STIFFNESS ARRANGEMENT

Figure 2 shows the relationships of top displacement and base acceleration, and the shear strain for the tested walls. It is noted that wall with stiff uniform reinforcement (Wall 2) have more stability. However, by substituting half of the stiff geogrid with soft geogrid in an alternating manner (Wall 4), the wall showed almost the same amount of displacement as Wall 2. By grouping the soft reinforcement either in the upper (Wall 5) or lower part (Wall 6) of the wall, the walls showed an increase in horizontal displacement and bulging phenomena at mid-height around critical stages. The shear strain was dependent on the geogrid stiffness arrangement. The lowest values of shear strain were observed for wall with stiff geogrid (Wall 2) followed by wall with alternating stiffness (Wall 4), while, walls with grouped schemes (Walls 5 and 6) showed larger values of shear strain, suggesting the backfill movement was more compared to Wall 2. The failure surface observed in shaking table test (blue line) and obtained in two-wedge analysis (red line) are shown in the figure. The failure surfaces of the walls with different geogrid stiffness arrangements were almost same as the wall with uniform stiffness geogrids.

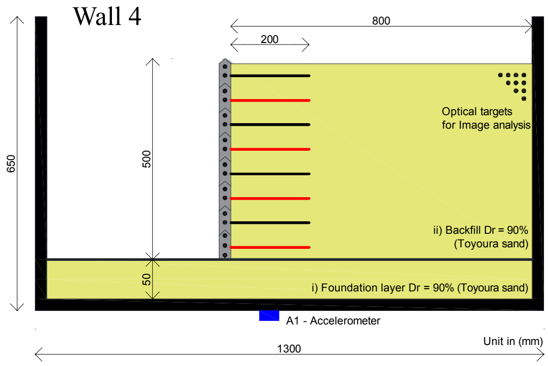

Figure 1. Test model (e.g rigid and soft alternatively)

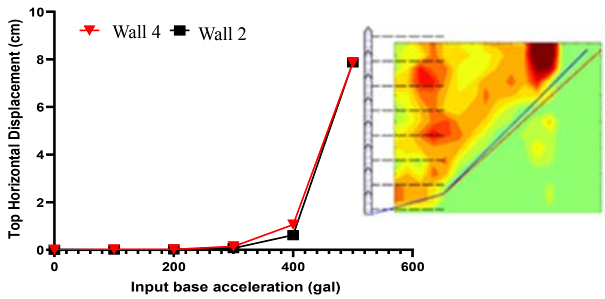

Figure 2. Top displacement and base accel. (Walls 4 &2)

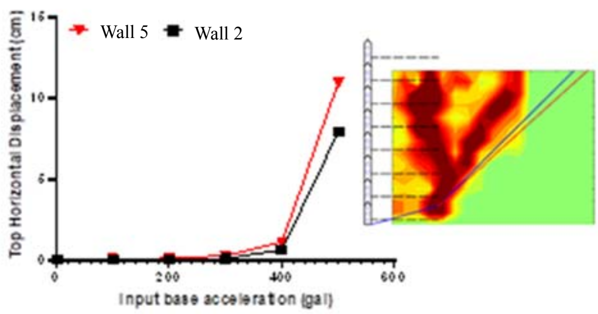

Figure 3. Top displacement and base accel. (Walls 5&2)

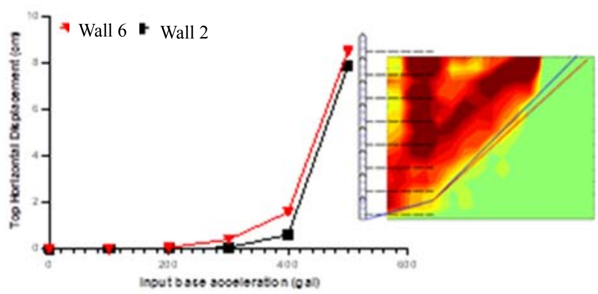

Figure 3. Top displacement and base accel. (Walls 6&2)

SESSION H

SPECIAL SESSION: SATREPS/ WATER RESOURCES, DISASTER MITIGATION AND URBAN PLANNNING

CLIMATE CHANGE SCENARIOS IN MYANMAR USING MRI-AGCM3.2S MODEL

W.W. ZIN[1]

[1] *Professor, Department of Civil Engineering, Yangon Technological University, Yangon, Myanmar, Correspond to Prof. Win Win Zin (winwinzin@gmail.com)*

Keywords: *Climate change, MRI-AGCM3.2S, Myanmar*

1. INTRODUCTION

Myanmar ranked second out of 183 countries most affected by extreme weather events between 1995 and 2014 in the Global Climate Risk Index [1]. Climate change threatens to compound the frequency and intensity of these events and, more importantly, to alter the conditions to which human and natural systems have adapted over millennia [2]. Myanmar is now facing the impacts of climate change, which threaten to undermine our development prospects and exacerbate the vulnerability of our communities. With projected changes in precipitation and temperature, considerable efforts would be required to prepare the Myanmar in dealing with the impacts of climate change on the different climate-sensitive sectors.

In the present study, MRI-AGCM3.2S was used to simulate both the present-day climate (1981-2005) and projected climate for near future (2020-2044) and far future (2075-99) under the IPCC A1B scenario. MRI-AGCM3.2S is developed by the Meteorological Research Institute (MRI) and Japan Meteorological Agency (JMA). In this research, 84 stations are considered to calculate the rainfall percentage departure of Myanmar. 43 stations are considered to calculate the temperature change of Myanmar.

2. RESULTS AND DISCUSSION

The bias-correction was performed using two different techniques: linear scaling and lumped quantile mapping. Bias correction is capable of improving the GCM-simulated outputs to a certain degree. When only few stations are located within the region, these data sets do not capture the realistic distribution in this large area. In that case, it is difficult to obtain actual distribution from very limited number of observation. It is seen that lumped quantile mapping method is better than linear scaling method. Performance of bias correction was quantified by coefficient of determination (R^2) and root mean square error (RMSE). It was seen that the projected precipitation will increase in 2030s and 2080s under A1B scenario. Average annual precipitation change in future (2075-2099) relative to 1981-2005 base period is shown in Figure 1.

3. CONCLUSIONS

The present and future average rainfall of Myanmar was observed to fluctuate, but have shown an increasing trend.

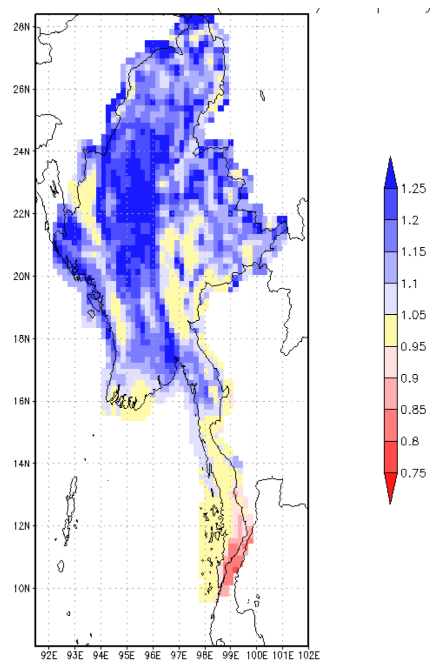

Figure 1. Average Annual Precipitation Change in Future (2075-2099) Relative to 1981-2005 Base Period

For future climate in 2030s and 2080s, outputs of the simulations under the A1B scenario are presented. The key findings are:

- Annual maximum temperatures are expected to rise by 0.2 °C to 1.6 °C in 2030s;
- Annual maximum temperatures are expected to rise by 0.7 °C to 3.6 °C in 2080s;
- In every region of Myanmar, rainfall is expected to increase by the middle and end of century

REFERENCES

[1] Kreft, S., Eckstein, D., Junghans, L., Kerestan, C., and Hagen, U. Global Climate Risk Index 2015: Who Suffers Most From Extreme Weather Events? Weather-Related Loss Events in 2013 and 1994 to 2013. In: G. K. Joanne Chapman-Rose, Daniela Baum (Ed.), Berlin, Germany: Germanwatch, 2014,pp. 32.

[2]. Horton, R., De Mel, M., Peters, D., Lesk, C., Bartlett, R., Helsingen, H., Bader, D., Capizzi, P., Martin, S. and Rosenzweig, C. Assessing Climate Risk in Myanmar. New York, NY, USA: Center for Climate Systems Research at Columbia University, WWF-US and WWF-Myanmar, 2016.

Development of flood inundation map using HEC-HMS and HEC-RAS

Wai Toe[1], Win Win Zin[2], Zin Mar Lar Tin San[3], and Akiyuki KAWASAKI[4]
[1] Master Student, Department of Civil Engineering, Yangon Technological University, Myanmar
waitoe.water7@gmail.com
[2] Professor, Department of Civil Engineering, Yangon Technological University, Myanmar
winwinzin@gmail.com
[3] Professor, Department of Civil Engineering, Yangon Technological University, Myanmar
zinmarlar@gmail.com
[4] Professor, Department of Civil Engineering, The University of Tokyo, Japan

ABSTRACT

Flood is a common natural disaster that causes damages to life and property and also effects the development of a country. 41990 people from Bago Township, 40 percent of the total population, were struck by Bago Riverine Flood in 2018. The flood inundation maps are developed using the Hydrologic Engineering Center – Hydrologic Modeling System (HEC-HMS) and Hydrologic Engineering Center – River Analysis System (HEC-RAS) models. Firstly, flood events from 2014 to 2018 were selected for calibration and validation of the rainfall-runoff correlation in the hydrologic modeling system. Furthermore, different return periods were also considered in the rainfall-runoff analysis. The steady flows with different return periods such as 10-year, 50-year, 100-year with the effect of Zaung Tu Dam were considered in the river analysis modeling system to evaluate the flooded depth. In addition, river cross-sections and High-Resolution Digital Elevation Model (DEM) were used to develop flood inundation maps using the 2D HEC-RAS model. The developed 2018 flood inundation map was compared with the 2018 flood inundation map extracted from the Synthetic Aperture Radar (SAR) image. Applications of the approach presented in this study lead to flood mitigation using different scenarios and approaches.
Keywords: Bago River, HEC-HMS, HEC-RAS, flood, rainfall-runoff analysis

1. INTRODUCTION

Floods are the most common natural disaster that can be occurred around the world. It causes significant damage to human life, infrastructures, social, health, and economy. A natural disaster such as flood obstruct the development of a country and it becomes no surprise that flood mitigation and flood risk reduction has become the most important consideration in many countries around the world. Some researcher say that Myanmar is the second most natural disaster-prone country in the world and also the most 15th country in the world which are struck by the floods due to climate change. In Myanmar, heavy storm rainfall from southwest monsoons causes many flooding from July to October. Flooding in the central plain and coastal areas caused by the heavy rainfall in the mountainous region mostly north, east and west sides of the country. Myanmar's climate is influenced by the circulation of India Monsoon and the central dry zone and the Ayeyarwady delta are facing extreme events such as extreme drought and extreme floods. In July 2015, eleven states and regions among fourteen states and regions in Myanmar were struck by seasonal monsoon flood, Kachin state, Chin state, Shan state, Rakhine state, Mon state, Kayin state, Sagaing region, Magway region, Mandalay region, Ayeyarwady region, Bago region, Yangon region. Among them, the worst four flooding areas, Magway region, Sagaing region, Chin state, and Rakhine state were declared by the Myanmar Government as a natural disaster zone. According to the Relief and Resettlement Department (RRD), the number of people between 67000 and 110000 throughout the whole country was affected by the 2015 monsoon flood and 125 people were killed by the flood. Ministry of Agriculture reported that 687200 acres of farmland have been inundated and damaged by the flood. 2015 monsoon floods in Myanmar caused by the tropical cyclone Komen and it impacted not only social but also economic of the country.

Just recently 2018, the Magway region, the Bago region, the Tanitharyi region, Kayin state, Mon state were hit by the 2018 monsoon flood. About 150000 people have been displaced by 2018 monsoon floods and at least 16 people had died as stated by the Department of Disaster Management (DDM). Although about 122000 people still displaced at 263 evacuation sites, some of them have returned to their homes from evacuation sites. The Union Government also led to a response in cooperation with the State and Regional Government and also with the help of international and national organizations such as the UN, NGOs and civil society. 71,898 people have evacuated their homes during the 2018 monsoon flood in the Bago region. In other areas, 25083 people in Kayin state, 18421 people in Mon State and 6583 people in Tanintharyi Region displaced to their home. There were also about six fatalities in Mon state and five fatalities in Tanintharyi Region.

Bago Region is the most affected region in the 2018 heavy monsoon flood and this region suffers the risk of flood year after year. According to historical flood records in the Bago region, the 2018 monsoon flood is the most severe flood within 53 years. The recorded water level of Bago City near Bago Bridge exceeded the danger water level (880 cm) and reached up to 936 cm on 29th July 2018. It was the highest record since 1966 and it kept on 6 days above the danger water level. Most of the floods in the Bago region occur in July and August of a year, that means monsoon floods mostly occur. In 2011, the heavy flood with the water level of 959 cm occurred in the Bago region and it damaged many agricultural lands. The flood record in 2014 was 936 cm hit the Bago Region with the loss of paddy fields. And another high flood occurred at the end of July 2018 and according to the Department of Disaster Management (DDM), 41990 of people displaced their home as a result of the flood. Moreover, A lot of agriculture land was damaged by the 2018 monsoon flood. Although structure countermeasures were constructed to mitigate the risk of floods at the upstream of Bago River Basin, suitable flood management and flood protection systems are needed to analyze.

In view of the above and severity of the damages and fatalities caused by extreme flood events, it is requisite to establish the near real-time flood protection techniques. There is no doubt that the flood hazard map is basic to analyze flood protection systems and flood risk management. Moreover, it can reduce the impacts of the flood on the likelihood and/or the impact of flood risk based on scientific research and findings. The mapping of the flood hazard integrates with the schemes of flood prevention, protection, preparedness, emergency response, risk reduction, and risk management. More importantly, the flood model can also be used to create hazard maps that indicate the levels of inundation due to rainfall events of varying recurrence intervals. In this research, the flood inundation map of the Bago River Basin was developed by coupling HEC-HMS (Hydrologic Engineering Center Hydrologic Modelling System) and HEC-RAS (Hydrologic Engineering Center - River Analysis System) with the geographical information system. And the flood hazard maps are developed with different scenarios to mitigate the risk of Bago riverine flood. Flood modeling to develop flood hazard maps includes the transformation of rainfall into a runoff hydrograph throughout a watershed and/or the transformation of runoff into an overland flow that is performed hydraulically. Modeling of flood applies to understand, assess and predict the flood risk on the human society and natural system. Additionally, it can generate the flood hazard maps which indicates the levels of inundation, consequently, a timely warning can be issued to the people in the affected area.

The general purpose of this research is to develop the flood inundation map by realizing the solutions which can mitigate the risk of flooding in the Bago River Basin. This goal is performed by addressing the following modeling systems; (1) hydrologic modeling system by using HEC-HMS in rainfall-runoff-inundation processes of the river basin and HEC-GeoHMS extension in ArcGIS to delineate the watershed from DEM; (2) hydraulic modeling system by using HEC-RAS for the river analysis system of the study area and HEC-GeoRAS in ArcGIS for the preprocessing and postprocessing of flood inundation map developing; (3) compare the flood inundation maps developed in (2) with the ones developed using SAR image for the same area. These all objectives are carried out by the high-resolution digital elevation model (DEM), surveyed cross-section data, meteorological and hydrological data from DMH, DHPI, and IWUMD.

2. STUDY AREA AND DATA ANALYSIS

2.1 Study Area

The hydrologic model and hydraulic model were applied to the study area; the Bago River Basin is listed in figure 1. Bago river originates from the Bago Yoma which is a range of upland between the Ayeyarwady river and Sittaung river. The river flows through Bago and Yangon regions and combines with Yangon river (Myitmaka river) and Pazundaung creek and then enters the Gulf of Mottama. The Bago River Basin approximately locates between 17° 13' 37.511" and 18° 25' 46.434" of North latitude and 95° 54' 36.623" and 96° 30' 45.228" of East longitude in Bago region, Myanmar. It has a drainage area of 2725 km2. It covers a majority of Bago Region especially 74 percent of the total catchment area in Bago District and 26 percent of the total catchment in Thar Yar Wady District. Bago river is used predominantly for the purpose hydropower generation by DHPI at the upstream of river and the other reservoirs Kodukwe, Salu, Shwe Laung, Mazin and Zalukhtaw reservoirs located at the upstream of Bago river's tributaries (Mazin and Zalukhtaw reservoirs are at the downstream). Most of the reservoir was constructed for the purpose of flood protection and irrigation in 2012. But the floods still occur many times. Figure 1 shows the location map of the study area and rainfall – water level stations in the Bago River Basin. The basin is composed by the mountainous region at the upstream of river and the low land areas at the downstream.

The length of Bago river from Zaung Tu Hydropower Dam to Zaung Tu Weir is about 90.38 km, the river starts from the downstream of Zaung Tu Dam and then flows freely. The length of the river from Zaung Tu Weir to Bago Bridge is about 33.08 km and the length from Bago Bridge up to Tarwa Gate is about 15.61 km long. Most of the river front areas are replaced by farm lands and residential areas. According to the information based on the year 2015 land-used-land-cover map derived from SERVIR Mekong Land Cover Portal, the Bago River Basin is composed of 0.3 % of built-up areas, 40 % of mixed Evergreen and deciduous, 23 % of Evergreen Broadleaf and 15% of crop land, 1.8 % of Rice Paddy Field and other types of land covers. Built-up areas and Agricultural lands are mostly located in the floodplains of Bago River and the Bago city is at the downstream of Bago River. Figure 2 lays out the land use map from SERVIR Mekong Land Cover Portal in (a), the soil map in (b) and the high-resolution digital elevation model in (c).

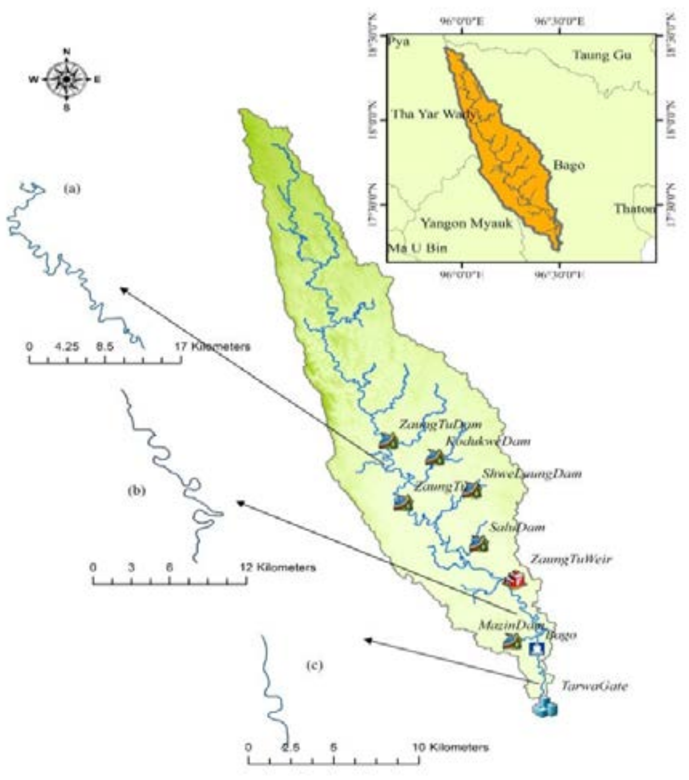

The hydrologic soil texture of Bago River Basin are Group C and Group D which constitute 81.03% of the total area followed by HSG Group C and 18.97% of the total area by HSG Group D. The four Hydrologic Soils Groups are A, B, C and D where soil group D has the greatest runoff potential. Group C soils are sandy clay loam. They have low infiltration rates when thoroughly wetted and consist chiefly of soils with a layer that impedes the downward movement of water and soils with moderately fine to fine structure. Clay, clay loam, silty clay, silty clay loam and sandy clay consist in the hydrologic soil group D. This HSG has the highest runoff potential and they have very low infiltration rates when thoroughly wetted and consist chiefly of clay soils with a high swelling potential and a permanent high-water table, moreover soil which is at or near the surface and over nearly impervious material.

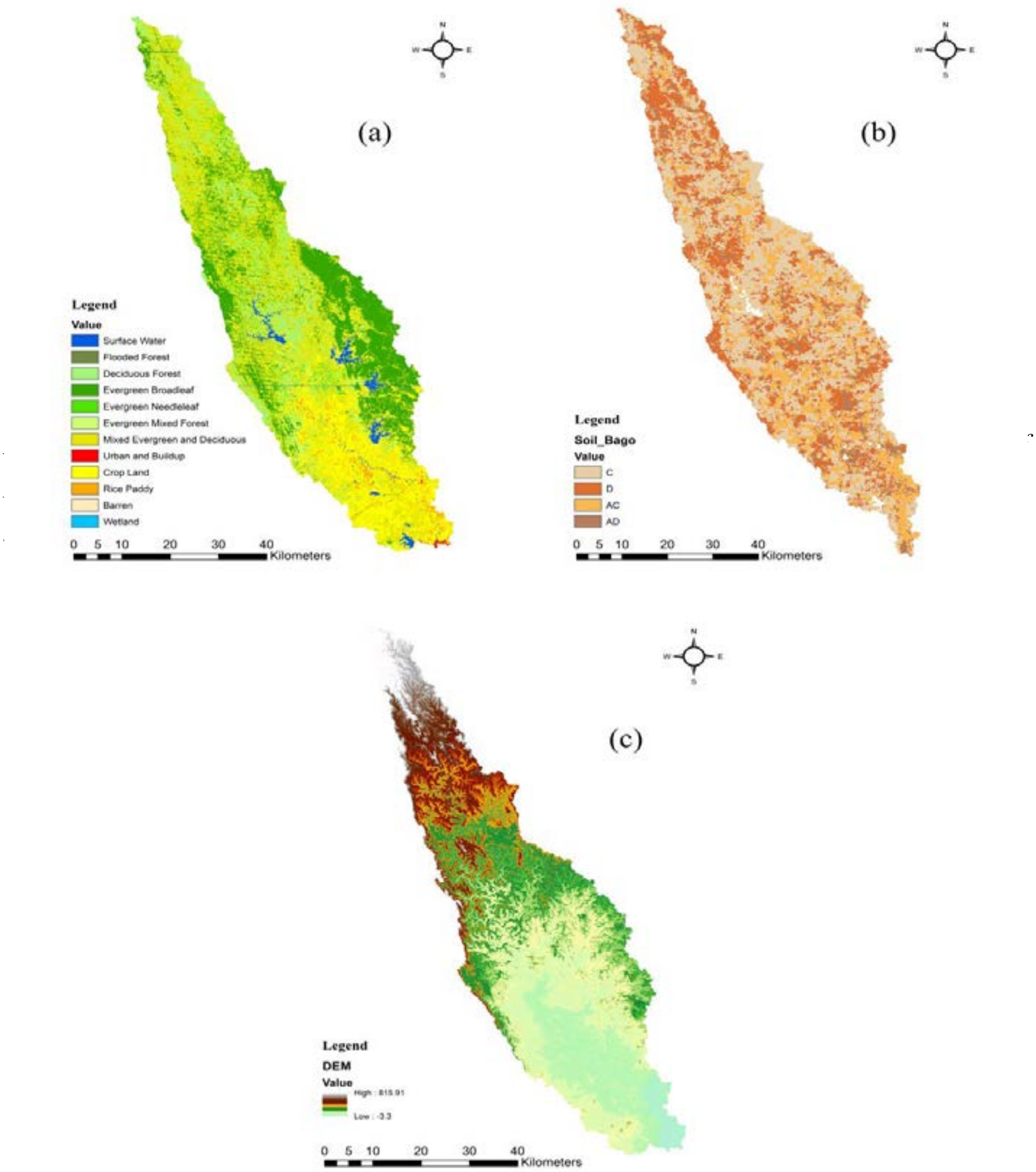

Figure 1. (a) land use map from SERVIR Mekong Land Cover Portal, (b) the soil map of Bago River Basin and (c) the high-resolution digital elevation model (Source: from Seemanta Bhagabati).

2.2. Data Analysis

The calibration and validation of the model based on the available data set from the Department of Meteorology and Hydrology (DMH), Department of Hydropower

Implementation (DHPI), Department of Irrigation and Water Utilization Management (IWUMD) and Irrigation Department (ID). The surveyed cross-sections data for the river analysis system were supported by Satreps Project. There are two rainfalls and water level stations from DMH, one station at Bago Bridge and one state at Zaung Tu village and only daily rainfall data and water levels are available. But the water level from Zaung Tu village is inappropriate to apply in this research. Furthermore, Daily rainfall data from dam sites are also available. Although the specific data for example hourly data or near real-time data should be used for flood modeling, detailed information cannot apply by the lack of certain data availability in the study area. The average rainfall and water level of the Bago river basin for calibrated and validated flood events are listed in figure 3. The red line shown in the figure is the danger water level. The danger water level of Bago River is 880 cm at Bago Bridge but some area is inundated before the river water level close to the danger level. In these flood events, the water level of 2014, 2015 and 2018 events was above the danger water level. The cumulative rainfall from 1967 to 2018 are in figure 4, the trend of the chart goes up slightly. But the cumulative rainfall will be less and less due to climate change, although the maximum rainfall occurred.

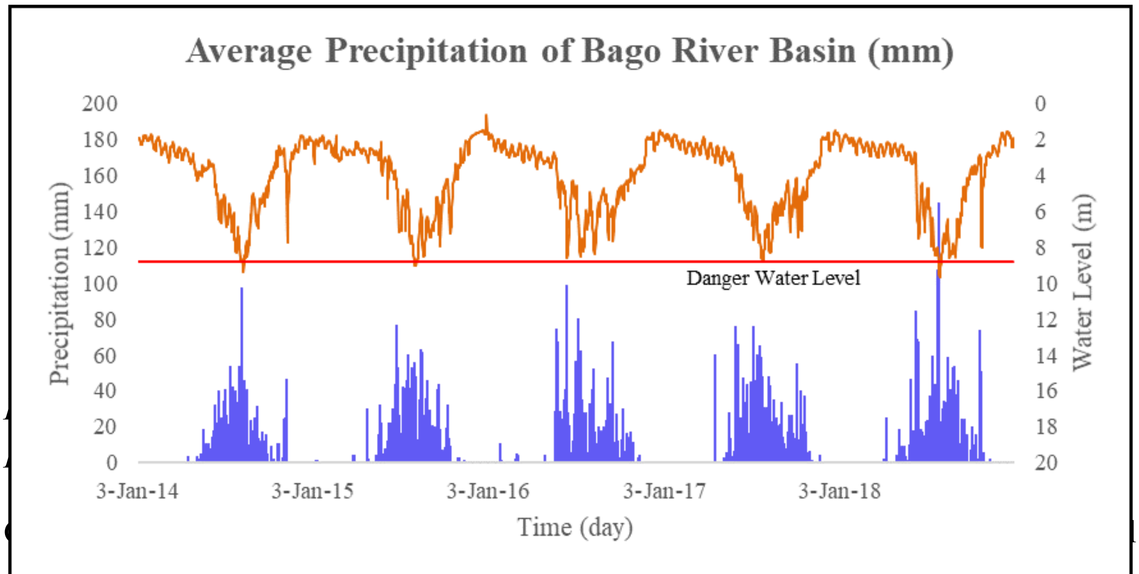

within 31 years. The cumulative rainfalls for simulation events are listed in figure 5 (a) and figure 5 (b) shows the Zaung Tu dam released flows for flood simulation events. Released flow from the dam is a key role in the Bago river basin's flood simulation.

Data required for hydrologic modeling (HEC-HMS) are:

(a) High-Resolution Digital Elevation Model (DEM):
(b) Land use and Soil cover
(c) Climate data (Precipitation)
(d) Flow data (Dam released flows, Water Level)

And the following data are required for the hydraulic modeling system.

(a) Terrain Data
(b) Geometry Data
(c) Flow Data

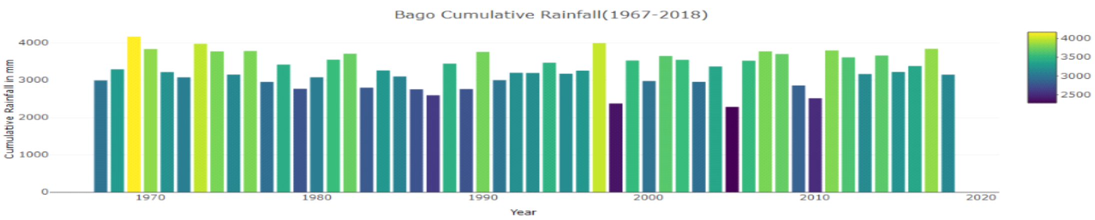

Figure 4. Bago Cumulative rainfall from 1967 to 2018

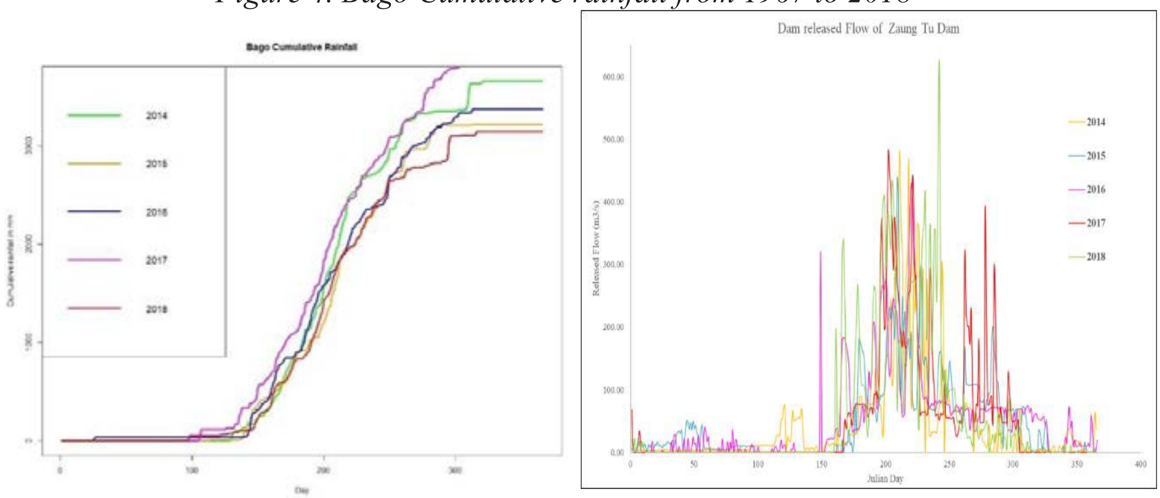

Figure 5. (a) Cumulative Rainfall for flood simulation events (b) Dame released flows for flood simulation events

3. Methodology

Hydrologic Modeling System, HEC-HMS and River Analysis System, HEC-RAS are two of the most commonly used models in hydrologic and hydraulic modeling systems. HEC-HMS and HEC-RAS have been developed by the U.S Army Corps of Engineers to deliver vital public and military engineering services, to energize the economy and reduce risks from disasters. HEC-HMS is a generalized modeling system designed to simulate the precipitation-runoff processes of watershed systems with a wide range of applicability. This includes large river basin water supply and flood hydrology, small urban or natural watershed runoff, forecasting stream flow, depth-area reduction, assessing model uncertainty, erosion and sediment transport, and water quality. Hydrologic modeling for a watershed involves infiltration, overland flow, computing rainfall excess, flood routing from the upstream of reach to the outlet and subsurface flow simulation.

Runoff volume and peak discharge calculation is the first step in hydrologic modeling. The rainfall losses involve tree canopy, land use and infiltration to the soil layer. Among them, infiltration through the soil is the key component in the calculation of runoff. Infiltration refers to the amount of rainfall which passes through the soil layer. The amount of infiltration rainfall is equivalent to the infiltration capacity of the soil layer. If the amount of rainfall is greater than the infiltration capacity, the actual rate of infiltration is equal to the rainfall amount. In other words, the actual infiltration rate is equal to the infiltration capacity, if the infiltration capacity is less than the rainfall amount.

$$f = i \; if \; f_p > i \qquad (1)$$

and

$$f = f_p \; if \; f_p < i \qquad (2)$$

where f_p = Infiltration capacity

f = Actual infiltration rate

I = Rate of rainfall

The excess rainfall is calculated from the following equation.

$$i_e = i - f \qquad (3)$$

where ie is the excess rainfall.

The various methods are used to evaluate the infiltration capacity. In this study, the initial and constant rate loss method is used for the excess rainfall based on the hydrologic soil group and land covers. The initial and constant method involves the parameters of constant rate, initial loss, and percent of impervious which show the physical characteristic of the soil layer and land use. The estimated infiltration loss rates for hydrologic soil groups are published by Skaggs and Khaleel in 1982. Table 1 shows the estimated infiltration loss rates for hydrologic soil groups.

Table 1. Hydrologic soil group and infiltration rates (Skaggs and Khaleel, 1982)

Soil Group	**Description**	**Infiltration loss rate (cm/hr)**
A	Deep sand, deep loss, aggregated silts	0.762 – 1.143
B	Shallow loess, sandy loam	0.381 – 0.762
C	Clay loams, shallow sandy loam, soils low in	0.127 – 0.381

	organic content, and soils usually high in clay	
D	Soils that swell significantly when wet, heavy plastic clays, and certain saline soils	0.00 – 0.127

For the transform method, the time of concentration, t_c was be calculated from the following equation developed by Kirpich (1940).

$$t_c = 0.0195 \, . L_c^{0.77} . S_c^{-0.385} \qquad (4)$$

where Lc is the watershed length in meter, the longest flow path in HEC-HMS and Sc is the slope (m/m) in the main channel.

The total runoff hydrograph involves direct runoff and baseflow. The separation of the distribution of baseflow from the total runoff hydrograph is also important in the hydrologic modeling system. It also impacts on the shape of the flow hydrographs.

The hydraulic modeling system requires river cross-sections and Manning's roughness coefficients as its geometric parameters. The basic computational procedure is based on the solution of the one-dimensional energy equation with energy losses evaluated by friction through Manning's equation and contraction and/or expansion. The one-dimensional energy equation is also called the standard step method.

$$y_1 + \frac{V_1^2}{2g} + S_0 \Delta x = y_2 + \frac{V_2^2}{2g} + S_f \Delta x \qquad (5)$$

Where Sf is the energy grade line slope, S0 is the channel bed slope.

3.2. HEC-HMS Model Development

The hydrologic model was developed using HEC-HMS Version 4.3 and has four components to simulate the basic hydrologic processes of runoff generation from precipitation, its transformation, and combination with baseflow, and it's routing towards the outlet. These four components are (i) infiltration loss, (ii) direct runoff, (iii) baseflow, and (iv) channel routing.

The infiltration loss component based on the Initial and Constant method computes for the volume of rainfall that falls on the watershed and addresses questions on how much of rainfall infiltrates on the surface and when does it run off.

The direct runoff component using the Snyder Unit Hydrograph method describes two critical processes in the transformation of excess precipitation to runoff which is 1) translation or movement of the excess precipitation from its origin throughout the drainage to the watershed outlet; and 2) attenuation or reduction of the magnitude of the discharge as the excess is stored throughout the watershed. The baseflow model based on the Recession method is used to explain the drainage from the natural storage of the watershed. The channel routing model, using the Lag method, simulate the flow in the channels towards the main outlet.

The development of the HEC-HMS model primarily involved the physical representation of watershed and streams within the Bago River Basin into hydrologic elements namely watersheds reaches, and junctions interconnected in a dendritic network to simulate rainfall-runoff processes. With a lumped-parameter approach, direct runoff is computed using the Initial and Constant method for each watershed and routed and translated toward each watershed's outlet using the Snyder Unit Hydrograph model. The computed direct runoff and baseflow hydrographs for each watershed are routed through channels (or "reaches") towards the main outlet of the Basin using the Lag method. Modeling in There are three specific components as a basin model, a meteorological model, and a set of control specifications. In the basin model, the termed "sub-basin", the physical representation of the basin model for each watershed and the river elements to simulate hydrologic processes are included. A meteorological model consists of a time series data of rainfall used for the simulation. The control specification determines the simulation time step and period or duration for model simulation and calibration. HEC-HMS's preprocessor, HEC-GeoHMS was used to prepare the basin model.

HEC-GeoHMS which is the extension of ArcView GIS software was applied to visualize spatial information, the characteristics of the watershed, watershed delineation, spatial analysis performance, and construct inputs to hydrologic models.

3.3. HEC-RAS Model Development

The HEC-RAS model of Bago River was developed by first constructing a geometric representation of the rivers and their flood plains. This includes cross-sections, riverbanks, and centerline, and the flood plain boundaries (i.e. the domain). A high-resolution 10-m DEM integrated with river observed cross-section data was used as the primary source of the cross-section data. Riverbanks and centerlines were digitized from the high-resolution Worldview-2 image. All the model pre-processing was done in ArcView GIS 10.4.1 using HEC-GeoRAS extension. HEC GeoRAS is the pre-processor of HEC RAS, and it prepares the model's geometric data. It is also used to assign basic model parameters. This geometric data is then imported in HEC RAS for further model setup. Some of the cross-sections from the pre-processing stage were extended beyond the model domain just to make sure all of the domains are covered. The flood depth and hazard maps for the model result after are got from the post-processing stage. Flow resistance coefficients, also called Manning's roughness coefficients n, were assigned to the cross-section segments (or the portion between cross-section points) using land-cover information from the SERVIR Mekong land-cover Portal. A look-up table based on the HEC RAS Hydraulic Reference Manual was used to transform the land-cover classes to Manning's n land-cover classes. As a hydraulic model, the HEC RAS model cannot run on its own to provide the required information (flood depths). In a simulation run, it requires information on how much water is entering at specific locations as well as water level conditions at the downstream-most portion (e.g., outlet) of the model domain. This required information is called boundary conditions that need to be set to reflect (i) the volume of water that the river receives (or inflow) from upstream watersheds and lateral inflows and (ii) the elevation of the water surface at the outlet.

4. RESULTS AND DISCUSSION

4.1. Calibration

HEC-HMS calibration was performed for six different flood events of 2014 to 2018 in the Bago River basin using daily flows discharge. Figures 3 (a), (b), (c), (d), (e) and (f) are the graphs that compare observed flow to simulated flow for the calibrated years, 2014 to 2016. The red dotted lines denote observed outflow measured at Bago gauge station, at Bago DMH. The blue dotted lines denote the total simulated outflow at the Discharge gauge. The calibration at event 2016B resulted in simulated outflow volume and peak flow almost the same as observed volume. At the outlet of the watershed, percent error in volume, PEV and percent error in peak discharge, PEPD for calibrated years is shown in Table 2.

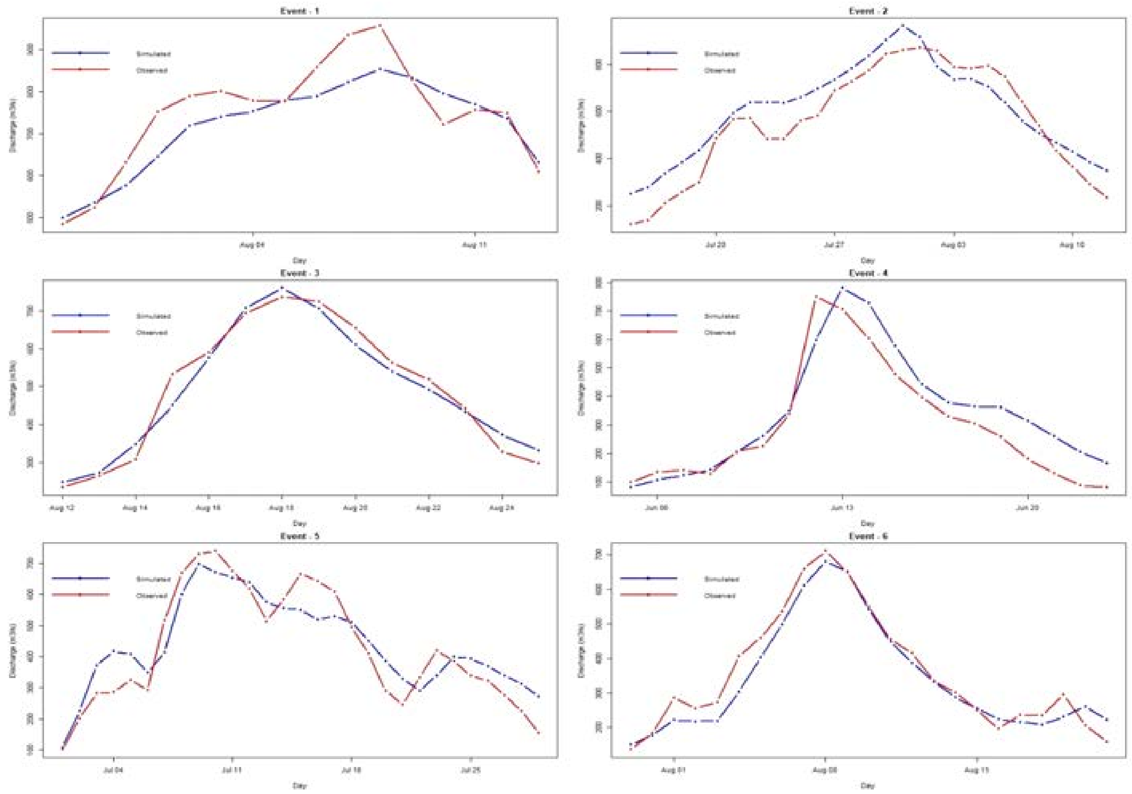

Figure 3. Observed and Simulated flow for Calibrated year (a) Event-1, 29-Jul-2014 to 13-Aug-2014 (b) Event-2, 15-Jul-2015 to 12-Aug-2015 (c) Event-3, 12-Aug-2015 to 25-Aug-2015 (d) Event-4, 5-Jun-2016 to 23-Jun-2016 (e) Event-5, 1-Jul-2016 to 29-Jul-2016 (f) Event-6, 30-Jul-2016 to 21-Aug-2016

Table 2. Percent Error in Volume (PEV) and Percent Error in Peak Discharge (PEPD) of the model for calibrated flood events

Events	**Observed Volume**	**Simulated Volume**	**PEV**	**Observed Discharge**	**Simulated Discharge**	**PEPD**
	(mm)	**(mm)**	**(mm)**	**(m3/s)**	**(m3/s)**	**(m3/s)**
Event - 1	430.82	392.53	8.9	956.7	853.4	10.8
Event - 2	597.59	639.62	7.0	872.2	963.3	10.4
Event - 3	250.13	237.96	4.9	737.1	760.7	3.2
Event - 4	207.64	235.34	13.3	749.3	780.5	4.2
Event - 5	461.87	465.53	0.8	739.5	697.5	5.7
Event - 6	303.75	279.32	8.0	710.5	680.4	4.2

Since the model was mainly calibrated considering the outflow volume and peak discharge, the calibrated flow pattern poorly represented the observed flow for Bago DMH station. Also, the flow pattern could not be calibrated accurately as the outflow of the watershed. Whereas, the flow trend of the event is similar to the observed flow at the outlet station. Hence, the model is unable to simulate the short-term events accurately at this outlet. Therefore the simulation for the short-term events must be performed. The initial peaks seen in the calibrated flow at all the junctions are due to model warmup period and thus can be ignored. Failure to simulate the peak flow and time of peak could also be due to ambiguity in the precipitation data. Apart from this, some important meteorological parameters such as wind speed and air pressure have not been included in the model whereas wind plays an important role in the hydrological cycle. The computational time step for simulation was set for 1day therefore; the computed outflow data were also for the one-day interval. In this computation, the data of the precipitation and discharge are daily averaged data. This mismatch between the time interval of input data and the output also created some level of error. Table 3 helps to evaluate the model performance for calibration.

Table 3. HEC HMS Model Performance Evaluation result for Calibration

Events	Nash-Sutcliffe	RMSE	Bias (%)	R-Squared`
Event-1	0.772	0.5	- 4.00	0.83
Event-2	0.837	0.4	9.37	0.9
Event-3	0.961	0.2	0.55	0.96
Event-4	0.829	0.4	15.42	0.88
Event-5	0.841	0.4	2.64	0.87
Event-6	0.935	0.3	5.41	0.95

The Nash-Sutcliffe Efficiency (NSE) for calibrated flood events found between 0.772 to 0.961 respectively. That is indicated a close relationship between the observed and simulated flow and the model performance is good. Nash Sutcliffe efficiency (NSE)are obtained as 0.772, 0.837, 0.961, 0.829, 0.841 and 0.935 respectively for 2014, 2015 and 2016 calibrated flood event. The validation process was done by these final parameter values for another two storm events (2017 and 2018). The validation results of the 2017 and 2018 flood events are as shown below in Figures 5 (a) and Figure 5 (b) respectively. That is indicated a close and good correlation between the observed and simulated flow.

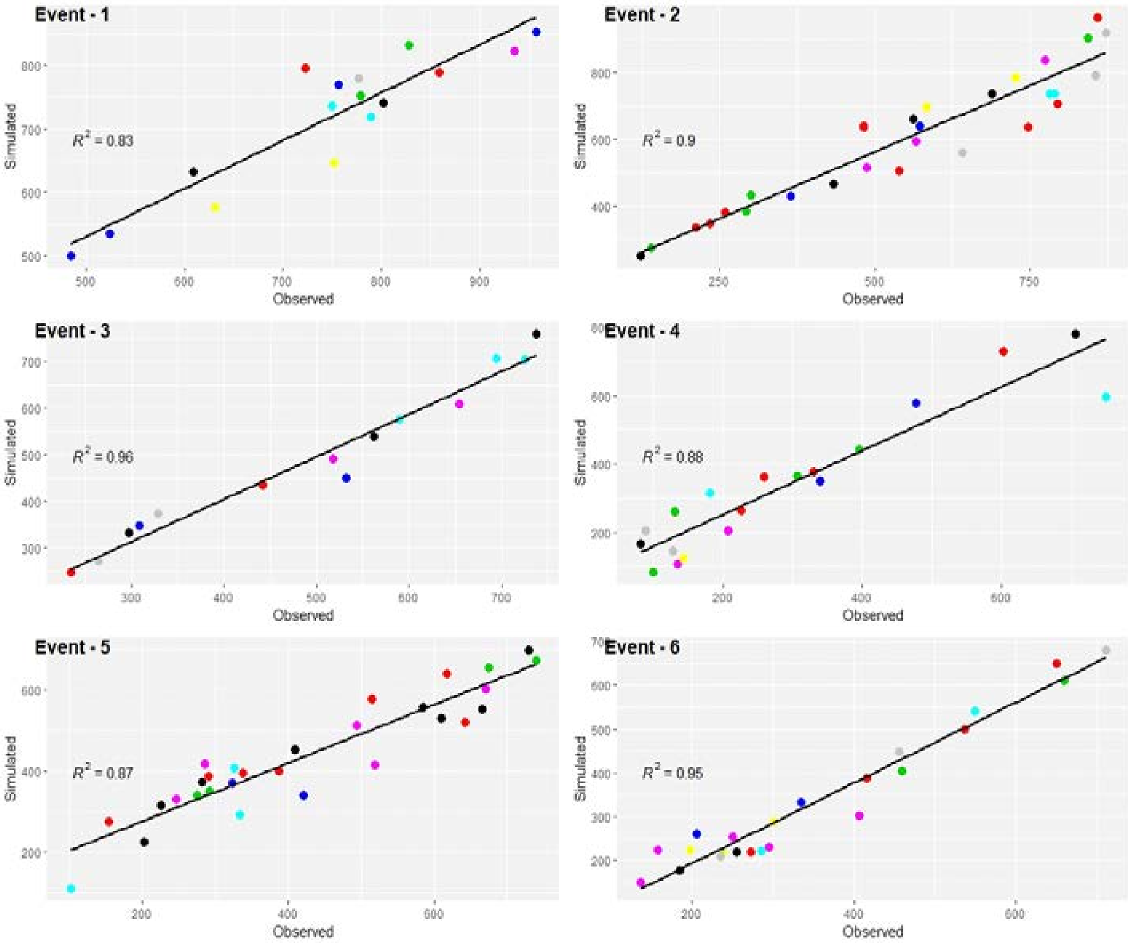

Figure 4. Coefficient of determination value for Calibrated years, (a)Event-1, (b) Event-2, (c) Event-3, (d) Event-4, (e) Event-5, (f) Event-6

4.2. Validation

To verify the output of this model, validation was also performed for validation events from the year 2017 to 2018. This was performed to check if the models were able to predict the runoff at the discharge stations for the period other than calibrated one or not. The resulting graphs for the validation period are shown in the figures below, Figures 5 (a) and Figure 5 (b). Nash Sutcliffe efficiency (NSE) is obtained as 0.527 for the 2017 Validation event and 0.559 for Validation event 2018 respectively and shown in table 4 and table 5.

From the above results, some similarities and differences between these basin models can be extracted and discussed herewith. There is no certainty for assigning values of parameters in HMS. Any value can be assigned to the parameter to get a well calibrated model. Therefore, even a set of values that do not have any physical relevance can result in a well-calibrated model. This could be possible in the HMS model. Therefore, seasonal parameterization may improve model performance. Simulation of rainfall-runoff modeling for dendritic basins was performed based on historical time-series data and was calibrated and validated with the observed flow in this research. With the ongoing global warming and climate change effects, precipitation and temperature are in increasing trend which implies higher runoff in the future.

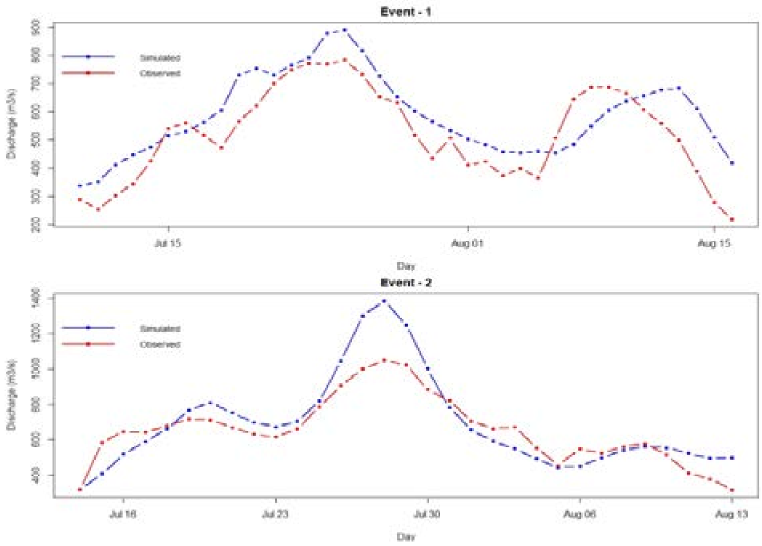

Figure 5. Observed and Simulated flow for Validated year (a) Event-1, 2017 flood event (b) Event-2, 2018 flood event

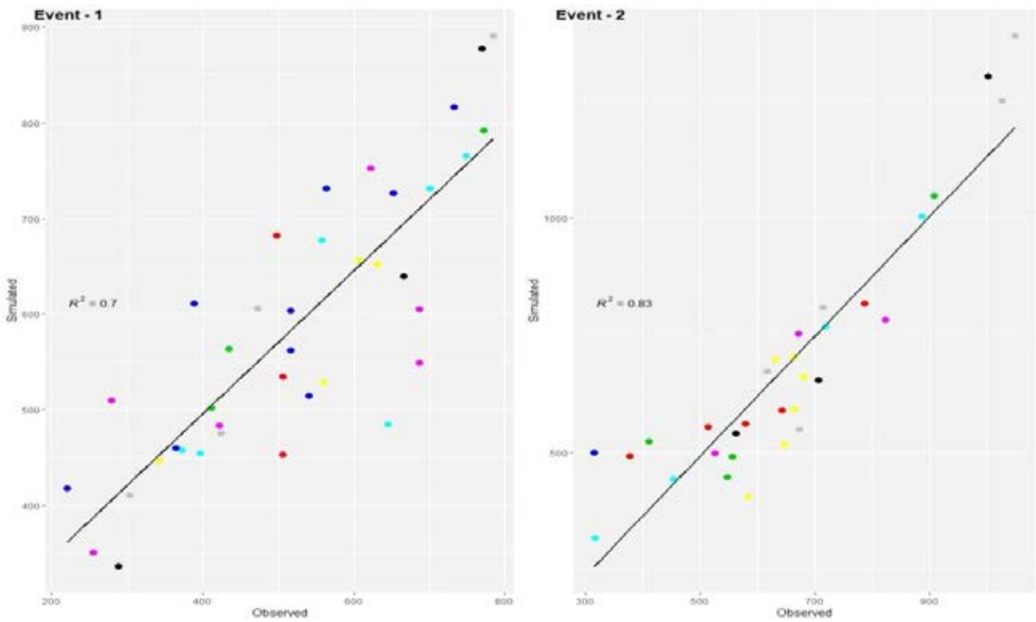

Figure 6. Coefficient of determination value for Validated years,(a) Event-1, (b) Event-2

Table 4. Percent Error in Volume (PEV) and Percent Error in Peak Discharge (PEPD) of the model for validated flood events

Events	**Observed Volume**	**Simulated Volume**	**PEV**	**Observed Discharge**	**Simulated Discharge**	**PEPD**
	(mm)	**(mm)**	**(mm)**	**(m3/s)**	**(m3/s)**	**(m3/s)**
Event - 1	740.05	815.60	75.55	784.2	891.0	106.8
Event - 2	752.62	777.45	24.83	1048.1	1387.7	339.6

Table 5. HEC HMS Model Performance Evaluation result for validated flood events

Events	**Nash-Sutcliffe**	**RMSE**	**Bias (%)**	**R-Squared`**
Event-1	0.527	0.7	12.42	0.7
Event-2	0.559	0.7	5.5	0.83

4.2. Hydraulic Modelling with HEC-RAS

The results in the HEC-RAS model are shown below. Calibration and Validation Results of HEC-RAS Model calibration was performed by the unsteady flow data option using the output flood hydrograph for two different flood events (2010, 2014, 2015, 2016, 2017 and 2018) that were simulated from HEC-HMS model. The friction slope is assumed and calibrated as 0.0001. The validation results with these final calibrated parameters for the 2018 flood hydrograph simulated form the HEC-HMS model are also shown below in Figure 4.9 respectively. In this flood inundation maps, the 2010 flood extent is the largest inundation area.

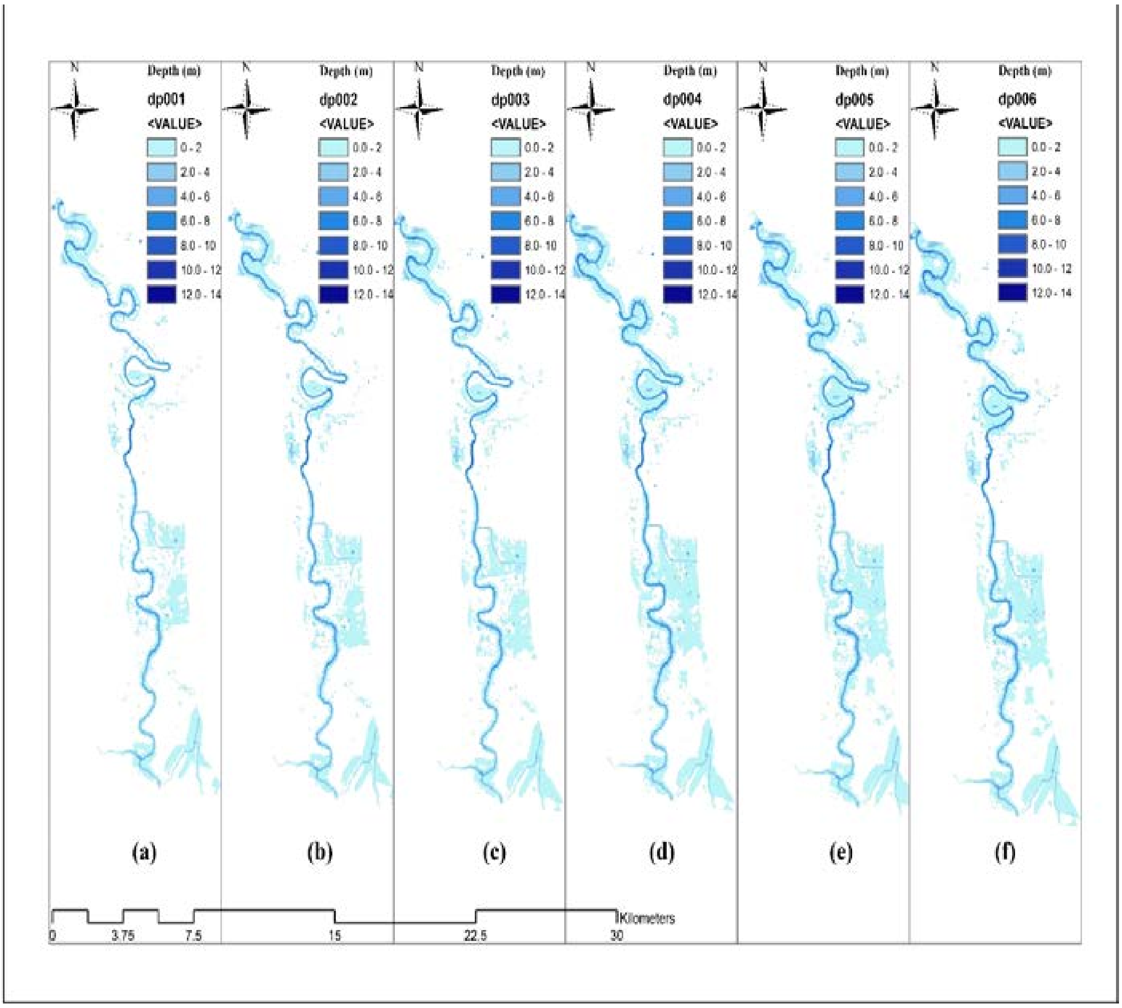

Figure 4.9. Flood Externts for different inundation events (a) Profile 2017 Flood Event (b) Profile 2016 Flood Event(c) Profile 2015 Flood Event (d) Profile 2018 Flood Event (e) Profile 2014 Flood Event (f) Profile 2010 Flood Event

5. Conclusions and Recommendation

The calibration for the hydrologic model was performed by the trial and error method in the HEC-HMS model. The values of calibrated parameters are sensitive to the characteristic of the basin as well as the resolution of the digital elevation model. It impacts the basin parameters such as slope which is important for the flood routing. The parameter changes incorrectly vary the scheme of water balance equation. For the study area which consists of a lot of topological changes, the resolution of the digital elevation model (DEM) is critical. For the hydraulic model, the cross-sections for the HEC-RAS model are extracted from DEM. The extracted cross-sections change the water surface elevation of the river analysis system. Therefore, the resolution of the DEM is important for both models. The result shows that parameters corresponding to the hillslope provide a large variation for different flood events.

As the author mention above, changes in the formation of cross-sections for the model affect the water surface elevation of a river. Moreover, the sedimentation, scour, urbanization, levee construction impact on the formation of cross-sections. For this reason, it is strongly recommended that the surveyed river cross-sections should be applied in the hydraulic model. Each surveyed river cross-section should have the minimum amount of cross-section filter to an extent over the flood-prone area.

Although the high-resolution digital elevation model was applied in this research, the resolution of the model doesn't extent over the whole river basin. The developer consolidates the 30 m and 10 m DEM for this model, so the resolution at the upstream of Zaung Tu Weir is not matched with the downstream resolution of the model. As possible, the high-resolution digital elevation model which covers the whole river basin should be used in the research.

There are only two rainfall and water level gauge stations form DMH in the river basin and the data from the stations are available daily. One station from Zaung Tu Village cannot be applied in this research because of data uncertainty. Therefore, new automatic rain gauges and water level stations should be installed at the places where the flow change, for example, the downstream of Zaung Tu weir and Zaung Tu Dam. One station from Zaung Tu Village cannot be applied in this research because of data uncertainty. To mitigate the flood risk in the Bago river basin, departments related to Bago river should be integrated.

But these current methods for managing facilities may not be sufficient to support planned design functions, so further study of operation methods is necessary. A coordination framework should be established between DMH, ID, and DHPI. This framework would utilize DMH hydrological and meteorological observation data for ID/HGPE/DHPI operation of hydropower and reservoir facilities.

FLOOD RISK ASSESSMENT BASED ON QUANTIFICATION OF FLOOD DAMAGE

B.B. SHRESTHA[1] and A. KAWASAKI[2]

[1] Project Researcher, Department of Civil Engineering, The University of Tokyo, Tokyo, Japan,
[2] Professor, Department of Civil Engineering, The University of Tokyo, Tokyo, Japan,
Correspond to Dr. B.B. SHRESTHA (shresthab@hydra.t.u-tokyo.ac.jp)

Keywords: *Flood Risk Modeling, Damage Quantification, Social Impact, Vulnerability, Myanmar*

1. INTRODUCTION

Floods are the most frequently occurring water-related disasters in the river basins of many countries, and the impact of floods is becoming greater due to their increasing frequency and scale of flood events, and the concentration of population and economic activities in the river basins. Flood disasters can cause serious damage such as loss of lives and destruction of infrastructures and properties. Therefore, flood disaster risk mitigation plans should be properly prepared and implemented for future floods. However, such mitigation plans require analysis of flood hazards and quantification of risk for mitigating and managing flood risk for the future. In this context, this study focuses on assessment of flood risk by quantifying flood damage in the Bago River basin of Myanmar, which is one of the most flood-prone river basins in Myanmar. Assessment of flood hazard and risk in the Bago River basin is very important since this basin plays an important role in economical contribution in the country's economy through agriculture production. Flood risk in the basin was thus assessed by quantifying flood damage to house building/assets and agriculture using hydrological and damage estimation models.

2. ASSESSMENT OF FLOOD HAZARD AND RISK

Figure 1 shows overview of flood damage/risk assessment in this study. Flood hazard and risk were assessed in the Bago River basin of Myanmar. Flood characteristics such as flood depth and duration were computed using hydrological model named Rainfall-Runoff-Inundation (RRI) model developed by Sayama et al. [1]. The horizontal resolution of RRI model was 15 arc-s grid cell (approximately 450m). The parameters of the RRI model were calibrated with 2014 flood by comparing calculated discharge with observed discharge at Bago Station as shown in Figure 2. The calibrated parameters were validated with 2015 and 2018 flood events.

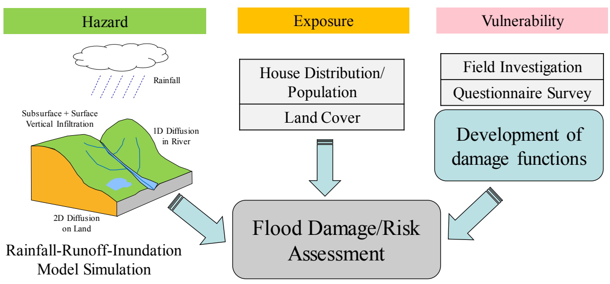

Figure 1. Overview of flood damage/risk assessment

After hazard analysis, flood damage to residential houses and agriculture sector (flood damage to rice-crops) was assessed and quantified based on flood damage curves. The population distribution data downloaded from the WorldPop were used to estimate distribution of residential houses, and the cropland areas in the study basin were extracted using global land cover map developed by International Steering Committee for Global Mapping (Figure 3).

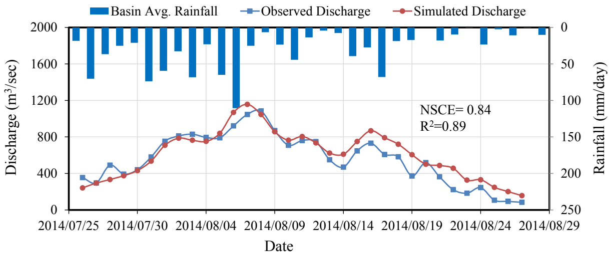

Figure 2. Comparison of calculated discharge with observed discharge at Bago Station for 2014 flood

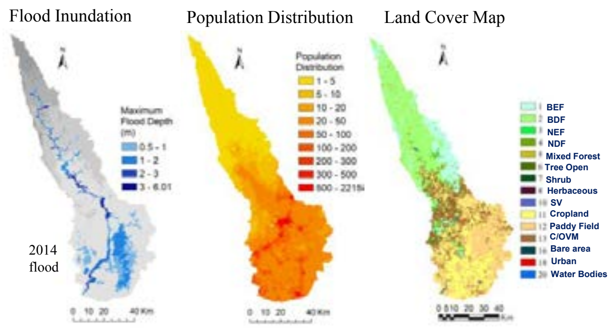

Figure 3. Flood inundation area during August 2014 flood, population distribution and land cover map of study area

Flood frequency analysis was also conducted to estimate the rainfall intensity for different return periods. Flood hazard and risk were assessed quantitatively for past largest flood and for different return period cases.

3. CONCLUSIONS

Flood hazard and risk were assessed quantitatively in the Bago River basin of Myanmar. Identifying areas of risk based on flood damage quantification provides essential information for designing future development activities. The results of risk assessment can also be useful to establish preventive measures, adaptation measures and policies required for flood damage reduction.

REFERENCES

[1] T. Sayama, G. Ozawa, T. Kawakami, S. Nabesaka, K. Fukami, Hydrol. Sci. J. 57 (2012) 298-312.

Estimation of Flood Discharge using with WEB-DHM model in Bago River Basin

Sann Win Maung[1], Zin Mar Lar Tin San[2], Win Win Zin[3] and Akiuki KAWASAKI[4]

[1] Ph.D Candidate, Department of Civil Engineering, Yangon Technological University, Myanmar
uswinmg@gmail.com

[2] Professor, Department of Civil Engineering, Yangon Technological University, Myanmar
zinmarlar@gmail.com

[3] Professor, Department of Civil Engineering, Yangon Technological University, Myanmar
winwinzin@gmail.com

[4] Professor, Department of Civil Engineering, The University of Tokyo, Japan
kawasaki@hydra.t.u-tokyo.ac.jp

ABSTRACT

Flooding has always been one of the major hazards in Myanmar, accounting for 11% of all disasters. In Myanmar, the Bago River Basin is a flood prone area. During the last decade, many severe floods occurred in the Bago River Basin, at the monsoon season about the period of July and August. Most of the floods are caused by the storm rainfall. The 2011 and 2018 floods are historical record of Bago. In this paper, the Water and Energy Budget-based Distributed Hydrological Model (WEB-DHM) was used for hydrological modeling as determined for the discharge of flood. In this study, Hydro-SHEDS DEM is used for elevation data of the Bago river basin. The Japanese 55*-year Reanalysis JRA-55 data from the Japan Meteorological Agency (JMA)is used for the meteorological data preparation of this hydrological model. This paper aim to compare the flood discharge from the hydrological modeling and the calculated observe data of the past three year 2014, 2015 and 2016.*

Keywords: Bago river basin, flood, rainfall, WEB-DHM

1. INTRODUCTION

A flood is a high flow or overflow of water from a river or similar source of water occurring over a period of time. Heavy rain spell can result in an extra volume of water in the waterways, leading to a rise in the water level of streams and rivers. A flood happens when the carrying capacity of the waterways fails to hold the total volume of increased water at any given time (UN-HABITAT, Myanmar, 2015).

Flooding has always been one of the major hazards in Myanmar, accounting for 11% of all disasters. In Myanmar, the Bago River Basin is a flood prone area. During the last decade, many severe floods occurred in the Bago River Basin, at the monsoon season about the period of July and August. Most of the floods are caused by the storm rainfall.

Flood protection measures can be structural ("hard") or non-structural ("soft"). The former refer to such defenses as dikes, dams and flood control reservoirs, diversions, floodways, etc. Structural defenses have a very old tradition, as dams and dikes have been built since more than four thousand years.

Non-structural flood protection measures are: source control, zoning, flood proofing, insurance, flood forecast-warning system, awareness raising and improving information, etc.

There is no flood protection measure guaranteeing complete safety. In many vulnerable areas, sufficient flood protection cannot be reached with the help of structural means only. Hence, further flood risk reduction via non-structural measures is often indispensable. An optimal, site-specific mix of structural and non-structural measures are being sought (Lucas Menzel, Zbigniew W. Kundzewicz. 2003).

Hydrologic models use relatively simple mathematical equations to conceptualize and aggregate the complex, spatially distributed, and highly interrelated water, energy, and vegetation processes in a watershed.

In this study, the WEB-DHM hydrological model is used for estimating and forecasting the flood discharge of the Bago river basin.

2. STUDY AREA

In Myanmar, the Bago River Basin is a flood prone area. During the last decade, many severe floods occurred in the Bago River Basin, at the monsoon season about the period of July and August. Most of the floods are caused by the storm rainfall. The 2011 and 2018 floods are historical record of Bago.

The Bago River is confluent with the Yangon River and reaches the coastal water body. It is located at about Latitude. 16°46'00"- 18°27'30" N and Longitude. 95°53'00"- 96°45'00" E. Its head is found 190 km from Yangon, lying on Pegu Yoma (mountain) at an elevation of 630 m. The length of the river-channel reaches, due to including complex meandering sections, over 340 km. However, its tributaries are not broadly developed, so the basin area is relatively small at about 5,030 km^2. The Bago River Basin is shown in Figure 1.

The Bago River is one of the most important and useful river basins in lower Myanmar for hydropower generation, irrigation use, fisheries, and navigation use (Shelly Win. 2014).

The two meteorological stations are located in the basin, Bago and Zaung Tu Station; the two points are the interesting points in this study. The average annual total rainfall at the Bago station is around 3,000 mm. Floods occur every year (sometimes even more than once) in the Bago River basin.

The Zaung Tu dam was constructed in 1996. The other three dams (Salu, Kodukwe, and Shwelaung) were constructed in 2012.

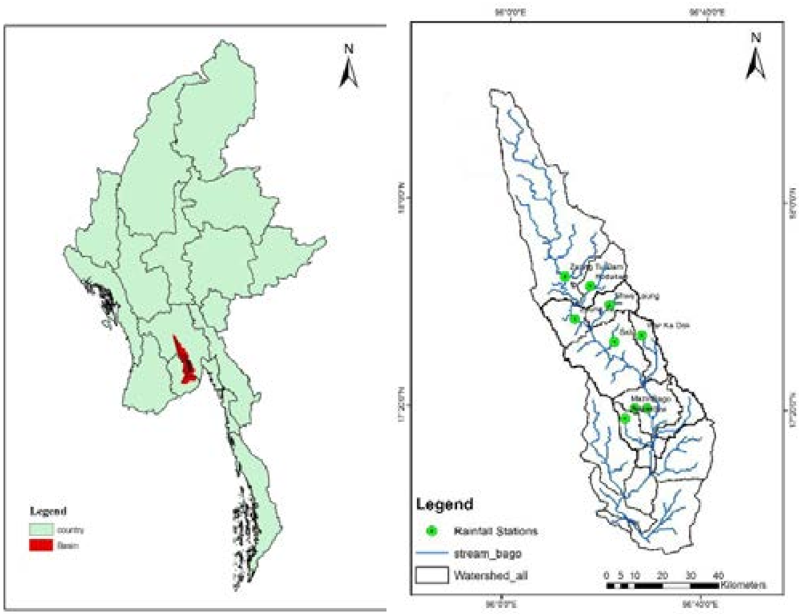

Figure 1: Location Map of Study Area

3. METHODOLOGY

3.1. Overview of WEB-DHM model

The Water and Energy Budget-based Distributed Hydrological Model (WEB-DHM), was developed by coupling a simple biosphere scheme (SiB2) with a geomorphology-based hydrological mode. The model can estimate the water, energy and CO2 fluxes at a basin scale. Contrary to traditional hydrological models, this model calculates evapo-transpiration based on both water as well as energy balances for each model grid, creating a much more solid physical foundation (Bhagabati, S.S, 2018).

Figure 2 show the overall structure of the WEBDHM model. The Figure. 2 (a) shows the sub-basin; (b) shows the sub-division from sub-basin to flow intervals; (c) shows the discretization from a model grid to a number of geometrically symmetrical hillslopes; and (d) shows the detailed process descriptions of the water moisture transfer from atmosphere to river, including downward solar radiation, downward long wave

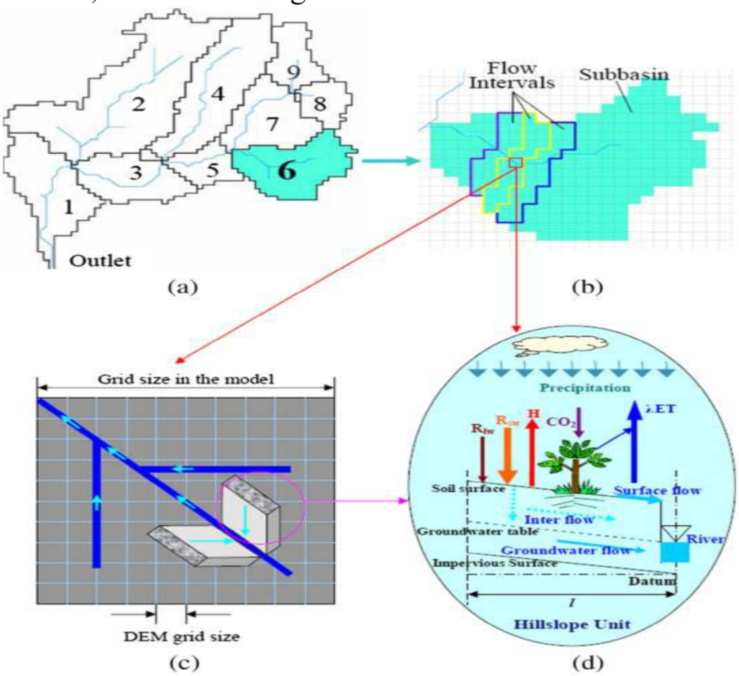

Figure 2: Overall Structure of WEB-DHM model (Lei WANG, Toshio KOIKE. 2009)

3.2. Model application

In this study, the first part of WEB-DHM model application is ArcGIS based tool analysis. The major geospatial input data includes Digital Elevation Model(DEM), soil data, land use and stream network layers.DEM is the geospatial raster data containing the continuous elevation values a topographic surface by the array of cells or pixels. It is used in ArcGIS to create the watersheds and river networks and streams, sub-basins, and parameters for Hydrological Response Units (HRUs) analysis. In this study, Hydro-SHEDS DEM is processed in a GIS environment using

In this study, land use and land cover data were acquired from the SERVIR MEKONG LAND COVER image (http://servir-rlcms.appspot.com/, n.d.).This data is used for HRU definition, and then allocate

The soil data for the study area was extracted from FAO (Food and Agricultural Organization of the United Nations) Digital Soil Map of the World (DSMW)(http://www.fao.org/soils-portal/soil-survey/soil-maps-and-databases/en/, n.d.).

3.2.1. Terrain preprocessing

Terrain Preprocessing includes the projection of DEM (Digital Elevation Model) (Figure 3(a)), DEM preprocessing as fill, flow accumulation and flow direction. Similarly, it includes the delineation of the watershed and the hill slope calculation.
DEM preprocessing involves various internal processes required for the model. It involves fill, flow accumulation, flow direction and stream generation.
Watershed delineation is a process of extracting the boundary of a watershed. This can be delineated from a DEM using the flow direction (Figure 3(b)), flow accumulation (Figure 3(c)) and the outlet of the watershed.
Hill slope calculation includes all the processing and calculation needed for the WEB DHM model. Above three preprocessing steps are required to create the input for the Hill slope calculation (The University of Tokyo. 2016).

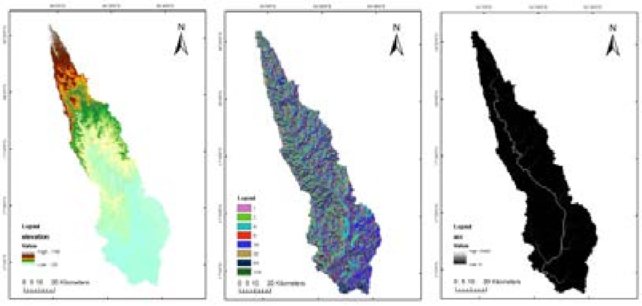

(a) (b) (c)

Figure 3: Elevation model, flow direction and flow accumulation of Bago River Basin

3.2.2. Basin division processing

WEB-DHM uses the Pfafstetter algorithm developed by Otto Pfafstetter in 1989. Based on the topology of the watershed, this algorithm can assign watershed IDs in a systematic manner. It is a hierarchal system where watersheds are delineated from junctions on a river network. The continental watersheds are represented as level 1. Higher level (Levels 2, 3, 4 etc.) represents even finer tessellations of the land surface into smaller watersheds, which are sub watersheds of lower level watersheds. The Pfafstetter code for each basin is unique and is based on its location on the overall drainage system and on the total drainage area upstream of the watershed's outlet. This file contains the information about the minimum and maximum width, height and roughness coefficient of all the sub basins. Sub-catchment number should be arranged in the descending order. These parameters can also be used for the model calibration purpose. In this paper, 9 sub basins of Bago river basin were divided by using Pfafstetter algorithm's first level codification as shown in Figure 4 (a).

3.2.3. Soil data processing

The Soil data is processed from the FAO global soil map. The soil properties from the soil map data are spatially distributed at approximately 9 km resolution grid size. The input data for WEB DHM models is static. Soil data preparation in this study is shown in Figure 4 (b).

3.2.4. Land use data processing

The USGS Land Cover map which has global land cover characteristic database was developed on a continent basis. All continents in the global database share the same map projection (Lambert Azimuthal Equal area) and have a 1-km nominal spatial resolution and are based on

1-km AVHRR data spanning April 1992 through March 1993. Land use data preparation in this study is shown in Figure 4 (c).

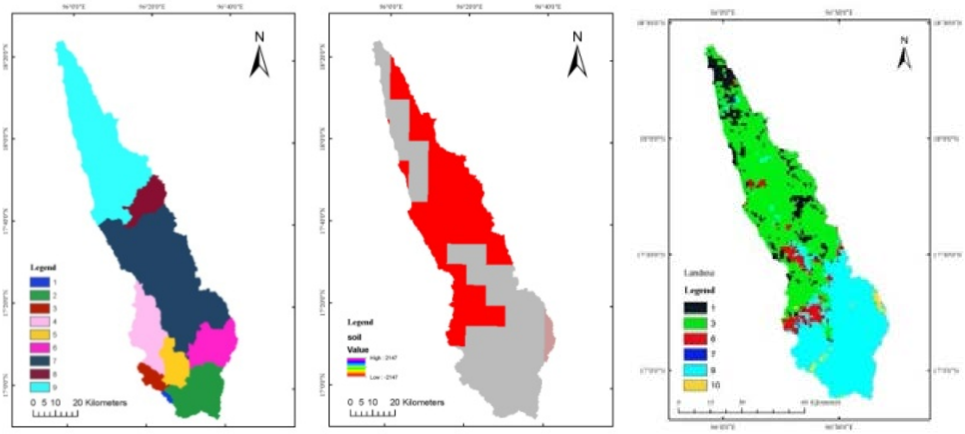

(a) (b) (c)

Figure 4: Basin Division, Soil and Land use Map of Bago River Basin

3.2.5. LAI and FPAR processing

The Leaf Area index (LAI) defines an important structural property of a plant canopy as the one-sided leaf area per unit ground area. LAI is the ratio of total upper leaf surface of vegetation divided by the surface area of the land on which the vegetation grows. LAI is a dimensionless value typically ranging from 0 for bare ground to 6 for dense forest. The fraction of incident radiation absorbed by greed canopy (FPAR) measures the proportion of available radiation in the photo synthetically active wave lengths that a canopy absorbs. LAI and FPAR and biophysical variables which describe the canopy structure and are related to functional process rates of energy and mass exchange. These parameters can be derived from satellite data MODIS.

3.2.6. Rainfall data processing

Rainfall is one of the main driving forcing for any hydrological model. This includes all form of water deposited on the earth’s surface and derived from atmospheric water vapor. Basically rainfall source can be of two types one is observed gauge data and another is satellite derived or re-analysis data. There are several global datasets for precipitation that is freely available online in the form of gridded raster dataset or asci files. In this study, observed guage data of the two target stations are used.

3.3 Meteorological Data Preparation

Besides Rainfall data, the Japanese 55-year Reanalysis JRA-55 meteorological data from the Japan Meteorological Agency (JMA) are used for WEB-DHM model. JRA-55 data are included the time series datasets of air temperature, humidity, wind (u, v), pressure, long wave radiation and short wave radiation.

3.4 Efficiency value of Model Simulation

The efficiency criteria used in this study are presented and evaluated with (i) Coefficient of determination (R^2), (ii) Nash-Sutcliffe efficiency (E_{NS}) and (iii) Root Mean Square Error (RMSE) (P. Krause, D. P. Boyle, F. B’ase, 2005)

3.4.1 Coefficient of determination (R^2)

The coefficient of determination R^2 is defined as the squared value of the coefficient of correlation according to Bravais-Pearson. It is calculated as:

$$R^2 = \frac{\left[\sum_{i=1}^{n} (qsi-qs)(qoi-qo)\right]^2}{\sum_{i=1}^{n} (qsi-qs)^2 \sum_{i=1}^{n} (qoi-qo)^2} \tag{1}$$

Where,

q_{oi} = observed value at the i time interval
q_{si} = simulated value at the i time interval
q_o = average value of the observed discharge

3.4.2 Nash-Sutcliffe efficiency (E_{NS})

The efficiency E proposed by Nash and Sutcliffe (1970) is defined as one minus the sum of the absolute squared differences between the predicted and observed values normalized by the variance of the observed values during the period under investigation. It is calculated as:

$$E_{NS} = 1 - \frac{\sum_{i=1}^{n} (qoi-qsi)^2}{\sum_{i=1}^{n} (qoi-qo)^2} \tag{2}$$

Where,

q_{oi} = observed value at the i time interval
q_{si} = simulated value at the i time interval
q_o = average value of the observed discharge

3.4.3 Root Mean Square Error

The Root Mean Square Error (RMSE) value is the parameter error test and its value approached to the zero means the least error parameter.

$$RMSE = \sqrt{\frac{\sum_{i=1}^{n} (Xoi-Ysi)^2}{n}} \tag{3}$$

Where,

X_{oi} = observed value at the i time interval
Y_{si} = simulated value at the i time interval
n = number of sample data

4. RESULTS AND DISCUSSIONS

In this study, the simulation of the flood discharge in 2014, 2015 and 2016 were carried out for the model calibration.

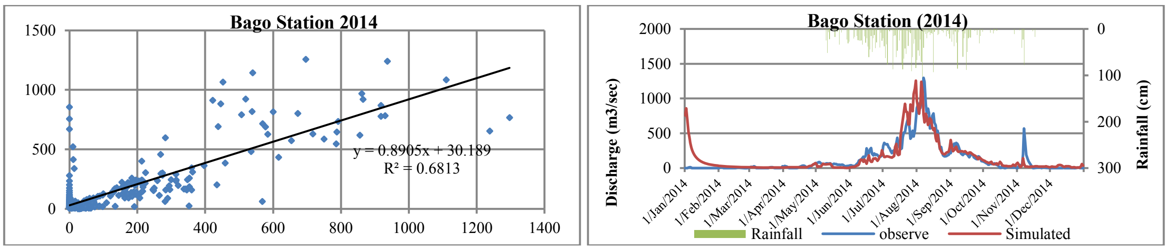

Figure 5: Comparison of Observed and Simulated Discharge at Bago Station in 2014

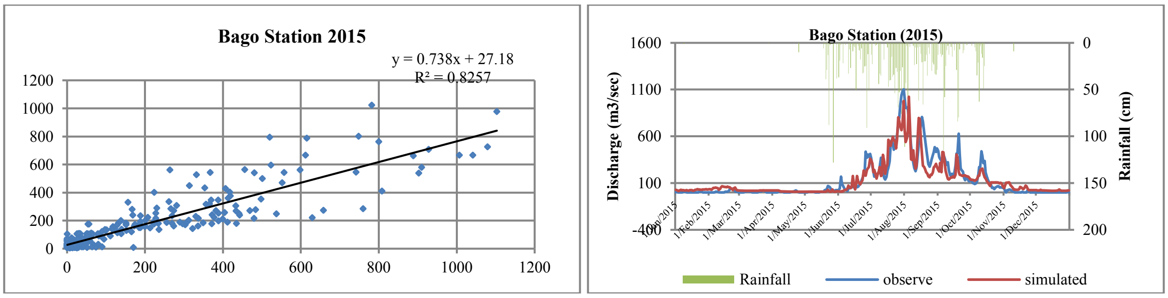

Figure 6: Comparison of Observed and Simulated Discharge at Bago Station in 2015

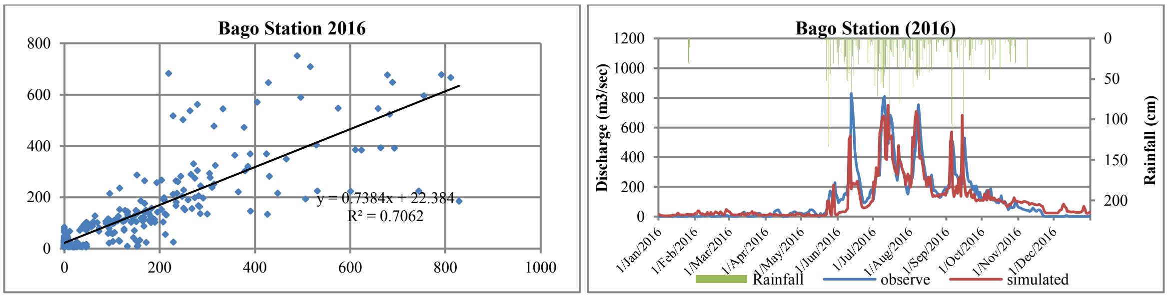

Figure 7: Comparison of Observed and Simulated Discharge at Bago Station in 2016

Table 1. Statistical Parameters for Simulation Results of Bago Station

Events	R^2	E_{NS}	RMSE
2014	0.681	0.612	137.07
2015	0.825	0.815	93.33
2016	0.706	0.702	92.99

The comparisons of observed and simulated discharge at Bago station from 2014 to 2016 time series are shown in Figure 5 to 7. According to the Table 1, the statistical parameters for the model simulation results of Bago station are acceptable level.

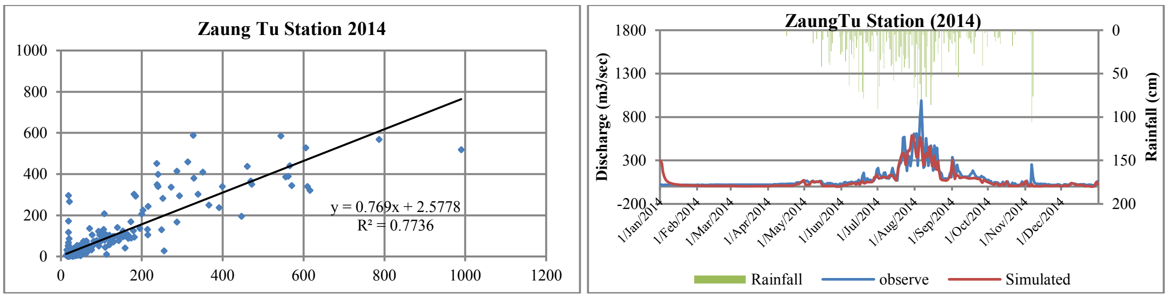

Figure 8: Comparison of Observed and Simulated Discharge at Zaung Tu Station in 2014

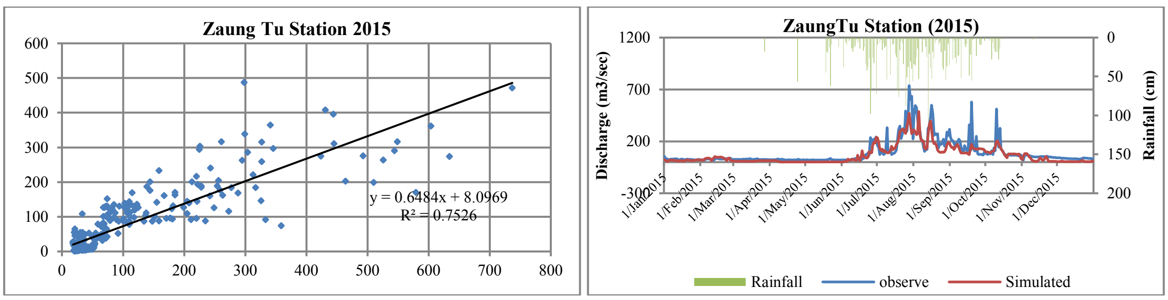

Figure 9: Comparison of Observed and Simulated Discharge at Zaung Tu Station in 2015

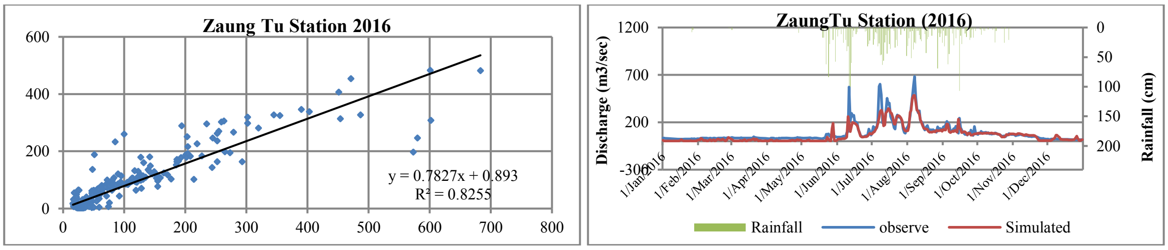

Figure 10: Comparison of Observed and Simulated Discharge at Zaung Tu Station in 2016

Table 2. Statistical Parameters for Simulation Results of Zaung Tu Station

Events	R^2	E_{NS}	RMSE
2014	0.773	0.756	62.51
2015	0.752	0.697	64.59
2016	0.825	0.793	46.26

The comparisons of observed and simulated discharge at Zaung Tu station from 2014 to 2016 time series are shown in Figure 8 to 10. According to the Table 2, the statistical parameters for the model simulation results of Zaung Tu station are also acceptable level.

5. CONCLUSION

At the Bago river basin, the topography of the upstream basin area is quite steep and the downstream basin area is normal flat condition. Most of the flooded areas in Bago are the residential area of the downstream basin area of Bago river basin. In this study, the simulated discharge was compared with the daily observed discharge values of the two meteorological stations. All the results of WEB-DHM simulation showed reliable values and acceptable level in statistical parameters for the selected three year. In this model simulation results, the statistical parameters of Zaung Tu station are more reliable than Bago station.

REFERENCES

Bhagabati, S.S. 2018. "*Development of a Near-Real Time Flood Inundation Analysis System for a Deltaic Flat River Basin in a Data Scarce Region; Case of the Bago River basin, Myanmar*". PhD Thesis. Department of Civil Engineering, School of Engineering, The University of Tokyo.

Lei WANG, Toshio KOIKE. 2009. "*Comparison of a Distributed Biosphere Hydrological Model with GBHM*". Annual Journal of hydraulic Engineering- JSCE 53, 103-108

Lucas Menzel, Zbigniew W. Kundzewicz. 2003. "*Non- Structural Flood Protection – A Challenge*". International conference 'Towards natural flood reduction strategies', Warsaw, 6-13 September 2003

P. Krause, D. P. Boyle, F. B¨ase. 2005. "*Comparison of Different Efficiency Criteria for Hydrological Model Assessment*". Advances in Geosciences, 5, 89–97, 2005

Shelly Win. 2014. "*Development of Flood Inundation Map for the Bago River*". M.E Thesis, Department of Civil Engineering, Yangon Technological University, Myanmar.

The University of Tokyo. 2016. "*GIS Tools for WEB-DHM using ArcGIS, User's Maunual, Version 2.0*". The University of Tokyo, Japan.

UN-HABITAT, Myanmar, 2015. "*Manual of Flood; Causes, Effects and Preparedness*". UN-HABITAT, Myanmar.

Seismic Risk Assessment of Existing Timber Building: A Case Study of Pyay Hostel in Yangon University

[1]Wai Yan Soe, [2]Kyaw Kyaw

[1]Department of Civil Engineering, Yangon Technological University
Yangon, the Republic of the Union of Myanmar
swaiyan304@gmail.com

[2]Department of Civil Engineering, Yangon Technological University
Yangon, the Republic of the Union of Myanmar
kyaw.u.kyaw@gmail.com

Abstract

Seismic Risk Assessment (SRA) involves determining the adverse consequences that people and society might suffer as a result of future earthquakes. There are three components to seismic risk assessment: the seismic hazard, the vulnerability of structures in the region and the expected losses that result from damage. Myanmar lays one of the two main earthquake belts of the world with a complex seismo-tectonic process. Most of the major cities in Myanmar including Yangon are located near the active Sagaing Fault and seismicity of those areas is very high, in which most of historical buildings had been constructed of timber frame. Among buildings in Myanmar, 82% of buildings are made of timber and bamboo, 2014 Myanmar Census. Due to the lack of maintenance, most of the timber buildings in Myanmar may be needed to renovate. When renovating buildings it is necessary to assess the physical condition. Therefore, seismic risk assessment of existing timber building: A Case Study of Pyay Hostel in Yangon University is presented in this study. Pyay hostel (two-storey timber building) in Yangon University has been established since 1924 and life time is about 100 years. It is necessary to investigate the existing seismic performance condition of this building. According to the FEMA guideline, Rapid Visual Screening technique (RVS) is an efficient method to quickly identify the seismic resistance of the building. To implement this study, the seismicity of region, soil information and determination of pre-code building were considered as pre-field survey data. According to the RVS data evaluation, detailed structural evaluation is required for high seismicity performance and also not required for moderate seismic performance.

Keywords: *Seismic Risk Assessment (SRA), Pyay Hostel (two-storey timber building), Rapid Visual Screening (RVS), Yangon*

1. INTRODUCTION

Earthquake is one of the most serious natural hazards. Myanmar had experienced several high magnitude earthquakes. Many of these events had a magnitude of 7 or greater and resulted in several damages and significant causalities. Seismic Risk Assessment (SRA) involves determining the adverse consequences that people and society might suffer as a result of future earthquakes. There are three components to seismic risk assessment: the seismic hazard, the vulnerability of structures in the region and the expected losses that result from damage. Myanmar lays one of the two main earthquake belts of the world with a complex seismo-tectonic process. Most of the major cities in Myanmar including Yangon are located near the active Sagaing Fault and seismicity of those areas is very high, in which most of historical buildings had been constructed of timber frame. According to seismicity and records of previous high magnitude earthquakes, some of the large earthquakes caused damages to some buildings and some casualties in and around Yangon Region. Among buildings in Myanmar, 82% of buildings are made of timber and bamboo, 2014 Myanmar Census. Due to the lack of maintenance, most of the timber buildings in Myanmar may be needed to renovate. When renovating buildings it is necessary to assess the physical condition. . Although timber framed buildings are known to have a relatively low risk of damage in earthquakes, failure of timber framed buildings due to seismic excitation was largely limited to sites that sustained ground deformations from liquefaction or landslide, or to vulnerable elements. Pyay hostel (two-storey timber building) in Yangon University has been established since 1924. The structural system of the building is the valuable timber building technique in Myanmar. Now, its life time is about 100 years old. According to the historical data, this building is one of the largest timber building and valuable historic timber building in Myanmar. Due to the visual survey, it has some circumstances: alteration of use and detection of deterioration (corrosion defects, termite, seasoning defects and etc.). Some of the timber beams and posts are suffering from those defects such as seasoning defects, corrosion, and other environmental conditions. If it is not repaired by proper technique, the strength properties, workability and serviceability will be reduced more. Thus, Seismic Risk Assessment of Existing Timber Building especially for Pyay Hostel Building is presented.

2. OBJECTIVE

The main objective of this study is to advocate the importance of building vulnerability assessment process and performance condition of existing timber building for the safety assessment and evaluation of Pyay Hostel in Yangon University.

3. OVERVIEW OF THE CASE STUDY BUILDING

Pyay Hostel in Yangon University is now utilized for 111 female students from the Yangon Education University. As the building was constructed on isolated reinforced concrete footings with timber post and beam structural system, the building's timber members lasted nearly a hundred years old. Pyay hostel (two-storey timber building) in Yangon University has been established since 1924 and life time is near 100 years. The dimensions of the building are 481ft. long, 52 ft. wide, 29 ft. height and the each of the floor area is about 25000 sq.ft. This building is composed of timbers, such as Pyinkado (Ironwood) and Teak as shown in Figure (1).

Figure (1) Location Map and Photo of Pyay Hostel in Yangon University

4. RAPID VISUAL SCREENING OF BUILDINGS FOR POTENTIAL SEISMIC HAZARD PROCEDURE (RVS PROCEDURE)

Vulnerability of the buildings is a critical determinant for earthquake risks. Experts say "Earthquakes don't kill people, but unsafe buildings do". Structural vulnerability is as measure of the damage, a building is likely to experience when subjected to ground shaking of a specific intensity. In general, dynamic response of a structure during ground shaking is a very complex behaviour. It depends on a number of inter- related parameters that are often very difficult to predict precisely. These include ground shaking that the building will experience, the extent to which the structure will be excited by response to the ground shaking: the strength of the materials in the structure; the quality of construction and condition of individual structural elements; the interaction of the structural and non- structural elements of the building; furnishings and contents present in the building at the time. Most of these factors can be estimated, but never precisely known.

Seismic evaluation of existing buildings demands a three- tiered process Screening Phase (Tier 1), Evaluation Phase (Tier 2) and Detailed Evaluation Phase (Tier 3) to assess either life safety or immediate occupancy performance level of the building. Screening Phase (Tier 1) uses a Rapid Visual Screening (RVS) methodology, while tier (2) and tier (3) needs more detailed and sophisticated analysis. Since Myanmar is adopting Myanmar National Building Code (MNBC) that is following International Building Code for design as a first step, FEMA 154 is considered relevant for adaption as shown in Figure (2).

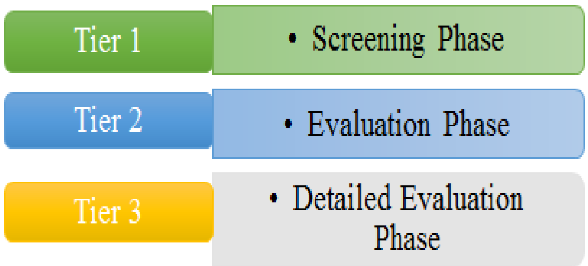

Figure (2) Three-tiered Process of Seismic Evaluation for Existing Buildings

Rapid Visual Screening (RVS) is a quick way of assessing the building vulnerability based on visual inspection. Once identified as potentially hazardous, such buildings should be further evaluated by a design professional experienced in seismic design to determine if, in fact they are seismically hazardous. The RVS procedure uses a methodology based on a sidewalk survey of a building and a data collection form, which the person conducting the survey completes, based on visual observation of the building from the exterior, and if possible, the interior. If large number of buildings needed to be evaluated, carrying out RVS of buildings minimizes the number of building that requires detailed assessment. Therefore, Rapid Visual Screening will be useful for all buildings except lifeline structures where detailed vulnerability assessment is always necessary. RVS procedure can be implemented relatively quickly and inexpensively to develop a list of potentially hazardous buildings without the high cost of a detailed seismic analysis of individual buildings. FEMA has updated the Rapid Visual Screening of Buildings for Potential Seismic Hazards: A Handbook (Third Edition) FEMA P-154/ January 2015.

5. SEISMICITY OF YANGON REGION

According to the Table 1, Ground motion for 0.2 sec Spectral Response acceleration for 0.2 S_s and motion for 1 sec spectral response acceleration at 2% of Yangon are 0.77 and 0.31 accordingly.

Table 1. Seismicity region determination from MECER spectral acceleration response

Seismicity Region	Spectral Acceleration Response, S_s (Short- period or 0.2 seconds)	Spectral Acceleration Response, S_1 (Long- period or 1 seconds)
Low	$S_s < 0.25g$	$S_1 < 0.10g$
Moderate	$0.25g \leq S_s < 0.50g$	$0.10g \leq S_1 < 0.20g$
Moderate High	$0.50g \leq S_s < 1.00g$	$0.20g \leq S_1 < 0.40g$
High	$1.00 \leq S_s < 1.50g$	$0.40g \leq S_1 < 0.60g$
Very High	$S_s \geq 1.50g$	$S_1 \geq 0.6g$

Note:** ***g = acceleration of gravity in horizontal direction

For Yangon Region according to the MNBC, S_A (0.2s) falls under Moderately High Seismicity Region category (0.50g < S_s < 1.00g) and SA (1s) falls under High Seismicity Region category (0.40g < S_1 < 0.60g).

6. SOIL INVESTIGATION OF CASE STUDY BUILDING

Soil Type, also known as Site Class, has a major influence on amplitude and duration of shaking and thus structural damage. The soil type should be identified during the planning stage and put into a readily usable map format for use during RVS. For the purpose of a rapid visual screening, the use of geotechnical engineering reports may be impractical. If soil maps of the area are not available, soil type can be estimated based on average shear wave velocity in the top 30 meters of soil, V_s^{30}. The investigation result of shear wave velocity for Pyay hostel area is 300 m/sec.The shear wave velocity of Kamaryut area is between 200 and 300 m/sec. Soil type D is mostly found in Yangon according to MNBC 2016.Therefore, soil type D is chosen for this building. Soil information map of Yangon area is shown in Figure (3).

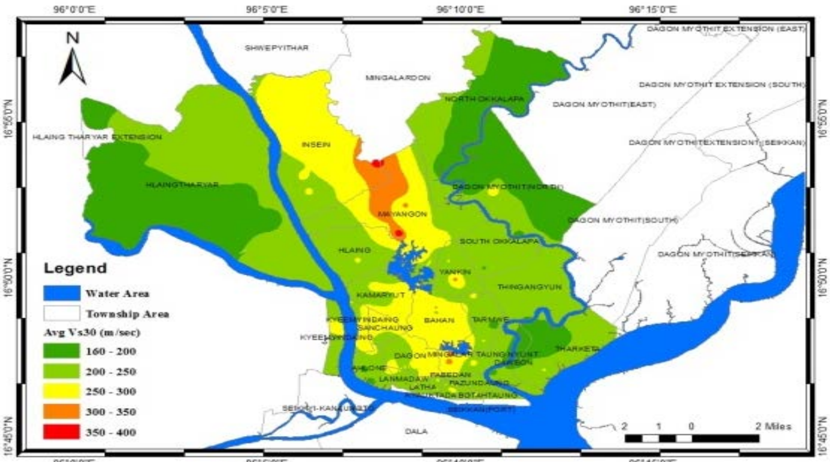

Figure (3) Soil Information Map of Yangon area

7. MATERIAL PROPERTIES OF CASE STUDY BUILDING

The experimental study on physical and mechanical properties of existing timber members (Pyay Hostel) are determined based on the ASTM Standard as shown in Figure 4.

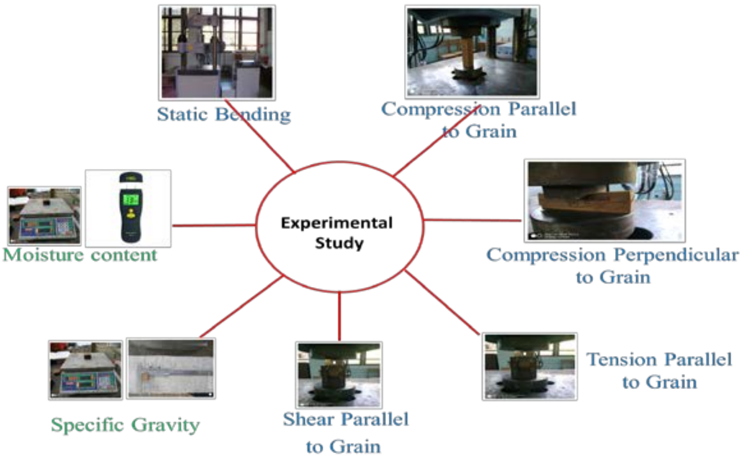

Figure 4. Experimental Study of Existing Timber Members (Pyay Hostel)

According to the experimental results, it is found that the physical properties of teak and pyingado used in this building are 10% and 14% of moisture content, and 0.56 and 0.8 for specific gravity. In the mechanical properties of timber members, the modulus of elasticity values for teak and pyingado are obtained 2.79×10^6 psi and 3.88×10^6 psi, and the modulus of rupture values of teak and pyingado are 1.94×10^4 psi and 2.81×10^4 psi respectively. On the other hand, it is found that the compressive strength of teak and pyingado are 636.69 psi and 1210.75 psi respectively.

8. CONDITIONAL SURVEY OF CASE STUDY BUILDING

A timber condition survey provides an assessment of the physical condition of timber within a building. It can evaluate the load-bearing properties of the structural timbers such as beams, joists, posts, rafters and purlins. It can also determine the condition of non-structural timber elements, such as floorboards, staircases, wood paneling, windows, doors, architrave and skirting as shown in Figure (4).

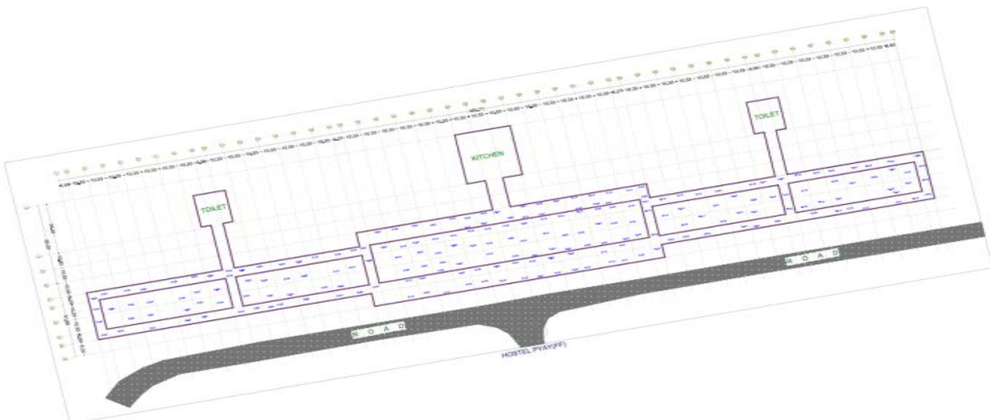

Figure 4. Plan View of Case Study Building

A condition survey provides the project architect, engineer or contractor with confidence that the original timber elements will meet the specified performance and appearance for the completed project. The extent of a condition survey can vary depending on the client's needs. It may involve a preliminary inspection to assess the general condition of the timber and to identify whether there are significant defects. This is then usually followed by a more detailed survey. The objective of the more detailed survey is to assess the condition and strength of the individual timber elements. This more detailed survey will identify and evaluate any damage which may have been caused by decay, fungi, wood destroying insects and other defects. Timber bearing structures can have, under normal circumstances, a shorter working life than other structures. During an inspection of timber structures we observe material characteristics, structural model and actual dimensions of elements and the possible actions of wood-decaying fungi or wood-destroying insects as shown in Figure (5).

Figure (5) Natural & Seasoning Defect of Case Study Building

9. DETERMINATION OF CUT-OFF SCORES OF CASE STUDY BUILDING

Use of the RVS methodology on a community-wide basis enables the RVS Authority to divide screened buildings into two categories: (1) those that are expected to have acceptable seismic performance; and (2) those that may be seismically hazardous and should be studied further. This requires that the RVS Authority determines, preferably as part of the pre-planning process, an appropriate cut-off score.

RVS Cut-off score is calculated by equation (1).

$$\mathbf{S = -\log_{10} (Probability\ of\ Collapse)} \qquad \text{(1)}$$

For this building, 2% Maximum Considered Earthquake probability in 50 years described in MNBC;

$$S = -\log_{10} (0.02) = 1.699 \qquad \text{(taken as 1.7)}$$

The score of 1.7 for MNBC is suggested as a cut-off for standard occupancy buildings, based on present seismic design criteria. Using this cut-off level, buildings having a score of 1.7 or less for MNBC 2016 should be investigated by a design professional experienced in seismic design. In some cases, a higher cut-off score may be warranted for critical or essential facilities. A higher score indicates a smaller probability of collapse. It does not, however, indicate a greater probability of other performance objectives being met, such as continued operation.

10. INSTRUCTION OF FILLING DATA COLLECTION FORM LEVEL (I) and (II)

Level (I) and (II) Data Collection forms can be seen in Figure 6 and 7. Level (I) form can be performed by a wide range of individuals, including civil engineers, structural engineers, architects, design professionals, building officials, construction contractors, facility mangers, fire-fighters, or other individual with a general background in building design or construction. The screeners fill out the forms and determine the scores to get seismic performance of the building. There are five different types of Level I Data Collection Form, representing different seismicity regions; Very High, High, Moderately High, Moderate and Low. The basic scores and score modifiers vary with seismicity regions.

Level (II) Data Collection Form is optional type and it should be filled by a civil or structural engineering professional, architect, or graduate student who has experiences and background knowledge on seismic evaluation of design of buildings. It should be noted that the screener applies same type of seismicity region to both Level I and II Form. If possible, Level I and II should be screened by same person. In Level II Data Collection Form, it includes four main sections;

(1) Building information and adjusted base line score,
(2) Structural modifiers to add to adjusted baseline score,
(3) Observable non-structural hazard, and
(4) Comments

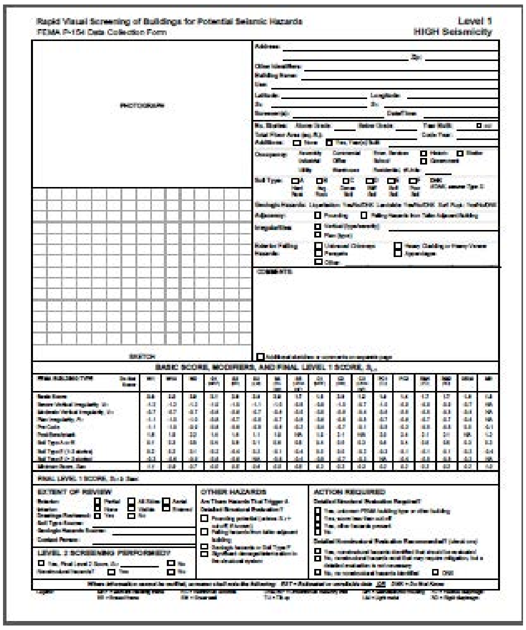
Rapid Visual Screening of Buildings for Potential Seismic Hazards
FEMA P-154 Data Collection Form
Level 1
HIGH Seismicity

Figure.6 Level (I) Data Collection Form

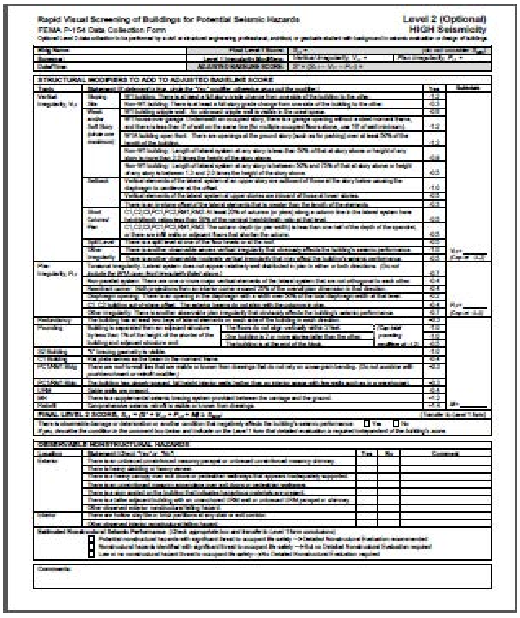
Rapid Visual Screening of Buildings for Potential Seismic Hazards
FEMA P-154 Data Collection Form
Level 2 (Optional)
HIGH Seismicity

Figure.7 Level (II) Data Collection Form

11. RVS RESULTS FOR CASE STUDY BUILDING

The main purpose of RVS results is to know the current situation of existing building in relation to seismic hazard and other related hazards. The final RVS score of case study building for moderate high seismicity region is higher than cut-off score and for high seismic region is lower than cut-off score.

12. CONCLUSION

As a result of all experimental investigated of teak and pyingado, their results are reasonable and applicable to use seismic safety assessment and evaluation of existing timber building. , the chemical treatment should be added to this building member for usage due to its nature of likely to be attacked by insects. The investigation result of shear wave velocity for Pyay hostel area is 300 m/sec.The shear wave velocity of Kamaryut area is between 200 and 300 m/sec. Soil type D is mostly found in Yangon according to MNBC 2016. According to the FEMA guideline, Rapid Visual Screening technique (RVS) is an efficient method to quickly identify the seismic resistance of the building. To implement this study, the seismicity of region, soil information and determination of pre-code building were considered as pre-field survey data. According to the RVS data evaluation, detailed structural evaluation is required for high seismicity performance and also not required for moderate seismic performance.

ACKNOWLEDGMENT

At first, the author would like to express deep appreciation to Dr. Nyan Myin Kyaw, for his insight suggestion and advice. And then, the author wishes to express his sincere gratitude to the Department of Engineering, Yangon Educational University ,NDT Engineering Teams for their invaluable help and guidance. Finally, the author would like to express grateful thanks to all teachers and parents for their supports, kindness and unconditional love and all his friends for their helps and advices on his studying.

REFERENCES

[1] Khin Maung Zaw. 2002 “An Evaluation of Ultimate Strength and the Performance of Timber Beams.” M.Engg. Thesis. University Teknologi Malaysia.
[2] Anon.1983. ASTM Standard Methods of Testing Small Clear Specimens of Timber D 143-09. 100 Barr Harbour Dr. PO Box C700 West Conshohocken, Pennsylvania 19428-2959, United States.
[3] MNBC2016, "Myanmar National Building Code 2016"
[4] Hélder S. Sousaa, Jorge M. Brancoa, Paulo B. Lourençoa, “Use of bending tests and visual inspection for multi-scale experimental evaluation of chestnut timber beams stiffness”.
[5] FEMA. 2000. Rapid Visual Screening of Buildings for the Seismic Rehabilitation of Buildings. FEMA 154, Federal Emergency Management Agency, Washington, D.C.
[6] FEMA. 2000. Prestandard and Commentary for the Seismic Rehabilitation of Buildings. FEMA 155, Federal Emergency Management Agency, Washington, D.C.

DIFFERENCE IN BUILDING COLLAPSE RISK IN YANGON DUE TO APPLICABLE DATASET

O. MURAO[1], T. IKEDA[2], M. KOSHIHARA[3], K. MEGURO[3], and T. SHWE[4]

[1] Professor, IRIDeS, Tohoku University, Japan,
[2] Professor, Nagaoka University of Technology, Japan,
[3] Professor, ICUS, IIS, The University of Tokyo, Japan,
[4] Professor, Yangon Technological University, Japan,
Correspond to Prof. O. MURAO (murao@irides.tohoku.ac.jp)

Keywords: *urban vulnerability, Myanmar, vulnerability function, ground condition, building structure*

1. INTRODUCTION

Myanmar has been increasingly thriving since the civilian government led by President U Thein Sein was established in 2011. However, similar to other Southeast Asian countries, it is vulnerable to natural disasters such as cyclones, floods, and earthquakes. Myanmar is at the greatest urban disaster risk for earthquakes. This is largely due to several populated, major cities such as Mandalay, Naypyidaw, Bago, and Yangon developed along the Sagaing Fault—a continental transform fault between the Indian and Sunda plates. In the 20th century, 6 earthquakes at or above 7.0 magnitude have occurred along the fault.

The authors have been involved in the SATREPS project "Development of a Comprehensive Disaster Resilience System and Collaboration Platform in Myanmar" since 2014 and were responsible for developing a vulnerability map in terms of building collapse risk for Yangon as the earthquake-related disaster group. However, Yangon City has not catalogued enough data for the assessment. Then, in 2019, we tried to evaluate its building collapse risk, as shown in Figure 1, with existing ground condition data which was published in 1934 [1-2], and vulnerability functions for Japanese buildings developed by the actual building damage dataset due to the 1995 Great Kobe Earthquake. The results are clarified as follows:

(1) Wooden buildings and RC account for 93.8% of all buildings.

(2) Based on Tokyo Metropolitan Government's method, the 567 objective wards were categorized into five ranks according to the building collapse risk value. It indicated that wards in the Dawpon and Tharkayta Townships, located in the west side of Pazundaung Creek, were the highest. Some newly developed outskirts areas, such as Hlaingtharyar or Dala, also appeared as vulnerable with Rank 4 and 5.

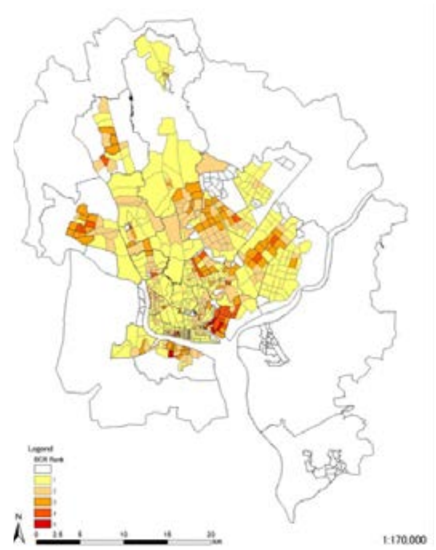

Figure 1. Distribution of building collapse risk in Yangon

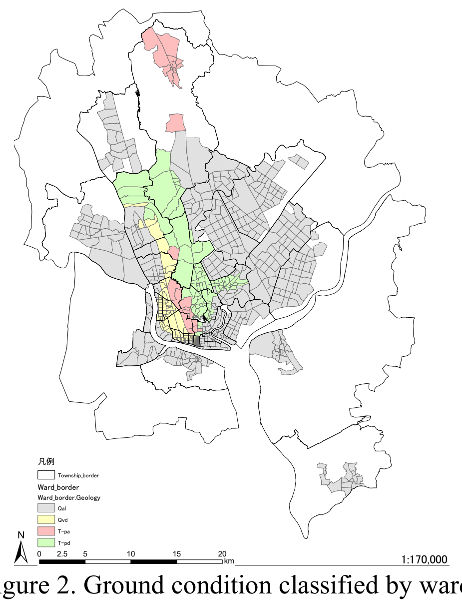

Figure 2. Ground condition classified by wards

2. DATA USED FOR REVISION

By the end of August 2019, we collected ground condition dataset and constructed vulnerability functions for the buildings in Yangon based on field surveys conducted in the SATREPS Myanmar Project. From the viewpoints above, this paper examines building collapse risk for Yangon using the latest dataset.

These will be demonstrated in the presentation.

REFERENCES

[1] H. H. Aung: "Potential Seismicity of Yangon Regeon (Geological Approach)," Advances in Geosciences, Vol.26, 139-151, 2010.

[2] H. L. Chhibber: "The Geology of Burma," Macmillan and Co. Limited, St. Martin's Street, London, 1934.

Opening ceremony

YTU main gate

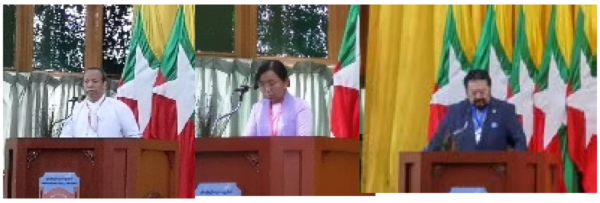

Prof. Myint Thein Rector of YTU, Prof .Khin Than Yu,
Prof. Kimiro Meguro, Director of ICUS, IIS, UTokyo (from left)

Key note speakers
Dr. Takayuki Miyoshi Nippon Koei Co., LTD (left) Dr. Toe Aung Direcotr of YCDC

Group photo of participants

Exhibitions

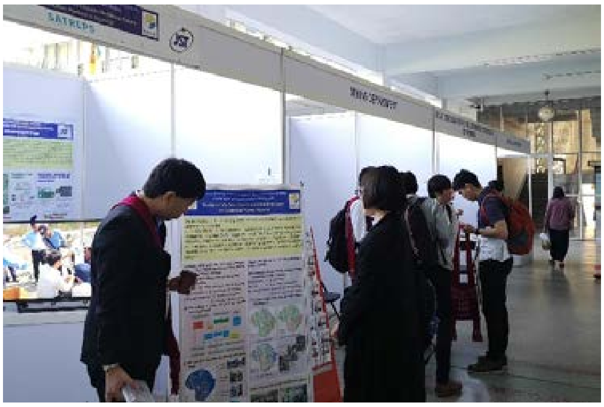

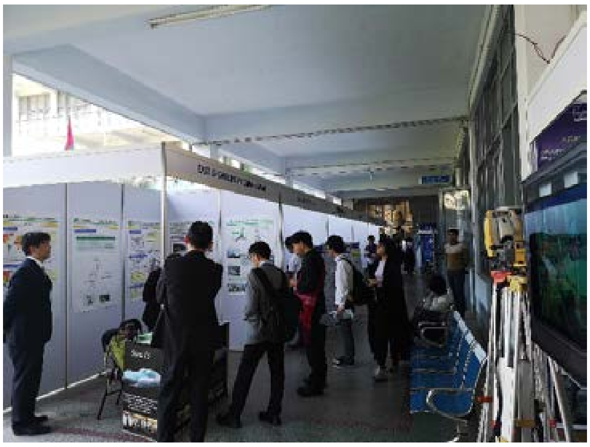

Presentation

Seminar Room 1 (Session B, D, F, H)

Presentation
Conference Room 1 (Session A, C, E, G)

Speakers

Closing Ceremony

Prof. Tun Naing, YTU

Prof. Kimiro Meguro, UTokyo

Prof. Pennung Warnitchai, AIT

Young-Researcher-Award recipients with Prof. Meguro (left) and Prof. TunNaing

Banquet party at Inya Lake Hotel, 9th night

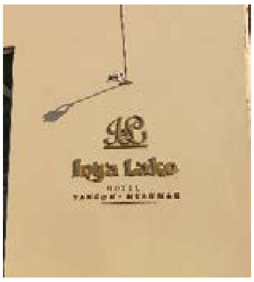

Opening Speech, Prof. TunNaing, YTU

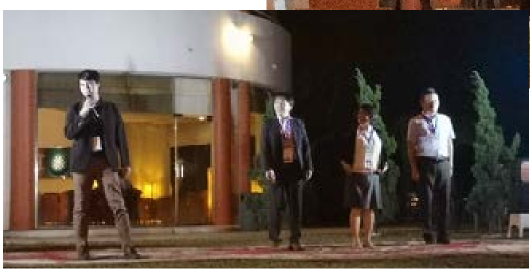

Closing Speech,
Prof. Kaori Hayashi, UTokyo

Lunch, Break time





Farewell Party at Esperade Lake View Hotel, 10th night


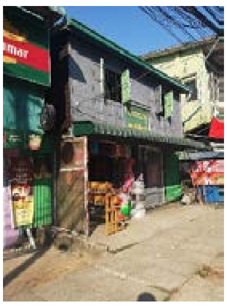



– ITINERARY

Day 1

5:30 Pick-up at Hotel

6:00 Check in at the Yangon Airport Domestic Terminal (T3)

7:15 Flight 7Y121 Departure from Yangon Airport

8:35 Arrival at Nyaung-U airport

9:15 Bagan Viewing Tower

10:30-12:00

Bagan Seminar at Ball Room, Bagan Umbra Hotel, Nyaung U Township, Bagan

Moderator Mr. Miyoshi

10:30 – 11:00 "The history and cultural significance of Bagan (TBC)"

U Aung Aung Kyaw, Head of Bagan region, Ministry of Religious Affairs and Culture

11:00 – 11:30 "Bagan as a UNESCO World Heritage site (TBC)"

U Than Zaw Oo, in charge of World Heritage registration, Ministry of Religious Affairs and Culture

11:30 – 11:45 Q & A

11:45 – 12:00 "Introduction to Bagan: temples and famous sites to visit (TBC)" YTU students

12:30- Lunch at Riverside restaurant

14:00- Visit to historical area

18:30- Dinner

Day 2

9:00-16:00 Visit to Historical area

- Thase Pyin Taw Village
- Sally
- Mount Popa

16:30 Check in

17:35 Flight Y5201 Departure from Nyaung-U airport

18:55 Arrival at Yangon airport

Technical Tour on 11-12th, visit to Bagan

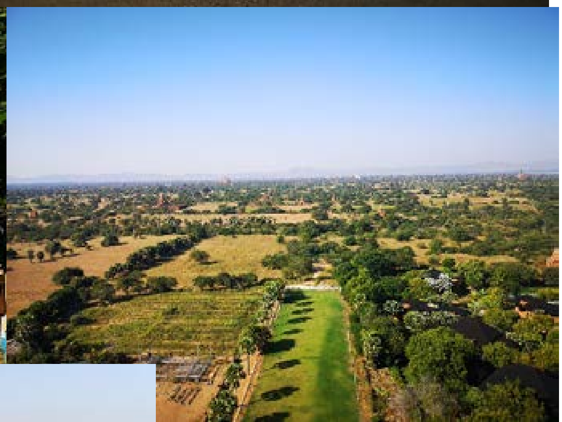

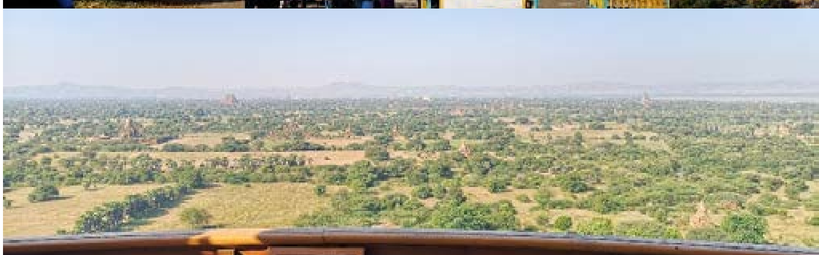

Group photo from Bagan Viewing Tower

Seminar at Bagan Umbra hotel







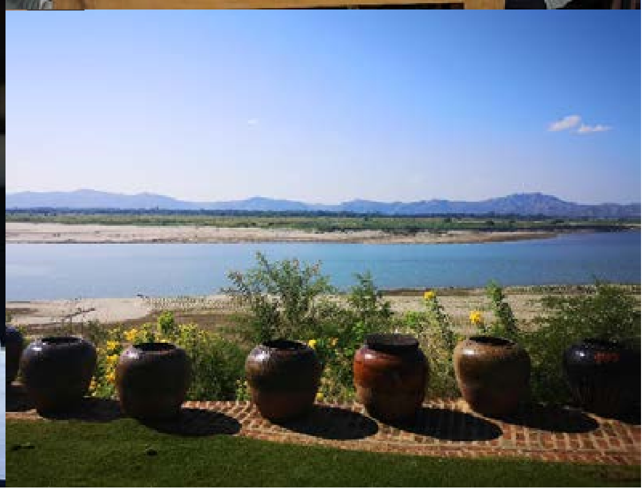

Lunch time

Visit to historical area

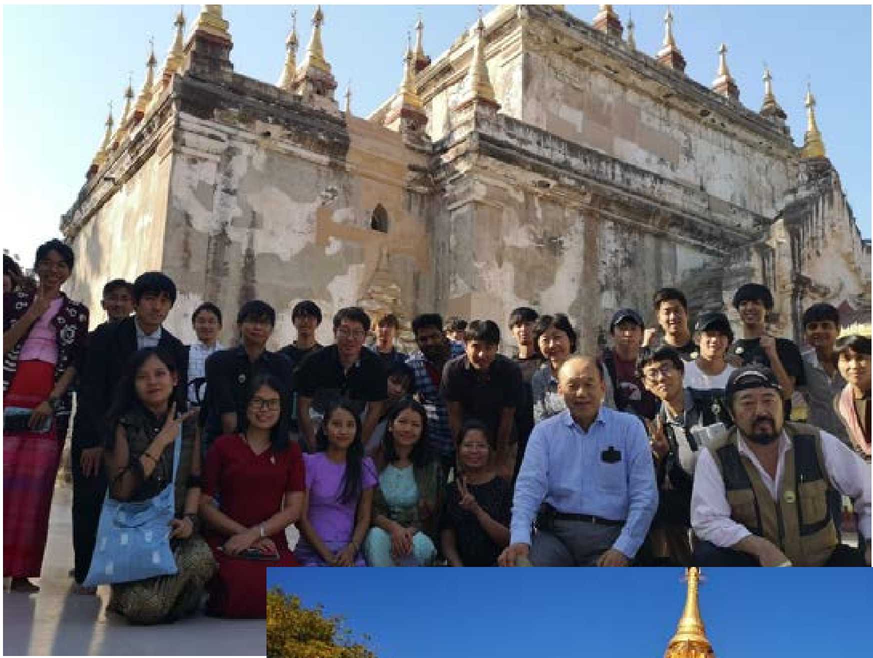

Manuha Temple

Ananda Temple

Shwezigon Pagoda

View of sunset

Dinner time

Nyaung-U Morning Market

Salay Yoke Sone Monastery at Salay

Group photo at Salay Yoke Sone Monastery

Lunch time at Salay

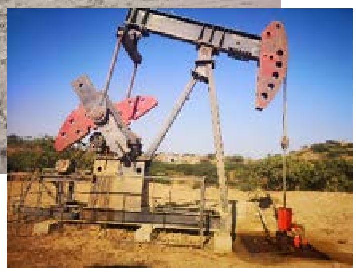

Oil mining around Chauk

Thabyinnyu Temple

International Center for Urban Safety Engineering
Institute of Industrial Science, The University of Tokyo
4-6-1 Komaba, Meguro-ku,
Tokyo 153-8505, Japan
Tel: +81-3-5452-6472
Fax: +81-3-5452-6476
http://icus.iis.u-tokyo.ac.jp
E-mail: icus@iis.u-tokyo.ac.jp